MEDICINAL PLANTS FOR PREVENTING AND TREATING CARDIOVASCULAR DISEASES AND THE DISCOVERY OF ACTIVE NATURAL PRODUCTS : ADVANCED MODELS, NOVEL PARADIGMS AND NEW MECHANISMS

EDITED BY: Ling Zhang, Yi Wang and Mirko Baruscotti
PUBLISHED IN: Frontiers in Pharmacology

frontiers Research Topics

ISSN 1664-8714
ISBN 978-2-83250-234-1
DOI 10.3389/978-2-83250-234-1

About Frontiers

Frontiers is more than just an open-access publisher of scholarly articles: it is a pioneering approach to the world of academia, radically improving the way scholarly research is managed. The grand vision of Frontiers is a world where all people have an equal opportunity to seek, share and generate knowledge. Frontiers provides immediate and permanent online open access to all its publications, but this alone is not enough to realize our grand goals.

Frontiers Journal Series

The Frontiers Journal Series is a multi-tier and interdisciplinary set of open-access, online journals, promising a paradigm shift from the current review, selection and dissemination processes in academic publishing. All Frontiers journals are driven by researchers for researchers; therefore, they constitute a service to the scholarly community. At the same time, the Frontiers Journal Series operates on a revolutionary invention, the tiered publishing system, initially addressing specific communities of scholars, and gradually climbing up to broader public understanding, thus serving the interests of the lay society, too.

Dedication to Quality

Each Frontiers article is a landmark of the highest quality, thanks to genuinely collaborative interactions between authors and review editors, who include some of the world's best academicians. Research must be certified by peers before entering a stream of knowledge that may eventually reach the public - and shape society; therefore, Frontiers only applies the most rigorous and unbiased reviews.
Frontiers revolutionizes research publishing by freely delivering the most outstanding research, evaluated with no bias from both the academic and social point of view. By applying the most advanced information technologies, Frontiers is catapulting scholarly publishing into a new generation.

What are Frontiers Research Topics?

Frontiers Research Topics are very popular trademarks of the Frontiers Journals Series: they are collections of at least ten articles, all centered on a particular subject. With their unique mix of varied contributions from Original Research to Review Articles, Frontiers Research Topics unify the most influential researchers, the latest key findings and historical advances in a hot research area! Find out more on how to host your own Frontiers Research Topic or contribute to one as an author by contacting the Frontiers Editorial Office: frontiersin.org/about/contact

MEDICINAL PLANTS FOR PREVENTING AND TREATING CARDIOVASCULAR DISEASES AND THE DISCOVERY OF ACTIVE NATURAL PRODUCTS : ADVANCED MODELS, NOVEL PARADIGMS AND NEW MECHANISMS

Topic Editors:
Ling Zhang, Zhejiang Chinese Medical University, China
Yi Wang, Zhejiang University, China
Mirko Baruscotti, University of Milan, Italy

Citation: Zhang, L., Wang, Y., Baruscotti, M., eds. (2023). Medicinal Plants for Preventing and Treating Cardiovascular Diseases and the Discovery of Active Natural Products : Advanced Models, Novel Paradigms and New Mechanisms. Lausanne: Frontiers Media SA. doi: 10.3389/978-2-83250-234-1

Table of Contents

frontiers in Pharmacology

REVIEW
published: 13 May 2021
doi: 10.3389/fphar.2021.675999

Chinese Herbal Medicines and Active Metabolites: Potential Antioxidant Treatments for Atherosclerosis

Luxia Song[1,2], *Jie Zhang*[1,2], *Runmin Lai*[1,2], *Qiuyi Li*[1,2], *Jianqing Ju*[2] *and Hao Xu*[2]*

[1]*Graduate School, Beijing University of Chinese Medicine, Beijing, China,* [2]*National Clinical Research Center for Chinese Medicine Cardiology, Xiyuan Hospital, China Academy of Chinese Medical Sciences, Beijing, China*

Atherosclerosis is a complex chronic disease that occurs in the arterial wall. Oxidative stress plays a crucial role in the occurrence and progression of atherosclerotic plaques. The dominance of oxidative stress over antioxidative capacity generates excess reactive oxygen species, leading to dysfunctions of the endothelium and accelerating atherosclerotic plaque progression. Studies showed that Chinese herbal medicines and traditional Chinese medicine (TCM) might regulate oxidative stress; they have already been used to treat diseases related to atherosclerosis, including stroke and myocardial infarction. This review will summarize the mechanisms of oxidative stress in atherosclerosis and discuss studies of Chinese herbal medicines and TCM preparations treating atherosclerosis, aiming to increase understanding of TCM and stimulate research for new drugs to treat diseases associated with oxidative stress.

Keywords: oxidative stress, atherosclerosis, anti-oxidant treatment, traditional Chinese medicine, Chinese herbal medicines

OPEN ACCESS

Edited by:
Ling Zhang,
Zhejiang Chinese Medical University, China

Reviewed by:
Mingbao Lin,
Chinese Academy of Medical Sciences and Peking Union Medical College, China
Zhenzhong Yang,
Zhejiang University, China

***Correspondence:**
Hao Xu
xuhaotcm@hotmail.com

Specialty section:
This article was submitted to Ethnopharmacology, a section of the journal Frontiers in Pharmacology

Received: *04 March 2021*
Accepted: *16 April 2021*
Published: *13 May 2021*

Citation:
Song L, Zhang J, Lai R, Li Q, Ju J and Xu H (2021) Chinese Herbal Medicines and Active Metabolites: Potential Antioxidant Treatments for Atherosclerosis. Front. Pharmacol. 12:675999. doi: 10.3389/fphar.2021.675999

INTRODUCTION

Atherosclerosis is one of the primary causes of death and is becoming one of the greatest threats to human health. Lancet Global Health reported that the number of patients with carotid plaques and stenosis worldwide increased significantly from 2000 to 2020 (Song et al., 2020). Atherosclerotic plaques cause vessel stenosis, which hinders the normal blood flow and leads to ischemia changes in tissues and organs (Willeit et al., 2003). Depending on the location of the atherosclerotic plaque, it may cause coronary artery disease, cerebrovascular disease (stroke), or peripheral arterial disease. Several factors induce atherosclerosis (Libby et al., 2019), including hypertension, hyperlipidemia, diabetes, long-term smoking, obesity; there are also non-disease factors such as gender and age (Gress et al., 2000; McClelland et al., 2006; Tyrrell and Goldstein, 2021). The pathogenesis of atherosclerosis is hypothesized to include inflammation, lipid infiltration, oxidative stress, platelet hyperfunction, immune dysfunction, and shear stress (Mury et al., 2018). Oxidative stress and inflammation are two primary factors in the progression of atherosclerosis (Hulsmans and Holvoet, 2010). When the antioxidant activity is insufficient to reduce reactive oxygen species (ROS), excess of the latter jeopardizes arterial endothelial function and threatens plaque stability (Davignon and Ganz, 2004; Laufs et al., 2005).

In this review, we collected the relevant clinical and experimental studies and reviews by searching papers published from January 2000 to February 2021 in Pubmed, Web of science, the China National Knowledge Internet (CNKI), and the China academic database, Wanfang, using "atherosclerosis", "oxidative stress", "TCM" or "TCM formula" or "TCM preparation" or "Chinese herbal medicine" or "herbal active compounds" or "herbal active ingredients" or

"herbal monomer" as the term. We will first review the mechanism of atherosclerotic plaque formation and progression. Then we discuss oxidative stress in the development of atherosclerotic plaques. Finally, we summarize experimental and clinical research on Chinese herbal medicines, active metabolites, and TCM prescriptions to treat atherosclerosis. The purpose of our review is to summarize the efficacy and mechanism of the Chinese herbal medicines in treating atherosclerosis from the perspective of antioxidants and provide evidence and deeper insights for future drug exploration and application in this area.

FORMATION AND PROGRESSION OF ATHEROSCLEROSIS

The structure of typical arterial walls includes vascular intima, media, and adventitia. Typical atherosclerotic are characterized by intimal thickening, excessive deposition of lipid, and infiltration of monocytes and lymphocytes. Endothelial injury dysfunction initiates atherosclerosis. Endothelial cells attach to the inner sides of arterial walls, where they help mediate immune functions by expressing adhesion molecules during inflammation that mediate the removal of swallowing foreign bodies (Libby et al., 2011). NO, prostacyclin, and bradykinin are generated by endothelial cells (Davignon and Ganz, 2004); these factors dilate blood vessels and prevent white blood cell adhesion and platelet aggregation. Endothelial cells also produce endothelin and angiotensin II that regulate vasoconstriction, promoting the proliferation of smooth muscle cells and affecting plaque progression.

Hypertension (Li et al., 2020a), hyperlipidemia (Drechsler et al., 2010), chronic smoking (Naya et al., 2011), and changes in shear stress (Chatzizisis et al., 2007) are risk factors for atherosclerosis; all result in inflammation and endothelial cell dysfunction, causing changes in permeability and expression of adhesion molecules such as vascular cell adhesion molecule-1 (VCAM-1) and E-selectin (Tabas et al., 2015). Adhesion molecules recruit inflammatory monocytes to adhere to endothelial cells and infiltrate the arterial intima (Tabas et al., 2007). Low-density lipoprotein (LDL) is transported to the arterial wall by recognizing guanine nucleotide exchange factor 4 (DOCK4) and scavenger receptor type B (SR-B1) in endothelial cells and modified to oxidized LDL (ox-LDL) (Huang et al., 2019). Leukocytes transform into macrophages and express SRs such as SR-A1, lipoxygenase 1 (Lox1), and CD36, recognizing the oxidized epitope of ox-LDL and internalizing ox-LDL to form foam cells (Canton et al., 2013; Chistiakov et al., 2017). Macrophages are the primary inflammatory cells in atherosclerotic plaques and are significant in plaque formation; they modulate plaque stability by polarizing into M1 and M2 macrophages (Canton et al., 2013).

M1 macrophages secrete pro-inflammatory factors TNF-α, IL-6, IL-1β, inducible nitric oxide synthesis (iNOS), and other effectors that promote early plaque formation, thinning fibrous caps, and enhancing immune response (Moore and Tabas, 2011; Barrett et al., 2019; Liao et al., 2020). Reverse cholesterol transport (RCT) is an important mechanism that maintains balanced lipid metabolism. High-density lipoprotein (HDL) transports cholesterol from extrahepatic tissue such as foam cells and atherosclerotic plaques to the liver for catabolism (Yu et al., 2019). HDL participates in RCT and exerts antioxidant and anti-inflammatory functions. In atherosclerosis, the structure and composition of HDL changes, hindering RCT and accelerating plaque progression (Ouimet et al., 2019). LXRα (liver X receptorα)/ABCA1 (ATP binding cassette subfamily A member 1) is a critical signal in RCT. Changes in this pathway promote the entry and retention of cholesterol-containing LDL particles in the arterial wall, causing early atherosclerosis lesions characterized by accumulation of macrophages, foam cells, and lipid droplets.

In atherogenesis, smooth muscle cells (SMCs) migrate to the inner membranes of the arterial walls and secrete extracellular matrix (ECM) components such as collagen and proteoglycan. Proteoglycan regulates ECM remodeling and cytokine function, interacting with apolipoprotein B, and retaining LDL under the endothelium (Stephens et al., 2011), forming a fibrous cap with proliferated SMCs covering the plaques. The fibrous cap covers macrophage derived foam cells. As the disease continues, these foam cells undergo apoptosis, causing the accumulation of extracellular lipids to form lipid-rich plaque cores, enlarged lipid or necrotic cores, that protrude into the artery. In advanced stages of atherosclerosis, the apoptosis of SMCs and the decomposition of collagen and elastin (exacerbated by the inflammatory process (Karunakaran et al., 2021)) cause rupture of the fibrous cap around the lipid core and incite coagulation factors to interact with tissue factors, leading to thrombus formation and associated complications (**Figure 1**).

OXIDATIVE STRESS AND ATHEROSCLEROSIS

Oxidative stress refers to the increased production of ROS in tissues or cells that weaken scavenging ability. Oxidative stress and inflammation are two major mechanisms of atherosclerosis. They interact with one another and form a vicious cycle in plaque progression. ROS include superoxide (compounds containing superoxide ion), hydrogen peroxide (H_2O_2), hydroxyl radicals, and nitric oxide radicals. These ROS participate in cell growth, proliferation, apoptosis, endothelial activation, mitochondrial damage, adhesion, and vascular inflammation process in atherosclerosis (Li and Shah, 2004; Madamanchi et al., 2005; Zhang et al., 2020a) (**Figure 2**). Major sources of ROS include nicotinamide adenine dinucleotide phosphate oxidase (NADPH oxidase or Nox), mitochondrial enzymes, Lox, uncoupled endothelial nitric oxide synthase (eNOS or NOS3), myeloperoxidases (MPO), cyclooxygenase (COX), mitochondria, and xanthine oxidase (XO). NADPH oxidase is the primary enzyme of ROS generation and has seven isoforms, namely Nox1-Nox5, Duox1, and Duox2, found in endothelial cells, vascular SMCs, fibroblasts, or perivascular adipocytes (Konior et al., 2014). Malondialdehyde (MDA), a lipid oxidation product, modifies LDL particles, leading to vascular

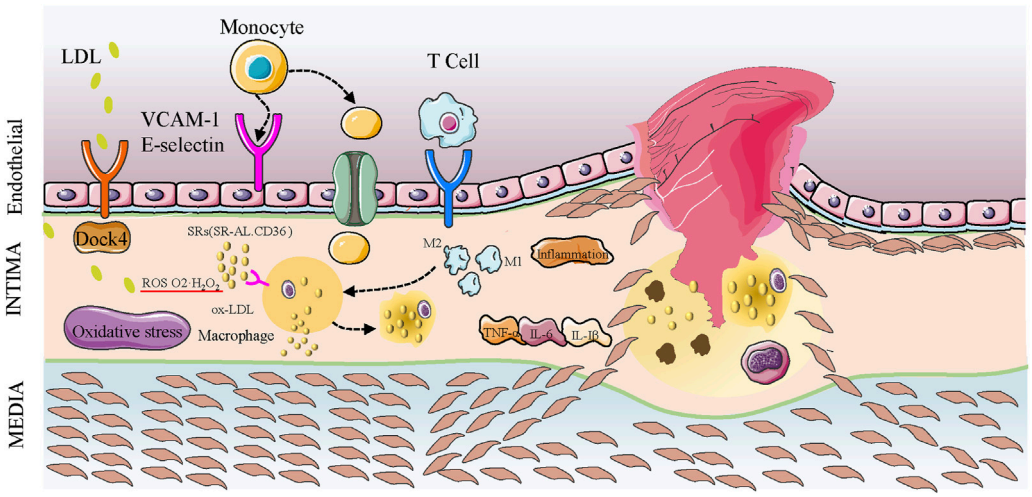

FIGURE 1 | Development of atherosclerotic plaques. LDL enters the arterial intima via endothelial cells expressing SR-B1 receptors in combination with DOCK4 action. LDL particles are oxidized to ox-LDL, and the monocytes entering the intima are transformed into macrophages that phagocytize ox-LDL mediated by surface SR (SR-A1, CD36). They also phagocytize other cholesterols in the intima to form foam cells. Macrophages are polarized into M1 and M2 forms. M1 macrophages release pro-inflammatory factors such as IL-6 to promote plaque progression, and oxidative stress promotes inflammatory factors. SMCs enter the intima to form fibrous caps, and oxidative stress and inflammation promote apoptosis and cell death in the plaque, leading to the accumulation of lipid and lipid cores. The continuous inflammation and oxidative stress causes the lipid nuclei to enlarge, the fibrous cap dilutes and ruptures, and platelets accumulate to form thrombi.

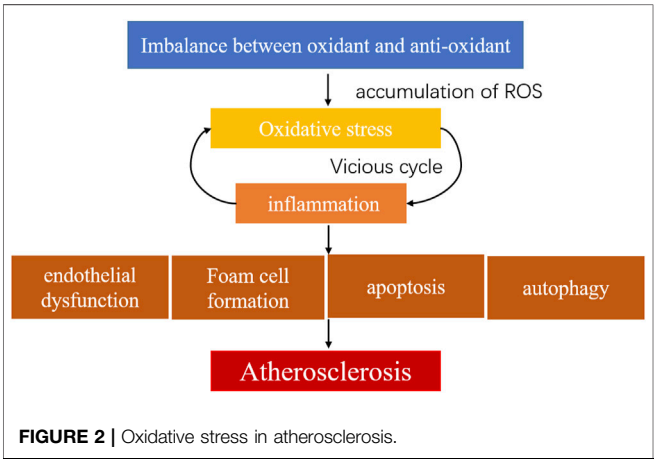

FIGURE 2 | Oxidative stress in atherosclerosis.

endothelial cell structure changes and jeopardizing endothelial function. Superoxide dismutase (SOD), glutathione (GSH), catalase (CAT), paraoxonase (PON), and nitric oxide (NO) are antioxidants that degrade excessive ROS to maintain internal homeostasis. The dominance of oxidation over antioxidant capabilities leads to excess accumulation of oxygen free radicals and metabolites (Cadenas, 2018). This disequilibrium leads to oxidative stress in atherosclerotic diseases (Griendling and FitzGerald, 2003a; Griendling and FitzGerald, 2003b; Sies, 2015). ROS produced by macrophages and SMCs may participate in inflammation, endothelial dysfunction, apoptosis, autophagy, and increased plaque vulnerability (Channon, 2002; Lin et al., 2012). Over-activation of Nox increases superoxide formation and ROS generation, impairing the NO production in the arterial wall and causing vascular endothelial dysfunction. For example, eNOS is associated with arterial endothelial function. Tetrahydrobiopterin (BH4) and L-arginine are cofactors for eNOS production. Insufficient synthesis of either of these two factors cause eNOS reduction or uncoupling, impairs NO production, and accelerates superoxide accumulation, causing endothelial dysfunction and hastening atherosclerosis (Antoniades et al., 2006; Antoniades et al., 2007; Daiber and Chlopicki, 2020). However, the evidence also suggests that the endothelial isoform Nox4 produces protective H_2O_2, maintains endothelial function, reduces macrophage adhesion to endothelial surfaces, and provide anti-atherosclerotic functions (Schürmann et al., 2015; Langbein et al., 2016). XO produces ROS through molecular oxygen as an electron acceptor (Förstermann et al., 2017). After ROS accumulation in the arterial walls, the inhibition of xanthine dehydrogenase (XDH) and the activation of XO activity causes active oxygen production, creating a vicious cycle (McNally et al., 2003). XO also stimulates macrophages and vascular smooth muscle cells (VSMCs) to generate Lox-1 and increase ROS accumulation. Lox-1, a specific receptor for ox-LDL, activates ROS generation and NF-κB (Murdocca et al., 2021), impairing eNOS expression and causing endothelial dysfunction. ROS converts XDH into XO, causing mitochondrial damage (Zhang et al., 2020b). MPO is an oxidant highly expressed in neutrophils that produces hypochlorous acid (HOCI) from H_2O_2 and becomes a significant ROS generator in inflammatory response. In atherosclerosis-related diseases, MPO oxidizes apolipoprotein A1 (ApoA1) in high-density lipoprotein (HDL) (Huang et al., 2013) and impairs cholesterol acceptor function (Huang et al., 2014). Overproduction of HOCI, which MPO generates, can directly jeopardize macrophages, causing cell death and increasing plaque inflammation by recruiting neutrophils and

accelerating plaque progression (Hickey, 2011; Duivenvoorden et al., 2013; Guo et al., 2020). The adhesion molecules expressed on endothelium recruit monocytes, and inflammatory cells stimulate monocytes to infiltrate into the intima, which mutually affects endothelial function. Oxidative stress occurring in plaques activates inflammatory pathways, such as NF-κB, and enhances adhesion molecule production, promoting plaque progression and thrombus formation via platelet activation (Liu et al., 2021). It also participates in macrophage polarization and increases M1 production, activating inflammation and reducing stability of vulnerable plaques (Yang et al., 2020a). ROS induces SRs in SMCs, leading to transformation into foam cells and promoting the release of matrix metalloproteinases, causing dilution of fibrous caps and plaque disruption (Kattoor et al., 2017).

Many studies examined ROS-stimulating arterial walls producing cytokines to activate signal pathways. The mechanism and critical targets of oxidative stress in the occurrence and development of atherosclerosis have also been further explored. Nrf2 eliminates ROS production, increasing the expression of antioxidant enzyme genes and maintaining oxidation/antioxidant balance in atherosclerosis (Zhu et al., 2019a). Sirtuin (Sirt) family proteins, the silent information regulators of deacetylase activity, are also crucial in the process of oxidative stress in atherosclerosis. Overexpression of Sirt1 up-regulates antioxidant-related expression, promotes the generation of transcription factor forkhead protein O subfamily 3a (FOXO3a)/PGC-1α complex, and up-regulates SOD secretion, exerting an antioxidant role against the progression of atherosclerosis (Olmos et al., 2013). Uncoupling proteins (UCPs), members of the mitochondrial transporter proteins family, act as proton transporters on the inner mitochondrial membrane related to ROS production, endothelial dysfunction, cell apoptosis, and proliferation; these also become target genes in atherosclerosis (Kim et al., 2007). An in-depth study of the specific mechanisms of oxidative stress in atherosclerosis would help identify new medications to treat atherosclerosis.

TCM FOR TREATMENT OF ATHEROSCLEROSIS, TARGETING OXIDATIVE STRESS

Chinese Herbal Medicines and Active Metabolites of Herbs

Resveratrol

Resveratrol is a natural phenolic compound found in varieties of plants, such as grapes and peanut, as well as Chinese herbal medicine, including *Reynoutria japonica* Houtt [Polygonaceae; Polygoni cuspidati rhizoma et radix] and *Veratrum nigrum* L. [Melanthiaceae]. Studies revealed that resveratrol mediates anti-atherosclerosis and heart protection. It protects endothelial cells from lipid damage, promotes vasodilation by regulating nitric oxide synthesis, and scavenges oxygen radicals and superoxide radicals by limiting lipid peroxidation, inhibiting platelet aggregation, and SMCs proliferation (Mohar and Malik, 2012; Bonnefont-Rousselot, 2016; Wiciński et al., 2018). Resveratrol reduces MDA, COX-1, and Nox production and activates SOD and GSH to balance the oxidation and antioxidant capacities, leading to eNOS generation to reduce endothelial dysfunction and pathological atherosclerotic changes (Szewczuk et al., 2004; Chow et al., 2007; Vivancos and Moreno, 2008; Bruedigam et al., 2011; Li et al., 2018a; Haimei et al., 2019; Li et al., 2019c; Yang et al., 2019). Transcription factor EB (TFEB) regulates homeostasis and maintains oxidant/antioxidant balance. Resveratrol promotes the translocation of TFEB from the cytoplasm to the nucleus in human umbilical vein endothelial cells (HUVECs) to activate TFEB and exert antioxidant effects, reducing autophagy and relieving endothelial dysfunction (Zhou et al., 2019). Similar results were found in clinical trials showing a beneficial effect of resveratrol in atherosclerosis by reducing oxidative stress (Imamura et al., 2017; Mansur et al., 2017). However, Gliemann et al. revealed that, instead of heart protection, supplementation of resveratrol did not affect Sirt 1, eNOS, or SOD expression and may impair the beneficial effects of physical exercise on cardiovascular health in older men (Gliemann et al., 2013). While affirming the effect of resveratrol on atherosclerosis, some researchers raised doubts. Berbée et al. compared resveratrol with statins in the treatment of ApoE*3-Leden CETP atherosclerotic mice, and showed that resveratrol alone reduced plaque volume (similar to use atorvastatin alone), but did not affect oxidative stress-related indicators PON1, COX-1, COX2, Lox-1, and MnSOD (Berbée et al., 2013). These findings suggest that more evidence is needed to confirm resveratrol's antioxidant effects on atherosclerosis (**Table 1**).

Curcumin and Its Analogues

Curcumin is the active ingredient of *Curcuma longa* L. [Zingiberaceae; Curcumae radix; Curcumae longae rhizoma]. It is a polyphenol demonstrated to act as a free radical scavenger and antioxidant that benefits in treating cardiovascular diseases (Zingg et al., 2013; Panahi et al., 2018; Li et al., 2019b; Li et al. 2020b). Curcumin inhibits ROS generation, limits lipid peroxidation (Panahi et al., 2018), and enhances NO bioavailability (Goel et al., 2008; Li et al., 2019a). Studies demonstrated that curcumin suppresses ROS production in both animal models and *in vitro* by inhibiting ROS-related inflammation pathways and cytokines (Zingg et al., 2013), such as ERK1/2 pathway (Ouyang et al., 2019; Zhang et al., 2020a), the high-mobility-group protein B1(HMGB1)- toll-like receptor (TLRS)-NF-κB pathway (Lv et al., 2020), COX-2 (Lee et al., 2020), and others (Shi et al., 2017; Saji et al., 2018; Asadi et al., 2020), preventing endothelial dysfunction and adhesion molecules secretion. Pu et al. found that curcumin alleviated ROS-induced endothelial dysfunction through UCP2 and increased eNOS activity (Pu et al., 2013; Treviño-Saldaña and García-Rivas, 2017). Arterial dysfunction and oxidative stress caused by vascular aging are vital factors in the development of atherosclerosis. Laboratory studies revealed some mechanisms of curcumin's effect on aging arteries. Fleenor et al. (Fleenor et al., 2013) explored the effect of curcumin on carotid artery function and vascular oxidative stress in aged mice. They discovered that

TABLE 1 | Resveratrol for treatment of atherosclerosis by regulating oxidative stress.

Active ingredients	Subjects in study	Full botanical taxonomic names (yes/no)	Relevant gene targets	Impact on ROS related targets	Potential mechanism of AS protection	References
Resveratrol	$ApoE^{-/-}$ mice HAECs	No	PKA-CREB	↓ROS ↑eNOS	↓endothelial dysfunction ↓plague formation	Zhong et al. (2020)
	High fat diet C57BL/6J mice	No	Orai1	↓peroxynitrite anion (ONOO-) ↑eNOS	↓endothelial dysfunction	Haimei et al. (2019)
	HUVECs	No	TyrRS-PARP1	↓MDA ↑SOD	↓endothelial damage	Yang et al. (2019)
		No	$gp91^{Phox}$ rac1	↓Nox ↓ROS	↓ ox-LDL induced oxidative stress	Chow et al. (2007)
		No	TFEB	↓ROS ↓MDA	↓autophagy ↓oxidative stress	Zhou et al. (2019)
	RAW 264.7	No	—	↓ROS ↓H_2O_2 ↓PGE2	↓oxidative stress and inflammation	Vivancos and Moreno (2008)
	type 2 diabetes arteriosclerosis patients	No	—	↓diacron-reactive oxygen metabolites (d-ROM)	Improve arterial stiffness in patients with T2DM	Imamura et al. (2017)
	healthy and slightly overweight volunteers	No	Sirt1	↓ROS	↑ Sirt1 ↓oxidative stress	Mansur et al. (2017)
	healthy aged physically inactive men	No	Sirt 1	No effect on eNOS, SOD, CAT, GPx-1, Nox	no effect on oxidative stress indicators	Gliemann et al. (2013)
	ApoE*3-Leiden.CETP mice	No	—	No effect on PON-1, Lox-1, MnSOD	↓ plagues volume no effect on oxidative stress indicators	Berbée et al. (2013)

curcumin increased eNOS in the aged carotid artery, reversed endothelial-dependent dilation, reduced superoxide, and inhibited NADPH oxidase p67 subunit activity. After up-regulating ABCA1 expression and inhibiting SR-A and CD36 in macrophages, curcumin reduced ROS production and foam cell formation to stabilize vulnerable plaques (Soltani et al., 2017). Curcumin analogs, such as L3, tetrahydrocurcumin (THC), Cur-NPs(Meng et al., 2019), HASF (a dual ROS-sensitive and CD44 receptor targeting amphiphilic carrier) (Hou et al., 2020), and curcumin compounds, are synthetic compounds that have similar effects; for example, they elevate glutathione peroxidase (GPx) catalyze GSH, and have higher bioavailability than common curcumin, showing anti-oxidative stress in atherosclerosis through multiple gene targets (Naito et al., 2002; Huang et al., 2015; Zheng et al., 2016). In summary, the antioxidant effects of curcumin combat atherosclerosis by the following mechanisms: 1) Blocking enzymes that promote ROS generation; 2) increasing antioxidant enzyme activity; 3) reducing damage to endothelial cells by anti-inflammatory actions, enhancing eNOS, and reducing adhesion factors; and 4) reducing foam cell formation (more details in **Table 2**).

Salidroside

Salidroside is an active ingredient that exists in Chinese herbal medicine Hongjingtian (*Rhodiola crenulata* (Hook.f. & Thomson) H.Ohba [Crassulaceae; Rhodiolae crenulatae radix et rhizoma]); this agent reduces oxidative stress (Mao et al., 2010; Li et al., 2011a)and is used to treat atherosclerosis. In terms of relieving endothelial dysfunction after impaired ROS production, salidroside enhances eNOS production and activates several pathways, including Sirt1/Foxo1, AMPK, and Sirt3, regulating oxidative stress, inflammation, cell apoptosis, autophagy, and mitochondrial function (Xing et al., 2014; Xing et al., 2018; Zhao et al., 2019; Zhu et al., 2019b). Hemoxygenase 1(HO-1) is an important antioxidant enzyme in cell microsomes that mediates anti-inflammation and anti-oxidation and suppresses the activity of adhesion molecules (Zhang et al., 2018). Zhu et al. (Zhu et al., 2016) found that salidroside promotes the expression of HO-1 and NAD(P)H dehydrogenase-quinone oxidoreductase 1(NQO1), lowers MDA and ROS production by regulating Nrf2, and subsequently alleviates enthothelial dysfunction. Ni et al. believed that salidroside impaired the combination of ox-LDL with Lox-1 and affected foam cell formation and apoptosis in atherosclerosis by regulating Lox-1 content; during this process, there were no changes in HO-1 expression (Ni et al., 2017a). Although the anti-oxidation effect of salidroside has been determined, its specific mechanism still needs to be further explored (**Table 3**).

Active Ingredients of Danshen

The traditional Chinese herbal medicine Danshen (*Salvia miltiorrhiza* Bunge [*Lamiaceae*; *Salviae miltiorrhizae* radix et rhizoma]) has been widely applied in the treatment of atherosclerotic diseases in Asia with encouraging results (Li et al., 2018b; Ren et al., 2019). The chemical components in *Salvia* are divided into fat-soluble and water-soluble components. Salvianolic acids (A-G) are water-soluble components. Tanshinone I, tanshinone IIA, tanshinone IIB, methyl tanshinate, and danshendiol are fat-soluble components. Investigators discovered that salvianolic acids have a good therapeutic effect on atherosclerosis (Xiang et al., 2018; Ma et al., 2020; Yang et al., 2020b). In a diabetic rat model, salvianolic acid B (Ren et al., 2016) decreased Nox2 and Nox4

TABLE 2 | Curcumin and its analog for treatment of atherosclerosis by regulating oxidative stress.

Active ingredients	Subjects in study	Full botanical taxonomic names (yes/no)	Relevant gene targets	Impact on ROS related targets	Potential mechanism of AS protection	References
Curcumin	VSMCs	Yes	ERK1/2	↓ROS ↓CRP	↓inflammation	Zhang et al. (2020b)
		—	TGF-β Non-smad signal pathway	↓ROS	↓oxidative stress and inflammation	Asadi et al. (2020)
	THP-1	No	ERK1/2 HIF-1α	↓ROS	↓oxidative stress and inflammation ↓ macrophage apoptosis	Ouyang et al. (2019)
		No	SR-A, ABCA1	↓ROS ↑GSH	↓oxidative stress and inflammation ↓foam cell formation	Soltani et al. (2017)
	ApoE$^{-/-}$ mice and human cytomegalovirus (HCMV)	No	HMGB1-TLRS-NF-κB	↓ROS	↓oxidative stress and inflammation ↓endothelial dysfunction	Lv et al. (2020)
	HUVECs	No	PKC-CREB	↓ROS ↓COX-2	↓oxidative stress and inflammation ↓endoplasmic reticulum stress	Lee et al. (2020)
	Human peripheral blood mononuclear cells (HPBMCs)	No	NF-κBp65	↓ROS ↓MDA ↓PGE2 ↓COX ↓iNOS	↓oxidative stress and inflammation	Saji et al. (2018)
	human microvascular endothelial cells (HMEC)	No	NF-κB	↓ROS ↓MDA ↑SOD	↓oxidative stress and inflammation ↓adhesion molecules	Deng et al. (2017)
	C57BL6/N mice	No	—	↑SOD ↓Nox p67	↓endothelial dysfunction ↓oxidative stress ↓artery aging	Fleenor et al. (2013)
	SD rats UCP2-/- rats	No	AMPK/UCP2	↓ROS ↑eNOS	↓endothelial dysfunction ↓oxidative stress	Pu et al. (2013)
Curcumin analogsand compounds	L3 Diabetic mice	No	—	↓ROS ↓iNOS ↓MDA ↑SOD ↑GPx ↑NO	↓endothelial dysfunction ↓oxidative stress	Zheng et al. (2016)
	compounds THP1	No	PKCδ/Nox/ROS	↓ROS ↓Nox2	↓oxidative stress ↓matrix invasion during monocyte-macrophage differentiation	Huang et al. (2015)
	THC Rabbit	No	—	↓ox-LDL	↓oxidative stress	Naito et al. (2002)

TABLE 3 | Salidroside for treatment of atherosclerosis by regulating oxidative stress.

Active ingredients	Subjects in study	Full botanical taxonomic names (yes/no)	Relevant gene targets	Impact on ROS related targets	Potential mechanism of AS protection	References
Salidroside	Wistar rats HUVECs	No	NF-κB AMPKα —	↑SOD ↑NO ↑eNOS ↓ROS ↓Superoxide anion	↓endothelial dysfunction ↓Mitochondrial dysfunction ↓oxidative stress and inflammation	Xing et al. (2014)
	HUVECs	No	Nrf2	↓ROS ↓MDA ↑SOD ↑CAT ↑HO-1 ↑NAD(P)H dehydrogenase (quinone1) (NQO1)	↓endothelial dysfunction —	Zhu et al. (2016)
		No	AMPK, SIRT1 —	↓ROS ↓MDA ↓Nox2 ↑SOD ↑GPx	↓oxidative stress ↓mitochondrial dysfunction ↓cell apoptosis	Zhao et al. (2019)
		No	SIRT1, FOXO1	↓ROS ↓MDA ↓Nox ↑SOD	↓oxidative stress ↑Autophagy	Zhang et at. (2020a)
	THP1	No	MAPK, AKT, JNK, ERK	↓Lox-1	↓foam cell formation ↓foam cell apoptosis	Ni et al. (2017a)
	BABLc mice HUVECs	No	SIRT3	↑eNOS	↓oxidative stress induced premature senescence ↓inflammation	Xing et al. (2018)

TABLE 4 | Active ingredients in Danshen for treatment of atherosclerosis by regulating oxidative stress.

Active ingredients	Subjects in study	Full botanical taxonomic names (yes/no)	Relevant gene targets	Impact on ROS related targets	Potential mechanism of AS protection	References
Salvianolic acid B	diabetic rat	No	Bcl-2	↓MDA ↑SOD ↑eNOS↑NO ↓Nox2↓Nox4	↓oxidative stress ↓endothelial dysfunction	Ren et al. (2016)
Tanshinone IIA	LDL solution	Yes	—	↑SOD ↓ONOO-	↓LDL oxidation ↓oxidative stress	Niu et al. (2000)
	$ApoE^{-/-}$ mice	Yes	miR-146b miR-155	↓ox-LDL	↓oxidative stress and inflammation	Xuan et al. (2017)
		No	ERK, NF-κB	↓MDA ↑SOD	↓oxidative stress and inflammation	Liu et al. (2015)
	$ApoE^{-/-}$ mice Macrophages of mice	Yes	PPARγ	↓SR-A ↓ox-LDL	↓oxidative stress	Tang et al. (2011)
	rabbit	Yes	—	↓ROS ↓MDA	↓oxidative stress and inflammation	Fang et al. (2008)
		No		↓ox-LDL ↑SOD ↑GPx		Chen et al. (2012)
	HUVECs	Yes	Pregnane X receptor (PxR)	↑GSH disulfide	↓Mitochondrial Apoptosis ↓endothelial injury	Zhu et al. (2017a)
	HUVECs	No	—	↑SOD ↑NO	↓oxidative stress and inflammation ↓endothelial injury	Lin et al. (2006)
	J774 macrophage	No	—	↑GPx	↓apoptosis ↓oxidative stress	Li et al. (2008)
	HUVECs	No	PI3K/Akt/mTOR?LC3-I? LC3-II	↓MDA ↑SOD	↓oxidative stress ↓autophagy	Huimin et al. (2017)

expression, limiting ROS that caused endothelial dysfunction. The vasoprotective factors eNOS and NO also improved in this process, preventing the occurrence of atherosclerosis. Tanshinone IIA is one of the pharmacologically active ingredients derived from Danshen that participates in maintaining vascular homeostasis; it is widely used to prevent and treat coronary heart disease (CHD) in Asia (Gao et al., 2012; Feng et al., 2021). Tanshinone IIA competes with LDL oxidation induced by diverse oxidizing systems, like copper-, peroxyl radical-, and peroxynitrite, scavenging peroxyl radicals and preventing atherosclerosis (Niu et al., 2000). In animal experiments (the $ApoE^{-/-}$ model and high fatty diet rabbit), tanshinone IIA exerted antioxidant and anti-inflammatory effects by reducing ox-LDL, ROS, MDA, and other

TABLE 5 | Berberine for treatment of atherosclerosis by regulating oxidative stress.

Active ingredients	Subject in study	Full botanical taxonomic names (yes/no)	Relevant gene targets	Impact on ROS related targets	Potential mechanism of AS protection	References
Berberine	ApoE-/- mice AMPKα2$^{-/-}$/ ApoE$^{-/-}$mice HUVECs	No	UCP2 AMPK	↓MDA ↓ROS ↓IL-6	↓endothelial injury ↓oxidative stress	Wang et al. (2011); Tan et al. (2020)
	J774A.1	No	AMPK/mTOR	—	↓ox-LDL induced inflammation ↓autophagy	Fan et al. (2015)
	THP-1	No	NF-κB NLRP3	↓Nox	↓oxidative stress and inflammation	Jiang et al. (2017)
		No	NADPHgp91(Nox2 subunit)	↑SOD	↓endothelial dysfunction	Sarna et al. (2010)
		No	LXRα ABCA1	—	regulate lipid homeostasis ↓ox-LDL induced lipid accumulation	Lee et al. (2010)
	ApoE-/- mice THP-1	No	Nrf2/HO-1		↓foam cell formation	Yang et al. (2020c)
	Fibroblast cell 2BS	No	sirt1	↓ROS	↓oxidative stress ↓H_2O_2 induced Damage of mitochondrial membrane	Zhu et al. (2017b)
	SD rats Monocyte-derived macrophages (MDM)	No	ET-1	↓Lox-1 ↓MDA ↑SOD	↓oxidative stress ↓foam cell formation	Chi et al. (2014)
	HUVECs	No	TNFα NF-κB MAPK/Erk1/2	↓ROS↓Lox-1 ↓Nox2	↓oxidative stress and inflammation. ↓endothelial dysfunction	Caliceti et al. (2017)
	VSMCs	No	ERK1/2	↓ROS	↓VSMCs proliferation and migration	Cho et al. (2005)

pro-oxidative stress products to reduce lipid peroxidation and inhibit atherosclerosis progression via multiple targets (ERK, NF-κB, PPARγ, and miR) (Fang et al., 2008; Tang et al., 2011; Chen et al., 2012; Liu et al., 2015; Xuan et al., 2017). *In vitro* experiments showed that tanshinone IIA reduced the damage caused by H_2O_2, increased the production of antioxidant enzymes, and prevented endothelial cell injury from oxidative stress (Lin et al., 2006; Zhu et al., 2017a). Adjusting antioxidant enzyme GPx generation may be a critical step in reducing ROS-related functions like apoptosis, endothelial injury, and inflammation (Li et al., 2008; Fang et al., 2008; Zhu et al., 2017a). Tanshinone IIA also alleviates ROS-induced subsequent autophagy and apoptosis (Ni et al., 2017b; Chen et al., 2012; Huimin et al., 2017; Li et al., 2008), presenting potential anti-atherosclerosis effects (**Table 4**).

Berberine

Berberine is an active ingredient derived from the Chinese herbal medicine *Coptis chinensis* Franch. [Ranunculaceae; Coptidis rhizoma] that helps to treat atherosclerosis-related cardiovascular diseases (Mulvihill and Huff, 2010; Wu et al., 2010). It inhibits endothelial cell dysfunction via multiple mechanisms (Fatahian et al., 2020). By regulating UCP2 and Nox2, berberine blocks MDA and enhances SOD production, inhibiting the AMPK pathway to relieve inflammation and autophagy; it also protects against endothelial cell dysfunction in atherosclerosis (Sarna et al., 2010; Wang et al., 2011; Fan et al., 2015; Caliceti et al., 2017; Tan et al., 2020). Accumulation of foam cells and apoptosis leads to increased lipid core volume and thinning of the fibrous caps, resulting in rupture of vulnerable plaques. Studies showed that berberine maintained lipid homeostasis and reduced foam cells formation via LXRα/ABCA1 and Nrf/HO-1, limiting macrophage ox-LDL uptake and cholesterol efflux and inhibiting macrophages superoxide anion production (Lee et al., 2010; Yang et al., 2020c). Berberine also decreased endothelin-1 (ET-1) induced Lox-1 expression in monocyte-derived macrophages, acting as an antioxidant and reducing foam cell formation (Chi et al., 2014; Caliceti et al., 2017). Zhu X et al. (Zhu et al., 2017b) established a premature aging model using low-concentration berberine to interfere with hydrogen peroxide; they found that berberine combated premature aging in human diploid fibroblasts via Sirt1-mediated ROS reduction, protecting loss of mitochondrial membrane potential and showing an antioxidant effect. Berberine may inhibit cell senescence caused by reducing oxidative stress associated with age-related diseases. Berberine also inhibited the proliferation and migration of VSMCs by suppressing Nox activity (Cho et al., 2005) and suppressed ROS-dependent NLRP3 inflammasomes in human peripheral blood mononuclear cells (PBMCs) (Jiang et al., 2017), providing research targets for berberine in treating atherosclerosis. (**Table 5**).

Quercetin

Quercetin is widely distributed in the plant kingdom. Chinese herbal medicines such as *Styphnolobium japonicum* (L.) Schott [Fabaceae; Sophorae flos], *Platycladus orientalis* (L.) Franco [Cupressaceae; Platycladi cacumen], *Alpinia officinarum* Hance [Zingiberaceae; Alpiniae officinarum rhizoma], *Tussilago farfara* L. [Asteraceae; Farfarae flos], *Morus alba* L. [Moraceae; Mori folium; Mori cortex], and *Ginkgo biloba* L. [Ginkgoaceae; Ginkgo

TABLE 6 | Quercetin for treatment of atherosclerosis by regulating oxidative stress.

Active ingredients	Subjects in study	Full botanical taxonomic names (yes/no)	Relevant gene targets	Impact on ROS related targets	Potential mechanism of AS protection	References
Quercetin	$ApoE^{-/-}$ mice mouse peritoneal macrophages (MPMs)	no	—	↓ROS ↓p47phox ↓p67phox	↓oxidative stress	Xiao et al. (2017)
	ApoE-/- mice HUVECs	no		↓ROS ↓p47phox ↑NO ↑HO-1	↓oxidative stress ↓endothelial dysfunction	Luo et al. (2020)
	ApoE-/- mice HAEC	no		↑eNOS ↑HO-1	↓endothelial dysfunction	Shen et al. (2013)
	HAEC	no		↑GSH	↓oxidant production	Li et al. (2016a)
	HUVECs	no	p38 Nrf2	↓oxidant production ↑HO-1 ↑GCL	↓endothelial damage	Li et al. (2016b)
		no	SIRT1 AMPK NF-κB	↓Nox2 ↓Nox4	↓oxidative stress ↓endothelial dysfunction	Hung et al. (2015)
		no	—	↓MDA ↑NO	↓oxidative stress ↓endothelial dysfunction	Yi et al. (2011)
	ApoE-/- mice bone marrow-derived macrophages	no	CD36	↓MDA	↓oxidative stress and inflammation	Loke et al. (2010); Lara-Guzman et al. (2012)
			$gp91^{Phox}$ rac1	↓Vascular superoxide ↑HO-1 ↑eNOS	↓foam cell formation ↓endothelial dysfunction	
		no	Sirt1	↓ROS	↓oxidative stress ↓apoptosis	Jiang et al. (2020)
		no	PCSK9 CD36 PPARγ LXRα	↓ox-LDL	↓oxidative stress and inflammation ↓lipid deposition	Jia et al. (2019)
		no	—	↓MDA ↓oxidized phosphocholine	↓HDL oxidation	Cui et al. (2017)
	RAW264.7	no	—	↓ROS ↓Lox-1	↓oxidative stress and inflammation ↓lipid deposition	Xue et al., (2017)
	C57BL/6	no	PI3K/AKT	↓ROS	↓oxidative stress and inflammation	Lu et al. (2017)
	VSMCs		NF-κB		↓apoptosis	
	HUVECs	no	TLR/NF-κB	↓MPO ↓COX	↓inflammation ↓endothelial dysfunction	Bhaskar et al. (2016)
	RAW264.7	no	MST1 LC3-II/I	↓ROS	↓autophagy	Cao et al. (2019)
			SA-β-GAL		↓foam cell formation	
			—		↓aging	

folium; Ginkgo semen] (Zhanxia et al., 2019) are major sources of quercetin. Quercetin is also found in fruits, nuts, and vegetables (Stromsnes et al., 2020). Studies showed that quercetin has potential to treat atherosclerosis by reducing inflammation and resisting oxidative stress (Deng et al., 2020). The antioxidant effects of quercetin occur first by inhibition of p47phox and p67phox activity, reducing NADPH oxidase activation to decrease ROS production (Xiao et al., 2017). Sirt1 and AMPK may be potential key targets for reducing Nox2 and Nox4 expression (Hung et al., 2015) and regulating ROS, superoxide (Loke et al., 2010), and MDA production (Yi et al., 2011; Lara-Guzman et al., 2012). Quercetin also increases generation of antioxidants such as HO-1 (Shen et al. 2013; Luo et al., 2020), NAD(P)H dehydrogenase, and glutamate-cysteine ligase (GCL) by activating Nrf2 (Li et al., 2016b). Li et al. (Li et al., 2016a) studied the mechanism of quercetin restoring the expression of GSH in human aortic endothelial cells (HAEC) that was relevant to GCL. In this manner, quercetin inhibited oxidative stress. After balancing oxidation and anti-oxidation, NO and eNOS bioavailability improved, reducing inflammation (Lara-Guzman et al., 2012; Bhaskar et al., 2016; Lu et al., 2017; Xue et al., 2017; Jia et al., 2019), autophagy (Cao et al., 2019), and apoptosis (Lu et al., 2017; Jiang et al., 2020), and inhibiting the recruitment of monocytes by adhesion factors, thereby protecting endothelial cell function. By elevating HDL cholesterol absorption capacity, quercetin increased HDL anti-oxidation

and reduced lipid accumulation (Lara-Guzman et al., 2012; Cui et al., 2017; Xue et al., 2017; Jia et al., 2019) (**Table 6**).

Other Active Ingredients of Herbs

The Chinese herbal medicine Sanqi (*Panax notoginseng* (Burkill) F.H.Chen [*Araliaceae*; Notoginseng radix et rhizoma]) is a traditional medicine widely used to treat CHD in China. It was shown to have good efficacy and safety in clinical practice (Sun et al., 2016; Duan et al., 2017). Panax notoginseng saponins, including ginsenoside Rb1, ginsenoside Rg1, and notoginsenoside R1, are the active ingredients extracted from Sanqi; they reduce ROS generation by inhibiting NOX4 activity and block recruitment of adhesion molecules to monocytes induced by multiple pathways (Dou et al., 2012; Qiao et al., 2015; Fan et al., 2016), protecting endothelial function and preventing atherosclerosis. Ginsenoside, derived from the Chinese herbal medicine *Panax ginseng* C.A.Mey. [*Araliaceae*; Ginseng radix et rhizoma], includes ginsenosides Rg1 and Rb1 (also abstracted from Sanqi), Rb2, Rb3, Rg2, Rg3, Rf, F1, F2, Rd, and Rh2 (Jin et al., 2019). Lü et al. (Lü et al., 2019) found that Rb1 competitively inhibited the expression of the estrogen receptor ER-β, reducing ROS generation in endothelial cells and increasing eNOS and SOD, thereby reducing endothelial dysfunction. Coupled with ROS reduction, the inflammatory response was also suppressed to alleviate atherosclerosis (Fan et al., 2016; Zhou et al., 2017). Similar results were also found in ginsenoside F1, which reduced LDL-induced endothelial dysfunction; it may be considered a new medication to treat atherosclerosis (Li et al., 2011b; Qin et al., 2017). *Ginko biloba* L. [Ginkgoaceae; Ginkgo folium; Ginkgo semen]is a dioecious tree species native to China. Flavonoids and terpenoids are the primary active compounds in *Ginkgo biloba* leaves. They have various pharmacological effects, including anti-oxidation, anti-platelet, and anti-apoptosis, preventing and treating cardiovascular and cerebrovascular diseases, Alzheimer's disease, and atherosclerosis (Li et al., 2020c; Tian et al., 2017). *Ginkgo biloba* extract (GBE) is used in modern medicine. The standard GBE- EGB761 synthesized by Willmar Schwabe Pharmaceuticals includes terpenoids, flavonoids, alkylphenols, polypentanol, and organic acids (van Beek and Montoro, 2009). To reduce ROS, GBE inhibits NADPH oxidase subunits p47 (Phox) and rac-1; it also reduces gp91 and p22 (Phox) expression caused by ox-LDL induced AMPK and PKC activation (Ou et al., 2013). GBE also enhances HO-1 expression through the Akt/eNOS and p38/MAPK pathways (Tsai et al., 2013). It reduces the adhesion molecules such as monocyte chemokine-1 (MCP-1) and VCAM-1 mediated by ROS and prevents the adhesion of monocytes to endothelial cells, protecting endothelial cells' function (Chen et al., 2003; Ou et al., 2009; Piazza et al., 2019). In terms of inhibiting the formation of foam cells, Li et al. (Tonghua, 2019) found that EGb761 inhibited the uptake of cholesterol by VSMC smooth muscle cells and enhanced the efflux of cholesterol by smooth muscle cells. EGb761 treatment inhibited the expression of SR-A1 and LOX-1, thereby inhibiting the uptake of ox-LDL by smooth muscle cells. Ginkgolide B, another active component abstracted from *Ginkgo biloba* leaves, presented similar mechanisms to EGB761 (Li et al., 2009; Ma et al., 2013; Feng et al., 2018; Wang et al., 2019). The antioxidant effect of GBE on atherosclerosis is mediated by reducing ROS generation, thereby preventing endothelial dysfunction caused by the adhesion of monocytes and endothelial cells (Jung et al., 2012) (**Table 7**).

TCM Preparations and Related Drugs

TCM preparations and its patent drugs include many Chinese herbs containing various ingredients. Clinical studies and laboratory research have shown positive effects on oxidative stress in atherosclerosis-related diseases (Hanqing et al., 2018; Feng et al., 2019; Xibin et al., 2019; Yonggang, 2020; Zhong et al., 2020). Tongqiao Huoxue decoction and Yiqi Huoxue decoction reduce MDA and ox-LDL production in ischemic stroke patients, relieve oxidative stress, and improve cerebral blood flow (Yonggang, 2020; Liu and Cui, 2016). Liang et al. (Hao et al., 2019) found that combined use of acupuncture and Dan-Lou tablets in patients with hypertension and atherosclerosis inhibited ROS production, enhanced SOD, and reduced inflammatory factors. Huatan Quzhuo fang exerted antioxidant effects in carotid atherosclerotic plaque patients (Quan et al., 2019). Dachaihu decoction (Gexuan et al., 2019) and Buyang Huanwu decoction (Zhixin et al., 2019) may reduce angina pectoris frequency in CHD patients through increasing SOD, total antioxidant capacity, and other antioxidant indicators. Xuefu Zhuyu decoction, which is frequently applied to treat blood stasis diseases in China, also shows alleviated atherosclerosis (Xibin et al., 2019; Feng et al., 2019; Zhao et al., 2020a), revealing a protective effect on oxidative stress (**Table 8**). According to Liu et al. (Liu et al., 2020), Buyang Huanwu decoction regulated oxidative stress and inflammation through TGF-β and NF-κB pathways, reducing MDA production and increasing CAT expression in a rat model of atherosclerosis. And the antioxidant effect achieved by Gualou Xiebai Banxia decoction was the inhibition of Lox-1 in aorta and enhancement of SOD and GPx generation (Jianen et al., 2017). Similar findings were also observed in Chinese medicine patent medications as well (Yu et al., 2016; Lanbin et al., 2017; Tong et al., 2018; Cailian and Zhang, 2019; Shibai et al., 2019; Yufeng et al., 2019; Zhu et al., 2019c; Yansheng et al., 2020). In CHD patients, clinical studies revealed that *Salvia miltiorrhiza* polyphenolate downregulated endothelin-1 expression, reducing the frequency of angina pectoris and improving heart function by protecting endothelial function and moderating oxidative stress (Jingshu et al., 2019; Feilong et al., 2020) (more details in **Table 8** and **Table 9**, raw herbs of each preparation listed in **Table 10**).

DISCUSSION

The application of antioxidants in the treatment of atherosclerosis are still under exploration. Clinical studies showed that natural antioxidants such as vitamin C and vitamin E did not reduce cardiovascular events (Libby et al., 2011). ACE inhibitors, ARB, aspirin, and statins reduce ROS generation and improve antioxidant effects (Kattoor et al., 2017).

TABLE 7 | Other active ingredients in herbs that treat atherosclerosis by regulating oxidative stress.

Active ingredients	Subjects in study	Full botanical taxonomic names (yes/no)	Relevant gene targets	Impact on ROS related targets	Potential mechanism of AS protection	References
Panax-notoginseng saponins	ApoE$^{-/-}$ mice No Yes Yes	No Yes Yes	RAGE/MAPK NF-κB Nrf2 TNF-α-p38	↓Nox4 ↓ROS ↓MDA ↑SOD ↑GSH ↑HO-1	↓oxidative stress and inflammation ↓endothelial dysfunction ↓adhesion molecules expression and adhesion to monocytes	Dou et al. (2012) Qiao et al. (2015) Fan et al. (2016)
Ginsenoside Rb1	ApoE$^{-/-}$ mice HUVECs	No	JNK TNF-α NF-κB ER-β —	↓ROS↓MDA ↓GPx ↑SOD ↑CAT ↑eNOS ↓Superoxide anion ↑eNOS	↓oxidative stress and inflammation ↓oxidative stress ↓endothelial dysfunction	Zhou et al. (2017); Lü et al. (2019)
Ginsenoside F1	ApoE$^{-/-}$ mice	Yes	NF-κB	↓MPO ↓Lox-1	↓endothelial dysfunction ↓inflammation	Qin et al. (2017)
EGB761	HUVECs HAECs VSMCs	No	AMPK PKC NF-κB	↓p47 (phox) ↓ Rac-1 ↓gp91 (phox) ↓p22 (phox) ↓ROS ↓Lox-1 ↑HO-1 ↓MCP-1 ↓VCAM-1 ↓ ICAM ↓E-selectin	↓endothelial dysfunction ↓inflammation ↓oxidative stress ↓adhesion molecules expression and adhesion to monocytes ↓foam cells formation	Ou et al. (2013) Tsai et al. (2013); Ou et al. (2009); Chen et al. (2003); Tonghua (2019)
Ginkgolide B	HUVECs	No	PCSK-9 LDL-R sirt1 Akt Nrf2	↓Lox-1 ↓Nox4 ↓MCP-1 ↓ROS ↓VCAM-1 ↓ ICAM ↓E-selectin ↓inflammatory factors	↓endothelial dysfunction ↓inflammation ↓oxidative stress ↓adhesion molecules expression and adhesion to monocytes	Feng et al. (2018); Li et al. (2009); Ma et al. (2013); Wang et al. (2019)

However, clear evidence of atherosclerotic antioxidant effects of these drugs remains insufficient. Probucol is a synthetic antioxidant used to regulate lipids and treat atherosclerosis. Kim et al. (Joon et al., 2018) found that combination use of aspirin or cilostazol with probucol can reduce vascular events in ischemic stroke at high risk of cerebral hemorrhage patients; however, they failed to demonstrate decreased risk of myocardial infarction. AGI-1067, an equivalent antioxidant and modifier of probucol, reduced restenosis after PCI without prolonging the QTc interval (Tardif et al., 2003). In a randomized double-blind placebo trial of acute coronary syndrome, AGI-1067 reduced composite secondary endpoint events such as primary outcome with all deaths, cardiovascular death, non-fatal myocardial infarction, or non-fatal stroke. Nevertheless, the agent insufficiently reduced the primary endpoint events, including cardiovascular death, myocardial infarction (non-fatal), stroke (non-fatal), and unstable angina, and was more likely to cause adverse events such as anemia and bleeding (Tardif et al., 2008). Further evaluation is required before the drug is officially used in the clinical treatment of atherosclerosis.

Chinese herbal medicine has a history spanning thousands of years and has been widely used to treat atherosclerosis in China. Based on our summary, current evidence from the studies illustrates that Chinese herbal medicines, herbal active metabolites, and TCM preparations have made progress in the antioxidant-mediated treatment of atherosclerosis. And the underlying mechanisms of these ingredients are also elucidated in a more specific manner, such as preventing plaque progression through protecting endothelial function, lipid metabolism, and foam cell formation. Researchers provided experimental bases for and clinical verifications of antioxidant targets of TCM. These ingredients may serve as alternatives for treatment of atherosclerosis via management of oxidative stress.

Nevertheless, there are limitations and controversies that hinder the promotion of these results. Most studies concluded in this review failed in stating the source plants of the active ingredients in appropriate botanical nomenclature (shown in **Tables 1–8** and **Table 10**). Ambiguous or incorrect use of botanical nomenclature may hinder the accuracy and promotion of research results since readers may not recognize which plants are being referenced (Rivera et al., 2014).

Most clinical studies have an insufficient number of patients and a lack of large-scale multi-center clinical studies. TCM preparations consist of various Chinese herbs that may involve multiple chemical components. Their complexity and diversity creates challenges in determining the mechanisms of these compounds in treating atherosclerosis: are the therapeutic effects mediated by an active metabolite alone? Or do several ingredients work together? The questions remain open.

Choosing a suitable research model guarantees the accuracy of the TCM mechanism exploration and the reliability of the results. *In vitro* models, including mouse or human cell lines, are feasible tools to explore cellular functions and mechanisms, as well as gene targets and drug transport. Most of the atherosclerosis-related *in vitro* inflammation models used human or animal-derived macrophage cell lines, such as murine leukemia cell line RAW264.7 and J774 and human leukemia monocyte cell line THP-1. After intervening with phorbol-12-myristate-13- acetate (PMA), 1α, 25-dihydroxyvitamin D3 (vD3), or macrophage colony-stimulating factor (M-CSF), THP-1 could differentiate into macrophages (Chanput et al., 2014). Researchers analyzed the inflammation mechanisms in atherosclerosis by constructing a biology network model and found that HAECs expressed a richer mechanism map compared with immortalized endothelial cell lines (De Leon et al., 2014). Since the macrophages in human

TABLE 8 | TCM preparations that treat atherosclerosis by regulating oxidative stress.

Preparations	Subjects in study	Full botanical taxonomic names (yes/no)	Impact on ROS related targets	Potential mechanism in treating atherosclerotic diseases	Single (1) or combined with basic treatment (2)	References
Tongqiao Huoxue decoction	acute ischemic stroke patients	No	↓MDA ↓ox-LDL ↑SOD ↑GPx	↓oxidative stress	(2)	Yonggang (2020)
Yiqi Huoxue decoction	ischemic stroke patients	No	↓MDA ↓ox-LDL ↑SOD ↑GPx	↓oxidative stress	(2)	Liu and Cui (2016)
Yangmai Huatan decoction	Hypertension with atherosclerosis patients	No	↓MDA ↑SOD	↓oxidative stress and inflammation	(2)	Hao et al. (2019)
Huatan Quzhuo fang	carotid atherosclerotic plaque patients	No	↓MDA ↑SOD	↓oxidative stress ↑lipid regulation	(2)	Quan et al. (2019)
Dachaihu decoction	unstable angina patients	No	↓MDA ↓LPO ↑SOD ↑eNOS ↑TAC	↓endothelial dysfunction ↓oxidative stress	(2)	Gexuan et al. (2019)
Buyang Huanwu decoction	unstable angina patients	No	↑SOD ↑GSH ↑TAC ↑NOS	↓oxidative stress	(2)	Zhixin et al. (2019)
	SD rats	No	↓MDA ↑SOD ↑GPx ↑CAT	↓oxidative stress and inflammation	(1)	Liu et al. (2020)
Xuefu Zhuyu decoction	PCI patients	No	↓MDA ↑SOD	—	(2)	Zhao et al. (2020b)
	SD rats	No	↓ROS ↓Nox2		(1)	Xibin et al. (2019)
	domestic rabbits	No	↓ROS ↓MDA ↓Nox2 ↑TAC ↑SOD ↑GSH		(2)	Hanqing et al. (2018)
	acute cerebral infarction patients	No	↓MDA ↑SOD ↑NO	↓oxidative stress ↓endothelial dysfunction	(2)	Feng et al. (2019)
Gualou Xiebai Banxia decoction	ApoE$^{-/-}$ mice	No	↓MDA ↓ox-LDL ↑SOD ↑GPx	↓oxidative stress	(1)	Jianen et al. (2017)
Huotan Jiedu Tongluo decoction	Japanese white rabbit	No	↓ROS ↓ox-LDL ↓eNOS uncoupling	↓oxidative stress	(1)	Tong et al. (2018)
Dingxin fang	ApoE$^{-/-}$ mice	No	↓MDA ↓ox-LDL ↑SOD ↑GPx ↑TAC	↓oxidative stress	(1)	Yu et al. (2016)
Huanglian Jiedu decoction	SD rats	No	↓MDA ↓ox-LDL ↑SOD	↓oxidative stress and inflammation	(1)	Lanbin et al. (2017)

TABLE 9 | Patent drugs that treat atherosclerosis by regulating oxidative stress.

Patent drugs	Subjects in study	Full botanical taxonomic names (yes/no)	Impact on ROS related targets	Potential mechanism in treating atherosclerotic diseases	Single (1) or combined with basic treatment (2)	References
Danshen granules, capsules, tablets, and drop pills	unstable angina patients	no	↓MDA ↑SOD ↑GPx ↑TAC	↓oxidative stress and inflammation	(2)	Yansheng et al. (2020)
Shexiang Baoxin pills	post PCI patients	no	↓MDA ↓LPO ↑SOD ↑TAC	↓oxidative stress	(2)	Yufeng et al. (2019)
Qishen Yiqi drip pills	coronary heart disease	no	↓MDA ↑SOD	↓oxidative stress	(2)	Cailian and Zhang (2019)
Dan-Lou tablet	Wistar rats	no	↓MDA ↓ox-LDL ↑SOD	↓oxidative stress and inflammation	(1)	Zhu et al. (2019c)
Ginkgo Leaf Capsules	angina pectoris patients	no	↓MDA ↑SOD ↑TAC	↓oxidative stress and inflammation	(2)	Shibai et al. (2019)
Salvia miltiorrhiza polyphenolate	CAD patients	no	↓MDA ↑SOD ↑NO	↓oxidative stress ↓endothelial dysfunction	(2)	Jingshu et al. (2019)
	CAD and angina pectoris patients	no	↓LPO ↓MDA ↑SOD ↑total anti-oxidative capacity (TAC)	↓oxidative stress	(2)	Feilong et al. (2020)

TABLE 10 | Raw herbs in TCM preparations.

Preparations	Raw herbs
Tongqiao Huoxue decoction	*Prunus persica* (L.) Batsch [Rosaceae; Persicae semen], *Carthamus tinctorius* L. [Asteraceae; Carthami Flos], *Zingiber officinale* Roscoe [Zingiberaceae; Zingiberis rhizoma praeparatum], *Paeonia lactiflora* Pall. [Paeoniaceae; Paeoniae radix alba], *Conioselinum anthriscoides 'Chuanxiong'* [Apiaceae; Chuanxiong rhizoma], *Ziziphus jujuba* Mill. [Rhamnaceae; Jujubae fructus]
Yiqi Huoxue decoction	*Astragalus mongholicus* Bunge [Fabaceae; Astragali radix], *Salvia miltiorrhiza* Bunge [Lamiaceae; Salviae miltiorrhizae radix et rhizoma], *Paeonia lactiflora* Pall. [Paeoniaceae; Paeoniae radix alba], *Angelica sinensis* (Oliv.) Diels [Apiaceae; Angelicae sinensis radix], *Conioselinum anthriscoides 'Chuanxiong'* [Apiaceae; Chuanxiong rhizoma], *Achyranthes bidentata* Blume [Amaranthaceae; Achyranthis bidentatae radix], *Dioscorea oppositifolia* L. [Dioscoreaceae; Dioscoreae rhizoma], *Prunus persica* (L.) Batsch [Rosaceae; Persicae semen], *Spatholobus suberectus* Dunn [Fabaceae; Spatholobi caulis], *Rehmannia glutinosa* (Gaertn.) DC. [Orobanchaceae; Rehmanniae radix], *Carthamus tinctorius* L. [Asteraceae; Carthami Flos], *Glycyrrhiza glabra* L. [Fabaceae; Glycyrrhizae radix et rhizoma]
Yangmai Huatan decoction	*Astragalus mongholicus* Bunge [Fabaceae; Astragali radix], *Smilax glabra* Roxb. [Smilacaceae; Smilacis glabrae rhizoma], *Salvia miltiorrhiza* Bunge [Lamiaceae; Salviae miltiorrhizae radix et rhizoma], *Carthamus tinctorius* L. [Asteraceae; Carthami Flos], *Prunus persica* (L.) Batsch [Rosaceae; Persicae semen], *Pinellia ternata* (Thunb.) Makino [Araceae; Pinelliae rhizoma], *Atractylodes macrocephala* Koidz. [Asteraceae; Atractylodis macrocephalae rhizoma], *Wurfbainia villosa* (Lour.) Skornick. & A.D.Poulsen [Zingiberaceae; Amomi fructus], *Gastrodia elata* Blume [Orchidaceae; Gastrodiae rhizoma], *Crataegus pinnatifida* Bunge [Rosaceae; Crataegi fructus], *Hordeum vulgare* L. [Poaceae; Hordei fructus germinatus]
Huatan Quzhuo fang	*Panax ginseng* C.A.Mey. [Araliaceae; Ginseng radix et rhizoma], *Atractylodes macrocephala* Koidz. [Asteraceae; Atractylodis macrocephalae rhizoma], *Pinellia ternata* (Thunb.) Makino [Araceae; Pinelliae rhizoma], *Smilax glabra* Roxb. [Smilacaceae; Smilacis glabrae rhizoma], *Crataegus pinnatifida* Bunge [Rosaceae; Crataegi fructus], *Citrus × aurantium* L. [Rutaceae; Citri exocarpium rubrum], *Citrus × aurantium* L. [Rutaceae; Aurantii fructus immaturus], *Nelumbo nucifera* Gaertn. [Nelumbonaceae; Nelumbinis folium], *Alisma plantago-aquatica subsp. orientale* (Sam.) Sam. [Alismataceae; Alismatis rhizoma], *Reynoutria multiflora* (Thunb.) Moldenke [Polygonaceae; Polygoni multiflori radix], *Salvia miltiorrhiza* Bunge [Lamiaceae; Salviae miltiorrhizae radix et rhizoma]
Dachaihu decoction	*Bupleurum chinense* DC. [Apiaceae; Bupleuri radix], *Citrus × aurantium* L. [Rutaceae; Aurantii fructus immaturus], *Scutellaria baicalensis* Georgi [Lamiaceae; Scutellariae radix], *Paeonia lactiflora* Pall. [Paeoniaceae; Paeoniae radix alba], *Salvia miltiorrhiza* Bunge [Lamiaceae; Salviae miltiorrhizae radix et rhizoma], *Smilax glabra* Roxb. [Smilacaceae; Smilacis glabrae rhizoma], *Citrus × aurantium* L. [Rutaceae; Citri exocarpium rubrum], *Rheum officinale* Baill. [Polygonaceae; Rhei radix et rhizoma], *Pinellia ternata* (Thunb.) Makino [Araceae; Pinelliae rhizoma], *Glycyrrhiza glabra* L. [Fabaceae; Glycyrrhizae radix et rhizoma]
Buyang Huanwu decoction	*Astragalus mongholicus* Bunge [Fabaceae; astragali radix], *Angelica sinensis* (Oliv.) Diels [Apiaceae; angelicae sinensis radix], *Paeonia lactiflora* Pall. [Paeoniaceae; paeoniae radix alba], *Rehmannia glutinosa* (Gaertn.) DC. [Orobanchaceae; rehmanniae radix], *Conioselinum anthriscoides 'Chuanxiong'* [Apiaceae; chuanxiong rhizoma], *Prunus persica* (L.) Batsch [Rosaceae; persicae semen], *Carthamus tinctorius* L. [Asteraceae; Carthami Flos]
Xuefu Zhuyu decoction	*Prunus persica* (L.) Batsch [Rosaceae; Persicae semen], *Carthamus tinctorius* L. [Asteraceae; Carthami Flos], *Angelica sinensis* (Oliv.) Diels [Apiaceae; Angelicae sinensis radix], *Bupleurum chinense* DC. [Apiaceae; Bupleuri radix], *Rehmannia glutinosa* (Gaertn.) DC. [Orobanchaceae; Rehmanniae radix], *Citrus × aurantium* L. [Rutaceae; Citri reticulatae pericarpium], *Conioselinum anthriscoides 'Chuanxiong'* [Apiaceae; Chuanxiong rhizoma], *Paeonia lactiflora* Pall. [Paeoniaceae; Paeoniae radix alba], *Platycodon grandiflorus* (Jacq.) A.DC. [Campanulaceae; Platycodonis radix], *Glycyrrhiza glabra* L. [Fabaceae; Glycyrrhizae radix et rhizoma], *Achyranthes bidentata* Blume [Amaranthaceae; Achyranthis bidentatae radix]
Gualou Xiebai Banxia decoction	*Trichosanthes kirilowii* Maxim. [Cucurbitaceae; Trichosanthis fructus], *Allium chinense* G.Don [Amaryllidaceae; Allii macrostemonis bulbus], *Pinellia ternata* (Thunb.) Makino [Araceae; Pinelliae rhizoma]
Huotan Jiedu Tongluo decoction	*Lonicera japonica* Thunb. [Caprifoliaceae; Caulis lonicerae japonicae], *Angelica sinensis* (Oliv.) Diels [Apiaceae; Angelicae sinensis radix], *Trichosanthes kirilowii* Maxim. [Cucurbitaceae; Trichosanthis fructus]
Dingxin fang	*Salvia miltiorrhiza* Bunge [Lamiaceae; Salviae miltiorrhizae radix et rhizoma], *Panax notoginseng* (Burkill) F.H.Chen [Araliaceae; Notoginseng radix et rhizoma], *Sophora flavescens* Aiton [Fabaceae; Sophorae flavescentis radix], *Coptis chinensis* Franch. [Ranunculaceae, Coptidis rhizoma], *Ziziphus jujuba* Mill. [Rhamnaceae; Ziziphi Spinosae Semen], *Codonopsis pilosula* (Franch.) Nannf. [Campanulaceae; Codonopsis radix], *Trichosanthes kirilowii* Maxim. [Cucurbitaceae; Trichosanthis fructus], *Paeonia lactiflora* Pall. [Paeoniaceae; Paeoniae radix alba], *Smilax glabra* Roxb. [Smilacaceae; Smilacis glabrae rhizoma]
Huanglian Jiedu decoction	*Coptis chinensis* Franch. [Ranunculaceae, Coptidis rhizoma], *Scutellaria baicalensis* Georgi [Lamiaceae; Scutellariae radix], *Phellodendron chinense* C.K.Schneid. [Rutaceae; Phellodendri chinensis cortex], *Gardenia jasminoides* J.Ellis [Rubiaceae; Gardeniae fructus]

and mouse atherosclerotic lesions have been affected by microenvironmental factors, the results obtained from immortal cell lines may differ from the *in vivo* data. Primary macrophages, bone marrow-derived macrophages, and peritoneal macrophages, including large peritoneal macrophages (LPMs) and small peritoneal macrophages (SPMs), are also commonly used cell models in atherosclerosis. Both LPMs and SPMs can coordinate immune responses, but these two peritoneal macrophages subtypes show heterogeneous cellular markers (Lee and Choi, 2020). ApoE$^{-/-}$ mouse model, high-fat diet mouse, and rabbit model constitute the primary *in vivo* platforms for studying underlying pharmaceutical mechanisms in atherosclerosis. However, the location of atherosclerotic lesions in mice is different from that in humans. In the mouse model, plaques locate in the aortic sinus and innominate arteries, while the coronary

arteries and carotid arteries are the primary lesions in human (Zhao et al., 2020b; Basu and Bornfeldt, 2020). The experimental models involved in this review can indeed explain the potential mechanisms of TCM in treating atherosclerosis via antioxidants. Nevertheless, due to the limitations of the *in vitro* and *in vivo* models, there is still a long way to go before basic research results can be transformed into the clinic.

In conclusion, translation from the bench to the bedside remains challenging. Oxidative stress is a critical component in the progression of atherosclerosis. Therefore, it is essential to develop medications or supplements to treat atherosclerosis from the perspective of enhancing antioxidant enzyme induction, inhibiting ROS generation, or blocking subsequent reactions, such as inhibition of inflammation process; all of these form vicious cycles in oxidative stress. Further exploration of the therapeutic effect of TCM on atherosclerosis from the perspective of oxidative stress and elucidating the mechanisms and targets will provide reliable evidence for the use of Chinese herbal medicine.

AUTHOR CONTRIBUTIONS

LS searched the relevant literature and drafted the manuscript. HX and JJ provided helpful advice and organized the work. JZ, RL, and QL assisted in literature searching and revised the manuscript. All authors have read and approved the final version of the manuscript.

FUNDING

This article is supported by the National Natural Science Foundation of China (No. 81874412 and 82074215).

ACKNOWLEDGMENTS

The authors would like to thank the National Natural Science Foundation of China.

REFERENCES

Antoniades, C., Shirodaria, C., Crabtree, M., Rinze, R., Alp, N., Cunnington, C., et al. (2007). Altered Plasma versus Vascular Biopterins in Human Atherosclerosis Reveal Relationships between Endothelial Nitric Oxide Synthase Coupling, Endothelial Function, and Inflammation. *Circulation* 116 (24), 2851–2859. doi:10.1161/circulationaha.107.704155

Antoniades, C., Shirodaria, C., Warrick, N., Cai, S., de Bono, J., Lee, J., et al. (2006). 5-methyltetrahydrofolate Rapidly Improves Endothelial Function and Decreases Superoxide Production in Human Vessels: Effects on Vascular Tetrahydrobiopterin Availability and Endothelial Nitric Oxide Synthase Coupling. *Circulation* 114 (11), 1193–201. doi:10.1161/circulationaha.106.612325

Asadi, A., Yaghobi Nezhad, D., Rafie Javazm, A., Khanicheragh, P., Mashouri, L., Shakeri, F., et al. (2020). *In Vitro* Effects of Curcumin on Transforming Growth Factor-β-Mediated Non-smad Signaling Pathway, Oxidative Stress, and Pro-inflammatory Cytokines Production with Human Vascular Smooth Muscle Cells. *Iran J. Allergy Asthma Immunol.* 19 (1), 84–93. doi:10.18502/ijaai.v19i1.2421

Barrett, T. J., Distel, E., Murphy, A. J., Hu, J., Garshick, M. S., Ogando, Y., et al. (2019). Apolipoprotein AI) Promotes Atherosclerosis Regression in Diabetic Mice by Suppressing Myelopoiesis and Plaque Inflammation. *Circulation* 140 (14), 1170–1184. doi:10.1161/circulationaha.119.039476

Basu, D., and Bornfeldt, K. E. (2020). Hypertriglyceridemia and Atherosclerosis: Using Human Research to Guide Mechanistic Studies in Animal Models. *Front. Endocrinol. (Lausanne)* 11, 504. doi:10.3389/fendo.2020.00504

Berbée, J. F., Wong, M. C., Wang, Y., van der Hoorn, J. W., Khedoe, P. P., van Klinken, J. B., et al. (2013). Resveratrol Protects against Atherosclerosis, but Does Not Add to the Antiatherogenic Effect of Atorvastatin, in APOE*3-Leiden.CETP Mice. *J. Nutr. Biochem.* 24 (8), 1423–1430. doi:10.1016/j.jnutbio.2012.11.009

Bhaskar, S., Sudhakaran, P. R., and Helen, A. (2016). Quercetin Attenuates Atherosclerotic Inflammation and Adhesion Molecule Expression by Modulating TLR-NF-Kb Signaling Pathway. *Cell Immunol* 310, 131–140. doi:10.1016/j.cellimm.2016.08.011

Bonnefont-Rousselot, D. (2016). Resveratrol and Cardiovascular Diseases. *Nutrients* 8 (5). doi:10.3390/nu8050250

Bruedigam, C., Eijken, M., Koedam, M., Chiba, H., and van Leeuwen, J. P. (2011). Opposing Actions of Rosiglitazone and Resveratrol on Mineralization in Human Vascular Smooth Muscle Cells. *J. Mol. Cel Cardiol* 51 (5), 862–871. doi:10.1016/j.yjmcc.2011.07.020

Cadenas, S. (2018). ROS and Redox Signaling in Myocardial Ischemia-Reperfusion Injury and Cardioprotection. *Free Radic. Biol. Med.* 117, 76–89. doi:10.1016/j.freeradbiomed.2018.01.024

Cailian, C., and Zhang, Lu. (2019). Effect of Qishen Yiqi Dripping Pills Combined with Ticagrelor on Plasma Visfatin Levels and Serum Oxidative Stress Markers in Patients with Coronary Heart Disease. *Drug Eval. Res.* 42 (05), 917–920. doi:10.7501/j.issn.1674-6376.2019.05.019

Caliceti, C., Rizzo, P., Ferrari, R., Fortini, F., Aquila, G., Leoncini, E., et al. (2017). Novel Role of the Nutraceutical Bioactive Compound Berberine in Lectin-like OxLDL Receptor 1-mediated Endothelial Dysfunction in Comparison to Lovastatin. *Nutr. Metab. Cardiovasc. Dis.* 27 (6), 552–563. doi:10.1016/j.numecd.2017.04.002

Canton, J., Neculai, D., and Grinstein, S. (2013). Scavenger Receptors in Homeostasis and Immunity. *Nat. Rev. Immunol.* 13 (9), 621–634. doi:10.1038/nri3515

Cao, H., Jia, Q., Yan, L., Chen, C., Xing, S., and Shen, D. (2019). Quercetin Suppresses the Progression of Atherosclerosis by Regulating MST1-Mediated Autophagy in Ox-LDL-Induced RAW264.7 Macrophage Foam Cells. *Int. J. Mol. Sci.* 20 (23). doi:10.3390/ijms20236093

Channon, K. M. (2002). Oxidative Stress and Coronary Plaque Stability. *Arterioscler Thromb. Vasc. Biol.* 22 (11), 1751–1752. doi:10.1161/01.atv.0000042203.08210.17

Chanput, W., Mes, J. J., and Wichers, H. J. (2014). THP-1 Cell Line: an In Vitro Cell Model for Immune Modulation Approach. *Int. Immunopharmacol* 23 (1), 37–45. doi:10.1016/j.intimp.2014.08.002

Chatzizisis, Y. S., Coskun, A. U., Jonas, M., Edelman, E. R., Feldman, C. L., and Stone, P. H. (2007). Role of Endothelial Shear Stress in the Natural History of Coronary Atherosclerosis and Vascular Remodeling: Molecular, Cellular, and Vascular Behavior. *J. Am. Coll. Cardiol.* 49 (25), 2379–2393. doi:10.1016/j.jacc.2007.02.059

Chen, J. W., Chen, Y. H., Lin, F. Y., Chen, Y. L., and Lin, S. J. (2003). Ginkgo Biloba Extract Inhibits Tumor Necrosis Factor-Alpha-Induced Reactive Oxygen Species Generation, Transcription Factor Activation, and Cell Adhesion Molecule Expression in Human Aortic Endothelial Cells. *Arteriosclerosis, Thromb. Vasc. Biol.* 23 (9), 1559–1566. doi:10.1161/01.atv.0000089012.73180.63

Chen, W., Tang, F., Xie, B., Chen, S., Huang, H., and Liu, P. (2012). Amelioration of Atherosclerosis by Tanshinone IIA in Hyperlipidemic Rabbits through Attenuation of Oxidative Stress. *Eur. J. Pharmacol.* 674 (2-3), 359–364. doi:10.1016/j.ejphar.2011.10.040

Chi, L., Peng, L., Hu, X., Pan, N., and Zhang, Y. (2014). Berberine Combined with Atorvastatin Downregulates LOX-1 Expression through the ET-1 Receptor in

Monocyte/macrophages. *Int. J. Mol. Med.* 34 (1), 283–290. doi:10.3892/ijmm.2014.1748

Chistiakov, D. A., Melnichenko, A. A., Myasoedova, V. A., Grechko, A. V., and Orekhov, A. N. (2017). Mechanisms of Foam Cell Formation in Atherosclerosis. *J. Mol. Med. (Berl)* 95 (11), 1153–1165. doi:10.1007/s00109-017-1575-8

Cho, B. J., Im, E. K., Kwon, J. H., Lee, K. H., Shin, H. J., Oh, J., et al. (2005). Berberine Inhibits the Production of Lysophosphatidylcholine-Induced Reactive Oxygen Species and the ERK1/2 Pathway in Vascular Smooth Muscle Cells. *Mol. Cell* 20 (3), 429–434.

Chow, S. E., Hshu, Y. C., Wang, J. S., and Chen, J. K. (2007). Resveratrol Attenuates oxLDL-Stimulated NADPH Oxidase Activity and Protects Endothelial Cells from Oxidative Functional Damages. *J. Appl. Physiol.* 102 (4), 1520–1527. doi:10.1152/japplphysiol.00881.2006

Cui, Y., Hou, P., Li, F., Liu, Q., Qin, S., Zhou, G., et al. (2017). Quercetin Improves Macrophage Reverse Cholesterol Transport in Apolipoprotein E-Deficient Mice Fed a High-Fat Diet. *Lipids Health Dis.* 16 (1), 9. doi:10.1186/s12944-016-0393-2

Daiber, A., and Chlopicki, S. (2020). Revisiting Pharmacology of Oxidative Stress and Endothelial Dysfunction in Cardiovascular Disease: Evidence for Redox-Based Therapies. *Free Radic. Biol. Med.* 157, 15–37. doi:10.1016/j.freeradbiomed.2020.02.026

Davignon, J., and Ganz, P. (2004). Role of Endothelial Dysfunction in Atherosclerosis. *Circulation* 109 (23 Suppl. 1), Iii27–32. doi:10.1161/01.CIR.0000131515.03336.f8

De Leon, H., Boue, S., Schlage, W. K., Boukharov, N., Westra, J. W., Gebel, S., et al. (2014). A Vascular Biology Network Model Focused on Inflammatory Processes to Investigate Atherogenesis and Plaque Instability. *J. Transl Med.* 12, 185. doi:10.1186/1479-5876-12-185

Deng, Q., Li, X. X., Fang, Y., Chen, X., and Xue, J. (2020). Therapeutic Potential of Quercetin as an Antiatherosclerotic Agent in Atherosclerotic Cardiovascular Disease: A Review. *Evid. Based Complement. Alternat Med.* 2020, 5926381. doi:10.1155/2020/5926381

Dou, L., Lu, Y., Shen, T., Huang, X., Man, Y., Wang, S., et al. (2012). Panax Notogingseng Saponins Suppress RAGE/MAPK Signaling and NF-kappaB Activation in Apolipoprotein-E-Deficient Atherosclerosis-Prone Mice. *Cell Physiol Biochem* 29 (5-6), 875–882. doi:10.1159/000315061

Drechsler, M., Megens, R. T., van Zandvoort, M., Weber, C., and Soehnlein, O. (2010). Hyperlipidemia-triggered Neutrophilia Promotes Early Atherosclerosis. *Circulation* 122 (18), 1837–1845. doi:10.1161/circulationaha.110.961714

Duan, L., Xiong, X., Hu, J., Liu, Y., Li, J., and Wang, J. (2017). Panax Notoginseng Saponins for Treating Coronary Artery Disease: A Functional and Mechanistic Overview. *Front. Pharmacol.* 8, 702. doi:10.3389/fphar.2017.00702

Duivenvoorden, R., Mani, V., Woodward, M., Kallend, D., Suchankova, G., Fuster, V., et al. (2013). Relationship of Serum Inflammatory Biomarkers with Plaque Inflammation Assessed by FDG PET/CT: the Dal-PLAQUE Study. *JACC Cardiovasc. Imaging* 6 (10), 1087–1094. doi:10.1016/j.jcmg.2013.03.009

Fan, J., Liu, D., He, C., Li, X., and He, F. (2016). Inhibiting Adhesion Events by Panax Notoginseng Saponins and Ginsenoside Rb1 Protecting Arteries via Activation of Nrf2 and Suppression of P38 - VCAM-1 Signal Pathway. *J. ethnopharmacology* 192, 423–430. doi:10.1016/j.jep.2016.09.022

Fan, X., Wang, J., Hou, J., Lin, C., Bensoussan, A., Chang, D., et al. (2015). Berberine Alleviates Ox-LDL Induced Inflammatory Factors by Up-Regulation of Autophagy via AMPK/mTOR Signaling Pathway. *J. Transl Med.* 13, 92. doi:10.1186/s12967-015-0450-z

Fang, Z. Y., Lin, R., Yuan, B. X., Yang, G. D., Liu, Y., and Zhang, H. (2008). Tanshinone IIA Downregulates the CD40 Expression and Decreases MMP-2 Activity on Atherosclerosis Induced by High Fatty Diet in Rabbit. *J. Ethnopharmacol* 115 (2), 217–222. doi:10.1016/j.jep.2007.09.025

Fatahian, A., Haftcheshmeh, S. M., Azhdari, S., Farshchi, H. K., Nikfar, B., and Momtazi-Borojeni, A. A. (2020). Promising Anti-atherosclerotic Effect of Berberine: Evidence from *In Vitro*, *In Vivo*, and Clinical Studies. *Rev. Physiol. Biochem. Pharmacol.* 178, 83–110. doi:10.1007/112_2020_42

Feilong, Chen., Wang, Xiuling., and Ma, Bin. (2020). Evaluation for the Treatment Effect of Salvianolate and its Influence on the Hemorheologyand Oxidative Stress in Angina Pectoris Patients. *Chin. J. Disaster Med.* 8 (03), 137–141. doi:10.13919/j.issn.2095-6274.2020.03.005

Feng, Chen., Wu, Xi., Mu, Yingtao., Xu, Taotao., and Liu, Renbin. (2019). Effects of Xuefu Zhuyu Decoction Combined with Conventional Treatment on Inflammatory Response, Oxidative Stress, Endothelium and Related Factors in Patients with Acute Cerebral Infarction. *J. Hainan Med. Univ.* 25 (10), 762–765. doi:10.13210/j.cnki.jhmu.20190327.001

Feng, J., Liu, L., Yao, F., Zhou, D., He, Y., and Wang, J. (2021). The Protective Effect of Tanshinone IIa on Endothelial Cells: a Generalist Among Clinical Therapeutics. *Expert Rev. Clin. Pharmacol.* 14 (2), 239–248. doi:10.1080/17512433.2021.1878877

Feng, Z., Yang, X., Zhang, L., Ansari, I. A., Khan, M. S., Han, S., et al. (2018). Ginkgolide B Ameliorates Oxidized Low-Density Lipoprotein-Induced Endothelial Dysfunction via Modulating Lectin-like Ox-LDL-Receptor-1 and NADPH Oxidase 4 Expression and Inflammatory Cascades. *Phytotherapy Res. : PTR* 32 (12), 2417–2427. doi:10.1002/ptr.6177

Fleenor, B. S., Sindler, A. L., Marvi, N. K., Howell, K. L., Zigler, M. L., Yoshizawa, M., et al. (2013). Curcumin Ameliorates Arterial Dysfunction and Oxidative Stress with Aging. *Exp. Gerontol.* 48 (2), 269–276. doi:10.1016/j.exger.2012.10.008

Förstermann, U., Xia, N., and Li, H. (2017). Roles of Vascular Oxidative Stress and Nitric Oxide in the Pathogenesis of Atherosclerosis. *Circ. Res.* 120 (4), 713–735. doi:10.1161/circresaha.116.309326

Gao, S., Liu, Z., Li, H., Little, P. J., Liu, P., and Xu, S. (2012). Cardiovascular Actions and Therapeutic Potential of Tanshinone IIA. *Atherosclerosis* 220 (1), 3–10. doi:10.1016/j.atherosclerosis.2011.06.041

Gexuan, R., Li, X., Tan, H., and Chen, J. (2019). A Multicenter, Randomized, Double-Blind Controlled Clinical Trial of Dachaihu Decoction for Unstable Angina Pectoris. *World Chin. Med.* 14 (04), 882–886. doi:10.3969/j.issn.1673-7202.2019.04.018

Gliemann, L., Schmidt, J. F., Olesen, J., Biensø, R. S., Peronard, S. L., Grandjean, S. U., et al. (2013). Resveratrol Blunts the Positive Effects of Exercise Training on Cardiovascular Health in Aged Men. *J. Physiol.* 591 (20), 5047–5059. doi:10.1113/jphysiol.2013.258061

Goel, A., Kunnumakkara, A. B., and Aggarwal, B. B. (2008). Curcumin as "Curecumin": from Kitchen to Clinic. *Biochem. Pharmacol.* 75 (4), 787–809. doi:10.1016/j.bcp.2007.08.016

Gress, T. W., Nieto, F. J., Shahar, E., Wofford, M. R., and Brancati, F. L. (2000). Hypertension and Antihypertensive Therapy as Risk Factors for Type 2 Diabetes Mellitus. Atherosclerosis Risk in Communities Study. *N. Engl. J. Med.* 342 (13), 905–912. doi:10.1056/nejm200003303421301

Griendling, K. K., and FitzGerald, G. A. (2003a). Oxidative Stress and Cardiovascular Injury: Part I: Basic Mechanisms and In Vivo Monitoring of ROS. *Circulation* 108 (16), 1912–1916. doi:10.1161/01.Cir.0000093660.86242.Bb

Griendling, K. K., and FitzGerald, G. A. (2003b). Oxidative Stress and Cardiovascular Injury: Part II: Animal and Human Studies. *Circulation* 108 (17), 2034–2040. doi:10.1161/01.CIR.0000093661.90582.c4

Guo, C., Davies, M. J., and Hawkins, C. L. (2020). Role of Thiocyanate in the Modulation of Myeloperoxidase-Derived Oxidant Induced Damage to Macrophages. *Redox Biol.* 36, 101666. doi:10.1016/j.redox.2020.101666

Haimei, L., Xu, J., Guan, L., Lin, Y., and Yan, F. (2019). Mechanism of Resveratrol Regulating Orai1 Expression in Aorta of Mice and Inhibiting Oxidative Stress Injury in Atherosclerosis. *Pharmacol. Clin. Chin. Materia Med.* 35 (01), 71–76. doi:10.13412/j.cnki.zyyl.2019.01.016

Hanqing, T., Pang, L., Zhang, S., Yue, F., Ning, W., and Wang, L. (2018). Effects of Xuefu Zhuyu Decoction on Oxidative Stress in Rabbits with Blood Stasis Syndrome of Coronary Heart Disease. *Prog. Vet. Med.* 39 (08), 31–35. doi:10.16437/j.cnki.1007-5038.2018.08.007

Hao, L., Yu, Y., and Zhou, Z. (2019). Clinical Observation on Acupuncture and Medicine Combined Treatment of Hypertension with Atherosclerosis. *China Med. Herald* 16 (30), 147–150.

Hickey, M. J. (2011). MPO and Neutrophils: a Magnetic Attraction. *Blood* 117 (4), 1103–1104. doi:10.1182/blood-2010-11-317479

Hou, X., Lin, H., Zhou, X., Cheng, Z., Li, Y., Liu, X., et al. (2020). Novel Dual ROS-Sensitive and CD44 Receptor Targeting Nanomicelles Based on Oligomeric Hyaluronic Acid for the Efficient Therapy of Atherosclerosis. *Carbohydr. Polym.* 232, 115787. doi:10.1016/j.carbpol.2019.115787

Huang, L., Chambliss, K. L., Gao, X., Yuhanna, I. S., Behling-Kelly, E., Bergaya, S., et al. (2019). SR-B1 Drives Endothelial Cell LDL Transcytosis via DOCK4 to Promote Atherosclerosis. *Nature* 569 (7757), 565–569. doi:10.1038/s41586-019-1140-4

Huang, S. L., Chen, P. Y., Wu, M. J., Tai, M. H., Ho, C. T., and Yen, J. H. (2015). Curcuminoids Modulate the PKCδ/NADPH Oxidase/Reactive Oxygen Species Signaling Pathway and Suppress Matrix Invasion during Monocyte-Macrophage Differentiation. *J. Agric. Food Chem.* 63 (40), 8838–8848. doi:10.1021/acs.jafc.5b04083

Huang, Y., DiDonato, J. A., Levison, B. S., Schmitt, D., Li, L., Wu, Y., et al. (2014). An Abundant Dysfunctional Apolipoprotein A1 in Human Atheroma. *Nat. Med.* 20 (2), 193–203. doi:10.1038/nm.3459

Huang, Y., Wu, Z., Riwanto, M., Gao, S., Levison, B. S., Gu, X., et al. (2013). Myeloperoxidase, Paraoxonase-1, and HDL Form a Functional Ternary Complex. *J. Clin. Invest.* 123 (9), 3815–3828. doi:10.1172/jci67478

Huimin, Cao., Song, Nan., Zhang, Ni., Yang, Guanlin., Chen, Wenzhe., Zhang, Zhe., et al. (2017). Regulation on Autophagy with Tanshinone ⅡA for Anti-oxidative Stress Damage of Endothelial Cells through PI3K/Akt/mTOR Pathway. *J. Beijing Univ. Traditional Chin. Med.* 40 (11), 933–939. doi:10.3969/j.issn.1006-2157.2017.11.011

Hulsmans, M., and Holvoet, P. (2010). The Vicious Circle between Oxidative Stress and Inflammation in Atherosclerosis. *J. Cel Mol Med* 14 (1-2), 70–78. doi:10.1111/j.1582-4934.2009.00978.x

Hung, C. H., Chan, S. H., Chu, P. M., and Tsai, K. L. (2015). Quercetin Is a Potent Anti-atherosclerotic Compound by Activation of SIRT1 Signaling under oxLDL Stimulation. *Mol. Nutr. Food Res.* 59 (10), 1905–1917. doi:10.1002/mnfr.201500144

Imamura, H., Yamaguchi, T., Nagayama, D., Saiki, A., Shirai, K., and Tatsuno, I. (2017). Resveratrol Ameliorates Arterial Stiffness Assessed by Cardio-Ankle Vascular Index in Patients with Type 2 Diabetes Mellitus. *Int. Heart J.* 58 (4), 577–583. doi:10.1536/ihj.16-373

Jia, Q., Cao, H., Shen, D., Li, S., Yan, L., Chen, C., et al. (2019). Quercetin Protects against Atherosclerosis by Regulating the Expression of PCSK9, CD36, PPARγ, LXRα and ABCA1. *Int. J. Mol. Med.* 44 (3), 893–902. doi:10.3892/ijmm.2019.4263

Jianen, G., Shubin, M., Yan, X., Xin, S., Gao, F., Liang, G., et al. (2017). Effects of Gualou Xiebai Banxia Decoction on Blood Lipid Metabolism, Oxidative Stress and Aortic Lox-1 Expression in ApoE-/- Mice. *Zhongguo Zhong yao za zhi* 42 (04), 752–757. doi:10.19540/j.cnki.cjcmm.20161222.076

Jiang, Y. H., Jiang, L. Y., Wang, Y. C., Ma, D. F., and Li, X. (2020). Quercetin Attenuates Atherosclerosis via Modulating Oxidized LDL-Induced Endothelial Cellular Senescence. *Front. Pharmacol.* 11, 512. doi:10.3389/fphar.2020.00512

Jiang, Y., Huang, K., Lin, X., Chen, Q., Lin, S., Feng, X., et al. (2017). Berberine Attenuates NLRP3 Inflammasome Activation in Macrophages to Reduce the Secretion of Interleukin-1β. *Ann. Clin. Lab. Sci.* 47 (6), 720–728.

Jin, S., Jeon, J. H., Lee, S., Kang, W. Y., Seong, S. J., Yoon, Y. R., et al. (2019). Detection of 13 Ginsenosides (Rb1, Rb2, Rc, Rd, Re, Rf, Rg1, Rg3, Rh2, F1, Compound K, 20 (S)-Protopanaxadiol, and 20 (S)-Protopanaxatriol) in Human Plasma and Application of the Analytical Method to Human Pharmacokinetic Studies Following Two Week-Repeated Administration of Red Ginseng Extract. *Molecules* 24 (14). doi:10.3390/molecules24142618

Jingshu, G., Zhou, Y., Miao, Z., Gao, S., and Jia, C. (2019). Effect of Salvianolate on Endothelial Function and Oxidative Stress in Patients with Coronary Heart. *China Pharmaceuticals* 28 (24), 75–77. doi:10.3969/j.issn.1006-4931.2019.24.024

Joon, K. B., Lee, E-J., Kwon Sun, U., Park Jong-Ho, S., Kim, Y-J., Hong, K-S., et al. (2018). Prevention of Cardiovascular Events in Asian Patients with Ischaemic Stroke at High Risk of Cerebral Haemorrhage (PICASSO): a Multicentre, Randomised Controlled Trial. *Lancet Neurol.* 17 (6).

Jung, I. H., Lee, Y. H., Yoo, J. Y., Jeong, S. J., Sonn, S. K., Park, J. G., et al. (2012). Ginkgo Biloba Extract (GbE) Enhances the Anti-atherogenic Effect of Cilostazol by Inhibiting ROS Generation. *Exp. Mol. Med.* 44 (5), 311–318. doi:10.3858/emm.2012.44.5.035

Karunakaran, D., Nguyen, M. A., Geoffrion, M., Vreeken, D., Lister, Z., Cheng, H. S., et al. (2021). RIPK1 Expression Associates with Inflammation in Early Atherosclerosis in Humans and Can Be Therapeutically Silenced to Reduce NF-Kb Activation and Atherogenesis in Mice. *Circulation* 143 (2), 163–177. doi:10.1161/circulationaha.118.038379

Kattoor, A. J., Pothineni, N. V. K., Palagiri, D., and Mehta, J. L. (2017). Oxidative Stress in Atherosclerosis. *Curr. Atheroscler. Rep.* 19 (11), 42. doi:10.1007/s11883-017-0678-6

Kim, H. S., Park, K. G., Koo, T. B., Huh, S., and Lee, I. K. (2007). The Modulating Effects of the Overexpression of Uncoupling Protein 2 on the Formation of Reactive Oxygen Species in Vascular Cells. *Diabetes Res. Clin. Pract.* 77 (Suppl. 1), S46–S48. doi:10.1016/j.diabres.2007.01.032

Konior, A., Schramm, A., Czesnikiewicz-Guzik, M., and Guzik, T. J. (2014). NADPH Oxidases in Vascular Pathology. *Antioxid. Redox Signal.* 20 (17), 2794–2814. doi:10.1089/ars.2013.5607

Lanbin, Y., Chen, Y., Xu, G., Yang, L., Hu, J., Duan, J., et al. (2017). Study on the Mechanism of Huanglian Jiedu Decoction on Atherosclerotic Rats Based on Anti-inflammatory and Oxidative Stress. *Modernization Traditional Chin. Med. Materia Medica-World Sci. Techn.* 19 (11), 1841–1845. doi:10.11842/wst.2017.11.013

Langbein, H., Brunssen, C., Hofmann, A., Cimalla, P., Brux, M., Bornstein, S. R., et al. (2016). NADPH Oxidase 4 Protects against Development of Endothelial Dysfunction and Atherosclerosis in LDL Receptor Deficient Mice. *Eur. Heart J.* 37 (22), 1753–1761. doi:10.1093/eurheartj/ehv564

Lara-Guzman, O. J., Tabares-Guevara, J. H., Leon-Varela, Y. M., Álvarez, R. M., Roldan, M., Sierra, J. A., et al. (2012). Proatherogenic Macrophage Activities Are Targeted by the Flavonoid Quercetin. *J. Pharmacol. Exp. Ther.* 343 (2), 296–306. doi:10.1124/jpet.112.196147

Laufs, U., Wassmann, S., Czech, T., Münzel, T., Eisenhauer, M., Böhm, M., et al. (2005). Physical Inactivity Increases Oxidative Stress, Endothelial Dysfunction, and Atherosclerosis. *Arterioscler Thromb. Vasc. Biol.* 25 (4), 809–814. doi:10.1161/01.ATV.0000158311.24443.af

Lee, J., and Choi, J. H. (2020). Deciphering Macrophage Phenotypes upon Lipid Uptake and Atherosclerosis. *Immune Netw.* 20 (3), e22. doi:10.4110/in.2020.20.e22

Lee, S. E., Park, H. R., Jeon, S., Han, D., and Park, Y. S. (2020). Curcumin Attenuates Acrolein-Induced COX-2 Expression and Prostaglandin Production in Human Umbilical Vein Endothelial Cells. *J. Lipid Atheroscler.* 9 (1), 184–194. doi:10.12997/jla.2020.9.1.184

Lee, T. S., Pan, C. C., Peng, C. C., Kou, Y. R., Chen, C. Y., Ching, L. C., et al. (2010). Anti-atherogenic Effect of Berberine on LXRalpha-ABCA1-dependent Cholesterol Efflux in Macrophages. *J. Cel Biochem* 111 (1), 104–10. doi:10.1002/jcb.22667

Li, C., Miao, X., Li, F., Adhikari, B. K., Liu, Y., Sun, J., et al. (2019a). Curcuminoids: Implication for Inflammation and Oxidative Stress in Cardiovascular Diseases. *Phytother Res.* 33 (5), 1302–1317. doi:10.1002/ptr.6324

Li, C., Zhang, W. J., Choi, J., and Frei, B. (2016a). Quercetin Affects Glutathione Levels and Redox Ratio in Human Aortic Endothelial Cells Not through Oxidation but Formation and Cellular Export of Quercetin-Glutathione Conjugates and Upregulation of Glutamate-Cysteine Ligase. *Redox Biol.* 9, 220–228. doi:10.1016/j.redox.2016.08.012

Li, C., Zhang, W. J., and Frei, B. (2016b). Quercetin Inhibits LPS-Induced Adhesion Molecule Expression and Oxidant Production in Human Aortic Endothelial Cells by P38-Mediated Nrf2 Activation and Antioxidant Enzyme Induction. *Redox Biol.* 9, 104–113. doi:10.1016/j.redox.2016.06.006

Li, F., Tang, H., Xiao, F., Gong, J., Peng, Y., and Meng, X. (2011a). Protective Effect of Salidroside from Rhodiolae Radix on Diabetes-Induced Oxidative Stress in Mice. *Molecules* 16 (12), 9912–9924. doi:10.3390/molecules16129912

Li, H., Sureda, A., Devkota, H. P., Pittalà, V., Barreca, D., Silva, A. S., et al. (2020a). Curcumin, the Golden Spice in Treating Cardiovascular Diseases. *Biotechnol. Adv.* 38, 107343. doi:10.1016/j.biotechadv.2019.01.010

Li, J. M., and Shah, A. M. (2004). Endothelial Cell Superoxide Generation: Regulation and Relevance for Cardiovascular Pathophysiology. *Am. J. Physiol. Regul. Integr. Comp. Physiol.* 287 (5), R1014–R1030. doi:10.1152/ajpregu.00124.2004

Li, J., Xie, Z. Z., Tang, Y. B., Zhou, J. G., and Guan, Y. Y. (2011b). Ginsenoside-Rd, a Purified Component from Panax Notoginseng Saponins, Prevents Atherosclerosis in apoE Knockout Mice. *Eur. J. Pharmacol.* 652 (1-3), 104–10. doi:10.1016/j.ejphar.2010.11.017

Li, J., Zhong, Z., Yuan, J., Chen, X., Huang, Z., and Wu, Z. (2019b). Resveratrol Improves Endothelial Dysfunction and Attenuates Atherogenesis in Apolipoprotein E-Deficient Mice. *J. Nutr. Biochem.* 67, 63–71. doi:10.1016/j.jnutbio.2019.01.022

Li, R., Chen, B. W. Wu., Bao, L., Li, J., and Qi, R. (2009). Ginkgolide B Suppresses Intercellular Adhesion Molecule-1 Expression via Blocking Nuclear Factor-kappaB Activation in Human Vascular Endothelial Cells Stimulated by Oxidized Low-Density Lipoprotein. *J. Pharmacol. Sci.* 110 (3), 362–369. doi:10.1254/jphs.08275fp

Li, X., Lu, L., Chen, J., Zhang, C., Chen, H., and Huang, H. (2020b). Ginkgo BilobaNew Insight into the Mechanisms of Extract in Vascular Aging Prevention. *Curr. Vasc. Pharmacol.* 18 (4), 334–345. doi:10.2174/1570161117666190621150725

Li, Y., Aziz, Q., Anderson, N., Ojake, L., and Tinker, A. (2020c). Endothelial ATP-Sensitive Potassium Channel Protects against the Development of Hypertension and Atherosclerosis. *Hypertension* 76 (3), 776–784. doi:10.1161/hypertensionaha.120.15355

Li, Y. I., Elmer, G., and Leboeuf, R. C. (2008). Tanshinone IIA Reduces Macrophage Death Induced by Hydrogen Peroxide by Upregulating Glutathione Peroxidase. *Life Sci.* 83 (15-16), 557–562. doi:10.1016/j.lfs.2008.08.003

Li, Y. R., Li, S., and Lin, C. C. (2018a). Effect of Resveratrol and Pterostilbene on Aging and Longevity. *Biofactors* 44 (1), 69–82. doi:10.1002/biof.1400

Li, Y., Tian, L., Sun, D., and Yin, D. (2019c). Curcumin Ameliorates Atherosclerosis through Upregulation of miR-126. *J. Cel Physiol* 234 (11), 21049–21059. doi:10.1002/jcp.28708

Li, Z. M., Xu, S. W., and Liu, P. Q. (2018b). Salvia miltiorrhizaBurge (Danshen): a Golden Herbal Medicine in Cardiovascular Therapeutics. *Acta Pharmacol. Sin* 39 (5), 802–824. doi:10.1038/aps.2017.193

Liao, J., An, X., Yang, X., Lin, Q. Y., Liu, S., Xie, Y., et al. (2020). Deficiency of LMP10 Attenuates Diet-Induced Atherosclerosis by Inhibiting Macrophage Polarization and Inflammation in Apolipoprotein E Deficient Mice. *Front Cel Dev Biol* 8, 592048. doi:10.3389/fcell.2020.592048

Libby, P., Buring, J. E., Badimon, L., Hansson, G. K., Deanfield, J., Bittencourt, M. S., et al. (2019). Atherosclerosis. *Nat. Rev. Dis. Primers* 5 (1), 56. doi:10.1038/s41572-019-0106-z

Libby, P., Ridker, P. M., and Hansson, G. K. (2011). Progress and Challenges in Translating the Biology of Atherosclerosis. *Nature* 473 (7347), 317–325. doi:10.1038/nature10146

Lin, C. J., Lee, C. C., Shih, Y. L., Lin, T. Y., Wang, S. H., Lin, Y. F., et al. (2012). Resveratrol Enhances the Therapeutic Effect of Temozolomide against Malignant Glioma In Vitro and In Vivo by Inhibiting Autophagy. *Free Radic. Biol. Med.* 52 (2), 377–391. doi:10.1016/j.freeradbiomed.2011.10.487

Lin, R., Wang, W. R., Liu, J. T., Yang, G. D., and Han, C. J. (2006). Protective Effect of Tanshinone IIA on Human Umbilical Vein Endothelial Cell Injured by Hydrogen Peroxide and its Mechanism. *J. Ethnopharmacol* 108 (2), 217–222. doi:10.1016/j.jep.2006.05.004

Liu, B., Song, Z., Yu, J., Li, P., Tang, Y., and Ge, J. (2020). The Atherosclerosis-Ameliorating Effects and Molecular Mechanisms of BuYangHuanWu Decoction. *Biomed. Pharmacother.* 123, 109664. doi:10.1016/j.biopha.2019.109664

Liu, X., Lu, B., Fu, J., Zhu, X., Song, E., and Song, Y. (2021). Amorphous Silica Nanoparticles Induce Inflammation via Activation of NLRP3 Inflammasome and HMGB1/TLR4/MYD88/NF-Kb Signaling Pathway in HUVEC Cells. *J. Hazard. Mater.* 404, 124050. doi:10.1016/j.jhazmat.2020.124050

Liu, X., Guo, C. Y., Ma, X. J., Wu, C. F., Zhang, Y., Sun, M. Y., et al. (2015). Anti-inflammatory Effects of Tanshinone IIA on Atherosclerostic Vessels of Ovariectomized ApoE Mice Are Mediated by Estrogen Receptor Activation and through the ERK Signaling Pathway. *Cel Physiol Biochem* 35 (5), 1744–1755. doi:10.1159/000373986

Liu, X., and Cui, Y. (2016). Effect of Yiqi Huoxue Decoction on Oxidative Stress Response and Neurologic Deficit in Patients with Ischemic Stroke. *Mod. J. Integrated Traditional Chin. West. Med.* 25 (22), 2422–2424. doi:10.3969/j.issn.1008-8849.2016.22.009

Loke, W. M., Proudfoot, J. M., Hodgson, J. M., McKinley, A. J., Hime, N., Magat, M., et al. (2010). Specific Dietary Polyphenols Attenuate Atherosclerosis in Apolipoprotein E-Knockout Mice by Alleviating Inflammation and Endothelial Dysfunction. *Arterioscler Thromb. Vasc. Biol.* 30 (4), 749–757. doi:10.1161/atvbaha.109.199687

Lü, J. M., Jiang, J., Jamaluddin, M. S., Liang, Z., Yao, Q., and Chen, C. (2019). Ginsenoside Rb1 Blocks Ritonavir-Induced Oxidative Stress and eNOS Downregulation through Activation of Estrogen Receptor-Beta and Upregulation of SOD in Human Endothelial Cells. *Int. J. Mol. Sci.* 20 (2). doi:10.3390/ijms20020294

Lu, X. L., Zhao, C. H., Yao, X. L., and Zhang, H. (2017). Quercetin Attenuates High Fructose Feeding-Induced Atherosclerosis by Suppressing Inflammation and Apoptosis via ROS-Regulated PI3K/AKT Signaling Pathway. *Biomed. Pharmacother.* 85, 658–671. doi:10.1016/j.biopha.2016.11.077

Luo, M., Tian, R., and Lu, N. (2020). Quercetin Inhibited Endothelial Dysfunction and Atherosclerosis in Apolipoprotein E-Deficient Mice: Critical Roles for NADPH Oxidase and Heme Oxygenase-1. *J. Agric. Food Chem.* 68 (39), 10875–10883. doi:10.1021/acs.jafc.0c03907

Lv, Y. L., Jia, Y., Wan, Z., An, Z. L., Yang, S., Han, F. F., et al. (2020). Curcumin Inhibits the Formation of Atherosclerosis in ApoE(-/-) Mice by Suppressing Cytomegalovirus Activity in Endothelial Cells. *Life Sci.* 257, 117658. doi:10.1016/j.lfs.2020.117658

Ma, L., Liu, X., Zhao, Y., Chen, B., Li, X., and Qi, R. (2013). Ginkgolide B Reduces LOX-1 Expression by Inhibiting Akt Phosphorylation and Increasing Sirt1 Expression in Oxidized LDL-Stimulated Human Umbilical Vein Endothelial Cells. *PloS one* 8 (9), e74769. doi:10.1371/journal.pone.0074769

Ma, Q., Yang, Q., Chen, J., Yu, C., Zhang, L., Zhou, W., et al. (2020). Salvianolic Acid A Ameliorates Early-Stage Atherosclerosis Development by Inhibiting NLRP3 Inflammasome Activation in Zucker Diabetic Fatty Rats. *Molecules* 25 (5). doi:10.3390/molecules25051089

Madamanchi, N. R., Vendrov, A., and Runge, M. S. (2005). Oxidative Stress and Vascular Disease. *Arterioscler Thromb. Vasc. Biol.* 25 (1), 29–38. doi:10.1161/01.Atv.0000150649.39934.13

Mansur, A. P., Roggerio, A., Goes, M. F. S., Avakian, S. D., Leal, D. P., Maranhão, R. C., et al. (2017). Serum Concentrations and Gene Expression of Sirtuin 1 in Healthy and Slightly Overweight Subjects after Caloric Restriction or Resveratrol Supplementation: A Randomized Trial. *Int. J. Cardiol.* 227, 788–794. doi:10.1016/j.ijcard.2016.10.058

Mao, G. X., Wang, Y., Qiu, Q., Deng, H. B., Yuan, L. G., Li, R. G., et al. (2010). Salidroside Protects Human Fibroblast Cells from Premature Senescence Induced by H(2)O(2) Partly through Modulating Oxidative Status. *Mech. Ageing Dev.* 131 (11-12), 723–731. doi:10.1016/j.mad.2010.10.003

McClelland, R. L., Chung, H., Detrano, R., Post, W., and Kronmal, R. A. (2006). Distribution of Coronary Artery Calcium by Race, Gender, and Age: Results from the Multi-Ethnic Study of Atherosclerosis (MESA). *Circulation* 113 (1), 30–37. doi:10.1161/circulationaha.105.580696

McNally, J. S., Davis, M. E., Giddens, D. P., Saha, A., Hwang, J., Dikalov, S., et al. (2003). Role of Xanthine Oxidoreductase and NAD(P)H Oxidase in Endothelial Superoxide Production in Response to Oscillatory Shear Stress. *Am. J. Physiol. Heart Circ. Physiol.* 285 (6), H2290–H2297. doi:10.1152/ajpheart.00515.2003

Meng, N., Gong, Y., Zhang, J., Mu, X., Song, Z., Feng, R., et al. (2019). A Novel Curcumin-Loaded Nanoparticle Restricts Atherosclerosis Development and Promotes Plaques Stability in Apolipoprotein E Deficient Mice. *J. Biomater. Appl.* 33 (7), 946–954. doi:10.1177/0885328218815328

Mohar, D. S., and Malik, S. (2012). The Sirtuin System: The Holy Grail of Resveratrol? *J. Clin. Exp. Cardiolog* 3 (11). doi:10.4172/2155-9880.1000216

Moore, K. J., and Tabas, I. (2011). Macrophages in the Pathogenesis of Atherosclerosis. *Cell* 145 (3), 341–355. doi:10.1016/j.cell.2011.04.005

Mulvihill, E. E., and Huff, M. W. (2010). Antiatherogenic Properties of Flavonoids: Implications for Cardiovascular Health. *Can. J. Cardiol.* 26 (Suppl. l), 17a–21a. doi:10.1016/s0828-282x(10)71056-4

Murdocca, M., C De Masi, S., Pucci, R. M., Novelli, G., Di Natale, C., and Sangiuolo, F. (2021). LOX-1 and Cancer: an Indissoluble Liaison. *Cancer Gene Ther.* doi:10.1038/s41417-020-00279-0

Mury, P., Chirico, E. N., Mura, M., Millon, A., Canet-Soulas, E., and Pialoux, V. (2018). Oxidative Stress and Inflammation, Key Targets of Atherosclerotic Plaque Progression and Vulnerability: Potential Impact of Physical Activity. *Sports Med.* 48 (12), 2725–2741. doi:10.1007/s40279-018-0996-z

Naito, M., Wu, X., Nomura, H., Kodama, M., Kato, Y., Kato, Y., et al. (2002). The Protective Effects of Tetrahydrocurcumin on Oxidative Stress in Cholesterol-Fed Rabbits. *J. Atheroscler. Thromb.* 9 (5), 243–250. doi:10.5551/jat.9.243

Naya, M., Morita, K., Yoshinaga, K., Manabe, O., Goto, D., Hirata, K., et al. (2011). Long-term Smoking Causes More Advanced Coronary Endothelial Dysfunction in Middle-Aged Smokers Compared to Young Smokers. *Eur. J. Nucl. Med. Mol. Imaging* 38 (3), 491–498. doi:10.1007/s00259-010-1647-2

Ni, J., Li, Y., Li, W., and Guo, R. (2017a). Salidroside Protects against Foam Cell Formation and Apoptosis, Possibly via the MAPK and AKT Signaling Pathways. *Lipids Health Dis.* 16 (1), 198. doi:10.1186/s12944-017-0582-7

Ni, Z., Cao, H., Song, N., Yang, G., Jia, L., and Zhang, Z. (2017b). The Protective Effect of Tanshinone ⅡA on Ox-LDL Induced Endothelial Cell Oxidative Stress Injury through Regulating Autophagosome. *Chin. J. Arteriosclerosis* 25 (03), 244–249.

Niu, X. L., Ichimori, K., Yang, X., Hirota, Y., Hoshiai, K., Li, M., et al. (2000). Tanshinone II-A Inhibits Low Density Lipoprotein Oxidation In Vitro. *Free Radic. Res.* 33 (3), 305–312. doi:10.1080/10715760000301471

Olmos, Y., Sánchez-Gómez, F. J., Wild, B., García-Quintans, N., Cabezudo, S., Lamas, S., et al. (2013). SirT1 Regulation of Antioxidant Genes Is Dependent on the Formation of a FoxO3a/PGC-1α Complex. *Antioxid. Redox Signal.* 19 (13), 1507–1521. doi:10.1089/ars.2012.4713

Ou, H. C., Hsieh, Y. L., Yang, N. C., Tsai, K. L., Chen, K. L., Tsai, C. S., et al. (2013). Ginkgo Biloba Extract Attenuates oxLDL-Induced Endothelial Dysfunction via an AMPK-dependent Mechanism. *J. Appl. Physiol.* 114 (2), 274–285. doi:10.1152/japplphysiol.00367.2012

Ou, H. C., Lee, W. J., Lee, I. T., Chiu, T. H., Tsai, K. L., Lin, C. Y., et al. (2009). Ginkgo Biloba Extract Attenuates oxLDL-Induced Oxidative Functional Damages in Endothelial Cells. *J. Appl. Physiol.* 106 (5), 1674–1685. doi:10.1152/japplphysiol.91415.2008

Ouimet, M., Barrett, T. J., and Fisher, E. A. (2019). HDL and Reverse Cholesterol Transport. *Circ. Res.* 124 (10), 1505–1518. doi:10.1161/circresaha.119.312617

Ouyang, S., Yao, Y. H., Zhang, Z. M., Liu, J. S., and Xiang, H. (2019). Curcumin Inhibits Hypoxia Inducible Factor-1α-Induced Inflammation and Apoptosis in Macrophages through an ERK Dependent Pathway. *Eur. Rev. Med. Pharmacol. Sci.* 23 (4), 1816–1825. doi:10.26355/eurrev_201902_17145

Panahi, Y., Ahmadi, Y., Teymouri, M., Johnston, T. P., and Sahebkar, A. (2018). Curcumin as a Potential Candidate for Treating Hyperlipidemia: A Review of Cellular and Metabolic Mechanisms. *J. Cel Physiol* 233 (1), 141–152. doi:10.1002/jcp.25756

Piazza, S., Pacchetti, B., Fumagalli, M., Bonacina, F., Dell'Agli, M., and Sangiovanni, E. (2019). Comparison of Two Ginkgo Biloba L. Extracts on Oxidative Stress and Inflammation Markers in Human Endothelial Cells. *Mediators Inflamm.*, 6173893. doi:10.1155/2019/6173893

Pu, Y., Zhang, H., Wang, P., Zhao, Y., Li, Q., Wei, X., et al. (2013). Dietary Curcumin Ameliorates Aging-Related Cerebrovascular Dysfunction through the AMPK/uncoupling Protein 2 Pathway. *Cel Physiol Biochem* 32 (5), 1167–1177. doi:10.1159/000354516

Qiao, Y., Zhang, P. J., Lu, X. T., Sun, W. W., Liu, G. L., Ren, M., et al. (2015). Panax Notoginseng Saponins Inhibits Atherosclerotic Plaque Angiogenesis by Down-Regulating Vascular Endothelial Growth Factor and Nicotinamide Adenine Dinucleotide Phosphate Oxidase Subunit 4 Expression. *Chin. J. Integr. Med.* 21 (4), 259–265. doi:10.1007/s11655-014-1832-4

Qin, M., Luo, Y., Lu, S., Sun, J., Yang, K., Sun, G., et al. (2017). Ginsenoside F1 Ameliorates Endothelial Cell Inflammatory Injury and Prevents Atherosclerosis in Mice through A20-Mediated Suppression of NF-kB Signaling. *Front. Pharmacol.* 8, 953. doi:10.3389/fphar.2017.00953

Quan, Li., Zhang, Xuexin., and Liu, Yanjun. (2019). Clinical Observation of Huatan Quzhuo Prescription in the Treatment of Carotid Atherosclerosis Plaque with Spleen Deficiency and Phlegm Turbidity Repression Type. *Hebei J. Traditional Chin. Med.* 41 (01), 42–46. doi:10.3969/j.issn.1002-2619.2019.01.009

Ren, J., Fu, L., Nile, S. H., Zhang, J., and Kai, G. (2019). Salvia Miltiorrhiza in Treating Cardiovascular Diseases: A Review on its Pharmacological and Clinical Applications. *Front. Pharmacol.* 10, 753. doi:10.3389/fphar.2019.00753

Ren, Y., Tao, S., Zheng, S., Zhao, M., Zhu, Y., Yang, J., et al. (2016). Salvianolic Acid B Improves Vascular Endothelial Function in Diabetic Rats with Blood Glucose Fluctuations via Suppression of Endothelial Cell Apoptosis. *Eur. J. Pharmacol.* 791, 308–315. doi:10.1016/j.ejphar.2016.09.014

Rivera, D., Allkin, R., Obon, C., Alcaraz, F., Verpoorte, R., and Heinrich, M. (2014). What Is in a Name? the Need for Accurate Scientific Nomenclature for Plants. *J. Ethnopharmacol* 152 (3), 393–402. doi:10.1016/j.jep.2013.12.022

Saji, S., Asha, S., Svenia, P. J., Ratheesh, M., Sheethal, S., Sandya, S., et al. (2018). Curcumin-galactomannoside Complex Inhibits Pathogenesis in Ox-LDL-Challenged Human Peripheral Blood Mononuclear Cells. *Inflammopharmacology* 26 (5), 1273–1282. doi:10.1007/s10787-018-0474-0

Sarna, L. K., Wu, N., Hwang, S. Y., Siow, Y. L., and O, K. (2010). Berberine Inhibits NADPH Oxidase Mediated Superoxide Anion Production in Macrophages. *Can. J. Physiol. Pharmacol.* 88 (3), 369–378. doi:10.1139/y09-136

Schürmann, C., Rezende, F., Kruse, C., Yasar, Y., Löwe, O., Fork, C., et al. (2015). The NADPH Oxidase Nox4 Has Anti-atherosclerotic Functions. *Eur. Heart J.* 36 (48), 3447–3456. doi:10.1093/eurheartj/ehv460

Shen, Y., Ward, N. C., Hodgson, J. M., Puddey, I. B., Wang, Y., Zhang, D., et al. (2013). Dietary Quercetin Attenuates Oxidant-Induced Endothelial Dysfunction and Atherosclerosis in Apolipoprotein E Knockout Mice Fed a High-Fat Diet: a Critical Role for Heme Oxygenase-1. *Free Radic. Biol. Med.* 65, 908–915. doi:10.1016/j.freeradbiomed.2013.08.185

Shi, J., Deng, H., and Zhang, M. (2017). Curcumin Pretreatment Protects against PM2.5-induced Oxidized Low-Density Lipoprotein-Mediated Oxidative Stress and Inflammation in Human Microvascular Endothelial Cells. *Mol. Med. Rep.* 16 (3), 2588–2594. doi:10.3892/mmr.2017.6935

Shibai, Li., Liu, Jun., and Wu, Zhisheng. (2019). Clinical Evaluation on Ginkgo Leaf Capsules Combined with Nicorandil in the Treatment of Angina Pectoris of Coronary Heart Disease. *China Pharmaceuticals* 28 (11), 77–80. doi:10.3969/j.issn.1006-4931.2019.11.024

Sies, H. (2015). Oxidative Stress: a Concept in Redox Biology and Medicine. *Redox Biol.* 4, 180–183. doi:10.1016/j.redox.2015.01.002

Soltani, B., Bodaghabadi, N., Ghaemi, N., and Sadeghizadeh, M. (2017). Radiation-induced Surge of Macrophage Foam Cell Formation, Oxidative Damage, and Cytokine Release Is Attenuated by a Nanoformulation of Curcumin. *Int. J. Radiat. Biol.* 93 (3), 303–314. doi:10.1080/09553002.2016.1242817

Song, P., Fang, Z., Wang, H., Cai, Y., Rahimi, K., Zhu, Y., et al. (2020). Global and Regional Prevalence, Burden, and Risk Factors for Carotid Atherosclerosis: a Systematic Review, Meta-Analysis, and Modelling Study. *Lancet Glob. Health* 8 (5), e721–e729. doi:10.1016/s2214-109x(20)30117-0

Stephens, E. H., Saltarrelli, J. G., Baggett, L. S., Nandi, I., Kuo, J. J., Davis, A. R., et al. (2011). Differential Proteoglycan and Hyaluronan Distribution in Calcified Aortic Valves. *Cardiovasc. Pathol.* 20 (6), 334–342. doi:10.1016/j.carpath.2010.10.002

Stromsnes, K., Mas-Bargues, C., Gambini, J., and Gimeno-Mallench, L. (2020). Protective Effects of Polyphenols Present in Mediterranean Diet on Endothelial Dysfunction. *Oxid Med. Cel Longev* 2020, 2097096. doi:10.1155/2020/2097096

Sun, Y., Liu, Y., and Chen, K. (2016). Roles and Mechanisms of Ginsenoside in Cardiovascular Diseases: Progress and Perspectives. *Sci. China Life Sci.* 59 (3), 292–298. doi:10.1007/s11427-016-5007-8

Szewczuk, L. M., Forti, L., Stivala, L. A., and Penning, T. M. (2004). Resveratrol Is a Peroxidase-Mediated Inactivator of COX-1 but Not COX-2: a Mechanistic Approach to the Design of COX-1 Selective Agents. *J. Biol. Chem.* 279 (21), 22727–22737. doi:10.1074/jbc.M314302200

Tabas, I., García-Cardeña, G., and Owens, G. K. (2015). Recent Insights into the Cellular Biology of Atherosclerosis. *J. Cel Biol* 209 (1), 13–22. doi:10.1083/jcb.201412052

Tabas, I., Williams, K. J., and Borén, J. (2007). Subendothelial Lipoprotein Retention as the Initiating Process in Atherosclerosis: Update and Therapeutic Implications. *Circulation* 116 (16), 1832–1844. doi:10.1161/circulationaha.106.676890

Tan, W., Wang, Y., Wang, K., Wang, S., Liu, J., Qin, X., et al. (2020). Improvement of Endothelial Dysfunction of Berberine in Atherosclerotic Mice and Mechanism Exploring through TMT-Based Proteomics. *Oxidative Med. Cell. longevity* 2020, 8683404. doi:10.1155/2020/8683404

Tang, F. T., Cao, Y., Wang, T. Q., Wang, L. J., Guo, J., Zhou, X. S., et al. (2011). Tanshinone IIA Attenuates Atherosclerosis in ApoE(-/-) Mice through Down-Regulation of Scavenger Receptor Expression. *Eur. J. Pharmacol.* 650 (1), 275–284. doi:10.1016/j.ejphar.2010.07.038

Tardif, J. C., Grégoire, J., Schwartz, L., Title, L., Laramée, L., Reeves, F., et al. (2003). Effects of AGI-1067 and Probucol after Percutaneous Coronary Interventions. *Circulation* 107 (4), 552–558. doi:10.1161/01.cir.0000047525.58618.3c

Tardif, J. C., McMurray, J. J., Klug, E., Small, R., Schumi, J., Choi, J., et al. (2008). Effects of Succinobucol (AGI-1067) after an Acute Coronary Syndrome: a Randomised, Double-Blind, Placebo-Controlled Trial. *Lancet* 371 (9626), 1761–1768. doi:10.1016/s0140-6736(08)60763-1

Tian, J., Liu, Y., and Chen, K. (2017). Ginkgo Biloba Extract in Vascular Protection: Molecular Mechanisms and Clinical Applications. *Curr. Vasc. Pharmacol.* 15 (6), 532–548. doi:10.2174/1570161115666170713095545

Tong, L., Zhao, M. J., Han, X. W., Deng, Y., Zhao, Y. Z., Yang, T., et al. (2018). [Huotan Jiedu Tongluo Decoction Alleviates Early Atherosclerosis of Rabbits by Inhibiting eNOS Uncoupling Pathway]. *Zhongguo Zhong yao Za Zhi = Zhongguo zhongyao zazhi = China J. Chin. materia Med.* 43 (21).

Tonghua, Li. (2019). "Ginkgo Biloba Extract (EGb761) Inhibiting Smoothmuscle Foam Cell Formation and the Underlyingmechanisms," in *Doctoral Dissertation* (Cnki: PLA Air Force Military Medical University).

Treviño-Saldaña, N., and García-Rivas, G. (2017). Regulation of Sirtuin-Mediated Protein Deacetylation by Cardioprotective Phytochemicals. *Oxid Med. Cel Longev* 2017, 1750306. doi:10.1155/2017/1750306

Tsai, H. Y., Huang, P. H., Lin, F. Y., Chen, J. S., Lin, S. J., and Chen, J. W. (2013). Ginkgo Biloba Extract Reduces High-Glucose-Induced Endothelial Reactive Oxygen Species Generation and Cell Adhesion Molecule Expression by Enhancing HO-1 Expression via Akt/eNOS and P38 MAP Kinase Pathways. *Eur. J. Pharm. Sci. : official J. Eur. Fed. Pharm. Sci.* 48, 803–811. doi:10.1016/j.ejps.2013.01.002

Tyrrell, D. J., and Goldstein, D. R. (2021). Ageing and Atherosclerosis: Vascular Intrinsic and Extrinsic Factors and Potential Role of IL-6. *Nat. Rev. Cardiol.* 18 (1), 58–68. doi:10.1038/s41569-020-0431-7

van Beek, T. A., and Montoro, P. (2009). Chemical Analysis and Quality Control of Ginkgo Biloba Leaves, Extracts, and Phytopharmaceuticals. *J. Chromatogr. A* 1216 (11), 2002–2032. doi:10.1016/j.chroma.2009.01.013

Vivancos, M., and Moreno, J. J. (2008). Effect of Resveratrol, Tyrosol and Beta-Sitosterol on Oxidised Low-Density Lipoprotein-Stimulated Oxidative Stress, Arachidonic Acid Release and Prostaglandin E2 Synthesis by RAW 264.7 Macrophages. *Br. J. Nutr.* 99 (6), 1199–207. doi:10.1017/s0007114507876203

Wang, G., Liu, Z., Li, M., Li, Y., Alvi, S. S., Ansari, I. A., et al. (2019). Ginkgolide B Mediated Alleviation of Inflammatory Cascades and Altered Lipid Metabolism in HUVECs via Targeting PCSK-9 Expression and Functionality. *Biomed. Research International* 2019, 7284767. doi:10.1155/2019/7284767

Wang, Q., Zhang, M., Liang, B., Shirwany, N., Zhu, Y., and Zou, M. H. (2011). Activation of AMP-Activated Protein Kinase Is Required for Berberine-Induced Reduction of Atherosclerosis in Mice: the Role of Uncoupling Protein 2. *PLoS One* 6 (9), e25436. doi:10.1371/journal.pone.0025436

Wiciński, M., Socha, M., Walczak, M., Wódkiewicz, E., Malinowski, B., Rewerski, S., et al. (2018). Beneficial Effects of Resveratrol Administration-Focus on Potential Biochemical Mechanisms in Cardiovascular Conditions. *Nutrients* 10 (11). doi:10.3390/nu10111813

Willeit, J., Kiechl, S., Weimer, T., Mair, A., Santer, P., Wiedermann, C. J., et al. (2003). Marburg I Polymorphism of Factor VII-Aactivating Protease: a Prominent Risk Predictor of Carotid Stenosis. *Circulation* 107 (5), 667–670. doi:10.1161/01.cir.0000055189.18831.b1

Wu, M., Wang, J., and Liu, L. T. (2010). Advance of Studies on Anti-atherosclerosis Mechanism of Berberine. *Chin. J. Integr. Med.* 16 (2), 188–92. doi:10.1007/s11655-010-0188-7

Xiang, Y., Ye, S., Cai, C., Chen, J., Zhao, X., Zhu, N., et al. (2018). Salvianolic Acid a Attenuates Limb Ischemia/reperfusion Injury in Skeletal Muscle of Rats. *Biomed. Pharmacother.* 97, 551–556. doi:10.1016/j.biopha.2017.10.094

Xiao, L., Liu, L., Guo, X., Zhang, S., Wang, J., Zhou, F., et al. (2017). Quercetin Attenuates High Fat Diet-Induced Atherosclerosis in Apolipoprotein E Knockout Mice: A Critical Role of NADPH Oxidase. *Food Chem. Toxicol.* 105, 22–33. doi:10.1016/j.fct.2017.03.048

Xibin, Dou., Tang, Hanqing., Zhao, Yufeng., Zhao, Qiuhua., Li, Keming., and Wang, Luyao. (2019). Effects of Xuefuzhuyu Decoction on Blood Fat and Myocardial Enzymes in the Coronary Heart Disease Rat Model. *Guangdong Med. J.* 40 (06), 767–771. doi:10.13820/j.cnki.gdyx.20185097

Xing, S. S., Li, J., Chen, L., Yang, Y. F., He, P. L., Li, J., et al. (2018). Salidroside Attenuates Endothelial Cellular Senescence via Decreasing the Expression of Inflammatory Cytokines and Increasing the Expression of SIRT3. *Mech. Ageing Dev.* 175, 1–6. doi:10.1016/j.mad.2017.12.005

Xing, S., Yang, X., Li, W., Bian, F., Wu, D., Chi, J., et al. (2014). Salidroside Stimulates Mitochondrial Biogenesis and Protects against H_2O_2-induced Endothelial Dysfunction. *Oxid Med. Cel Longev* 2014, 904834. doi:10.1155/2014/904834

Xuan, Y., Gao, Y., Huang, H., Wang, X., Cai, Y., and Luan, Q. X. (2017). Tanshinone IIA Attenuates Atherosclerosis in Apolipoprotein E Knockout Mice Infected with Porphyromonas Gingivalis. *Inflammation* 40 (5), 1631–1642. doi:10.1007/s10753-017-0603-8

Xue, F., Nie, X., Shi, J., Liu, Q., Wang, Z., Li, X., et al. (2017). Quercetin Inhibits LPS-Induced Inflammation and Ox-LDL-Induced Lipid Deposition. *Front. Pharmacol.* 8, 40. doi:10.3389/fphar.2017.00040

Yang, J., Zhou, X., Zeng, X., Hu, O., Yi, L., and Mi, M. (2019). Resveratrol Attenuates Oxidative Injury in Human Umbilical Vein Endothelial Cells through Regulating Mitochondrial Fusion via TyrRS-PARP1 Pathway. *Nutr. Metab. (Lond)* 16, 9. doi:10.1186/s12986-019-0338-7

Yang, X. J., Liu, F., Feng, N., Ding, X. S., Chen, Y., Zhu, S. X., et al. (2020a). Berberine Attenuates Cholesterol Accumulation in Macrophage Foam Cells by Suppressing AP-1 Activity and Activation of the Nrf2/HO-1 Pathway. *J. Cardiovasc. Pharmacol.* 75 (1), 45–53. doi:10.1097/fjc.0000000000000769

Yang, Y., Wang, J., Guo, S., Pourteymour, S., Xu, Q., Gong, J., et al. (2020b). Non-lethal Sonodynamic Therapy Facilitates the M1-To-M2 Transition in Advanced Atherosclerotic Plaques via Activating the ROS-AMPK-mTORC1-Autophagy Pathway. *Redox Biol.* 32, 101501. doi:10.1016/j.redox.2020.101501

Yang, Y., Pei, K., Zhang, Q., Wang, D., Feng, H., Du, Z., et al. (2020c). Salvianolic Acid B Ameliorates Atherosclerosis via Inhibiting YAP/TAZ/JNK Signaling Pathway in Endothelial Cells and Pericytes. *Biochim. Biophys. Acta Mol. Cel Biol Lipids* 1865 (10), 158779. doi:10.1016/j.bbalip.2020.158779

Yansheng, K., Liu, J., Zhang, W., Wang, T., Wang, X., Wen, L., et al. (2020). Effect of Compound Danshen Granules, Capsules, Tablets, and Drop Pills on Curative Effect, Inflammatory Factors, and Oxidative Stress Indexes of Angina Pectoris Patients with Coronary Heart Disease. *Drug Eval. Res.* 43 (02), 287–292. doi:10.7501/j.issn.1674-6376.2020.02.021

Yi, L., Jin, X., Chen, C. Y., Fu, Y. J., Zhang, T., Chang, H., et al. (2011). Chemical Structures of 4-Oxo-Flavonoids in Relation to Inhibition of Oxidized Low-Density Lipoprotein (LDL)-induced Vascular Endothelial Dysfunction. *Int. J. Mol. Sci.* 12 (9), 5471–5489. doi:10.3390/ijms12095471

Yonggang, Li. (2020). Effects of Tongqiao Huoxue Decoction on Oxidative Stress and Cerebral Blood Flow in Patients with Acute Ischemic Stroke. *Hunan J. Traditional Chin. Med.* 36 (03), 36–37. doi:10.16808/j.cnki.issn1003-7705.2020.03.014

Yu, X. H., Zhang, D. W., Zheng, X. L., and Tang, C. K. (2019). Cholesterol Transport System: An Integrated Cholesterol Transport Model Involved in Atherosclerosis. *Prog. lipid Res.* 73, 65–91. doi:10.1016/j.plipres.2018.12.002

Yu, Zhang., Cheng, Saibo., Zhao, Dandan., Su, Zhijie., Zhang, Lei., Xu, Yuling., et al. (2016). Dingxin Recipe Attenuates Atherosclerosis by Up-Regulating PTEN Expression in Apo E Knockout Mice. *Chin. J. Exp. Traditional Med. Formulae* 22 (24), 111–115. doi:10.13422/j.cnki.syfjx.2016240111

Yufeng, Qian., Fang, Cunming., and Chen, Guoyou. (2019). Effects of Shexiang Baoxin Pills on Serum Cyclophilin A and Oxidative Stress in Patients with Coronary Heart Disease after PCI. *Mod. J. Integrated Traditional Chin. West. Med.* 28 (25), 2822–2825. doi:10.3969/j.issn.1008-8849.2019.25.024

Zhang, M, K. Nakamura. S. Kageyama., AO, Lawal., Gong, K. W., Bhetraratana, M., Fujii, T., Sulaiman, D., et al. (2018). Myeloid HO-1 Modulates Macrophage Polarization and Protects against Ischemia-Reperfusion Injury. *JCI insight* 3 (19). doi:10.1172/jci.insight.120596

Zhang, X., Liu, J., Pang, X., Zhao, J., and Xu, S. (2020a). Curcumin Suppresses Aldosterone-Induced CRP Generation in Rat Vascular Smooth Muscle Cells via Interfering with the ROS-Erk1/2 Signaling Pathway. *Evid. Based Complement. Alternat Med.* 2020, 3245653. doi:10.1155/2020/3245653

Zhang, Y., Murugesan, P., Huang, K., and Cai, H. (2020b). NADPH Oxidases and Oxidase Crosstalk in Cardiovascular Diseases: Novel Therapeutic Targets. *Nat. Rev. Cardiol.* 17 (3), 170–194. doi:10.1038/s41569-019-0260-8

Zhanxia, H., Liang, S., Lu, B., and Ji, L. (2019). Effect of PI3K-Mediated Nrf2 Phosphorylated Activation in Quercetin in Inhibiting Clivorine-Induced Hepatotoxicity. *Chin. J. Exp. Traditional Med. Formulae* 25 (05), 112–118. doi:10.13422/j.cnki.syfjx.20190423

Zhao, D., Sun, X., Lv, S., Sun, M., Guo, H., Zhai, Y., et al. (2019). Salidroside Attenuates Oxidized Low-Density Lipoprotein-Induced Endothelial Cell Injury via Promotion of the AMPK/SIRT1 Pathway. *Int. J. Mol. Med.* 43 (6), 2279–2290. doi:10.3892/ijmm.2019.4153

Zhao, J., Liu, H., Xu, B., Peng, J., Xing, Y., Tang, W., et al. (2020a). The Role of Xuefu Zhuyu Decoction in Prevention of Contrast-Induced Nephropathy after Percutaneous Coronary Intervention. *Evid. Based Complement. Alternat Med.* 2020, 5419016. doi:10.1155/2020/5419016

Zhao, Y., Qu, H., Wang, Y., Xiao, W., Zhang, Y., and Shi, D. (2020b). Small Rodent Models of Atherosclerosis. *Biomed. Pharmacother.* 129, 110426. doi:10.1016/j.biopha.2020.110426

Zheng, B., Yang, L., Wen, C., Huang, X., Xu, C., Lee, K. H., et al. (2016). Curcumin Analog L3 Alleviates Diabetic Atherosclerosis by Multiple Effects. *Eur. J. Pharmacol.* 775, 22–34. doi:10.1016/j.ejphar.2016.02.016

Zhixin, D., Gu, X., and Li, J. (2019). Clinical Study on Modified Buyang Huanwu Tang Combined with Routine Western Medicine Therapy for Angina Pectoris. *Xin Zhong Yi* 51 (06), 93–97. doi:10.13457/j.cnki.jncm.2019.06.028

Zhong, D-y., Li, H-y., Lan, L., Ma, R-m., Jiang, C-t., Ding-xiang, L., et al. (2020). Effect of Tongqiao Huoxue Decoction Combined with Western Medicine on Ischemic Stroke: A Systematic Review. *Evidence-Based Complement. Altern. Med.* 2020, 8877998. doi:10.1155/2020/8877998

Zhou, P., Lu, S., Luo, Y., Wang, S., Yang, K., Zhai, Y., et al. (2017). Attenuation of TNF-α-Induced Inflammatory Injury in Endothelial Cells by Ginsenoside Rb1 via Inhibiting NF-Kb, JNK and P38 Signaling Pathways. *Front. Pharmacol.* 8, 464. doi:10.3389/fphar.2017.00464

Zhou, X., Yang, J., Zhou, M., Zhang, Y., Liu, Y., Hou, P., et al. (2019). Resveratrol Attenuates Endothelial Oxidative Injury by Inducing Autophagy via the Activation of Transcription Factor EB. *Nutr. Metab. (Lond)* 16, 42. doi:10.1186/s12986-019-0371-6

Zhu, H., Chen, Z., Ma, Z., Tan, H., Xiao, C., Tang, X., et al. (2017a). Tanshinone IIA Protects Endothelial Cells from H_2O_2-Induced Injuries via PXR Activation. *Biomol. Ther. (Seoul)* 25 (6), 599–608. doi:10.4062/biomolther.2016.179

Zhu, L., Liu, Y., Liu, Y., Xu, H., Wang, S., Liu, Y., et al. (2019a). Anti-inflammatory and Antioxidative Effects of Dan-Lou Tablets in the Treatment of Coronary Heart Disease Revealed by Metabolomics Integrated with Molecular Mechanism Studies. *J. ethnopharmacology* 240, 111911. doi:10.1016/j.jep.2019.111911

Zhu, X., Yue, H., Guo, X., Yang, J., Liu, J., Liu, J., et al. (2017b). The Preconditioning of Berberine Suppresses Hydrogen Peroxide-Induced Premature Senescence via Regulation of Sirtuin 1. *Oxid Med. Cel Longev* 2017, 2391820. doi:10.1155/2017/2391820

Zhu, Y., Zhang, Y., Huang, X., Xie, Y., Qu, Y., Long, H., et al. (2019b). Z-ligustilide Protects Vascular Endothelial Cells from Oxidative Stress and Rescues High Fat Diet-Induced Atherosclerosis by Activating Multiple NRF2 Downstream Genes. *Atherosclerosis* 284, 110–120. doi:10.1016/j.atherosclerosis.2019.02.010

Zhu, Y., Zhang, Y. J., Liu, W. W., Shi, A. W., and Gu, N. (2016). Salidroside Suppresses HUVECs Cell Injury Induced by Oxidative Stress through Activating the Nrf2 Signaling Pathway. *Molecules* 21 (8). doi:10.3390/molecules21081033

Zhu, Z., Li, J., and Zhang, X. (2019c). Salidroside Protects against Ox-LDL-Induced Endothelial Injury by Enhancing Autophagy Mediated by SIRT1-FoxO1 Pathway. *BMC Complement. Altern. Med.* 19 (1), 111. doi:10.1186/s12906-019-2526-4

Zingg, J. M., Hasan, S. T., and Meydani, M. (2013). Molecular Mechanisms of Hypolipidemic Effects of Curcumin. *Biofactors* 39 (1), 101–21. doi:10.1002/biof.1072

Conflict of Interest: The authors declare that the research was conducted in the absence of any commercial or financial relationships that could be construed as a potential conflict of interest.

frontiers in Pharmacology

REVIEW
published: 06 August 2021
doi: 10.3389/fphar.2021.726528

Traditional Uses, Phytochemistry, Pharmacology, and Quality Control of *Dendrobium officinale* Kimura et. Migo

Wenhua Chen, Jiemiao Lu, Jiahao Zhang, Jianjun Wu, Lilong Yu, Luping Qin and Bo Zhu**

School of Pharmaceutical Sciences, Zhejiang Chinese Medical University, Hangzhou, China

Dendrobium officinale, a well-known plant used as a medicinal and food homologous product, has been reported to contain various bioactive components, such as polysaccharides, bibenzyls, phenanthrenes, and flavonoids. It is also widely used as a traditional medicine to strengthen "Yin", nourish heart, tonify five viscera, remove arthralgia, relieve fatigue, thicken stomach, lighten body, and prolong life span. These traditional applications are in consistent with modern pharmacological studies, which have demonstrated that *D. officinale* exhibits various biological functions, such as cardioprotective, anti-tumor, gastrointestinal protective, anti-diabetes, immunomodulatory, anti-aging, and anti-osteoporosis effects. In this review, we summarize the research progress of *D. officinale* from November 2016 to May 2021 and aim to better understand the botany, traditional use, phytochemistry, and pharmacology of *D. officinale*, as well as its quality control and safety. This work presents the development status of *D. officinale*, analyzes gaps in the current research on *D. officinale*, and raises the corresponding solutions to provide references and potential directions for further studies of *D. officinale*.

Keywords: *Dendrobium officinale*, phytochemistry, pharmacology, quality control, traditional use

OPEN ACCESS

Edited by:
Yi Wang,
Zhejiang University, China

Reviewed by:
José Blanco-Salas,
University of Extremadura, Spain
Ambrose Okem,
University of the Witwatersrand, South Africa

****Correspondence:***
Luping Qin
lpqin@zcmu.edu.cn
Bo Zhu
zhubo@zcmu.edu.cn

Specialty section:
This article was submitted to Ethnopharmacology, a section of the journal Frontiers in Pharmacology

Received: *17 June 2021*
Accepted: *26 July 2021*
Published: *06 August 2021*

Citation:
Chen W, Lu J, Zhang J, Wu J, Yu L, Qin L and Zhu B (2021) Traditional Uses, Phytochemistry, Pharmacology, and Quality Control of Dendrobium officinale *Kimura et. Migo. Front. Pharmacol. 12:726528. doi: 10.3389/fphar.2021.726528*

INTRODUCTION

The genus *Dendrobium* (Orchidaceae) includes more than 1,000 species (Teixeira and Ng, 2017). Among them, *Dendrobium officinale* Kimura et. Migo is a precious medicinal plant recorded in Chinese Pharmacopoeia, which is widely used as a traditional Chinese medicine (Editorial Board of China Pharmacopoeia Committee, 2020). Moreover, there is a synonym of "*Dendrobium catenatum* Lindl." in the plant list (http://ipni.org/urn:lsid:ipni.org:names:628140-1). It is well known that *D. officinale* is distributed in several countries around the world, such as the United States, Japan, and Australia. In particular, *D. officinale* exhibits a broader distribution in the different regions of China, including Anhui, Zhejiang, Hunan, Fujian, Guangxi, Sichuan, and Yunnan Provinces (Guo et al., 2020a). Due to the overexploitation and depletion of its wild plant resources, it has been considered as a secondary endangered plant in the "China Plant Red Data Book" (Fu, 1992). On the other hand, the artificial cultivation technology of *D. officinale* has made a significant breakthrough (Cheng Y et al., 2019). However, the existing cultivation resources of *D. officinale* are mixed, which results in the uneven product quality and the unsound evaluation system, greatly affecting the practical and reasonable development and utilization of *D. officinale*.

Pharmacological results published in the literature have revealed multiple promising bioactivities of *D. officinale*, including cardioprotective (Xiao et al., 2018), anti-tumor (Guo et al., 2019), gastrointestinal protective (Liu et al., 2020), anti-diabetes (Zeng et al., 2020),

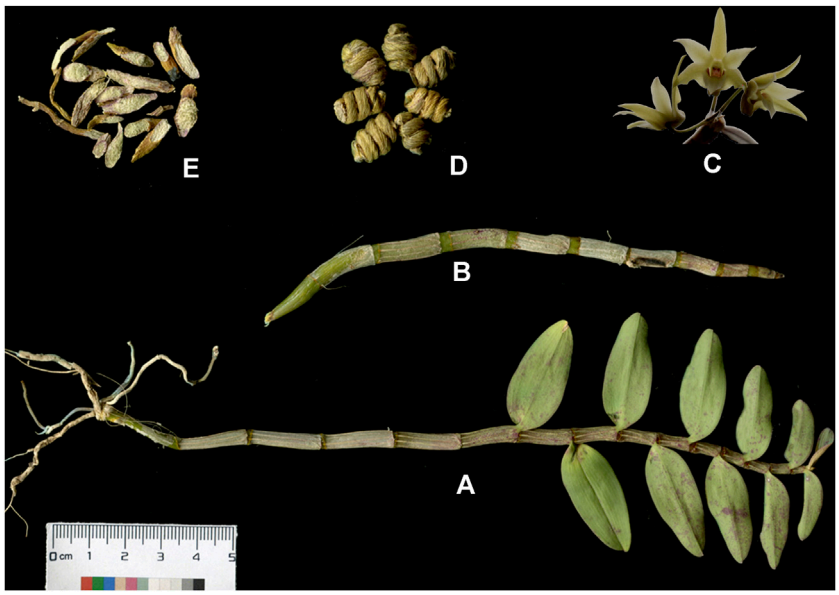

FIGURE 1 | The whole plant **(A)**, fresh strips **(B)**, flowers **(C)**, commercial product named *Tiepifengdou* **(D)**, and decoction pieces **(E)** of *Dendrobium officinale* Kimura et. Migo.

immunomodulatory (Huang et al., 2018), anti-aging (Liang et al., 2017), and anti-osteoporosis (Wang et al., 2018) effects. Besides, it is usually prescribed as one of the ingredients of herbal formula, such as "Tin maple crystal" (Tiepifengdoujing: *D. officinale* and *American ginseng*), for regulating the gastrointestinal tract in traditional and contemporary clinical practice (Qin et al., 2019). According to currently available phytochemical investigations, the bioactive chemical components of *D. officinale* mainly consist of polysaccharides (Zhao et al., 2019), bibenzyls (Zhao et al., 2020), phenanthrenes (Liu et al., 2019), flavonoids (Xing et al., 2018), and alkaloids (Chu et al., 2019). In contrast, according to the literature, only few of these compounds have been evaluated in bioactivity assays (Zhao et al., 2018a; Liu et al., 2018; Xing et al., 2018; Chu et al., 2019; Liu et al., 2019; Lee et al., 2020; Zhao et al., 2020). Additionally, although *D. officinale* is utilized as an effective matter to treat various diseases, its quality control and safety have yet to be defined.

The present review provides an up-to-date and comprehensive literature analysis of *D. officinale* on the basis of botany, traditional applications, phytochemistry, pharmacology, quality control, and safety, which may provide new insights into the development and applications of *D. officinale* as a novel therapeutic agent for the prevention and treatment of diseases.

MATERIALS AND METHODS

All the information available about *D. officinale* was obtained from scientific databases, including Web of Science, PubMed, Google Scholar, Baidu Scholar, Springer, Sci Finder, and ScienceDirect, CNKI, from November 2016 to May 2021, and classic books of Chinese herbal medicines. The keywords included *Dendrobium officinale*, *Dendrobium catenatum*, ethnopharmacology, phytochemistry, biological activity, pharmacology, clinic, traditional uses, safety, quality control, toxicology, and other related words. In this paper, *D. catenatum* was also written as *D. officinale*. However, the other species in *Dendrobium* genera were excluded.

BOTANY

According to the Chinese Pharmacopoeia (Editorial Board of China Pharmacopoeia Committee, 2020), *D. officinale* can be twisted into a spring or spiral shape, which can be further heated and dried to prepare *Tiepifengdou*. *D. officinale* typically has 2–6 whorls with a length of 3–12 cm and a diameter of 0.2–0.4 cm after straightening. The surface color of *D. officinale* is yellow-green or light golden yellow, with fine longitudinal wrinkles, obvious nodes. Moreover, sometimes residual gray-white leaf sheaths can be seen on the nodes. The short fibrous roots remaining at the stem base can be observed at one end (Flora of China Editorial Committee, 2009). *D. officinale* is solid and fragile with a flat section while showing gray-white to gray-green color and slightly horny (**Figure 1**).

"Flora of China" records: *D. officinale* grows upright to a height of 9–35 cm and a thickness of 2–4 mm and is usually cylindrical. The stem is vertical without branches while having many nodes above the middle and 3–5 leaves alternate. The leaves are biseriate, papery, and oblong-lanceolate. The apex is obtuse and slightly hooked. The leaf-sheaths often exhibit purple spots. Its inflorescence racemes usually come from the upper part of old stems, with deciduous leaves and 2–3 flowers. The inflorescence axis is bent back and is 2–4 cm long. Sepals and petals show

TABLE 1 | Summary of traditional medicinal uses of *D. officinale*.

Traditional use	Part used	Ref.
Removing arthralgia, tonifying five viscera, relieving fatigue, strengthening Yin, thickening stomach, lightening body, and prolonging life	Stem	Shennong's Herbal Classic (《神农本草经》) (Dong Han Dynasty, A.D. 25–220)
Raw stone, fine and solid, color of gold, and the shape of grasshopper legs is better	Stem	Variorum of Classic of Herbology (《本草经集注》) (Liang Dynasty, A.D. 502–557)
Nourishing the essence, reinforcing kidney, calming stomach, building muscles, expeling evil heat, relieving foot and knee pain, and removing convulsion	Stem	Records of Famous Doctors (《名医别录》) (Weijin Dynasty, A.D. 220–450)
Replenishing Qi and removing heat	Stem	Theory of Property (《药性论》) (Tang Dynasty, A.D. 618–907)
Nourishing the essence, calming stomach, building muscles, expelling skin evil heat, relieving foot and knee pain	Stem	Herbal Medicines for Kaibao (《开宝本草》) (Song Dynasty, A.D. 960–1,279)
Treating asthenia heat in stomach	Stem	Amplified Herbology (《本草衍义》) (Song Dynasty, A.D. 960–1,127)
Treating fever, spontaneous sweating, ulcer, and pus	Stem	Compendium of Herbology (《本草纲目》) (Ming Dynasty, A.D. 1,552–1,578)
Removing dampness of spleen and stomach	Stem	Herbal classics (《本草经疏》) (Ming Dynasty, A.D. 1,552–1,578)
Treating deficiency of spleen and stomach, and relieve internal heat or fever	Stem	Herbal Medicines for Mengquan (《本草蒙荃》) (Ming Dynasty, A.D. 1,552–1,578)
Invigorating spleen and kidney	Stem	Essential Herbs (《本草备要》) (Qing Dynasty, A.D. 1,636–1912)
Entering the spleen to remove deficiency heat and kidney astringency	Stem	Herbal Medicines for Qiuzhen (《本草求真》) (Qing Dynasty, A.D. 1,636–1912)
Removing stomach deficiency heat and check polydipsia	Stem	Match Medica (《得配本草》) (Qing Dynasty, A.D. 1,636–1912)

yellow-green color and comparable sizes, which are usually end-rounded and have five veins (Flora of China Editorial Committee, 2009). The flowering period is from March to June (Zhao et al., 2018a; Liu et al., 2018).

D. officinale is well-known for its nutritional and medicinal value (Flora of China Editorial Committee, 2009), which often grows in semi-humid mountain rocks over 1,600 m and is widely distributed in Anhui, Zhejiang, Fujian, Guangxi, Sichuan, Yunnan Provinces in China. Moreover, *D. officinale* displays a broad geographical distribution in other countries or regions, including India, Australia, Japan, and United States (Guo et al., 2020a).

TRADITIONAL USES

D. officinale is mainly used as traditional medicine and healthy food in China. *D. officinale* was initially recorded in "Shennong's Herbal Classic" (《神农本草经》, Dong Han Dynasty, A.D. 25–220), which has the ability to strengthen "Yin", tonify five viscera, nourish heart, remove arthralgia, relieve fatigue, thicken stomach, lighten the body, and prolong life span. In "Variorum of Classic of Herbology" (《本草经集注》, Liang Dynasty, A.D. 502–557), the appearance of *D. officinale* was mentioned to be rough, fine, and solid with a golden color. Moreover, the quality is better if the shape is like grasshopper legs. In "Records of Famous Doctors" (《名医别录》, Weijin Dynasty, A.D. 220–450), *D. officinale* was recorded to be non-toxic and could be widely used to nourish the essence, reinforce kidney, calm the stomach, build muscles, expel evil heat, relieve foot and knee pain, and remove convulsion. In "Theory of Property" (《药性论》, Tang Dynasty, A.D. 618–907), it was stated that *D. officinale* could replenish "Qi" and remove heat. Moreover, Herbal Medicines for Kaibao (《开宝本草》, Song Dynasty, A.D. 960–1,279) also had similar description regarding the medical benefits of *D. officinale* as described above. In addition, it was also recorded in "Amplified Herbology" (《本草衍义》, Song Dynasty, A.D. 960–1,127) that *D. officinale* could treat asthenia heat in the stomach. In "Compendium of Herbology" (《本草纲目》, Ming Dynasty, A.D. 1,552–1,578), *D. officinale* was described as a therapeutic approach for fever, spontaneous sweating, ulcer, and pus. According to the record in "Herbal classics" (《本草经疏》, Ming Dynasty, A.D. 1,552–1,578), *D. officinale* shows the function to remove dampness of spleen and stomach. It was reported that *D. officinale* could treat deficiency of spleen and stomach and relieve internal heat or fever in "Herbal Medicines for Mengquan" (《本草蒙荃》, Ming Dynasty, A.D. 1,552–1,578). In "Essential Herbs" (《本草备要》, Qing Dynasty, A.D. 1,636–1,912), it was documented that *D. officinale* could invigorate spleen and kidney. Similarly, in "Herbal Medicines for Qiuzhen" (《本草求真》, Qing Dynasty, A.D. 1,636–1,912), it was registered that *D. officinale* has the ability to enter the spleen to remove deficiency heat and kidney astringency. Additionally, it was recorded that *D. officinale* could mitigate stomach deficiency and heat (inflammation) and check for polydipsia in "Match Medica" (《得配本草》, Qing Dynasty, A.D. 1,636–1,912). The summary of the traditional medicinal uses is shown in **Table 1**.

D. officinale has been reported to have effects on benefiting heart and stomach to produce saliva and nourishing "Yin" to clear heat in China Pharmacopoeia Committee, which is mainly utilized in the treatment of fluid injury, deficiency of "Yin" in the heart and stomach, no regression of inflammation after the disease, hyperactivity of heat due to "Yin" deficiency, dark eyes, muscles, and bone weakness in accordance with China Pharmacopoeia Committee (Committee for the Pharmacopoeia of PR China, 2015). On the other hand, *D. officinale* stems can be used as ordinary food (National Health and Family Planning Commission of the People's Republic of

TABLE 2 | The main compounds isolated from *D. officinale*.

Class	No	Name	Formula	Plant parts	Ref.
Bibenzyls	1	4,4′-Dihydroxy-3,5-dimethoxybibenzyl	$C_{16}H_{18}O_4$	Leaves	Ren et al. (2020a); Ren et al. (2020b)
	2	3,4′-Dihydroxy-5-methoxybibenzyl	$C_{15}H_{16}O_3$	Stems	Liu et al. (2018)
	3	3,4-Dihydroxy-4′,5-dimethoxybibenzyl	$C_{16}H_{18}O_4$	Leaves	Ren et al. (2020a); Ren et al. (2020b)
	4	Gigantol	$C_{16}H_{18}O_4$	Stems, Leaves	He et al. (2020); Ren et al. (2020b)
	5	Moscatilin	$C_{17}H_{20}O_5$	Leaves	Ren et al. (2020a); Ren et al. (2020b)
	6	Tristin	$C_{15}H_{16}O_4$	Stems	He et al. (2020)
	7	Erianin	$C_{18}H_{22}O_5$	Stems	Peng et al. (2020)
	8	3,4,4′-Trihydroxy-5-methoxybibenzyl	$C_{15}H_{16}O_4$	Stems	Chu et al. (2019)
	9	3-Hydroxy-4′,5-dimethoxybibenzy	$C_{16}H_{18}O_3$	Stems	Chu et al. (2019)
	10	Amoenylin	$C_{17}H_{20}O_4$	Stems	Chu et al. (2019)
	11	Dendrophenol	$C_{17}H_{20}O_5$	Stems	Peng et al. (2020)
	12	Dihydroresveratrol	$C_{14}H_{14}O_3$	Stems	Liu et al. (2018)
	13	Dendrocandin B	$C_{27}H30O_8$	Leaves	Ren et al. (2020a); Ren et al. (2020b)
	14	Denofficin	$C_{36}H_{38}O_{10}$	Leaves	Ren et al. (2020b)
	15	Dendrocandin U	$C_{26}H_{28}O_8$	Stems, Leaves	Liu et al. (2018); Ren et al. (2020a); Ren et al. (2020b)
	16	Dendrocandin W	$C_{26}H_{28}O_8$	Stems	Zhu et al. (2020)
	17	Dendrocandin V	$C_{26}H_{28}O_7$	Stems	Zhu et al. (2020)
	18	Trigonopol B	$C_{25}H_{26}O_7$	Stems	Zhu et al. (2020)
	19	3,4, α-Trihydroxy-5,4′-dimethoxybibenzyl	$C_{16}H_{18}O_5$	Laves	Ren et al. (2020a); Ren et al. (2020b)
	20	Dendrocandin N	$C_{25}H_{26}O_7$	Stems	Zhu et al. (2020)
	21	Dendrocandin P1	$C_{26}H_{24}O_8$	Stems	He et al. (2020)
	22	Dendrocandin P2	$C_{26}H_{26}O_8$	Stems	He et al. (2020)
Phenanthrenes	23	Ephemeranthol A	$C_{16}H_{16}O_4$	Stems	Cui et al. (2019); He et al. (2020)
	24	Erianthridin	$C_{16}H_{16}O_4$	Stems	Cui et al. (2019)
	25	Orchinol	$C_{15}H_{14}O_3$	Stems	He et al. (2020)
	26	2,4,7-Trihydroxy-9, 10-dihydrophenanthrene	$C_{14}H_{12}O_3$	Stems	He et al. (2020)
	27	Confusarin	$C_{17}H_{16}O_5$	Stems	Cui et al. (2019); He et al. (2020)
	28	2,7-Dihydroxy-3, 4-dimethoxyphenanthrene	$C_{16}H_{14}O_4$	Stems	Cui et al. (2019)
Penylpropanoids	29	1-O-Caffeoyl-β-D-glucoside	$C_{15}H_{18}O_9$	Flowers	Zhang et al. (2019)
	30	1-O-*p*-Coumaroyl-β-D-glucoside	$C_{15}H_{18}O_8$	Flowers	Zhang et al. (2019)
	31	ethyl *p*-Hydroxyhydrocinnamate	$C_{11}H_{14}O_3$	Leaves	Ren et al. (2020a)
	32	ω-Hydroxypropioguaiacone	$C_{10}H_{12}O_4$	Stems	Zhu et al. (2020)
	33	trans-3,4,5-Trimethoxyl-cinnamyl alcohol	$C_{12}H_{16}O_4$	Stems	Cui et al. (2019)
	34	Dihydroconiferyldihydro-*p*-coumarate	$C_{19}H_{22}O_5$	Stems	Ye et al. (2017)
	35	6-Hydroxy-3-oxo-α-ionol	$C_{13}H_{20}O_3$	Stems	Zhu et al. (2020)
	36	Scoparone	$C_{11}H_{10}O_4$	Stems	Peng et al. (2020)
	37	Syringaresinol	$C_{22}H_{26}O_8$	Stems, Leaves	Ye et al. (2017); Ren et al. (2020a)
	38	Magnolenin C	$C_{28}H_{36}O_{14}$	Stems	Cui et al. (2019)
	39	Officinalioside	$C_{28}H_{34}O_{14}$	Stems	Cui et al. (2019)
	40	Moellenoside A	$C_{26}H_{32}O_{11}$	Stems	Cui et al. (2019)
	41	Pinoresinol-4-O-β-D-glucopyranoside	$C_{28}H_{36}O_{14}$	Stems	Cui et al. (2019)
	42	5, 5′-Dimethoxy-lariciresinol	$C_{23}H_{30}O_8$	Stems	He et al. (2020)
	43	Lyoniresinol	$C_{22}H_{28}O_8$	Stems	He et al. (2020)
	44	(+)-Syringaresinol-4′-O-β-D-glucopyranoside	$C_{28}H_{36}O_{13}$	Stems	Chen et al. (2018)
Flavonoids	45	Apigenin	$C_{15}H_{10}O_5$	Roots, Stems, Leaves	Yu et al. (2018); Ren et al. (2020c)
	46	Naringenin	$C_{15}H_{12}O_5$	Stems	Ye et al. (2017); Peng et al. (2020)
	47	Naringin	$C_{27}H_{32}O_{14}$	Stems	Zhou et al. (2018)
	48	2-Hydroxynaringenin	$C_{15}H_{12}O_6$	Roots, Stems, Laves	Ren et al. (2020c)
	49	Phloretin	$C_{15}H_{14}O_5$	Roots, Stems	Ren et al. (2020c)
	50	Eriodictyol	$C_{15}H_{12}O_6$	Stems	Lv et al. (2017)
	51	Chrysoeriol	$C_{16}H_{12}O_6$	Stems	Lv et al. (2017)
	52	Quercetin	$C_{15}H_{10}O_7$	Stems	Lv et al. (2017)
	53	Taxifolin	$C_{15}H_{12}O_7$	Stems	Lv et al. (2017)
	54	Isorhamnetin	$C_{16}H_{12}O_7$	Stems	Lv et al. (2017)
	55	Rutin	$C_{27}H_{30}O_{16}$	Stems, Leaves, Flowers	Ye et al. (2017); Zhou et al. (2018); Ren et al. (2020a); Zhang et al. (2019)
	56	Cosmosiin	$C_{21}H_{20}O_{10}$	Flowers	Ren et al. (2020c)
	57	Genistin 7-O-gentiobioside	$C_{27}H_{30}O_{15}$	Stems	Yu et al. (2018)
	58	Pelargonidin 3,5-O-diglucoside	$C_{27}H_{31}O_{15}$	Stems	Yu et al. (2018)
	59	Pelargonidin 3-O-rutinoside	$C_{27}H_{31}O_{14}$	Stems	Yu et al. (2018)
	60	Malvidin 3-O-glucosid	$C_{23}H_{25}O_{12}$	Stems	Yu et al. (2018)
	61	Vicenin I	$C_{26}H_{28}O_{14}$	Roots, Stems, Leaves, Flowers	Ye et al. (2017); Ren et al. (2020c); Zhang et al. (2017b)

(Continued on following page)

TABLE 2 | (*Continued*) The main compounds isolated from *D. officinale*.

Class	No	Name	Formula	Plant parts	Ref.
	62	Vicenin II	$C_{27}H_{30}O_{15}$	Roots, Stems, Leaves, Flowers	Lv et al. (2017); Zhang et al. (2017b); Luo et al. (2019)
	63	Vicenin III	$C_{26}H_{28}O_{14}$	Stems	Lei et al. (2018)
	64	Violanthin	$C_{27}H_{30}O_{14}$	Stems	(Ye et al. 2017; Lei et al. 2018; Zhou et al. 2018)
	65	Isoschaftoside	$C_{26}H_{28}O_{14}$	Stems, Flowers	Ye et al. (2017); Zhou et al. (2018); Zhang et al. (2019)
	66	Schaftoside	$C_{26}H_{28}O_{14}$	Stems, Flowers	Ye et al. (2017); Zhou et al. (2018); Zhang et al. (2019)
	67	Vitexin-2″-O-β-D-glucopyranoside	$C_{26}H_{27}O_{14}$	Stems	Ye et al. (2017)
	68	Isovitexin apigenin-6-C-glucoside	$C_{21}H_{20}O_{10}$	Stems	Ren et al. (2020c)
	69	Apigenin-6-C-β-D-xyloside-8-C-β-D-arabinoside	$C_{25}H_{26}O_{13}$	Stems	Ye et al. (2017)
	70	Apigenin-6,8-di-C-α-L-arabinoside	$C_{25}H_{26}O_{13}$	Stems, Flowers	Ye et al. (2017); Zhang et al. (2019)
	71	Isoviolanthin	$C_{27}H_{30}O_{14}$	Stems, Leaves	Ye et al. (2017); Zhang et al. (2019)
	72	Apigenin-6-C-α-L-arabinoside-8-C-β-D-xyloside	$C_{25}H_{26}O_{13}$	Stems	Ye et al. (2017)
	73	Apigenin-6-C-(2″-O-β-Dglucopyranoside)-α-L-arabinoside	$C_{26}H_{27}O_{13}$	Stems	Ye et al. (2017)
	74	Neoschaftoside	$C_{26}H_{28}O_{14}$	Flowers	Zhang et al. (2019)
	75	Vitexin-2″-O-glucoside	$C_{27}H_{30}O_{15}$	Flowers	Zhang et al. (2019)
	76	Apigenin-6,8-di-C-β-D-glucoside	$C_{27}H_{30}O_{15}$	Flowers	Zhou et al. (2018); Zhang et al. (2019)
	77	Apigenin-8-C-β-D-glucosyl-(1→4)-O-β-D-glucoside	$C_{27}H_{30}O_{15}$	Flowers	Zhang et al. (2019)
	78	Apigenin-6-C-β-D-xyloside-8-C-α-L-arabinoside	$C_{25}H_{26}O_{13}$	Flowers	Zhang et al. (2019)
	79	Apigenin-6-C-α-L-arabinoside-8-C-β-D-xyloside	$C_{25}H_{26}O_{13}$	Flowers	Zhang et al. (2019)
	80	Apigenin-6-C-α-L-rhamnoside-8-C-β-D-xyloside	$C_{26}H_{28}O_{13}$	Flowers	Zhang et al. (2019)
	81	Apigenin-6-C-arabinosyl-2″-O-β-D-glucoside	$C_{26}H_{28}O_{14}$	Flowers	Zhang et al. (2019)
	82	Apigenin-8-C-glucosyl-(1→2)-α-L-arabinoside	$C_{26}H_{28}O_{14}$	Flowers	Zhang et al. (2019)
	83	Apigenin 6-C-glucosyl-(1→2)-α-L- arabinoside	$C_{26}H_{28}O_{14}$	Leaves	Zhang et al. (2017b)
	84	Apigenin-6-C-β-D-xyloside-8-C-β-D-glucoside	$C_{26}H_{28}O_{15}$	Leaves	Zhou et al. (2018)
	85	Apigenin-6-C-β-D-glucoside-8-C-β-D-xyloside	$C_{26}H_{28}O_{15}$	Leaves	Zhou et al. (2018)
	86	Isoquercitrin	$C_{21}H_{20}O_{12}$	Flowers	Zhang et al. (2019)
	87	Kaempferol-3-O-α-L-rutinoside	$C_{27}H_{30}O_{15}$	Flowers	Zhang et al. (2019)
	88	Kaempferol-3-O-β-D-glucoside	$C_{21}H_{20}O_{11}$	Flowers	Zhang et al. (2019)
	89	Isorhamnetin-3-O-β-D-glucoside	$C_{22}H_{22}O_{12}$	Flowers	Zhang et al. (2019)
	90	Tamarixin	$C_{22}H_{22}O_{12}$	Flowers	Zhang et al. (2019)
	91	Nothofagin Glc	$C_{21}H_{24}O_{10}$	Flowers	Ren et al. (2020c)
	92	3′,5′-Di-C-glucosylphloretin	$C_{27}H_{34}O_{15}$	Stems	Ren et al. (2020c)
	93	Cyanidin 3-O-rutinoside	$C_{27}H_{31}O_{15}$	Stems	Ren et al. (2020d)
	94	Cyanidin 3-O-glucoside	$C_{21}H_{21}O_{11}$	Stems	Yu et al. (2018)
	95	Cyanidin 3-O-galactoside	$C_{21}H_{21}O_{11}$	Stems	Yu et al. (2018)
	96	Cyanidin 3-[6-(sinapoyl) glucoside]-5-glucoside	$C_{38}H_{41}O_{20}$	Stems	Ren et al. (2020d)
	97	Cyanidin 3-[2-(glucosyl)-6-(sinapoyl) glucoside]-5-glucoside	$C_{44}H_{51}O_{25}$	Stems	Ren et al. (2020d)
	98	Cyanidin 3-[6-sinapoyl-2-O-(2-(sinapoyl) glucosyl)-glucoside]	$C_{49}H_{51}O_{24}$	Stems	Ren et al. (2020d)
	99	Cyanidin 3-[6-sinapoyl-2-O-(2-(sinapoyl) glucosyl)-glucoside]-5-glucoside	$C_{55}H_{61}O_{29}$	Stems	Ren et al. (2020d)
	100	Cyanidin 3-[6-(sinapoyl)glucoside]	$C_{32}H_{31}O_{15}$	Stems	Ren et al. (2020d)
	101	Delphinidin 3-glucoside-7, 3′-di-[6-(sinapoyl) glucoside]	$C_{55}H_{61}O_{30}$	Stems	Ren et al. (2020d)
	102	Delphinidin 3,5-O-diglucoside	$C_{27}H_{31}O_{17}$	Stems	Yu et al. (2018)
	103	Peonidin 3,5-O-diglucoside	$C_{28}H_{33}O_{16}$	Stems	Yu et al. (2018)
Alkaloids	104	Anosmine	$C_{11}H_{17}N_2$	Stems	Chen et al. (2018)
	105	2-Benzothiazolol	C_7H_5NOS	Leaves	Ren et al. (2020a)
	106	3,5-Dimethoxyphenethylamines	$C_{10}H_{15}NO_2$	Stems	Zhu et al. (2020)
	107	N-*p*-coumaroyltyramine	$C_{17}H_{17}NO_3$	Stems	Chu et al. (2019)
	108	N-*trans*-*p*-feruloyltyramine	$C_{18}H_{19}NO_4$	Stems	Chu et al. (2019)
Acids	109	Malic acid	$C_4H_6O_5$	Stems	Chen et al. (2018)
	110	Ferulic acid	$C_{10}H_{10}O_4$	Stems	Ye et al. (2017)
	111	Vanillic acid	$C_8H_8O_4$	Stems	Ye et al. (2017)
	112	Syringic acid	$C_9H_{10}O_5$	Stems	Ye et al. (2017)
	113	Protocatechuic acid	$C_7H_6O_4$	Leaves	Ren et al. (2020a)
	114	*p*-Hydroxycinnamic acid	$C_9H_8O_3$	Stems	Ye et al. (2017)
	115	*p*-Hydroxylbenzoic acid	$C_7H_6O_3$	Leaves	Ren et al. (2020a)
	116	Palmitic acid	$C_{16}H_{32}O_2$	Leaves	Ren et al. (2020a)

(Continued on following page)

TABLE 2 | (*Continued*) The main compounds isolated from *D. officinale*.

Class	No	Name	Formula	Plant parts	Ref.
Others	117	Flifimdioside A	$C_{32}H_{52}O_{13}$	Stems	Chen et al. (2018)
	118	Flickinflimoside B	$C_{31}H_{50}O_{13}$	Stems	Chen et al. (2018)
	119	Loliolide	$C_{11}H_{16}O_3$	Leaves	Ren et al. (2020a)
	120	1-Glycerol linolenate	$C_{21}H_{36}O_4$	Leaves	Ren et al. (2020a)
	121	Densiflorol A	$C_{16}H_{16}O_4$	Leaves	Ren et al. (2020a); Ren et al. (2020b)
	122	2-Butoxyethyl linolenate	$C_{24}H_{42}O_3$	Leaves	Ren et al. (2020a)
	123	Catechol	$C_6H_6O_2$	Leaves	Ren et al. (2020a)
	124	Octadecadienoic acid-2,3-dihydroxypropyl ester	$C_{21}H_{40}O_4$	Leaves	Ren et al. (2020a)
	125	Stigmast-5-en-3β-ol-7-one	$C_{29}H_{48}O_2$	Stems	Zhu et al. (2020)
	126	Dendrofindlaphenol B	$C_{27}H_{30}O_6$	Stems	Liu et al. (2018)

China, 2013). In traditional Chinese therapies, *D. officinale* is often combined with other Chinese herbal medicines, including *Adenophora stricta*, *Ophiopogon japonicus*, *Paeonia lactiflo*ra, *Astragalus membranaceus* and *Polygonatum odoratum*. In recent years, pharmacological research mainly focused on the cardioprotective (Xiao et al., 2018), anti-tumor (Guo et al., 2019), gastrointestinal protective (Liu et al., 2020), and anti-diabetes (Zeng et al., 2020) effects of *D. officinale*. Therefore, it is encouraged to combine the traditional pharmacological actions of *D. officinale* and advanced research technologies in order to explore the potential mechanisms and establish the foundation for its clinical applications in the future.

PHYTOCHEMISTRY

Extensive phytochemistry studies have demonstrated that *D. officinale* mainly contains polysaccharides, bibenzyls (**1–22**), phenanthrenes (**23–28**), phenylpropanoids (**29–44**), flavonoids (**45–103**), alkaloids (**104–108**), acids (**109–116**), and others (**117–126**). Among them, polysaccharides, bibenzyls, and flavonoids are considered the main bioactive compounds responsible for various pharmacological properties and therapeutic efficacy of *D. officinale*. All compounds identified in *D. officinale* are summarized and shown in **Table 2**, and the corresponding structures are shown in **Figures 2–8**.

Polysaccharides

Polysaccharides are the main medicinal components of *D. officinale*, with a wide range of medicinal properties. A large number of polysaccharides have been isolated from *D. officinale*, including DWDOP1, DWDOP2, DWDOP3, FWDOP1, FWDOP2, FWDOP3 (Yu et al., 2018), DOP-50, DOP-60, DOP-70 (Xing et al., 2018), DO (Ma et al., 2018), DOPA-1 (Wei et al., 2018), DOP1-DES, DOP2-DES (Liang J et al., 2018), LDOP-1 (Yang et al., 2020), UDP-1, FLP-1, and FDP-1 (Liang K. L et al., 2018), which are identified by various analytical technologies, such as high performance liquid chromatography (HPLC), high performance gel permeation chromatography (HPAEC), gas chromatography-mass spectrometry (GC-MS), and gel permeation chromatography (GPC). The molecular weights of *D. officinale* polysaccharides range from 30 to 1,415 kDa (Liang J et al., 2018; Ma et al., 2018; Wei et al., 2018; Yu et al., 2018). It has been demonstrated that *D. officinale* polysaccharides are composed of glucose, mannose, galactose, xylose, arabinose, ribose and rhamnose (Tian et al., 2019). Among them, glucomannan is considered to be the main component of *D. officinale* polysaccharides with 1,4-β-D-Man*p* and 1,4-β-D-Glc*p*, comprising acetyl groups in varying degrees and positions with or without branches (Liang et al., 2019). It should be mentioned that a lot of factors may impact the biological activity of polysaccharides, including molecular structure, main chain composition, molecular branching degree, the configuration of the main chain, and chemical modification (Yue et al., 2017; Huang et al., 2020). Importantly, according to the literature, polysaccharides have exhibited various therapeutic potentials, including cardioprotective (Zhang et al., 2017a; Su et al., 2021), anti-tumor (Wei et al., 2018; Zhao et al., 2019), gastrointestinal protective (Ke et al., 2020; Zhang et al., 2020), immunomodulatory (Huang et al., 2018), anti-aging (Liang et al., 2017; Wei et al., 2017), and pulmonary protective effects (Chen et al., 2020).

Bibenzyls

Bibenzyl components in *D. officinale* have attracted a lot of attention due to their promising anti-tumor properties (He et al., 2020). To date, 19 bibenzyls have been isolated, which were identified predominantly from the stems and leaves of *D. officinale*. The typical parent nucleus structure of bibenzyls presented in the stems of *D. officinale* is two benzene rings, which can be replaced by different substituents. Some bibenzyls (**4**, **5**, and **7**) were found to have significant anti-tumor activity (Tian et al., 2019; Zhao et al., 2020), which attracted further research and development. The chemical structures of these bibenzyls are shown in **Figure 2**.

Phenanthrenes

The phenanthrenes are abundantly found in the stems of *D. officinale*, including ephemeranthol A (**23**), erianthridin (**24**), orchinol (**25**), 2, 4, 7-trihydroxy-9, 10-dihydrophenanthrene (**26**), confusarin (**27**), and 2,7-dihydroxy-3,4-dimethoxyphenanthrene (**28**). Notably, orchinol (**25**) possesses anti-tumor activity, which can potentially be used to develop new anti-tumor drugs (Zhao et al., 2018a). The chemical structures of these phenanthrenes are shown in **Figure 3**.

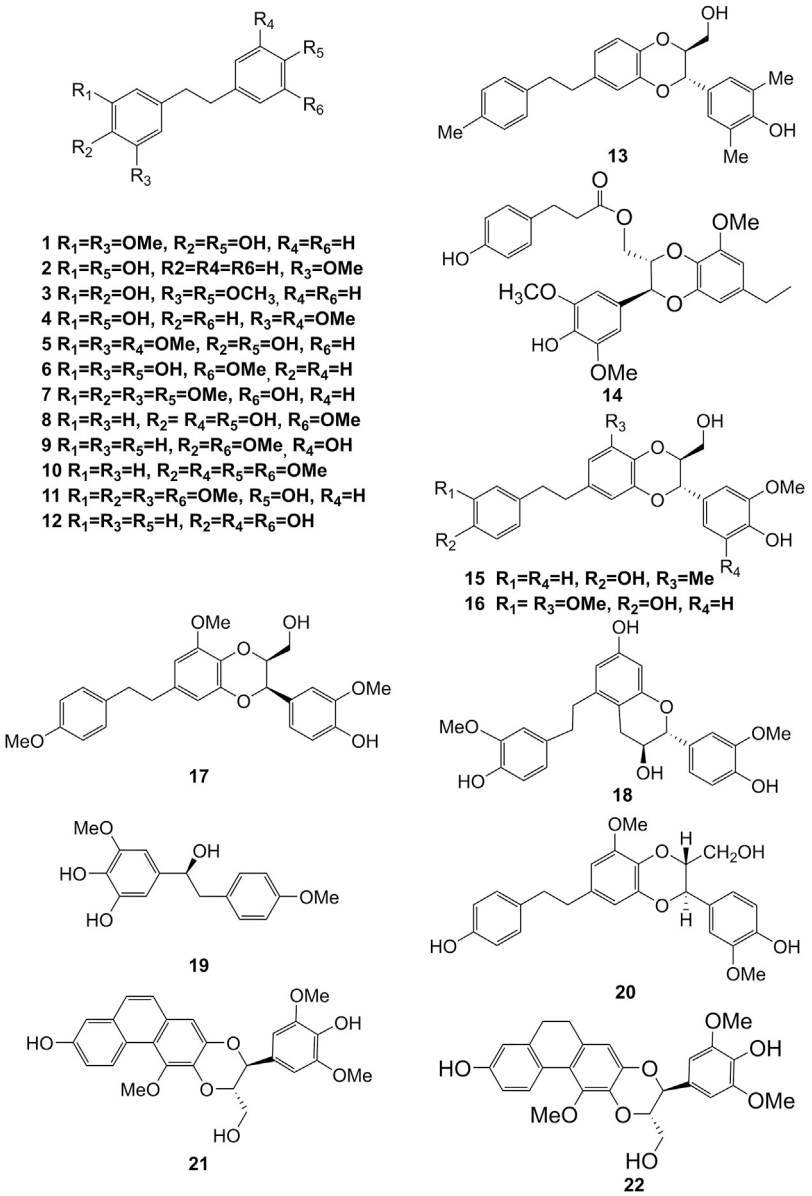

FIGURE 2 | Structures of bibenzyls (**1–22**) isolated from *D. officinale*.

Phenylpropanoids

Phenylpropanoid compounds refer to natural organic compounds with one or more C_6-C_3 units in the basic parent nucleus, mainly including simple phenylpropanoids, coumarins, and lignans. To date, 16 phenylpropanoids (**29–44**) have been identified in *D. officinale*, including simple phenylpropanoids (**29–35**), coumarin (**36**), and lignans (**37–44**). The chemical structures of these phenylpropanoids are presented in **Figure 4**.

Flavonoids

It has been reported that flavonoids belong to a large group of secondary metabolites in *D. officinale*, which possess anti-tumor activity (Xing et al., 2018). Most flavonoids isolated and identified from the roots, stems, leaves, and flowers of *D. officinale* are *C*-glycosides, while the rest of flavonoids are *O*-glycosides. It is well known that the foundational skeletons of flavonoids are apigenin, vitexin, quercetin, and kaempferol. Nowadays, mass spectrometry technologies coupled with liquid chromatography, such (HPLC-ESI-MS) (Ye et al., 2017), ultra-high-performance liquid chromatography (UPLC-ESI-MS/MS) (Zhou et al., 2018), and UPLC-quadrupole time of flight mass spectrometry (UPLC-QTOF-MS) (Yu et al., 2018), have been widely implemented for the identification and quantification of these flavonoid compounds. Interestingly, it is generally believed that glucoside derivatives (anthocyanins) delphinidin 3,5-*O*-diglucoside and cyanidin 3-*O*-glucoside are responsible for

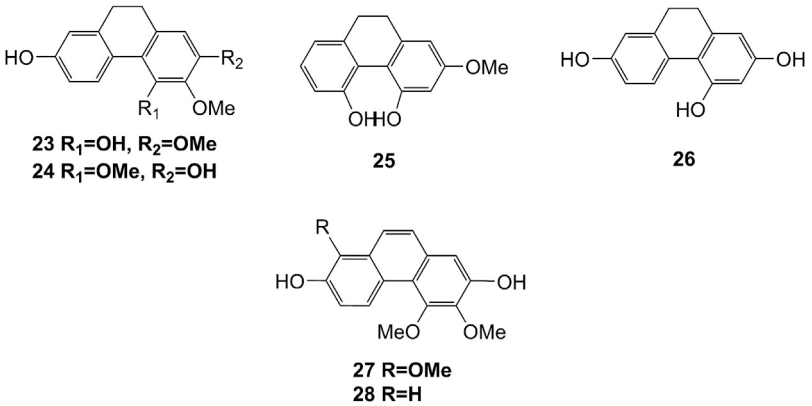

FIGURE 3 | Structures of phenanthrenes (**23–28**) isolated from *D. officinale*.

the red color stems of *D. officinale* (Yu et al., 2018). In addition, the transcriptome and component metabolism analyses have become the typical approaches to investigate flavonoid biosynthesis mechanisms in *D. officinale* (Lei et al., 2018). The chemical structures of these flavonoids are shown in **Figures 5**–**7**.

Alkaloids

Alkaloids are a class of nitrogenous organic compounds possessing various biological activities. They are also active constituents of *Dendrobium* plants. It is worth noting that the regulation of genes related to alkaloid biosynthetic pathways through comparative transcriptomic analysis has gradually become a research interest (Jiao et al., 2018). The chemical structures of these alkaloids are shown in **Figure 8**.

Organic Acids

Organic acids are a kind of acid organic compounds containing a carboxyl group. Eight types of organic acids have been identified in *D. officinale*. The chemical structures of these organic acids are displayed in **Figure 9**.

Other Compounds

Some other types of compounds have also been isolated from the stems and leaves of *D. officinale*, including flifimdioside A (**117**), flickinflimoside B (**118**) (Chen et al., 2018), loliolide (**119**), 1-glycerol linolenate (**120**), densiflorol A (**121**), 2-butoxyethyl linolenate (**122**), catechol (**123**) (Ren et al., 2020a), octadecadienoic acid-2,3-dihydroxypropyl ester (**124**) stigmast-5-en-3β-ol-7-one (**125**) (Zhu et al., 2020), and dendrofindlaphenol B (**126**) (Liu et al., 2018). The chemical structures of these compounds are shown in **Figure 10**.

PHARMACOLOGY

D. officinale has been found to possess multiple biological functions, including cardioprotective (Zhang et al., 2017a; Su et al., 2021), anti-tumor (Guo et al., 2019), gastrointestinal protective (Liu et al., 2020), anti-diabetes (Zeng et al., 2020), immunomodulatory (Huang et al., 2018), anti-aging (Liang et al., 2017), and anti-osteoporosis (Wang et al., 2018) effects. Among them, modern pharmacological studies of *D. officinale* majorly focus on its cardioprotective, anti-tumor, gastrointestinal protective, and hypoglycemic effects. The biological activities of *D. officinale* and corresponding mechanisms are shown in **Figure 11**.

Cardioprotective Activity

Cardiovascular diseases are the major causes of mortality globally, and the main cause of more than 10 million people death. Among cardiovascular diseases risk factors, cardiomyopathy and high blood pressure are the most common ones. Oral administration of *D. officinale* fine powders at the doses of 0.09, 0.18, and a very high dose of 1.1 g/kg for 30 days protected isoproterenol (ISO)-induced cardiac hypertrophy, indicated by the decreased myocardial collagen synthesis, increased myocardial fibrosis and ventricular remodeling, and significantly reduced levels of atrial natriuretic peptide (ANP), brain natriuretic peptide (BNP), and cardiac troponin I (cTN-I) in plasma relative to the model group (ISO = 5 mg/kg) (Xiao et al., 2018). In addition, it was well known that diabetic cardiomyopathy was a typical cardiovascular complication mediated *via* hyperglycemia. One study indicated that *D. officinale* water-soluble extracts prevented diabetic cardiomyopathy and might be a candidate for therapeutic use (Zhang et al., 2016). *D. officinale* water extracts (75, 150, and 300 mg/kg) intragastrically once daily for 2 weeks could protect left anterior descending coronary artery (LAD)-induced myocardial ischemia through decreasing creatine kinase (CK)-MB, lactate dehydrogenase (LDH), malondialdehyde (MDA), and increasing superoxide dismutase (SOD) and Meis 1 levels (Dou et al., 2016). Treatment with *D. officinale* stems polysaccharide DOP-GY at the doses of 6.25, 12.5, and 25 μg/ml exhibited protective effects on hydrogen peroxide (H_2O_2)-induced H9c2 cardiomyocyte apoptosis *via* phosphatidylinositol/protein kinase B (PI3K)/Akt and mitogen-activited protein kinase (MAPK) signaling pathways, as demonstrated by the decreased levels of LDH, lipid peroxidation damage (LPD), reactive oxygen species (ROS), and pro-apoptosis protein (Zhang et al., 2017a).

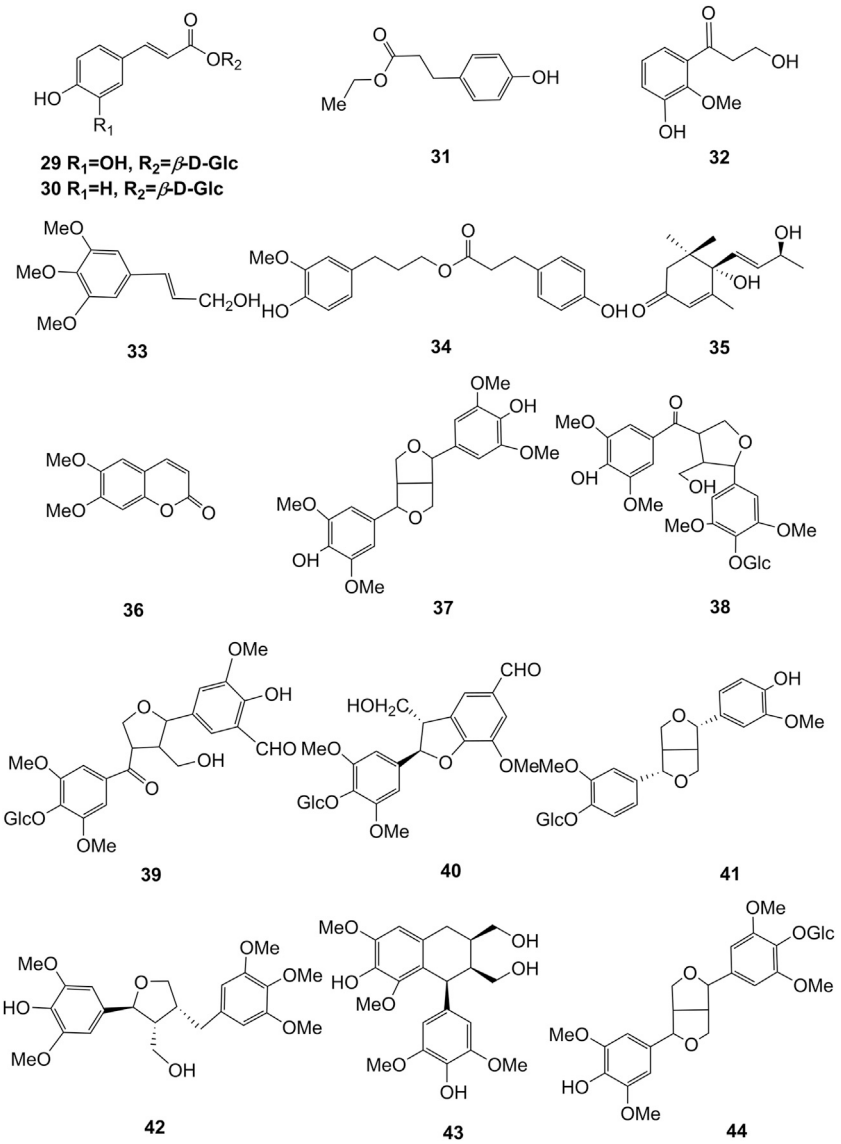

FIGURE 4 | Structures of phenylpropanoids (**29–44**) isolated from *D. officinale*.

Another study demonstrated that *D. officinale* polysaccharides could decrease malondialdehyde levels, increase SOD activities, and inhibit the generation of intracellular ROS in H9c2 cardiomyocytes (Zhao et al., 2017). Besides, Yue et al. (2017) obtained a novel homogeneous heteroxylan from alkali-extracted *D. officinale* crude polysaccharide (S32), which possessed significant anti-angiogenic effects (S32, 13.51 μM) on human microvascular endothelial cells (HMEC-1) by inhibiting their migration and disruption of tube formation in a dose-dependent manner, compared with a vehicle group (Yue et al., 2017). However, some of these experimental doses were too high and there was a lack of positive controls.

It has been suggested that *D. officinale* has cardioprotective activity by treating hypertension. It was reported that blood pressure was significantly reduced after treating with *D. officinale* (10 g/d) (Wu et al., 2018b). The treatment of *D. officinale* ultrafine powder (DOFP) at very high doses of 200 and 400 mg/kg for 20 weeks exhibited anti-hypertensive activity on overeating greasy-induced metabolic hypertension in rats by inhibiting the activation of lipopolysaccharide/toll-like receptor 4 (LPS/TLR4) signal pathway, as demonstrated by the decreased levels of total cholesterol (TC), triglyceride (TG), low-density lipoprotein cholesterol (LDL-c), LPS, C-reactive protein (CRP), interleukin 6 (IL-6), TLR4, myeloid differentiation factor (MyD88), IL-1β, and tumor necrosis factor alpha (TNF-α) and the increased levels of high-density lipoprotein cholesterol (HDL-c) and nitric oxide (NO) relative to valsartan (8 mg/kg)-treated positive control (Su et al., 2021). Moreover, Yan et al. (2019a) reported that the effective component of alcohol extract of *D. officinale* in the treatment

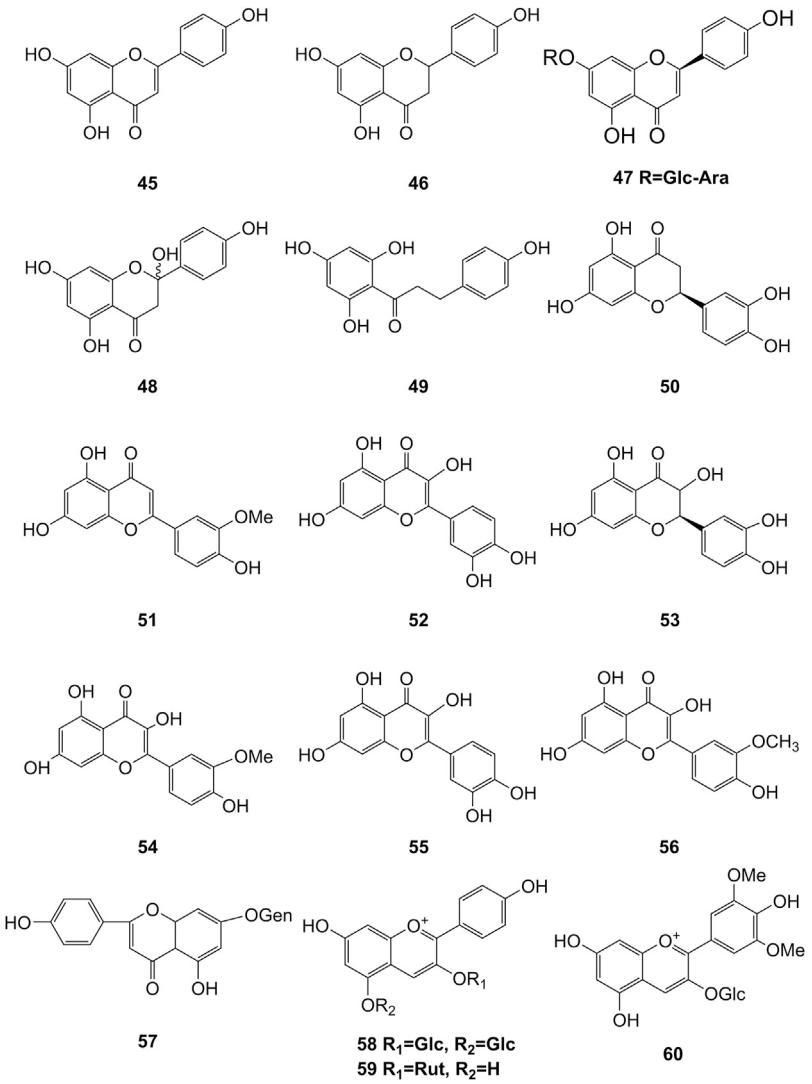

FIGURE 5 | Structures of flavonoids (**45–60**) isolated from *D. officinale*.

of metabolic hypertension was apigenin flavonoid glycosides (Yan et al., 2019a). In contrast, more investigations are still needed to reveal the underlying mechanism of the anti-hypertensive effect of apigenin flavonoid glycosides. The results showed that treatment with *D. officinale* flowers at a very high dose of 3.1 g/kg for 6 weeks could significantly improve vascular diastolic function by reducing systolic blood pressure and mean arterial pressure in high glucose and fat compound alcohol-induced hypertensive rats, inhibiting the thickening of thoracic aorta and the loss of endothelial cells, reducing plasma content of endothelin 1 (ET-1) and thromboxane B2 (TXB2), and increasing the content of prostacycline (PGI2) and NO, compared with model control group and valsartan (5.7 mg/kg) positive control group (Liang K. L et al., 2018). Treating with *D. officinale* ultrafine powder DOFP could improve the intestinal flora and increase the production, transportation, and utilization of short-chain fatty acid (SCFA), activate the intestinal-vascular axis SCFA-GPCR43/41 pathway, increase vascular endothelial function, and finally decrease the blood pressure in alcohol, and high sugar and fat diets (ACHSFD)-induced metabolic hypertension model rats (Li et al., 2021). These results suggested that *D. officinale* may have a potential clinical application in the treatment of hypertension. In this study, however, the optimal dose, constituents, and side effects of *D. officinale* are not assessed. Moreover, further detailed clinical trials should be employed to assess the value of *D. officinale* as a drug for the treatment of hypertension. In addition, this evidence is still tenuous; no double-blind trials involving *D. officinale* have been performed, and more evidence from randomized controlled trials is required to elucidate other mechanisms that may be responsible for anti-hypertension effects.

Although *D. officinale* possesses a potential therapeutic effect on cardiovascular diseases, especially cardiomyopathy and hypertension (**Figure 12**), more in-depth investigations on its

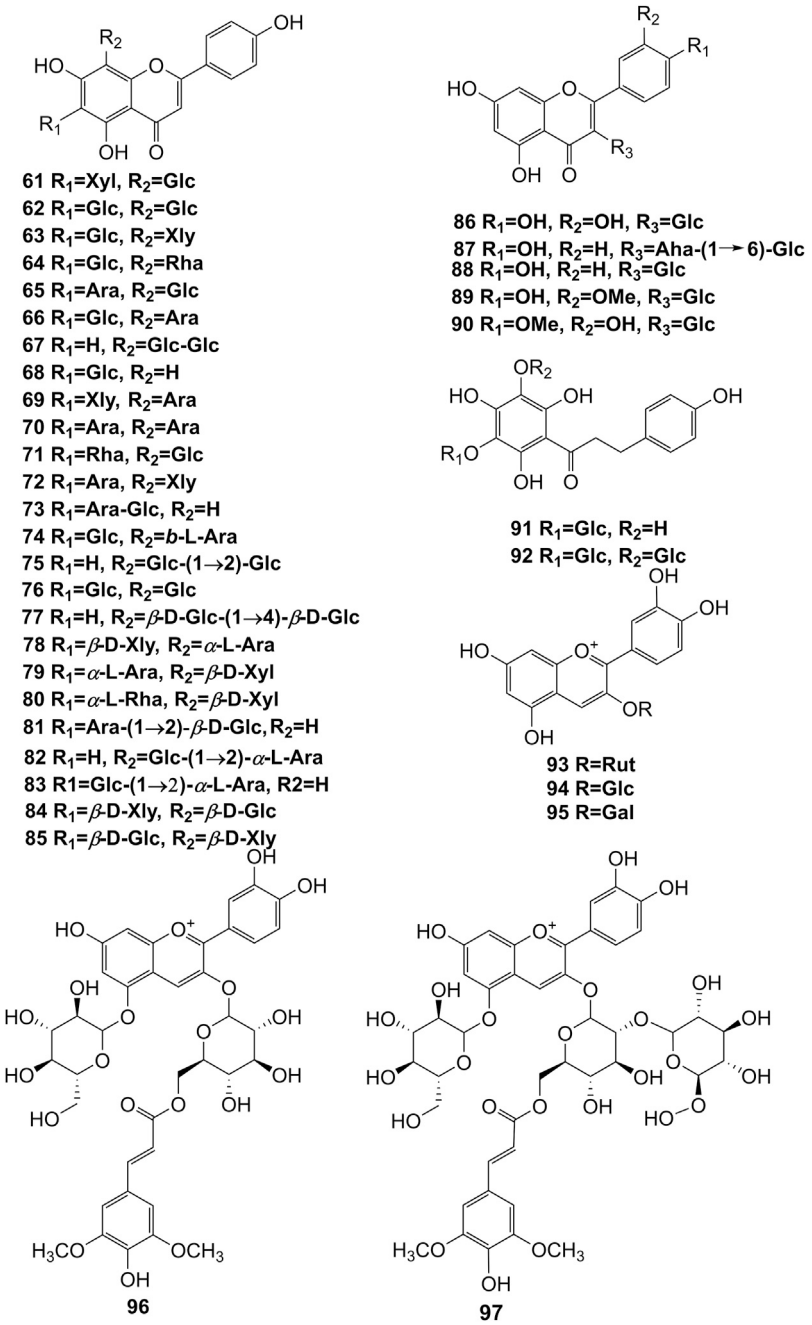

FIGURE 6 | Structures of flavonoids (**61–97**) isolated from *D. officinale*.

effective monomer compounds, molecular mechanism, and clinical trials are warranted to identify effective cardioprotective agents with minimized side effects.

Anti-Tumor Activity

As a type of traditional medicine and ordinary food, *D. officinale* has benefits on human health supported by its effectiveness in the prevention and treatment of cancer diseases (Guo et al., 2019). Several studies have reported all crude extracts, polysaccharides, and other pure compounds isolated from *D. officinale* exhibited anti-tumor activities (Wei et al., 2018; Guo et al., 2019; Zhao et al., 2020).

Administration of *D. officinale* methanol extracts at a dose of 0.25, 0.5, and 1 mg/ml could inhibit the growth of SMMC-7721, BEL-7404 cells, and primary liver cancer cells, and promote their apoptosis *via* activating mitochondria apoptosis pathway and suppressing the Wnt/β-catenin pathway (Guo et al., 2019). Similarly, another study demonstrated that *D. officinale*

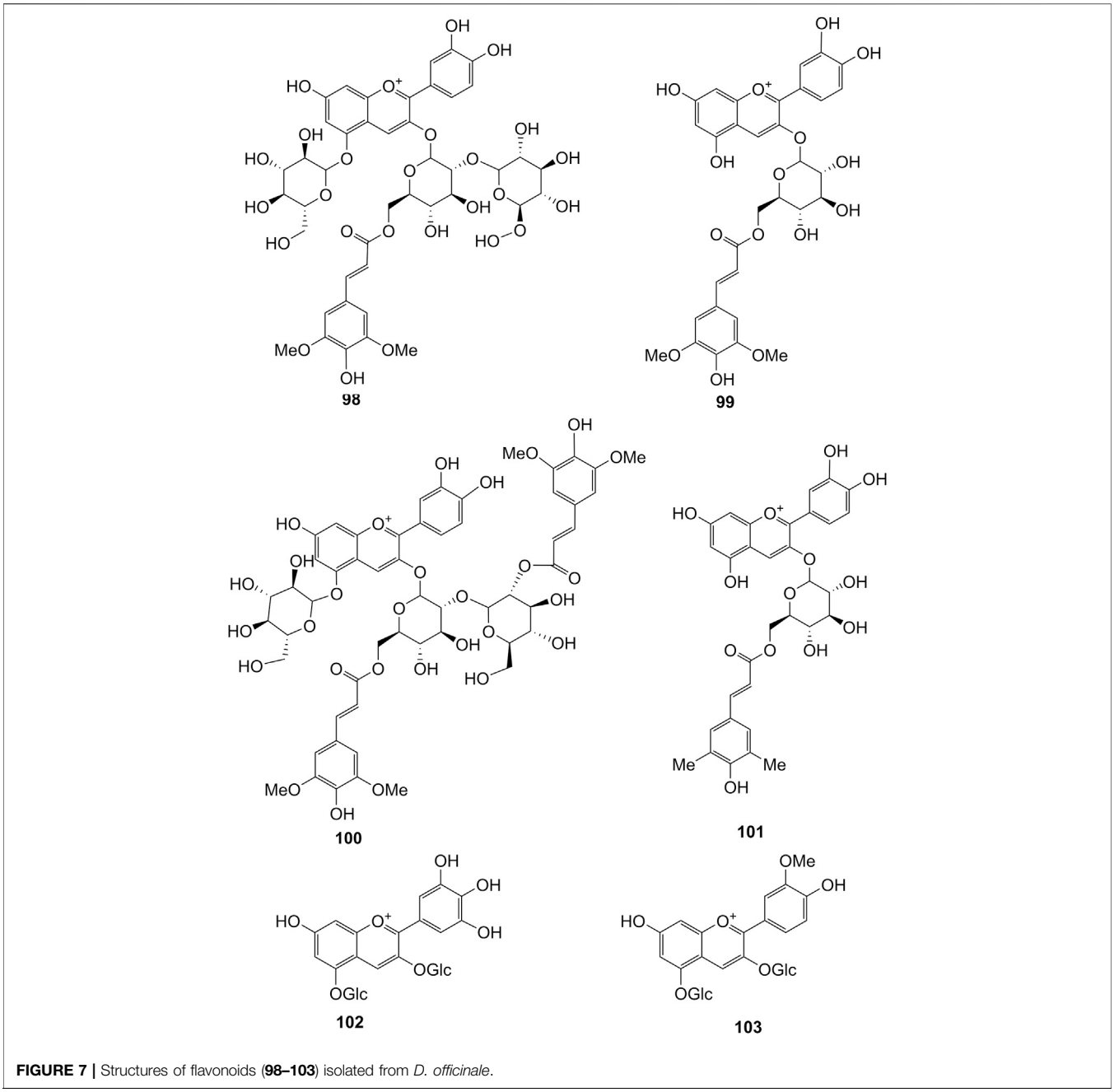

FIGURE 7 | Structures of flavonoids (**98–103**) isolated from *D. officinale*.

polysaccharide (DOPA-1) induced HepG-2 cell apoptosis by influencing mitochondrial function, ROS production, and apoptosis-related protein expression (Wei et al., 2018). Importantly, a rat study also confirmed the anti-tumor effects of *D. officinale in vivo*. The 2-weeks administration of *D. officinale* polysaccharide DOP at very doses of 2.4, 4.8, and 9.6 g/kg suppressed 1-methyl-2-nitro-1-nitrosoguanidine-(MNNG)-induced (150 μg/ml) precancerous lesions of gastric cancer in rats *via* modulating Wnt/β-catenin pathway and altering endogenous serum metabolites (Zhao et al., 2019). In addition to crude extracts and polysaccharides, it is more evident that gigantol (**4**), moscatilin (**5**), erianin (**7**), orchinol (**25**), and isoviolanthin (**71**) isolated from *D. officinale* are also responsible for the anticancer activity of *D. officinale* (Xing et al., 2018; Liu et al., 2019; Lee et al., 2020; Zhao et al., 2020). Gigantol (**4**) was found to repress invasiveness and growth of SW780, 5,637, and T24 human bladder cancer cells by inhibiting the Wnt/epithelial-mesenchymal transition (EMT) signaling (Guo et al., 2019). Likewise, moscatilin (**5**) was demonstrated to induce apoptosis in FaDu human head and neck squamous carcinoma cells (HNSCC) *via* c-Jun N-terminal kinase (JNK) signaling pathway (Lee et al., 2020). The anti-tumor function of erianin (**7**) was investigated by two independent studies. The results suggest that erianin (**7**) induced cell apoptosis through the

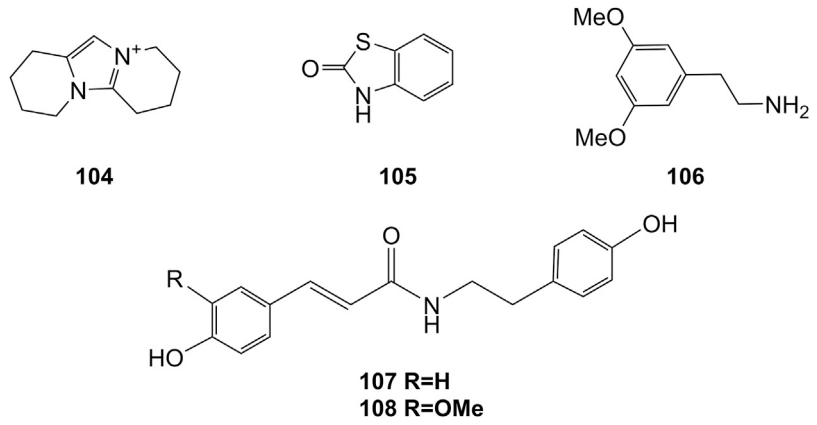

FIGURE 8 | Structures of alkaloids (**104–108**) isolated from *D. officinale*.

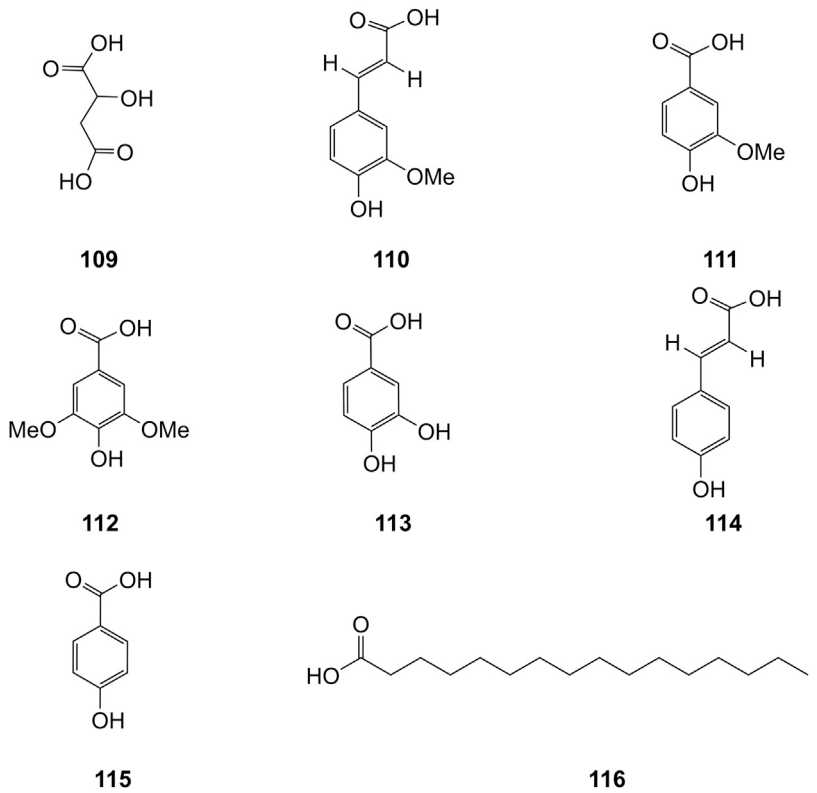

FIGURE 9 | Structures of acids (**109–116**) isolated from *D. officinale*.

ERK pathway in nasopharyngeal carcinoma (NPC) (Liu et al., 2019) while suppressing the growth of bladder cancer cells EJ and T24 through JNK pathways with the IC_{50} values of 65.04 and 45.9 nM, respectively (Zhu et al., 2019). Moreover, it was demonstrated that orchinol (**25**) exhibited strong cytotoxic activity in HI-60 and THP-1 cells with the IC_{50} values of 11.96 and 8.92 μM, respectively (Lee et al., 2020). Additionally, isoviolanthin (**71**) was revealed to suppress transforming growth factor (TGF)-β1-induced EMT through the regulation of TGF-β/Smad and PI3K/Akt/mTOR signaling pathways in HepG2 and Bel-7402 hepatocellular carcinoma (HCC) cells (Xing et al., 2018). However, the dose of *D. officinale* polysaccharide DOP was too high in the treatment of gastric cancer, attention should be paid to the possible side-effects in clinical applications.

Overall, the anti-tumor mechanisms of *D. officinale* are mainly attributed to promoting tumor cell apoptosis, inhibiting tumor

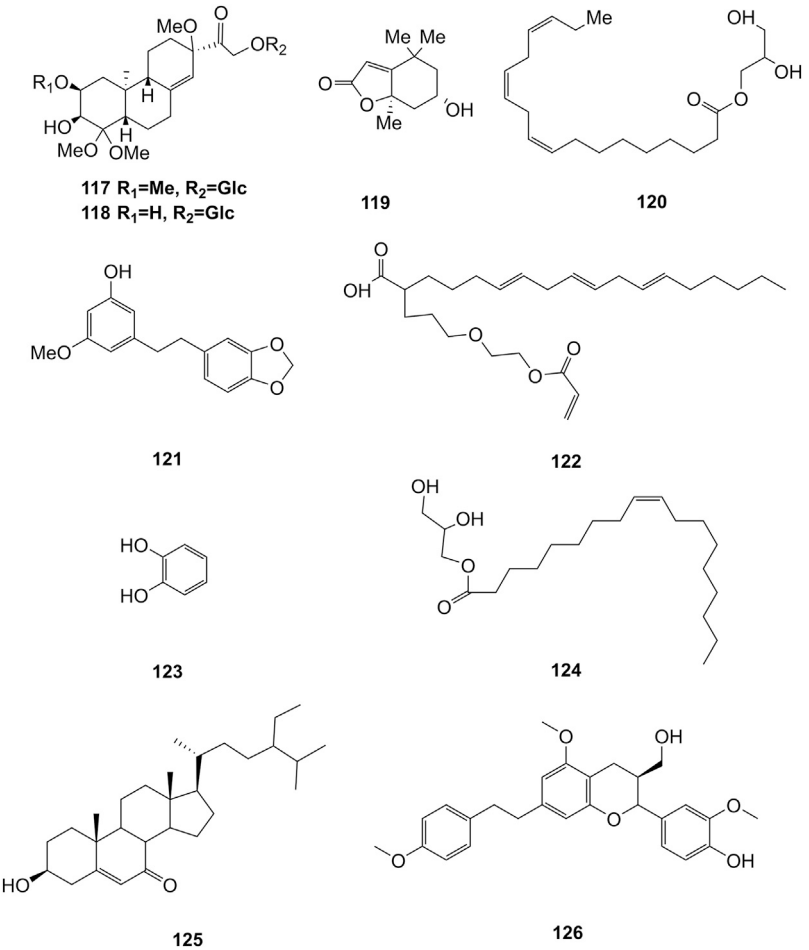

FIGURE 10 | Structures of other compounds (**117–126**) isolated from *D. officinale*.

cell proliferation, repressing tumor cell migration and invasion, and improving body immunity (**Figure 13**). The studies described above suggest that the compounds identified in *D. officinale* demonstrate significant inhibitory effects on different types of tumor cells, such as SMMC-7721, BEL-7404, HepG-2, SW780, and HCC cell lines. Further investigations may explore the structural modification and the structure-activity relationship (SAR) studies for these bioactive compounds of *D. officinale*, thereby facilitating the further discovery and development of new anti-tumor candidates, along with the characterization of the key regulatory genes, metabolic pathways, and heterologous biosynthesis pathways of active ingredients from *D. officinale*. The currently published studies on the anti-tumor effects of the compounds from *D. officinale* are mainly focused on *in vitro* and *in vivo* experiments, while clinical studies have yet to be conducted and the exact molecular mechanisms remain elusive.

Gastrointestinal Protective Effect

D. officinale is traditionally used to nourish "Yin" and thicken stomach. *D. officinale* extracts have thus been frequently applied to treat gastrointestinal diseases as a traditional Chinese medicine. It was reported that polyphenols from fermentation liquid of *D. officinale* improved intestinal health *via* the regulation of intestinal microbiota and their metabolites, thereby relieving oxazolone-induced intestinal inflammation in Zebrafish (Gong et al., 2020). Moreover, *D. officinale* is often used in combination with other traditional Chinese medicines to achieve its better therapeutic effects. It was found that the mixture of *D. officinale* and American ginseng at a dose of (0.32 × the dog's weight × 6 g)/12 kg) could function as a prebiotic agent to enhance SCFA-producing genera and reverse gut dysbiosis (Liu et al., 2020). Likewise, the combination of *D. officinale* and other Chinese herbal medicine, such as *Acanthopanax senticosus*, *Panaxnotoginseng*, *Didymocarpus hancei* and *Valeriana officinalis* can also alleviate gastric mucosal injury (Guo, 2020b).

The 14-days treatment of *D. officinale* glucomannans at 0.16 g/kg produced more SCFAs (mainly acetate and butyrate) in cecum and colon (Shi et al., 2020). It should be noted that polysaccharides LDOP-1 isolated from *D. officinale* could protect ethanol-induced gastric mucosal injury *in vitro* (250, 125, and 62.5 mg/ml for 2 h) and *in vivo* (100 and a very high dose of 400 mg/kg for 30 days) by regulating AMP-activated protein

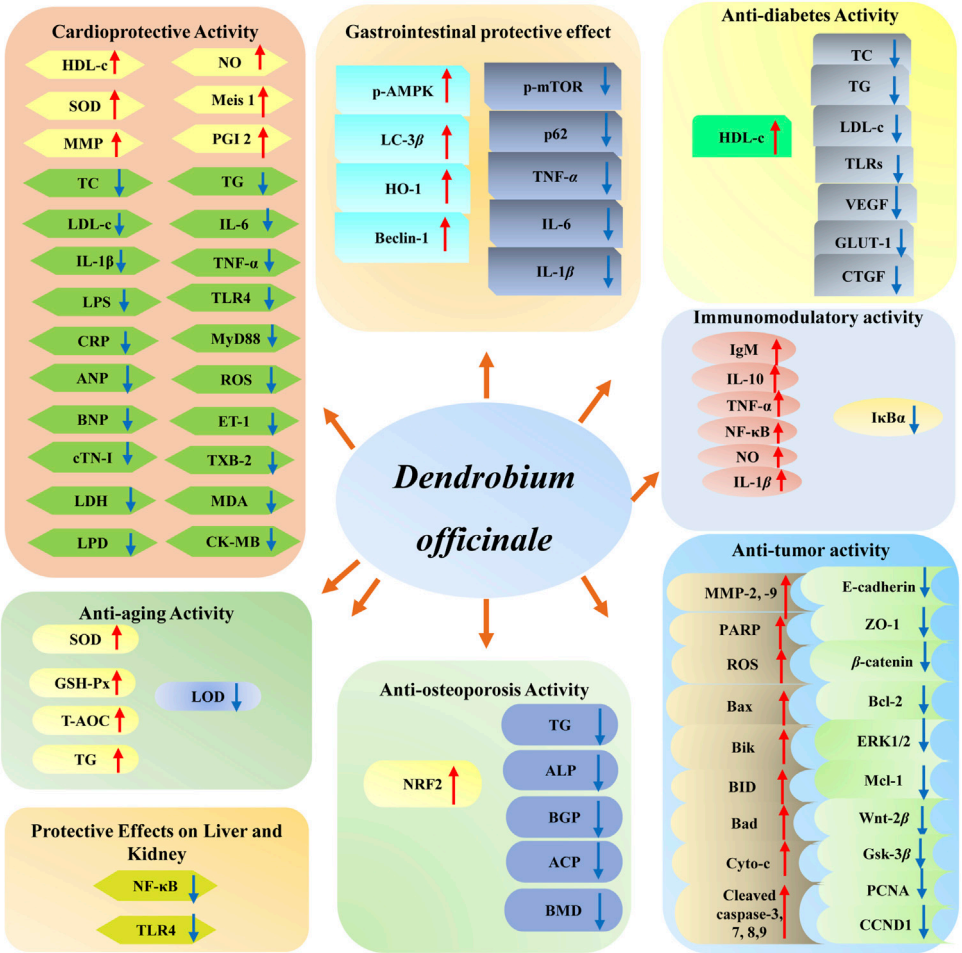

FIGURE 11 | The bioactivities of main compounds isolated from *D. officinale* and their underlying mechanisms.

kinase (AMPK)/mTOR signaling pathway demonstrated by the increased levels of p-AMPK, light chain 3β (LC-3β), heme oxygenase-1 (HO-1) and Beclin-1, the decreased levels of p-mTOR and p62, and the reversed levels of caspase3, Bax, and Bcl-2 detected both *in vitro* and *in vivo* (Ke et al., 2020). Furthermore, it was suggested that *D. officinale* polysaccharide (200 mg/kg/d) exhibited protective effects against DSS-induced colitis by inhibiting pro-inflammatory cytokines TNF-α, IL-6, and IL-1β in the colonic mucosa, modulating the abundance of gut microbiota, and promoting the production and utilization of SCFAs in the colon (Zhang et al., 2020). However, positive control or dose-dependent effect analysis was not performed, which might require further validation. In addition, the structure of the correlation between polysaccharide administration and health outcomes, as well as the functional role of the polysaccharides themselves has not been examined in depth.

Anti-Diabetes Activity

Diabetes is a common disease with glucose metabolism disorder, which seriously affects human health around the world (Ye et al., 2017). Numerous ethnomedicinal studies supported the traditional use of *D. officinale* for clearing heat, nourishing "Yin", benefiting the stomach, and promoting body fluid, thereby leading *D. officinale* to become an essential medicine to treat "Xiao Ke" disease (Diabetes) for thousands of years (Yan et al., 2019b).

Over the past few years, the hypoglycemic effect of *D. officinale* has become an attractive research field. One study has confirmed that the administration of water extracts from the stems of *D. officinale* at the doses of 75, 150, and a very high dose of 300 mg/kg for 12 weeks decreased serum insulin, TC, TG, LDL-c, and increase HDL-c in high-fat diet/streptozotocin (HFD/STZ) (30 mg/kg)-induced diabetic mice in a dose-dependent manner (Zeng et al., 2020). The possible mechanism of *D. officinale* water extracts can be associated with improving lipid transport and suppressing insulin resistance and fibrosis *via* EMT. Another study similarly found that a 4-weeks treatment with *D. officinale* water extracts at very high doses of 350 and 700 mg/kg elevated the liver glycogen synthesis, energy, and amino acid metabolism as well as taurine-mediated defense against oxidative stress in STZ-induced diabetic mice (Zheng et al., 2017). It was found that the

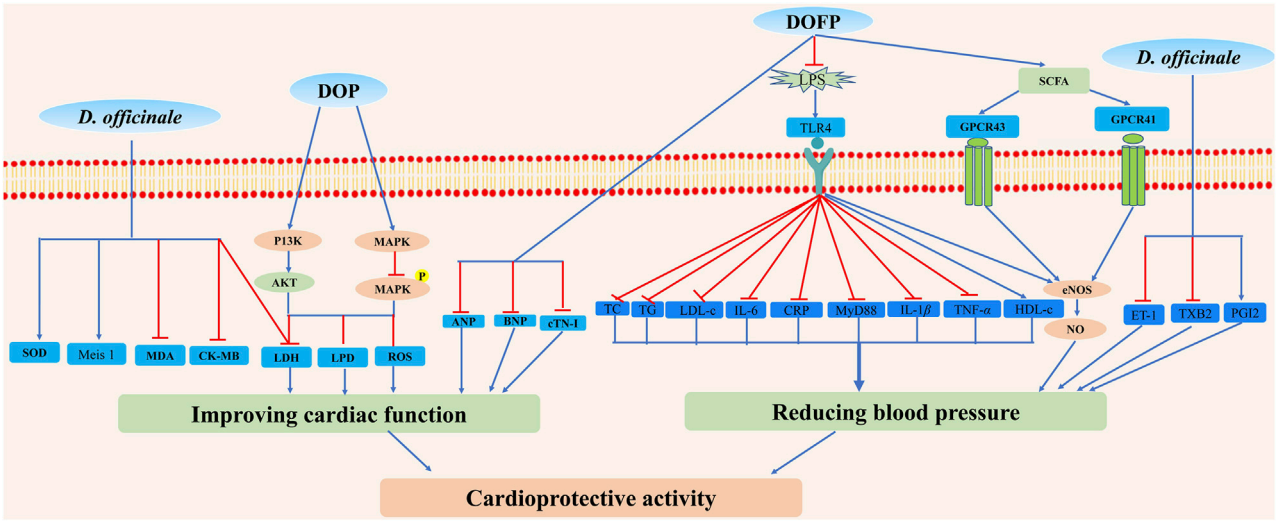

FIGURE 12 | Possible mechanisms for cardioprotective activity properties of *D. officinale*. *D. officinale* exhibited cardioprotective activity by improving cardiac function *via* inhibiting oxidative stress, inflammation, and by reducing blood pressure *via* inhibiting the activation of LPS/TLR4 signal pathway, decreasing ET-1 and TXB2 levels, and increasing SCFA and PGI2 levels.

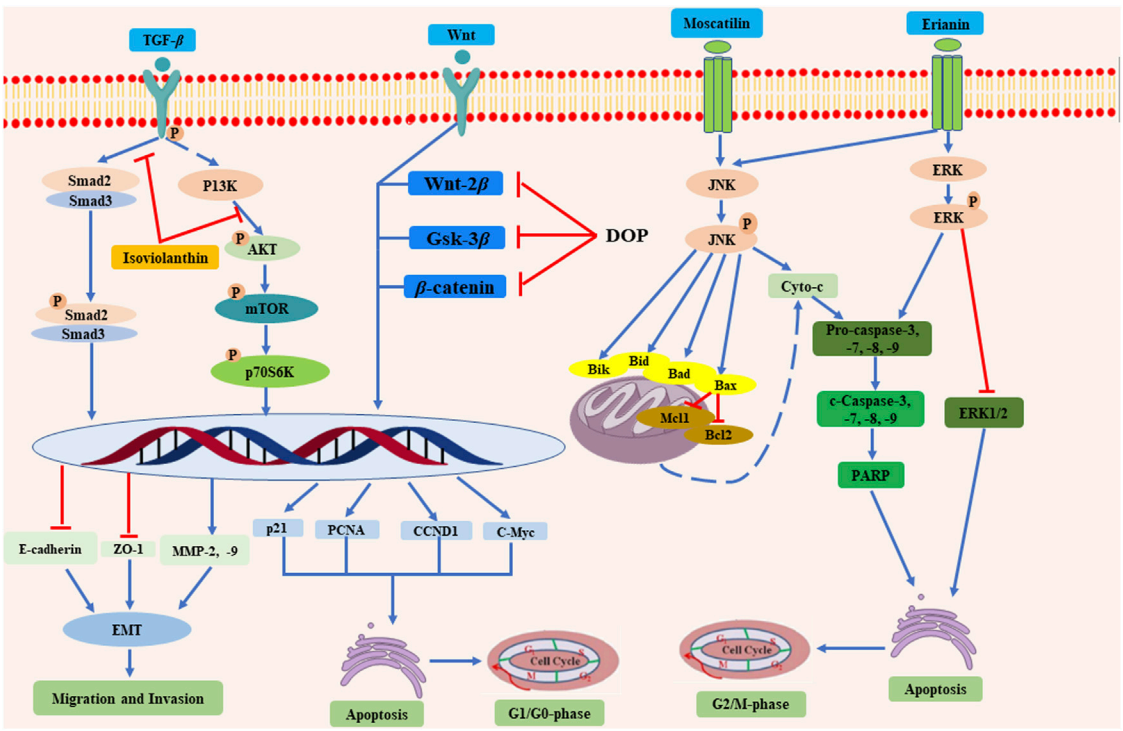

FIGURE 13 | The anti-tumor mechanisms of the compounds from *D. officinale*. *D. officinale* exhibited anti-tumor activity by promoting the tumor cells apoptosis *via* inhibiting the G1/G0 and G2/M phases, and inhibiting the migration and invasion of tumor cells.

treatment of *D. officinale* stem's water extracts at very high doses of 10 and 20 g/kg for 4 weeks ameliorated insulin resistance by decreasing toll-like receptors (TLRs) and inflammatory response in STZ-induced diabetic rats in comparison with the treatment of dimethyl biguanide (DMBG, 0.0042 g/kg) as a positive control (Zhao and Han 2018b). Moreover, it was reported that the administration of *D. officinale* at the doses of 0.2, 0.4, and 0.8 g/kg for 8 weeks protected against diabetic kidney lesions

in STZ-induced (60 mg/kg) rats *via* suppressing vascular endothelial growth factor (VEGF), glucose transporter 1 (GLUT-1), and connective tissue growth factor (CTGF) relative to the irbesartan (17.5 mg/kg)-treated positive control (Chang et al., 2019). Additionally, a previous study also revealed that the hypoglycemic effect of the 3-months combined treatment of *D. officinale* (10 g/d) and metformin (0.5 g/d) was superior to the single-use (Wu et al., 2017). However, these studies have important limitations—only one or two doses of *D. officinale* are used in these studies. In addition, the evaluation of *D. officinale* doses that are much higher, and it has no translational value from a therapeutic viewpoint.

It is evident that the hypoglycemic effect of *D. officinale* is closely related to the inhibition of α-glucosidase and α-amylase (Zhu et al., 2020). Notably, 3,4′-dihydroxy-5-methoxybibenzyl (**2**) and dihydroresveratrol (**12**) isolated from *D. officinale* extracts have been reported to exhibit hypoglycemic activity in an α-glucosidase inhibitory assay with IC_{50} values of 36.05 ± 0.67 and 159.59 ± 0.86 μM, respectively, relative to the acarbose as a positive control (IC_{50} = 152.86 ± 1.43 μM) (Liu et al., 2018). Likewise, 3,4-dihydroxy-4′,5-dimethoxybibenzyl (**3**), 3,4,4′-trihydroxy-5-methoxybibenzyl (**8**), dendrocandin U (**15**), *N-p*-coumaroyltyramine (**107**), and *N-trans-p*-feruloyltyramine (**108**) have been identified as α-glucosidase inhibitors with IC_{50} values of 199.5 μM, 9.46 *m*M, 403.4, 0.4 and 234.1 μM, respectively, compared with acarbose (IC_{50} = 763.5 μM). Furthermore, the inhibitory effect of 3,4-dihydroxy-4′,5-dimethoxybibenzyl (**3**) on α-amylase (an IC_{50} value of 5.99 mM) was weaker than acarbose (IC_{50} = 0.12 μM) (Chu et al., 2019). Several studies have demonstrated the definite hypoglycemic effect of *D. officinale*, while further investigations are required to identify the specific bioactive components responsible for this activity and clarify the hypoglycemic mechanism of *D. officinale*.

Immunomodulatory Activity

A large number of experiments have provided evidence for the immunomodulatory activity of *D. officinale*. Polysaccharide is the main active component for immunoregulation. Oral administration of 0.25% *D. officinale* polysaccharide DOW-5B (w/v) for 25 days displayed significant immunomodulatory effects *via* increasing the content of butyrate, immunoglobulin M (IgM), IL-10, and TNF-α *in vivo* (Li et al., 2020a). Another study also demonstrated that *D. officinale* polysaccharide DOP-1-1 stimulated immunity by enhancing the level of nuclear factor kappa-B (NF-κB) while inhibiting the level of IκBα through TLR4 signaling (Huang et al., 2018). Moreover, it was found that *D. officinale* polysaccharides (FDP-1) treatments, ranging from 12.5 to 200 μg/ml, exhibited immunomodulatory activity through increasing cell proliferation and NO and IL-1β production in a dose-dependent manner (Tian et al., 2019). Neither positive control nor dose-effect analysis *in vivo* was assessed in these studies. In addition, there is a general lack of systematic research on the relationship between immune activity and structure of *D. officinale* polysaccharides.

Anti-Aging Activity

The oral administration with a very high dose of 1 g/kg of *D. officinale* juice and a very high dose of 0.32 g/kg of *D. officinale* polysaccharide for 9 weeks exhibited an anti-aging effect in D-galactose-induced (0.125 g/kg) aging mice, supported by the significantly increased contents of SOD, glutathione peroxidase (GSH-Px) and total antioxidant capacity (T-AOC) in serum, as well as the enhanced SOD level in heart, liver, kidney, and cerebrum (Liang et al., 2017). Similar to this study, the treatment with *D. officinale* polysaccharide (DOP) at the doses of 50 and 100 mg/kg for 4 weeks exhibited more potent anti-fatigue activity than *Rhodiola rosea* extract as a positive control in BALB/c mice, as revealed by the increased TG (or fat) mobilization and the decreased lipid oxidation (LOD) and cell variability of T and B lymphocytes in the weight-loaded swimming test (Wei et al., 2017). However, the underlying mechanisms by which *D. officinale*'s anti-aging effects remain unclear. Additionally, the current pharmacological research lacks component analysis and clinical pharmacological experiments.

Anti-Osteoporosis Activity

A previous study revealed that the administration of *D. officinale* water extracts at very high doses of 150, 300, and 600 mg/kg for 13 weeks prevented ovariectomy (OVX)-induced bone loss in Wistar rats by decreasing the levels of TG, alkaline phosphatase (ALP), bone glucose protein (BGP) while increasing acid phosphatase (ACP) and bone mineral density (BMD) in comparison with Xian-Ling-Gu-Bao capsule (240 mg/kg) as a positive control (Wang et al., 2018). Meanwhile, *D. officinale* water extract treatments (10, 40, 80 μg/ml) were found to suppress receptor activator expression of the nuclear factor-κB ligand (RANKL)-induced osteoclastogenesis in RAW264.7 cells (Wang et al., 2018). In addition, *D. officinale* polysaccharide DOP treatments at very high doses of 200 or 400 μg/ml exhibited an anti-osteoporosis effect through the activation of NRF2 signaling, thereby attenuating adipogenic differentiation and promoting osteogenic differentiation in BMSCs (Peng et al., 2019). Notably, no reports about the anti-osteoporosis effect of small molecule compounds from *D. officinale* have been documented so far.

Protective Effects on Liver and Kidney

One study has demonstrated that the treatment with *D. officinale* ethanol extracts at the doses of 4.375 and 17.5 mg/kg for 9 weeks prevented liver and kidney damage in hyperuricemic rats by suppressing the protein levels of NF-κB and TLR4 compared with the model group (0.15% adenine, 10% yeast extract, and 89.85% standard diet) (Lou et al., 2020). Likewise, another study revealed that *D. officinale* flower water extracts (50, 100, 150, and 200 mg/kg) showed protective effects on alcohol-induced (10 ml/kg) liver injury by its anti-steatosis, anti-oxidative, and anti-inflammatory effects (Wu et al., 2020). However, additional evidence from randomized controlled trials is required to identify other regulatory mechanisms that may be responsible for the protective effects on liver and kidney. The bioactive constituents of these extracts also remain unknown.

Other Activities

In addition to the bioactivities described above, *D. officinale* was also found to have other therapeutic effects, such as neuroprotective effect, anti-photoaging effect, and pulmonary protective function. For instance, in hypoxic-ischemic brain damage (HIBD) neonatal rat model (vehicle group, normal saline = 10 ml/kg), the administration of aqueous extracts of *D. officinale* at the doses of 75, 150, and 300 mg/kg for 14 days suppressed the neuronal apoptosis by reducing cleaved caspase-3 and Bax, increasing Bcl-2, enhancing the expression of neurotrophic factors and K + -Cl—cotransporter 2 (KCC2), and decreasing the expression of hypoxia-inducible factor-1α (HIF-1α) and histone deacetylase 1 (HDAC1), leading to neuroprotective effects in neonatal rats against HIBD (Li and Hong, 2020b). *D. officinale* protocorm treatments at the doses of 10, 25, and 50 mg/ml exerted an anti-photoaging effect through decreasing erythema and protected skin from dryness by increasing CAT, SOD, and GSH-Px expression levels and decreasing thiobarbituric acid reactive substances (TBARS) and MMPs levels relative to the model group (UV irradiation) and positive control group (UV irradiation and a formulation of matrixyl) (Mai et al., 2019). In addition, *D. officinale* polysaccharides prevented lung injury by ameliorating cigarette smoke-induced mucus hypersecretion and viscosity by decreasing the expression of mucin-5AC (MUC5AC) mRNA and secretory protein *in vitro* and *in vivo* (Chen et al., 2020).

QUALITY CONTROL

The wild resources of *D. officinale* have gradually decreased, while the supply of artificially cultivated *D. officinale* has increased correspondingly. Consequently, wild resource collection has progressively become a non-mainstream, and the artificial cultivation mode occupies a dominant position in *D. officinale* industry (Ni et al., 2018). According to the description in the Editorial Board of Chinese Pharmacopoeia (2020) edition, the peak area ratio of mannose to glucose, moisture content, total ash content, ethanol extract, and polysaccharide content should reach 2.4–8.0%, less than 12.0%, more than 6.0, 6.5, and 25.0% of *D. officinale* stem, respectively (China Pharmacopoeia Committee, 2020). However, the quality of *D. officinale* may be affected by regions, tissues, harvest time, cultivation techniques, growth years, endophytes, and others which may disturb the long growth cycle (Cheng J et al., 2019). For instance, Li et al. (2017a) found that the contents of polysaccharides in *D. officinale* from Yunnan, Fujian, Jiangsu, and Zhejiang were variable (Li et al., 2017b). Among them, the highest content of polysaccharides was 54.42% in Zhejiang, followed by 43.26% in Fujian (Li et al., 2017a). Previous studies have revealed that the contents of polysaccharides in stems, leaves, and flowers of *D. officinale* are 34.61%, 23.51%, and 13.47%, respectively (Cao et al., 2018). It was also found that the polysaccharide content of *D. officinale* is gradually increased during the entire flower-opening process from buds to full bloom, in which the polysaccharide content is the highest in the full bloom stage (13.75%), followed by the micro bloom stage (11.52%). In contrast, the lowest content appears in the bud stage (9.50%) (Huang et al., 2017). In addition, *D. officinale* is usually planted on trees (fixed to the trunk with fine twine). Therefore, the polysaccharide content of *D. officinale* is significantly affected by different auxiliary tree species. Those planted on the evergreen tree *Phoebe zhennan* as the accessory hosts exhibit the highest polysaccharide content (37.8%) substantially different from those grown on the *Michelia ilsonii*, *Davidia nvolucrate* and *Taxus chinensis* var. *mairei* (Gu and Xie, 2021). Moreover, the polysaccharide content of 5-year-old *D. officinale* stems is the highest, followed by 3-year-old, 4-year-old, 2-year-old, and 1-year-old ones (Qin et al., 2017). Besides, endophytes play an important role in promoting the accumulation of polysaccharides. For example, DO14 (*Pestalotiopsis* sp.) isolated from *D. officinale* treated with 240 mg/L protein-polysaccharide fractions (PPF) can promote the accumulation of polysaccharides. This endophytic fungus could be used as biological fertilizer to improve the yield and quality of *D. officinale* (Zhu et al., 2018). In addition, exploiting suitable artificial-sheltered cultivation mode, screening the best cultivation substrate, and developing aseptic germination technology could be utilized to enhance the quality production of *D. officinale* in current agronomical practices (Cheng Y et al., 2019; Zuo et al., 2020).

It is well known that the polysaccharides' bioactivities vary from different sources, production regions, and cultivation conditions of *D. officinale*. Moreover, it has been reported that the bioactivities of *D. officinale* polysaccharides are related to their chemical characteristics and advanced structures. However, *D. officinale* polysaccharides are macromolecular compounds with large molecular weight and complex structure, thereby generating a great challenge to implement analytical technologies (Ma et al., 2018). Therefore, it is necessary to establish a safe and effective quality assessment method for the quality control and clinical application of *D. officinale*. Herein, the qualitative and quantitative analytic methods of *D. officinale* polysaccharides are summarized and discussed.

There are several rapid and accurate methods for quantitative estimation of natural polysaccharides and their different fractions in *D. officinale* (Wu et al., 2018a). Generally, the large *D. officinale* polysaccharides are acid hydrolyzed into oligosaccharides, and then LC-MS is used to separate and characterize the products efficiently. The previous results indicate that the variations in the mass values of different peaks present structural differences of various metabolized products. Moreover, MS can be used to explore the oligosaccharide hydrolysates of *D. officinale* polysaccharides in detail from the aspects of identity, structure, and properties (Ma et al., 2018). An oligosaccharide-marker approach by labeling them with fluorescence reagent paminobenzoic acid ethyl ester (ABEE) (Te-Man-ABEE and Pen-Man-ABEE) was recently applied for quality assessment of *D. officinale* polysaccharides using UHPLC-QTOF-MS (Wong et al., 2019). The results revealed that the two oligosaccharide markers exhibited a satisfactory linearity relationship with *D. officinale* polysaccharides ($R^2 \geq 0.997$) in the range of 0.68–16.02 μg. These markers also revealed satisfactory precision (relative standard deviation, RSD <7.0%) and recovery (91.41–118.30%) in unknown sample

determination. It is speculated that the oligosaccharide-marker method is a simple, rapid, and reliable approach for the qualitative and quantitative determination of specific polysaccharides from *D. officinale* and other herb formulas (Wong et al., 2019).

Although single-component quality assessment can be used to control the quality of natural Chinese herbal medicine (Wei et al., 2020), the chemical compositions of *D. officinale* are complex. *D. officinale* contains a lot of effective nutritional compositions, including flavonoids, crude fiber, amino acids, proteins, and fat. These active components of *D. officinale* are affected by tissues and harvest times. A previous study found that the contents of flavonoids in the stems, leaves, and flowers of *D. officinale* were 0.052%, 0.251%, and 1.835%, respectively (Li et al., 2019a). Another research reported that the content of total flavonoids in the flowers of *D. officinale* is the highest at the full flowering stage (1.66%) followed by the bract stage (1.52%) and micro flowering stage (1.41%) (Huang et al., 2017). It should be noted that the contents of five representative flavonoid glucosides from *D. officinale* in 25 batches with different sources were determined by UHPLC-ESI-MS/MS, where principal component analysis (PCA) and hierarchical cluster analysis (HCA) were applied (Ye et al., 2017). The content of crude fiber in the autumn stem is 59.7% higher than that in the spring stem, and the fiber in the autumn leaf is 122.9% higher than that in the spring leaf (Li et al., 2017a). The total protein content of *D. officinale* stems in autumn is 10.9% higher than that in spring, while that of the leaves in autumn is 9.3% higher than that in spring. The results also revealed that the total protein content in the leaves is higher than that in the stems, and the ratio of total protein in the autumn leaves is 67.03 mg/g, which is 31.4% higher than that in the autumn stems (51.02 mg/g). The content of fat in the stems and leaves of *D. officinale* ranges from 10.0 to 15.0 mg/g. The average content of fat in the leaves (13.90 mg/g) is slightly higher than that in the stems (11.50 mg/g) (Liao et al., 2018). In particular, Wu and Feng (2019) revealed that the content of polysaccharides is the highest in those samples collected from October to the following March (Wu and Feng, 2019). Yu et al. (2014) found that it is more reasonable to harvest *D. officinale* at biennials pre-bloom than at specific harvesting months according to the content of polysaccharides (Xu et al., 2021). According to the Editorial Board of Chinese Pharmacopoeia (2020) edition, however, *D. officinale* should be harvested from November to the following March (China Pharmacopoeia Committee, 2020).

Additionally, there are some noteworthy scientific gaps, which can be resolved from the following aspects. First, the genuine, defective, and counterfeit varieties of *D. officinale* are mixed together, so there is an urgent need to breed varieties with better agronomic characters, high yield, high quality, and intense stress resistance. (Guo et al., 2019). Second, it is also an effective way to ensure the quality of *D. officinale* by controlling pesticide residues and using endophytes to control diseases and pests (Yu et al., 2014; Zhou et al., 2018). Third, at present, chemical methods are primarily used to evaluate the quality of *D. officinale*, while the quality evaluation of traditional Chinese medicine is closely related to its biological activity. Therefore, the evaluation methods are suggested to be improved by combining chemical approaches and bioassays, providing a foundation for the industrial production and clinic use of *D. officinale* (Wei et al., 2020).

SAFETY

The stems and leaves of *D. officinale* were approved by National Health and Family Planning Commission (NHFPC) of People's Republic (PR) of China to be utilized as a novel food material on Jan 15, 2013 and Jan 15, 2017 (National Health and Family Planning Commission of the People's Republic of China, 2013; National Health and Family Planning Commission of the People's Republic of China, 2017), respectively. Therefore, several safety studies of *D. officinale* have been performed. It has been reported that acute toxicity test (12.0 g/kg), genetic toxicity tests (Ames test, micronucleus test of bone marrow, and sperm shape abnormality test in mice) (1,000, 2000, and 4,000 mg/kg), and 90-days feeding test (1.08, 1.67, and 5.00 g/kg) in rats were employed to assess the safety of the stems from *D. officinale*. These results indicated that *D. officinale* was a type of health food product without noticeable toxicity, genetic toxicity, and mutagenicity within the range of the test doses (Li Z. et al., 2019). Moreover, oral administration with *D. officinale* stems at the doses of 25, 1,250, and 2,500 mg/kg did not exhibit any apparent effect on pregnant rats or deformity effect on fetal rats (Qin et al., 2019). Likewise, oral administration with the leaves and flowers of *D. officinale* at the doses of 0, 2.0, 4.0, and 6.4 g/kg for 90 days did not exhibit apparent adverse effects on sperm quality and testicular tissue morphology in parent and offspring rats (Fu et al., 2017; Fu et al., 2020a). Besides, *D. officinale* flowers (0, 2.0, 6.4 g/kg) had no apparent adverse effects on pregnant and offspring rats before birth (Fu et al., 2020b).

D. officinale is considered to have edible and medicinal values. However, due to its thermal tonic property, it is prohibited for patients with wind-heat cold, dampness, and allergies, teenagers, and pregnant women. According to the Pharmacopoeia of the People's Republic of China (China Pharmacopoeia Committee, 2020), the dosage of 6–12 g/d of *D. officinale* is appropriate, and intake of trace elements recommended by the Food and Drug Administration of the United States will not induce poisonous effects.

CONCLUSION AND FUTURE PROSPECTS

D. officinale, as a medicinal or food homologous product, plays a crucial role in healthcare. This study summarizes and updates the botany, traditional uses, bioactive components, pharmacology, quality control, and safety of *D. officinale*. Available data indicate that over 120 compounds have been isolated and identified from *D. officinale*, including polysaccharides, bibenzyls, flavonoids, alkaloids, phenanthrenes, etc. *D. officinale* is associated with multiple beneficial pharmacological properties, such as cardioprotective, anti-tumor, gastrointestinal protective,

anti-diabetes, anti-aging, and anti-osteoporosis activities. Furthermore, it is evident that *D. officinale* is a non-toxic, which can be listed as a toxicologically safe functional food. However, its clinical applications has been rarely described, and critical improvements are still required for its industrial applications.

Firstly, phytochemical studies have demonstrated that *D. officinale* mainly contains polysaccharides, bibenzyls, phenanthrenes, and flavonoids while little is known about the analysis and function of organic compounds such as protein and fatty acid. Growing evidence has shown that structure-based drug design plays a vital role in developing novel drugs, and a series of strategies can be adopted to obtain effective therapeutic drugs. Further studies need to be conducted to isolate and identify more compounds from *D. officinale* with novel structures, emphasizing on bioactivity-guided, structurally modified, and chemically synthesized molecules. Besides, most of the *D. officinale* containing health products are mainly derived from its stems rich in chemical compounds, while non-medicinal parts are rarely exploited. Therefore, it may be interesting to extend the research to the non-medicinal parts of the inexpensive flowers, leaves, and roots of *D. officinale* to ensure the fully utilization of its edible and medicinal values (Zhang et al., 2017a).

Second, *D. officinale* is traditionally used to relieve fatigue, nourish "Yin", heart, and stomach, and expel evil heat, which is closely related to its preventive effects on cardiac, gastrointestinal and diabetes diseases according to modern pharmacology. Pharmacological research of the cardioprotective, gastrointestinal tract and anti-diabetes protective effects of *D. officinale* mainly concentrates on its crude extracts and polysaccharides. However, the optimal dose, constituents, and side effects of *D. officinale* are not assessed. Besides, there is a lack of in-depth study on the mechanism of action of *D. officinale* monomeric compounds or the specific mechanism of *D. officinale* in animals is not comprehensive enough. Therefore, the high-quality and well-designed *in vivo*, *in vitro*, and clinical studies are encouraged to be carried out and to explore the molecular mechanisms and relationship between active chemical constituents and potential cardioprotective, gastrointestinal tract regulatory and anti-diabetes effects.

Third, the dosage of *D. officinale* used in previous studies were different (ranging from 4.375 mg/kg to 20 g/kg). It is not possible to define an exact upper cut-off dose, and the test dose needs to be pharmacologically relevant. In many cases, 100–200 mg/kg extracts for *in vivo* studies should be assumed as the upper limit for meaningful pharmacological studies. For pure compounds, a much lower dose range (e.g., 30–50 μM) should be considered for *in vitro* studies (Heinrich et al., 2020). In some cases, the pharmacological activity of *D. officinale* is present only with doses that might be too high for clinical use. According to the Chinese Pharmacopoeia, 6–12 g/day administration of *D. officinale* extract is common for human, but any clinical application at such doses should be accompanied with conservative safety insurance. Besides, the acute toxicity and sub-toxicity assessments of *D. officinale* were mostly carried out based on animal experiments. Furthermore, comprehensive placebo-controlled and double-blind clinical trials are necessary to provide sufficient evidence ensuring drug efficacy and patient safety.

Finally, *D. officinale* possesses various biological activities, which has been applied as health care medicine, health food, and health tea. In addition, with the development of analytical techniques and quality control methods, such as the improvement and update in chromatography techniques and molecular identification methods, new quality markers and quality control measures are likely to be adopted for better quality assessment of Chinese herbal medicine in the future (Leong et al., 2020).

In conclusion, *D. officinale* is one of the most popular medicinal and food homologous products in China. Modern pharmacology investigations have revealed its cardio-protective, gastrointestinal protective, anti-diabetes, and anti-aging effects, which robustly support its traditional application in nourishing "Yin", heart, and stomach, expelling evil heat, and relieving fatigue. This paper provides a full-scale review about the progress of botany, traditional uses, phytochemistry, pharmacology, quality control, and toxicology of *D. officinale*. The information summarized in this work can provide a foundation for further applying the medicinal and edible value of *D. officinale* in the future.

AUTHOR CONTRIBUTION

WC collated documents and wrote the manuscript; JL and JZ helped to perform the arrangement of tables and pictures; JW and LY helped to check chemical structure formula; LQ and BZ contributed significantly to analysis and manuscript preparation. All authors have read and approved the final version of the manuscript.

FUNDING

This work was supported by the National Natural Science Foundation of China (82003896).

REFERENCES

Cao, X. Y., Tang, Y. N., Jiang, X. M., Shao, W., and Gao, D. M. (2018). Study on contents and antioxidant activity of polysaccharides in different parts of *Dendrobium officinale* Kimura et Migo. *Food Drug* 20, 227–230. doi:10.3969/j.issn.1672-979X.2018.03.015

Chang, J., Zhou, Y., Cong, G., Guo, H., Guo, Y., Lu, K., et al. (2019). Dendrobium Candidum Protects against Diabetic Kidney Lesions through Regulating Vascular Endothelial Growth Factor, Glucose Transporter 1, and Connective Tissue Growth Factor Expression in Rats. *J. Cel. Biochem.* 120, 13924–13931. doi:10.1002/jcb.28666

Chen, H., Li, X., Xu, Y., Lo, K., Zheng, H., Hu, H., et al. (2018). Study on the Polar Extracts of *Dendrobium Nobile, D. Officinale, D. Loddigesii*, and *Flickingeria Fimbriata*: Metabolite Identification, Content Evaluation, and Bioactivity Assay. *Molecules* 23, 1185–1194. doi:10.3390/molecules23051185

Chen, R., Liang, Y., Ip, M. S. M., Zhang, K. Y., and Mak, J. C. W. (2020). Amelioration of Cigarette Smoke-Induced Mucus Hypersecretion and Viscosity by *Dendrobium Officinale* Polysaccharides *In Vitro* and *In Vivo*. *Oxid. Med. Cel. Longev.* 2020, 8217642–8217651. doi:10.1155/2020/8217642

Chen, Y., Wang, Y., Lyu, P., Chen, L., Shen, C., and Sun, C. (2019). Comparative Transcriptomic Analysis Reveal the Regulation Mechanism Underlying MeJA-Induced Accumulation of Alkaloids in Dendrobium Officinale. *J. Plant Res.* 132, 419–429. doi:10.1007/s10265-019-01099-6

Cheng, J., Dang, P.-P., Zhao, Z., Yuan, L.-C., Zhou, Z.-H., Wolf, D., et al. (2019). An Assessment of the Chinese Medicinal Dendrobium Industry: Supply, Demand and Sustainability. *J. Ethnopharmacology* 229, 81–88. doi:10.1016/j.jep.2018.09.001

Chu, C., Li, T., Pedersen, H. A., Kongstad, K. T., Yan, J., and Staerk, D. (2019). Antidiabetic Constituents of Dendrobium Officinale as Determined by High-Resolution Profiling of Radical Scavenging and α-glucosidase and α-amylase Inhibition Combined with HPLC-PDA-HRMS-SPE-NMR Analysis. *Phytochemistry Lett.* 31, 47–52. doi:10.1016/j.phytol.2019.03.002

Committee for the Pharmacopoeia of PR China (2015). *Pharmacopoeia of the People's Republic of China, Part 1*. Beijing, China: China Medical Science Press, 295–296.

Cui, Y. D., Lu, Y. L., Zhao, Y. M., Liu, M. X., and Zhang, G. G. (2019). Isolation and identification of chemical constituents from *Dendrobium officinale* Kimura et Migo. *J. Shenyang. Pharm. Univer.* 36, 7–11. doi:10.14066/j.cnki.cn21-1349/r.2019.01.002

Dou, M.-M., Zhang, Z.-H., Li, Z.-B., Zhang, J., and Zhao, X.-Y. (2016). Cardioprotective potential of *Dendrobium officinale* Kimura et Migo against myocardial ischemia in mice. *Mol. Med. Rep.* 14, 4407–4414. 2016. doi:10.3892/mmr.2016.5789

Editorial Board of Chinese Pharmacopoeia (2020). *Chinese Pharmacopoeia*, Vol. 1. Beijing, China: China Medical Science Press, 94–97, pp. 295–296.

Flora of China Editorial Committee (2009). *Flora of the People's Republic of China, Part 25 (English)*. Beijing, China: Science Press, 139.

Fu, J. Y., Song, Y. H., He, J. W., Zhu, Z. J., Song, S., and Xia, Y. (2017). A Study on the Effects of *Dendrobium Officinale* Leaves on Sperm Quality and Testicular Tissue Morpholohy in Parent and Offspring Rats. *Pre. Med.* 29, 782–789. doi:10.1002/elan.201600787

Fu, J. Y., Song, Y. H., Zhang, Y. Y., Zhu, Z. J., He, J. W., and Xia, Y. (2020a). Effects of *Dendrobium Officinale* Flowers on Testivular Tissue and Sperm Quality in Parent and Offspring Rats. *Pre. Med.* 32, 442–445. doi:10.19485/j.cnki.issn2096-5087.2020.05.003

Fu, J. Y., Xia, Y., Zhang, Y. Y., Cai, D. L., He, J. W., and Song, Y. H. (2020b). Toxicity of *Dendrobium Officinale* Flowers to Pregnant Rats and Offspring Rats before Birth. *Pre. Med.* 32, 1000–1003. doi:10.19485/j.cnki.issn2096-5087.2020.10.007

Fu, L. G. (1992). *China Plant Red Data Book Rare and Endangered Plants*. Beijing, China: Science Press, 492–493.

Gong, X. Y., Jiang, S. M., Tian, H. Y., Xiang, D., and Zhang, J. C. (2020). Polyphenols in the Fermentation Liquid of *Dendrobium Candidum* Relieve Intestinal Inflammation in Zebrafish through the Intestinal Microbiome-Mediated Immune Response. *Front. Immunol.* 11, 1542–1558. doi:10.3389/fimmu.2020.01542

Gu, H. Y., and Xie, K. P. (2021). Study on Epiphytic Cultivation Techniques of *Dendrobium Officinale* under Forestin in Emei Mountain. *S. Chin. For. Sci.* 49, 40–43. doi:10.16259/j.cnki.36-1342/s.2021.01.010

Guo, L., Qi, J., Du, D., Liu, Y., and Jiang, X. (2020a). Current Advances of *Dendrobium Officinale* Polysaccharides in Dermatology: a Literature Review. *Pharm. Biol.* 58, 664–673. doi:10.1080/13880209.2020.1787470

Guo, Y. (2020b). Efficacy of the Tiepishihu Yangwei Quwei Mixture on Intestinal Metathesis of Gastric Mucosa. *Clin. J. Chin. Med.* 12, 81–83. doi:10.3969/j.issn.1674-7860.2020.28.029

Guo, Z., Zhou, Y., Yang, J., and Shao, X. (2019). Dendrobium Candidum Extract Inhibits Proliferation and Induces Apoptosis of Liver Cancer Cells by Inactivating Wnt/β-Catenin Signaling Pathway. *Biomed. Pharmacother.* 110, 371–379. doi:10.1016/j.biopha.2018.11.149

He, L., Su, Q., Bai, L., Li, M., Liu, J., Liu, X., et al. (2020). Recent Research Progress on Natural Small Molecule Bibenzyls and its Derivatives in *Dendrobium* Species. *Eur. J. Med. Chem.* 204, 112530–112546. doi:10.1016/j.ejmech.2020.112530

Heinrich, M., Appendino, G., Efferth, T., Fürst, R., Izzo, A. A., Kayser, O., et al. (2020). Best Practice in Research - Overcoming Common Challenges in Phytopharmacological Research. *J. Ethnopharmacology* 246, 112230–112237. doi:10.1016/j.jep.2019.112230

Huang, S., Chen, F., Cheng, H., and Huang, G. (2020). Modification and Application of Polysaccharide from Traditional Chinese Medicine Such as *Dendrobium Officinale*. *Int. J. Biol. Macromolecules* 157, 385–393. doi:10.1016/j.ijbiomac.2020.04.141

Huang, X. H., Wang, Z. H., Li, J., Miao, A. Q., and Ye, Q. S. (2017). Comparative Analysis of Quality Properties and Main Nutrients in *Dendrobium* Flowers during Different Flowering Phases. *Chin. J. Trop. Crop* 38, 45–52.

Huang, Y.-P., He, T.-B., Cuan, X.-D., Wang, X.-J., Hu, J.-M., and Sheng, J. (2018). 1,4-β-d-Glucomannan from Dendrobium Officinale Activates NF-Kb *via* TLR4 to Regulate the Immune Response. *Molecules* 23, 2658–2672. doi:10.3390/molecules23102658

Jiao, C., Song, C., Zheng, S., Zhu, Y., Jin, Q., Cai, Y., et al. (2018). Metabolic Profiling of *Dendrobium Officinale* in Response to Precursors and Methyl Jasmonate. *Ijms* 19, 728–746. doi:10.3390/ijms19030728

Ke, Y., Zhan, L. H., Lu, T. T., Zhou, C., Chen, X., Dong, Y. J., et al. (2020). Polysaccharides of *Dendrobium Officinale* Kimura & Migo Leaves Protect against Ethanol-Induced Gastric Mucosal Injury *via* the AMPK/mTOR Signaling Pathway *In Vitro* and *Vivo*. *Front. Pharmacol.* 11, 526349–526363. doi:10.3389/fphar.2020.526349

Lee, E., Han, A.-R., Nam, B., Kim, Y.-R., Jin, C. H., Kim, J.-B., et al. (2020). Moscatilin Induces Apoptosis in Human Head and Neck Squamous Cell Carcinoma Cells *via* JNK Signaling Pathway. *Molecules* 25, 901–912. doi:10.3390/molecules25040901

Lei, Z. X., Zhou, C. H., Ji, X. Y., Wei, G., Huang, Y. C., Yu, W. X., et al. (2018). Transcriptome Analysis Reveals Genes Involved in Flavonoid Biosynthesis and Accumulation in *Dendrobium Officinale* from Different Locations. *Sci. Rep.* 8, 6373–6388. doi:10.1038/s41598-018-24751-y

Leong, F., Hua, X., Wang, M., Chen, T. K., Song, Y. L., Tu, P. F., et al. (2020). Quality Standard of Traditional Chinese Medicines: Comparison between European Pharmacopoeia and Chinese Pharmacopoeia and Recent Advances. *Chin. Med.* 15, 76–95. doi:10.1186/s13020-020-00357-3

Li, B., He, X., Jin, H.-Y., Wang, H.-Y., Zhou, F.-C., Zhang, N.-Y., et al. (2021). Beneficial Effects of *Dendrobium Officinale* on Metabolic Hypertensive Rats by Triggering the Enteric-Origin SCFA-Gpcr43/41 Pathway. *Food Funct.* 12, 5524–5538. doi:10.1039/d0fo02890h

Li, D.-l., Zheng, X.-l., Duan, L., Deng, S.-w., Ye, W., Wang, A.-h., et al. (2017a). Ethnobotanical Survey of Herbal tea Plants from the Traditional Markets in Chaoshan, China. *J. Ethnopharmacology* 205, 195–206. doi:10.1016/j.jep.2017.02.040

Li, F., Wei, Y., and Chen, Y. J. (2019a). Study on the content of flavonoids in stems, leaves and flowers of *Dendrobium officinale* Kimura et Migo and its antioxidant activity *In Vitro*. *Acta Chin. Med.* 34, 1020–1023. doi:10.16368/j.issn.1674-8999.2019.05.242

Li, L. Y., Ding, Q., and Sun, P. F. (2017b). Study on Quality of *Dendrobium Officinale* in Different Regions. *Mod. Chin. Med.* 19, 1702–1707. doi:10.13313/j.issn.1673-4890.2017.12.009

Li, M., Yue, H., Wang, Y., Guo, C., Du, Z., Jin, C., et al. (2020a). Intestinal Microbes Derived Butyrate Is Related to the Immunomodulatory Activities of *Dendrobium Officinale* Polysaccharide. *Int. J. Biol. Macromolecules* 149, 717–723. doi:10.1016/j.ijbiomac.2020.01.305

Li, X. L., and Hong, M. (2020b). Aqueous Extract ofDendrobium Officinaleconfers Neuroprotection against Hypoxic-ischemic Brain Damage in Neonatal Rats. *Kaohsiung J. Med. Sci.* 36, 43–53. doi:10.1002/kjm2.12139

Li, Z., Liu, M., Hu, J., and Qin, G. H. (2019b). Effects of *Dendrobium Officinale* on Blood Biochemical Indexes of Rats. *J. Food Safe. Qual.* 1, 3579–3583.

Liang, C. Y., Liang, Y. M., Liu, H. Z., Zhu, D. M., Hou, S. Z., Wu, Y. Y., et al. (2017). Effect of *Dendrobium Officinale* on D-Galactose-Induced Aging Mice. *Chin. J. Integr. Med.*, 1–9. doi:10.1007/s11655-016-2631-x2017

Liang, J., Li, H., Chen, J., He, L., Du, X., Zhou, L., et al. (2019). *Dendrobium Officinale* Polysaccharides Alleviate colon Tumorigenesis *via* Restoring Intestinal Barrier Function and Enhancing Anti-tumor Immune Response. *Pharmacol. Res.* 148, 104417–104429. doi:10.1016/j.phrs.2019.104417

Liang, J., Zeng, Y., Wang, H., and Lou, W. (2018). Extraction, Purification and Antioxidant Activity of Novel Polysaccharides from *Dendrobium Officinale* by Deep Eutectic Solvents. *Nat. Product. Res.* 33, 3248–3253. doi:10.1080/14786419.2018.1471480

Liang, K. L., Fang, P., Shi, Q. Q., Su, J., Li, B., Chen, S. H., et al. (2018). [Antihypertensive Effect and Mechanism of Dendrobium Officinale Flos on High-Blood Pressure Rats Induced by High Glucose and High Fat Compound Alcohol]. *Zhongguo Zhong Yao Za Zhi* 43, 147–153. doi:10.19540/j.cnki.cjcmm.20171027.020

Liao, X. Y., Xu, H. M., Liu, P., Chen, C. J., Li, X. K., and Huang, J. Y. (2018). Analysis on the Basic Nutritional Components of *Dendrobium Officinale* "Yanshangxian. *J. Food Sci. Tech.* 36, 61–67. doi:10.1200/jco.2018.78.4652

Liu, C.-Z., Chen, W., Wang, M.-X., Wang, Y., Chen, L.-Q., Zhao, F., et al. (2020). *Dendrobium officinale* Kimura et Migo and *American ginseng* mixture: A Chinese herbal formulation for gut microbiota modulation. *Chin. J. Nat. Medicines* 18, 446–459. doi:10.1016/s1875-5364(20)30052-2

Liu, M. X., Cui, Y. D., Deng, B. W., Shi, S., Zhang, C. Y., and Zhang, G. G. (2018). Isolation and identification of chemical constituents from *Dendrobium officinale* Kimura et Migo. *J. Shenyang. Pharm. Univer.* 35, 739–743. doi:10.14066/j.cnki.cn21-1349/r.2018.09.007

Liu, Y.-T., Hsieh, M.-J., Lin, J.-T., Chen, G., Lin, C.-C., Lo, Y.-S., et al. (2019). Erianin Induces Cell Apoptosis through ERK Pathway in Human Nasopharyngeal Carcinoma. *Biomed. Pharmacother.* 111, 262–269. doi:10.1016/j.biopha.2018.12.081

Lou, X. J., Wang, Y. Z., Lei, S. S., He, X., Lu, T. T., Zhan, L. H., et al. (2020). Beneficial Effects of Macroporous Resin Extract of *Dendrobium Officinale* Leaves in Rats with Hyperuricemia Induced by a High-Purine Diet. *Evid. Based. Complement. Alternat. Med.* 2020, 3086106–3086115. doi:10.1155/2020/3086106

Luo, Y., Ren, Z., Du, B., Xing, S., Huang, S., Li, Y., et al. (2019). Structure Identification of ViceninII Extracted from Dendrobium Officinale and the Reversal of TGF-B1-Induced Epithelial-Mesenchymal Transition in Lung Adenocarcinoma Cells through TGF-β/Smad and PI3K/Akt/mTOR Signaling Pathways. *Molecules* 24, 144–159. doi:10.3390/molecules24010144

Lv, C. G., Yang, J., Kang, C. Z., Li, Z. H., M, Z. H., G, L. P., et al. (2017). Determination of 10 Flavonoids by UPLC-MS/MS and Analysis of Polysaccharide Contents and Compositions in *Dendrobium Officinale* Caulis from Different Habitats. *Chin. J. Exper. Tradi. Med. Formu.* 23, 47–52. doi:10.13422/j.cnki.syfjx.2017170047

Ma, H., Zhang, K., Jiang, Q., Dai, D., Li, H., Bi, W., et al. (2018). Characterization of Plant Polysaccharides from *Dendrobium Officinale* by Multiple Chromatographic and Mass Spectrometric Techniques. *J. Chromatogr. A* 1547, 29–36. doi:10.1016/j.chroma.2018.03.006

Mai, Y., Niu, Z., He, W., Lai, X., Huang, S., and Zheng, X. (2019). The Reparative Effect of *Dendrobium Officinale* Protocorms against Photodamage Caused by UV-Irradiation in Hairless Mice. *Biol. Pharm. Bull.* 42, 728–735. doi:10.1248/bpb.b18-00901

National Health and Family Planning Commission of the People's Republic of China (2013). *NHFPC-approved Seven New Food Materials*. Announcement No. 1, 2013.

National Health and Family Planning Commission of the People's Republic of China (2017). *NHFPC-approved Seven New Food Materials*. Announcement No. 1, 2017.

Ni, Z., Chen, Z., Bai, R., and Tang, F. (2018). Determination of Trace Elements in *Dendrobium Officinale* Cultivated in Various Conditions. *Anal. Lett.* 51, 648–658. doi:10.1080/00032719.2017.1345931

Peng, H., Yang, M., Guo, Q., Su, T., Xiao, Y., and Xia, Z. Y. (2019). *Dendrobium Officinale* Polysaccharides Regulate Age-Related Lineage Commitment between Osteogenic and Adipogenic Differentiation. *Cell. Prolif.* 52, 12624–12633. doi:10.1111/cpr.12624

Peng, L.-Q., Dong, X., Zhen, X.-T., Yang, J., Chen, Y., Wang, S.-L., et al. (2020). Simultaneous Separation and Concentration of Neutral Analytes by Cyclodextrin Assisted Sweeping-Micellar Electrokinetic Chromatography. *Analytica Chim. Acta* 1105, 224–230. doi:10.1016/j.aca.2020.01.037

Qin, G. H., Liu, M., Wang, W., Hu, J. X., and Li, Z. (2019). Effects of *Dendrobium Officinale* on Pregnant Rats and Embryonic Development of Offspring Mice. *J. Food Safe. Qual.* 10, 3971–3974.

Qin, Z. F., Tan, X. Y., Ning, H. J., H, J., Miao, Y. X., and Zhang, X. Q. (2017). Quantification and Characterization of Polysaccharides from Different Aged *Dendrobium Officinale* Stems. *Food Sci.* 39, 189–193. doi:10.7506/spkx1002-6630-201806030

Ren, G., Chen, Y. T., Ye, J. B., Zhong, G. Y., Xiao, C. Y., Deng, W. Z., et al. (2020a). Phytochemical Investigation of Leaves of *Dendrobium Officinale*. *Chin. Trad. Herb. Drug* 55, 3637–3644. doi:10.7501/j.issn.0253-2670.2020.14.005

Ren, G., Deng, W. Z., Xie, Y. F., Wu, C. H., Li, W. Y., Xiao, C. Y., et al. (2020b). Bibenzyl Derivatives from Leaves of *Dendrobium Officinale*. *Nat. Prod. Comm.* 15, 1–5. doi:10.1177/1934578x20908678

Ren, Z., Ji, X., Jiao, Z., Luo, Y., Zhang, G. Q., Tao, S., et al. (2020c). Functional Analysis of a Novel C-Glycosyltransferase in the Orchid *Dendrobium Officinale*. *Hortic. Res.* 7, 111–128. doi:10.1038/s41438-020-0330-4

Ren, Z. Y., Qiu, F. N., Wang, Y. J., Yu, W. X., Liu, C. X., Sun, Y. Y., et al. (2020d). Network Analysis of Transcriptome and LC-MS Reveals a Possible Biosynthesis Pathway of Anthocyanins in *Dendrobium Officinale*. *Biomed. Res. Int.* 2020, 6512895–65129906. doi:10.1155/2020/6512895

Shi, X.-D., Yin, J.-Y., Cui, S. W., Wang, Q., Wang, S.-Y., and Nie, S.-P. (2020). Comparative Study on Glucomannans with Different Structural Characteristics: Functional Properties and Intestinal Production of Short Chain Fatty Acids. *Int. J. Biol. Macromolecules* 164, 826–835. doi:10.1016/j.ijbiomac.2020.07.186

Su, J., Wang, T., Yan, M. Q., Yu, J. J., Xu, J., Zhuge, R. C., et al. (2021). Effect of *Dendrobium Officinale* Superfine Powder on Overeating Greasy-Induced Metabolic Hypertension in Rats. *China. J. Chin. Mater. Med.* 2021, 1–11. doi:10.19540/j.cnki.cjcmm.20201027.403

Teixeira, D. S. J. A., and Ng, T. B. (2017). The Medicinal and Pharmaceutical Importance of *Dendrobium* Species. *Appl. Microbiol. Biotechnol.* 101, 2227–2239. doi:10.1007/s00253-017-8169-9

Tian, W., Dai, L., Lu, S., Luo, Z., Qiu, Z., Li, J., et al. (2019). Effect of *Bacillus* Sp. DU-106 Fermentation on *Dendrobium Officinale* Polysaccharide: Structure and Immunoregulatory Activities. *Int. J. Biol. Macromolecules* 135, 1034–1042. doi:10.1016/j.ijbiomac.2019.05.203

Wang, Q., Zi, C. T., Wang, J., Wang, Y. N., Huang, Y. W., Fu, X. Q., et al. (2018). *Dendrobium Officinale* Orchid Extract Prevents Ovariectomy-Induced Osteoporosis *In Vivo* and Inhibits RANKL-Induced Osteoclast Differentiation *In Vitro*. *Front. Pharmacol.* 8, 966–978. doi:10.3389/fphar.2017.00966

Wei, W., Li, Z.-P., Zhu, T., Fung, H.-Y., Wong, T.-L., Wen, X., et al. (2017). Anti-fatigue Effects of the Unique Polysaccharide Marker of *Dendrobium Officinale* on BALB/c Mice. *Molecules* 22, 155–166. doi:10.3390/molecules22010155

Wei, X. C., Cao, B., Luo, C. H., Huang, H. Z., Tan, P., Xu, X. R., et al. (2020). Recent Advances of Novel Technologies for Quality Consistency Assessment of Natural Herbal Medicines and Preparations. *Chin. Med.* 15, 56–78. doi:10.1186/s13020-020-00335-9

Wei, Y., Wang, L. W., Wang, D. J., Wang, D., Wen, C. W., and Han, B. (2018). Characterization and Anti-tumor Activity of a Polysaccharide Isolated from *Dendrobium Officinale* Grown in the Huoshan County. *Chin. Med.* 13, 47–57. doi:10.1186/s13020-018-0205-x

Wong, T.-L., Li, L.-F., Zhang, J.-X., Bai, S.-P., Zhou, L.-S., Fung, H.-Y., et al. (2019). Oligosaccharide-marker Approach for Qualitative and Quantitative Analysis of Specific Polysaccharide in Herb Formula by Ultra-high-performance Liquid Chromatography-Quadrupole-Time-Of-Flight Mass Spectrometry: *Dendrobium Officinale*, a Case Study. *J. Chromatogr. A* 1607, 460388–460396. doi:10.1016/j.chroma.2019.460388

Wu, D.-T., Guo, H., Lin, S., Lam, S.-C., Zhao, L., Lin, D.-R., et al. (2018a). Review of the Structural Characterization, Quality Evaluation, and Industrial Application of *Lycium Barbarum* Polysaccharides. *Trends Food Sci. Tech.* 79, 171–183. doi:10.1016/j.tifs.2018.07.016

Wu, J. Y., and Feng, Y. (2019). The Determination and Comparison of Main Components of *Dendrobium Officinale* in Different Harvesting Periods. *Chin. J. Ethnomed. Ethnophar.* 2, 39–42. 1007-8517(2019)10-0039-04

Wu, J., Zhuang, H. H., Mao, Z. T., Li, T. M., Li, W., and Wu, H. Q. (2018b). Clinical Observation of *Dendrobium Officinale* in Mount Longhu in the Treatment of Hypertension. *Clin. J. Trad. Chin. Med.* 30, 297–300. doi:10.16448/j.cjtcm.2018.0088

Wu, J., Zhuang, H. H., Mao, Z. T., Li, T. M., Li, W., and Wu, H. Q. (2017). Comparison of the Clinical Efficacy of *Dendrobium Officinale* in Mount Longhu in the Treatment of Type 2 Diabetes Mellitus. *Jiangxi. J. Trad. Chin. Med.* 48, 45–47.

Wu, Y. L., Huang, S. H., He, C. M., Qiu, B., Liu, J. J., Li, J., et al. (2020). *Dendrobium Officinale* Flower Extraction Mitigates Alcohol-Induced Liver Injury in Mice: Role of Anti-steatosis, Anti-oxidative, and Anti-inflammatory. *Evid. Based. Complement. Alternat. Med.* 2020, 1421853–1421864. doi:10.1155/2020/1421853

Xiao, X. C., Chen, W. H., Cao, Y. Y., Lou, Y. J., Liu, Y., Wang, J., et al. (2018). Protective Effect of *Dendrobium Officinale* on Isoproterenol Induced Cardiac Hypertrophy in Rats. *China. J. Chin. Mater. Med.* 43, 800–804. doi:10.19540/j.cnki.cjcmm.2018.0021

Xing, S., Yu, W., Zhang, X., Luo, Y., Lei, Z., Huang, D., et al. (2018). Isoviolanthin Extracted from Dendrobium Officinale Reverses TGF-B1-Mediated Epithelial-Mesenchymal Transition in Hepatocellular Carcinoma Cells *via* Deactivating the TGF-β/Smad and PI3K/Akt/mTOR Signaling Pathways. *Ijms* 19, 1556–1572. doi:10.3390/ijms19061556

Xu, Z., Li, L., Xu, Y., Wang, S., Zhang, X., Tang, T., et al. (2021). Pesticide multi-residues in *Dendrobium officinale* Kimura et Migo: Method validation, residue levels and dietary exposure risk assessment. *Food Chem.* 343, 128490–128517. doi:10.1016/j.foodchem.2020.128490

Yan, M. Q., Su, J., Yu, J. J., Yang, Z. Y., Wang, T., Chen, S. H., et al. (2019a). [Effects and Active Substances of Ethanol Extract from Dendrobium Officinale on Metabolic Hypertensive Rats Induced by Comprehensive Dietary]. *Zhongguo Zhong Yao Za Zhi* 44, 4896–4904. doi:10.19540/j.cnki.cjcmm.20190610.401

Yan, M. Q., Yang, Z. Y., Shi, Q. Q., Wang, T., Chen, S. H., and Lv, G. Y. (2019b). Research Progress on Protective Effects and Mechanism of *Dendrobium Officinale* on Metabolic Disturbances. *Chin. Trad. Herb. Drug* 50, 2491–2497. doi:10.7501/j.issn.0253-2670.2019.10.033

Yang, K., Lu, T., Zhan, L., Zhou, C., Zhang, N., Lei, S., et al. (2020). Physicochemical Characterization of Polysaccharide from the Leaf of *Dendrobium Officinale* and Effect on LPS Induced Damage in GES-1 Cell. *Int. J. Biol. Macromolecules* 149, 320–330. doi:10.1016/j.ijbiomac.2020.01.026

Ye, Z., Dai, J. R., Zhang, C. G., Lu, Y., Wu, L. L., Gong, A. G. W., et al. (2017). Chemical Differentiation of *Dendrobium Officinale* and *Dendrobium Devonianum* by Using HPLC Fingerprints, HPLC-ESI-MS, and HPTLC Analyses. *Evid. Based. Complement. Alternat. Med.* 2017, 8647212–8647219. doi:10.1155/2017/8647212

Yu, Q. X., Guo, Y. Y., Si, J. P., Wu, L. S., and Wang, L. H. (2014). [Variation of Polysaccharides and Alcohol-Soluble Extracts Content of Dendrobium Officinale]. *Zhongguo Zhong Yao Za Zhi* 39, 4769–4772. doi:10.4268/cjcmm20142414

Yu, Z., Liao, Y., Teixeira da Silva, J., Yang, Z., and Duan, J. (2018). Differential Accumulation of Anthocyanins in *Dendrobium Officinale* Stems with Red and green Peels. *Ijms* 19, 2857–2870. doi:10.3390/ijms19102857

Yue, H., Liu, Y., Qu, H., and Ding, K. (2017). Structure Analysis of a Novel Heteroxylan from the Stem of *Dendrobium Officinale* and Anti-angiogenesis Activities of its Sulfated Derivative. *Int. J. Biol. Macromolecules* 103, 533–542. doi:10.1016/j.ijbiomac.2017.05.097

Zeng, J., Li, D., Li, Z., Zhang, J., and Zhao, X. (2020). *Dendrobium Officinale* Attenuates Myocardial Fibrosis *via* Inhibiting EMT Signaling Pathway in HFD/STZ-induced Diabetic Mice. *Biol. Pharm. Bull.* 43, 864–872. doi:10.1248/bpb.b19-01073

Zhang, J.-y., Guo, Y., Si, J.-p., Sun, X.-b., Sun, G.-b., and Liu, J.-j. (2017a). A Polysaccharide of *Dendrobium Officinale* Ameliorates H2O2-Induced Apoptosis in H9c2 Cardiomyocytes *via* PI3K/AKT and MAPK Pathways. *Int. J. Biol. Macromolecules* 104, 1–10. doi:10.1016/j.ijbiomac.2017.05.169

Zhang, X., Zhang, S., Gao, B., Qian, Z., Liu, J., Wu, S., et al. (2019). Identification and Quantitative Analysis of Phenolic Glycosides with Antioxidant Activity in Methanolic Extract of Dendrobium Catenatum Flowers and Selection of Quality Control Herb-Markers. *Food Res. Int.* 123, 732–745. doi:10.1016/j.foodres.2019.05.040

Zhang, Y., Wu, Z., Liu, J., Zheng, Z., Li, Q., Wang, H., et al. (2020). Identification of the Core Active Structure of a *Dendrobium Officinale* Polysaccharide and its Protective Effect against Dextran Sulfate Sodium-Induced Colitis *via* Alleviating Gut Microbiota Dysbiosis. *Food Res. Int.* 137, 109641–109652. doi:10.1016/j.foodres.2020.109641

Zhang, Y., Zhang, L., Liu, J., Liang, J., Si, J., and Wu, S. (2017b). *Dendrobium Officinale* Leaves as a New Antioxidant Source. *J. Funct. Foods* 37, 400–415. doi:10.1016/j.jff.2017.08.006

Zhang, Z., Zhang, D., Dou, M., Li, Z., Zhang, J., and Zhao, X. (2016). *Dendrobium officinale* Kimura et Migo attenuates diabetic cardiomyopathy through inhibiting oxidative stress, inflammation and fibrosis in streptozotocin-induced mice. *Biomed. Pharmacother.* 84, 1350–1358. doi:10.1016/j.biopha.2016.10.074

Zhao, G.-Y., Deng, B.-W., Zhang, C.-Y., Cui, Y.-D., Bi, J.-Y., and Zhang, G.-G. (2018a). New Phenanthrene and 9, 10-dihydrophenanthrene Derivatives from the Stems of *Dendrobium Officinale* with Their Cytotoxic Activities. *J. Nat. Med.* 72, 246–251. doi:10.1007/s11418-017-1141-2

Zhao, M., and Han, J. (2018b). *Dendrobium officinale* Kimura et Migo ameliorates insulin resistance in rats with diabetic nephropathy. *Med. Sci. Monit. Basic Res.* 24, 84–92. doi:10.12659/msmbr.909242

Zhao, M., Sun, Y., Gao, Z., Cui, H., Chen, J., Wang, M., et al. (2020). Gigantol Attenuates the Metastasis of Human Bladder Cancer Cells, Possibly through Wnt/EMT Signaling. *Ott* Vol. 13, 11337–11346. doi:10.2147/ott.s271032

Zhao, X., Dou, M., Zhang, Z., Zhang, D., and Huang, C. (2017). Protective Effect of Dendrobium Officinale Polysaccharides on H2O2-Induced Injury in H9c2 Cardiomyocytes. *Biomed. Pharmacother.* 94, 72–78. doi:10.1016/j.biopha.2017.07.096

Zhao, Y., Li, B., Wang, G., Ge, S., Lan, X., Xu, G., et al. (2019). Dendrobium Officinale Polysaccharides Inhibit 1-Methyl-2-Nitro-1-Nitrosoguanidine Induced Precancerous Lesions of Gastric Cancer in Rats through Regulating Wnt/β-Catenin Pathway and Altering Serum Endogenous Metabolites. *Molecules* 24, 2660–2673. doi:10.3390/molecules24142660

Zheng, H., Pan, L., Xu, P., Zhu, J., Wang, R., Zhu, W., et al. (2017). An NMR-Based Metabolomic Approach to Unravel the Preventive Effect of Water-Soluble Extract from Dendrobium Officinale Kimura & Migo on Streptozotocin-Induced Diabetes in Mice. *Molecules* 22, 1543–1556. doi:10.3390/molecules22091543

Zhou, C. H., Xie, Z. S., Lei, Z. X., Huang, Y. C., and Wei, G. (2018). Simultaneous Identification and Determination of Flavonoids in *Dendrobium Officinale*. *Chem. Cent. J.* 12, 40–48. doi:10.1186/s13065-018-0403-8

Zhu, B., Wu, L. S., Wan, H. T., Yang, K., Si, J. P., and Qin, L. P. (2018). Fungal Elicitors Stimulate Biomass and Active Ingredients Accumulation in *Dendrobium Officinale* Plantlets. *China. J. Chin. Mater. Med.* 73, 1–10. doi:10.2478/s11756-018-0091-9

Zhu, L.-J., Wang, M.-Q., Qin, Y., Wang, M.-N., Zhang, G.-Q., Niu, L.-T., et al. (2020). Two New Dibenzyl Derivatives from the Stems of Dendrobium Catenatum. *J. Asian Nat. Prod. Res.* 2020, 1–6. doi:10.1080/10286020.2020.1826937

Zhu, Q., Sheng, Y., Li, W., Wang, J., Ma, Y., Du, B., et al. (2019). Erianin, a Novel Dibenzyl Compound in *Dendrobium* Extract, Inhibits Bladder Cancer Cell Growth *via* the Mitochondrial Apoptosis and JNK Pathways. *Toxicol. Appl. Pharmacol.* 371, 41–54. doi:10.1016/j.taap.2019.03.027

Zuo, S.-M., Yu, H.-D., Zhang, W., Zhong, Q., Chen, W., Chen, W., et al. (2020). Comparative Metabolomic Analysis of *Dendrobium Officinale* under Different Cultivation Substrates. *Metabolites* 10, 325–338. doi:10.3390/metabo10080325

Conflict of Interest: The authors declare that the research was conducted in the absence of any commercial or financial relationships that could be construed as a potential conflict of interest.

Publisher's Note: All claims expressed in this article are solely those of the authors and do not necessarily represent those of their affiliated organizations, or those of the publisher, the editors and the reviewers. Any product that may be evaluated in this article, or claim that may be made by its manufacturer, is not guaranteed or endorsed by the publisher.

GLOSSARY

D. officinale Dendrobium officinale

HPLC high performance liquid chromatography

HPAEC high performance gel permeation chromatography

GC-MS gas chromatography-mass spectrometry

GPC gel permeation chromatography

HPLC-ESI-MS high performance liquid chromatography electrospray ionization mass spectrometry

UHPLC ultra-high performance liquid chromatography

QTOF quadrupole time of flight mass spectrometry

ISO isoproterenol

ANP atrial natriuretic peptide

BNP brain natriuretic peptide

cTN-I cardiac troponin I

LAD anterior descending coronary artery

CK creatine kinase

LDH lactate dehydrogenase

MDA malondialdehyde

SOD superoxide dismutase

H2O2 hydrogen peroxide

PI3K phosphatidylinositol

Akt protein kinase B

MAPK mitogen-activited protein kinase

LPD lipid peroxidation damage

ROS reactive oxygen species

HMEC-1 human microvascular endothelial cells

DOFP D. officinale ultrafine powder

LPS lipopolysaccharide

TLR4 toll-like receptor 4

TC total cholesterol

TG triglyceride

LDL-c low-density lipoprotein cholesterol

CRP C-reactive protein

IL-6 interleukin 6

MyD88 myeloid differentiation factor

TNF-α tumor necrosis factor alpha

HDL-c high-density lipoprotein cholesterol

NO nitric oxide

ET-1 endothelin 1

TXB2 thromboxane B2

PGI2 prostacycline

SCFA short-chain fatty acid

ACHSFD alcohol, and high sugar and fat diets

MNNG methyl-2-nitro-1-nitrosoguanidine

EMT epithelial-mesenchymal transition

HNSCC human head and neck squamous carcinoma cells

JNK jun N-terminal kinase

NPC nasopharyngeal carcinoma

TGF transforming growth factor

HCC hepatocellular carcinoma

SAR structure-activity relationship

AMPK AMP-activated protein kinase

LC-3β light chain 3β

HO-1 heme oxygenase-1

HFD/STZ high-fat diet/streptozotocin

TLRs toll-like receptors

DMBG dimethylbiguanide

VEGF vascular endothelial growth factor

GLUT-1 glucose transporter 1

CTGF connective tissue growth factor

IgM immunoglobulin M

NF-κB, nuclear factor kappa-B

GSH-Px glutathione peroxidase

T-AOC total antioxidant capacity

DOP D. officinale polysaccharide

LOD lipid oxidation

OVX ovariectomy

ALP alkaline phosphatase

BGP bone glucose protein

ACP acid phosphatase

BMD bone mineral density

RANKL receptor activator expression of the nuclear factor-κB ligand

Nrf2 nuclear factor E2-related factor 2

KCC2 K + -Cl -cotransporter 2

HIF-1α hypoxia-inducible factor-1α

HDAC1 Histone deacetylase 1

HIBD hypoxic-ischemic brain damage

TBARS thiobarbituric acid reactive substances

MUC5AC mucin-5AC

ABEE aminobenzoic acid ethyl ester

RSD relative standard deviation

PCA principal component analysis

HC hierarchical cluster analysis

NHFPC national health and family planning commission

PR people's republic

frontiers in Pharmacology

ORIGINAL RESEARCH
published: 02 November 2021
doi: 10.3389/fphar.2021.734671

Attenuation and Structural Transformation of Crassicauline A During Sand Frying Process and Antiarrhythmic Effects of its Transformed Products

Pei Tao[1], *Yan Wang*[1] *and Yujie Wang*[2]*

[1]School of Pharmacy, Chengdu University of Traditional Chinese Medicine, Chengdu, China, [2]School of Ethnic Medicine, Chengdu University of Traditional Chinese Medicine, Chengdu, China

To ensure safety and efficacy, most *Aconitum* herbs should be processed before clinical application. The processing methods include boiling, steaming, and sand frying. Among these methods, the transformation pathways of diterpenoid alkaloids in the process of sand frying are more complicated. Therefore, crassicauline A, a natural product with two ester bonds, was chosen as the experimental object. Consequently, a known alkaloid, together with three new alkaloids, was derived from crassicauline A. Meanwhile, the cardiotoxicity of converted products was reduced compared with their parent compound. Interestingly, some diterpenoid alkaloids have similar structures but opposite effects, such as arrhythmia and antiarrhythmic. Considering the converted products are structural analogues of crassicauline A, herein, the antiarrhythmic activity of the transformed products was further investigated. In a rat aconitine-induced arrhythmia assay, the three transformed products, which could dose-dependently delay the ventricular premature beat (VPB) incubation period, reduce the incidence of ventricular tachycardia (VT), combined with the increasing arrhythmia inhibition rate, exhibited prominent antiarrhythmic activities. Our experiments speculated that there might be at least two transformation pathways of crassicauline A during sand frying. The structure-activity data established in this paper constructs the critical pharmacophore of diterpenoid alkaloids as antiarrhythmic agents, which could be helpful in searching for the potential drugs that are equal or more active and with lower toxicity, than currently clinical used antiarrhythmic drugs.

Keywords: crassicauline A, processing, sand frying, antiarrhythmic, cardiotoxicity

OPEN ACCESS

Edited by:
Yi Wang,
Zhejiang University, China

Reviewed by:
Attila Hunyadi,
University of Szeged, Hungary
Yi Tao,
Zhejiang University of Technology, China
Xianli Zhou,
Southwest Jiaotong University, China

***Correspondence:**
Yujie Wang
superwangyj@126.com

Specialty section:
This article was submitted to Ethnopharmacology, a section of the journal Frontiers in Pharmacology

Received: *01 July 2021*
Accepted: *18 October 2021*
Published: *02 November 2021*

Citation:
Tao P, Wang Y and Wang Y (2021) Attenuation and Structural Transformation of Crassicauline A During Sand Frying Process and Antiarrhythmic Effects of its Transformed Products. Front. Pharmacol. 12:734671. doi: 10.3389/fphar.2021.734671

INTRODUCTION

Aconitum L. (Ranunculaceae) is a large herbal medicinal genus, which has 300 species widely distributed in the temperate regions of the northern hemisphere. In China, over 200 species are distributed mainly in western Sichuan, northwestern Yunnan, and eastern Tibet Autonomous Region. Among which 76 species can be extensively employed in traditional Chinese medicine and ethnomedicine (The Flora Committee of Chinese Academy of Sciences, 1979; Xiao et al., 2006). For example, *Aconitum carmichaelii* Debx. and *A. kusnezoffii* Reichb. are commonly used in traditional

Chinese medicine (Chinese Pharmacopoeia Commission, 2020), while *A. pendulum* Busch and *A. vilmorinianum* Kom. are usually used in Tibetan medicine and Qiang medicine. They have been employed for the clinical treatment of pains, rheumatics, and neurological disorders (Wang et al., 2007; Wang et al., 2009; Li et al., 2017).

Diterpenoid alkaloids, as the bioactive compounds of *Aconitum* herbs, exert anti-inflammatory and analgesic activities, but also have the drawbacks of cardiotoxicity and neurotoxicity (Chen and Zheng, 1987; Wu et al., 2018). For example, aconitine, a famous diester diterpenoid alkaloid (DDA), can specifically bind with the voltage-sensitive sodium channels on the cell membranes of cardiomyocytes and nerve cells, causing a persistent activation of the sodium channels (Ameri, 1998; Coulson et al., 2017), and continuing sodium influx, destroying the homeostasis of the internal environment, resulting in numbness of limbs, respiratory depression, and arrhythmia (Chan, 2009). In severe cases, it can lead to multiple organ dysfunction and even death.

It must be noted that, in the clinical practice of traditional Chinese medicine and ethnomedicine, most *Aconitum* herbs should be processed with conventional methods to reduce the toxicity, such as boiling, steaming, and sand frying. The boiling (boiling with water for 4~6 h) and steaming (steaming for 6~8 h) methods are diffusely applied in traditional Chinese medicine, of which the structural transformation pathways of DDAs have been elucidated clearly, mainly because DDAs are successively hydrolyzed into less toxic monoester- and amines-diterpenoid alkaloids (Gong, 2005). The method of sand frying is a unique processing method for *Aconitum* herbs in ethnomedicine, which requires only 10–15 min of stir-frying with sand to achieve toxicity reduction. However, the transformation pathways of DDAs are more complicated in the sand frying process, and the transformation mechanism is not clear by far.

The processing mechanisms for different processing methods (boiling, steaming, and sand frying) of *A. pendulum* Busch were investigated in our previous studies (Wang et al., 2010a; Wang et al., 2010b; Wang et al., 2011). It was confirmed that aconitine, deoxyaconitine, and 3-acetylaconitine, three main ingredients of *A. pendulum* Busch, were converted into the corresponding monoester- or amines-diterpenoid alkaloids by hydrolyzing the ester bonds at the C-8 and C-14 position during the boiling and steaming process (Wang et al., 2010a; Wang et al., 2010b). However, 16-epi-pyroaconitine and 16-epi-pyrodeoxyaconitine, the corresponding products of aconitine and deoxyaconitine, have been isolated from the sand-fried processed *A. pendulum* Busch (Wang et al., 2010b; Wang et al., 2011). It was found that, by comparing the chemical characteristics of the above four compounds, the substituents at C-15 of aconitine and deoxyaconitine, which were hydroxyl groups, were converted into carbonyl groups after processing. It is speculated that the prototype alkaloids with different substituents at the C-15 position may have different structural transformation pathways.

Crassicauline A (bulleyaconitine A), the main component of many *Aconitum* drugs produced in Yunnan province (Xiao et al., 2006), such as *Aconitum hemsleyanum* E. Pritz. (syn. *A. crassicaule* W. T. Wang) (Wang and Fang, 1981), is a commonly used analgesic in China, whose structural analogues have more potential to be developed as drugs. Besides, crassicauline A does not bear a hydroxyl group at C-15, making it less susceptible to oxidation during the sand frying process, which may have different transformation pathways from aconitine and deoxyaconitine during processing (Wang et al., 2010b; Wang et al., 2011). Therefore, crassicauline A was chosen as the experimental object, and the oil bath heating was used to simulate the sand frying process. Simultaneously, the temperature and time parameters for the structural transformation of crassicauline A were screened via high-performance liquid chromatography (HPLC) method. Moreover, the corresponding processed products of crassicauline A were obtained by processing based on screened parameters. The transformed components were further separated and identified. By comparing the structure changes and toxicity between prototype compound and converted products, the structural transformation pathways of crassicauline A were clarified, as well as whether the sand frying method could attenuate the toxicity.

Notably, some diterpenoid alkaloids exhibit opposite effects, though their structures are extremely similar. For example, aconitine has serious proarrhythmic effects, while aconitine-like compounds such as 14-benzoyltalatisamine, 14-benzoyldelcosine, and 14-benzoyldictyocarpine (Lin et al., 2004; Wang, 2009) have antiarrhythmic effects. Considering crassicauline A is structurally similar to its transformed products. It was unclear, with the transformation of structure, whether the transformed products have antiarrhythmic effects on the premise of reduced toxicity. This intriguing problem beckoned for an explicit solution, to clarify this question, we were engaged in relative experiments to elucidate above speculation.

MATERIALS AND METHODS

General Experimental Procedures

Shimadzu LC-2030C system (Shimadzu Corporation, Japan) and LabSolutions software program were used for chromatographic separation of components and analyzing HPLC data. Preparative-HPLC (Gelaipu Corporation, Chengdu, China), equipping with a GL6000-cp1000 high-pressure infusion pump, GL6000-UV3292 ultraviolet detector, and GelaiInst software program. The packing used in the pre-HPLC column (200 × 100 mm, 10 μm) was purchased from Acchrom Co., Ltd. (Wenling, China). BL-420F Organism Functional Experimental System (Chengdu Techman Co., Ltd. Chengdu, China) was used to record the lead II electrocardiograms (ECGs). CPA2250 electronic analytical balance (Sartorius, Germany) was used to correctly weigh the lab samples. The process of sand frying was simulated by oil bath heating using an HH-SJ heat-collecting magnetic stirrer (Jintan Chengdong Xinrui Instrument Factory, Changzhou, China). Optical rotations were obtained on a Perkin-Elmer 341 polarimeter (PerkinElmer, United States). Melting points were measured on an X-4 micro-melting point apparatus and uncorrected (Shanghai Precision Scientific Instrument

Corporation, Shanghai, China). NMR spectra were measured on a Bruker Avance 600 spectrometer (Bruker, Germany) in $CDCl_3$ with tetramethylsilane (TMS) as internal standard. Mass spectra were carried out on a micrO-TOF-Q-II mass spectrometer (Bruker, Germany). RE-3000B rotary evaporator (Shanghai Yarong Biochemical Instrument Factory, Shanghai, China) was used to evaporate the solvent. Silica gel G (200–300 mesh) for column chromatography and TLC plates (silica gel G) were obtained from Qingdao Sea Chemical Factory (Qingdao, China).

Chemicals and Reagents

Crassicauline A (purity ≥98%) was purchased from Chengdu Desite Bio-Technology Co., Ltd. (Chengdu, China), aconitine (purity = 99%) from Shaanxi Herbchem Bio-Technology Co., Ltd. (Xi'an, China). Propafenone hydrochloride (purity = 99.8%) and lidocaine hydrochloride (purity = 93.4%) were purchased from National Institutes for Food and Drug Control (Beijing, China), urethane from Chengdu Kelong Chemical Reagent Factory (Chengdu, China). Compounds **1**–**4** (purity ≥95%) were separated and identified from processed crassicauline A, the structures were verified by ^{1}H NMR, ^{13}C NMR, and HR-ESI-MS.

HPLC-grade acetonitrile was supplied by Fisher Chemical Co. (New Jersey, United States). Ultrapure water was directly obtained from a ULUP-I-10T water purification system (Chengdu, China). The remaining reagents were all of analytical grade. Spots on TLC plates were visualized with Dragendorff's reagent or iodine vapor.

Animals

SPF grade Sprague Dawley rats (male and female) weighing between 180 and 220 g [certificate No. SCXK (CHUAN) 2015-030 and 2020-030] were supplied from Chengdu Dossy experimental animals Co., Ltd. (Chengdu, China) and maintained under a controlled light/dark cycle and temperature (20 ± 2°C), with free access to food and water. They were left for 2 days for acclimatization to animal room conditions. The animal study was reviewed and approved by the Animal Experimentation Ethics Committee of Chengdu University of Traditional Chinese Medicine (permission No. 2020-15).

Screening of Processing Parameters

Chromatographic Conditions

Quantitative analyses were performed with a Shimadzu LC-2030C system (Shimadzu Corporation, Japan), using a Supersil ODS-B C_{18} column (250 × 4.6 mm, 5 μm-Elite, China) maintained at 40°C. The detection wavelength was 260 nm. The mobile phase comprised acetonitrile (A) and 0.03 moL/L NH_4HCO_3 (The aqueous was alkalized to pH 9.5 using 25% NH_4OH, B) with a gradient program of 37% A at 0–40 min, 37–70% A at 40–60 min, and 70% A at 60–85 min. The injection volume was 10 μl and the flow rate was 1 ml/min.

Preparation of Standard Solution

100.60 mg crassicauline A standard was weighed accurately into a 250 ml volumetric flask and dissolved in dichloromethane to make a concentration of 402.4 μg/ml reaction stock solution. 4 ml of the reaction stock solution was added into a 10 ml volumetric flask, with dichloromethane evaporating, 0.1% (v/v) HCl-methanol was added for dissolution to prepare a final concentration of 160.96 μg/ml. The standard solution was filtered with 0.45 μm syringe filter before injection into the HPLC.

Preparation of Processed Product Sample Solution

Twenty-four 100 ml round-bottomed flasks were divided into four temperature groups (120°C, 140°C, 160°C, and 180°C), six reaction time points (1, 5, 10, 20, 30, and 40 min) were set at each temperature. Accurately adding 4 ml of the reaction stock solution into each flask, and the solvent was evaporated. The flasks were subsequently immersed in an oil bath and processing according to set parameters, cooling to room temperature after reaction. The residue was diluted with 0.1% (v/v) HCl-methanol in a 10 ml volumetric flask and subsequently filtered with 0.45 μm syringe filter before injection into the HPLC.

Preparation and Separation of Compounds 1-3

1.83 g crassicauline A was dissolved in a 250 ml round-bottomed flask with a proper amount of dichloromethane, and the solvent was evaporated with a rotary evaporator at 40°C to make crassicauline A uniformly adhere to the inner wall of the flask, and processed in an oil bath at 160°C for 30 min, obtaining a crude residue of crassicauline A (1.65 g) for column chromatography.

The residue obtained was purified over silica gel column chromatography (120 g, 200–300 mesh) and eluted with petroleum ether-acetone-triethylamine 8:1:0.01 (0.4 L), 6:1:0.01 (3 L), and 3:1:0.01 (1.2 L) to furnish three fractions (A-C). Fraction B (1 g) was further separated by preparative TLC on silica gel G (petroleum ether-acetone-triethylamine, 3:3:0.01) to obtain Frs T_1 (*Rf* 0.41), Frs T_2 (*Rf* 0.51), and Frs T_3 (*Rf* 0.77). Frs T_3 was recrystallized from dichloromethane-methanol to generate compound **3** (100 mg). Frs T_1 (200 mg) and Frs T_2 (430 mg) were further purified by preparative HPLC, with the chromatographic condition of acetonitrile −0.03 moL/L NH_4HCO_3 at 42:58 (The aqueous was basified to pH 9.5 using 25% NH_4OH, and the detection wavelength was 260 nm), the collected fractions were evaporated under reduced pressure to no acetonitrile, leaving only the aqueous phase. Following this, the aqueous phase was extracted twice with dichloromethane. The combined extracts were subsequently dried over Na_2SO_4, the solvent was removed in vacuo to obtain compounds **1** (110 mg) and **2** (310 mg).

Preparation and Separation of Compound 4

1.11 g crassicauline A was weighed and processed upon above-mentioned processing method, the processing parameters were set at 180°C for 30 min, to obtain a crude residue of crassicauline A (1 g) for column chromatography.

The residue was subjected to column chromatography (silica gel, 120 g, 200–300 mesh) and eluted with dichloromethane-acetone-methanol-triethylamine 60:2:1:0.01 (5.7 L) and 10:2:1:0.01 (0.8 L) to obtain three fractions (D-F). Fraction D

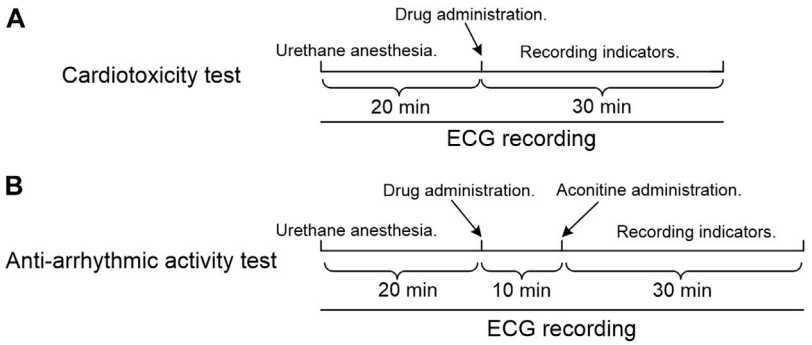

FIGURE 1 | Experimental timeline. **(A)** Cardiotoxicity test; **(B)** Anti-arrhythmic activity test.

(400 mg) was further separated by preparative TLC on silica gel G (petroleum ether-acetone-triethylamine, 2:1:0.01) to generate fraction T_4 (R*f* 0.55), which was recrystallized from petroleum ether-acetone-methanol to afford compound **4** (300 mg).

Electrocardiography

The rats were anesthetized by intraperitoneal (*i.p.*) injection of 20% urethane (1.2 g/kg), with their back fixed and four limbs in subcutaneous penetration of needle-electrodes. Lead II ECGs were recorded after the administration of urethane.

Cardiotoxicity Test

In vivo studies were carried out to assess the cardiotoxicity of crassicauline A and its converted products. 40 rats were equally divided into four groups, five female and five male rats for each group were intravenously injected with the same dose of compounds. Lead II ECGs were recorded for 20 min prior to drug administration, recording the ECG changes within 30 min after administration (**Figure 1**).

Through the preliminary experiment, it was found that 0.10 mg/kg crassicauline A could cause ventricular premature beat (VPB), ventricular tachycardia (VT), and ventricular fibrillation (VF) in rats. Comparing under the same dose, whether the converted products caused arrhythmias can directly reflect the cardiotoxicity pre- and post-processing.

Aconitine-Induced Arrhythmia Test

To further investigate the antiarrhythmic activity of the three converted alkaloids, the testing was performed *in vivo* in 233 rats. The rats were randomly divided into the following 15 groups, a minimum of ten animals were used in each group: the blank solvent group (Take 4 ml of 1% HCl-ethanol solution, dilute it with saline, add 5% NaOH to adjust pH 7, and fixed volume with saline to 100 ml), the control group (Aconitine, 0.03 mg/kg body weight), the positive control groups (Lidocaine, 5.0 mg/kg (Hong et al., 2019) body weight; propafenone, 3.2 mg/kg (Li et al., 2006) body weight), the compound **1** groups (0.05, 0.20, 0.40, and 0.60 mg/kg body weight), the compound **2** groups (0.05, 0.20, 0.30, and 0.40 mg/kg body weight), and the compound **4** groups (0.05, 0.20, and 0.40 mg/kg body weight). The preparation methods of aconitine, positive drugs, and the experimental compounds were the same as the blank solvent. To confirm whether the blank solvent had an influence on rats, the rats of solvent group were only administered the same volume of blank solvent to observe ECG changes during the recording time.

The rats were anesthetized using 20% urethane (1.2 g/kg, *i.p.*) (Bai et al., 2012; Mohamed et al., 2016). Recording the lead II ECGs for 20 min prior to administration, the experimental compounds, positive drugs, and equal volume of saline were subsequently administered *via* the exposed vena femoral, respectively. After stabilization for 10 min (Zhang et al., 2006), aconitine was administered into the uncovered vena femoral at a dosage of 0.03 mg/kg (Bartosová et al., 2005; Klekot, 2006; Bartosova et al., 2007) to establish arrhythmia (**Figure 1**). The onset time of VPB (Qiu et al., 2016) was recorded within 30 min (Sun et al., 2006; Zhang and Xiong, 2015; Qiu et al., 2016) after aconitine. Meanwhile, the VT (Meng et al., 1992; Ma et al., 2018) or arrhythmia (Wang et al., 1997a; Wang et al., 1997b), if any, was recorded for each group at the end of the observation period.

Statistical Analysis

The data obtained were analysed using statistical package for social sciences (SPSS) version 20 software. Experimental data were expressed as mean ± SD or proportion. Descriptive statistics were examined individually. When the data conformed to the normal distribution, the one-way ANOVA would be used for those with homogeneous variance. If the variance was not homogeneous, Tamhane's T2 test would be used for comparison between groups. Comparisons of proportions were made with the Pearson's chi-square (χ^2) test. Statistical significance was set at $p < 0.05$.

RESULTS

Method Validation

Analysis of the peak area of the standard sample resulted from HPLC as well as linear regression ($Y = 21239X\text{-}3038.8$, $r = 0.9996$), the obtained results showed that crassicauline A exhibited satisfactory linearity within the range of 2–200 μg/ml. The LOD and LOQ of crassicauline A under the chromatographic conditions were 0.18 μg/ml and 0.60 μg/ml, respectively.

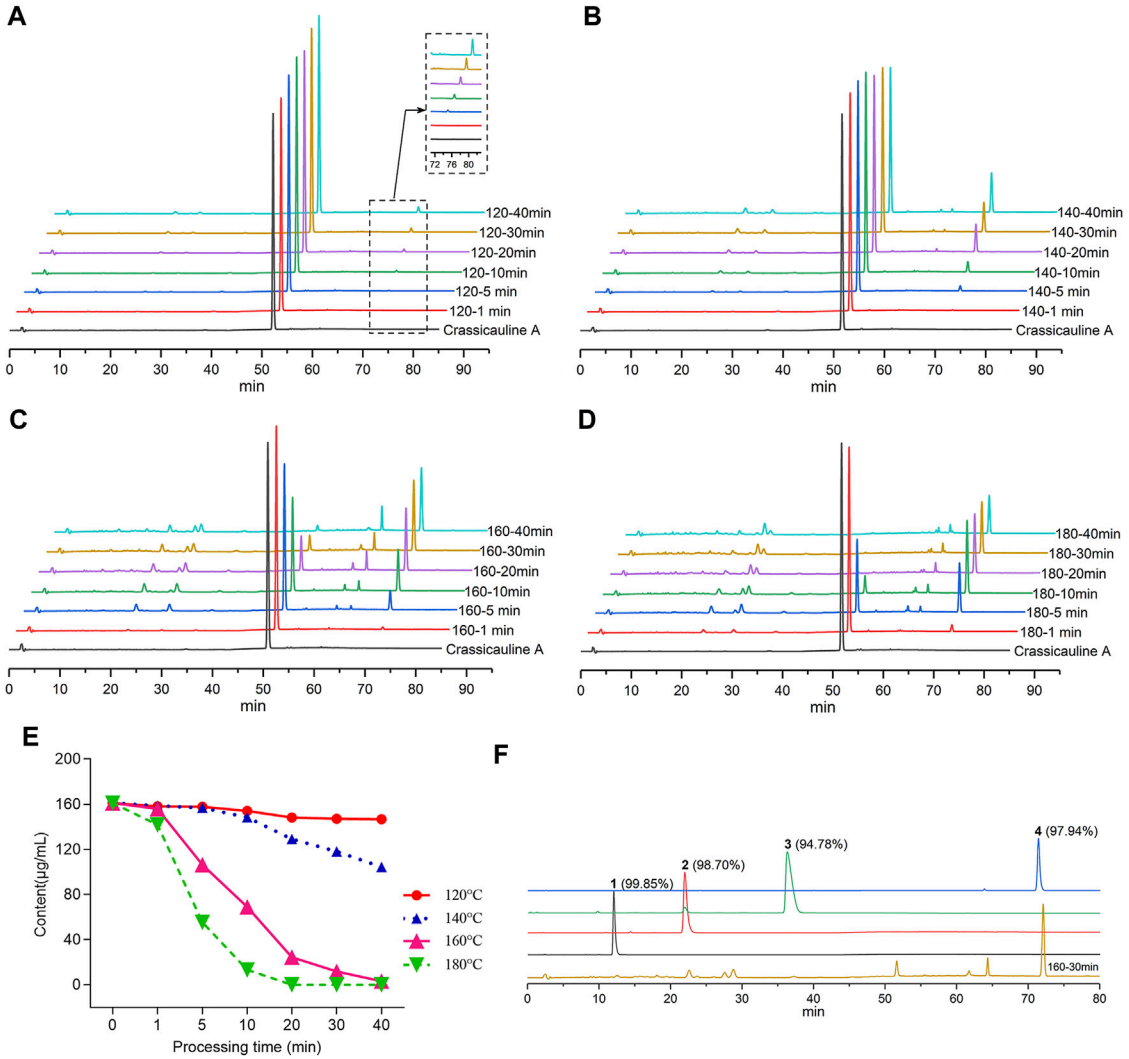

FIGURE 2 | Contents for crassicauline A of different processed products and purity test. **(A–D)** HPLC chromatograms of different carssicauline A processed products. (A: 120°C, B: 140°C, C: 160°C, D: 180 °C). **(E)** Content variety of crassicauline A under different processing temperatures and time. **(F)** Purity of the transformed products.

Precision, stability, and repeatability of the method were additionally verified. During the determination, the RSD values of crassicauline A for the precision, stability, and repeatability were 1.29, 2.33, and 2.69%, respectively, indicating that the established method was precise, stable, and accurate enough for determination.

Temperature and Time for the Structural Transformation of Crassicauline A

To screen out the temperature and time range for the structural transformation of crassicauline A in the sand frying process, the sample solutions, acquired under different processing temperatures and time, along with the standard solutions, were injected into the HPLC, respectively. The chromatograms were obtained after determination, which could visually reflect the dynamic change of crassicauline A. The chromatograms are shown in **Figures 2A–D**.

In light of the above experimental findings (**Figures 2A–E**), it could be found that the content of crassicauline A before processing was 160.96 μg/ml. When crassicauline A was processed at 140–180°C, with the elevation of temperature and prolongation of processing time, the content of crassicauline A decreased. For instance, the content of crassicauline A was 69.07 μg/ml after being processed for 10 min at 160°C and continuously dropped to 24.42 μg/ml for 20 min. When processed at 180°C for 5 min, the content decreased to 55.47 μg/ml, even declined to 0 μg/ml for another 15 min. Meanwhile, some unknown chromatographic peaks emerged in chromatograms. As a result, the quantity and content of the above transformed products were increased obviously when processed at 160°C for 30 min. Therefore, in this paper, the

TABLE 1 | ^{1}H (600 MHz) and ^{13}C (150 MHz) NMR data for compound **1** ($CDCl_3$).

Position	δ_H (*J* in Hz)	δ_C, type	HMBC	NOESY	^{1}H-^{1}H COSY
1	3.05 m	85.1, CH	C-10, C-17, 1-OCH_3	H-3β, H-10, 1-OCH_3	H-2α, β
2α	2.29 m	25.9, CH_2	—	—	H-1, H-2β, H-3α, β
2β	1.91 m		—	—	H-1, H-2α, H-3α, β
3α	1.70 m	34.7, CH_2	—	H-18α, β	H-2α, β, H-3β
3β	1.58 m		C-19	H-1, H-5	H-2α, β, H-3α
4	—	39.4, C	—	—	—
5	2.07 d (6.6)	49.1, CH	C-7, C-10, C-17, C-19	H-3β, H-18β	H-6
6	4.19 d (6.6)	81.7, CH	C-4, C-8, C-17, 6-OCH_3	H-9, 6-OCH_3	H-5, H-7
7	2.11 s	49.1, CH	C-11, C-15	H-15, 6-OCH_3	H-6
8	—	73.9, C	—	—	—
9	2.55 m	47.0, CH	C-12, C-13, C-15	H-6	H-10, H-14
10	2.17 m	42.7, CH	C-8, C-17	H-1, H-14	H-9, H-12α, β
11	—	50.2, C	—	—	—
12α	3.02 m	40.9, CH_2	C-11, C-14, C-16	—	H-10, H-12β
12β	1.96 m		C-9, C-16	H-14	H-10, H-12α
13	—	76.9, C	—	—	—
14	5.17 d (5.1)	80.3, CH	C-8, C-16, ArC = O	H-10, H-12β	H-9
15	5.61 d (9.54)	130.1, CH	C-9, C-13	H-7, H-17	H-16
16	5.91 d (9.54)	134.8, CH	C-8	H-17	H-15
17	3.07 s	62.6, CH	C-6, C-8, C-10, C-19	H-15, H-16, H-21, H-22	—
18α	3.29 d (8.46)	80.6, CH_2	C-3, C-5, C-19, 18-OCH_3	H-3α, H-5, H-19α, β, 18-OCH_3	H-18β
18β	3.72 d (8.46)		C-3, C-19, 18-OCH_3	H-5, H-19β, 18-OCH_3	H-18α
19α	2.58 m	54.2, CH_2	C-3, C-5, C-17	H-18α	H-19β
19β	2.65 m		C-3	H-18α, β	H-19α
21α	2.51 m	49.3, CH_2	—	H-17	H-22
21β	2.59 m		—	H-17	H-22
22	1.06 t (7.32)	13.3, CH_3	—	H-17	H-21α, β
1-OCH_3	3.24 s	56.2, CH_3	C-1	H-1	—
6-OCH_3	3.30 s	57.6, CH_3	C-6	H-6, H-7	—
18-OCH_3	3.32 s	59.2, CH_3	C-18	H-18α, β	—
ArC = O	—	167.1, C	—	—	—
1′	—	121.6, C	—	—	—
2′, 6′	7.90 d (8.82)	131.7, CH	C-4′, ArC = O	—	H-3′, 5′
3′, 5′	6.92 d (8.82)	114.0, CH	C-1′	4′-OCH_3	H-2′, 6′
4′	—	163.9, C	—	—	—
4′-OCH_3	3.85 s	55.5, CH_3	C-4′	H-3′, 5′	—

processed products were prepared based on above processing parameters.

Structural Identification of Converted Products

Compounds **1**-**4** were subsequently isolated from processed crassicauline A by procedures described in the experimental section, and the purity of converted products was determined by re-injected into the HPLC (**Figure 2F**).

16-demethoxy-$\Delta^{15(16)}$-8-deacetylcrassicauline A (**1**) was isolated as an amorphous powder, $[\alpha]_D^{20}$ + 47.1°(*c* = 0.92, CH_3OH). It showed a positive reaction with Dragendorff's reagent. Its molecular formula was deduced to be $C_{32}H_{43}NO_8$ from a protonated molecule ion at *m/z* 570.3052 $(M + H)^+$ (calcd. 570.3061) in its HR-ESI-MS. The NMR spectra (**Table 1**) of compound **1** showed the presence of an *N*-ethyl group (δ_H 1.06, 3H, t, *J* = 7.32 Hz; δ_H 2.51, 2.59, each 1H, m; δ_C 13.3 q, 49.3 t), three methoxyl groups (δ_H 3.24, 3.30, 3.32, each 3H, s; δ_C 56.2 q, 57.6 q, 59.2 q), one *p*-methoxyl benzoyloxy group (δ_H 6.92, 7.90, each 2H, AA'BB' system, *J* = 8.82 Hz; 3.85, 3H, s; δ_C 167.1 s, 121.6 s, 131.7 d (2C), 114.0 d (2C), 163.9 s, 55.5 q), as well as four quaternary carbons (δ_C 39.4, 50.2, 73.9, 76.9). The aforementioned NMR features suggested an aconitine-type alkaloid for compound **1** (Pelletier et al., 1984). The ^{1}H-doublet signal at δ_H 5.17 (*J* = 5.1 Hz) was assigned to H-14β (Pelletier and Joshi, 1991; Gao et al., 2006), resulting in location of the *p*-methoxyl benzoyloxy group to C-14. Three methoxyl groups were attributed to C-1, C-6, and C-18 based on the cross-peaks between 1-OCH_3 (δ_H 3.24) and C-1, 6-OCH_3 (δ_H 3.30) and C-6, 18-OCH_3 (δ_H 3.32) and C-18 in its HMBC spectrum (**Figure 3**). Two hydroxyl groups were assigned to C-8 and C-13 based on the correlations between the C-8 and H-6, H-10, H-14, H-16, H-17, as well as C-13 and H-9, H-15 in the HMBC of **1**. The ^{1}H NMR signals at δ 5.61 (1H, d, *J* = 9.54 Hz, H-15), δ 5.91 (1H, d, *J* = 9.54 Hz, H-16), and the ^{13}C NMR signals at δ 130.1 and 134.8 indicated the existence of a disubstituted double bond in the molecule (Yue et al., 1994a; Yue et al., 1994b; Desai et al., 1998). Also, long-range correlations between C-13 and H-15, C-8 and H-16 confirmed the presence of a double bond between C-15 and C-16. In addition, the coupling constant between H-15 and H-16 was 9.54 Hz, suggesting that the two

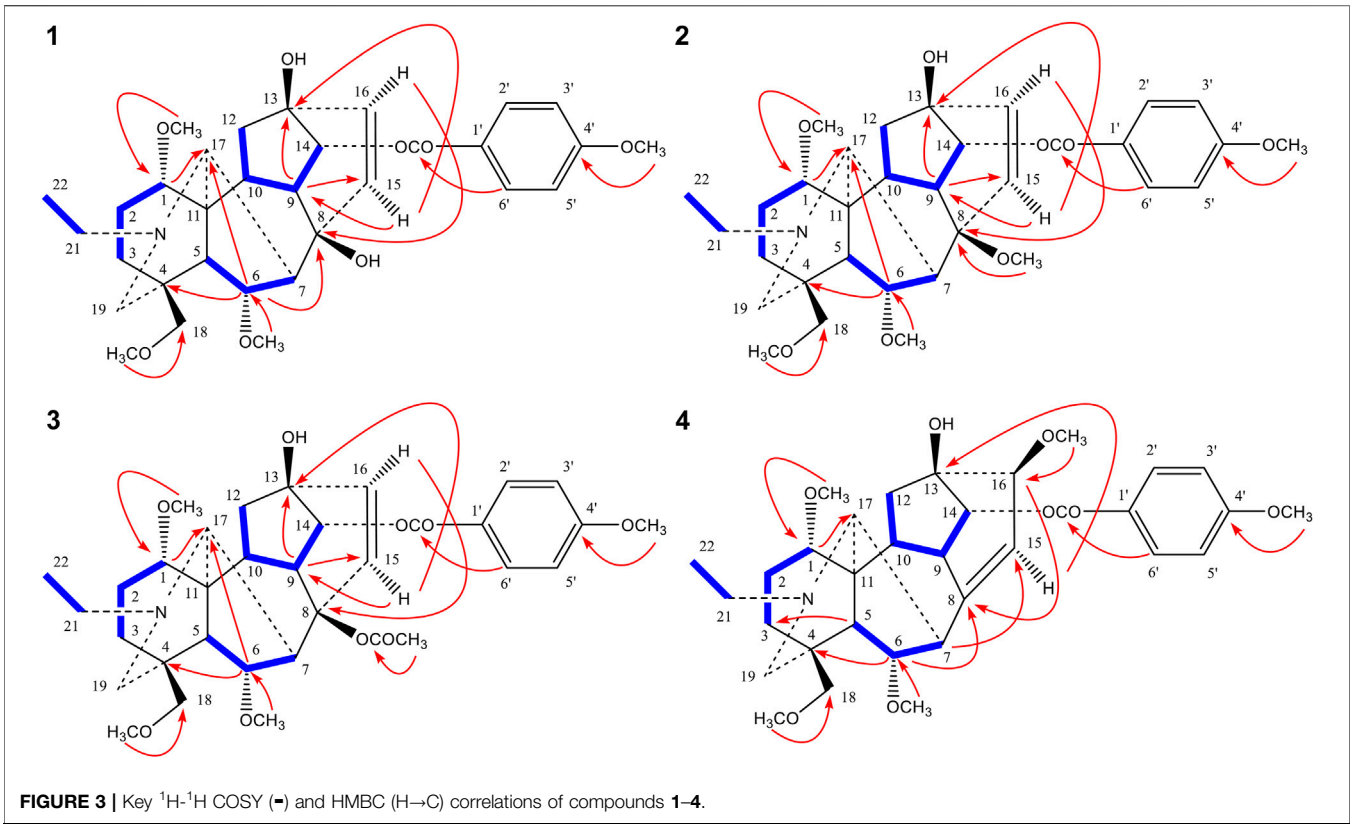

FIGURE 3 | Key ^{1}H-^{1}H COSY (▬) and HMBC (H→C) correlations of compounds **1**–**4**.

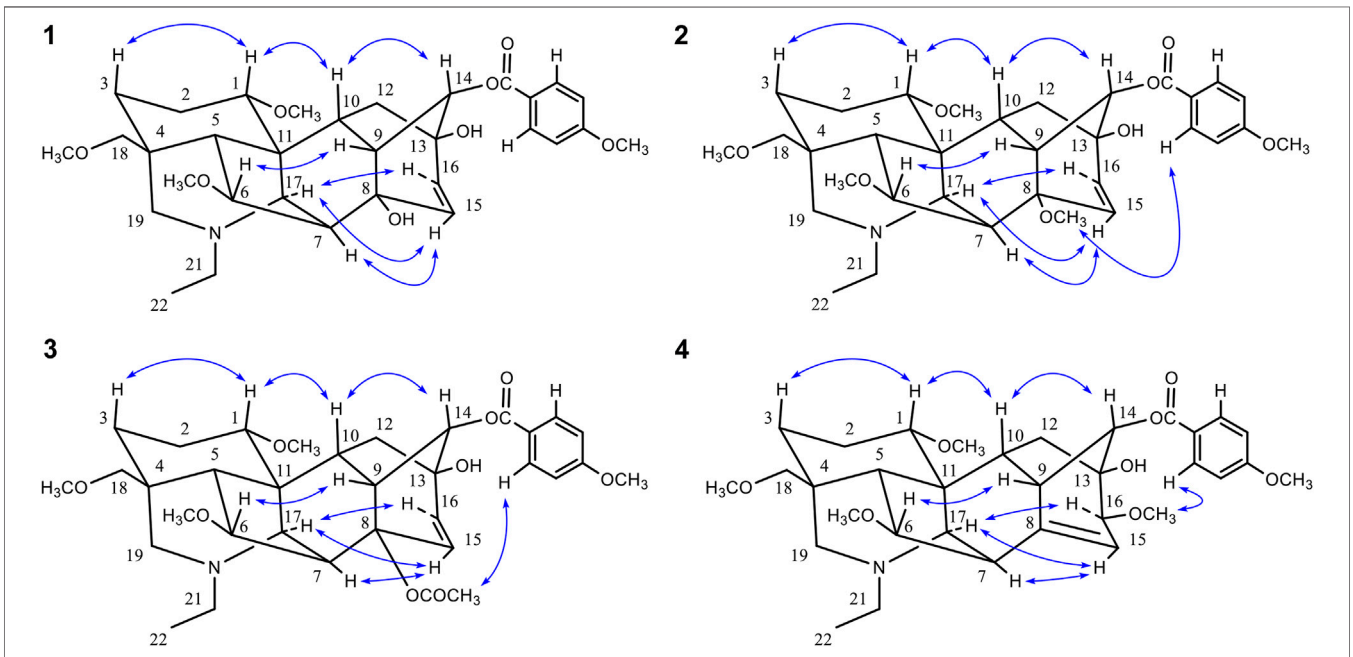

FIGURE 4 | Key NOE correlations (H↔H) of compounds **1**–**4**.

hydrogen atoms were CIS structures. The key NOE correlations (**Figure 4**) between H-15 and H-17, H-16 and H-17 also confirmed the configuration of H-15 and H-16 in **1** was α-orientation. The NMR spectra of compound **1** lacked a methoxyl group at C-16, when compared with crassicauline A (Chen et al., 2002), and the ^{13}C NMR spectra of **1** clearly showed

TABLE 2 | ^{1}H (600 MHz) and ^{13}C (150 MHz) NMR data for compound **2** ($CDCl_3$).

Position	δ_H (*J* in Hz)	δ_C, type	HMBC	NOESY	^{1}H-^{1}H COSY
1	3.03 m	85.3, CH	C-10, C-17, 1-OCH_3	H-3β, H-10, 1-OCH_3	H-2α, β
2α	2.27 m	26.1, CH_2	—	—	H-1, H-2β, H-3α, β
2β	1.93 m		—	—	H-1, H-2α, H-3α, β
3α	1.70 m	34.7, CH_2	—	H-18α	H-2α,β, H-3β
3β	1.59 m		C-19	H-1, H-5	H-2α,β, H-3α
4	—	39.3, C	—	—	—
5	2.03 d (6.6)	48.8, CH	C-7, C-10, C-17, C-18, C-19	H-3β, H-18α, β	H-6
6	4.10 d (6.6)	82.1, CH	C-4, C-8, C-17, 6-OCH_3	H-9, 6-OCH_3	H-5, H-7
7	2.32 s	44.6, CH	C-9, C-11, C-15	H-15, 6-OCH_3	H-6
8	—	76.9, C	—	—	—
9	2.63 m	45.7, CH	C-12, C-13, C-15	H-6	H-10, H-14
10	2.15 m	42.6, CH	C-8, C-17	H-1, H-14	H-9, H-12α, β
11	—	50.3, C	—	—	—
12α	2.99 m	40.1, CH_2	C-11, C-14, C-16	—	H-10, H-12β
12β	1.89 m		C-9, C-11, C-16	H-14	H-10, H-12α
13	—	76.9, C	—	—	—
14	4.95 d (4.08)	78.6, CH	C-8, C-16, ArC = O	H-10, H-12β	H-9
15	5.80 d (9.9)	125.2, CH	C-9, C-13	H-7, H-17, 8-OCH_3	H-16
16	6.03 d (9.9)	137.2, CH	C-8	H-17	H-15
17	2.96 s	62.4, CH	C-5, C-6, C-8, C-10, C-19	H-15, H-16, H-21, H-22	—
18α	3.29 d (8.76)	80.5, CH_2	C-3, C-5, C-19, 18-OCH_3	H-3α, H-5, H-19α, β, 18-OCH_3	H-18β
18β	3.65 d (8.76)		C-3, C-19, 18-OCH_3	H-5, H-19β, 18-OCH_3	H-18α
19α	2.56 m	54.1, CH_2	C-3, C-5, C-17	H-18α	H-19β
19β	2.62 m		C-3	H-18α,β	H-19α
21α	2.49 m	49.2, CH_2	—	H-17	H-22
21β	2.54 m		—	H-17	H-22
22	1.05 t (7.38)	13.3, CH_3	—	H-17	H-21α, β
1-OCH_3	3.23 s	56.2, CH_3	C-1	H-1	—
6-OCH_3	3.26 s	57.8, CH_3	C-6	H-6, H-7	—
8-OCH_3	3.12 s	49.1, CH_3	C-8	H-15, H-2′, 6′	—
18-OCH_3	3.29 s	59.2, CH_3	C-18	H-18α, β	—
ArC = O	—	167.3 C	—	—	—
1′	—	122.7, C	—	—	—
2′, 6′	7.98 d (8.82)	131.9, CH	C-4′, ArC = O	8-OCH_3	H-3′, 5′
3′, 5′	6.89 d (8.82)	113.5, CH	C-1′	4′-OCH_3	H-2′, 6′
4′	—	163.4, C	—	—	—
4′-OCH_3	3.84 s	55.4, CH_3	C-4′	H-3′, 5′	—

changes in the chemical shifts of C-8, C-15, and C-16 due to the absence of an acetoxyl group and the presence of a double bond. Except for these points, the ^{13}C NMR spectra of the two alkaloids were very similar. From these deductions, the structure of compound **1** was assigned as 16-demethoxy-$\Delta^{15(16)}$-8-deacetylcrassicauline A, a new diterpenoid alkaloid (**Supplementary Figures S1–S13**).

16-demethoxy-$\Delta^{15(16)}$-8-*O*-methylcrassicauline A (**2**) was isolated as a white amorphous powder, $[\alpha]_D^{20}$ + 61.5°(*c* = 0.78, CH_3OH). Its molecular formula $C_{33}H_{45}NO_8$ was derived from the HR-ESI-MS spectral data: *m/z* 584.3203 $(M + H)^+$ (cacld. 584.3218). ^{1}H- and ^{13}C-NMR spectra of **2** (**Table 2**) showed the distinct NMR features of an aconitine-type C_{19}-diterpenoid alkaloid skeleton (Pelletier et al., 1984), bearing an *N*-ethyl group (δ_H 1.05, 3H, t, *J* = 7.38 Hz; δ_H 2.49, 2.54, each 1H, m; δ_C 13.3 q, 49.2 t), four methoxyl groups (δ_H 3.12, 3.23, 3.26, 3.29, each 3H, s; δ_C 49.1 q, 56.2 q, 57.8 q, 59.2 q), a disubstituted double bond (δ_H 5.80, 1H, d, *J* = 9.9 Hz; δ_H 6.03, 1H, d, *J* = 9.9 Hz), and a *p*-methoxyl benzoyloxy group (δ_H 6.89, 7.98, each 2H, AA'BB' system, *J* = 8.82 Hz; 3.84, 3H, s; δ_C 167.3 s, 122.7 s, 131.9 d (2C), 113.5 d (2C), 163.4 s, 55.4 q). The ^{1}H-doublet signal at δ_H 4.95 (*J* = 4.08 Hz) was assigned to H-14β (Pelletier and Joshi, 1991; Gao et al., 2006), resulting in location of the *p*-methoxyl benzoyloxy group to C-14. Four methoxyl groups were assigned to C-1, C-6, C-8, C-18 due to the long-range correlations between 1-OCH_3 (δ_H 3.23) and C-1, 6-OCH_3 (δ_H 3.26) and C-6, 8-OCH_3 (δ_H 3.12) and C-8, 18-OCH_3 (δ_H 3.29) and C-18 in the HMBC spectrum of **2** (**Figure 3**). A remaining hydroxyl group was assigned to C-13 based on the correlations between the C-13 and H-9, H-15 in the HMBC of **2**. Also, the presence of a double bond between C-15 and C-16 could be corroborated by the HMBC correlations (**Figure 3**) from H-15 to C-13 and from H-16 to C-8 (Yue et al., 1994a; Yue et al., 1994b; Desai et al., 1998). The NOE correlations (**Figure 4**) could be observed between H-15 and H-17, H-16 and H-17 in compound **2**. As a result, the configuration of H-15 and H-16 in compound **2** was unambiguously established to have an α-orientation.

Comparison of the NMR spectra of **2** with that of crassicauline A (Chen et al., 2002), it was showed that compound **2** bore a

TABLE 3 | ^{1}H (600 MHz) and ^{13}C (150 MHz) NMR data for compound **3** ($CDCl_3$).

Position	δ_H (*J* in Hz)	δ_C, type	HMBC	NOESY	^{1}H-^{1}H COSY
1	3.09 m	85.1, CH	1-OCH_3	H-3β, H-10, 1-OCH_3	H-2α, β
2α	2.27 m	26.2, CH_2	—	—	H-1, H-2β, H-3α, β
2β	1.93 m		—	—	H-1, H-2α, H-3α, β
3α	1.70 m	35.1, CH_2	—	H-18α	H-2α, β, H-3β
3β	1.65 m		—	H-1, H-5	H-2α, β, H-3α
4	—	39.3, C	—	—	—
5	2.09 d (6.6)	45.5, CH	—	H-3β, H-18α, β	H-6
6	4.10 d (6.6)	82.3, CH	C-4, C-8, C-17, 6-OCH_3	H-9, 6-OCH_3	H-5, H-7
7	3.00 brs	45.5, CH	C-9, C-11, C-15	H-15, 6-OCH_3	H-6
8	—	83.7, C	—	—	—
9	2.92 m	44.4, CH	C-12, C-13, C-15	H-6	H-10, H-14
10	2.20 m	42.1, CH	—	H-1, H-14	H-9, H-12
11	—	49.9, C	—	—	—
12α	3.06 m	39.3, CH_2	C-11	—	H-10, H-12β
12β	1.89 m		—	H-14	H-10, H-12α
13	—	76.2, C	—	—	—
14	4.92 d (4.8)	77.9, CH	C-8, C-16, ArC = O	H-10, H-12β	H-9
15	6.53 d (9.9)	125.4, CH	C-9, C-13	H-7, H-17	H-16
16	6.05 d (9.9)	137.3, CH	C-8	H-17	H-15
17	3.03 brs	62.8, CH	C-6, C-8, C-11	H-15, H-16, H-21, H-22	—
18α	3.26 d (8.82)	80.5, CH_2	C-3, 18-OCH_3	H-3α, H-5, H-19α, β, 18-OCH_3	H-18β
18β	3.65 d (8.82)		C-3, C-19, 18-OCH_3	H-5, H-19β, 18-OCH_3	H-18α
19α	2.52 m	53.8, CH_2	—	H-18α	H-19β
19β	2.56 m		—	H-18α, β	H-19α
21α	2.50 m	49.3, CH_2	—	H-17	H-22
21β	2.53 m		—	H-17	H-22
22	1.05 brs	13.3, CH_3	—	H-17	H-21α, β
1-OCH_3	3.24 s	56.1, CH_3	C-1	H-1	—
6-OCH_3	3.15 s	57.4, CH_3	C-6	H-6, H-7	—
18-OCH_3	3.27 s	59.2, CH_3	C-18	H-18α, β	—
8-C=O	—	169.6, C	—	—	—
CH_3	1.39 s	21.8, CH_3	8-C=O	H-2′, 6′	—
ArC = O	—	166.6, C	—	—	—
1′	—	122.4, C	—	—	—
2′, 6′	7.94 d (6.96)	131.7, CH	C-4′, ArC = O	8-CO-CH_3	H-3′, 5′
3′, 5′	6.88 d (6.96)	113.7, CH	C-1′, C-4′	4′-OCH_3	H-2′, 6′
4′	—	163.6, C	—	—	—
4′-OCH_3	3.85 s	55.4, CH_3	C-4′	H-3′, 5′	—

methoxyl group at C-8 instead of an acetoxyl group, except for the absence of a methoxyl group at C-16 and the induction of a double bond at C-15 and C-16. Compound **2** exhibited nearly identical ^{1}H and ^{13}C NMR resonances to those of **1**, and the distinction between the two sets of spectra was demonstrated by the presence of an additional methoxyl group at C-8 in **2** instead of a hydroxyl group in **1**. All of the above arguments determined the structure of **2** as 16-demethoxy-$\Delta^{15(16)}$-8-*O*-methylcrassicauline A, a new diterpenoid alkaloid (**Supplementary Figures S14–S26**).

16-demethoxy-$\Delta^{15(16)}$-crassicauline A (**3**) was obtained as colorless needles, mp 155–157°C, $[\alpha]_D^{20}$ + 25.4°(*c* = 0.80, CH_3OH). A protonated molecular ion at *m/z* 612.3163 $(M + H)^+$ (cacld. 612.3121) in the HR-ESI-MS spectrum suggested a molecular formula of $C_{34}H_{46}NO_9$. Compound **3** exhibited characteristic NMR features (**Table 3**) of an aconitine-type alkaloid (Pelletier et al., 1984), bearing an *N*-ethyl group (δ_H 1.05, brs, 3H; δ_H 2.50, 2.53, each 1H, m; δ_C 13.3 q, 49.3 t), three methoxyl groups (δ_H 3.15, 3.24, 3.27, each 3H, s; δ_C 57.4 q, 56.1 q, 59.2 q), an acetoxyl group (δ_H 1.39, 3H, s; δ_C 169.6 s, 21.8 q) (Joshi et al., 1987), as well as a *p*-methoxyl benzoyloxy group (δ_H 6.88, 7.94, each 2H, AA'BB' system, *J* = 6.96 Hz; 3.85, 3H, s; δ_C 166.6 s, 122.4 s, 131.7 d (2C), 113.7 d (2C), 163.6 s, 55.4 q). The one-proton double signal (*J* = 4.8 Hz) at δ_H 4.92 was attributed to H-14β (Pelletier and Joshi, 1991; Gao et al., 2006), implying the appearance of *p*-methoxyl benzoyloxy group at C-14 position. The location of three methoxyl groups was based on the long-range correlations between 1-OCH_3 (δ_H 3.24) and C-1, 6-OCH_3 (δ_H 3.15) and C-6, 18-OCH_3 (δ_H 3.27) and C-18 in HMBC spectrum (**Figure 3**). Furthermore, a hydroxyl group was assigned to C-13 based on the correlations between the C-13 and H-9, H-15 in the HMBC of **3**. The ^{13}C-NMR signals at δ 125.4 and 137.3 showed that a disubstituted double bond was located at C-15 and C-16. The ^{1}H-NMR signal at δ 6.53 (1H, d, *J* = 9.9 Hz, H-15) and δ 6.05 (1H, d, *J* = 9.9 Hz, H-16) also confirmed this deduction (Yue et al., 1994a; Yue et al., 1994b; Desai et al., 1998).

Comparison of the NMR data of **3** with crassicauline A (Chen et al., 2002) showed that except a disubstituted double bond, compound **3** lacked a methoxyl group at C-16. The NMR spectra

of compound **3** were also similar to those of **1** and **2** except for the substituents at C-8. The C-8 substituents of **1** and **2** were hydroxyl group and methoxyl group, respectively, while **3** was acetoxyl group. The key NOE correlations (**Figure 4**) could be observed between 8-OAc and H-2′, 6′ in compound **3**. Therefore, the configuration of 8-OAc in **3** was unambiguously established to have a β-orientation. Thus, the structure of **3** was elucidated 16-demethoxy-$\Delta^{15(16)}$-crassicauline A, a new diterpenoid alkaloid (**Supplementary Figures S27–S39**).

Pyrocrassicauline A (**4**) was obtained as colorless needles, mp 129–131°C, $[\alpha]_D^{20}$ + 182.4°(c = 0.81, CH_3OH). Its molecular formula, determined to be $C_{33}H_{45}NO_8$, was derived from HR-ESI-MS: m/z 584.3222 $(M + H)^+$ (calcd. 584.3218). ^1H and ^{13}C NMR spectra of **4** (**Supplementary Table S1**) showed the distinct NMR features of an aconitine-type C_{19}-diterpenoid alkaloid skeleton (Pelletier et al., 1984), bearing an *N*-ethyl group (δ_H 1.07, 3H, t, J = 7.2 Hz; δ_H 2.54, 2.66, each 1H, m; δ_C 13.6 q, 49.9 t), four methoxyl groups (δ_H 3.24, 3.28, 3.30, 3.38, each 3H, s; δ_C 56.4 q, 58.2 q, 59.3 q, 57.2 q), and a *p*-methoxyl benzoyloxy group (δ_H 6.88, 7.99, each 2H, AA'BB' system, J = 8.4 Hz; 3.84, 3H, s; δ_C 167.9 s, 122.9 s, 132.0 d (2C), 113.5 d (2C), 163.3 s, 55.4 q). The one-proton double signal (J = 3.0 Hz) at δ_H 4.93 was attributed to H-14β (Pelletier and Joshi, 1991; Gao et al., 2006), implying the appearance of a *p*-methoxyl benzoyloxy group at C-14. Four methoxyl groups were assigned to C-1, C-6, C-16, C-18 due to the long-range correlations between 1-OCH_3 (δ_H 3.24) and C-1, 6-OCH_3 (δ_H 3.28) and C-6, 16-OCH_3 (δ_H 3.38) and C-16, 18-OCH_3 (δ_H 3.30) and C-18 in the HMBC spectrum of **4** (**Figure 3**). Along with the above-mentioned signals, its ^{13}C NMR displayed eight oxygenated carbon signals, suggesting that compound **4** possessed an additional hydroxyl group, which could be located at C-13 due to the HMBC correlations between the C-13 and H-15 of **4**. Furthermore, the ^{13}C NMR signals at δ 146.9 and 116.0 showed that a trisubstituted double bond was located at C-8 and C-15. The ^1H NMR signal at δ 5.53 (1H, d, J = 6.0 Hz, H-15) also confirmed this deduction (Wang et al., 2009). The configuration of 16-OCH_3 in **4** was also determined to have a β-orientation according to the key NOE correlations between 16-OCH_3 and H-2′, 6′ (**Figure 4**). The ^{13}C NMR spectra of **4** and crassicauline A were very similar except for the chemical shifts of C-8, C-15 signal appeared at low field, caused by the absence of an acetoxyl group and the presence of a double bond (Yue et al., 1994a; Yue et al., 1994b; Desai et al., 1998; Chen et al., 2002). All of the above arguments determined the structure of **4** as pyrocrassicauline A (**Supplementary Figures S40–S53**).

Cardiotoxicity Assays

Intravenous injection of 0.10 mg/kg crassicauline A caused arrhythmias in normal rats, such as VPB, VT, and VF, accompanied by regular chest twitching and convulsions. The incubation period of crassicauline A induced arrhythmia was (182.8 ± 84.58) s. In contrast, the three converted products did not exhibit arrhythmias and behavioral manifestations under the same dose. Through this comparative experiment, it could be concluded that the cardiotoxicity was reduced after processing (**Table 4**; **Supplementary Figure S54**).

Effects of Converted Products on VPB Incubation Period

VPB is the initial manifestation of aconitine-induced arrhythmia model rats, and the ECG of VPB is characterized by premature and bizarrely shaped QRS complexes that appear wide on the ECG, these complexes are not preceded by a P wave, and a T wave is usually oriented in a direction opposite the major deflection of the QRS (Casas et al., 2018; Bae and Kwon, 2019). VPB incubation period refers to the time after the administration of aconitine to the first occurrence of VPB (Qiu et al., 2016). The length of VPB incubation period can reflect the antiarrhythmic effect of the experimental compounds, the longer the incubation period is, the better the antiarrhythmic effect is.

In the control group, the typical characteristic ECGs of VPB and VT occurred successively following the injection of aconitine, even VF occurred in parts of the rats, and lasted for more than 30 min, suggesting that the arrhythmia model was successfully replicated. The VPB incubation period of the control group was (116.5 ± 36.4) s, lidocaine and propafenone groups were (280.3 ± 128.7) s and (193.3 ± 39.9) s, respectively. Two positive drugs had a significant difference in comparison with the control group ($p < 0.05$).

The effects of compounds **1**, **2**, and **4** on VPB incubation period in rats are shown in **Table 5**; **Figure 5**. Compared with the control group, different dose groups of compound **1** (0.20, 0.40, and 0.60 mg/kg) significantly delayed the emerge of VPB ($p < 0.05$, **Figure 5A**). The VPB incubation periods in 0.40 and 0.60 mg/kg groups were (493.7 ± 148.7) s and (547.3 ± 241.8) s, respectively. They were significantly different from propafenone ($p < 0.05$). Similarly, there was a significant difference between 0.40 mg/kg group and lidocaine group ($p < 0.05$), indicating that a 0.40 mg/kg or more intravenous dose of compound **1** exhibited a marked activity relative to positive drugs.

As mentioned above, the differentiation between compounds **1** and **2** is the substituents at C-8 position. To explore the effects of these structural distinctions, the antiarrhythmic effect of compound **2** was further evaluated. In comparison with the control group, different dose groups of compound **2** (0.20, 0.30, and 0.40 mg/kg) had a significant delay on the VPB incubation period ($p < 0.05$, **Figure 5B**). The VPB incubation periods in 0.20, 0.30, and 0.40 mg/kg groups were (441.4 ± 202.3) s, (800.5 ± 353.2) s, and (920.5 ± 358.1) s, respectively, which were significantly different from propafenone ($p < 0.05$). Compared with lidocaine, 0.30 and 0.40 mg/kg groups had significant difference ($p < 0.05$). It was demonstrated that a 0.30 mg/kg or more dose of compound **2** exhibited superior antiarrhythmic activity relative to compound **1** and the positive drugs.

On the contrary, compound **3**, bearing two ester bonds at C-8 and C-14, belonging to DDAs, may exert relatively strong toxicity (Gong, 2005). Consequently, its antiarrhythmic activity was not investigated. Different from compounds **1** and **2**, the double bond of compound **4** is located at C-8/C-15 rather than C-15/C-16. To exemplify different positions of double bonds on the strength of the antiarrhythmic efficacy, we further investigated the antiarrhythmic effect of compound **4**. Different dose groups of compound **4** (0.20 and 0.40 mg/kg) significantly delayed the

TABLE 4 | Comparison of cardiotoxicity between crassicauline A and its converted products.

Compound	Dose (mg/kg)	VPB incubation period (s)	VT incidence (%)
Crassicauline A	0.10	182.8 ± 84.58	100
Compound **1**	0.10	—	0
Compound **2**	0.10	—	0
Compound **4**	0.10	—	0

"—"means that no arrhythmia occurred within 30 min after the administration of experimental compound. Data are expressed as mean ± S.D. (n = 10).

TABLE 5 | Effects of different compounds on VPB incubation period.

Group	Dose (mg/kg)	Number (with arrhythmia/total number)	VPB incubation period (s)
Control	—	10/10	116.5 ± 36.4
Lidocaine	5.0	12/21	280.3 ± 128.7*
Propafenone	3.2	10/10	193.3 ± 39.9*
Compound **1**	0.05	10/10	199.4 ± 79.7
	0.20	11/12	202 ± 56.4*
	0.40	10/13	493.7 ± 148.7*+#
	0.60	11/25	547.3 ± 241.8*#
Compound **2**	0.05	11/11	168.4 ± 74.0
	0.20	11/13	441.4 ± 202.3*#
	0.30	10/22	800.5 ± 353.2*+#
	0.40	10/28	920.5 ± 358.1*+#
Compound **4**	0.05	10/10	201.0 ± 84.9
	0.20	11/13	377.8 ± 184.0*
	0.40	19/25	382.9 ± 146.5*#

*Data are presented as mean ± S.D. *$p < 0.05$ compared with control group, +$p < 0.05$ compared with the lidocaine group, #$p < 0.05$ compared with the propafenone group.*

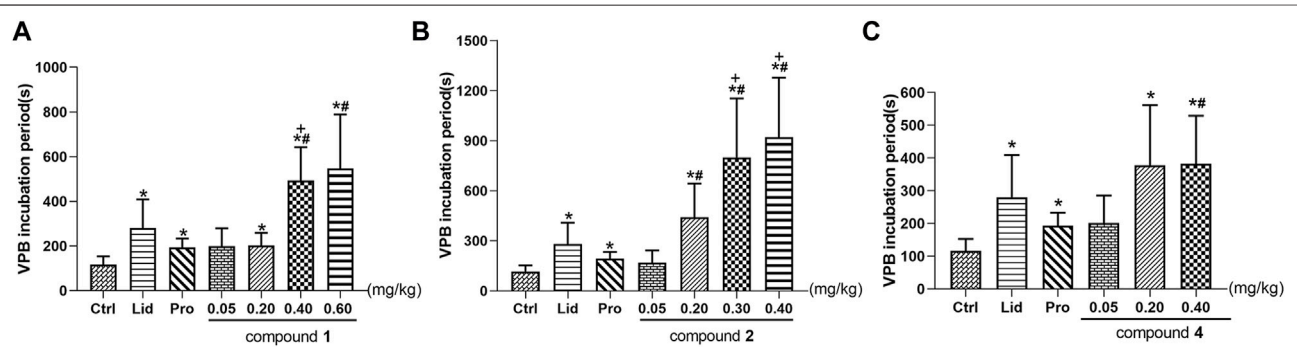

FIGURE 5 | Effects of different experimental compounds on VPB incubation period **(A)**: compound **1**; **(B)**: compound **2**; **(C)**: compound **3**. Data are presented as mean ± SD. *$p < 0.05$ compared with control group, +$p < 0.05$ compared with the lidocaine group, #$p < 0.05$ compared with the propafenone group. Ctrl, the control group. Lid, lidocaine; Pro, propafenone.

onset time of VPB compared with the control group ($p < 0.05$, **Figure 5C**). The incubation period of VPB was (382.9 ± 146.5) s in the 0.40 mg/kg group, and it was significantly different from propafenone ($p < 0.05$), but showed an equivalent effect relative to lidocaine ($p > 0.05$).

In summary, within their own dose ranges, compounds **1**, **2**, and **4** could delay the onset time of VPB in a dose-dependent manner. Additionally, at the dose of 0.40 mg/kg, the VPB incubation periods were compound **2** >compound **1** >compound **4**, indicating that compound **2** had the best antiarrhythmic effect among these compounds.

Effects of Converted Products on Incidence of VT

VT is the result of further progression of VPB, as well as an established risk factor for sudden cardiac death (Batiste et al., 2019). The ECGs of VT are characterized by three or more consecutive beats of apparent ventricular origin, the QRS complexes are wide and deformed, without constant P wave (Swerdlow et al., 1983; Baldzizhar et al., 2016; Brady et al., 2017). The incidence of VT can be used to evaluate whether the experimental compound can effectively prevent the progress of VPB, the lower the occurrence is, the better the efficacy is.

TABLE 6 | Chi-square analysis of the incidence of VT among different dose groups.

Compound	Dose (mg/kg)	VT (frequency)	Without VT (frequency)	χ^2	*p*
Compound **1**	0.05–0.20	18	3	14.704	0.001
	0.40	6	4		
	0.60	2	9		
Compound **2**	0.05	9	2	13.000	0.002
	0.20–0.30	13	8		
	0.40	1	9		
Compound **4**	0.05–0.20	18	3	10.165	0.001
	0.40	7	12		

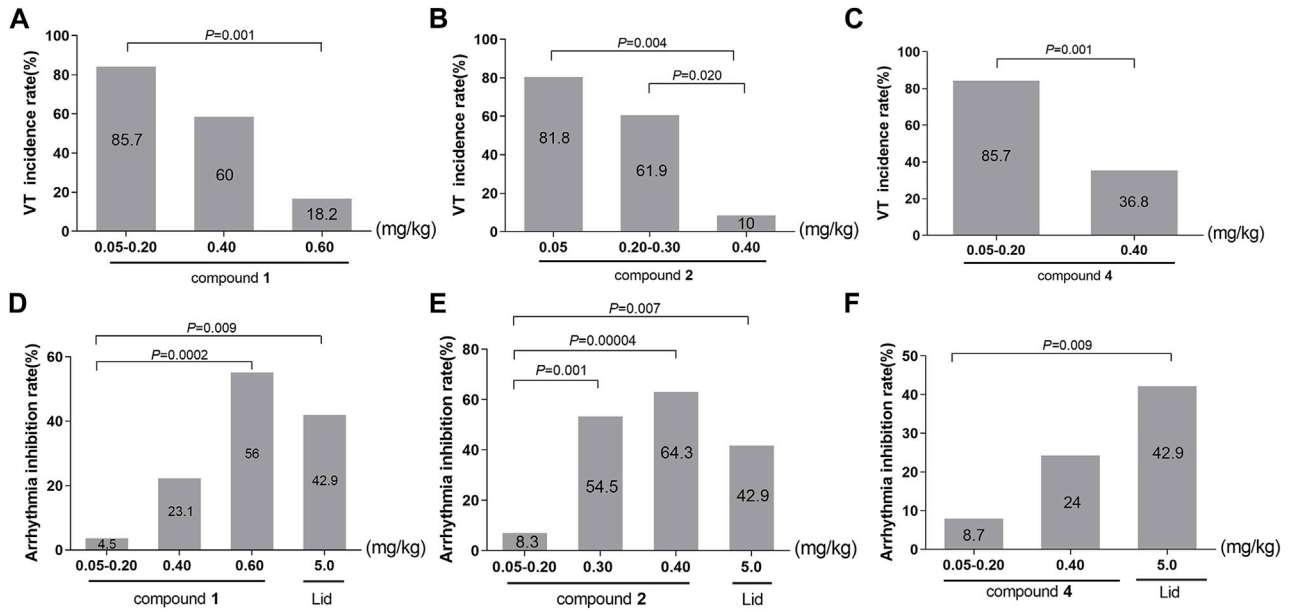

FIGURE 6 | (A–C) Effects of converted products on the incidence of VT. **(A)**: compound **1**; **(B)**: compound **2**; **(C)**: compound **3**. **(D–F)** Effects of converted products on arrhythmia inhibition rate. **(D)**: compound **1**; **(E)**: compound **2**; **(F)**: compound **3**.

In accordance with the data requirements of chi-square test, the adjacent dose groups with similar VT incidence should be combined to carry out chi-square test. The subgroups of compound **1** were 0.05–0.20, 0.40, and 0.60 mg/kg. As vividly displayed in **Table 6**; **Figure 6A**, chi-square test showed a significant difference in the incidence of VT among the three groups (χ^2 = 14.704, p = 0.001). The pairwise comparison revealed a highly significant drop in the incidence of VT from 85.7% in the 0.05–0.20 mg/kg group to only 18.2% in the 0.60 mg/kg group (χ^2 = 11.313, p = 0.001).

Following the identical research approach as VPB incubation period, we further investigated the incidence of VT in compounds **2** and **4**. Compound **2** was divided into the 0.05, 0.20–0.30, and 0.40 mg/kg groups. As described in **Table 6**; **Figure 6B**, chi-square test showed that there was a marked difference in the incidence of VT among the three groups (χ^2 = 13.000, p = 0.002). In comparison with the 0.05 mg/kg (81.8%) and 0.20–0.30 mg/kg (61.9%) groups, the incidence of VT was significantly dropped to 10% in 0.40 mg/kg group (χ^2 = 8.144, p = 0.004; χ^2 = 5.422, p = 0.020).

The subgroups of compound **4** were 0.05–0.20 and 0.40 mg/kg groups. As presented in **Table 6**; **Figure 6C**, the chi-square test showed a highly difference in the incidence of VT between the two subgroups (χ^2 = 10.165, p = 0.001). Furthermore, there was a greatly significant reduction in the incidence of the VT from 85.7% in 0.05–0.20 mg/kg group to 36.8% in 0.40 mg/kg group (χ^2 = 10.165, p = 0.001).

On the basic of aforementioned results, it can be concluded that compounds **1**, **2**, and **4** could reduce the incidence of VT in a dose-dependent manner, suggesting that they could effectively prevent the further progression of VPB.

Effects of Converted Products on Arrhythmia Inhibition Rate

The incidence of arrhythmia (Wang et al., 1997a; Wang et al., 1997b) is defined as the proportion of arrhythmia that occurs

TABLE 7 | Chi-square analysis of arrhythmia inhibition rate between different experimental compounds and lidocaine.

Compound	Dose (mg/kg)	Arrhythmia (frequency)	Without arrhythmia (frequency)	χ^2	*p*
Compound **1**	0.05–0.20	21	1	15.457	0.001
	0.40	10	3		
	0.60	11	14		
Lidocaine	5.0	12	9		
Compound **2**	0.05–0.20	22	2	18.123	0.0004
	0.30	10	12		
	0.40	10	18		
Lidocaine	5.0	12	9		
Compound **4**	0.05–0.20	21	2	6.908	0.032
	0.40	19	6		
Lidocaine	5.0	12	9		

within 30 min after pre-intravenous injections of test drugs, followed by an arrhythmia model established with aconitine. The occurrence of any kinds of ECGs such as VPB, VT, or VF should be judged as arrhythmia. Arrhythmia inhibition rate (%) = 100%-arrhythmia incidence rate (%), that is, the proportion that no arrhythmia occurs within 30 min, which can be used to evaluate whether the experimental compound could completely inhibit the proarrhythmic effect of aconitine. Arrhythmia inhibition rate is the most intuitive index reflecting the strength of the drug efficacy, the higher it gets, the better the efficacy is.

Considering the number of rats without arrhythmia in dose groups of 0.05 and 0.20 mg/kg was small, the original grouping could not meet the requirements of the chi-square test. Therefore, adopting the similar data analysis method as VT incidence, chi-square analysis was carried out in this paper by combining 0.05 and 0.20 mg/kg groups into 0.05–0.20 mg/kg group in each experimental compound.

In this paper, the effects of different doses of compound **1** (0.05–0.20, 0.40, and 0.60 mg/kg) and lidocaine on arrhythmia inhibition rate in rats were compared. Chi-square test showed that the arrhythmia inhibition rates in the four groups were significantly different (χ^2 = 15.457, p = 0.001), as shown in **Table 7**. Compared with 0.05–0.20 mg/kg group, the arrhythmia inhibition rates in 0.60 mg/kg and lidocaine groups significantly increased from 4.5% to 56% and 42.9%, respectively (χ^2 = 14.258, p = 0.0002; χ^2 = 6.820, p = 0.009). Notably, the arrhythmia inhibition rate in 0.60 mg/kg group was higher than lidocaine, exhibiting a better effect, as shown in **Figure 6D**.

To ascertain the influence of different substituents at C-8 and the location of double bond on drug efficacy, we further analysed the arrhythmia inhibition rate of compounds **2** and **4**, the result of chi-square test showed that the arrhythmia inhibition rates in compound **2** subgroups (0.05–0.20, 0.30, and 0.40 mg/kg) and lidocaine were statistically different (χ^2 = 18.123, p = 0.0004), as shown in **Table 7**. In comparison with 0.05–0.20 mg/kg group, the arrhythmia inhibition rate in 0.30 mg/kg, 0.40 mg/kg, and lidocaine groups significantly rose from 8.3% to 54.5%, 64.3%, and 42.9%, respectively (χ^2 = 11.578, p = 0.001; χ^2 = 17.093, p = 0.00004; χ^2 = 7.228, p = 0.007, respectively.), indicating that the antiarrhythmic effect of compound **2** was stronger with the increasing dose. Furthermore, a 0.30 mg/kg or more dosage of compound **2** exhibited a superior antiarrhythmic effect than lidocaine, as illustrated in **Figure 6E**.

Chi-square test showed that the arrhythmia inhibition rates in different dose groups (0.05–0.20 and 0.40 mg/kg) of compound **4** and lidocaine were significantly different (χ^2 = 6.908, p = 0.032), as shown in **Table 7**. The pairwise comparison result showed that the arrhythmia inhibition rate of lidocaine was significantly higher than 0.05–0.20 mg/kg group (χ^2 = 6.832, p = 0.009). However, a 0.40 mg/kg intravenously dose of compound **4** exhibited an equal antiarrhythmic activity relative to lidocaine (p > 0.05), as displayed in **Figure 6F**.

In summary, within their respective dose ranges, compounds **1**, **2**, and **4** could increase the arrhythmia inhibition rate in a dose-dependent manner. Among them, compound **1** in 0.60 mg/kg group (56%), compound **2** in 0.30 and 0.40 mg/kg groups (54.5%; 64.3%) had a higher arrhythmia inhibition rate than lidocaine (42.9%), manifesting that these two compounds possessed excellent antiarrhythmic effects.

DISCUSSION

In this paper, the HPLC method was used to investigate the structural transformation pathway of crassicauline A in sand frying process. Meanwhile, the cardiotoxicity between crassicauline A and its converted products was compared, the antiarrhythmic effect of the products was ultimately investigated. Considering crassicauline A is a monomer compound, readily adhering to the surface of the sand during processing, which is inconvenient to prepare and recover samples. In our previous study (Wang et al., 2020), it was confirmed that oil bath heating could simulate the process of sand frying, truly reflecting the dynamic variety of compounds during processing. In this paper, the processing parameters were determined according to the contents of crassicauline A and converted products in different processed samples. When processed at 160°C for 30 min, the converted products would get a relatively large quantity and higher content compared with other samples. As a result, the crassicauline A was processed, four converted products

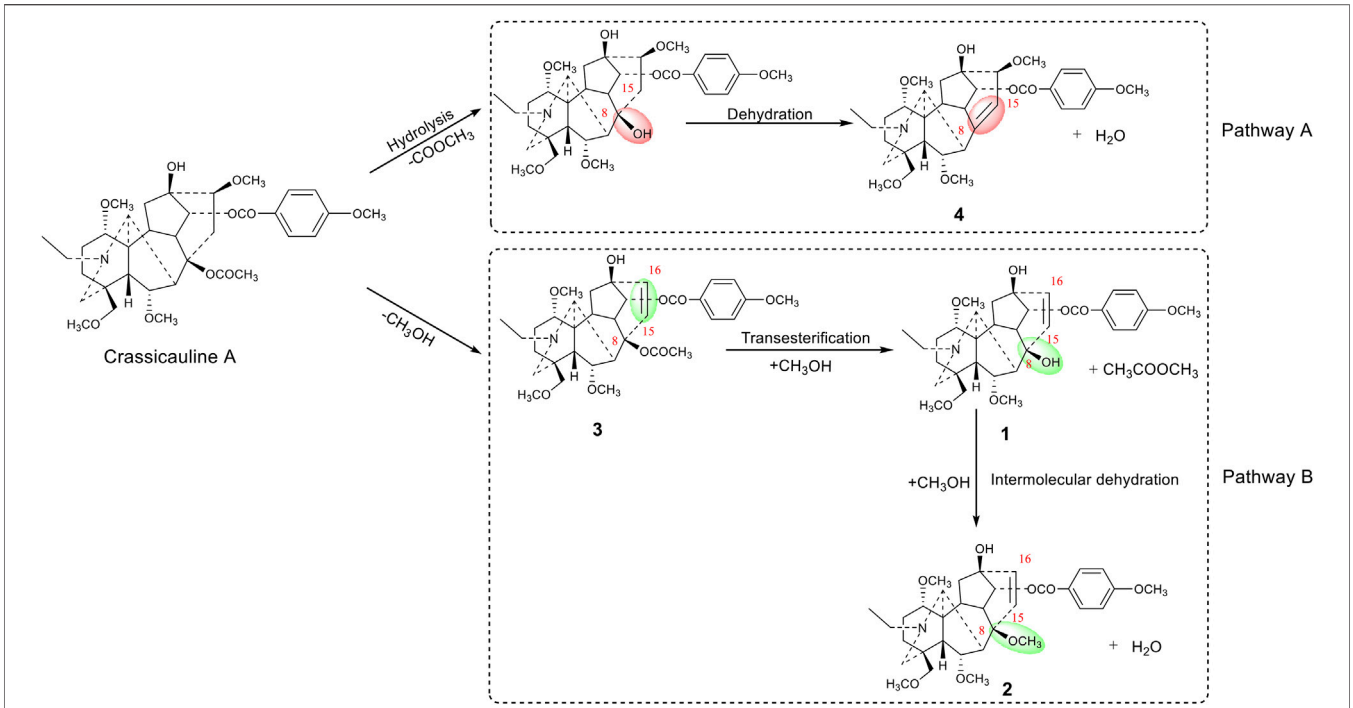

FIGURE 7 | Transformation pathways of crassicauline A during sand frying process.

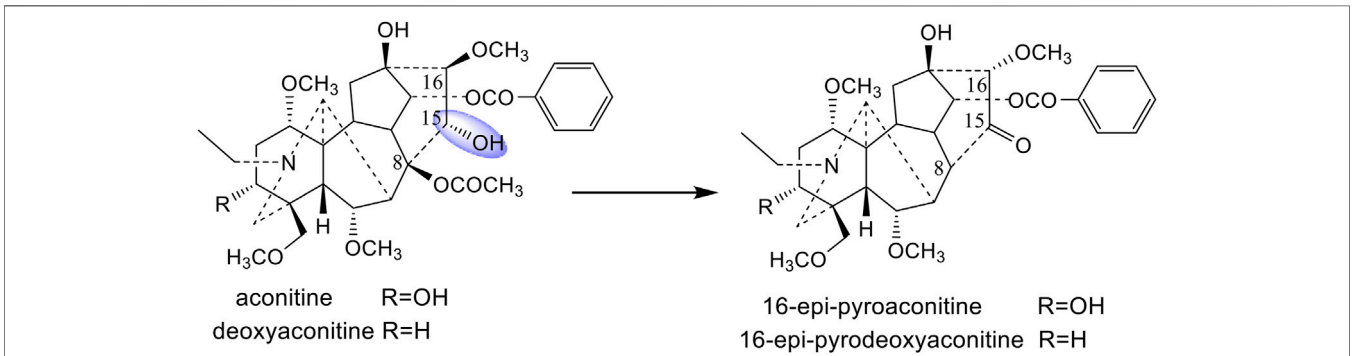

FIGURE 8 | Prototype compounds and the corresponding sand-fried products (Wang et al., 2010b; Wang et al., 2011).

were further obtained by chromatographic techniques and elucidated by spectroscopic methods, which were identified as compounds **1**, **2**, **3**, and **4**, respectively.

Crassicauline A is thermally unstable in structure and easily decomposed at high temperatures. Comparing the structures of the transformed products and the prototype compound, we found that the substituents at C-8, C-15, and C-16 of crassicauline A were converted after processing, and there might be at least two corresponding transformation pathways: (A) the acetoxyl group at C-8 of crassicauline A was firstly hydrolyzed to a hydroxyl group, a double bond was subsequently introduced at C-8/C-15 via further dehydration, which converted into compound **4**. (B) a double bond was firstly introduced at C-15/C-16 of crassicauline A by elimination of C-15 hydrogen atom and C-16 methoxyl group, to obtain compound **3**. The removed hydrogen atom and methoxyl group might generate methanol. The acetoxyl group at C-8 of compound **3** could undergo transesterification with methanol produced in the previous step, to generate compound **1** and methyl acetate. Finally, compound **2** was obtained by intermolecular dehydration of compound **1** with methanol (**Figure 7**). It was demonstrated that the structural transformation pathways of crassicauline A were different from those of aconitine and deoxyaconitine (**Figures 7**, **8**, Wang et al., 2010b; Wang et al., 2011), which confirmed our speculation, the prototype alkaloids with different substituents at the C-15 position may have different structural transformation pathways.

Cardiotoxicity assays showed that intravenously administration of 0.10 mg/kg crassicauline A caused VPB, VT, and VF in normal rats, but no arrhythmias occurred when injecting the same dose of converted products. The cardiotoxicity of the transformed products was reduced relative to crassicauline A, indicating that the sand frying method could attenuate the cardiotoxicity of the parent compound.

Aconitine-induced arrhythmia model, a classical experimental modeling for arrhythmia, has long been used to test the efficacy of antiarrhythmic agents (Winslow, 1980; Xu et al., 2005). Aconitine mainly targets sodium channels and prolongs the open state, the cells are depolarized by a sustained Na^+ influx, which accelerates the autonomy of the pacemaker and induces ectopic rhythm points, thus forming a multi-focal ectopic rhythm and shortening the myocardial refractory period, and finally leading to arrhythmia (Xu et al., 2005; Chan, 2009). The transformed products, as well as the parent compound, have structural similarities to aconitine. As mentioned above, some structurally similar diterpenoid alkaloids may exert opposite effects. We hypothesized that these converted alkaloids might have antiarrhythmic effects through an opposite mechanism to aconitine. Therefore, aconitine was chosen to establish the arrhythmia model in this paper for pharmacodynamic evaluation. Furthermore, concerning aconitine induces arrhythmia via continuously activating the sodium channel, two classical Class I sodium channel blockers, Class Ib lidocaine and Class Ic propafenone, were selected as positive drugs.

In this paper, three indicators, VPB incubation period, the incidence of VT, and the arrhythmia inhibition rate, were selected to comprehensively assess the antiarrhythmic activity of the three transformed products of crassicauline A. The experimental results manifested that, in their respective dose ranges, the transformed products could delay the VPB incubation period, decline the occurrence of VT and increase the arrhythmia inhibition rate. Within the dose ranges, if the optimal dose represented the strength of the antiarrhythmic activity of the tested compounds, the antiarrhythmic activities of the three transformed products would be ranked as follows. Compound **2** exhibited superior antiarrhythmic activity. At the dose of 0.40 mg/kg, 64.3% of the rats could not suffer from arrhythmia. And the onset time of VPB, among the rats undergoing arrhythmia, was found even at the point of approximately 15 min after aconitine administration, with the occurrence of VT being only 10%. Following compound **2**, compound **1** at a dose of 0.60 mg/kg exhibited a moderate antiarrhythmic activity, 56% of the rats were immune to arrhythmia. Within the rest rats, the arrhythmia was delayed for about 10 min. Among them, a 0.40 mg/kg intravenous dose of compound **4** produced the lowest antiarrhythmic effect. Only 24% of rats could be prevented from arrhythmia.

The antiarrhythmic structure-activity relationship acquired for the converted products exhibited promising antiarrhythmic effects relative to the parent compound crassicauline A. The activity can be manipulated by the positions of the double bond, as well as the substituents at the C-8 position. For example, compound **2** possessed a methoxyl group at C-8 instead of a hydroxyl group (compound **1**) exhibited superior antiarrhythmic activity. On the other hand, introduction of a double bond at C-8/C-15 (compound **4**) rather than at C-15/C-16 (compounds **1**, **2**) displayed a relatively weaker activity. These results indicated that a hydroxyl or a methoxyl group at C-8, elimination of C-16 methoxyl group, and a double bond at C-15/C-16 or C-8/C-15 might be important structural features to the antiarrhythmic activity of this kind of diterpenoid alkaloids. The structures of converted products could be beneficial in searching for the potential antiarrhythmic activity agents that are equal or more active, with lower toxicity, than antiarrhythmic drugs currently in clinical use.

CONCLUSION

In summary, this paper used oil bath heating to simulate the process of sand frying, and screened out the temperature and time parameters for the structural transformation of crassicauline A, which provided a reference for the standardization and quantification of sand frying processing technology. In addition, it was found that the prototype alkaloids, which had different substituents at the C-15 position, might have different transformation pathways. Furthermore, it also demonstrated from the *in vivo* experiments that, with the structural transformation of crassicauline A, the converted products displayed lower cardiotoxicity and relatively strong antiarrhythmic effects. However, the converted products were not completely isolated, there might be other structural transformation pathways that remained investigate.

DATA AVAILABILITY STATEMENT

The original contributions presented in the study are included in the article/**Supplementary Material**, further inquiries can be directed to the corresponding author.

ETHICS STATEMENT

The animal study was reviewed and approved by the Animal Experimentation Ethics Committee of Chengdu University of Traditional Chinese Medicine.

AUTHOR CONTRIBUTIONS

Y-JW, PT, and YW designed and performed the research. PT and Y-JW analysed data. PT and Y-JW wrote the paper. All authors read and approved the final manuscript.

FUNDING

This work was supported by the National Natural Science Foundation of China (No. 81403104), the Sichuan Science and Technology program (No. 2020YJ0131), and Xinglin Scholar Research Promotion Project of Chengdu University of TCM (No. QNXZ2018042).

ACKNOWLEDGMENTS

We are very grateful to our alma mater, Chengdu University of Traditional Chinese Medicine, for its convenience in collecting documents.

SUPPLEMENTARY MATERIAL

The Supplementary Material for this article can be found online at: https://www.frontiersin.org/articles/10.3389/fphar.2021.734671/full#supplementary-material

REFERENCES

Ameri, A. (1998). The Effects of *Aconitum* Alkaloids on the Central Nervous System. *Prog. Neurobiol.* 56 (2), 211–235. doi:10.1016/s0301-0082(98)00037-9

Bae, T. W., and Kwon, K. K. (2019). Efficient Real-Time R and QRS Detection Method Using a Pair of Derivative Filters and max Filter for Portable ECG Device. *Appl. Sci.* 9, 4128. doi:10.3390/app9194128

Bai, D. L., Chen, W. Z., Bo, Y. X., Dong, Y. L., Kang, A. L., Sun, W. K., et al. (2012). Discovery of N-(3,5-bis(1-pyrrolidylmethyl)-4-hydroxybenzyl)-4-methoxybenzenesulfamide (Sulcardine) as a Novel Anti-arrhythmic Agent. *Acta Pharmacol. Sin.* 33 (9), 1176–1186. doi:10.1038/aps.2012.119

Baldzizhar, A., Manuylova, E., Marchenko, R., Kryvalap, Y., and Carey, M. G. (2016). Ventricular Tachycardias: Characteristics and Management. *Crit. Care Nurs. Clin. North. Am.* 28 (3), 317–329. doi:10.1016/j.cnc.2016.04.004

Bartosova, L., Novak, F., Bebarova, M., Frydrych, M., Brunclik, V., Opatrilova, R., et al. (2007). Antiarrhythmic Effect of Newly Synthesized Compound 44Bu on Model of Aconitine-Induced Arrhythmia -- Compared to Lidocaine. *Eur. J. Pharmacol.* 575 (1-3), 127–133. doi:10.1016/j.ejphar.2007.07.044

Bartosová, L., Novák, F., Frydrych, M., Parák, T., Opatrilová, R., Brunclík, V., et al. (2005). Effect of a New Ultrashort Betalytic Agent on Aconitine-Induced Arrhythmia. *Biomed. Pap. Med. Fac. Univ. Palacky Olomouc Czech. Repub.* 149 (2), 339–343. doi:10.5507/bp.2005.054

Batiste, S. M., Blackwell, D. J., Kim, K., Kryshtal, D. O., Gomez-Hurtado, N., Rebbeck, R. T., et al. (2019). Unnatural Verticilide Enantiomer Inhibits Type 2 Ryanodine Receptor-Mediated Calcium Leak and Is Antiarrhythmic. *Proc. Natl. Acad. Sci. U S A.* 116 (11), 4810–4815. doi:10.1073/pnas.1816685116

Brady, W. J., Mattu, A., Tabas, J., and Ferguson, J. D. (2017). The Differential Diagnosis of Wide QRS Complex Tachycardia. *Am. J. Emerg. Med.* 35 (10), 1525–1529. doi:10.1016/j.ajem.2017.07.056

Casas, M. M., Avitia, R. L., Gonzalez-Navarro, F. F., Cardenas-Haro, J. A., and Reyna, M. A. (2018). Bayesian Classification Models for Premature Ventricular Contraction Detection on ECG Traces. *J. Healthc. Eng.* 2018, 2694768. doi:10.1155/2018/2694768

Chan, T. Y. (2009). Aconite Poisoning. *Clin. Toxicol. (Phila)* 47 (4), 279–285. doi:10.1080/15563650902904407

Chen, D. L., Jian, X. X., and Wang, F. P. (2002). C_{19}-diterpenoid Alkaloids of *Aconitum Transsecutum* Diels. *West. China J. Pharm. Sci.* 17, 326–328. doi:10.13375/j.cnki.wcjps.2002.05.002

Chen, J. S., and Zheng, S. (1987). *China Poisonous Plants*. Beijing, China: Science Press, 465–468.

Chinese Pharmacopoeia Commission (2020). *Pharmacopoeia of the People's Republic of China*. eleventh Edition. Beijing, China: China Medical Science Press, 867–868.

Coulson, J. M., Caparrotta, T. M., and Thompson, J. P. (2017). The Management of Ventricular Dysrhythmia in Aconite Poisoning. *Clin. Toxicol. (Phila)* 55 (5), 313–321. doi:10.1080/15563650.2017.1291944

Desai, H. K., Hart, B. P., Caldwell, R. W., Huang, J. Z., and Pelletier, S. W. (1998). Certain Norditerpenoid Alkaloids and Their Cardiovascular Action. *J. Nat. Prod.* 61 (6), 743–748. doi:10.1021/np970499j

Gao, F., Chen, D. L., and Wang, F. P. (2006). Two New C_{19}-Diterpenoid Alkaloids from *Aconitum Hemsleyanium* Var. Circinacum. *Chem. Pharm. Bull. (Tokyo)* 54 (1), 117–118. doi:10.1248/cpb.54.117

Gong, Q. F. (2005). *Science of Processing Chinese Materia Medica*. Beijing, China: China Medical Science Press, 310–312.

Hong, B., He, J., Le, Q., Bai, K., Chen, Y., and Huang, W. (2019). Combination Formulation of Tetrodotoxin and Lidocaine as a Potential Therapy for Severe Arrhythmias. *Mar. Drugs* 17 (12), 685–697. doi:10.3390/md17120685

Joshi, B. S., Wunderlich, J. K., and Pelletier, S. W. (1987). ^{13}C Nuclear Magnetic Resonance Spectroscopy in the Elucidation of Structures of Diterpenoid Alkaloids. *Can. J. Chem.* 65, 99–103. doi:10.1139/v87-016

Klekot, A. A. (2006). Antiarrhythmic Activity of a Membrane-Protecting Agent Sal'magin in Rats with Aconitine-Induced Arrhythmias. *Bull. Exp. Biol. Med.* 142 (2), 209–211. doi:10.1007/s10517-006-0329-3

Li, H., Niu, X., Li, G. Z., Shi, X. J., Wei, Z. Z., Xiao, J. P., et al. (2006). Study on Effect of Tiaomaiyin Injection on Experimental Arrhythmia. *Zhongguo Zhong Yao Za Zhi* 31 (9), 759–762. doi:10.3321/j.issn:1001-5302.2006.09.016

Li, X., Gu, L., Yang, L., Zhang, D., and Shen, J. (2017). Aconitine: A Potential Novel Treatment for Systemic Lupus Erythematosus. *J. Pharmacol. Sci.* 133 (3), 115–121. doi:10.1016/j.jphs.2017.01.007

Lin, L. Y., Chen, Q. H., and Wang, F. P. (2004). Advances in Pharmacological Activities of Norditerpenoid Alkaloids. *West. China J. Pharm. Sci.* 19 (3), 200–205. doi:10.13375/j.cnki.wcjps.2004.03.018

Ma, L. Q., Yu, Y., Chen, H., Li, M., Ihsan, A., Tong, H. Y., et al. (2018). Sweroside Alleviated Aconitine-Induced Cardiac Toxicity in H9c2 Cardiomyoblast Cell Line. *Front. Pharmacol.* 9, 1138. doi:10.3389/fphar.2018.01138

Meng, J. R., Wu, T., and Huang, L. (1992). Influence of Neural Regulation on Anti-arrhythmic Effects of GABA in Rats. *Zhongguo Yao Li Xue Bao* 13 (1), 66–68.

Mohamed, O. Y., Al-Masri, A. A., El Eter, E. A., and Lateef, R. (2016). SCH 79797, a Selective PAR1 Antagonist, Protects against Ischemia/reperfusion-Induced Arrhythmias in the Rat Hearts. *Eur. Rev. Med. Pharmacol. Sci.* 20 (22), 4796–4800.

Pelletier, S. W., and Joshi, B. S. (1991). "Carbon-13 and Proton NMR Shift Assignments and Physical Constants of Norditerpenoid Alkaloids," in *Alkaloids: Chemical and Perspectives* (New York: John Wiley), Vol. 7, 297–564. doi:10.1007/978-1-4612-3006-9_3

Pelletier, S. W., Mody, N. V., Joshi, B. S., and Schramn, L. C. (1984). *Alkaloids: Chemical and Biological Perspectives*, Vol. 2. New York: John Wiley.

Qiu, M., Dong, Y. H., Han, F., Qin, J. M., Zhang, H. N., Du, J. X., et al. (2016). Influence of Total Flavonoids Derived from *Choerospondias Axillaris* Folium on Aconitine-Induced Antiarrhythmic Action and Hemodynamics in Wistar Rats. *J. Toxicol. Environ. Health A.* 79 (19), 878–883. doi:10.1080/15287394.2016.1193117

Sun, G. B., Xu, H. B., Wen, F. C., Ding, T., and Sun, X. B. (2006). Anti-arrhythmic Effect of Deglucose-Chikusetsu-Saponin IVa. *Chin. J. Pharmacol. Toxicol.* 20, 377–380. doi:10.3321/j.issn:1000-3002.2006.05.004

Swerdlow, B., Axelrod, P., Kolman, B., Perry, D., and Mark, R. (1983). Ambulatory Ventricular Tachycardia: Characteristics of the Initiating Beat. *Am. Heart J.* 106 (6), 1326–1331. doi:10.1016/0002-8703(83)90041-8

The Flora Committee of Chinese Academy of Sciences (1979). *Flora of China*, Vol. 55. Beijing, China: Science Press, 156.1

Wang, F. P., and Fang, Q. C. (1981). Alkaloids from Roots of *Aconitum Crassicaule*. *Planta Med.* 42 (8), 375–379. doi:10.1055/s-2007-971658

Wang, C. F., Gerner, P., Wang, S. Y., and Wang, G. K. (2007). Bulleyaconitine A Isolated from *Aconitum* Plant Displays Long-Acting Local Anesthetic Properties *In Vitro* and *In Vivo*. *Anesthesiology* 107 (1), 82–90. doi:10.1097/01.anes.0000267502.18605.ad

Wang, F. P. (2009). A Deliberation on Methodology of Modernization of Traditional Chinese Medicines Based on the Research and Development of New Drugs from "Cao Wu". *Chem. Ind. Eng. Prog.* 21 (1), 63–65.

Wang, J. L., Shen, X. L., Chen, Q. H., Qi, G., Wang, W., and Wang, F. P. (2009). Structure-analgesic Activity Relationship Studies on the C(18)- and C(19)-diterpenoid Alkaloids. *Chem. Pharm. Bull. (Tokyo)* 57 (8), 801–807. doi:10.1248/cpb.57.801

Wang, P. D., Ma, X. M., Zhang, H. L., Yang, Y. M., Yang, Y. R., Wang, H., et al. (1997a). Effect of Lappaconitine on ECG in Anesthetized Rats and its Anti-arrhythmic Action. *Acta Pharmacol. Sin.* 13 (3), 263–265.

Wang, P. D., Zhang, H. L., Yang, Y. M., and Liu, H. L. (1997b). Comparison of the Effects of Two Kinds of Diterpenoid Alkaloids on Aconitine-Induced Arrhythmias in Rats. *J. Baotou Med. Coll.* 13 (2), 4–6. doi:10.16833/j.cnki.jbmc.1997.02.003

Wang, Y., Zhang, J., Tian, H., Zeng, C., Yao, Z., and Zhang, Y. (2010b). Study on Processing Principle of *Aconitum Pendulum*. *Zhongguo Zhong Yao Za Zhi* 35 (5), 588–592. doi:10.4268/cjcmm20100510

Wang, Y. J., Zeng, C. J., Yao, Z., Zhang, J., Zhang, Y., and Zhang, F. (2010a). Diterpene Alkaloids from Roots and Processed Products of *Aconitum Pendulum*. *Chin. Tradit. Herb. Drugs* 41 (3), 347–351.

Wang, Y. J., Zhang, J., Zeng, C. J., Yao, Z., and Zhang, Y. (2011). Study on the Diterpene Alkaloids from Processed Roots of *Aconitum Pendulum*. *West. China J. Pharm. Sci.* 26 (1), 11–13. doi:10.13375/j.cnki.wcjps.2011.01.020

Wang, Y., Tao, P., Wang, Y. J., and Deng, W. J. (2020). Study on Structural Transformation Pathway of Indaconitine in Stir-Frying with Sand Process and Toxicity of its Processing Products. *Chin. Tradit. Herb. Drugs* 51 (5), 1205–1213. doi:10.7501/j.issn.0253-2670.2020.05.017

Winslow, E. (1980). Evaluation of Antagonism of Aconitine-Induced Dysrhythmias in Mice as a Method of Detecting and Assessing Antidysrhythmic Activity. *Br. J. Pharmacol.* 71 (2), 615–622. doi:10.1111/j.1476-5381.1980.tb10981.x

Wu, J. J., Guo, Z. Z., Zhu, Y. F., Huang, Z. J., Gong, X., Li, Y. H., et al. (2018). A Systematic Review of Pharmacokinetic Studies on Herbal Drug Fuzi: Implications for Fuzi as Personalized Medicine. *Phytomedicine* 44 (2018), 187–203. doi:10.1016/j.phymed.2018.03.001

Xiao, P.-G., Wang, F. P., Gao, F., Yan, L. P., Chen, D. L., and Liu, Y. (2006). A Pharmacophylogenetic Study of *Aconitum* L. (Ranunculaceae) from China. *Acta Phytotaxonomica Sinica* 44 (1), 1–46. doi:10.1360/aps050046

Xu, S. Y., Bian, R. L., and Chen, X. (2005). *Experimental Methods in Pharmacology*. Beijing, China: People's Medical Publishing House, 1173–1174.

Yue, J. M., Chen, Y. Z., and Li, Y. Z. (1994a). C_{19}-diterpenoid Alkaloids of *Aconitum Kongboense*. *Phytochemistry* 35 (3), 829–831. doi:10.1016/S0031-9422(00)90619-8

Yue, J., Xu, J., Chen, Y., and Chen, S. (1994b). Diterpenoid Alkaloids from *Aconitum Talassicum*. *Phytochemistry* 37 (5), 1467–1470. doi:10.1016/S0031-9422(00)90435-7

Zhang, H. Y., Xu, C. Q., Li, H. X., Li, H. Z., Han, L. P., Sun, Y. H., et al. (2006). The Effect of Resveratrol on Arrhythmia and Cardiac Ischemia. *Acta Pharmacol. Sin.* 22 (3), 383–384. doi:10.3321/j.issn:1001-1978.2006.03.033

Zhang, J. H., and Xiong, Y. A. (2015). Effect of Paeonol on Rats' Ischemic Arrhythmia and miRNA-1 Expression. *Chin. J. Exp. Tradit. Med. Form.* 21 (5), 129–132. doi:10.13422/j.cnki.syfjx.2015050129

Conflict of Interest: The authors declare that the research was conducted in the absence of any commercial or financial relationships that could be construed as a potential conflict of interest.

Publisher's Note: All claims expressed in this article are solely those of the authors and do not necessarily represent those of their affiliated organizations, or those of the publisher, the editors and the reviewers. Any product that may be evaluated in this article, or claim that may be made by its manufacturer, is not guaranteed or endorsed by the publisher.

frontiers in Pharmacology

SYSTEMATIC REVIEW
published: 18 November 2021
doi: 10.3389/fphar.2021.722975

Comparison of Traditional Chinese Medicine in the Long-Term Secondary Prevention for Patients with Ischemic Stroke: A Systematical Analysis

Jiali Li[1†], Xixi Zhao[2†], Yangyang Zhang[2], Haitong Wan[2], Yu He[3], Xiaohong Li[3], Li Yu[2] and Weifeng Jin[3*]*

[1]The Second School of Clinical Medicine, Zhejiang Chinese Medical University, Hangzhou, China, [2]School of Life Sciences, Zhejiang Chinese Medical University, Hangzhou, China, [3]School of Pharmaceutical Sciences, Zhejiang Chinese Medical University, Hangzhou, China

OPEN ACCESS

Edited by:
Yi Wang,
Zhejiang University, China

Reviewed by:
You Yun,
China Academy of Chinese Medical Sciences, China
Lu Yan,
Institute of Botany (CAS), China

***Correspondence:**
Li Yu
yuli9119@126.com
Weifeng Jin
jin_weifeng@126.com

[†]*These authors have contributed equally to this work*

Specialty section:
This article was submitted to Ethnopharmacology, a section of the journal Frontiers in Pharmacology

Received: *09 June 2021*
Accepted: *05 October 2021*
Published: *18 November 2021*

Citation:
Li J, Zhao X, Zhang Y, Wan H, He Y, Li X, Yu L and Jin W (2021) Comparison of Traditional Chinese Medicine in the Long-Term Secondary Prevention for Patients with Ischemic Stroke: A Systematical Analysis. Front. Pharmacol. 12:722975. doi: 10.3389/fphar.2021.722975

Background: Keeping in view the high recurrence rate and risk of ischemic stroke, combinatorial therapy involving traditional Chinese medicine (TCM) with conventional Western medicine (WM) is receiving wider scientific attention. Thus, a systematical analysis was made to explore the efficacy of TCM+WM in the long-term secondary prevention for patients with ischemic stroke.

Methods: Qualified inclusion and exclusion criteria were set up beforehand, and two researchers independently read the articles, extracted data, and evaluated the quality of included articles according to Cochrane Reviewer's Handbook 5.1 method. For the sake of comprehensive data acquisition, seven databases from the time of their establishment to May 5, 2021, have been searched completely. Additionally, pairwise meta-analysis was made to compare TCM+WM vs. WM, and network meta-analysis was conducted by frequentist random effects models for the comparison of different kinds of TCM+WM via indirect evidence. The primary outcomes defined were recurrent stroke and NIHSS. Secondary outcomes were fibrinogen (Fib) fasting blood glucose (FBG), triglycerides (TG), and total cholesterol (TC). Safety outcomes were outlined as all-cause mortality and adverse events (AEs). Furthermore, Stata16.0 software was used to accomplish the systematical analysis and cluster analysis.

Results: In total, 47 qualified randomized controlled trials (RCTs) including 10,732 patients were taken into consideration. Seven traditional Chinese medicines included in the study are Naoxintong capsule (NXT), Tongxinluo capsule (TXL), Buyang Huanwu decoction (BYHW), Naomaitai capsule (NMT), Dengzhan Shengmai capsule (DZSM), Naoshuantong capsule (NST), and Maixuekang capsule (MXK). With respect to their primary outcomes, all kinds of TCM+WM were significantly more effective than WM (e.g., NXT in recurrent stroke (OR=0.54, P<0.01), TXL in NIHSS (WM=−1.4, P<0.01)). Additionally, the outcomes of cluster analysis indicated that MXK+WM and NST+WM had relatively good preventive effects for recurrent stroke, NIHSS, and all-cause mortality. There was no significant difference in the comparisons of AEs; however, this may arise from the lack of sufficient data.

Conclusion: According to our systematical analysis, MXK+WM and NST+WM had relatively good secondary prevention effects for patients with ischemic stroke regarding recurrent stroke, NIHSS, and all-cause mortality. Nevertheless, better, high-quality, large-sample randomized clinical trials (RCTs) are required to verify our conclusions in the future.

Systematic Review Registration: [https://inplasy.com/inplasy-2021-5-0036/], identifier [INPLASY202150036].

Keywords: traditional Chinese medicine, ischemic stroke, long-term, secondary prevention, recurrent stroke, stroke risk factors, systematical analysis

INTRODUCTION

Stroke causes nearly 5% of all disabilities (Collaborators, 2017b) and about 10% of deaths around the world (Collaborators, 2017a). In addition, ischemic stroke accounts for about 70% of the total death caused by stroke (Feigin et al., 2018). Moreover, a good volume of research showed that the cumulative long-term risk of recurrence of stroke is 11.1% at 1 year and 26.4% at 5 years (Mohan et al., 2011). Besides, patients with ischemic stroke are faced with a higher risk of vascular events or death (Kernan et al., 2014; Amarenco et al., 2016). Furthermore, some researchers said that taking secondary prevention on time will decrease the risk of stroke recurrence by about 80% (Hackam and Spence, 2007; Rothwell et al., 2007). Therefore, it is essential to take appropriate measures to avoid the recurrence of stroke.

According to the American Heart Association/American Stroke Association guideline (AHA/ASA), conventional Western medicine for stroke treatment includes hypoglycemic drugs, antihypertensive drugs, antiplatelet drugs, hypolipidemic drugs, etc. (Kernan et al., 2014). However, the combination of clopidogrel and aspirin is not any more effective than either aspirin or clopidogrel monotherapy, and gives rise to a higher risk of bleeding (Diener et al., 2004; Bhatt et al., 2006; Bhatt et al., 2007). Some patients are resistant to antiplatelet drugs (Guo et al., 2019). Moreover, one study has shown that statins for the treatment of stroke can increase the relative risk of new onset diabetes by 9% (Gao, 2015). New treatment methods are thus warranted.

Traditional Chinese medicine (TCM) is attracting increasing attention on account of its exact curative effect and low toxicity (Bu et al., 2020). In addition, in pre-thrombotic conditions, TCM is a multi-link, multi-target which effectively prevents the recurrence of ischemic stroke (Kang and Li, 2012). Furthermore, TCM plays a significant role in the prevention of cerebrovascular disease and recovery of limb function (Zhang et al., 2012).

For example, a randomized controlled trial (RCT) showed that Naoxintong capsule (NXT) had a positive effect on the prevention of recurrence of stroke (Sun, 2020), and another RCT indicated that Tongxinluo capsule (TXL) promoted the recovery of nerve function (Bo et al., 2017). In this study, NXT, TXL, Buyang Huanwu decoction (BYHW), Naomaitai capsule (NMT), Dengzhan Shengmai capsule (DZSM), Naoshuantong capsule (NST), and Maixuekang capsule (MXK) were made a part of the systematical analysis.

At present, there are only a few reviews and meta-analyses on the long-term secondary prevention of cerebral infarction by the combination of Western medicine (WM) and traditional Chinese medicine (TCM). One of the few studies showed that Buyang Huanwu decoction has no statistical significance in reducing the recurrence rate of ischemic stroke (Xie, 2015), possibly because of the lack of any significant literature at that time. Different from traditional pairwise meta-analysis, network meta-analysis (NMA) allows various treatments to be compared and ranked through direct and indirect contrasts to select the best ones (De Laat, 2017). However, comparisons of efficacy across different types of TCM are still inconclusive, causing confusion among physicians and patients.

Therefore, this study is intended to use systematical analysis including pairwise and network meta-analysis to compare the long-term secondary prevention effects and safety of the addition of different kinds of traditional Chinese medicines against ischemic stroke. In addition, the stroke risk factors of different kinds of TCM were also compared to provide references for the study regarding the cause of recurrence. This article will help researchers to better understand the advantages of TCM in the treatment of stroke and offer better assistance for clinical applications.

MATERIALS AND METHODS

Our systematical analysis was registered in the International Platform of Registered Systematic Review and Meta-Analysis Protocols (INPLASY) under the registration number INPLASY202150036. The analysis was carried out according to the Preferred Reporting Items for Systematic Reviews and Meta-Analyses (PRISMA) guidelines (Hutton et al., 2015) (**Supplementary Material S1**). The abbreviations used in this manuscript have been listed in **Supplementary Material S2**.

Eligibility and Exclusion Criteria

The (Patient/Intervention/Comparison/Outcome/Study design) PICOS framework was employed as our eligibility criteria, thus only randomized controlled trials (RCTs) consistent with the following requirements were taken into our consideration: (1) Participants: patients with the diagnosis of ischemic stroke with no limitation on nationality, race, gender, age, and disease duration; (2) Interventions and comparisons: the treatment group was given conventional WM plus TCM, and the control group adopted another kind of TCM plus WM or WM alone. In

TABLE 1 | The detailed search process of PubMed.

Serial number	Strategy
#1	Ischemic stroke (MeSH Terms) OR cerebral infarction (MeSH Terms)
#2	Cerebral Infarctions (Title/Abstract)) OR Infarctions, Cerebral (Title/Abstract)) OR Infarction, Cerebral (Title/Abstract)) OR Cerebral Infarction, Left Hemisphere (Title/Abstract)) OR Left Hemisphere Infarction, Cerebral (Title/Abstract)) OR Infarction, Left Hemisphere, Cerebral (Title/Abstract)) OR Left Hemisphere, Cerebral Infarction (Title/Abstract)) OR Cerebral, Left Hemisphere, Infarction (Title/Abstract)) OR Infarction, Cerebral, Left Hemisphere(Title/Abstract)) OR Subcortical Infarction(Title/Abstract)
#3	#1 AND #2
#4	secondary prevention (Title/Abstract)
#5	Naoxintong Capsule (Title/Abstract)
#6	Tongxinluo Capsule (Title/Abstract)
#7	Buyang Huanwu Decoction (Title/Abstract)
#8	Naomaitai Capsule (Title/Abstract)
#9	Dengzhan Shengmai Capsule (Title/Abstract)
#10	Naoshuantong Capsule (Title/Abstract)
#11	Maixuekang Capsule (Title/Abstract)
#12	AND/#5–#11
#13	randomized controlled trial (Publication Type) OR controlled clinical trial (Publication Type)
#14	randomized (Title/Abstract) OR placebo (Title/Abstract) OR randomly (Title/Abstract)
#15	#13 OR #14
#16	animals (MeSH Terms)
#17	humans (MeSH Terms)
#18	#16 NOT #17
#19	#12 NOT #18
#20	#3 AND #4 AND #12 AND #19

addition, the WM treatment must be the same between treatment and control groups. The common WM drugs were antiplatelet, statins, antihypertensive drugs, hypoglycemic drugs, etc. whereas TCM included NXT, TXL, BUHW, NMT, DZSM, NST, and MXK. Besides, there were no limitations on dosage and the follow-up time was defined as more than 2 months; (3) Outcomes: the primary outcomes of this systematical analysis were recurrent stroke and the National Institute of Health stroke scale (NIHSS). Additionally, the secondary outcomes were stroke risk factors including elevated fibrinogen (Fib), fasting blood glucose (FBG), triglycerides (TG), and total cholesterol (TC). Moreover, the safety outcomes were all-cause mortality and adverse events (AEs). In this systematical analysis, RCT which included one of the primary outcomes was sufficient. Furthermore, the reasons behind choosing these secondary outcomes are the fact that increases in Fib (Refaai et al., 2018), FBG (Lawes et al., 2004), TG (Yuan et al., 2020), and TC (Yuan et al., 2020) have a close association with ischemic stroke or cardiovascular events; and (4) Study design: Only RCTs were taken into consideration for the current investigation.

RCTs would be excluded if they were in accordance with the following criteria: (1) The follow-up time was less than 2 months; (2) the treatment methods include acupuncture or other kinds of TCM; (3) publications were duplicated; (4) data was incomplete; (5) there were no relevant outcomes; and (6) the patients had serious complications.

Search Strategy

PubMed, Web of Science, embase, China National Knowledge Infrastructure (CNKI), Chinese Biological Medicine Literature Service System (CBM), China Science and Technology Journal database (VIP), and Wan–fang database (WF) were searched for this investigation. The included studies were published in the period starting from the foundation of each database to May 5, 2021. The topic search used was the combination of medical topic title terminology and free text terminology. Searched terms included "ischemic stroke," "cerebral infarction," "secondary prevention," "Naoxintong Capsule," "Tongxinluo Capsule," "Buyang Huanwu Decoction," "Naomaitai Capsule," "Dengzhan Shengmai Capsule," "Naoshuantong Capsule," and "Maixuekang Capsule". The detailed search process of PubMed is outlined in **Table 1**. Furthermore, references in the literature were searched manually.

Literature Inclusion and Data Extraction

Endnote 20.0 software was utilized for creating a library of the obtained articles and the literature inclusion was done by two researchers independently. Duplicated articles were excluded first. The titles and abstracts of articles were then thoroughly read for primary screening in accordance with the inclusion and exclusion criteria. The next step involved the re-screening of the articles via reading full-text content based on the inclusion and exclusion criteria. A third researcher would additionally participate in the discussion if at any stage the results were controversial. Moreover, relevant data were extracted which included publication date, author's name, title, detailed characteristics of participants (sample capacity, age, sex), interventions (drug, dose, and follow-up time), outcomes (primary outcomes, secondary outcomes, and safety outcomes), and elements which were used to evaluate the risk of bias. Furthermore, since our research was related to ethnopharmacology, the compositions of included medicines were clearly recorded (Heinrich et al., 2020). In addition, all botanical plants were named according to the existing international standards in databases (Rivera et al., 2014).

TABLE 2 | Characteristic of the articles included in this systematical analysis.

Study ID	Sample size		Age		Sex(M/F)		Interventions		Dose of TCM	Follow–up time	Outcomes
	T	C	T	C	T	C	T	C			
Sun (2020)	75	75	56.18 ± 1.39	55.92 ± 1.47	43/32	41/34	NXT + WM	WM	3c/t,3t/d	1a	①③⑤⑥⑧
Shi et al. (2011a)	562	512	——	——	——	——	NXT + WM	WM	3c/t,3t/d	5a	①
Shi et al. (2011b)	46	45	62.1 ± 7.9	63.4 ± 8.6	24/22	24/21	NXT + WM	WM	3c/t,3t/d	3 m	②⑤⑥
Zang et al. (2011)	52	46	67 ± 9.3	65 ± 3.6	30/22	27/19	NXT + WM	WM	3c/t,3t/d	2a	①
Tian and Li (2010)	360	357	56.8 ± 7.9	58.2 ± 6.8	222/138	204/153	NXT + WM	WM	3c/t,3t/d	1a	①③④⑤⑥⑧
Jiang (2012)	46	50	58 ± 5	56 ± 6	24/22	28/22	NXT + WM	WM	3c/t,3t/d	2a	①③⑥
Tu et al. (2013)	108	106	59.9 ± 8.4		——	——	NXT + WM	WM	3c/t,3t/d	1a	①④⑧
Dang et al. (2018)	161	158	65.7 ± 10.8	65.9 ± 9.9	114/47	97/61	NXT + WM	WM	3c/t,2t/d	519d	①⑧
Zhang et al. (2008)	80	80	40–78(59)		88/72		NXT + WM	WM	4c/t,3t/d	2a	①
Xu (2017)	40	40	75.3 ± 3.2	76.7 ± 3.1	25/15	24/16	NXT + WM	WM	3c/t,3t/d	3a	①⑦
Zhou (2013)	38	48	41–79(60)		32/34		NXT + WM	WM	4c/t,3t/d	2a	①⑧
Meng (2009)	40	40	41–79(61)		44/36		NXT + WM	WM	4c/t,3t/d	2a	①⑧
Wang (2018)	40	40	55.5 ± 14		——	——	NXT + WM	WM	3c/t,3t/d	1a	①③
Zhou (2018)	70	70	41–83(62.08)	42–83(62.47)	45/25	41/29	NXT + WM	WM	4c/t,3t/d	6 m	②③⑤⑥
Chen (2012)	75	60	60 ± 4.3	58 ± 3.8	42/33	30/34	NXT + WM	WM	3c/t,3t/d	3 m	①⑤⑥
Lu et al. (2018)	35	35	62.4 ± 10.5	61.6 ± 9.4	20/15	18/17	TXL + WM	WM	2c/t,3t/d	6 m	①②⑤⑥⑧
Liu and Cao (2008)	30	30	61 ± 11	63 ± 10	17/13	19/11	TXL + WM	WM	2c/t,3t/d	3a	①⑦⑧
Song (2014)	86	76	58.48 ± 7.79	57.12 ± 7.4	45/41	41/35	TXL + WM	WM	3c/t,3t/d	6 m	①⑦
Bo et al. (2017)	68	77	66.88 ± 10.6	66.99 ± 10.24	32/36	33/44	TXL + WM	WM	4c/t,3t/d	1a	①⑦
Zhou (2014)	200	200	53.1 ± 9.7		268/132		TXL + WM	WM	4c/t,3t/d	1a	①⑤⑥
Yan et al. (2008)	182	178	——		——		TXL + WM	WM	3c/t,3t/d	1a	①
Chai (2015)	84	84	66.1 ± 7.2	65.8 ± 6.3	53/31	52/32	TXL + WM	WM	3c/t,3t/d	1a	⑤⑥
Xue et al. (2014)	74	74	66.1 ± 7.2	65.8 ± 6.3	42/32	43/31	TXL + WM	WM	4c/t,3t/d	1a	①⑤⑥⑦
Guo et al. (2013)	50	48	59.7 ± 5.4	60.4 ± 5.1	39/11	36/12	TXL + WM	WM	2c/t,3t/d	1a	①②⑤⑧
Jiao et al. (2011)	49	53	——		——		BYHW + WM	WM	1p/d	6 m	①②
Yu (2013)	49	53	——		——		BYHW + WM	WM	1p/d	6 m	①
Lin and Li (2012)	37	37	47–83	49–81	20/17	19/18	BYHW + WM	WM	1p/d	2a	①
Liu (2019)	24	24	56 ± 6.5	54.8 ± 6.8	15/9	14/10	BYHW + WM	WM	1p/d	3 m	①③
Chen and Cao (2016)	35	35	42–75		39/31		BYHW + WM	WM	1p/d	6 m	①②③
Sun (2008)	50	50	72.7 ± 10.2	71.3 ± 11.6	26/24	25/25	NMT + WM	WM	2c/t,3t/d	2a	①
Huang and Huang (2007)	218	200	62.46 ± 6.28	60.35 ± 6.73	143/75	131/69	NMT + WM	WM	2c/t,3t/d	3a	①
Liu and Wang (2006)	80	80	65.28 ± 13.12	64.41 ± 12.56	60/40	54/46	NMT + WM	WM	2c/t,3t/d	3a	①
Gan (2007)	58	60	48–75	45–78	33/25	38/22	NMT + WM	WM	2c/t,3t/d	3 m	①②⑧
Liu et al. (2014)	50	50	61.6 ± 8.6	63.3 ± 7.7	31/19	29/21	NMT + WM	WM	2c/t,3t/d	2 m	②③
Liu (2009)	21	21	57.9 ± 9.14	55.41 ± 9.42	10/11	8/13	DZSM + WM	WM	2c/t,2t/d	6 m	①③④⑤⑥⑦⑧
Nan and Li (2016)	63	63	61.94 ± 10.96	62.42 ± 10.17	35/28	36/27	DZSM + WM	WM	2c/t,3t/d	6 m	①②③⑤⑥⑧
Chao (2011)	620	620	60.82 ± 9.04	61.44 ± 8.77	225/395	215/405	DZSM + WM	WM	2c/t,2t/d	1a	①③⑧
Chen et al. (2008)	495	504	63.3 ± 9.1	66.3 ± 8.0	241/254	267/237	DZSM + WM	WM	2c/t,3t/d	1.5a	①③④⑤⑥⑧
Ma et al. (2014)	55	55	60.6 ± 5.8	60.9 ± 5.4	30/25	31/24	DZSM + WM	WM	2c/t,3t/d	6 m	①②⑥
Liu and Li (2012)	87	86	69 ± 5.04	68.2 ± 5.05	52/35	53/33	NST + WM	WM	3c/t,3t/d	1a	①②⑤⑥⑦
Ye et al. (2015)	345	352	62.37 ± 9.97	62.82 ± 9.97	232/113	231/121	NST + WM	WM	3c/t,3t/d	6 m	①⑧
Huang et al. (2014)	49	45	68.5 ± 6.3	68.7 ± 6.5	29/20	27/18	NST + WM	WM	3c/t,3t/d	3 m	①②
Peng et al. (2012)	45	45	60.26 ± 9.52	61.75 ± 10.26	22/23	26/19	NST + WM	WM	3c/t,3t/d	6 m	②
Ge et al. (2016)	200	198	——	——	——	——	MXK + WM	WM	3c/t,3t/d	1a	①⑧
Peng and Niu(2014)	124	124	65 ± 14	64 ± 13	69/55	67/57	MXK + WM	WM	2c/t,3t/d	1a	①③⑤⑥⑦
Zhen (2015)	49	49	70.22 ± 7.33	70.12 ± 7.19	27/22	28/21	MXK + WM	WM	3c/t,3t/d	3 m	②④⑤⑥
Wu and Xiang (2018)	65	65	62.3 ± 4.3	61.2 ± 4.1	34/31	36/29	MXK + WM	WM	3c/t,3t/d	3 m	②③

T, treatment group; C, control group; M, male; F, Female; NXT, Naoxintong capsule; TXL, Tongxinluo capsule; BYHW, Buyang Huanwu Decoction; NMT, Naomaitai capsule; DZSM, Dengzhan Shengmai capsule; NST, Naoshuantong capsule; MXK, Maixuekang capsule; WM, conventional Western medicine; c, capsule; p, package; t, time; d, day; m, month; a, year; ①, recurrent stroke; ②, NIHSS; ③, fibrinogen; ④, fasting blood glucose; ⑤, triglycerides; ⑥, total cholesterol; ⑦, all–cause mortality; ⑧, adverse events.

Risk of Bias Assessment

According to the Cochrane risk of bias tool (Higgins et al., 2011), the quality assessment of all included RCTs was conducted by two researchers independently. Every RCT was classified as low, unclear, or high risk of bias based on seven quality evaluation items precisely: selection bias (random sequence generation and allocation concealment), performance bias (blinding of participants and personnel), detection bias (blinding of outcome assessment),

attrition bias (incomplete outcome data), reporting bias (selective reporting), and other bias. In addition, when assessing outcomes, the objective outcomes (e.g., recurrent stroke) and subjective outcomes (e.g., NIHSS) were considered separately. When a discordance exists between two researchers, the ultimate outcomes would be resolved by consensus with a third researcher.

Statistical Analysis

For binary variables, the outcomes were shown as odds ratios (ORs) as well as 95% confidence intervals (95% CIs). For continuous variables, the outcomes were presented as the mean differences (MDs) as well as 95% CIs. Moreover, the results were significantly different when 95% CIs of ORs did not contain 1 or 95% CIs of MDs did not include 0. In addition, if each outcome had at least two studies, the pairwise meta-analysis would be performed with a random effects model. Besides, different interventions would be compared by network meta-analysis under a frequentist framework with a random effects model. League tables were also utilized to display the findings of the systematical analysis. The chance of each treatment included in the systematical analysis being the best was evaluated using the surface under the cumulative ranking curve area (SUCRA) to obtain the best treatment (Salanti et al., 2011). In addition, cluster analysis was used to determine the optimum therapy for ischemic stroke.

In the standard pairwise meta-analysis, the statistical heterogeneity was tested by the calculation of I^2 statistics and the clinical heterogeneity was assessed by comparisons of data on potential effect modifiers. If the $I^2 \leq$ is 50%, the heterogeneity is not obvious (Higgins et al., 2003). Since each network graph was not looped, the incoherence (the statistical disagreement between direct and indirect results) could not be evaluated. In systematical analysis, we also assumed a consistent estimate for the heterogeneity variance. The distribution of putative effect modifiers was examined to determine transitivity between treatment comparisons (Turner et al., 2012).

If the number of studies was adequate, funnel plots were used to determine the presence of publication bias. Furthermore, the GRADE evaluation would serve as the foundation for the quality assessment, which would cover the five aspects of research restriction: study limitation, indirectness, inconsistency, imprecision, and publication bias (Salanti et al., 2014). A subgroup meta-analysis was also performed to evaluate the following possible effect modifiers (source of heterogeneity): 1. Treatment dosage (low dose, median dose, and high dose). 2. The age of patients (mean age less than 60 and mean age not less than 60). 3. The specific methods of WM (with statins and without statins). Finally, a post hoc sensitivity analysis was made: we used a leave–one–out meta-analysis to identify the independent impact of each study on the pooled estimates. We use Stata 16.0 software to get the statistical outcomes and statistical graphing of this systematical analysis.

RESULTS

Literature Selection

A total of 2094 articles were obtained at first, including 541 articles from CNKI, 808 articles from WanFang data, 674 articles from CBM, 66 articles from VIP, 3 articles from PubMed, 0 and 2 articles, respectively, from the web of science and embase. After de-duplicating articles, a total of 1271 articles were taken into consideration. Then, following a thorough reading of the title and abstract of each publication, we excluded the publications that were not relevant to our systematical analysis. Furthermore, the full text of the remaining 196 articles was carefully read to find articles that met our PICOS principles. In the end, 47 articles were taken into consideration. In conclusion, only RCTs about the comparison between TCM + WM and WM were ultimately chosen. Furthermore, the conditions of patients and treatment methods must meet our pre-determined requisites. Moreover, the outcomes in the literature must have one of the primary outcomes. In addition, the follow-up time must be longer than 2 months. We show the PRISMA diagram about the further details of the article screening process in **Figure 1**.

Study Characteristics

On the whole, there were 47 RCTs (Liu and Wang, 2006; Gan, 2007; Huang and Huang, 2007; Chen et al., 2008; Liu and Cao, 2008; Sun, 2008; Yan et al., 2008; Zhang et al., 2008; Liu, 2009; Meng, 2009; Tian and Li, 2010; Shi D. H. et al., 2011; Shi F. H. et al., 2011; Chao, 2011; Jiao et al., 2011; Zang et al., 2011; Chen, 2012; Jiang, 2012; Lin and Li, 2012; Peng et al., 2012; Guo et al., 2013; Tu et al., 2013; Yu, 2013; Zhou, 2013; Huang et al., 2014; Liu et al., 2014; Ma et al., 2014; Peng and Niu, 2014; Song, 2014; Xue et al., 2014; Zhou, 2014; Chai, 2015; Ye et al., 2015; Zhen, 2015; Chen and Cao, 2016; Ge et al., 2016; Nan and Li, 2016; Bo et al., 2017; Xu, 2017; Dang et al., 2018; Lu et al., 2018; Wang, 2018; Wu and Xiang, 2018; Zhou, 2018; Liu, 2019; Sun, 2020) involving 10,732 patients. Most of the patients involved in the trial were middle-aged and elder. All articles were about two-arm comparisons between TCM + WM and WM, and seven comparisons were made a part of our systematical analysis: NXT + WM vs. WM (n = 15), TXL + WM vs. WM (n = 9), BYHW + WM vs. WM (n = 5), NMT + WM vs. WM (n = 5), DZSM + WM vs. WM (n = 5), NST + WM vs. WM (n = 4), MXK + WM vs. WM (n = 4). Moreover, the most used drugs were aspirin, statins, and antihypertensive drugs. The median follow-up time was found to be 1 year (range, 2 months to 5 years). More details of the included articles are described in **Table 2**. Additionally, the specific intervention methods of TCM in each publication have been demonstrated in **Supplementary material S3** Other detail information can be found in **Supplementary material S4** which demonstrated indications and chemical analysis of each TCM and **Supplementary material S5** which depicted compositions and extraction procedure of each TCM. Moreover, the network graphs of the above seven kinds of TCM + WM have been listed in **Figure 2**. About **Figure 2**, the size of the point is assigned by the total number of people in each study, and the width of the edge is assigned by the standard error.

Risk of Bias Assessment

When it comes to random sequence generation, 16 articles used random number tables or other random methods, therefore these articles were presumed to have a low risk of bias. On the contrary, two articles generated random sequences according to the admission time, which will lead to a high risk of bias. Regarding allocation concealment, three RCTs highlighted that

random sequences would be kept by a third party; they were thus evaluated to have a low risk of bias. In terms of performance bias, two articles mentioned the performance of the double-blind method leading to a low risk of bias. Nevertheless, seven articles did not use a placebo, thus the evaluation was "high." In terms of blinding of outcome assessment, two articles were assessed to have a low risk for using the double-blind method. Moreover, since all articles had no incomplete data, we classify them as low risk. Due to the lack of sufficient information, the biased entries of other aspects in each article were evaluated to be "unclear." In conclusion, the quality of included articles was poor. Summary of the risk of bias is demonstrated in **Figure 3** in which green indicates a low risk of bias, yellow indicates a medium risk of bias, and red indicates a high risk of bias.

Outcomes

Recurrent Stroke

In total, 40 studies involving 7 treatments regarding recurrent stroke were evaluated: NXT + WM vs. WM (n = 13), TXL + WM vs. WM (n = 8), BYHW + WM vs. WM (n = 5), NMT + WM vs. WM (n = 4), DZSM + WM vs. WM (n = 5), NST + WM vs. WM (n = 3), MXK + WM vs. WM (n = 2). All types of TCM + WM were superior to WM alone, and the results were significantly different. **Table 3** shows the detailed information of comparisons: NXT + WM vs. WM (OR = 0.54, 95%CIs (0.43, 0.66)), TXL + WM vs. WM (OR = 0.44, 95% CIs (0.31, 0.61)), BYHW + WM vs. WM (OR = 0.48, 95%CIs (0.26, 0.89)), NMT + WM vs. WM (OR = 0.20, 95%CIs (0.13, 0.32)), DZSM + WM vs. WM (OR = 0.53, 95%CIs (0.36, 0.79)), NST + WM vs. WM (OR = 0.36, 95%CIs (0.19, 0.68)), MXK + WM vs. WM (OR = 0.33, 95%CIs (0.16, 0.68)). Furthermore, NMT + WM vs. NXT + WM (OR = 0.37, 95%CIs (0.22, 0.62)), NMT + WM vs. TXL + WM (OR = 0.46, 95%CIs (0.26, 0.82)), NMT + WM vs. BYHW + WM (OR = 0.42, 95%CIs (0.19, 0.91)), NMT + WM vs. DZSM + WM (OR = 0.38, 95%CIs (0.20, 0.69)) were related to significantly reduce recurrent stroke. Other comparisons did not have statistically significant differences.

Based on the outcomes of SUCRA probabilities (**Table 4**; **Figure 4**), NMT + WM was most likely to be the best choice. In addition, the detailed ranking results of those seven kinds of TCM + WM were depicted as follows: NMT + WM (97.0%) > MXK + WM (71.1%) > NST + WM (66.5%) > TXL + WM (54.1%) > BYHW + WM (44.6%) > DZSM + WM (34.5%) > NXT + WM (32.1%) > WM (0.2%).

NIHSS

A total of 15 researches including 7 interventions referred to NIHSS: NXT + WM vs. WM (n = 2), TXL + WM vs. WM (n = 2), BYHW + WM vs. WM (n = 2), NMT + WM vs. WM (n = 2), DZSM + WM vs. WM (n = 2), NST + WM vs. WM (n = 3), MXK + WM vs. WM (n = 2). Compared with WM alone, all TCM + WM had significant effectiveness regarding NIHSS. In addition, the specific results are listed in **Table 3**: NXT + WM vs. WM (MD = −2.91, 95%CIs (−3.39, −2.43)), TXL + WM vs. WM (MD = −1.40, 95%CIs (−2.19, −0.61)), BYHW + WM vs. WM (MD = −3.51, 95%CIs (−5.11, −1.91)), NMT + WM vs. WM (MD = −1.37, 95%CIs (−2.15, −0.60)), DZSM + WM vs. WM (MD = −1.62, 95%CIs (−2.38, −0.85)), NST + WM vs. WM

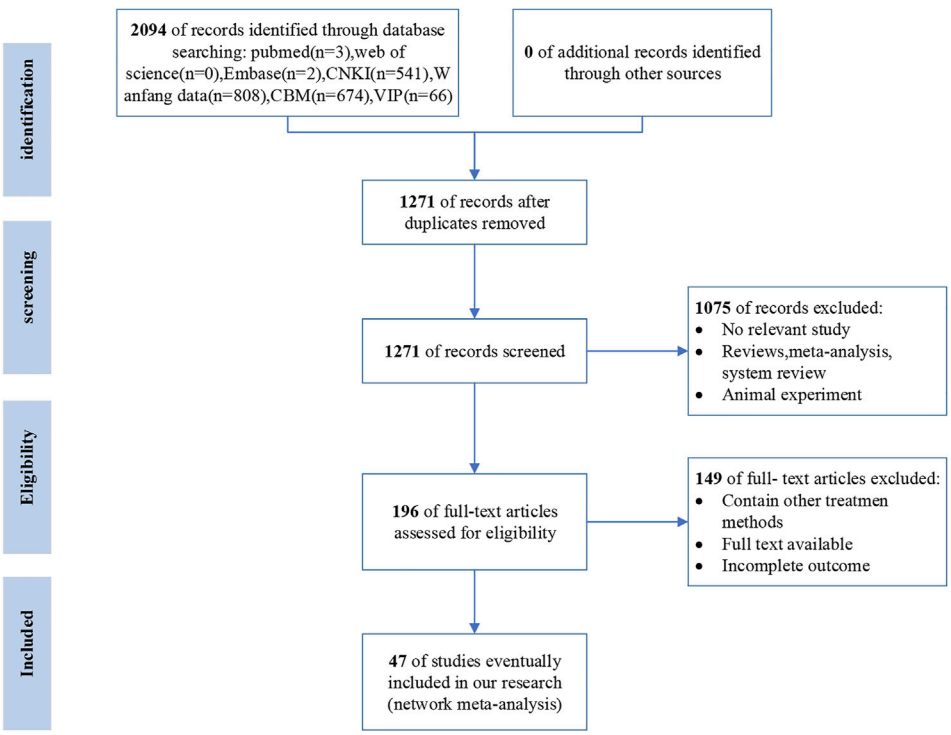

FIGURE 1 | Flow diagram of literature screening (CNKI, National Knowledge Infrastructure; CBM, the Chinese Biological Medicine Literature Service System; VIP, the Chinese Scientific Journal Full–text database; WF, the Wan–fang database; n, number of articles).

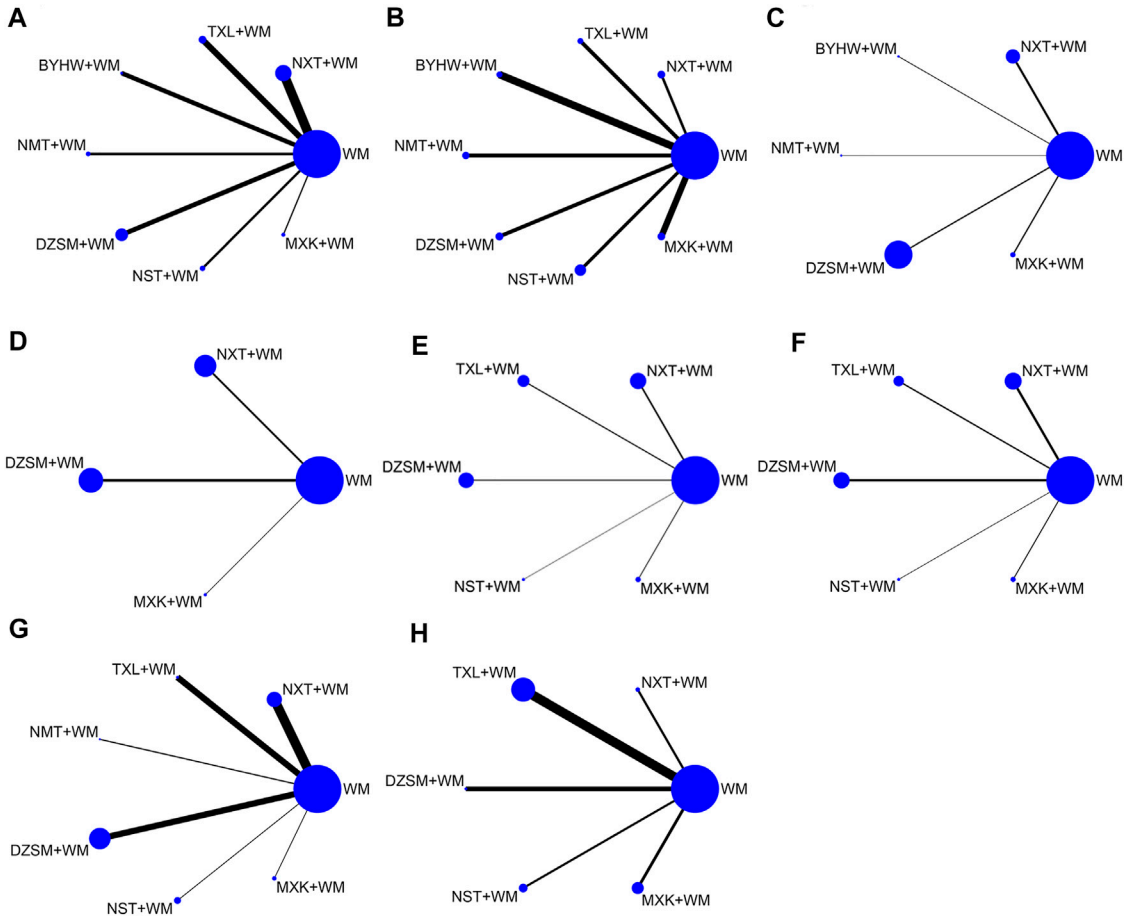

FIGURE 2 | Network graphs for various outcomes. The size of the point is assigned by the total number of people in each study, and the width of the edge is assigned by standard error. **(A)** Recurrent stroke; **(B)** NIHSS; **(C)** Fib; **(D)** FBG; **(E)** TG; **(F)** TC; **(G)** all−cause mortality; **(H)** AEs (NXT, Naoxintong capsule; TXL, Tongxinluo capsule; BYHW, Buyang Huanwu Decoction; NMT, Naomaitai capsule; DZSM, Dengzhan Shengmai capsule; NST, Naoshuantong capsule; MXK, Maixuekang capsule; WM, conventional Western medicine; Fib, fibrinogen; FBG, fasting plasma glucose; TG, triglycerides; TC, cholesterol; AEs, adverse events).

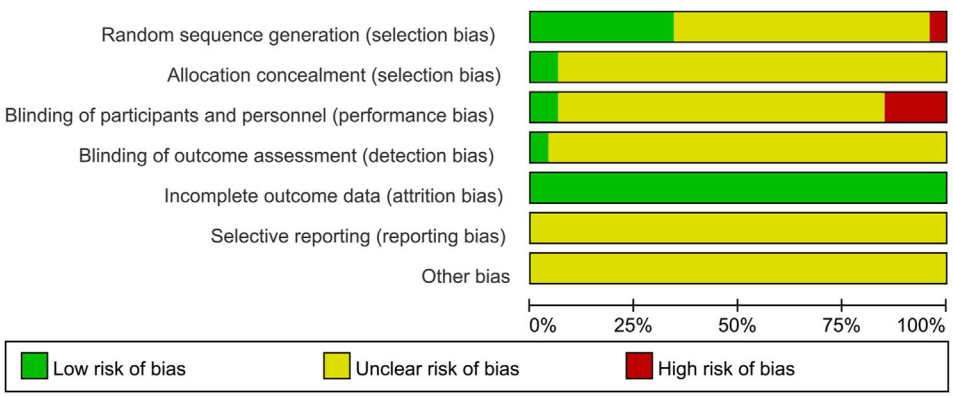

FIGURE 3 | Summary of the risk of bias. The vertical axis represents the quality evaluation items, and the horizontal axis represents the number of randomized controlled trials. Herein green indicates low risk of bias, yellow indicates medium risk of bias, and red indicates high risk of bias.

TABLE 3 | Final results of the systematical meta–analysis.

Outcomes	WM	NXT + WM	TXL + WM	BYHW + WM	NMT + WM	DZSM + WM	NST + WM	MXK + WM
Recurrent stroke (OR)	WM	— —	— —	— —	— —	— —	— —	— —
	1.86 (1.50,2.30)	NXT + WM	— —	— —	— —	— —	— —	— —
	2.29 (1.63,3.22)	1.23 (0.82,1.84)	TXL + WM	— —	— —	— —	— —	— —
	2.09 (1.12,3.90)	1.12 (0.58,2.17)	0.91 (0.45,1.86)	BYHW + WM	— —	— —	— —	— —
	5.00 (3.13,7.97)	2.68 (1.61,4.49)	2.18 (1.22,3.89)	2.39 (1.10,5.22)	NMT + WM	— —	— —	— —
	1.87 (1.26,2.79)	1.01 (0.64,1.58)	0.82 (0.48,1.38)	0.90 (0.43,1.88)	0.38 (0.20,0.69)	DZSM + WM	— —	— —
	2.79 (1.47,5.29)	1.50 (0.76,2.94)	1.22 (0.59,2.51)	1.34 (0.55,3.27)	0.56 (0.25,1.23)	1.49 (0.70,3.16)	NST + WM	— —
	2.99 (1.47,6.07)	1.61 (0.77,3.36)	1.30 (0.59,2.86)	1.43 (0.56,3.68)	0.60 (0.26,1.40)	1.59 (0.71,3.59)	1.07 (0.41,2.78)	MXK + WM
NIHSS (WM)	WM	— —	— —	— —	— —	— —	— —	— —
	2.91 (2.43,3.39)	NXT + WM	— —	— —	— —	— —	— —	— —
	1.40 (0.61,2.19)	−1.51 (−2.43,−0.58)	TXL + WM	— —	— —	— —	— —	— —
	3.51 (1.91,5.11)	0.60 (−1.07,2.27)	2.11 (0.33,3.89)	BYHW + WM	— —	— —	— —	— —
	1.37 (0.60,2.15)	−1.53 (−2.44,−0.62)	−0.03 (−1.13,1.08)	−2.14 (−3.92,−0.36)	NMT + WM	— —	— —	— —
	1.62 (0.85,2.38)	−1.29 (−2.19,−0.39)	0.21 (−0.88,1.31)	−1.90 (−3.67,−0.12)	0.24 (−0.85,1.33)	DZSM + WM	— —	— —
	2.47 (2.31,2.63)	−0.44 (−0.94,0.07)	1.07 (0.27,1.87)	−1.04 (−2.65,0.57)	1.10 (0.30,1.89)	0.86 (0.08,1.63)	NST + WM	— —
	2.63 (1.24,4.03)	−0.27 (−1.74,1.20)	1.23 (−0.37,2.83)	−0.88 (−3.00,1.24)	1.26 (−0.33,2.85)	1.02 (−0.57,2.61)	0.16 (−1.24,1.56)	MXK + WM
Fib (WM)	WM	— —	— —	— —	— —	— —	— —	— —
	1.04 (0.86,1.22)	NXT + WM	— —	— —	— —	— —	— —	— —
	1.09 (0.83,1.35)	0.05 (−0.26,0.36)	— —	BYHW + WM	— —	— —	— —	— —
	0.09 (−0.31,0.49)	−0.95 (−1.39,−0.51)	— —	−1.00 (−1.48,−0.52)	NMT + WM	— —	— —	— —
	0.28 (0.10,0.47)	−0.76 (−1.02,−0.50)	— —	−0.81 (−1.13,−0.49)	0.19 (−0.25,0.63)	DZSM + WM	— —	— —
	1.28 (0.93,1.62)	0.24 (−0.16,0.63)	— —	0.19 (−0.25,0.62)	1.19 (0.66,1.72)	1.00 (0.61,1.39)	— —	MXK + WM
FBG (WM)	WM	— —	— —	— —	— —	— —	— —	— —
	0.03 (−0.13,0.18)	NXT + WM	— —	— —	— —	— —	— —	— —
	0.19 (−0.01,0.40)	0.17 (−0.09,0.42)	— —	— —	— —	DZSM + WM	— —	— —
	0.41 (0.09,0.73)	0.38 (0.03,0.74)	— —	— —	— —	0.22 (−0.17,0.60)	— —	MXK + WM
TG (WM)	WM	— —	— —	— —	— —	— —	— —	— —
	0.38 (0.18,0.58)	NXT + WM		— —	— —	— —	— —	— —
	0.22 (0.03,0.41)	−0.16 (−0.43,0.12)	TXL + WM	— —	— —	— —	— —	— —
	0.03 (−0.23,0.28)	−0.35 (−0.68,−0.02)	−0.19 (−0.51,0.12)	— —	— —	DZSM + WM	— —	— —
	−0.42 (−0.89,0.05)	−0.80 (−1.31,−0.29)	−0.64 (−1.15,−0.14)	— —	— —	−0.45 (−0.98,0.09)	NST + WM	— —
	0.11 (−0.22,0.43)	−0.27 (−0.65,0.11)	−0.12 (−0.49,0.26)	— —	— —	0.08 (−0.33,0.49)	0.53 (−0.04,1.10)	MXK + WM
TC (WM)	WM	— —	— —	— —	— —	— —	— —	— —
	0.85 (0.37,1.34)	NXT + WM	— —	— —	— —	— —	— —	— —
	0.67 (0.08,1.26)	−0.18 (−0.95,0.58)	TXL + WM	— —	— —	— —	— —	— —
	0.39 (−0.22,1.00)	−0.47 (−1.24,0.31)	−0.28 (−1.13,0.57)	— —	— —	DZSM + WM	— —	— —
	−1.49 (−2.68,−0.29)	−2.34 (−3.63,−1.05)	−2.16 (−3.49,−0.82)	— —	— —	−1.87 (−3.21,−0.53)	NST + WM	— —
	0.54 (−0.30,1.39)	−0.31 (−1.29,0.66)	−0.13 (−1.16,0.90)	— —	— —	0.15 (−0.89,1.20)	2.03 (0.56,3.49)	MXK + WM
All-Cause mortality (OR)	WM	— —	— —	— —	— —	— —	— —	— —
	2.63 (1.27,5.45)	NXT + WM	— —	— —	— —	— —	— —	— —
	2.44 (0.43,13.88)	0.93 (0.14,6.11)	TXL + WM	— —	— —	— —	— —	— —
	0.63 (0.10,4.07)	0.24 (0.03,1.77)	0.26 (0.02,3.31)	— —	NMT + WM	— —	— —	— —
	3.07 (1.42,6.60)	1.17 (0.40,3.37)	1.26 (0.19,8.40)	— —	4.85 (0.65,36.29)	DZSM + WM	— —	— —

(Continued on following page)

TABLE 3 | (*Continued*) Final results of the systematical meta–analysis.

Outcomes	WM	NXT + WM	TXL + WM	BYHW + WM	NMT + WM	DZSM + WM	NST + WM	MXK + WM
	1.58 (0.48,5.14)	0.60 (0.15,2.40)	0.65 (0.08,5.29)	— —	2.49 (0.28,22.61)	0.51 (0.13,2.10)	NST + WM	— —
	1.70 (0.57,5.06)	0.65 (0.17,2.40)	0.70 (0.09,5.43)	— —	2.69 (0.31,23.27)	0.55 (0.15,2.10)	1.08 (0.22,5.39)	MXK + WM
AEs (OR)	WM	— —	— —	— —	— —	— —	— —	— —
	2.62 (0.36,19.24)	NXT + WM	— —	— —	— —	— —	— —	— —
	1.51 (0.57,4.01)	0.58 (0.06,5.32)	TXL + WM	— —	— —	— —	— —	— —
	1.00 (0.04,23.62)	0.38 (0.01,16.07)	0.66 (0.02,18.15)	— —	— —	DZSM + WM	— —	— —
	3.27 (0.47,22.60)	1.25 (0.08,20.11)	2.17 (0.25,18.92)	— —	— —	3.27 (0.08,133.13)	NST + WM	— —
	0.66 (0.07,6.46)	0.25 (0.01,5.23)	0.44 (0.04,5.24)	— —	— —	0.66 (0.01,32.60)	0.20 (0.01,4.01)	MXK + WM

The bolded and underlined results express statistically significant difference (NXT, Naoxintong capsule; TXL, Tongxinluo capsule; BYHW, Buyang Huanwu Decoction; NMT, Naomaitai capsule; DZSM, Dengzhan Shengmai capsule; NST, Naoshuantong capsule; MXK, Maixuekang capsule; WM, conventional Western medicine).

TABLE 4 | SUCRA of different treatments for various outcomes.

t	recurrent	NIHSS	Fib	FBG	TG	TC	AEs	all-cause mortality
WM	0.2	0	6.7	13.8	32.9	24.3	32.5	20.9
NXT+WM	32.1	83.4	70	25	95.4	89.5	68.8	72.5
TXL+WM	54.1	27.9	——	——	74.7	72.9	53.6	64.5
BYHW+WM	44.6	91.4	76.4	——	——	——	——	
NMT+WM	97	26.9	17.3	——	——	——	——	16.4
DZSM+WM	34.5	35	36	66.3	40.4	53	42	79.7
NST+WM	66.5	64.7	——	——	2.6	0.3	75.7	46.5
MXK+WM	71.1	70.6	93.6	94.9	54.1	63.7	27.5	49.5

The redder the data, the higher the ranking of the drug in the outcome indicator.

(MD = −2.47, 95%CIs (−2.63, −2.31)), MXK + WM vs. WM (MD = −2.63, 95%CIs (−4.03, −1.24)). In addition, comparisons of any one of the three drugs (BYHW + WM, NXT + WM, NST + WM) with any one of the other three drugs (DZSM + WM, NMT + WM, TXL + WM) performed statistically significantly different. Moreover, no statistically significant difference was found between other treatments.

According to the ranking of SUCRA probabilities (**Table 4**; **Figure 4**), the order of 7 types of TCM + WM was: BYHW + WM (91.4%) > NXT + WM (83.4%) > MXK + WM (70.6%) > NST + WM (64.7%) > DZSM + WM (35.0%) > TXL + WM (27.9%) > NMT + WM (26.9%) > WM (0.0%).

Fib

A total of 14 RCTs involving 5 interventions investigated Fib: NXT + WM vs. WM (n = 5), BYHW + WM vs. WM (n = 2), NMT + WM vs. WM (n = 1), DZSM + WM vs. WM (n = 4), MXK + WM vs. WM (n = 2). Except for NMT + WM, each TCM + WM's comparison with WM had significant difference. **Table 3** specifically expresses the following difference: NXT + WM vs. WM (MD = −1.04, 95%CIs (−1.22, −0.86)), BYHW + WM vs. WM (MD = −1.09, 95%CIs (−1.35, −0.83)), DZSM + WM vs. WM (MD = −0.28, 95%CIs (−0.47, −0.10)), MXK + WM vs. WM (MD = −1.28, 95%CIs (−1.62, −0.93)). Other detailed results can be found in **Table 3**.

Based on the SUCRA value (**Table 4**; **Figure 4**), the ranking of 5 types of TCM + WM was as follows: MXK + WM(93.6%) > BYHW + WM(76.4%) > NXT + WM(70.0%) > DZSM + WM(36%) > NMT + WM(17.3%) > WM(6.7%).

FBG

In total, 5 RCTs with three treatments referred to FBG were found: NXT + WM vs. WM (n = 2) DZSM + WM vs. WM (n = 2) MXK + WM vs. WM (n = 1). Only two comparisons in **Table 3** showed significant difference: MXK + WM vs. WM (MD = −0.41, 95%CIs (−0.73, −0.09)), MXK + WM vs. NXT + WM (MD = −0.38, 95%CIs: (−0.74, −0.03)). Other results showed no statistically significant difference.

Based on the ranking of SUCRA probabilities (**Table 4**; **Figure 4**), the ranking of the included three types of TCM + WM was as follows: MXK + WM (94.9%) > DZSM + WM (66.3%) > NXT + WM (25.0%) > WM (13.8%).

TG

A total of 16 articles with 5 interventions presented data about TG: NXT + WM vs. WM (n = 5), TXL + WM vs. WM (n = 5)

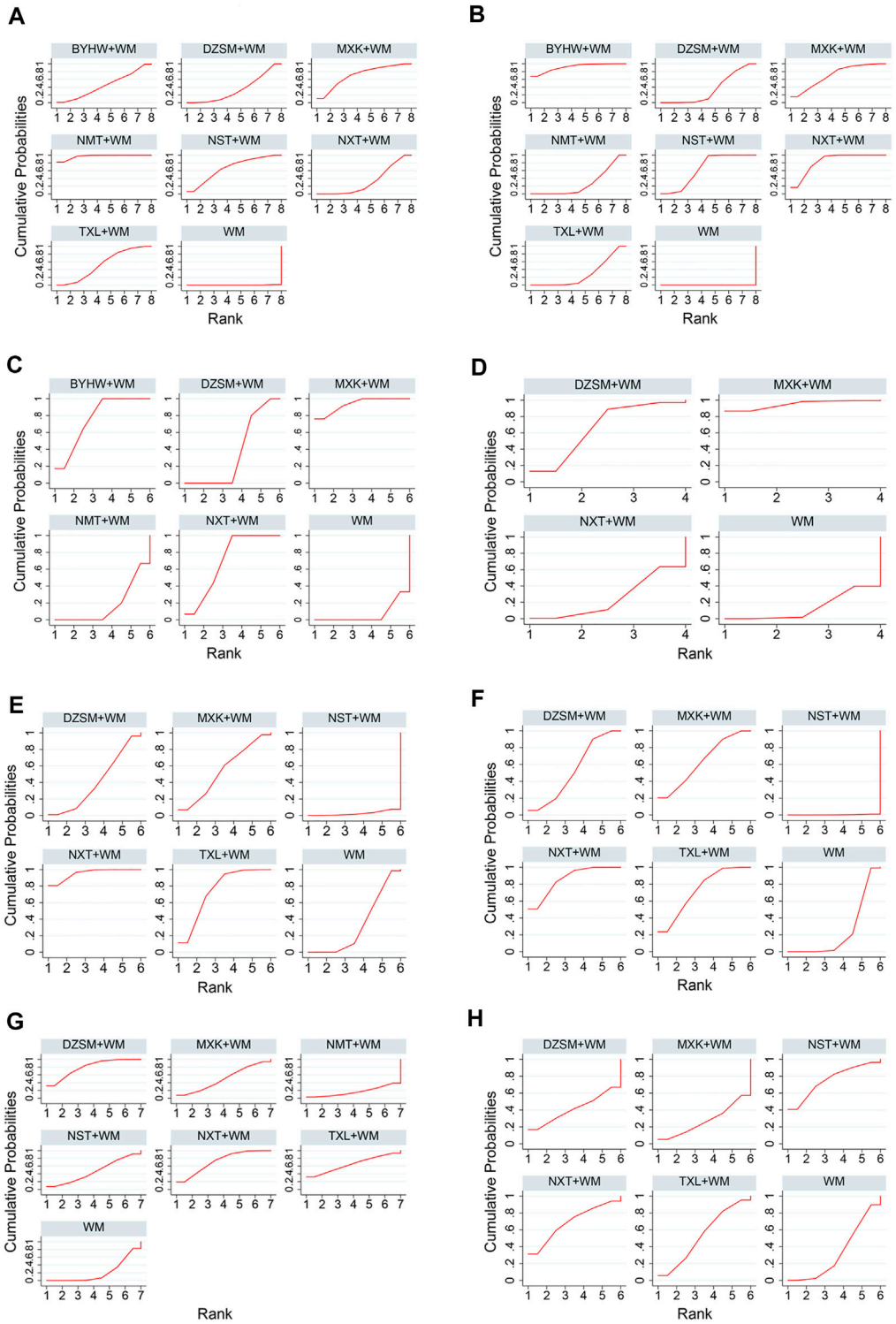

FIGURE 4 | SUCRA for various outcomes. The vertical axis represents cumulative probabilities, and the horizontal axis represents ranking of the treatment. **(A)** Recurrent stroke; **(B)** NIHSS; **(C)** Fib; **(D)** FBG; **(E)** TG; **(F)** TC; **(G)** All-cause mortality; **(H)** AEs (NXT, Naoxintong capsule; TXL, Tongxinluo capsule; BYHW, Buyang Huanwu Decoction; NMT, Naomaitai capsule; DZSM, Dengzhan Shengmai capsule; NST, Naoshuantong capsule; MXK, Maixuekang capsule; WM, conventional Western medicine; Fib, fibrinogen; FBG, fasting blood glucose; TG, triglycerides; TC, cholesterol; AEs, adverse events).

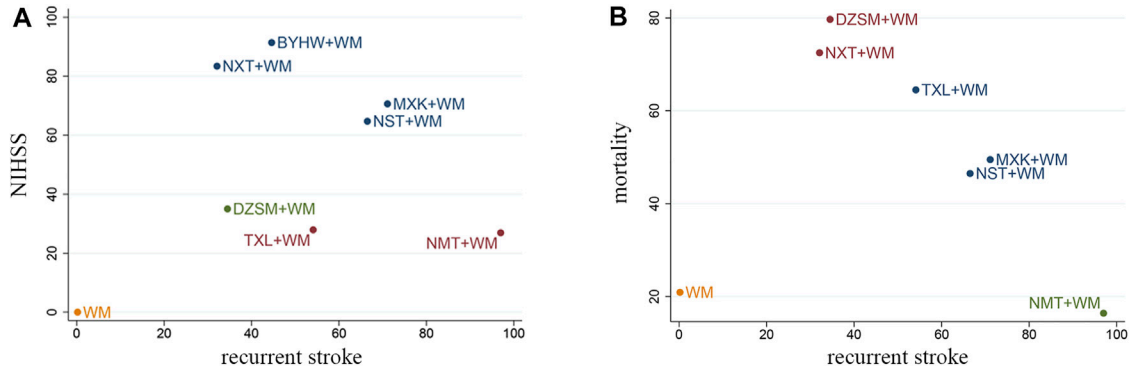

FIGURE 5 | Cluster analysis plots for three outcomes. **(A)** Recurrent stroke (*X* axis), NIHSS (*Y* axis); **(B)** recurrent stroke (*X* axis), all-cause mortality (*Y* axis). Herein blue indicates the best choice considering both outcomes, red indicates the second choice considering both outcomes, green indicates the third choice considering both outcomes, orange indicates the last choice considering both outcomes (NXT, Naoxintong capsule; TXL, Tongxinluo capsule; BYHW, Buyang Huanwu Decoction; NMT, Naomaitai capsule; DZSM, Dengzhan Shengmai capsule; NST, Naoshuantong capsule; MXK, Maixuekang capsule; WM, conventional Western medicine).

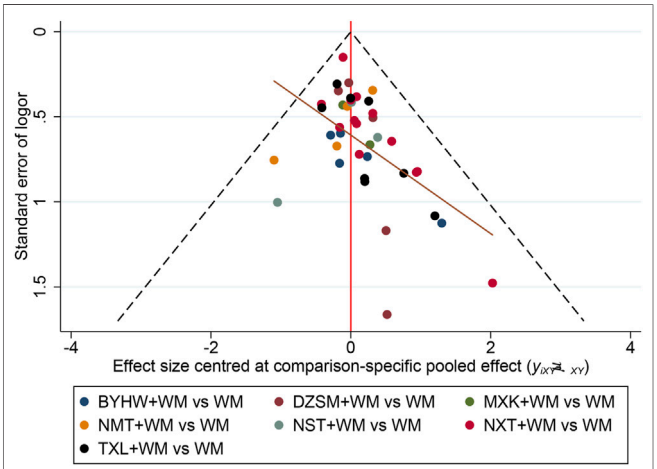

FIGURE 6 | Funnel plot for recurrent stroke. The vertical axis represents "standard error of effect size" and horizontal axis represents "effect size centered at comparison-specific pooled effect." (NXT, Naoxintong capsule; TXL, Tongxinluo capsule; BYHW, Buyang Huanwu Decoction; NMT, Naomaitai capsule; DZSM, Dengzhan Shengmai capsule; NST, Naoshuantong capsule; MXK, Maixuekang capsule; WM, conventional Western medicine).

DZSM + WM vs. WM (n = 3), NST + WM vs. WM (n = 1), MXK + WM vs. WM (n = 2). Compared with WM, only NXT + WM (MD = −0.80, 95%CIs (−1.31, −0.29)) and TXL + WM (MD = −0.64, 95%CIs (−1.15, −0.14)) significantly reduce TG. Also, the comparison results are demonstrated in **Table 3**.

According to the SUCRA values (**Table 4**; **Figure 4**), the order of 5 kinds of TCM + WM was: NXT + WM (95.4%) > TXL + WM (74.7%) > MXK + WM (54.1%) > DZSM + WM (40.4%) > WM (32.9%) > NST + WM (2.6%).

TC

The information of TC was available for 17 researches including 5 treatments: NXT + WM vs. WM (n = 6), TXL + WM vs. WM (n = 4) DZSM + WM vs. WM (n = 4), NST + WM vs. WM (n = 1), MXK + WM vs. WM (n = 2). As it is listed in **Table 3** that NXT + WM and TXL + WM significantly reduced TC compared with WM alone: NXT + WM vs. WM (MD = −2.34, 95%CIs (−3.63, −1.05)) and TXL + WM vs. WM (MD = −2.16, 95%CIs (−3.49, −0.82)). However, it is interesting to find that compared to WM alone, NST + WM (MD = 1.49, 95%CIs (0.29, 2.68)) significantly improved TC.

According to the ranking of SCURA probabilities (**Table 4**; **Figure 4**), the results of ranking of 5 treatments were as follows: NXT + WM (85.9%) > TXL + WM (72.9%) > MXK + WM (63.7%) > DZSM + WM (53%) > WM (24.3%) > NST + WM (0.3%).

All-Cause Mortality

In total, 16 studies involving 6 kinds of medicines investigated all-cause mortality: NXT + WM vs. WM (n = 6), TXL + WM vs. WM (n = 3), NMT + WM vs. WM (n = 1), DZSM + WM vs. WM (n = 4), NST + WM vs. WM (n = 1), MXK + WM vs. WM (n = 1). Only two results in **Table 3** demonstrate significant difference: DZSM + WM vs. WM (OR = 0.33, 95%CIs (0.15, 0.70)), NXT + WM vs. WM (OR = 0.38, 95%CIs (0.18, 0.79)).

It can be seen from SUCRA values (**Table 4**; **Figure 4**) that the six types of TCM + WM's rankings in reducing all-cause mortality were: DZSM + WM (79.7%) > NXT + WM (72.5%) > TXL + WM (64.5%) > MXK + WM (49.5%) > NST + WM (46.5%) > WM (20.9%) > NMT + WM (16.4%).

AEs

Most of the adverse events were gastrointestinal reaction, nausea, and giddiness(Peng and Niu, 2014; Bo et al., 2017; Xu, 2017). Our research showed that patients were tolerable for adverse reactions of TCM + WM or WM. In addition, the information of AEs was available for 8 researches involving 5 treatments: NXT + WM vs. WM (n = 1), TXL + WM vs. WM (n = 4) DZSM + WM vs. WM (n = 1), NST + WM vs. WM (n = 1), MXK + WM vs. WM (n = 1). All results performed no significant differences, which are listed in **Table 3.**

Based on the ranking of SUCRA probabilities (**Table 4**; **Figure 4**), the 5 interventions' rankings in reducing AEs were: NST + WM (75.7%) > NXT + WM (68.8%) > TXL + WM (53.6%) > DZSM + WM (42.0%) > WM (32.5%) > MXK + WM (27.5%).

TABLE 5 | GRADE assessment for recurrent stroke.

Summary of GRADE assessment for recurrent stroke					
Comparison effect	**Number of direct comparisons**	**Number of participants**	**Nature of evidence**	**Certainty**	**Reason for down grading**
NXT + WM vs. WM	13	1612 vs. 1687	Direct	Low	a, e
TXL + WM vs. WM	8	718 vs. 725	Direct	Moderate	a
BYHW + WM vs. WM	5	202 vs. 194	Direct	Low	b
NMT + WM vs. WM	4	408 vs. 388	Direct	Low	a, e
DZSM + WM vs. WM	5	1263 vs. 1254	Direct	Low	a, e
NST + WM vs. WM	3	483 vs. 480	Direct	Moderate	a
MXK + WM vs. WM	2	327 vs. 327	Direct	Low	a, e

[a]*The quality assessment of most studies is unclear (study limitation).*
[b]*The quality assessment of most studies is low (study limitation).*
[c]*The heterogeneity between pairwise comparisons was high (inconsistency). [no comparison effect needs to be downgraded for this reason].*
[d]*Small sample size or results show no obvious tendency to a drug (imprecision) [no comparison effect needs to be downgraded for this reason].*
[e]*Potential publication bias (publication bias).*

TABLE 6 | Subgroup analysis for recurrent stroke and NIHSS.

Outcome	**Average age**		***p* value for interaction**	**Dose**			***p* value for interaction**	**Western medicine**		***p* value for interaction**
	<60	**≥60**		**Low**	**Median**	**High**		**With stain**	**Without statin**	
Placebo(reference)										
Recurrent stroke										
NXT + WM	0.39 (0.18, 0.83)	0.43 (0.29, 0.66)	0.8	0.82 (0.35, 1.88)	0.53 (0.42, 0.69)	0.52 (0.31, 0.89)	0.62	0.52 (0.36, 0.75)	0.55 (0.43, 0.72)	0.79
TXL + WM	0.45 (0.28, 0.73)	0.35 (0.19, 0.64)	0.51	0.29 (0.11, 0.77)	0.46 (0.24, 0.89)	0.36 (0.15, 0.86)	0.74	0.44 (0.31, 0.63)	0.36 (0.06, 2.01)	0.81
BYHW + WM	0.13 (0.01, 1.18)	−−	−−	−−	0.48 (0.26, 0.89)	−−	−−	0.59 (0.28, 1.22)	0.28 (0.08, 0.92)	0.29
NMT + WM	−−	0.16 (0.10, 0.26)	−−	0.20 (0.11, 0.36)	−−	−−	−−	0.15 (0.09, 0.26)	0.36 (0.14, 0.97)	0.12
DZSM + WM	−−	0.54 (0.36, 0.80)	−−	0.54 (0.30, 0.96)	0.60 (0.31, 1.16)	−−	0.8	0.60 (0.31, 1.16)	0.50 (0.30, 0.82)	0.64
NST + WM	−−	0.32 (0.16, 0.62)	−−	−−	0.36 (0.19, 0.68)	−−	−−	0.32 (0.16, 0.62)	1.02 (0.14, 7.31)	0.27
MXK + WM	−−	0.33 (0.16, 0.67)	−−	0.25 (0.07, 0.94)	0.37 (0.16, 0.86)	−−	0.64	0.25 (0.07, 0.94)	−−	−−
NIHSS										
NXT + WM	−2.91 (−3.44, −2.38)	−2.90 (−3.99, −1.81)	0.99	−−	−2.91 (−3.44, −2.38)	−2.90 (−3.99, −1.81)	0.99	−2.91 (−3.39, −2.43)	−−	−−
TXL + WM	−1.12 (−2.61, 0.37)	−1.51 (−2.44, −0.58)	0.66	−1.40 (−2.19, −0.61)	−−	−−	−−	−1.40 (−2.19, −0.61)	−−	−−
BYHW + WM	−3.51 (−5.11, −1.91)	−−	−−	−−	−3.51 (−5.11, −1.91)	−−	−−	−3.51 (−5.11, −1.91)	−−	−−
NMT + WM	−−	−1.37 (−2.15, −0.60)	−−	−1.37 (−2.15, −0.60)	−−	−−	−−	−1.22 (−2.10, −0.34)	−1.90 (−3.53, −0.27)	0.47
DZSM + WM	−−	−1.89 (−2.18, −1.60)	−−	−1.89 (−2.18, −1.60)	−−	−−	−−	−1.90 (−2.78, −1.02)	−0.76 (−2.29, −0.77)	0.2
NST + WM	−−	−2.17 (−2.80, −1.53)	−−	−−	−2.17 (−2.80, −1.53)	−−	−−	−2.17 (−2.80, −1.53)	−−	−−
MXK + WM	−−	−2.63 (−4.03, −1.24)	−−	−−	−2.63 (−4.03, −1.24)	−−	−−	−2.63 (−4.03, −1.24)	−−	−−

All I^2<50%.

Cluster Analysis

Two-dimensional clustering was utilized to find the best TCM through different indicators of various drugs. Herein blue indicates the best choice considering both outcomes, red indicates the second choice considering both outcomes, green indicates the third choice considering both outcomes, and orange indicates the last choice considering both outcomes. When it comes to recurrent stroke and NIHSS, the cluster analysis depicted that BYHW + WM, NXT + WM, MXK + WM, NST + WM were dominant in comparison (**Figure 5A**). Furthermore, as cluster analysis related to recurrent stroke and al-cause mortality was made, we found that MXK + WM, NST + WM had relatively good curative effects (**Figure 5B**). In conclusion, the results of cluster analysis demonstrated that MXK + WM, NST + WM had relatively good secondary prevention effects with regard to recurrent stroke, NIHSS, and all-cause mortality.

Publication Bias

To test the publication bias, the comparison–adjusted funnel plots for recurrent stroke were plotted. As it is listed in **Figure 6**, we found the scatters were basically symmetrical along the center line and the angle between the center line and the adjusted auxiliary line was not large. The results indicated that there is little publication bias and the small sample effects were rare.

GRADE Assessment

Here, strength of evidence was evaluated through GRADE assessment which was about the comparisons between TCM + WM with WM on recurrent stroke. Except BYHW + WM had high risk of bias leading to low certainty evidence, other types of TCM + WM's study limitation were uncertain. Furthermore, there was no inconsistency in this systematical analysis which meant no study needs to be downgraded. In addition, all researches had enough sample size and demonstrated obvious tendency to TCM giving rise to no imprecision. Thus, all study didn't required to be downgraded. Moreover, some of the TCM + WM were downgraded for having publication bias. (**Table 5**).

Subgroup Analysis

For recurrent stroke and NIHSS, all calculation of potential effect modifier (potential source of heterogeneity) including age of patients (average age <60 vs. average age ≥60), treatment dose (low does vs. medium dose vs. high dose), and the specific methods of WM (with statins vs. without statins) demonstrated no significant difference (**Table 6**). Thus, we believe that the age of patients and treatment dose had little effect on the transitivity of our systematical analysis.

Sensitivity Analysis

In the standard pairwise meta-analysis, statistical heterogeneity was tested by the calculation of I^2 if the number of the study was at least 5 and we find all I^2<50%. Additionally, a leave–one–out meta-analysis was used to evaluate the independent effect of every study on summary results. The results suggested that no study needed to be excluded, thus we thought each study produced little bias in the results.

DISCUSSION

Unilateral weakness, unilateral sensory loss, speech disturbance, clumsiness or ataxia, and vertigo are all common stroke symptoms (Hankey and Blacker, 2015). Non-contrast CT is used to precisely diagnose the condition because of its sensitivity and rapidity. RI is also employed to refine the understanding of infarct location (Powers et al., 2019). In addition, most ischemic strokes originated from thromboembolism, the common source of embolism is atherosclerosis and heart disease, especially atrial fibrillation. Other causes of ischemic stroke involve small vessel disease, which has a close association with hypertension and diabetes, especially in Asia (Campbell et al., 2019).

The systematical analysis approach was taken to compare the secondary prevention effects and safety of TCM + WM in the treatment of stroke. In this study, a total of 47 RCTs including 10,732 patients were included in this work, and we evaluated 7 treatments in terms of 8 indicators involving recurrent stroke, NIHSS, Fib, FBG, TG, TC, all-cause mortality, and AEs. The results indicated that all kinds of TCM + WM were more effective on long-term secondary prevention of ischemic stroke than WM alone. Additionally, through cluster analysis, we concluded that MXK + WM and NST + WM had relatively good preventive effects.

In this systematical analysis, seven kinds of TCM were extracted from Astragali Radix, Radix, Chuanxiong Rhizoma, Persicae Semen, Carthami Flos, Pheretima, or other herbs through modern technological means (Bu et al., 2020). Guo et al. reported TCM has the effects of anti-oxidation, anti-inflammatory, anti-apoptosis, and protection of blood–brain barrier (Guo et al., 2017). Furthermore, Yan et al. found that the TCM can prevent stroke through a variety of signaling pathways (Yan et al., 2019), such as JAK2/STAT3 which regulates proinflammatory cytokine expression (Chen et al., 2017; Hu et al., 2017), NF–κB which is related to the inflammatory mechanism of brain tissue reperfusion injury (Fann et al., 2018; Fu et al., 2020), PI3K/Akt which participates in the pathological process of cerebral ischemia and plays a role in promoting survival and anti-apoptotic pathway (Samakova et al., 2019; Chen et al., 2020).

Nevertheless, there were few systematic reviews and meta-analyses to show the long-term secondary preventive effects of TCM on ischemic stroke. The comparisons between them were rather ambiguous leading to confusion in choosing the appropriate drugs. Thus, this study used pairwise meta-analysis as well as network meta-analysis thus better demonstrating the effects of different kinds of TCM. In addition, different types of TCM were quantitatively ranked to determine the best choice for treatment in clinical settings.

In terms of primary outcomes including recurrent stroke and NIHSS, the results suggested that all types of TCM + WM were better than WM, and results had a statistically significant difference. Some articles reported its origin from multi-channel and multi-target therapy of TCM (Li and Li, 2016;

Wei, 2016). Wang et al. said NXT can decrease recurrent stroke and NIHSS, which also corroborates well with our study (Wang et al., 2019). Also, Ma et al. pointed out DZSM is beneficial for recurrent stroke and NIHSS (Ma et al., 2014). However, Xie found there was no significant difference in the recurrent stroke between the BYHW + WM and WM (Xie, 2015), and we guessed it was caused by a small sample size at that time. Moreover, according to the ranking of SUCRA probabilities, NMT + WM, MXK + WM were most likely to become the best treatments for recurrent stroke, and BYHW + WM and NXT + WM were most probably to be the best choices for NIHSS.

The secondary outcomes were stroke risk factors including Fib, FBG, TG, and TC (Diener and Hankey, 2020). The SCURA ranking of WM alone was very low, implying that the combination of TCM and WM was superior to WM. NST was lower in SUCRA values compared with WM when it comes to TC and TG. We believe that the reason behind NST reducing stroke recurrence was due to other stroke risk factors. Moreover, Chen and Yu showed that MXK can decrease Fib which agrees with our results (Chen and Yu, 2020). Our conclusion was also consistent with Wang et al. who proved that NXT is beneficial for reducing TC and TG (Wang et al., 2019). Furthermore, our results were favored by the outcome of the experiments utilizing TCM to reduce blood lipid and blood glucose in mice (Chen et al., 2018; Li et al., 2018). Based on SUCRA value, MXK + WM and BYHW + WM were most likely to be the best choice for reducing Fib. In terms of FBG, MXK had the highest probability to be the best treatment. In TC, the most effective choices were NXT + WM and TXL + WM. Moreover, NXT + WM and TXL + WM were most likely to be the best in TG. However, the samples of some secondary outcome indicators of TCM were less, thus more RCTs are warranted to test our results.

For all-cause mortality, only DZSM and NXT were found to significantly decrease all-cause mortality, all other comparisons have no statistically significant difference. As regards AEs, there was no significant difference in all contrasts. Thus, this implied that all kinds of TCM + WM were more or less tolerable for patients, however, it may be limited to lack of data. Moreover, the AEs predominantly include gastrointestinal reactions, nausea, and giddiness (Peng and Niu, 2014; Bo et al., 2017; Xu, 2017).

In conclusion, TCM + WM were more effective than WM in the long–term secondary prevention for patients with ischemic stroke, and there was no significant difference in the comparisons of AEs. Regarding recurrent stroke, NIHSS, and all-cause mortality, MXK + WM and NST + WM had relatively good preventive effects on long-term secondary prevention through cluster analysis. The basis for confirming the secondary preventive effect of MXK and NST on cerebral infarction is as follows.

The main component of MXK is *Hirudo nipponic*a Whitman (Haemadipsidae, Hirudo) which is the strongest natural thrombin-specific inhibitor discovered yet (Junren et al., 2021). Hirudin inhibits thrombin activity by directly binding with thrombin and plays an anticoagulant role. Second, hirudin has a strong antiplatelet effect, which can inhibit thrombin-induced platelet thrombin binding, platelet activation as well as aggregation (Garcia et al., 2012; Han et al., 2020). Additionally, in comparison with heparin, hirudin has less bleeding and side effects, and it has no allergic reaction and no toxicity (Johnson, 1994; Markwardt, 1994). Furthermore, clinical trials (e.g., Peng, Zhen, Ge, and Wu) showed that MXK has a significant effect on the secondary prevention of ischemic stroke (Peng and Niu, 2014; Zhen, 2015; Ge et al., 2016; Wu and Xiang, 2018).

Typha orientalis C. Presl (Typhaceae, Typhae Pollen), *Paeonia lactiflora* Pall (Paeoniaceae, Paeoniae Radix Rubra), *Curcuma phaeocaulis* Valeton (Zingiberaceae, Curcumae Radix), *Gastrodia elata* Blume (Orchidaceae, Gastrodiae Rhizoma), *Rha ponticum uniflorum* (L.) DC (Compositae, Rhapontici Radix) make up NST, a Chinese medication (Luo et al., 2020). It is also extensively used for increasing blood circulation, eliminating blood stasis, and promoting nerve function recovery (Liu et al., 2014). Moreover, a meta-analysis showed that NST has the effect of increasing blood adiponectin, decreasing neurological deficits, and reducing the area of atherosclerotic plaque (Zhang et al., 2019). Since it has been widely used to treat ischemic stroke, Liu and Huang demonstrated that NST + WM is better than WM in recurrent stroke, and the results are significantly different (Liu and Li, 2012; Huang et al., 2014).

INNOVATIONS AND LIMITATIONS OF THE STUDY

This is for the first time that the secondary prevention effects of various kinds of TCM on ischemic stroke as well as their safety were systematically evaluated. Moreover, this is the pioneer study, ranking seven kinds of TCM based on SUCRA value from different indicators, which furnishes the high-quality basis for clinical practice. Finally, strict inclusion and exclusion criteria were established, and the articles were thereby searched comprehensively.

Nevertheless, the risk of bias in most included articles was unclear and no direct comparison between TCM was found, giving rise to a lack of evidence, but we included 47 articles involving a large sample size and the subgroup analysis showed that the transitivity was good. All included RCTs were conducted in China, therefore more RCTs are needed to see whether the findings of this study applied to patients from other regions. Furthermore, clinical heterogeneity might appear because of the diversity and different courses of treatment of Western medicine. Despite these shortcomings, this is the first comparison of the long-term secondary prevention effects of various TCM on ischemic stroke from multiple indexes and provide some valuable suggestions for clinical practice.

CONCLUSION

In summary, our systematical analysis revealed that TCM had positive secondary prevention effects on patients with cerebral infarction, and there was no significant difference in the comparisons of AEs. Additionally, MXK + WM and NST + WM had relatively good preventive effects for recurrent stroke, NIHSS, and all-cause mortality.

Nevertheless, on account of some limitations, more high-quality, and double-blinded multicenter RCTs with a larger sample size are needed to test and verify our results in the future.

DATA AVAILABILITY STATEMENT

The original contributions presented in the study are included in the article/**Supplementary Material**. Further inquiries can be directed to the corresponding authors.

AUTHOR CONTRIBUTIONS

JL and LY conceived and designed the study. XZ, YZ and HW extracted and analyzed the data. JL, YH and WJ performed this systematical analysis. JL and XL wrote this manuscript. LY, WJ and XZ played an important role in the revision of the manuscript. All authors contributed to the article and approved the final version of manuscript.

FUNDING

This work was supported by the National Key R&D Program of China (Nos. 2019YFC1708600, 2019YFC1708604) the National Natural Science Foundation of China (Nos.81630105, 81904083, 81973560), and the Key Laboratory of TCM Encephalopathy of Zhejiang Province (grant no. 2020E10012).

SUPPLEMENTARY MATERIAL

The Supplementary Material for this article can be found online at: https://www.frontiersin.org/articles/10.3389/fphar.2021.722975/full#supplementary-material

REFERENCES

Amarenco, P., Lavallée, P. C., Labreuche, J., Albers, G. W., Bornstein, N. M., Canhão, P., et al. (2016). One–Year Risk of Stroke after Transient Ischemic Attack or Minor Stroke. *N. Engl. J. Med.* 374 (16), 1533–1542. doi:10.1056/NEJMoa1412981

Bhatt, D. L., Flather, M. D., Hacke, W., Berger, P. B., Black, H. R., Boden, W. E., et al. (2007). Patients with Prior Myocardial Infarction, Stroke, or Symptomatic Peripheral Arterial Disease in the CHARISMA Trial. *J. Am. Coll. Cardiol.* 49 (19), 1982–1988. doi:10.1016/j.jacc.2007.03.025

Bhatt, D. L., Fox, K. A., Hacke, W., Berger, P. B., Black, H. R., Boden, W. E., et al. (2006). Clopidogrel and Aspirin versus Aspirin Alone for the Prevention of Atherothrombotic Events. *N. Engl. J. Med.* 354 (16), 1706–1717. doi:10.1056/NEJMoa060989

Bo, G., Wan, Y., Wang, G. H., and Xiong, H. (2017). The Clinical Research of Tongxinluo Capsule in Treating Ischemic Stroke Patients. *J. Chengdu Med. Coll.* 12 (03), 277–279. doi:10.3969/j.issn.1674–2257.2017.03.008

Bu, L., Dai, O., Zhou, F., Liu, F., Chen, J. F., Peng, C., et al. (2020). Traditional Chinese Medicine Formulas, Extracts, and Compounds Promote Angiogenesis. *Biomed. Pharmacother.* 132, 110855. doi:10.1016/j.biopha.2020.110855

Campbell, B. C. V., De Silva, D. A., Macleod, M. R., Coutts, S. B., Schwamm, L. H., Davis, S. M., et al. (2019). Ischaemic Stroke. *Nat. Rev. Dis. Primers* 5 (1), 70. doi:10.1038/s41572–019–0118–8

Chai, X. B. (2015). Observation on the Curative Effect of Tongxinluo Capsule Combined with Statins and Aspirin in the Treatment of Cerebral Infarction. *Inner Mongolia J. Traditional Chin. Med.* (7), 70–71. doi:10.3969/j.issn.1006–0979.2015.07.071

Chao, J. F. (2011). A Multicenter, Randomized, Double–Blind Clinical Study on Secondary Prevention of Ischemic Stroke with Yiqi Huoxue Yangyin Herbs. Doctor. *J. Chengdu Univ. Traditional Chin. Med.*

Chen, B., Fang, X. H., Wu, Y. H., Jing, S. L., Sun, H. J., and Li, S. T. (2008). Acute Ischemic Stroke: Paradigm for Treatment. *Chin. J. Neurol.* 41 (3), 195–230. doi:10.3321/j.issn:1006–7876.2008.03.015

Chen, W. F., and Yu, T. (2020). Meta Analysis of the Clinical Effect of Maixuekang Capsule in the Treatment of Acute Cerebral Infarction. *Hunan J. Traditional Chin. Med.* 36 (08), 134–139. doi:10.16808/j.cnki.issn1003–7705.2020.08.055

Chen, X., Chen, H., He, Y., Fu, S., Liu, H., Wang, Q., et al. (2020). Proteomics–Guided Study on Buyang Huanwu Decoction for its Neuroprotective and Neurogenic Mechanisms for Transient Ischemic Stroke: Involvements of EGFR/PI3K/Akt/Bad/14–3–3 and Jak2/Stat3/Cyclin D1 Signaling Cascades. *Mol. Neurobiol.* 57 (10), 4305–4321. doi:10.1007/s12035–020–02016–y

Chen, X., Li, G. M., Zhou, L. H., Sun, J. B., Huang, Y., and Luo, E. L. (2018). Effect of Dengzhanshengmai (DZSM) on Cognition Function, Blood Glucose and Blood Lipid Level for Mouse Model of Transient Ischemic Attack. *Anatomical Res.* 40 (03), 161–164+181. doi:10.3969/j.issn.1671–0770.2018.03.001

Chen, Y., and Cao, J. (2016). Clinical Observation on 35 Cases of Cerebral Infarction in Convalescence Treated with Integrated Traditional Chinese and Western Medicine. *Pract. Clin. J. Integrated Traditional Chin. West. Med.* 16 (5), 16–18. doi:10.13638/j.issn.1671–4040.2016.05.007

Chen, Y. (2012). Effect of Naoxintong Capsule Combined with Atorvastatin on Secondary Prevention of Acute Cerebral Infarction. *Chin. Manipulation Rehabil. Med.* 3 (8), 26.

Chen, Y., Huang, X. S., Wu, H. J., Luo, Y. L., Wang, Y., and Tan, L. H. (2017). Effect of Puerarin on JAK2/STAT3 Signaling Pathway after Cerebral Ischemia–Reperfusion Injury in Rats. *Hunan J. Traditional Chin. Med.* 33 (04), 144–147+165. doi:10.16808/j.cnki.issn1003–7705.2017.04.070

Collaborators, G. D. a. H. (2017a). Global, Regional, and National Age–Sex Specific Mortality for 264 Causes of Death, 1980–2016: a Systematic Analysis for the Global Burden of Disease Study 2016. *Lancet* 390 (10100), 1151–1210. doi:10.1016/S0140–6736(17)32152–9

Collaborators, G. D. a. H. (2017b). Global, Regional, and National Disability–Adjusted Life–Years (DALYs) for 333 Diseases and Injuries and Healthy Life Expectancy (HALE) for 195 Countries and Territories, 1990–2016: a Systematic Analysis for the Global Burden of Disease Study 2016. *Lancet* 390 (10100), 1260–1344. doi:10.1016/S0140–6736(17)32130–X

Dang, C. J., Yu, X. F., Cai, D. F., Zhu, X. Y., Zhang, H. Z., Wang, M. Z., et al. (2018). Secondary Prevention Effect of Naoxintong Capsule on Ischemic Stroke of Blood Stasis Type. *J. Traditional Chin. Med.* 59 (13), 1121–1125. doi:10.13288/j.11–2166/r.2018.13.011

De Laat, A. (2017). Network Meta–Analysis. *J. Oral Rehabil.* 44 (10), 735. doi:10.1111/joor.12540

Diener, H. C., Bogousslavsky, J., Brass, L. M., Cimminiello, C., Csiba, L., Kaste, M., et al. (2004). Aspirin and Clopidogrel Compared with Clopidogrel Alone after Recent Ischaemic Stroke or Transient Ischaemic Attack in High–Risk Patients (MATCH): Randomised, Double–Blind, Placebo–Controlled Trial. *Lancet* 364 (9431), 331–337. doi:10.1016/S0140–6736(04)16721–4

Diener, H. C., and Hankey, G. J. (2020). Primary and Secondary Prevention of Ischemic Stroke and Cerebral Hemorrhage: JACC Focus Seminar. *J. Am. Coll. Cardiol.* 75 (15), 1804–1818. doi:10.1016/j.jacc.2019.12.072

Fann, D. Y., Lim, Y. A., Cheng, Y. L., Lok, K. Z., Chunduri, P., Baik, S. H., et al. (2018). Evidence that NF–Kb and MAPK Signaling Promotes NLRP Inflammasome Activation in Neurons Following Ischemic Stroke. *Mol. Neurobiol.* 55 (2), 1082–1096. doi:10.1007/s12035–017–0394–9

Feigin, V. L., Feigin, V. L., Nguyen, G., Cercy, K., Johnson, C. O., Alam, T., et al. (2018). Global, Regional, and Country–specific Lifetime Risks of Stroke, 1990 and 2016. *N. Engl. J. Med.* 379 (25), 2429–2437. doi:10.1056/NEJMoa1804492

Fu, C., Zhang, X., Zeng, Z., Tian, Y., Jin, X., Wang, F., et al. (2020). Neuroprotective Effects of Qingnao Dripping Pills against Cerebral Ischemia via Inhibiting NLRP3 Inflammasome Signaling Pathway: *In Vivo* and *In Vitro*. *Front. Pharmacol.* 11, 65. doi:10.3389/fphar.2020.00065

Gan, Z. R. (2007). Effect of Naomaitai Capsule on Serum C–Reactive Protein and Prognosis in Patients with Cerebral Infarction. *Chin. Gen. Pract.* 10 (24), 2040–2042. doi:10.3969/j.issn.1007–9572.2007.24.007

Gao, C. Y. (2015). Thinking of Integrated Traditional Chinese and Western Medicine on Secondary Prevention of Ischemic Stroke. *Proc. 11th China Neurol. Conf. integrated traditional Chin. West. Med.*, 94.

Garcia, D. A., Baglin, T. P., Weitz, J. I., and Samama, M. M. (2012). Parenteral Anticoagulants: Antithrombotic Therapy and Prevention of Thrombosis, 9th Ed: American College of Chest Physicians Evidence–Based Clinical Practice Guidelines. *Chest* 141 (2 Suppl. l), e24S–e43S. doi:10.1378/chest.11–2291

Ge, Y. C., Zhao, H. Q., Shi, J., and Wu, Z. H. (2016). Value of Maixuekang Capsule in Secondary Prevention of Ischemic Stroke. *China J. Mod. Med.* 26 (21), 83–86. doi:10.3969/j.issn.1005–8982.2016.21.017

Guo, J. Q., Wang, X. J., Yao, B. L., Zhang, H., He, L. N., Lu, X., et al. (2013). Effect of Tongxinluo Capsule on Sequela of Cerebral Infarction. *Chin. J. Coal Industry Med.* 16 (2), 1972–1974.

Guo, L., Huang, G. L., Zhou, K., Zhou, D. W., and Lu, Y. (2017). Research Progress on the Mechanism of Traditional Chinese Medicine and its Effective Components in the Prevention and Treatment of Cerebral Apoplexy Ischemia–Reperfusion Injury. *Heilongjiang J. Traditional Chin. Med.* 46 (02), 69–71.

Guo, P. P., Chen, X. X., Wang, X. R., and Liu, Z. G. (2019). Progress in the Mechanism and Clinical Treatment of Antiplatelet Resistance of Aspirin and Clopidogrel. *Chin. J. Clin. Neurosciences* 27 (03), 321–328.

Hackam, D. G., and Spence, J. D. (2007). Combining Multiple Approaches for the Secondary Prevention of Vascular Events after Stroke: a Quantitative Modeling Study. *Stroke* 38 (6), 1881–1885. doi:10.1161/STROKEAHA.106.475525

Han, H. H., Zhang, H. T., Wang, R., Yan, Y., Liu, X., Wang, Y., et al. (2020). Improving Long Circulation and Procoagulant Platelet Targeting by Engineering of Hirudin Prodrug. *Int. J. Pharm.* 589, 119869. doi:10.1016/j.ijpharm.2020.119869

Hankey, G. J., and Blacker, D. J. (2015). Is it a Stroke? *BMJ* 350, h56. doi:10.1136/bmj.h56

Heinrich, M., Appendino, G., Efferth, T., Fürst, R., Izzo, A. A., Kayser, O., et al. (2020). Best Practice in Research – Overcoming Common Challenges in Phytopharmacological Research. *J. Ethnopharmacol* 246, 112230. doi:10.1016/j.jep.2019.112230

Higgins, J. P., Altman, D. G., Gøtzsche, P. C., Jüni, P., Moher, D., Oxman, A. D., et al. (2011). The Cochrane Collaboration's Tool for Assessing Risk of Bias in Randomised Trials. *BMJ* 343, d5928. doi:10.1136/bmj.d5928

Higgins, J. P., Thompson, S. G., Deeks, J. J., and Altman, D. G. (2003). Measuring Inconsistency in Meta–Analyses. *BMJ* 327 (7414), 557–560. doi:10.1136/bmj.327.7414.557

Hu, G. Q., Du, X., Li, Y. J., Gao, X. Q., Chen, B. Q., and Yu, L. (2017). Inhibition of Cerebral Ischemia/reperfusion Injury–Induced Apoptosis: Nicotiflorin and JAK2/STAT3 Pathway. *Neural Regen. Res.* 12 (1), 96–102. doi:10.4103/1673–5374.198992

Huang, H. M., Ding, Y. B., Deng, W. H., and Pan, X. P. (2014). Application Research on Aspirin Resistance in Patients with Cerebral Infarction Treated by Naoshuantong. *Guide China Med.* (5), 19–20.

Huang, X. H., and Huang, X. B. (2007). *Clinical Study on Naomaitai Capsule in Preventing Recurrence of strokeThe Third pan TCM Forum, TCM "preventive Treatment" and the First Fuyang Forum*, 306–308.

Hutton, B., Salanti, G., Caldwell, D. M., Chaimani, A., Schmid, C. H., Cameron, C., et al. (2015). The PRISMA Extension Statement for Reporting of Systematic Reviews Incorporating Network Meta–Analyses of Health Care Interventions: Checklist and Explanations. *Ann. Intern. Med.* 162 (11), 777–784. doi:10.7326/M14–2385

Jiang, Y. X. (2012). Effect of Buchang Naoxintong Capsule on Secondary Prevention of Ischemic Cerebrovascular Disease. *Chin. J. Pract. Med.* 39 (12), 111–112. doi:10.3760/cma.j.issn.1674–4756.2012.12.056

Jiao, J., Niu, Y., and Wei, X. (2011). Clinical Effect of Buyang Huanwu Decoction on Secondary Prevention of Qi Deficiency Cerebral Infarction in Convalescence. *J. Zhejiang Univ. Tradit. Chin. Med.* 35 (6), 836–838. doi:10.3969/j.issn.1005–5509.2011.06.009

Johnson, P. H. (1994). Hirudin: Clinical Potential of a Thrombin Inhibitor. *Annu. Rev. Med.* 45, 165–177. doi:10.1146/annurev.med.45.1.165

Junren, C., Xiaofang, X., Huiqiong, Z., Gangmin, L., Yanpeng, Y., Xiaoyu, C., et al. (2021). Pharmacological Activities and Mechanisms of Hirudin and its Derivatives – A Review. *Front. Pharmacol.* 12, 660757. doi:10.3389/fphar.2021.660757

Kang, z., and Li, y. (2012). Application of Integrated Traditional Chinese and Western Medicine in Secondary Prevention of Cerebral Infarction. *Acta Chin. Med.* 27 (02), 220–222.

Kernan, W. N., Ovbiagele, B., Black, H. R., Bravata, D. M., Chimowitz, M. I., Ezekowitz, M. D., et al. (2014). Guidelines for the Prevention of Stroke in Patients with Stroke and Transient Ischemic Attack: a Guideline for Healthcare Professionals from the American Heart Association/American Stroke Association. *Stroke* 45 (7), 2160–2236. doi:10.1161/STR.0000000000000024

Lawes, C. M., Parag, V., Bennett, D. A., Suh, I., Lam, T. H., Whitlock, G., et al. (2004). Blood Glucose and Risk of Cardiovascular Disease in the Asia Pacific Region. *Diabetes Care* 27 (12), 2836–2842. doi:10.2337/diacare.27.12.2836

Li, S. S., and Li, G. Y. (2016). Research Progress on Prevention and Treatment of Ischemic Stroke with Traditional Chinese Medicine. *Anat. Res.* 38 (03), 200–202.

Li, T. M., Wu, Y., Xu, L. Y., and Zhong, P. (2018). Effect of Buyang Huanwu Decoction on Blood Lipid and Inflammatory Reaction of Atherosclerotic Plaque in ApoE Gene Deficient Mice. *J. New Chin. Med.* 50 (02), 5–8.

Lin, R. F., and Li, P. k. (2012). Observation on Cerebral Infarction of Qi Deficiency and Blood Deficiency Treated with Modified Buyang Huanwu Decoction. *China Health Industry* (4), 49–50.

Liu, F. (2019). Treatment of 24 Cases of Ischemic Stroke with Buyang Huanwu Decoction Combined with Aspirin. *China Pract. Med.* 14 (3), 119–120. doi:10.14163/j.cnki.11–5547/r.2019.03.072

Liu, H., Peng, Y. Y., Liang, F. Y., Chen, S., Li, P. B., Peng, W., et al. (2014). Protective Effects of Traditional Chinese Medicine Formula NaoShuanTong Capsule on Haemorheology and Cerebral Energy Metabolism Disorders in Rats with Blood Stasis. *Biotechnol. Biotechnol. Equip* 28 (1), 140–146. doi:10.1080/13102818.2014.901678

Liu, J. X., and Li, X. M. (2012). Therapeutic and Preventive Effects of Naoshuantong Capsule on Cerebral Infarction. *Guide China Med.* 10 (18), 5–6. doi:10.3969/j.issn.1671–8194.2012.18.003

Liu, S. R., and Cao, J. (2008). Effect of Tongxinluo Capsule on Secondary Prevention of Ischemic Stroke. *The Fourth Int. Conf. collaterals*, 252–255.

Liu, W. J., and Wang, S. X. (2006). Observation on the Effect of Naomaitai Capsule on 80 Cases of Cerebral Infarction. *Henan Traditional Chin. Med.* 26 (12), 71–72. doi:10.3969/j.issn.1003–5028.2006.12.053

Liu, W. W. (2009). *Preliminary Study of Dengzhan Shengmai Capsule on Secondary Prevention of Ischemic Stroke (6 Months).* [dissertation/master's thesis]. Wuhan, China: Hubei University of traditional Chinese Medicine.

Lu, Y. L., Qiao, X. D., and Ye, F. (2018). Effect of Tongxinluo Capsule Combined with Aspirin and Atorvastatin on Secondary Prevention of Ischemic Stroke. *Guizhou Med. J.* 42 (3), 318–320. doi:10.3969/j.issn.1000–744X.2018.03.024

Luo, L., Wu, S., Chen, R., Rao, H., Peng, W., and Su, W. (2020). The Study of Neuroprotective Effects and Underlying Mechanism of Naoshuantong Capsule on Ischemia Stroke Mice. *Chin. Med.* 15 (1), 119. doi:10.1186/s13020–020–00399–7

Ma, L. S., Chu, Z. H., and Zhao, S. C. (2014). Effect of Dengzhan Shengmai Capsule on Secondary Prevention of Atherosclerotic Cerebral Infarction. *Chin. J. Clin. Pharmacol. Ther.* 19 (04), 442–445.

Markwardt, F. (1994). The Development of Hirudin as an Antithrombotic Drug. *Thromb. Res.* 74 (1), 1–23. doi:10.1016/0049–3848(94)90032–9

Meng, X. Q. (2009). Effect of Buchang Naoxintong on Preventing Recurrence of Cerebral Infarction. *Liaoning J. Traditional Chin. Med.* 36 (11), 1942.

Mohan, K. M., Wolfe, C. D., Rudd, A. G., Heuschmann, P. U., Kolominsky–Rabas, P. L., and Grieve, A. P. (2011). Risk and Cumulative Risk of Stroke Recurrence: a Systematic Review and Meta–Analysis. *Stroke* 42 (5), 1489–1494. doi:10.1161/STROKEAHA.110.602615

Nan, M. Z., and Li, D. D. (2016). Application Effect of Dengzhan Shengmai Capsule in Secondary Prevention of Ischemic Stroke. *China Foreign Med. Treat.* 35 (9), 146–148. doi:10.16662/j.cnki.1674–0742.2016.09.146

Peng, R. Q., and Niu, J. P. (2014). Clinical Study of Maixuekang Capsule on Secondary Prevention of Ischemic Stroke. *17th Natl. Conf. Neurol. Chin. Med. Assoc.* 1.

Peng, W., Zhou, J., and Yang, Y. (2012). Effect of Naoshuantong Capsule on Cerebral Blood Flow reserve in Patients with Cerebral Infarction. *Clin. J. Chin. Med.* 4 (24), 93–94.

Powers, W. J., Rabinstein, A. A., Ackerson, T., Adeoye, O. M., Bambakidis, N. C., Becker, K., et al. (2019). Guidelines for the Early Management of Patients

with Acute Ischemic Stroke: 2019 Update to the 2018 Guidelines for the Early Management of Acute Ischemic Stroke: A Guideline for Healthcare Professionals from the American Heart Association/American Stroke Association. *Stroke* 50 (12), e344–e418. doi:10.1161/STR.0000000000000211

Refaai, M. A., Riley, P., Mardovina, T., and Bell, P. D. (2018). The Clinical Significance of Fibrin Monomers. *Thromb. Haemost.* 118 (11), 1856–1866. doi:10.1055/s−0038−1673684

Rivera, D., Allkin, R., Obón, C., Alcaraz, F., Verpoorte, R., and Heinrich, M. (2014). What Is in a Name? the Need for Accurate Scientific Nomenclature for Plants. *J. Ethnopharmacol* 152 (3), 393–402. doi:10.1016/j.jep.2013.12.022

Rothwell, P. M., Giles, M. F., Chandratheva, A., Marquardt, L., Geraghty, O., Redgrave, J. N., et al. (2007). Effect of Urgent Treatment of Transient Ischaemic Attack and Minor Stroke on Early Recurrent Stroke (EXPRESS Study): a Prospective Population−Based Sequential Comparison. *Lancet* 370 (9596), 1432–1442. doi:10.1016/S0140−6736(07)61448−2

Salanti, G., Ades, A. E., and Ioannidis, J. P. (2011). Graphical Methods and Numerical Summaries for Presenting Results from Multiple−Treatment Meta−Analysis: an Overview and Tutorial. *J. Clin. Epidemiol.* 64 (2), 163–171. doi:10.1016/j.jclinepi.2010.03.016

Salanti, G., Del Giovane, C., Chaimani, A., Caldwell, D. M., and Higgins, J. P. (2014). Evaluating the Quality of Evidence from a Network Meta−Analysis. *PLoS One* 9 (7), e99682. doi:10.1371/journal.pone.0099682

Samakova, A., Gazova, A., Sabova, N., Valaskova, S., Jurikova, M., and Kyselovic, J. (2019). The PI3k/Akt Pathway Is Associated with Angiogenesis, Oxidative Stress and Survival of Mesenchymal Stem Cells in Pathophysiologic Condition in Ischemia. *Physiol. Res.* 68 (Suppl. 2), S131–S138. doi:10.33549/physiolres.934345

Shi, D. H., Zhang, H. T., Zhao, M. Y., He, L., Sun, Q., Tan, J. W., et al. (2011a). Effect of Naoxintong Capsule Combined with Atorvastatin on Secondary Prevention of Acute Cerebral Infarction. *Chin. Gen. Pract.* 14 (23), 2699–2700. doi:10.3969/j.issn.1007−9572.2011.23.041

Shi, F. H., Wu, Q. Z., and Hu, Y. L. (2011b). Efficacy Analysis of Naoxintong Capsule Combined with Aspirin Tablets and Aspirin Tablets Alone in Secondary Prevention of Cerebral Infarction. *Med. Innovation China* 8 (22), 45–46. doi:10.3969/j.issn.1674−4985.2011.22.028

Song, H. Q. (2014). Neoclassicism in Art. *Hebei J. Traditional Chin. Med.* (6), 890–892. doi:10.1002/9781118351352.wbve1436

Sun, H. J. (2020). The Value of Naoxintong Capsule in Secondary Prevention of Ischemic Stroke. *Sichuan J. Anat.* 28 (01), 26–27. doi:10.3969/j.issn.1005−1457.2020.01.012

Sun, X. Y. (2008). Effect of Sanjin Naomaitai Capsule on Cerebral Infarction. *Pract. J. Card. Cereb. Pneumal Vasc. Dis.* 16 (7), 30–31. doi:10.3969/j.issn.1008−5971.2008.07.016

Tian, D. F., and Li, X. X. (2010). Clinical Observation of Naoxintong Capsule on Secondary Prevention of 360 Cases of Ischemic Stroke. *Yunnan J. Traditional Chin. Med. Materia Med.* 31 (12), 36–37. doi:10.3969/j.issn.1007−2349.2010.12.020

Tu, Y. F., Guo, J. C., and Zeng, K. J. (2013). Preventive Effect of Combination of Chinese and Western Medicine on 108 Patients with Cerebral Infarction. *Guangming J. Chin. Med.* 28 (7), 1412–1414. doi:10.3969/j.issn.1003−8914.2013.07.062

Turner, R. M., Davey, J., Clarke, M. J., Thompson, S. G., and Higgins, J. P. (2012). Predicting the Extent of Heterogeneity in Meta−Analysis, Using Empirical Data from the Cochrane Database of Systematic Reviews. *Int. J. Epidemiol.* 41 (3), 818–827. doi:10.1093/ije/dys041

Wang, P. P., Li, X. L., Li, X. C., Zhang, M. L., Liu, S. Y., Li, B., et al. (2019). Meta Analysis of Clinical Efficacy and Safety of Naoxintong Capsule Combined with Aspirin and Statins in the Treatment of Cerebral Infarction. *Chin. J. Pharmacoepidemiol.* 28 (10), 636–642.

Wang, S. H. (2018). Application Effect Evaluation of Buchang Naoxintong Capsule in Preventing Recurrence of Cerebral Infarction. *Electron. J. Clin. Med. Lit.* 5 (71), 153. doi:10.3877/j.issn.2095−8242.2018.71.141

Wei, J. J. (2016). Progress in Treatment of Cerebral Infarction with Traditional Chinese and Western Medicine. *Tianjin Pharm.* 28 (04), 56–58.

Wu, X. H., and Xiang, Z. (2018). Clinical Effect of Maixuekang Capsule on Patients with Cerebral Infarction in Convalescence. *Chin. J. Mod. Drug Appl.* 12 (23), 3–5. doi:10.14164/j.cnki.cn11−5581/r.2018.23.002

Xie, J. H. (2015). *Buyang Huanwu Decoction In the Treatment of Ischemic Stroke in Convalescence: A Systematic Review*. [dissertation/master's thesis]. Chengde, China: Chengde Medical College.

Xu, H. X. (2017). Application Effect of Buchang Naoxintong in Preventing Recurrence of Cerebral Infarction. *Contemp. Med. Symp.* 15 (05), 139–140.

Xue, M. Z., Mi, G. Q., Wang, L. H., Li, L., and Sun, L. C. (2014). Tongxinluo Capsule Combined with Atorvastatin and Aspirin in the Treatment of Ischemic Stroke with Cerebral Artery Stenosis. *Mod. J. Integr. Tradit. Chin. West. Med.* (35), 3920–3922. doi:10.3969/j.issn.1008−8849.2014.35.015

Yan, B., Zhou, D., Guo, F. Q., Rao, P., Gao, L., Liu, F. Y., et al. (2008). A Randomized, Prospective, Multicenter, Controlled Clinical Study of Tongxinluo in Patients with Ischemic Stroke (Acute and Subacute). *West China Med. J.* 23 (5), 945–946.

Yan, F. Q., Yao, C. m., Qin, Y. Q., Chen, Y., Liu, T. Q., and Zhang, Q. P. (2019). Research Progress of Effective Components of Traditional Chinese Medicine in Prevention and Treatment of Cerebral Ischemia−Reperfusion Injury. *Acta Chin. Med.* 34 (10), 2108–2112.

Ye, X. Q., Xie, Y. M., Zhou, Y. H., Zhao, X. Q., Han, J. H., Wagn, X. Z., et al. (2015). Effect of Naoshuantong Capsule on Change of SSQOL index in Patients with Ischemic Stroke in Six Mouths Follow−Up. *Cjcmm* 40 (21), 4297–4300. doi:10.4268/cjcmm20152132

Yu, F. S. (2013). Clinical Effect Analysis of Buyang Huanwu Decoction in the Treatment of Cerebral Infarction Recovery. *Guide China Med.* (22), 263–264.

Yuan, S., Tang, B., Zheng, J., and Larsson, S. C. (2020). Circulating Lipoprotein Lipids, Apolipoproteins and Ischemic Stroke. *Ann. Neurol.* 88 (6), 1229–1236. doi:10.1002/ana.25916

Zang, W. P., Feng, L. H., and Wang, R. A. (2011). Effect of Buchang Naoxintong Capsule on Secondary Prevention of Cerebral Infarction. *Chin. J. Mod. Drug Appl.* 5 (2), 166. doi:10.3969/j.issn.1673−9523.2011.02.146

Zhang, H., Xing, Y., Chang, J., Wang, L., An, N., Tian, C., et al. (2019). Efficacy and Safety of NaoShuanTong Capsule in the Treatment of Ischemic Stroke: A Meta−Analysis. *Front. Pharmacol.* 10, 1133. doi:10.3389/fphar.2019.01133

Zhang, X. C., Cai, Y. F., and Huang, Y. (2012). Discussion on the Clinical Breakthrough point and Advantages of Traditional Chinese Medicine in the Prevention and Treatment of Stroke. *J. New Chin. Med.* 44 (05), 1–3.

Zhang, X. Z., Zhang, D. X., and Xu, H. Y. (2008). Effect of Buchang Naoxintong on Secondary Prevention of Ischemic Cerebrovascular Disease. *Pract. J. Card. Cereb. Pneumal Vasc. Dis.* 16 (12), 37. doi:10.3969/j.issn.1008−5971.2008.12.022

Zhen, W. X. (2015). Clinical Effect of Maixuekang Capsule on Patients with Cerebral Infarction in Convalescence. *Pharmacol. Clin. Chin. Mater. Med.* 31 (4), 247–249.

Zhou, D. S. (2013). Effect of Buchang Naoxintong on Preventing Recurrence of Cerebral Infarction. *Health Way* 12 (2), 119. doi:10.3969/j.issn.1671−8801.2013.02.121

Zhou, X. L. (2014). Clinical Observation of Tongxinluo in Reducing the Recurrence Rate of Cerebral Infarction. *Chin. J. Clin. Rational Drug Use* 7 (7), 67–68.

Zhou, Y. (2018). Community Clinical Efficacy of Buchang Naoxintong Capsule in the Treatment of Cerebral Infarction. *Mod. Diagn. Treat.* 29 (22), 3599–3600. doi:10.3969/j.issn.1001−8174.2018.22.011

Conflict of Interest: The authors declare that the research was conducted in the absence of any commercial or financial relationships that could be construed as a potential conflict of interest.

frontiers in Pharmacology

ORIGINAL RESEARCH
published: 22 November 2021
doi: 10.3389/fphar.2021.764388

Phenotype-Based HPLC-Q-TOF-MS/MS Coupled With Zebrafish Behavior Trajectory Analysis System for the Identification of the Antidepressant Components in Methanol Extract of Anshen Buxin Six Pills

Jiani Liu[1†], *Yue Shang*[2†], *Juanlan Xiao*[3], *Huirong Fan*[4], *Min Jiang*[1*], *Saijun Fan*[2*] and *Gang Bai*[1]

[1]State Key Laboratory of Medicinal Chemical Biology, College of Pharmacy and Tianjin Key Laboratory of Molecular Drug Research, Nankai University, Tianjin, China, [2]Institute of Radiation Medicine, Chinese Academy of Medical Sciences and Peking Union Medical College, Tianjin, China, [3]Graduate School, Tianjin University of Traditional Chinese Medicine, Tianjin, China, [4]The Institute of Radiation Medicine, Chinese Academy of Medical Sciences, Tianjin, China

Phenotype screening has become an important tool for the discovery of active components in traditional Chinese medicine. Anshen Buxin Six Pills (ASBX) are a traditional Mongolian medicine used for the treatment of neurosis in clinical settings. However, its antidepressant components have not been explicitly identified and studied. Here, the antidepressant effect of ASBX was evaluated in adult zebrafish. High performance liquid chromatography-mass spectrometry (HPLC-Q-TOF-MS/MS) was combined with zebrafish behavior trajectory analysis to screen and identify the antidepressant-active extract fraction and active components of ASBX. Finally, the antidepressant effect of the active ingredients were verified by the behavior, pathology, biochemical indices and protein level of adult fish. The novel tank driving test (NTDT) showed that ASBX can effectively improve the depressive effect of reserpine on zebrafish. Petroleum ether and dichloromethane extracts of ASBX were screened as antidepressant active extracts. Costunolide (COS) and dehydrocostus lactone (DHE) were screened as the active components of ASBX. COS had been shown to significantly improve the depressive behavior, nerve injury and neurotransmitter levels (5-hydroxytryptamine (5-HT) and norepinephrine (NE)) of zebrafish by inhibiting the high expression of serotonin transporter and norepinephrine transporter induced by reserpine suggesting the antidepressant effect of COS may be related to its effect on 5-HT and NE pathways. This study provided a phenotype based screening method for antidepressant components of traditional Chinese medicines, so as to realize the separation, identification and activity screening of components at the same time.

Keywords: Anshen Buxin Six Pills, anti-depression, costunolide, dehydrocostus lactone, phenotype-based screening method

OPEN ACCESS

Edited by:
Yi Wang,
Zhejiang University, China

Reviewed by:
Mario Aranda,
Pontificia Universidad Católica de Chile, Chile
Mingquan Guo,
Wuhan Botanical Garden (CAS), China
GAO Wenyuan,
Tianjin University, China

***Correspondence:**
Min Jiang
minjiang@nankai.edu.cn
Saijun Fan
fansaijun@irm-cams.ac.cn

†These authors have contributed equally to this work and share first authorship

Specialty section:
This article was submitted to Ethnopharmacology, a section of the journal Frontiers in Pharmacology

Received: *25 August 2021*
Accepted: *03 November 2021*
Published: *22 November 2021*

Citation:
Liu J, Shang Y, Xiao J, Fan H, Jiang M, Fan S and Bai G (2021) Phenotype-Based HPLC-Q-TOF-MS/MS Coupled With Zebrafish Behavior Trajectory Analysis System for the Identification of the Antidepressant Components in Methanol Extract of Anshen Buxin Six Pills. Front. Pharmacol. 12:764388. doi: 10.3389/fphar.2021.764388

Abbreviations: ASBX, Methanol extract of Anshen Buxin Six Pills; COS, Costunolide; DHE, dehydrocostus lactone; HPLC-Q-TOF-MS/MS, High-performance liquid chromatography coupled with quadrupole time-of-flight mass spectrometry; NTDT, Novel tank diving test; NE, Norepinephrine; NET, norepinephrine transporter; SERT, serotonin transporter; TCMs, traditional Chinese medicines; 5-HT, 5-hydroxytryptamine.

INTRODUCTION

Traditional Chinese medicines (TCM) have been shown to have an important role in the treatment of central nervous system (CNS) diseases (Li et al., 2016). As a result, the active components of TCM have become important sources of lead compounds (Gao et al., 2019). High-performance liquid chromatography-mass spectrometry (HPLC-Q-TOF-MS/MS) technology combined with target-based (Hou et al., 2020) and cell-based activity detection methods (Zhang et al., 2021), has been widely used in screening for lead compounds. However, it is not suitable for screening active ingredients where the target is unknown. Due to the complexity of the mechanism of central nervous system diseses (Krahn et al., 2020), such as depression, the screening methods based on cells and targets can not show the complex physiological activities of the nervous system. Therefore, phenotypic screening is more advantageous because it can detect the activity of drugs at the complete animal level (Henry and Wlodkowic, 2019). However, the traditional mammalian based screening method has the defects of large dosage and can not screen a large number of samples quickly. Therefore, a rapid screening method of neuroactive drugs needs to be established.

Depression has become one of the most common mental diseases (Yao et al., 2019). Monoamine metabolites levels, ability to cross the blood–brain barrier, and neuroprotective activity have been used as screening indices for antidepressant components (Zhang et al., 2019). Virtual screening methods, based on correlation analysis of metabolites and network pharmacology (Liu et al., 2021) with molecular docking technology (Dhiman et al., 2018) can predict the active ingredients of antidepressants. However, these methods cannot directly evaluate the efficacy of ingredients, and therefore, they may give false-positive and false-negative results. In recent years, more and more attention has been paid to phenotype-based drug screening, which has become an important method of early drug discovery. These methods, however, cannot directly evaluate the efficacy of ingredients, and therefore, there may be false-positive and false-negative results. In recent years, more and more attention has been paid to phenotype-based drug screening, which has become an important method of early drug discovery (Kuusanmaki et al., 2020). Neuroactive molecules usually have the characteristics of pleiotropy, phenotype-based screening methods can more directly reflect the pharmacological effects of chemical components in the whole organism, without assuming relevant molecular targets (Henry and Wlodkowic, 2019). Therefore, it is necessary to establish a high-throughput, phenotype-based screening method to identify new neuroactive compounds present in TCMs. Zebrafish larvae are important tool for screening large-scale components and discovering new neuroactive drug, as a phenotype-based drug screening model, because their advantages of requiring a low dosage of drug, exhibiting fast reproduction (Stewart et al., 2015) and homology with human genes in the monoaminergic nervous system (Aslanzadeh et al., 2019). The zebrafish swimming behavior-based screening method has been widely used in the exploration of mental diseases, such as Alzheimer's disease (Li et al., 2020).

Anshen Buxin Six Pills is a traditional Mongolian medicine preparation that has been, and still is clinically used to treat neurosis. Therefore, it has potential as a library of lead compounds used in the treatment of depression and other psychiatric diseases. It is composed of six traditional medicines, including the root of *Aucklandia costus* Falc., the seed of *Myristica fragrans* Houtt., the fruit of *Choerospondias axillaris* (Roxb.) B.L.Burtt & A.W.Hill., the flower of *Syzygium aromaticum* (L.) Merr. & L.M.Perry., the resin of *Liquidambar formosana* Hance. and the heart of Asian water buffaloes (*Bubalus bubalis* Linnaeus) or yellow cattle (*Bos taurus domesticus* Gmelin). The content radio of these six traditional Chinese medicines is the same, and the content is 100 g individually, the preparation method is crushed into fine powder, sieved, mixed evenly, pan pills with water, coated with 0.2 g cinnabar, polished and dried. Costunolide (COS) and dehydrocostus lactone (DHE) have been identified as the main active components of *Aucklandia costus* Falc (Dong et al., 2018). However, the antidepressant active components of the Anshen Buxin Six Pills are not clear.

In this study, the strategy of HPLC-Q-TOF-MS/MS technology combined with a zebrafish behavior trajectory analysis system is established to screen for antidepressant components of ASBX. This method can theoretically establish a phenotype-based screening platform to achieve the separation, identification, and activity screening of TCMs at the same time.

MATERIALS AND METHODS

Preparation of Plant Extracts

Anshen Buxin Six Pills (Lot number: 180908) was purchased from Ulanhot Sino-Mongolian Pharmaceutical Co. Ltd. (Ulanhot, Inner Mongolia, China). Anshen Buxin Six Pills powder (10 g) was dissolved in 100 ml of methanol and extracted via ultrasonication of 600 W for 1 h using a ultrasonic cleaning machine (SB-25-12-DT), which was purchased from Ningbo Scientz Biotechnology Co.,Ltd. (Ningbo, Zhejiang, China). After filtration, the methanol extract of Anshen Buxin Six Pills (ASBX) was obtained via rotary evaporation. The solvent of the extract was removed by the oil pump and vacuum freeze-dried into powder to obtain the lyophilized powder of ASBX, which was stored in −20°C for the next experiment. Follow the above steps to get ASBX, then, the ASBX were heated with water in 100 ml and resuspended. Then gradient extraction was carried out, each solvent was 300 ml each time, extracted for 3 times, and the solvent was removed by rotary distillation, petroleum ether extract (PEE), dichloromethane extract (DME), ethyl acetate extract (EAE), water-saturated *n*-butanol extract (BUE), and aqueous extracts (AQE) were

obtained. Finally, the solvent was evaporated by oil pump and vacuum freeze-dried to obtain the samples of each extraction layer.

Chemicals and Reagents

Reserpine (83580, purity ≥ 99.0%) was purchased from Sigma-Aldrich (St. Louis, MO, United States). Fluoxetine (FLX, F830634, purity ≥98.0%) was purchased from Shanghai Macklin Biomedical Co., Ltd. (Shanghai, China), and Costunolide (COS, AB0612, purity ≥98.0%) was purchased from Chengdu Alfa Biotechnology Co., Ltd. (Chengdu, Sichuan, China). Dehydrocostus lactone (DHE, D91141, purity ≥98.0%) was purchased from Shanghai Acmec Biochemical Co. Ltd. (Shanghai, China). ELISA kit for 5-hydroxytryptamine (5-HT) and dopamine (DA) was purchased from Wuhan Genomei Technology Co., Ltd. (Wuhan, Hubei, China). ELISA kit for norepinephrine (NE), serotonin transporter (SERT) and norepinephrine transporter (NET) was purchased from Shanghai Jianglai Industrial Co., Ltd. (Shanghai, China).

Experimental Animals

Adult zebrafish (AB strains, 5 months-old, male:female, 1:1) were purchased from Shanghai FishBio Co. Ltd. (Shanghai, China) and acclimated in fish tanks purchased from Shanghai Haisheng Biotech Co., Ltd. (Shanghai, China) with a recirculating aquatic system. The system water contained KCl 0.05 g/L, $NaHCO_3$ 0.025 g/L, NaCl 3.5 g/L and $CaCl_2$ 0.1 g/L. The zebrafish embryos were incubated with Holt buffer (15 mM NaCl, 0.67 mM KCl, 0.03 mM $NaHCO_3$, 0.90 mM $CaCl_2$, pH 7.2). Adult zebrafish and zebrafish embryos were maintained under a photoperiod of 14 h light/10 h dark. All the animal studies have been approved by the Tianjin University of Traditional Chinese Medicine of Laboratory Animals Care and Use Committee (TCM-LAEC2016032).

Establishment of Depression Adult Zebrafish Model and Experimental Grouping of ASBX

The configuration of solutions of ASBX groups was the lyophilized powder of ASBX was dissolved with DMSO, and dilute to 0.8% DMSO with system water. The experimental grouping is described as follows. To investigate the antidepressant activity of ASBX, adult zebrafish were randomly divided into six groups (n = 10): control group (Con, 0.8% DMSO system water), model group (Mod, 0.8% DMSO system water), Fluoxetine group (FLX, 10 μmol/kg), and ASBX groups (ASBX-80 mg/kg, ASBX-20 mg/kg, and ASBX-5 mg/kg). The FLX group was used as the positive control. Except for the Con group, zebrafish were soaked with reserpine (40 μg/ml) for 1 h every day for 7 days to induce a depressive phenotype (Tang et al., 2019). After treatment with reserpine daily, adult zebrafish were injected intraperitoneally with the above sample solutions.

Novel Tank Diving Test

The experimental procedure for the NTDT is described below. The experiment was conducted according to the protocol (Liu et al., 2020), with little change. The part of the tank with water was equally divided into two analysis areas, which was defined as top and bottom. After the zebrafish adapted to the tank environment for 5 min, the swimming trajectory of zebrafish in the first 10 min was recorded and analyzed using Noldus Ethvision XT 15 software (Noldus Information Technology, Leesburg, VA, United States). The following parameters were measured: total distance traveled (cm), average velocity (cm/s), freezing duration(s), number of transitions from bottom to top, first latency to enter the top area (s), and time spend in the top area.(s).

Nissl Staining and Determination of Content of Neurotransmitter

The experimental procedure for Nissl staining and the determination of neurotransmitter content are described below. The brains of the zebrafish were stained with Nissl stain solution (Beijing SolarBio Science & Technology Co., Ltd., Beijing, China) according to the manufacturer's instructions, and digital images were taken with a Nikon CiS microscope (Nikon). Image-Pro Plus software (version 6.0) was used to analyze the images and count the number of Nissl-positive cells in the periglomerular gray zone (PGZ) and ventrolateral nucleus of the semicircular torus (TSvl). The concentrations of 5-HT, DA, and NE in the brain tissues of zebrafish were detected using Enzyme-linked immunosorbent assay (ELISA) kits for 5-HT, DA and NE, according to the manufacturer's instructions.

Establishment of Depression Zebrafish Larvae Model and Preparation of Different Extraction Layers and Components of ASBX

The light/dark preference test was used to examine the effects of the extract layer and components of ASBX on reserpine-induced depression-like behavior in zebrafish larvae, analyzed by the zebrafish behavior trajectory analysis system. Reserpine was dissolved in 3 ml of Holt buffer containing 0.1% DMSO. The embryos (30/plate) were kept in 12-well plates with Holt buffer containing reserpine (4 μg/ml) or 0.1% DMSO Holt Buffer (Con group) at 6 h post fertilization and maintained in the dark for 6 days to obtain zebrafish larvae for the test. The establishment of depression phenotype of zebrafish larvae was referred to the methods (Wang et al., 2019) in the literature.

Freeze-dried extraction layers different extraction layers (PEE, DME, EAE, BUE, AQE) and lyophilized powder of ASBX were dissolved with DMSO and diluted with Holt buffer to the content of DMSO was 0.1%. The experimental groups are described as follows. To screen the anti-depression extraction layer(s) in ASBX, zebrafish larvae treated with reserpine were transferred to solutions of different extraction layers (PEE, DME, EAE, BUE, AQE, 80 μg/ml), ASBX methanol extract (80 μg/ml), Mod (0.1% DMSO Holt Buffer), and FLX (Fluoxetine, 10 μM) in 12-well plates. The actual drug amount of each extraction layer is

calculated according to the equivalent crude drug amount, indicating the proportion of substances in each extraction layer in ASBX of 80 μg/ml. The FLX group was used as the positive control. The fractions (1–46 min) of PEE (10 mg/ml) from HPLC were collected into 10 ml EP tubes every 2 min for 23 fractions total. The contents of the EP tubes were then evaporated to dryness in a vacuum drying oven and dissolved in 3 ml Holt buffer. A sample that matches a peak of the corresponding time in the chromatogram is considered one component. COS and DHE groups (0.1, 1 and 10 μmol/L) were used to verify the antidepressant activity of the screened components from the light/dark preference test.

Light/Dark Preference Test on Zebrafish Larvae

The light/dark preference test was then conducted according to the protocol (Wang et al., 2019) with some modifications. Briefly, the culture medium with reserpine of zebrafish larvae was replaced with drug solutions, soaked for 2 h. Zebrafish larvae treated with above mentioned drug solutions were transferred to each well of a 96-well plate (length × width: 125 × 85 mm, well diameter 10 mm), with 300 μl of Holt buffer, and adapted for 3 min before the test.

The light conditions are described as follows. The setting of the light and dark stimulus program was started 5 min after beginning video recording of the behavior trajectory. For light stimulation, the program was set as follows: light was applied for 3 min, off for 3 min, and repeated for three cycles. The video recordings were analyzed using Noldus Ethovision XT 15 software (Noldus Information Technology, Leesburg, VA, United States) by tracking the center of mass of the individual fish over time. Parameters were measured as the total distance traveled (mm) and average velocity (mm/s).

HPLC-Q-TOF-MS/MS Analysis of PEE

After determining PEE was the active extraction layer, PEE was dissolved in methanol with concentration of 0.1 mg/ml, then subjected to HPLC-Q-TOF-MS/MS analysis. A diamonsil® C18(2) (250 × 4.6 mm, 5 μm) column was used to separate and detect the components of ASBX extraction, with the column temperature maintained at 40°C. The mobile phase was a gradient elution system of A (CH_3OH) and B ($HCOOH:H_2O$ = 0.05:100), and elution was performed at a flow rate of 0.5 ml/min. The injection volume was 10 μl, and the gradient duration program was 0–2 min, 96% B; 2–6 min, 96–35% B; 6–41 min, 35%–0% B; 41–48 min, 0% B; 48–48.5 min, 0%–96% B; 48.5–56 min, 96% B.

Accurate mass measurements were collected using an AB Sciex Triple-TOF™ 4600^+ mass spectrometer (Framingham, MA, United States) with an electrospray ionization (ESI) system. The ESI/MS spectra were acquired in the positive ion mode, and the ionizing voltage was set to 5,500 V. The temperature of the source was 300°C. The sample cone voltage was set to 30 V. High-purity nitrogen was used for nebulization and as the auxiliary gas. Ion source gases (N_2) 1 and 2 were maintained at 60 psi, and the curtain gas (N_2) pressure was maintained at 35 psi. The relative impact energy was 10 eV. The de-clustering voltage was 40 V. Peak View 2.2 was employed to process the data.

Experimental Grouping of COS in NTDT

To study the antidepressant activity of COS, adult, reserpine-treated zebrafish were randomly divided into six groups (n = 10): control group (Con, 0.8% DMSO system water), model group (Mod, 0.8% DMSO system water), FLX group (Fluoxetine, 10 μmol/kg), and COS groups (COS-10 μmol/kg, COS-40 μmol/kg, and COS-160 μmol/kg). Other experimental conditions were the same as those described in section *Novel Tank Diving Test*.

Protective Effect of COS on Reserpine-Induced Neuronal Injury

The experimental conditions for Nissl staining and determination of the content of neurotransmitters (5-HT, DA, and NE) were the same as in Section *Nissl Staining and Determination of Content of Neurotransmitter*.

Determination of Expression Level of Monoamine Transporter

The expression levels of SERT and NET were quantified using ELISA kits (Shanghai Jianglai Industrial Co., Ltd., Shanghai, China) according to the manufacturer's instructions.

Statistical Analysis

GraphPad Prism Software (version 6.0) was used for the statistical analysis of results, and one-way analysis of variance was applied for data analysis, followed by the Tukey's test for comparison of significant differences between the means. The results are expressed as the mean ± SEM. Statistical significance was set at $p < 0.05$.

RESULTS

Anti-Depressive Effect of ASBX on Zebrafish Behavior

To study the antidepressant effect of ASBX on zebrafish behavior, a NTDT was conducted. The NTDT takes advantage of the stress response of zebrafish in a new environment, which can be used to simulate anxiety, depression, and other behaviors (Benneh et al., 2017). As shown in the heat map in **Figure 1A**, exposure to reserpine resulted in low-frequency swimming at the top of the tank (simulating the effects of depression); this behavior was reversed by ASBX and FLX. Compared with the model group, the ASBX-80 mg/kg and FLX groups showed significantly improved swimming ability (total distance traveled and average velocity) (***$p < 0.001$, **Figures 1B,C**), freezing behavior (shortened freezing time) (*$p < 0.05$, **Figure 1D**), and exploration behavior (increased transitions from bottom to top and shortened first latency to top area) (*$p < 0.05$, **Figure 1E**). But

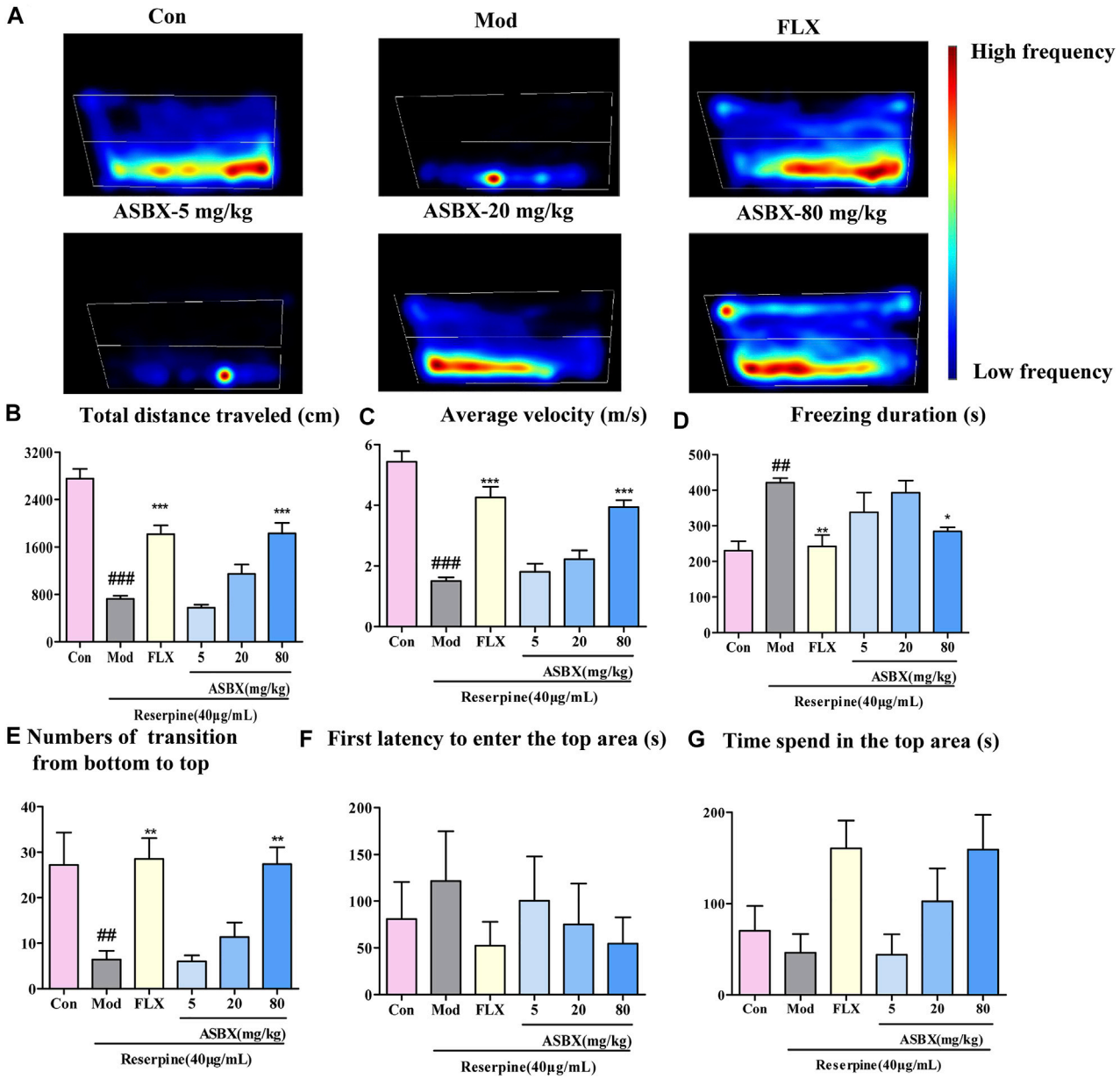

FIGURE 1 | Antidepressant effect of Anshen Buxin Six Pills (ASBX) was tested using a novel tank diving test. **(A)** Heat maps of the behavior trajectory. The bar chart shows the swimming ability, exploratory behavior, and freezing behavior of adult zebrafish. **(B)** Total distance travelled (cm) **(C)** Average velocity (cm/s) **(D)** Freezing duration (s) **(E)** Number of transitions from bottom to top **(F)** First latency to enter top area (s) **(G)**. Time spend in the top area. Data are expressed as the mean ± SEM) (n = 10/group). Significance was defined as $^{\#\#}p < 0.01$, $^{\#\#\#}p < 0.001$ compared with Con group, $^{*}p < 0.05$, $^{**}p < 0.01$, $^{***}p < 0.001$ compared with Mod group.

there was no siginificant diffrences in First latency to enter the top area and Time sped inthe top area (**Figures 1 F,G**).

Protective Effect of ASBX on Reserpine-Induced Neuronal Injury

Based on the improved effect of ASBX on the swimming behavior of zebrafish, we further verified its antidepressant effect at the level of histopathology and biochemical indexes by Nissl staining and enzyme-linked immunosorbent assay (ELISA). Neuronal regeneration dysfunction is one cause of depression (Fang et al., 2018). Exposure to reserpine led to the reduction and disordered arrangement of Nissl bodies in cytoplasm, the distance between cells became larger, and the boundary is not clear in periglomerular gray zone (PGZ) (**Figures 2A,C**), conversely, ASBX-80 mg/kg and FLX groups reversed the reduction in the number of neurons in the PGZ and TSvl induced by reserpine, there are significant differences in statistical results.($^{*}p < 0.05$, **Figures 2B,D**).

Neurotransmitters are closely associated with the neurobiological mechanisms of depression (Liu et al., 2018). ASBX-80 mg/kg and

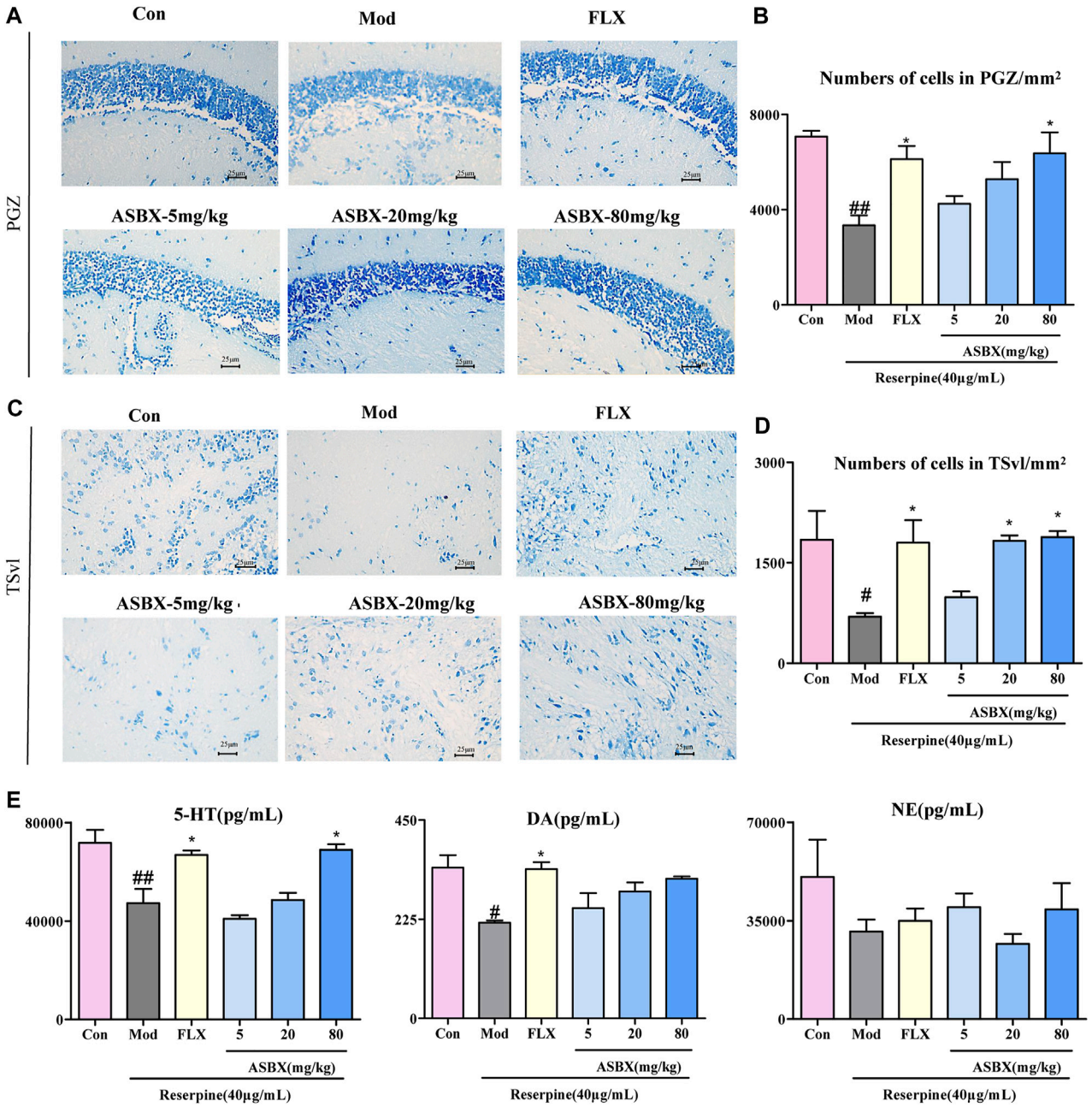

FIGURE 2 | Protective effect of Anshen Buxin Six Pills (ASBX) on reserpine-induced neuronal injury. **(A)**. Nissl stain of zebrafish brain (400×) in periglomerular gray zone (PGZ) **(C)**. Nissl stain of zebrafish brain in ventrolateral nucleus of the semicircular torus (TSvl). **(B and D)** are the quantitative statistics of neurons in the PGZ and TSvl, respectively. **(E)**. The content of 5-HT, DA, NE in zebrafish brain was measured by ELISA. Data are expressed as the mean ± SEM (n = 3/group). Significance was defined as $^{\#}p < 0.05$, $^{\#\#}p < 0.01$, $^{*}p < 0.05$.

FLX groups significantly reversed the reduction in the levels of 5-HT ($^{*}p < 0.05$) after exposure to reserpine (**Figure 2E**).

Discovery of Antidepressant Components of ASBX Through HPLC-Q-TOF-MS/MS

Based on the antidepressant effect exhibited by ASBX, we further screened its components. We tested the survival rate of zebrafish embryos by ASBX, PEE, DME, EAE, BUE and AQE to determine the toxicity of each extract. There was no significant difference in the survival rate between each extract and the Con group, which proved that each extract had no obvious toxicity at this concentration (**Supplementary Figure S2**). Under photoperiod (dark/light alternating) stimulation, neurotoxic phenotypes at higher doses of reserpine show decreased swimming behavior in the

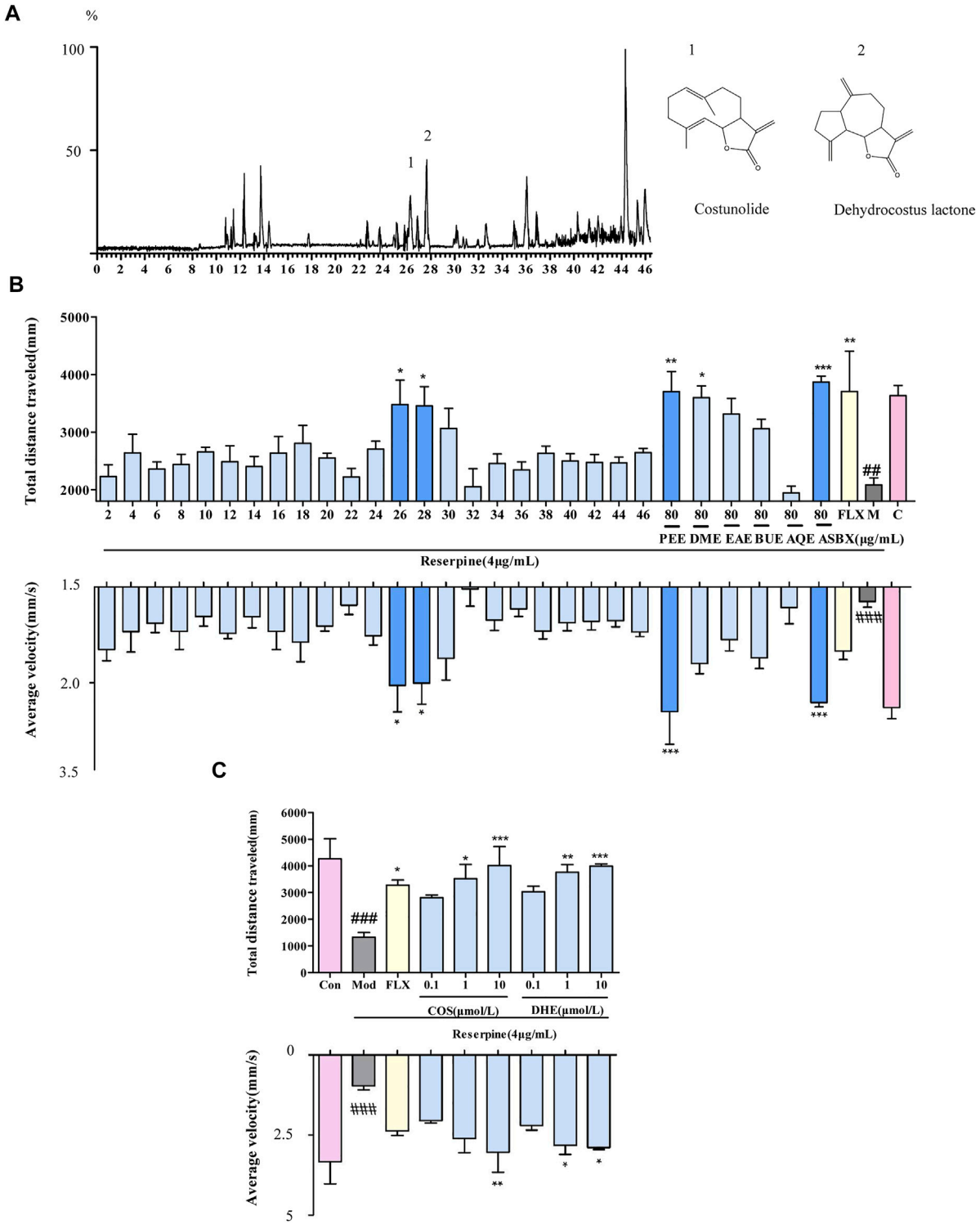

FIGURE 3 | Screening for the antidepressant components of methanolic extract of Anshen Buxin Six Pills (ASBX) on the swimming ability of zebrafish larvae. **(A)**. Total ion chromatograms (TIC) of the petroleum ether extract (PEE) of ASBX in positive ESI mode **(B)**. Bioactivity histogram obtained via zebrafish behavior trajectory analysis system are analyzed as total distance traveled (mm) and average velocity (mm/s). **(C)**. The swimming behavior of costunolide (COS) and dehydrocostus lactone (DHE) obtained via zebrafish behavior trajectory analysis system are analyzed as total distance traveled (mm) and average velocity (mm/s). Data are expressed as the mean ± SEM (n = 8/group). Significance was defined as $^{\#\#}p < 0.01$, $^{\#\#\#}p < 0.001$,$^{*}p < 0.05$, $^{**}p < 0.01$, $^{***}p < 0.001$.

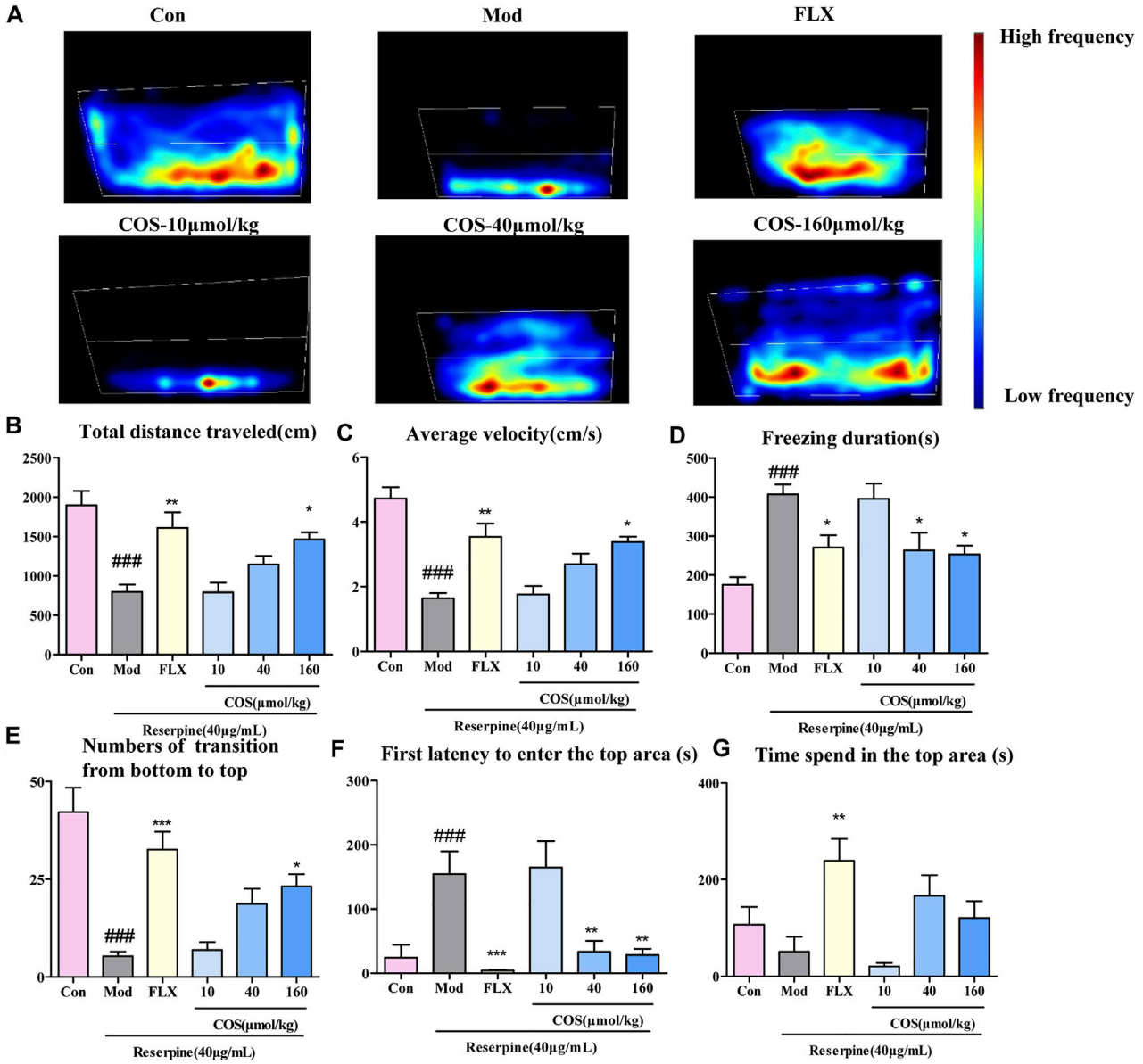

FIGURE 4 | Antidepressant effect of costunolide (COS) was tested using a novel tank diving test. **(A)**. Heat maps of the behavior trajectory. The bar chart shows the swimming ability, freezing behavior and exploratory behavior of adult zebrafish. **(B)**. Total distance travelled (cm) **(C)**. Average velocity (cm/s) **(D)**. Freezing duration (s) **(E)**. Numbers of transition from bottom to top **(F)**. First latency to enter top area (s) **(G)**. Time spend in the top area Data are expressed as the mean ± SEM (n = 10/group). . Significance was defined as $^{###}p < 0.001$ $^{*}p < 0.05$, $^{**}p < 0.01$, $^{***}p < 0.001$.

zebrafish larvae (Wang et al., 2019). Compared with the Mod group, PEE had the best activity among the extraction layers, in terms of total swimming distance and average swimming speed (**Figure 3B**). Therefore, the PEE layer was chosen for further identification and separation by HPLC-Q-TOF-MS/MS (**Figure 3A**), and the antidepressant activity of the 23 fractions was evaluated (**Figure 3B**). Among them, fractions 26 and 28 improved the swimming ability of zebrafish larvae depression model induced by reserpine. Fraction 26 corresponds to the substance flowing out in 25–27 min in the ion flow diagram, and stream 28 corresponds to the substance flowing out in 27–29 min. According to the mass spectrum information, we identified that the components contained in fraction 26 are costunolide and costic acid, and the components contained in fraction 28 are dehydrocostus lactone (See for mass spectrum information in **Supplementary Table S1**). The antidepressant activities of compounds 1 and 2 were again verified by light/dark preference test. Zebrafish larvae treated with COS or DHE showed improved swimming activity of zebrafish larvae induced by reserpine (**Figure 3C**). The results thereby showed that COS and DHE were potentially the antidepressant components of ASBX.

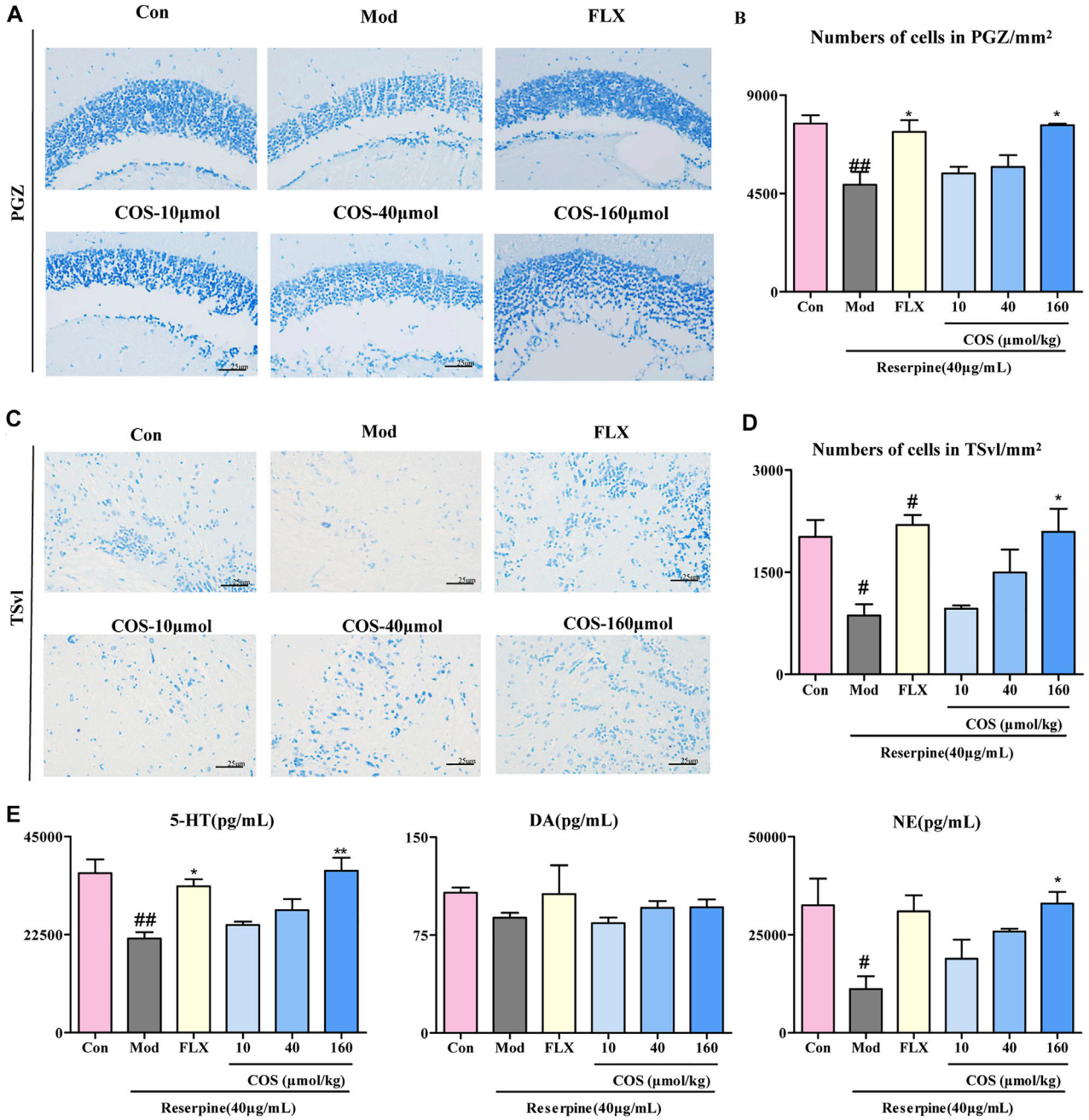

FIGURE 5 | Protective effect of costunolide (COS) on reserpine-induced neuronal injury. **(A)**. Nissl stain of the zebrafish brain (400×) in periglomerular gray zone (PGZ) **(C)**. Nissl stain of the zebrafish brain (400×) in ventrolateral nucleus of the semicircular torus (TSvl). **(B and D)** are the quantitative statistics of neurons of the PGZ and TSyl, respectively. **(E)**. The content of 5-HT, DA, NE in zebrafish brain was measured via ELISA. Data are expressed as the mean ± SEM (n = 3/group). Significance was defined as $^{\#}p < 0.05$, $^{\#\#}p < 0.01$, $^{*}p < 0.05$, $^{**}p < 0.01$.

Anti-Depressive Effect of COS on Zebrafish Behavior

To verify the antidepressant activity of COS, the NTDT was conducted, and the heat map shows that the depressive phenotype could be reversed by COS and FLX (**Figure 4A**). Compared with the Mod group, the COS-160 μmol/kg group showed improved swimming capacity (**Figures 4B,C**), freezing behavior (**Figure 4D**), and exploration behavior (**Figures 4E,F**). The COS-40 μmol/kg group showed improved depressive behavior with respect to freezing duration, first latency to enter the top (**Figures 4D,F**). There was no sigificant difference in time spend in the top area between the COS

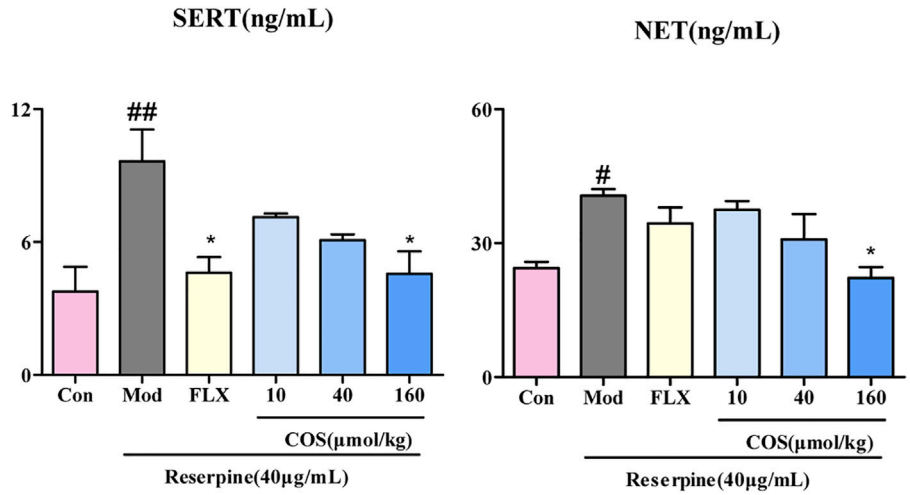

FIGURE 6 | Effect of costunolide (COS) on the expression of serotonin transporter (SERT) and norepinephrine transporter (NET). The content of SERT and NET in zebrafish brain was measured via ELISA. Data are expressed as the mean ± SEM (n = 3/group). Significance was defined as $^{\#}p < 0.05$, $^{\#\#}p < 0.01$, $^{*}p < 0.05$.

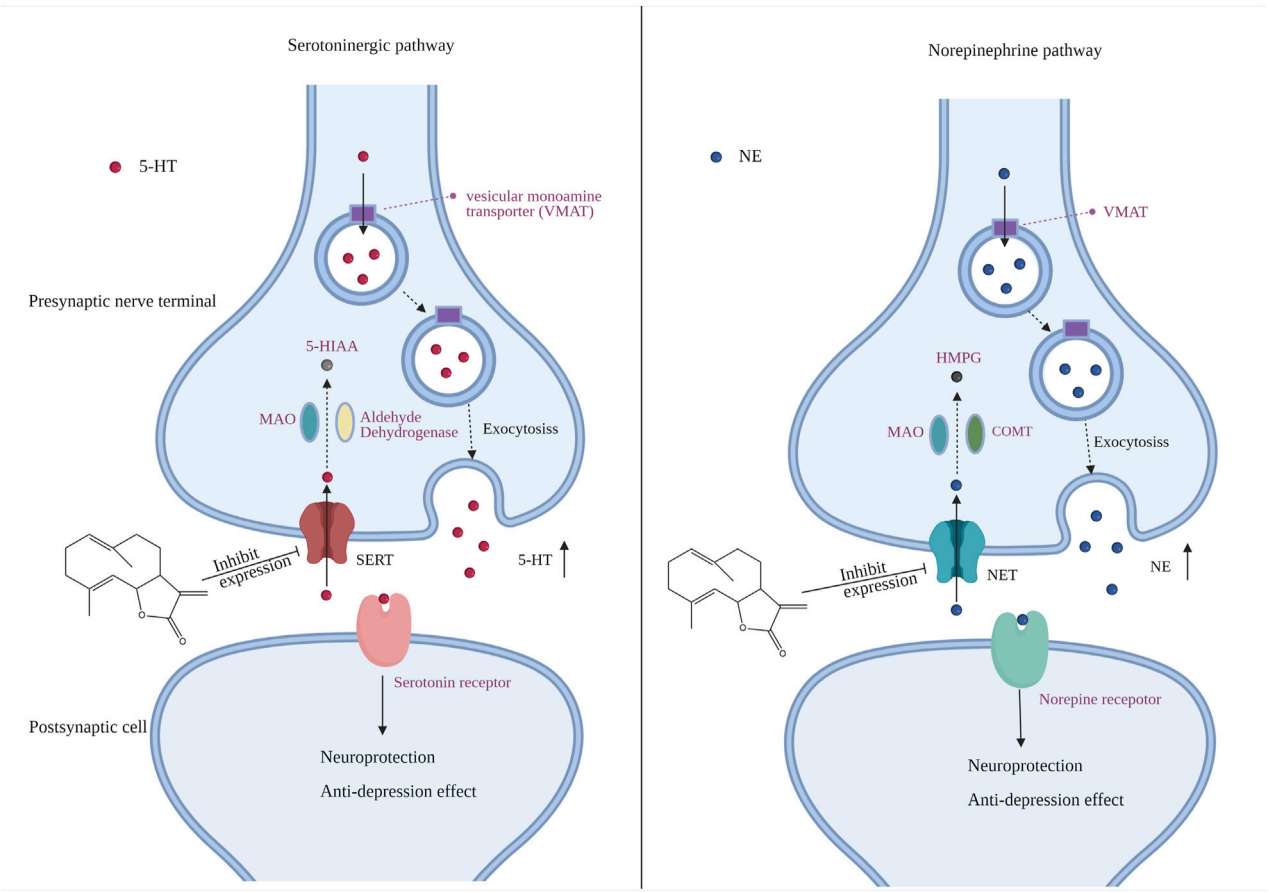

FIGURE 7 | Potential mechanism of the antidepressant effect of costunolide (COS). Through inhibiting the expression of SERT and NET, COS inhibits the reuptake function of 5-HT and NE in the process of synaptic transmission, to increase the level of 5-HT and NE and activate related receptors, which is the potential mechanism of its antidepressant effect. The Figure 7 was created with BioRender.com.

groups and Mod group (**Figures 4G**). The results showed that COS could improve the swimming behavior of zebrafish with reserpine induced depression.

Protective Effect of COS on Reserpine-Induced Neuronal Injury

The anti-depression effect of COS was also verified at the histopathological and biochemical levels. The results of Nissl staining showed that the neuronal loss in PGA and TSvl in the Mod group was improved by COS (COS-160 μmol/kg) and FLX. (**Figures 5A–D**). Compared with the Mod group, in the COS-160 μmol/kg group, the levels of 5-HT and NE was increased. (**Figure 5E**). The results showed that cos had a protective effect on reserpine induced nerve injury, which may be related to the increase of 5-HT and NE.

COS Decreased the Expression Level of SERT and NET

The upregulation of SERT and NET leads to a lack of 5-HT and NE in the synaptic cleft, which may be one of the causes of depression (Chen et al., 2012; Li et al., 2019). The COS-160 μmol/kg treatment showed inhibition of expression of SERT and NET compared with Mod group (**Figure 6**).

DISCUSSION

The active components of TCMs are usually complex and found in trace quantities (Liao et al., 2020). How to achieve rapid separation and enrichment of components in complex samples, and how to detect the activity on the basis of trace compounds, are problems that still need to be solved. In this study, a phenotype-based screening strategy, utilizing HPLC-Q-TOF-MS/MS technology combined with a zebrafish behavior trajectory analysis system, was established and used to screen the antidepressant components of ASBX. Firstly, we found the antidepressant effect of ASBX through the new tank diving experiment of adult fish. Secondly, a depression model of zebrafish larvae induced by reserpine was established, which showed a significant decline in swimming behavior (**Figure 3B**), which was consistent with the literature reports (Wang et al., 2019). Thirdy, the light/dark preference test was used to detect the activity of the components of ASBX separated by HPLC. The screened components showed the ability to affect the swimming behavior of zebrafish larvae at the micromolar range (**Figures 3B,C**), which indicates that the method can realize the activity detection of trace components. In addition, the zebrafish behavior trajectory analysis system can automatically image and digitally analyze the swimming behavior of a large scale of zebrafish larvae in microplates (i.e. 96 per plate and many plates consecutively), to evaluate the influence of multiple components on behavior function at the same time. Finally, the active components were identified as COS and DHE by HPLC-Q-TOF-MS/MS, Here, the antidepressant effect of DHE is reported for the first time. It is a sesquiterpene with a structure similar to COS. Volatile and fat-soluble components have been shown to be psychoactive (Brillatz et al., 2020). We speculate that the antidepressant activity of COS and DHE may be that these sesquiterpenoids are fat soluble components and easy to penetrate into the brain, so as to achieve the required concentration of antidepressants.

Monoamine neurotransmitters such as serotonin (5-HT), DA and NE are widely distributed in the developing and adult central nervous system (CNS), affecting numerous physiological processes, including depression and anxiety (Wilhelm et al., 2008). Neurotransmitters such as 5-HT are synthesized by presynaptic neurons and stored in vesicles through vesicle transporters. They are transported to nerve endings through vesicles, exocytosis is released to synaptic space, activate postsynaptic receptors and stimulate postsynaptic neurons, resulting in changes in a series of signal pathways (Ochi et al., 2019). Reserpine is an inhibitor of vesicle monoamine transporter (Wilhelm et al., 2008), which inhibits the entry of neurotransmitters into vesicles. Our results indicated that COS improves the contents of 5-HT and NE in zebrafish brain tissue of reserpine induced depression model, and improved swimming behavior and nerve injury (**Figure 5C**, **6**). These results also further confirmed the important role of 5-HT and NE system in the regulation of depression by the central nervous system (**Figure 7**). The inhibition of monoamine transporter can lead to its aggregation in synaptic space and prolong the activation time of receptor (Taciak et al., 2018). Therefore, transporters play a very important role in the transmission of neurotransmitters. SERT is a monoamine transporter,which can terminate 5-HT transmission through rapid presynaptic uptake (Orlando et al., 2020). The fuction of SERT may be related to several different mechanisms, such as the increase of expression of SERT (Li et al., 2019) and the change of SERT conformation (Plenge et al., 2020). NET is also a neurotransmitter transporter, which accelerates the inactivation of NE through the reabsorption of NE released from the synaptic space of central and peripheral nervous system (Fentress et al., 2013). Both SERT and NET belong to sodium/chloride dependent transporters. After binding to the substrate, sodium and chloride ions are transferred to the cytoplasm together with the substrate (Loland et al., 2003). The function of NET can be changed by many drugs. These drugs can directly bind to transporters, for example, NET after glycosylation will be expressed on the cell surface, so as to have functionality, or inhibit its function, such as changing the activity of cell membrane Na^+/K^+ adenosine triphosphatase, affecting the supply of energy during transport, acting as antagonists, or competing with substrates to change function (Mandela and Ordway, 2006). The knockout of SERT and NET reduced immobility in forced swimming test and tail suspension test (Kalueff et al., 2007; Solich et al., 2020). Chronic stress leads to the increase of content of SERT and NET, which may be the reason for the decrease of NE and SERT level in brain tissue (Pidathala et al., 2021). Therefore, regulating the expression of SERT and NET plays an important role in the occurrence of depression. Studies have shown that both corticotropin releasing factor (CRF) and CRF receptor agonists can

increase the expression of NET (Huang et al., 2015). CRF is a neuropeptide that plays an important role in the regulation of hypothalamic pituitary adrenal axis (HPA) (Bijlsma et al., 2011). CRF receptor blockers can block the activation of noradrenergic neurons induced by stress, CRFR1 or CRFR2 antagonists can restore the expression of net to normal level and increase the level of NE (Huang et al., 2015), so as to further play a regulatory role in depression. The absence of SERT leads to obvious fear learning defect, and the blocker of CRF1 receptor can restore this phenotype to normal, which means the interaction between signal pathway of CRF and 5-HT in nervous system (Bijlsma et al., 2015). Previous studies have revealed that COS may form hydrogen bonds by occupying the allosteric sites of SERT, affecting the binding of 5-HT to the active pocket, so as to inhibit the reuptake of 5-HT (Li et al., 2021). In our study, COS can inhibit the high expression of SERT and NET induced by reserpine, which indicates that the inhibition of SERT and NET may be the potential mechanism of antidepressant effect of COS. In the next study, we may further study the antidepressant target of COS, which may be related to inhibition of CRF receptor.

Traditional screening methods can be divided into two categories, the method based on target and cell (Qian and Tcw, 2021), and the method based on animal (Paunovic et al., 2017). Affinity based biological separation methods, such as affinity chromatography (Krahn et al., 2020) and activity detection methods based on receptor (Gao et al., 2019) are used to characterize the active components and targets in traditional Chinese medicine. However, it is not suitable for screening active ingredients which target is unknown. The occurrence of depression is usually the result of multiple target regulation, which is usually characterized by behavioral phenotype. The efficacy of drugs in the nervous system cannot be explained at the level of cells and targets. Therefore, it is necessary to establish a phenotype based screening method.

Traditional mammalian based screening methods usually can not detect a large number of components at the same time and use a large amount of drugs (Geng et al., 2019). The antidepressant screening method of HPLC-Q-TOF-MS/MS technology combined with a zebrafish behavior trajectory screening system has significant advantages. Firstly, the method can detect the drug concentration at the micro molar level and can be used to detect trace samples. Secondly, this method can detect a large number of samples in 96 well plate at the same time, so it can realize the rapid screening of a large number of compounds. Finally, zebrafish larvae can sensitively show photokinetic response under strong light stimulation, and can respond to low concentration drug stimulation (Kokel et al., 2012). This method is simple and rapid for screening antidepressant components, but it still faces some challenges. The development of phenotype screening research relies more and more on the advancement of automatic video recording and digital behavior analysis systems. These systems have the purpose of analyzing and learning cognitive behavior through three-dimensional motion tracking. Digital behavior analysis can provide light, sound, heat and other signal stimulations (Henry and Wlodkowic, 2019). At the same time, it is necessary to enrich the behavior evaluation indexes of screening methods, such as establishing behavior fingerprints and behavior digital bar codes (Fuller et al., 2018), to further systematically and comprehensively analyze the pharmacodynamic characteristics of chemical components.

CONCLUSION

In this study, the strategy of HPLC-Q-TOF-MS/MS technology combined with a zebrafish behavior trajectory screening system was successfully applied to screen and identify two antidepressant components, COS and DHE, from ASBX. The antidepressant effect of COS may be related to the inhibition of high expression of SERT and NET, the improvement of 5-HT and NE levels,and the repair of neuronal damage.

DATA AVAILABILITY STATEMENT

The original contributions presented in the study are included in the article/**Supplementary Material**, further inquiries can be directed to the corresponding authors.

ETHICS STATEMENT

The animal study was reviewed and approved by Tianjin University of Traditional Chinese Medicine of Laboratory Animals Care and Use Committee (TCM-LAEC2016032).

AUTHOR CONTRIBUTIONS

JL and YS performed the experiments and wrote the manuscript. JX and HF analyzed the data. MJ, GB, and SF designed the experiment and revised the manuscript.

FUNDING

This research was supported by grants funded by the National Key R&D Program of China (grant number 2018YFC1708200, 2018YFC1708203) and the Science and Technology Plan Project of Inner Mongolia Autonomous Region (grant number 2019ZD004).

SUPPLEMENTARY MATERIAL

The Supplementary Material for this article can be found online at: https://www.frontiersin.org/articles/10.3389/fphar.2021.764388/full#supplementary-material

REFERENCES

Aslanzadeh, M., Ariyasiri, K., Kim, O. H., Choi, T. I., Lim, J. H., Kim, H. G., et al. (2019). The Body Size of Stimulus Conspecifics Affects Social Preference in a Binary Choice Task in Wild-type, but Not in Dyrk1aa Mutant, Zebrafish. *Zebrafish* 16 (3), 262–267. doi:10.1089/zeb.2018.1717

Benneh, C. K., Biney, R. P., Mante, P. K., Tandoh, A., Adongo, D. W., and Woode, E. (2017). Maerua Angolensis Stem Bark Extract Reverses Anxiety and Related Behaviours in Zebrafish-Involvement of GABAergic and 5-HT systemsMaerua Angolensis Stem Bark Extract Reverses Anxiety and Related Behaviours in Zebrafish—Involvement of GABAergic and 5-HT Systems. *J. Ethnopharmacol* 207, 129–145. doi:10.1016/j.jep.2017.06.012

Bijlsma, E. Y., Hendriksen, H., Baas, J. M., Millan, M. J., and Groenink, L. (2015). Lifelong Disturbance of Serotonin Transporter Functioning Results in Fear Learning Deficits: Reversal by Blockade of CRF1 Receptors. *Eur. Neuropsychopharmacol.* 25 (10), 1733–1743. doi:10.1016/j.euroneuro.2015.07.004

Bijlsma, E. Y., van Leeuwen, M. L., Westphal, K. G., Olivier, B., and Groenink, L. (2011). Local Repeated Corticotropin-Releasing Factor Infusion Exacerbates Anxiety- and Fear-Related Behavior: Differential Involvement of the Basolateral Amygdala and Medial Prefrontal Cortex. *Neuroscience* 173, 82–92. doi:10.1016/j.neuroscience.2010.11.026

Brillatz, T., Jacmin, M., Queiroz, E. F., Marcourt, L., Slacanin, I., Petit, C., et al. (2020). Zebrafish Bioassay-Guided Isolation of Antiseizure Compounds from the Cameroonian Medicinal Plant Cyperus Articulatus L. *Phytomedicine* 70, 153175. doi:10.1016/j.phymed.2020.153175

Chen, P., Fan, Y., Li, Y., Sun, Z., Bissette, G., and Zhu, M. Y. (2012). Chronic Social Defeat Up-Regulates Expression of Norepinephrine Transporter in Rat Brains. *Neurochem. Int.* 60 (1), 9–20. doi:10.1016/j.neuint.2011.11.003

Dhiman, P., Malik, N., and Khatkar, A. (2018). Hybrid Caffeic Acid Derivatives as Monoamine Oxidases Inhibitors: Synthesis, Radical Scavenging Activity, Molecular Docking Studies and In Silico ADMET Analysis. *Chem. Cent. J.* 12 (1), 112. doi:10.1186/s13065-018-0481-7

Dong, S., Ma, L. Y., Liu, Y. T., Yu, M., Jia, H. M., Zhang, H. W., et al. (2018). Pharmacokinetics of Costunolide and Dehydrocostuslactone after Oral Administration of Radix Aucklandiae Extract in normal and Gastric Ulcer Rats. *J. Asian Nat. Prod. Res.* 20 (11), 1055–1063. doi:10.1080/10286020.2018.1489379

Fang, Y. Y., Zeng, P., Qu, N., Ning, L. N., Chu, J., Zhang, T., et al. (2018). Evidence of Altered Depression and Dementia-Related Proteins in the Brains of Young Rats after Ovariectomy. *J. Neurochem.* 146 (6), 703–721. doi:10.1111/jnc.14537

Fentress, H. M., Klar, R., Krueger, J. J., Sabb, T., Redmon, S. N., Wallace, N. M., et al. (2013). Norepinephrine Transporter Heterozygous Knockout Mice Exhibit Altered Transport and Behavior. *Genes Brain Behav.* 12 (8), 749–759. doi:10.1111/gbb.12084

Fuller, T. D., Westfall, T. A., Das, T., Dawson, D. V., and Slusarski, D. C. (2018). High-throughput Behavioral Assay to Investigate Seizure Sensitivity in Zebrafish Implicates ZFHX3 in Epilepsy. *J. Neurogenet.* 32 (2), 92–105. doi:10.1080/01677063.2018.1445247

Gao, X., Yang, L., Bai, Y., Li, Q., Zhao, X., Bian, L., et al. (2019). Screening of Bioactive Components from Traditional Chinese Medicine by Immobilized β2 Adrenergic Receptor Coupled with High Performance Liquid Chromatography/mass Spectrometry. *J. Chromatogr. B Analyt Technol. Biomed. Life Sci.* 1134-1135, 121782. doi:10.1016/j.jchromb.2019.121782

Geng, C. A., Yang, T. H., Huang, X. Y., Ma, Y. B., Zhang, X. M., and Chen, J. J. (2019). Antidepressant Potential of Uncaria Rhynchophylla and its Active Flavanol, Catechin, Targeting Melatonin Receptors. *J. Ethnopharmacol* 232, 39–46. doi:10.1016/j.jep.2018.12.013

Henry, J., and Wlodkowic, D. (2019). Towards High-Throughput Chemobehavioural Phenomics in Neuropsychiatric Drug Discovery. *Mar. Drugs* 17 (6), 370. doi:10.3390/md17060340

Hou, X., Sun, M., Bao, T., Xie, X., Wei, F., and Wang, S. (2020). Recent Advances in Screening Active Components from Natural Products Based on Bioaffinity Techniques. *Acta Pharm. Sin B* 10 (10), 1800–1813. doi:10.1016/j.apsb.2020.04.016

Huang, J., Tufan, T., Deng, M., Wright, G., and Zhu, M. Y. (2015). Corticotropin Releasing Factor Up-Regulates the Expression and Function of Norepinephrine Transporter in SK-N-BE (2) M17 Cells. *J. Neurochem.* 135 (1), 38–49. doi:10.1111/jnc.13268

Kalueff, A. V., Fox, M. A., Gallagher, P. S., and Murphy, D. L. (2007). Hypolocomotion, Anxiety and Serotonin Syndrome-like Behavior Contribute to the Complex Phenotype of Serotonin Transporter Knockout Mice. *Genes Brain Behav.* 6 (4), 389–400. doi:10.1111/j.1601-183X.2006.00270.x

Kokel, D., Rennekamp, A. J., Shah, A. H., Liebel, U., and Peterson, R. T. (2012). Behavioral Barcoding in the Cloud: Embracing Data-Intensive Digital Phenotyping in Neuropharmacology. *Trends Biotechnol.* 30 (8), 421–425. doi:10.1016/j.tibtech.2012.05.001

Krahn, A. I., Wells, C., Drewry, D. H., Beitel, L. K., Durcan, T. M., and Axtman, A. D. (2020). Defining the Neural Kinome: Strategies and Opportunities for Small Molecule Drug Discovery to Target Neurodegenerative Diseases. *ACS Chem. Neurosci.* 11 (13), 1871–1886. doi:10.1021/acschemneuro.0c00176

Kuusanmäki, H., Leppä, A. M., Pölönen, P., Kontro, M., Dufva, O., Deb, D., et al. (2020). Phenotype-based Drug Screening Reveals Association between Venetoclax Response and Differentiation Stage in Acute Myeloid Leukemia. *Haematologica* 105 (3), 708–720. doi:10.3324/haematol.2018.214882

Li, X., Liu, Q., Yu, J., Zhang, R., Sun, T., Jiang, W., et al. (2021). Costunolide Ameliorates Intestinal Dysfunction and Depressive Behaviour in Mice with Stress-Induced Irritable Bowel Syndrome via Colonic Mast Cell Activation and central 5-hydroxytryptamine Metabolism. *Food Funct.* 12 (9), 4142–4151. doi:10.1039/d0fo03340e

Li, X. Y., Q, W. W., Zhang, Y. X., Jiang, S. Y., Yang, B., Xiong, L., et al. (2019). Helicid Ameliorates Learning and Cognitive Ability and Activities cAMP/PKA/CREB Signaling in Chronic Unpredictable Mild Stress Rats. *Biol. Pharm. Bull.* 42 (7), 1146–1154. doi:10.1248/bpb.b19-00012

Li, Y., Li, L., and Hölscher, C. (2016). Therapeutic Potential of Genipin in Central Neurodegenerative Diseases. *CNS Drugs* 30 (10), 889–897. doi:10.1007/s40263-016-0369-9

Li, Y. Q., Chen, Y., Fang, J. Y., Jiang, S. Q., Li, P., and Li, F. (2020). Integrated Network Pharmacology and Zebrafish Model to Investigate Dual-Effects Components of Cistanche Tubulosa for Treating Both Osteoporosis and Alzheimer's Disease. *J. Ethnopharmacol* 254, 112764. doi:10.1016/j.jep.2020.112764

Liao, M., Yan, P., Liu, X., Du, Z., Jia, S., Aybek, R., et al. (2020). Spectrum-effect Relationship for Anti-tumor Activity of Shikonins and Shikonofurans in Medicinal Zicao by UHPLC-MS/MS and Chemometric Approaches. *J. Chromatogr. B Analyt Technol. Biomed. Life Sci.* 1136, 121924. doi:10.1016/j.jchromb.2019.121924

Liu, M., Wei, W., Stone, C. R., Zhang, L., Tian, G., and Ding, J. N. (2018). Beneficial Effects of Trimetazidine on Expression of Serotonin and Serotonin Transporter in Rats with Myocardial Infarction and Depression. *Neuropsychiatr. Dis. Treat.* 14, 787–797. doi:10.2147/NDT.S157441

Liu, S., Yu, M., Xie, X., Ru, Y., and Ru, S. (2020). Carbofuran Induces Increased Anxiety-like Behaviors in Female Zebrafish (*Danio rerio*) through Disturbing Dopaminergic/norepinephrinergic System. *Chemosphere* 253, 126635. doi:10.1016/j.chemosphere.2020.126635

Liu, X., Wei, F., Liu, H., Zhao, S., Du, G., and Qin, X. (2021). Integrating Hippocampal Metabolomics and Network Pharmacology Deciphers the Antidepressant Mechanisms of Xiaoyaosan. *J. Ethnopharmacol* 268, 113549. doi:10.1016/j.jep.2020.113549

Loland, C. J., Norgaard-Nielsen, K., and Gether, U. (2003). Probing Dopamine Transporter Structure and Function by Zn2+-Site Engineering. *Eur. J. Pharmacol.* 479 (1-3), 187–197. doi:10.1016/j.ejphar.2003.08.068

Mandela, P., and Ordway, G. A. (2006). The Norepinephrine Transporter and its Regulation. *J. Neurochem.* 97 (2), 310–333. doi:10.1111/j.1471-4159.2006.03717.x

Ochi, T., Vyalova, N. M., Losenkov, I. S., Paderina, D. Z., Pozhidaev, I. V., Loonen, A. J. M., et al. (2019). Limited Associations between 5-HT Receptor Gene Polymorphisms and Treatment Response in Antidepressant Treatment-free Patients with Depression. *Front. Pharmacol.* 10, 1462. doi:10.3389/fphar.2019.01462

Orlando, A., Clemente, C., D'Attoma, B., and Russo, F. (2020). Effects of Lactobacillus Rhamnosus GG on the Serotonergic Pathway in a Gliadin-Induced Enteropathy Animal Model. *J. Funct. Foods* 72, 104077. doi:10.1016/j.jff.2020.104077

Paunovic, A. I., Drowley, L., Nordqvist, A., Ericson, E., Mouchet, E., Jonebring, A., et al. (2017). Phenotypic Screen for Cardiac Regeneration Identifies Molecules with Differential Activity in Human Epicardium-Derived Cells versus Cardiac Fibroblasts. *ACS Chem. Biol.* 12 (1), 132–141. doi:10.1021/acschembio.6b00683

Pidathala, S., Mallela, A. K., Joseph, D., and Penmatsa, A. (2021). Structural Basis of Norepinephrine Recognition and Transport Inhibition in Neurotransmitter Transporters. *Nat. Commun.* 12 (1), 2199. doi:10.1038/s41467-021-22385-9

Plenge, P., Abramyan, A. M., Sørensen, G., Mørk, A., Weikop, P., Gether, U., et al. (2020). The Mechanism of a High-Affinity Allosteric Inhibitor of the Serotonin Transporter. *Nat. Commun.* 11 (1), 1491. doi:10.1038/s41467-020-15292-y

Qian, L., and Tcw, J. (2021). Human iPSC-Based Modeling of Central Nerve System Disorders for Drug Discovery. *Int. J. Mol. Sci.* 22 (3), 1203. doi:10.3390/ijms22031203

Solich, J., Kusmider, M., Faron-Gorecka, A., Pabian, P., and Dziedzicka-Wasylewska, M. (2020). Restraint Stress in Mice Alters Set of 25 miRNAs Which Regulate Stress- and Depression-Related mRNAs. *Int. J. Mol. Sci.* 21 (24), 9469. doi:10.3390/ijms21249469

Stewart, A. M., Gerlai, R., and Kalueff, A. V. (2015). Developing highER-Throughput Zebrafish Screens for *In-Vivo* CNS Drug Discovery. *Front. Behav. Neurosci.* 9, 14. doi:10.3389/fnbeh.2015.00014

Taciak, P. P., Lysenko, N., and Mazurek, A. P. (2018). Drugs Which Influence Serotonin Transporter and Serotonergic Receptors: Pharmacological and Clinical Properties in the Treatment of Depression. *Pharmacol. Rep.* 70 (1), 37–46. doi:10.1016/j.pharep.2017.07.011

Tang, Y. Q., Li, Z. R., Zhang, S. Z., Mi, P., Chen, D. Y., and Feng, X. Z. (2019). Venlafaxine Plus Melatonin Ameliorate Reserpine-Induced Depression-like Behavior in Zebrafish. *Neurotoxicol Teratol* 76, 106835. doi:10.1016/j.ntt.2019.106835

Wang, S., Duan, M., Guan, K., Zhou, X., Zheng, M., Shi, X., et al. (2019). Developmental Neurotoxicity of Reserpine Exposure in Zebrafish Larvae (*Danio rerio*). *Comp. Biochem. Physiol. C Toxicol. Pharmacol.* 223, 115–123. doi:10.1016/j.cbpc.2019.05.008

Wilhelm, C. J., Johnson, R. A., Eshleman, A. J., and Janowsky, A. (2008). Lobeline Effects on Tonic and Methamphetamine-Induced Dopamine Release. *Biochem. Pharmacol.* 75 (6), 1411–1415. doi:10.1016/j.bcp.2007.11.019

Yao, T., Cui, Q., Liu, Z., Wang, C., Zhang, Q., and Wang, G. (2019). Metabolomic Evidence for the Therapeutic Effect of Gentiopicroside in a Corticosterone-Induced Model of Depression. *Biomed. Pharmacother.* 120, 109549. doi:10.1016/j.biopha.2019.109549

Zhang, L., Yi, X., Wang, S., Liang, P., Zhou, H., Fu, J., et al. (2021). Construction of Graphene Quantum Dots-Decorated EGFR Cell Membrane Chromatography for Screening Active Components from Peucedanum Praeruptorum Dunn. *Anal. Bioanal. Chem.* 413 (7), 1917–1927. doi:10.1007/s00216-021-03161-6

Zhang, Y., Lv, X., Liu, R., Zhang, M., Liu, H., Gao, H., et al. (2019). An Integrated Strategy for Ascertaining Quality Marker of Schisandra Chinensis (Turcz.) Baill Based on Correlation Analysis between Depression-Related Monoaminergic Metabolites and Chemical Components Profiling. *J. Chromatogr. A.* 1598, 122–131. doi:10.1016/j.chroma.2019.03.056

Conflict of Interest: The authors declare that the research was conducted in the absence of any commercial or financial relationships that could be construed as a potential conflict of interest.

Publisher's Note: All claims expressed in this article are solely those of the authors and do not necessarily represent those of their affiliated organizations, or those of the publisher, the editors, and the reviewers. Any product that may be evaluated in this article, or claim that may be made by its manufacturer, is not guaranteed or endorsed by the publisher.

frontiers in Pharmacology

ORIGINAL RESEARCH
published: 10 December 2021
doi: 10.3389/fphar.2021.769021

Identifying of Anti-Thrombin Active Components From Curcumae Rhizoma by Affinity-Ultrafiltration Coupled With UPLC-Q-Exactive Orbitrap/MS

Zhenwei Lan[1†], Ying Zhang[2†], Yue Sun[1†], Lvhong Wang[1], Yuting Huang[1], Hui Cao[2], Shumei Wang[1]* and Jiang Meng[1]**

[1]School of Traditional Chinese Medicine, Guangdong Pharmaceutical University, Key Laboratory of Digital Quality Evaluation of Chinese Materia Medica, State Administration of Traditional Chinese Medicine (TCM), Engineering Technology Research Center for Chinese Materia Medica Quality of Universities in Guangdong Province, Guangzhou, China, [2]College of Pharmacy, Jinan University, Research Center for Traditional Chinese Medicine of Lingnan, Guangdong Provincial Key Laboratory of Traditional Chinese Medicine Informatization, Guangzhou, China

Recent studies concerning products that originate from natural plants have sought to clarify active ingredients, which both explains the mechanisms of the function and aids in quality control during production. As a traditional functional plant, Curcumae Rhizoma (CR) has been proven to be effective in promoting blood circulation and removing blood stasis. However, the components that play a role in its huge compound library are still unclear. The present study aimed to develop a high-throughput screening method to identify thrombin inhibitors in CR and validate them by *in vitro* and *in vivo* experiments. The effect of CR on thrombin in HUVECs cells was determined by ELISA, then an affinity-ultrafiltration-UPLC-Q-Exactive Orbitrap/MS approach was applied. Agatroban and adenosine were used as positive and negative drugs respectively to verify the reliability of the established method. The *in vitro* activity of the compounds was determined by specific substrate S-2238. The *in vivo* effect of the active ingredients was determined using zebrafish. Molecular docking was used to understand the internal interactions between compounds and enzymes. ELISA results showed that CR had an inhibitory effect on thrombin. The screening method established in this paper is reliable, by which a total of 15 active compounds were successfully identified. This study is the first to report that C7, 8, and 11 have *in vitro* thrombin-inhibitory activity and significantly inhibit thrombosis in zebrafish models at a safe dose. Molecular docking studies were employed to analyze the possible active binding sites, with the results suggesting that compound 16 is likely a better thrombin inhibitor compared with the other compounds. Based on the affinity-ultrafiltration-UPLC-Q-Exactive Orbitrap/MS approach, a precisely targeted therapy method using bio-active compounds from CR might be successfully established, which also provides a valuable reference for targeted therapy, mechanism exploration, and the quality control of traditional herbal medicine.

Keywords: curcumae rhizoma, affinity-ultrafiltration-MS, diarylheptanoid, antithrombosis, zebrafish, thrombin inhibitors

OPEN ACCESS

Edited by:
Ling Zhang,
Zhejiang Chinese Medical University, China

Reviewed by:
Junzeng Zhang,
National Research Council
Michal Blazej Ponczek,
University of Łódź, Poland

****Correspondence:***
Hui Cao
Kovhuicao@aliyun.com
Shumei Wang
shmwang@sina.com
Jiang Meng
jiangmeng666@126.com

[†]These authors have contributed equally to this work and share first authorship

Specialty section:
This article was submitted to Ethnopharmacology, a section of the journal Frontiers in Pharmacology

Received: *01 September 2021*
Accepted: *11 November 2021*
Published: *10 December 2021*

Citation:
Lan Z, Zhang Y, Sun Y, Wang L, Huang Y, Cao H, Wang S and Meng J (2021) Identifying of Anti-Thrombin Active Components From Curcumae Rhizoma by Affinity-Ultrafiltration Coupled With UPLC-Q-Exactive Orbitrap/MS. Front. Pharmacol. 12:769021. doi: 10.3389/fphar.2021.769021

INTRODUCTION

Thrombus, as one of the most commonly observed etiological factors causing a variety of cardiovascular and cerebrovascular diseases such as hypertension and cerebral ischemic stroke, has been attributed to the injury of vascular endothelial cells, including serious injuries related to surgery and childbirth, as well as changes in blood rheology and other pathological changes (Naghavi et al., 2017; Zhao et al., 2019). By abnormally activating the coagulation pathways, these pathological changes disturb the normal clotting mechanisms, ultimately leading to unnecessary thrombus formation. Unfortunately, as we age, the potential risk of thrombogenesis is ever increasing due to higher exposure to these changes, along with the aging of blood vessels. Many scholars have dedicated themselves to the exploration of suitable targets in coagulation pathways and attempted to develop a solution that aids the treatment and prevention of thrombosis-relevant diseases by manipulating these targets (Liu et al., 2021).

Thrombin (FIIα), a key enzyme in thrombosis, is a downstream factor of the coagulation pathway. *In vivo*, it converts fibrinogen into fibrin monomer, or factor XIII into factor XIIIα, thus binding with calcium ions to form a fibrin network, which is already known to be a critical link in thrombosis. Therefore, great attention has been paid to thrombin as an antithrombotic target. Vorapaxar was the first thrombin receptor inhibitor (THRI) approved by the Food and Drug Administration (FDA) in 2014 (Poole and Elkinson, 2014), but clinical trials have shown that its use increases the rate of severe bleeding, including intracranial haemorrhage in patients with a history of stroke (Vranckx et al., 2016). The research and development of Atopaxar (O'Donoghue et al., 2011) PZ-128 became trapped in a dilemma during phase II clinical trials for similar reasons (Gurbel et al., 2016). Part of the latest generation of oral direct thrombin inhibitors, Dabigatran (Pradaxa) has minimal side effects with other foods and drugs, a rapid clotting effect, and a wide treatment window (Lee and Ansell, 2011; van Ryn et al., 2013); however, there is still a risk of causing life-threatening bleeding after kidney damage (Summers and Sterling, 2016). These setbacks in antithrombosis studies have led researchers to seek safer sources, for instance, the vast compound library of natural products, aiming to anchor some new alternatives to those thrombin inhibitors mentioned above, since potential active components with a thrombin-inhibitory effect, such as salvianolic acid A, B, C, and protocatechuic acid, have been obtained from natural products in previous studies (Cao et al., 2016; Wu et al., 2020).

Natural plants have been used, especially in China, Japan, and Southeast Asia, as a functional food and phytomedicine for thousands of years (Liu and Nair, 2012; Zhang L. et al., 2017). Although many of the specific pharmaco-mechanisms remain unexplored, their long-term use has been well documented, which lays a solid foundation for further exploration (Zhou et al., 2016). According to the Chinese Pharmacopoeia, Curcumae Rhizoma (CR), the dried rhizome of *Curcuma phaeocaulis* Val., *Curcuma kwangsiensis* (S.G. Lee and C.F. Liang) or *Curcuma wenyujin* (Y.H. Chen and C.Ling), which is a synonym for *Curcuma aromatica* Salisb., has long been used in China and Japan as a medicinal plant for promoting blood circulation. It has two existing medicinal products—raw CR (RCR) and vinegar-processed CR (PCR), both bearing, but in various intensity, an effect of promoting blood circulation and removing blood stasis (Chinese Pharmacopoeia Commission, 2020). Previous network pharmacological studies have preliminarily revealed that CR may have an active effect on thrombin receptor (THR) (Tao et al., 2013). A recent study in our laboratory with a representative sample size showed that RCR was generally stronger *in vitro* than PCR in inhibiting THR, and this inhibition was highly correlated with the near infrared ray (NIR) spectrum, which reflects the overall chemical composition of CR products. This study, for the first time, proved the inhibitory effect of CR products on THR (Lan et al., 2021). However, the specific molecular mechanism of their THRI activity is still not clear, thus necessitating deeper research to further identify and verify the molecular compositions of the active substances in CR products.

In recent studies, affinity ultrafiltration coupled with ultra-performance liquid chromatography-mass spectrometry (AUF-LC-MS) has proved to be effective for the rapid characterization of the target molecules in a given compound (Xie et al., 2020, 2021). Although the spectrum-effect relationship analysis is also a useful screening method, false positive results may easily occur if the toxicity of the compound to the enzyme is considered. In the process of AUF-LC-MS identification, AUF can screen ligand-protein complexes from unbound substances, while LC-MS can identify target substances with varying contents. Being a high throughput method, AUF-LC-MS has a good performance in active substance screening without a high demand in sample size, in addition to some other benefits such as simple operation and strong targeting. Besides, the formation of protein-ligand complexes takes place in a condition that mimics the degrees of freedom in the actual biological system, making this screening method more practical and reliable (Wei et al., 2016). However, there are also some problems associated with this technique, which often compromise the experimental results. For instance, positive drugs are typically used to explore the AUF conditions (Wang S. et al., 2020), whereas, the drugs, as a compound monomer, usually cannot well represent a condition that simulates the rich compounds library in natural plants. In addition, false-positive results caused by various factors are usually formed during the dissociation of ligand-protein complexes. As a solution, the chromatic substrate method was applied in this study to explore the experimental conditions of AUF for the total extract. Meanwhile, unbound fraction analysis (UFA), an approach validated to be effective in a variety of previous studies (Tao et al., 2015), was also employed here by comparing it with bound fraction analysis (BFA) (Qin et al., 2015), with the deactivated-THR experimental group established as the control to analyze the filtrate and reduce the impact of non-specific binding.

In summary, to further explore the internal mechanism of CR in promoting blood circulation and removing blood stasis, an appropriate AUF-LC-MS method was developed in this study to identify potential inhibitors from CR extracts. As a result, a series

of diarylheptanoid compounds were identified to be active in thrombin inhibition. To the best of our knowledge, the activity of diarylheptanoid compounds against THR has not been previously reported, therefore, this finding reveals potential new applications for these compounds. In the present study, the *in vivo* inhibition ability of the samples was also evaluated using established zebrafish thrombosis models. Molecular docking technology was used to preliminarily explore the binding mechanism between the active molecules and THR.

MATERIALS AND METHODS

Materials and Animals

The reagents used in this study and the sources were as follows: human recombinant THR, Yeasen Biotech Co., Ltd. (Shanghai, China); chromogenic substrate S-2238 (98%), Yuanye Bio-technology Co., Ltd. (Shanghai, China); phosphate buffer saline (PBS, pH = 6.5), CORNING, Inc. (New York, United States); 4,4′-[3,5-bis(acetyloxy)-1,7-heptanediyl]bis-1,2-benzenediol (C7), 3-acetate-1,7-bis(4-hydroxyphenyl)-3,5-heptanediol (C8), and 4-[3,5-bis(acetyloxy)-7-(4-hydroxyphenyl)heptyl]-1,2-benzenediol (C11), Grint Biological Technology Co., Ltd. (Wuhan, China); arachidonic acid (AA, 99%, No. C2123090), aspirin (99%, No. H2017088) and O-dianisidine (3,3′Dimethoxybenzidine, 97%, No. C2009167), Shanghai Aladdin Biochemical Technology Co., Ltd. (Shanghai, China). All of the reagents were of corresponding analytical grade.

Centrifugal ultrafiltration filters (Amicon Ultra-0.5, 10 kDa) was purchased from Millipore Co., Ltd. (Bedford, MA, United States). FIIα ELISA kit was supplied by Shanghai Fusheng Biotechnology Co., Ltd., (Shanghai, China).

The RCR (batch number: 200101231) and PCR samples (batch number: 191200361) were procured from Kangmei Pharmaceutical Co., Ltd., (Guangdong, China) and identified by Professor Jizhu Liu from the School of Traditional Chinese Medical Materials, Guangdong Pharmaceutical University. Voucher specimens were deposited at the Herbarium Centre, Guangdong Pharmaceutical University. To facilitate extraction, the samples were crushed in a rocking pulverizer (DFY-400-D) and passed through an 80 mesh sieve, and then dried at 45°C and sealed for preservation. Liquid extract was prepared from CR powder using methanol (1:3, w/v) with sonication, and finally, a rotary evaporator and freeze dryer were used to obtain the CR extract, which was then sealed and stored at 4°C.

Zebrafish AB strains from the National Zebrafish Resource Center were used in the antithrombotic activity experiment. Tail thrombus staining intensity reportedly, which has a high negative correlation with cardiac staining intensity (Zhu et al., 2016), was used to evaluate the degree of thrombosis (Jagadeeswaran et al., 2016; Wang AK. et al., 2020). The zebrafish were fed on live brine shrimp twice a day in an automatic circulating tank system in the key laboratory of digital quality evaluation of Chinese Materia Medica, Guangdong Pharmaceutical University (Guangzhou, China), with the condition controlled steadily for a 14 h light/10 h dark cycle. Water temperature was maintained at 28 ± 0.5°C and pH at 7.0 ± 0.5. The embryos were produced naturally by the zebrafish. After spawning, the fertilized eggs were collected and washed with culture water 3 times. Then, they were placed in a 28°C-light incubator, and the activity evaluation experiment was conducted with 3 dpf fish. All the animal procedures in our study were carried out according to the Regulations of Experimental Animal Administration issued by the State Committee of Science and Technology of China and approved by the institutional ethical committee (IEC) of Guangdong Pharmaceutical University.

Determination of thrombin Inhibitory Activity

The thrombin inhibition assay was performed based on a previous examination (Lan et al., 2021). To be specific, the reaction mixture, 20 μL of 5 mg/ml CR extract solution (diluted in methanol) and 5 U/mL thrombin solution (diluted in PBS), was properly shaken for 30 s and incubated at 37°C for 40 min. Afterward, 20 μL of S-2238 was added to each well for analysis using a microplate reader (Thermo Fisher Scientific) under the mode of dynamic method. The testing was conducted for 10 min at a 6 s interval, with a detection wavelength of 405 nm. After the decomposition kinetics of the chromogenic substrates was characterized, an appropriate linear time range was selected to calculate the thrombin inhibition rate. The results showed that the linearity of 0–6 min was good, which was related to the amount of chromogen substrate added. Therefore, the inhibitory activity was determined by the slope of the linear regression between 0 and 6 min, and the inhibition rate was calculated by comparing it with the blank control.

ELISA Evaluation

Although network pharmacology (Tao et al., 2013) and NIR modeling (Lan et al., 2021) studies have shown the presence of potential THRI in CR, the results of Tao's network pharmacology experiment were not verified by specific *in vitro* or *in vivo* experiments. The modeling study on NIR was also essentially a spectroscopy-effect relationship experiment based on a single target, so the effect of CR on thrombin in an intracellular environment should be further evaluated. For this reason, ELISA was employed to quantify the release of thrombin.

Before the ELISA experiment, the cells in the logarithmic growth phase were digested and centrifuged and then transferred into the medium to obtain cell suspension under gentle blow. Hemacytometry was applied to count cells. The total number of the cells on the counting plate was counted under an inverted microscope, and for the cells crossing the grooves of the counting plate, only those on the left or the top of the counting chambers were counted. The calculation was as follows: the number of cells/mL= the total number of cells in five chambers $\times 5\times 10^{4.}$

We then collected HUVEC cells in the logarithmic growth stage and diluted them to 8×10^{4} cells/mL. The cells were then transferred to a culture plate, 100 μL/well, to gain adherent cells. After removing the medium, 100 μL of CR extract and PCR extract in 0.25, 0.5, 1.0, 5.0 and 10.0 μg/ml was added, respectively. In addition, a blank control group was

established. All the samples, each with quintuple culture wells, were placed in a CO_2 incubator for a 12 h continuous culture at 5% CO_2 and 37°C. Then 10 μL of 5 mg/ml MTT solution was added to each well. Following another 4 h incubation at 37°C in dark, the medium was discarded, and 100 μL of DMSO solution was added to each well. The samples were then placed in a 37°C incubator for 20 min to fully dissolve the blue crystals. The absorbance value of each well was measured at 490 nm with a microplate reader. Tests were performed in triplicate, with the average taken as the result. The concentration at which the cell survival rate was above 80% was identified as the non-toxic concentration of the extract.

The HUVECs were then cultured in an endothelial cell growth medium, with fresh medium supplied every 48–72 h, and then plated in 24-well culture plates at a density of 1×10^6 cells per well for a 24 h culture in a 5% CO_2 incubator at 37°C. After the medium was changed, the HUVECs were respectively treated with RCR and PCR solutions for 12 h. The cell suspension was diluted with PBS (pH 7.2–7.4) to about 1 million cells/mL, and the cells were dissociated by repeated freeze-thaw procedures to release the contents, followed by 20 min centrifugation at 3,000 *g* to collect the supernatant. The absorbance of each well was detected strictly in accordance with the instructions of the FIIα ELISA kit at 450 nm wavelength, with the blank wells used for alignment. The tests were carried out in triplicate to take the average for analysis. The data were analyzed by GraphPad Prism Version 8.4.3 (La Jolla, CA, United States). Multiple group comparison was conducted by one-way ANOVA, and $p < 0.05$ was considered statistically significant.

Optimization of AUF Experimental Conditions

To obtain stable ultrafiltration results and maintain steady enzyme activity, the pH was set at 6.5 in this experiment, as recommended by the manufacturer.The incubation temperature was fixed at 37°C, approximately equal to human body temperature, considering the meaningful active substances should function under an *in vivo* environment. At the same time, current studies suggest that 37°C was the optimal temperature (Qin et al., 2019; Xie et al., 2021). The enzyme concentration was set at 5 U/mL due to the analytical requirements of S-2238. All experiments were carried out simultaneously to avoid the impact of repeated freeze-thawing. Based on previous research (Lan et al., 2021), the CR extract was tested, respectively, in three concentrations (1, 2.5, and 5 mg/ml; CR extract was dissolved in DMSO to 2.5, 5, and 10 mg/ml, and then diluted with culture medium) with various incubation times (30, 40 and 50 min), aiming to optimize the screening conditions. In the experimental group, CR extract was mixed with active THR, in contrast to the control group where an equal volume of methanol was used to form a mixture with THR. The absorbance value was determined at 405 nm. Besides, PBS with a volume equal to CR extract was added in each experimental group to counteract the influence of the color caused by CR extraction. We also observed whether the extract has a decomposition effect on S-2238 through the kinetic curve. All the tests were repeated three times.

Procedures of AUF and Effective Peaks Characterization

100 μL of 2.5 mg/ml CR solution (CR extract was dissolved in methanol to prepare 25 mg/ml solution, which was diluted with PBS to 2.5 mg/ml, followed by centrifugation to obtain the working liquid) was transferred to an Eppendorf tube, then 100 μL of 5 U/mL active and inactivated THR were added for incubation at 37°C for 50 min without light. After being transferred to an ultrafiltration centrifuge tube, the samples were centrifugated at 12000 g for 15 min. The filtrate was preserved at −80°C for freezing and then transferred to a lyophilized machine to prepare the lyophilized powder. Finally, the lyophilized product was dissolved with 100 μL of LC-MS grade methanol, centrifuged to remove most of the buffer salts in the system, and then filtered by 0.22 μm microporous membrane to obtain the sample solution for LC-MS analysis.

In this experiment, compounds with an enzyme-binding rate of more than 1/3 were considered meaningful, which was calculated by the ratio of the peak area of inactive enzyme components to that of active enzyme components (Qin et al., 2015; Cai et al., 2020). It is worth noting that the use of an inactive enzyme group also played an important role in eliminating the nonspecific binding interference.

METHODS VALIDATION

Argatroban is a known inhibitor of THR (Lewis et al., 2001). To verify whether the established method can be used to identify THRI in CR, argatroban at a variety of concentrations (20, 50, 100, 200, 500, 1,000, 2000 nM) was used to test THR activity (Wu et al., 2020). The IC_{50} of THR was determined by adding different concentrations of argatroban to 2.5 mg/mL S-2238 solution under the conditions of the optimized method. Then, the determined IC_{50} was used to further validate the efficacy of the established AUF-UPLC-MS method in which a mixture of argatroban and negative control adenosine (Zhang Q. et al., 2017) was employed as the working solution. The inhibition rate was calculated by the following formula:

$$\text{Inhibition ratio } (\%) = \left[(dA/dt)_{blank} - (dA/dt)_{sample} \right] / (dA/dt)_{blank} \times 100\% \quad (1)$$

Where $(dA/dt)_{blank}$ is the reaction rate of the blank group, and $(dA/dt)_{sample}$ is the reaction rate of the sample group. The period of dA/dt is 0–6 min. The IC_{50} values of the active compounds were calculated three times in parallel at 7 concentrations. Statistical analysis and IC_{50} value calculation were conducted using GraphPad Prism Version 8.4.3 (GraphPad Software Inc., La Jolla, CA, United States).

HPLC and LC-MS Conditions

Verification of the AUF method was performed by HPLC (Shimadzu Corporation, Japan) equipped with a vacuum degasser, binary pump, automatic sampler, and diode array

detector (DAD), with combined use of an Ultimatetm XB-C18 (250 × 4.6 mm, 5 μm). According to the improved method reported in the literature (Zhang Q. et al., 2017), the mobile phase for separation was solvent A—water-acetic acid (1,000:1, v/v) and solvent B—methanol, with an elution program of 0–18 min, 15–80% B; 18–20 min, 80–15% B; and 20–25 min, 15% B. The other key conditions were set as follows: flow rate, 0.6 ml/min; DAD detection wavelength, 254 nm, and 330 nm; column temperature, 35°C; and injection volume, 10 μL.

UPLC-Q-Exactive Orbitrap/MS was performed using Ultimate 3,000 Ultra-performance liquid chromatograph and Thermo Scientific Orbitrap Fusion Tribrid Mass Spectrometer (Thermo Fisher Scientific, United States) to characterize the compounds in AUF. Waters ACQUITY UPLC BEH RP18 (2.1 mm × 100 mm, 1.7 μm) was employed for chromatographic analysis, and the mobile phases consisted of solvent A—water-acetic acid (1,000:1, v/v) and solvent B—acetonitrile. The separation followed the gradient elution program: 0–5 min: 95–75% solvent A; 5–13 min: 75–70% solvent A; 13–20 min: 70–65% solvent A; 20–35 min: 65–20% solvent A; 35–43 min: 20–10% solvent A; 43–45 min: 10–95% solvent A; and 45–48 min: 95–95% solvent A. The flow rate was 0.2 ml·min-1, with a column temperature of 25°C and an injection volume of 2 μL. The detection wavelength was set at 210, 254, and 415 nm, respectively. The MS parameters were as follows: Scanning mode was Full MS/dd MS2, and the switching mode was used in the system; Nebulizer voltage was 3.5 kV; Sheath gas pressure and aux gas pressure were 35 arb and 15 arb, respectively; Ion transport temperature and evaporation temperature were 320°C, CES was 10 eV, and the average EPI scanning spectrum was obtained when CE was 15, 35, and 45. Moreover, Orbitrap Fusion Tune and Xcalibur 4.0 were employed for mass spectrometry and data acquisition. Electrospray (ESI) ion sources were used for compounds analysis, with MS frontier 8.0 and Compound Discovery 3.1 applied to analyze the structure of the compounds.

In vitro thrombin Inhibition Assays

To evaluate the thrombin inhibition ability of the compounds and verify the results of AUF-LC-MS, an *in vitro* thrombin inhibition assay was developed based on the previous studies (Lan et al., 2021). The determination was carried out on a 96-well microplate. 100 μL of 2 U/mL THR was firstly placed in micro-well at 37°C for 10 min for activating, and then the identified THR ligands were added into the pores in equal volume (diluted into 7 concentrations with buffer solution) and incubated for 50 min. After completion of incubation, 35 μL of 2.5 mg/mL S-2238 was added to each well by volley, followed by 20 min of dynamical measurement at a 6 s interval under 405 nm. The blank group and the control group followed the same procedure, except for the active enzyme or samples replaced by the denaturing enzyme and buffer in the same volume. In addition, argatroban was applied as the positive control. All assays were done in triplicate, with the average value of the inhibition ratios taken as the final results. The concentration-inhibition response curve was plotted by GraphPad Prism Version 8.4.3, and the sample concentration producing 50% inhibition (IC_{50}) was calculated.

Antithrombotic Assay in Zebrafish

To further verify whether the monomer compounds that were active *in vitro* have an equivalent *in vivo* effect on preventing or treating thrombus, we used arachidonic acid (AA) to construct zebrafish thrombus models in the antithrombotic test. Zebrafish (3pdf) selected under stereomicroscopy were randomly placed in a 24-well plate containing 2 ml of embryo culture water, 12 fish in each well. In the following procedures, they were divided into four groups to be treated with different reagents—blank group, 0.1% DMSO; model group, AA (80 μM); positive control group, a mixture of aspirin (ASP, 20 μg/ml) and AA (80 μM); and administration group, a mixture of drugs (the concentration gradient was determined by the maximum tolerable concentration) and AA (80 μM). The 24-well plate was then placed at 28°C for 1.5 h, and O-dianisidine dyeing solution was added for a 10 min staining procedure without light. 10 zebrafish from each group were randomly selected and observed under a fluorescence microscope to evaluate the staining intensity of the tail thrombosis (Sun et al., 2021). Image Pro Plus 6.0 software was used to process the images for calculation.

Molecular Docking Analysis

One purpose of molecular docking is to explore the binding force and binding energy of molecule-enzyme conjugates, and identify the most likely target molecules from a large number of compounds for further verification, while another is to locate the sites for molecule–enzyme binding. In our experiment, the crystallographic structures of THR and argatroban were obtained from the Protein Database (PDB code 1DWC). SYBYL-X 2.0 scoring function was applied to compare the selected compounds with positive and negative drugs verified in this paper. Software was used to analyze the main and side chains of the protein and repair the parts that need to be repaired, and crystal water was removed. The protein coming with ligand argatroban was used for verification, and the optimal total score was taken as the score of the compound. To verify the binding sites of the compounds, the docking box was determined by the ligand that comes with the protein, within 5 Å. Chem 3D software was employed to construct the molecules, with the compound configuration optimized by MM2 molecular mechanics. After the ligand was hydrogenated and charged, the root of the ligand was detected to search and define the rotatable bonds. All the hydrogen atoms were added to the acceptor, followed by Gasteiger charge computation with the mergence ofnon-polar hydrogens. Besides, molecular docking coordinates were determined to increase the calculation accuracy, the maximum iteration was set as 2000 to find the lowest binding free energy. Default values were used for all parameters unless otherwise stated. Finally, semi-flexible docking was employed, and the conformation with the best affinity was selected as the final docking conformation. The molecular docking was performed using the Surflex-Dock method. The target molecules were screened according to the total score. The conformation with the lowest docking score was used for docking binding mode analysis, and docking sites were

analyzed using PyMOL 2.5 and Discovery Studio 4.5 software to observe the interaction between enzymes and inhibitors.

RESULTS AND DISCUSSION

ELISA Assay and AUF Condition

Although our preliminary experiments have confirmed the thrombin-inhibitory effect of CR, further study is necessary to identify the active components that play key roles in thrombin inhibition. Therefore, we conducted an ELISA assay using HUVECs endothelial cells. To optimize the AUF experimental conditions, RCR and PCR working solution at three concentrations—2.5, 5, and 10 μg/ml, were used as instructed in the maximum tolerated dose experiment. The results are shown in **Supplementary Figure S1A**. Compared with the blank group, the CR products showed a significant thrombin-inhibitory effect at all three concentrations, making the establishment of the AUF-LC-MS method valuable for further analysis.

In the previous experiments based on a large number of samples, it was concluded that RCR was generally stronger than PCR in inhibiting THR. Taking this into account, the RCR solution was used in this AUF experiment for condition screening. Meanwhile, the decomposition rate of S-2238 under different experimental conditions was used to characterize the inhibition rate of the enzyme. During the whole screening process, the concentration of the enzyme was fixed, so the concentration of the working solution was considered to be a key factor for the optimization of experimental conditions. As shown in **Supplementary Figure S1B**, under a certain incubation time, when the concentration of the working solution increased from 2.5 to 5 μg/ml, its inhibition rate elevated slightly and unsubstantially, and the increase in inhibition rate was even smaller when the concentration was 10 μg/ml, which indicated that even the active substance in the 2.5 μg/ml working solution could occupy most of the binding sites. Moreover, keeping increasing the concentration of the working solution may lead to false positive results due to the competitive binding of active substances in the system. On the other hand, incubation time also affects the binding rate of ligand and target protein. Too short incubation time is not enough for the ligand to fully interact with the target protein, thus causing difficulties in subsequent analysis. On the contrary, an overlong incubation time could compromise the experimental efficiency. Therefore, it is also necessary to choose an appropriate reaction time. In this experiment, with other conditions unchanged, significant changes, not only in enzyme activity but also in the binding ability to intrinsic ligands, were observed under different incubation times, with a result showing that the strongest enzyme activity and enzyme inhibitor-binding capability were detected at an incubation time of 50 min. By summarizing the findings as mentioned above, the optimal screening conditions were set as follows: THR concentration, 5 U/mL; incubation time, 50 min; incubation temperature, 37°C; pH value of the incubation solution, 6.5; and concentration of the working solution, 2.5 mg/ml.

Validation of the Established Approach

Aratroban is an excellent THR inhibitor with an IC_{50} of 0.243 μM under the established conditions, therefore it was used to validate the affinity ultrafiltration operation and served as a reference for activity validation experiments. A mixture of positive control (aratroban) and negative control (adenosine) was used to verify the specificity of the affinity ultrafiltration method. The results are shown in **Supplementary Figure S2**. The peak of aratroban was detected at 5.974 min under 254 nm, while the curve of adenosine peaked at 9.032 min under 330 nm. The peak value of argatroban was significantly reduced in the active THR co-incubated group compared with the inactive enzyme group and blank group (the mixture of positive and negative drugs, with the same amount of enzyme diluent PBS added). Whereas, no significant difference was shown between the denatured enzyme group and the blank group. In addition, there was no change in the level of adenosine in the three groups, indicating that the established method had good specificity for THR, and the established method in the inactive enzyme group could effectively prevent non-specific binding without generating additional false positive results. The denatured enzymes were produced by boiling active enzymes in a test tube over a water bath for 20 min.

Screening Potential thrombin Inhibitors by AUF-LC-MS

There are some disadvantages to traditional methods for enzyme inhibitors screening, such as high labor intensity, time consuming and extensive material consumption. Therefore, an affinity ultrafiltration approach based on ligand-enzyme complex was applied here to solve these problems. Subsequently, a combination with ultra-performance liquid chromatography-mass spectrometry (UPLC-MS) was developed to further refine the screening of bioactive compounds and study ligand-receptor binding properties. Hence, by directly comparing the chromatographic peak areas of active-enzyme group and inactive-enzyme group after affinity ultrafiltration, the bioactive compounds in complex plant extracts were very likely to be identified. In addition, positive and negative control groups were used to verify the reliability of the method established in this study, and to exclude the interference from other inactive components.

The results are shown in **Figure 1**. After affinity ultrafiltration screening, we found a total of 15 significantly reduced CR components with a binding rate of more than 1/3 in both the negative and positive modes. By observing the peak number of these compounds (C1—C15) based on time sequence, we found that C1, C4, C5, C6, C7, C10, C11, C12, and C13 and C15 with active enzymes disappeared after incubation, suggesting that these substances may have a strong thrombin inhibitory effect or at least a high binding ability. Yet a definite conclusion cannot be drawn because the competitive binding of the compounds in CR extract with the same targets should also be considered. Competition for the same targets will result in fewer binding sites. Under this circumstance, trace amounts of active substances are more likely to bind completely, while larger amounts of active substances will bind insufficiently due to the lack of sufficient

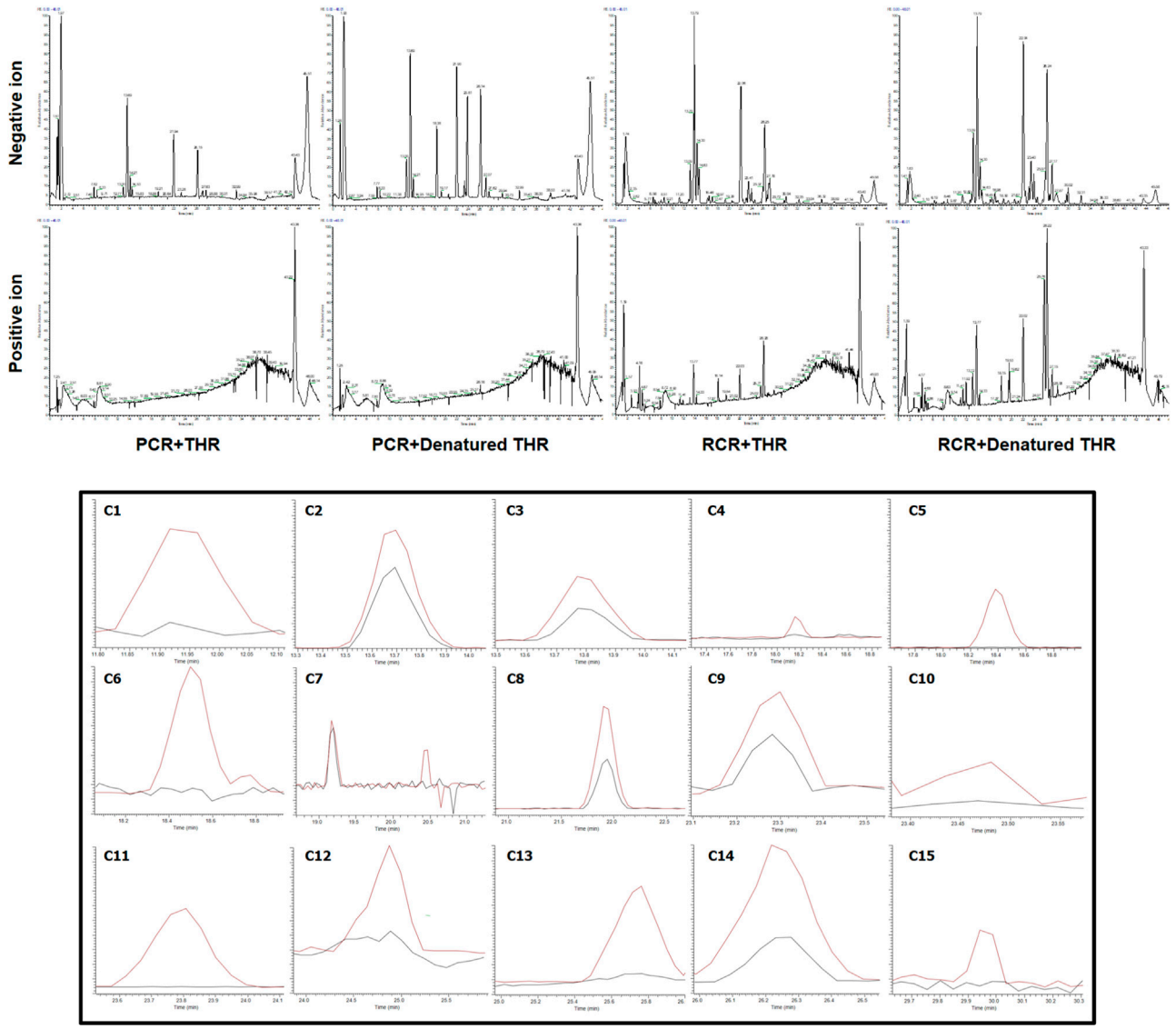

FIGURE 1 | Selective ion monitoring chromatograms for screening potential THR inhibitors by combined use of affinity ultrafiltration and high-performance liquid chromatography-mass spectrometry (AUF-LC-MS). (Black line, experimental group with active enzyme; red line, control group with denatured enzyme).

binding sites. UPLC-Q-Exactive-MS, which has been widely used in the study of complex mixtures owing to its high resolution and mass accuracy, was employed for further identification. In this study, the structure of AUF ultrafiltrate was identified and characterized based on the real standard, accurate mass, fragment ions, and relevant literature (Zhou et al., 2016, 2018; Alberti et al., 2018; Vanucci-bacqu and Bedos-belval, 2021). The structure and other details of the compounds are shown in **Figure 2A**; **Table 1**. Based on the chemical structures, CR mainly consists of sesquiterpenes, diterpenoids, and diarylheptanoids. Amongst the 15 compounds mentioned above, 13 are diarylheptanoid structures, which means that the diarylheptanoids play a major role in CR activity. This type of structure bears some common fragmentation patterns resulting in molecular breakdown, usually at positions 1 and 7 of the skeleton and the benzene ring, or at the double bonds formed on the left and right of positions 3 and 5 due to the hydroxyl group. Moreover, acetyloxy existing on position 3 and 5 carbon atoms are also subject to the cracking law common to diarylheptanoids, which is a special structure of some compounds in this class and has characteristic fragments. In this study, compounds 1 and 6 were taken as examples for specific analytical rules, as shown in **Figure 2B**.

The back search, which focused on the experimental activity studies of monomer molecules, was applied for these compounds in the database ZINC 15, SciFinder, and PubChem. We searched these databases for bioactive-related researches using precise molecular formulas. No bioactivity was reported for ZINC 15. Results in SciFinder and PubChem showed a great potential of diarylheptanoids in antioxidant and anti-inflammatory

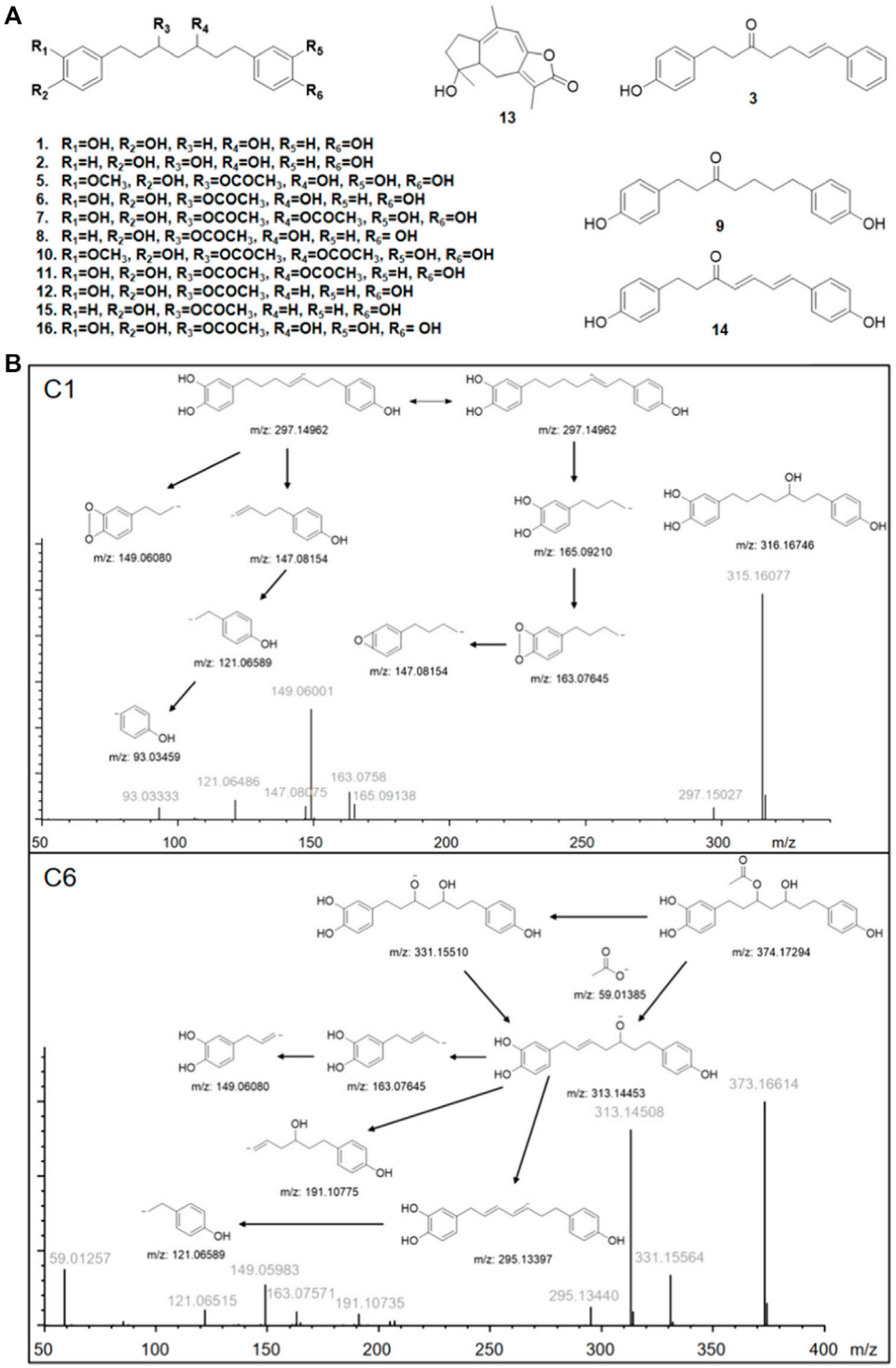

FIGURE 2 | (A) Structures of identified bioactive compounds in *Curcumae* Rhizoma; **(B)** Proposed fragmentation pathways of C1 and C6 in negative ion mode. m/z represents the calculated theoretical mass value of the fragments; gray font represents the actual value of the measurements.

properties. In particular, C1 (He et al., 2011), C3, C8, C9, C11 (Li et al., 2011), C12 (Li et al., 2010) showed the inhibitory effects on nitric oxide production in lipopolysaccaride-activated macrophages. Antioxidant test results suggested that C2 (Liu et al., 2018) and C7 (Li et al., 2012) were active. C2 and C14 could increase glucose consumption in differentiated L6 myotubes (Zhang Y. et al., 2017)

TABLE 1 | Identification and molecular docking of active compounds in AUF step.

No.	t_R/min	Molecular formula	m/z	Measured ions	Mass error/ ppm	Fragment ions	Tentative identification	Docking scores
1	11.942	$C_{19}H_{24}O_4$	317.1593	$[C_{19}H_{25}O_4]^+$	0.870	283.1332,255.1382,237.1276,227.1432,171.0805,147.0441,133.0650,107.0496	4-[5-Hydroxy-7-(4-hydroxyphenyl)heptyl]-1,2-benzenediol	7.5702
2	13.695	$C_{19}H_{24}O_4$	315.1608	$[C_{19}H_{23}O_4]^-$	5.439	163.0758,149.0600,145.0807121.0649,93.0334	1,7-Bis(4-hydroxyphenyl)-3,5-heptanediol	7.0134
3	13.801	$C_{19}H_{20}O_2$	281.1539	$[C_{19}H_{21}O_2]^+$	0.617	187.1120,161.0963,147.0801,133.0651,107.0497	(6E)-1-(4-Hydroxyphenyl)-7-phenyl-6-hepten-3-one	6.0415
4	18.151	-	274.2743	$[-]^+$	-	247.1331,229.1226,205.0603, 183.0783,154.9904,143.0397, 102.0344	NI, Sesquiterpenes	-
5	18.412	$C_{22}H_{28}O_7$	403.1769	$[C_{22}H_{27}O_7]^-$	4.490	361.1662,343.1555,328.1324,221.1183,207.1025,165.0549,163.0758,161.0601,135.0443,59.0125	4-[5-(Acetyloxy)-3-hydroxy-7-(4-hydroxy-3-methoxyphenyl) heptyl]-1,2-benzenediol	9.8642
6	18.482	$C_{21}H_{26}O_6$	373.1662	$[C_{21}H_{25}O_6]^-$	4.221	331.1556,131.1451,195.1344,191.1074,136.0757,149.0598,131.0283,59.0125	4-[3-(Acetyloxy)-5-hydroxy-7-(4-hydroxyphenyl)heptyl]-1,2-benzenediol	6.7434
7	20.465	$C_{23}H_{28}O_8$	431.1716	$[C_{23}H_{27}O_8]^-$	4.165	371.1505,311.1293,293.1190,249.1134,189.0916,163.0757,147.0442,59.0125	4,4'-[3,5-Bis(acetyloxy)-1,7-heptanediyl]bis-1,2-benzenediol	10.0157
8	22.025	$C_{21}H_{26}O_5$	357.1714	$[C_{21}H_{25}O_5]^-$	4.507	315.1606,297.1500,191.1073,149.0600,147.0806,145.0650,59.0125	3-Acetate-1,7-bis(4-hydroxyphenyl)-3,5-heptanediol	9.6972
9	23.391	$C_{19}H_{22}O_3$	297.1500	$[C_{19}H_{21}O_3]^-$	4.944	191.1074,149.0600,93.0334	1,7-Bis(4-hydroxyphenyl) heptan-3-one	6.2109
10	23.482	$C_{24}H_{30}O_8$	445.1876	$[C_{24}H_{29}O_8]^-$	4.258	385.1662,343.1556,325.1450,189.0917,161.0601,147.0443,121.0285,59.0125	4-[3,5-Bis(acetyloxy)-7-(4-hydroxy-3-methoxyphenyl) heptyl]-1,2-benzenediol	8.5073
11	23.811	$C_{23}H_{28}O_7$	415.1769	$[C_{23}H_{27}O_7]^-$	4.361	355.1555,313.1450,295.1343,189.0916,147.0443,121.0284,59.0125	4-[3,5-Bis(acetyloxy)-7-(4-hydroxyphenyl)heptyl]-1,2-benzenediol	9.2422
12	24.714	$C_{21}H_{26}O_5$	357.1713	$[C_{21}H_{25}O_5]^-$	4.703	315.1606,297.1499,279.1391,163.0757,147.0442,121.0284,59.0125	4-[3-(Acetyloxy)-7-(4-hydroxyphenyl)heptyl]-1,2-benzenediol	7.0544
13	25.761	$C_{15}H_{18}O_3$	247.1331	$[C_{15}H_{19}O_3]^+$	1.048	229.1225,201.1275,139.0391,123.0444,107.0860,81.0706	Zedoalactone F	4.1909
14	26.137	$C_{19}H_{18}O_3$	293.1188	$[C_{19}H_{17}O_3]^-$	5.387	187.0759,119.0492,93.0334	1,7-Bis(4-hydroxyphenyl)-4,6-heptadien-3-one	6.2413
15	30.020	$C_{21}H_{26}O_4$	341.1762	$[C_{21}H_{25}O_4]^-$	4.145	299.1656,281.1550,175.1122,59.0125	1,7-bis(4-hydroxyphenyl) heptan-3-yl acetate	8.0456

Docking scores are the total scores calculated by SYBYL-X 2.0. The total score of the positive drug argatroban and negative drug adenosine is 7.9147 and 5.4534, respectively. "-" represents no data, "NI" represents not identified.

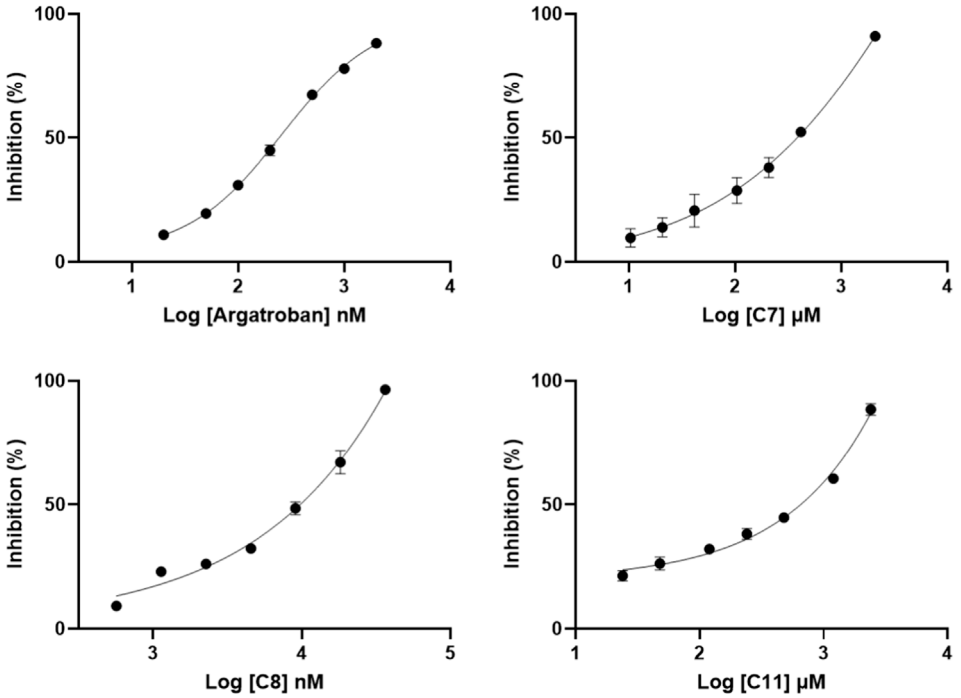

FIGURE 3 | Dose-response curves of *in vitro* inhibition assays.

and exhibited good anti-tumor activity against tested tumor cell lines (HepG-2, SMMC-7721, Hela and A549) (Zhang et al., 2015). C3 had estrogen-like effects (Suksamrarn et al., 2008). C6 were evaluated for inhibitory effects on the proliferation of HH cells and HaCaT cells (Chen et al., 2015), and inhibited the release of β-hexanosidase from rat basophilic leukemic leukemia (RBL-2H3) cells to produce antiallergic activity (Matsumoto et al., 2015). C9 was reported to have strong HT-22 cytotoxicity (Jirásek et al., 2014). C14 suppressed adipocyte differentiation by inhibiting PPARγ. C/EBPα inhibits the differentiation of 3T3-L1 adipocytes (Yang et al., 2014a) and reduced pancreatic lipase activity at low concentrations (Yang et al., 2014b). In addition, C14 was also considered a selective inhibitor of COX2 (Yang et al., 2009) and has been shown to inhibit B16 melanoma cells (Matsumoto et al., 2013). C10 has been described only as a plant metabolic component and its specific activity has not been studied because it is not readily available (He et al., 2018; Wang et al., 2021). From the point of view of structure, diarylheptanoids belong to polyphenol, which means they have potentially good antioxidant activity. These identical structures were similar to curcumin to a significant extent, meaning that most studies have focused on their anti-inflammatory activity. It is worth noting that the role of these compounds in the coagulation system had not yet been reported.

In vitro THR Inhibition Assays

In order to evaluate the THR inhibitory activity of the identified compounds from CR, the enzyme activity was determined *in vitro* using compounds 7, 8, and 11 (C7, C8, and C11), as shown in **Figure 3**. The IC_{50} was determined by the validated method. The results showed that the IC_{50} values of C7, C8, and C11 were 358.44, 9.92, and 654.29 μM, respectively. Although the inhibition ability of these compounds is weaker than the positive drug argatroban, as extracts from natural plant species, they probably could be used as an effective and safe substitute for argatroban. The skeleton structure is very different from that of argatroban, so they are worthy of further exploration to optimize potential thrombin inhibitors. In addition, these compounds have been reported to carry a variety of other beneficial biological activities. For instance, C11 has an anti-allergic activity and can inhibit melanoma formation (Matsumoto et al., 2015). C7 and C8, as well as some other diarylheptanoid compounds, have a good antioxidant and anti-inflammatory activity (Alonso-Amelot, 2016; Jivishov et al., 2020; Nair and Paliwal, 2021; Vanucci-bacqu and Bedos-belval, 2021). Free radicals, inflammation, and thrombosis are interrelated in complex ways to each other. Inflammation can promote thrombosis in a variety of ways, and thrombogenic factors can also participate in the regulation of inflammatory response. Oxidative stress usually leads to oxidative damage of biomolecules, causing the generation of damage-associated molecular patterns (DAMPs) and the release of cytokines in the body. These changes will consequently result in increased release of cytokines and chemokines, recruitment and activation of more inflammatory cells, as well as systemic chronic inflammatory response in the body. These chronic injuries will in turn further activate the clotting pathways abnormally, and finally trigger the formation of clots (Wang et al., 2017; Yang et al., 2017; Li et al., 2018). These natural compounds with multiple synergistic biological activities show

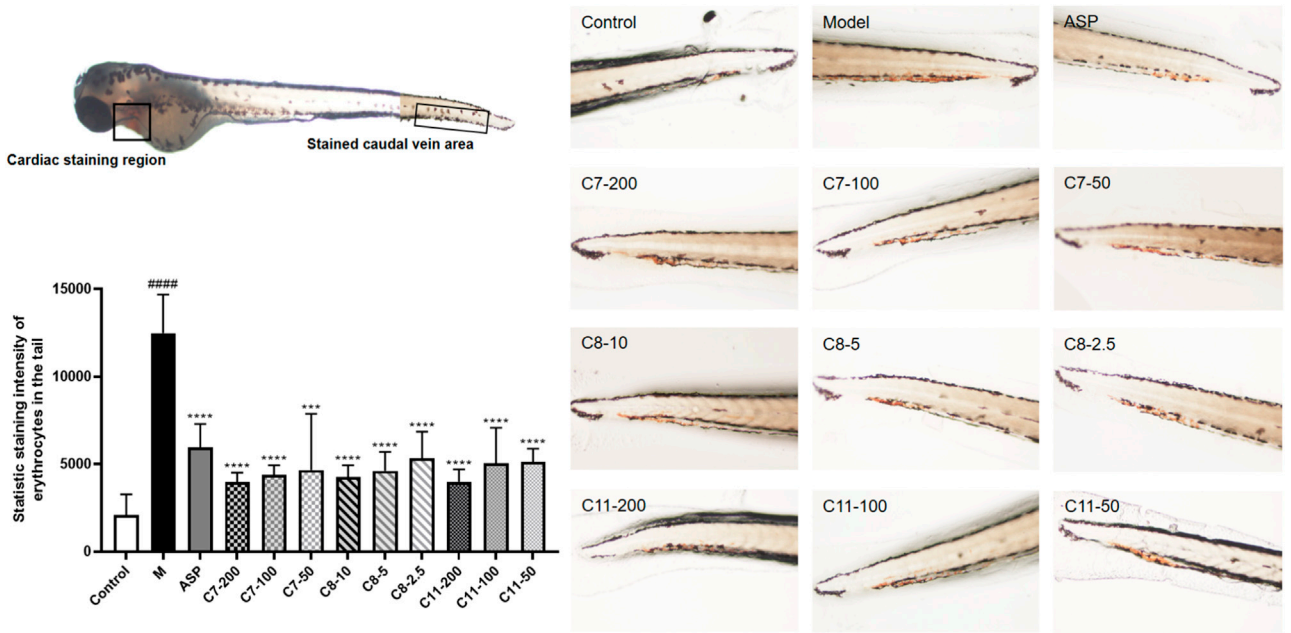

FIGURE 4 | Antithrombotic activity of C7, 8, and 11 in zebrafish (n = 10, mean ± standard deviation). *In vivo* visualization of the erythrocytes of zebrafish tails, and statistic staining intensity of the erythrocytes in zebrafish tails of all the groups. ***p < 0.001 compared to the model (M) group. ****p < 0.0001 compared to the M group.

great potential to be developed as a functional dietary supplement. In brief, our experiment has demonstrated that certain diarylheptanoid compounds have a good THR inhibitory activity while at the same time having some other benefits. It is also worth mentioning that the target substance can be obtained more conveniently by affinity ultrafiltration as compared to the complex procedures of traditional methods, which require continuous purification by HPLC and activity verification of each fragment (Nongonierma and Fitzgerald, 2018). The results of the study have shown that AUF-LC-MS is a rapid and effective approach for the isolation and identification of bioactive constituents.

Antithrombotic Activity in Zebrafish Larvae

By using zebrafish thrombosis, we also analyzed the *in vivo* effects of the three compounds (C7, C8, and C11) that have been validated to be effective *in vitro* thrombin-inhibitory substances. The toxicity of these compounds at different concentrations was assessed within 24 h before testing using juvenile zebrafish (3 dpf), and a 100% survival rate was obtained when the concentration of C7, C8, and C11 was 200, 10, and 200 μg/ml, respectively. Three concentration gradients were employed for the administration group according to the maximum tolerated concentration, as shown in **Figure 4**. The staining intensity (SI) of the erythrocytes in zebrafish tails in the model group was significantly increased, implicating the successful formation of tail vein thrombosis. As a result, the administration group at the experimental concentrations showed similar antithrombotic activity as the positive group, indicating that all three compounds have *in vivo* activity to downregulate the risk of peripheral circulation blockage in AA thrombotic zebrafish. Compared with the other compounds, C8 showed a stronger effect, which was consistent with the results from *in vitro* experiments. Nevertheless, the three identified compounds all showed a significant antithrombotic activity within their safe concentration ranges (C7 less than 200 μg/ml, C8 less than 10 μg/ml, and C9 less than 200 μg/ml).

Interaction Determination

Computer-aided interactive molecular docking can be used to predict and analyze the structure-activity relationship between receptor and ligand. The three compounds that were verified *in vitro* were selected for visualized molecular docking, and the results are shown in **Figure 5**. In the structure of thrombin, the most critical catalytic triads (His57, Asp102, and Ser195) are located in the middle of the active site, others are in the exosite I, exosite II, and Na+ binding sites (Zheng et al., 2021). Only the active site was tested. It can be seen that the three compounds can be inserted into the catalytic active center in THR to produce a variety of forces inhibiting the enzyme activity, thereby blocking the process of thrombosis by preventing fibrinogen (FI) from turning into fibrin monomer (Flα). Specifically, C7 can form a Pi-Pi interaction with His57 and interacts with Asp102 and Ser195 via a weak van der Waals force. C8 can form a strong conventional hydrogen bond with Ser195 and a carbon hydrogen bond with His57. C11 can also interact with His57 and Ser195 by van der Waals force. Ser195 is located in a position that makes it act directionally and participate in nucleophilic attacks to cleavage amide bonds of substrates. His57 is involved in proton transfer and plays the catalytic role on a generalized base. In contrast, Asp102 mainly performs an adjuvant function of

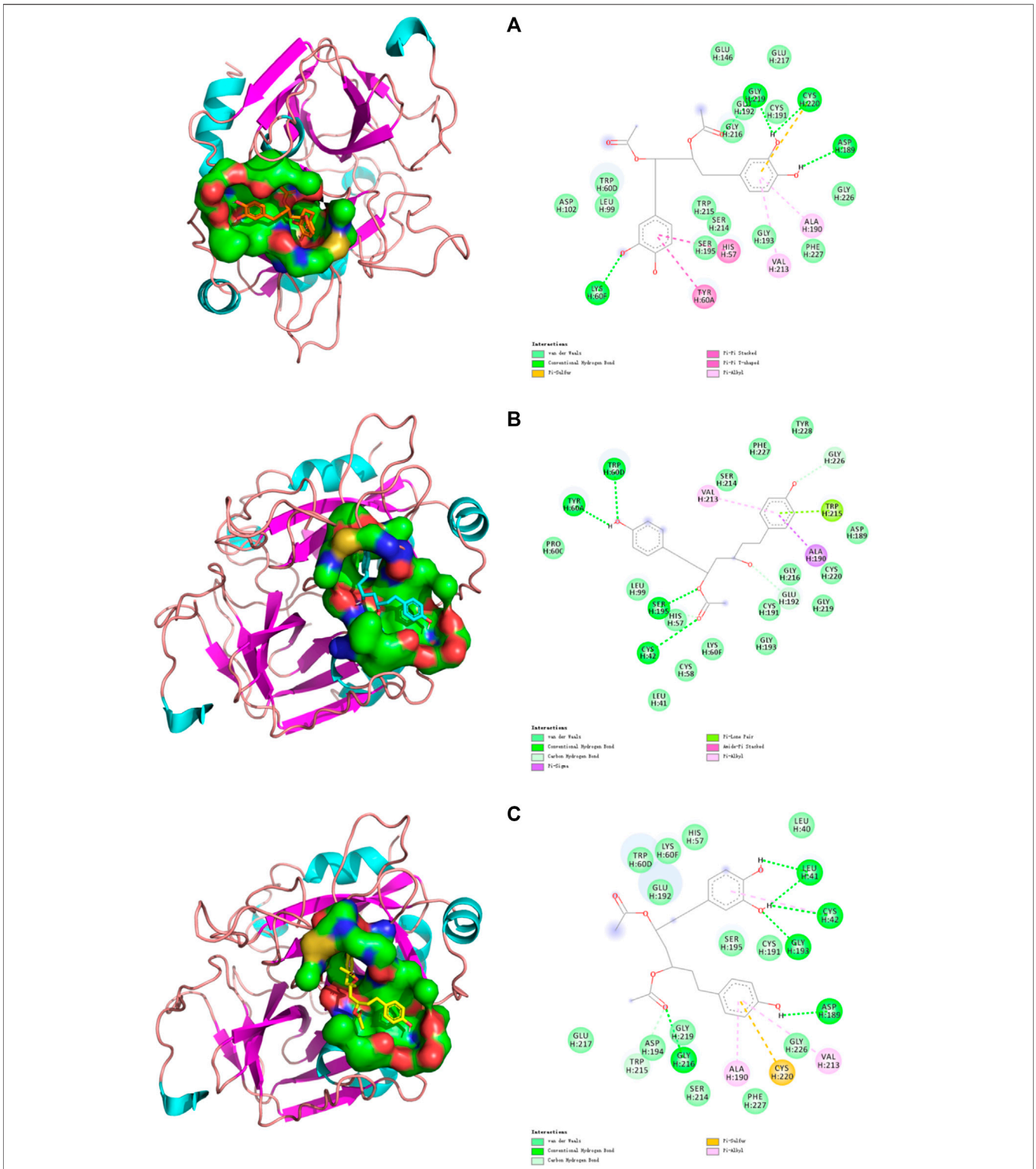

FIGURE 5 | Docking models of **(A)** C7, **(B)** C8, and **(C)** C11 in THR active site. (Van der Waals are colored in light green; Hydrogen bonds are colored in deep green; Yellow, purple, deep pink, and light pink indicate hydrophobic interactions and represent Pi-Sulful, Pi-sigma, Amide-Pi Stacked, and Pi-Alkyl, respectively).

correctly locating His57 and has little involvement in the formation of interactions (Böhm et al., 1999). In addition, three important residues (Ala190-Cys191-Glu192) remain at the base of the active site. Ala190 can form a Pi-Alkyl interaction with the benzene rings of C7 and C11 and a strong Pi-sigma interaction with the benzene rings of C8.

TABLE 2 | Binding sites of the compounds and the interaction forces between monomer and thrombin.

Compounds	Hydrogen bond amino acids	Pi-interaction amino acids	Van der Waals interaction amino acids
C7	Gly219, Cys220, Asp189, Lys60F	His57, Tyr60A, Val213, Ala190, Cys220	Asp102, Leu99, Trp60D, Trp215, Ser214, Ser195, Gly193, Phe227, Gly226, Cys191, Glu192, Gly216, Glu217, Glu146
C8	Trp60D, Tyr60A, Ser195, His57, Cys42, Glu192, Gly226	Ala190, Trp215, Val213	Pro60C, Leu99, Leu41, Cys58, Lys60F, Gly193, Cys191, Gly216, Gly219, Cys220, Asp189, Tyr228, Phe227, Ser214
C11	Asp194, Gly216, Asp189, Gly193, Cys42, Leu41	Cys42, Val213, Cys220, Ala190	His57, Lys60F, Trp60D, Glu192, Leu40, Cys191, Ser195, Gly226, Phe227, Ser214, Gly219, Trp215, Glu217
Argatroban	Asp189, Gly219, Gly226, Gly216, Ser195, Glu217	Trp60D, His57, Tyr60A, Leu99, Ile174, Trp215	Asn98, Val213, Glu192, Cys191, Cys220, Ser214, Lys60F

Cys191 interacts with the phenol hydroxyl groups of C7 and C11, and also with the hydroxyl group at position 3 of C8 to form van der Waals force. Glu192 can form van der Waals forces with C7 and C11, and carbon hydrogen bond with the hydroxyl group at position 3 of C8. Plus, some interactions demonstrated the compound's effect on the Na^+ binding site of thrombin, Leu99, LLE174, and Trp215 form s-hydrophobic cysts (Brandstetter et al., 1996), which facilitate the binding of aromatic residues. C7 forms van der Waals forces with Leu99 and Trp215, C8 forms van der Waals forces and Pi-Lone pair interaction with Leu99 and Trp215, respectively, while C11 forms a carbon hydrogen bond with Trp215. The Trp60D residue and S2 region extends to the active region, forming a closed hydrophobic pocket that makes it difficult to access the larger structure of the substrate. The amino acid residue forms van der Waals force interaction with C7 and C11, and strong hydrogen bonds with C8. Glu217 is the key residue of the sodium-binding allosteric site, and both C7 and C11 interacted with it (Abdel Aziz and Desai, 2018).

Table 2 shows the complete molecular docking details and the interaction of the protein 1DWC with the carrying ligand agatroban. The docking score is calculated by G_score, PMF_score, D_score, and ChemScore. The higher the score, the stronger the binding ability of the target. Among all the groups, the docking score of positive drug agatroban is 7.9147, while that of negative drug adenosine is 5.4534. Therefore, structures with a docking score of less than 5.4534 were considered less important, whereas, those with a docking score greater than 7.9147 should be valued. In our experiment, some compounds, such as C13, had a docking score of less than 5 but were also selected, possibly because their binding site was not the catalytic active site of thrombin. The results showed that the docking score of C5, C7, C8, and C11 were all higher than that of the positive drug agatroban, but this was not the case for C7, C8, and C11 in actual *in vitro* tests. The docking score represents an ideal binding ability, but in practice, factors such as solubility and toxicity of compounds also play an important role in their efficacy. In addition, as mentioned above, the amino acid residues have different degrees of importance in realizing thrombin catalytic activity but this was not considered by the molecular docking systems.

By comprehensive analysis of the results, it can be seen that when the acetoxyl group is present at positions 3 and 5, one end of the catechol structure with more hydroxyl groups is more likely to enter the active site for binding. However, when 4-hydroxyphenyl is present at positions 1 and 7, the side with less steric hindrance at positions 3 and 5, the side near the hydroxyl group at positions 3 or 5, is more likely to enter and exert forces on multiple amino acid residues. While C7, which shows symmetry, has different binding sites at both ends, demonstrating the advantage of the catechol structure at both ends of the long chain. Based on this, a relatively ideal structure should be 4,4'-[3-(acetyloxy)-5-hydroxy-1,7-heptanediyl]bis[1,2-benzenediol], as shown in **Figure 2A** C16. The compound with this structure had a trace content in the samples collected in this study, which was due to a failure in considering the absorption of this compound (more than 80%) to avoid the baseline noise fluctuation. However, this compound is confirmed to be one of the diarylheptanoid compounds of CR (Vanucci-bacqu and Bedos-belval, 2021).

CONCLUSION

Curcumae Rhizoma and its relatives are widely used as functional plants in Asia because of its rich existence in the beneficial pigment curcumin and the evident effect of promoting blood circulation and removing blood stasis. In our study, an AUF-LC-MS method based on THR affinity was successfully established for rapid, efficient, and targeted screening and identification of the bioactive compounds in CR. A total of 15 active compounds (13 diarylheptanoid, 1 diterpenoids, and 1 sesquiterpenes) were found and identified, with some of them verified to be effective in in vitro THR inhibition experiments. Further analysis was conducted by molecular docking to study the structure-activity relationship of the compounds, and the *in vivo* antithrombotic activity of these compounds was also evaluated using a zebrafish model. The results confirmed the discovery of a new biological activity--thrombin inhibition--of specific diarylheptanoid structures, suggesting that this natural skeleton may have the potential to be further developed and modified as THRI. Additionally, as mentioned above, some studies have shown that the ingredients verified in this paper have antioxidant and anti-inflammatory effects. Since the process of thrombotic disease is closely related to oxidative stress and inflammatory response as known to all, treatments consider that in addition to their direct role in the clotting pathway, antioxidants, and anti-inflammatory work together to produce antithrombotic

activity. For this reason, these substances have shown great potential as a dietary supplement to protect the cardiovascular system. This method can accelerate and simplify the study of bioactive compounds in natural products. The analysis of its bioactive components is also helpful for its quality evaluation and clinical application.

DATA AVAILABILITY STATEMENT

The original contributions presented in the study are included in the article/**Supplementary Material**, further inquiries can be directed to the corresponding authors.

ETHICS STATEMENT

The animal study was reviewed and approved by Guangdong Pharmaceutical University.

AUTHOR CONTRIBUTIONS

ZL developed the paper draft. JM and ZL were responsible for draft revision. JM and SY worked as the supervisor of experiments. ZL and YH performed the experiments. Other contributions of the authors are summarised as follows—ZL: investigation design, resourcing, conceptualization, methodology development, software operation, as well as data curation, visualization, and validation. YZ: investigation design. SY: methodology development. LW: methodology development. YH: investigation design and software operation. HC: investigation design. SW: funding acquisition. JM: funding acquisition and resourcing. All data were generated in-house without any paper mill used. All authors agreed to be accountable for all aspects of the work to ensure integrity and accuracy.

FUNDING

Innovation and Strong School Project of Guangdong Pharmaceutical University and Guangdong Provincial Education Department (2016KTSCX064, 2018KZDXM040), the sixth batch of national experts of Traditional Chinese Medicine Academic Experience Inheritance Teacher and Apprentice Project (2017 no. 29), National Standardization Project of Traditional Chinese Medicine (ZYBZH-Y-SC-40).

ACKNOWLEDGMENTS

We sincerely thank Guangdong Pharmaceutical University for providing the platform for the experiment. We are also grateful to the staff from SY Laboratory for their valuable advice, as well as Gang Chen laboratory for providing the necessary resources for Zebrafish research.

SUPPLEMENTARY MATERIAL

The Supplementary Material for this article can be found online at: https://www.frontiersin.org/articles/10.3389/fphar.2021.769021/full#supplementary-material

REFERENCES

Abdel Aziz, M. H., and Desai, U. R. (2018). Novel Heparin Mimetics Reveal Cooperativity between Exosite 2 and Sodium-Binding Site of Thrombin. *Thromb. Res.* 165, 61–67. doi:10.1016/j.thromres.2018.03.013

Alberti, Á., Riethmüller, E., and Béni, S. (2018). Characterization of Diarylheptanoids: An Emerging Class of Bioactive Natural Products. *J. Pharm. Biomed. Anal.* 147, 13–34. doi:10.1016/j.jpba.2017.08.051

Alonso-Amelot, M. E. (2016). "Chapter 4-Multitargeted Bioactive Materials of Plants in the Curcuma Genus and Related Compounds: Recent Advances," in *Studies in Natural Products Chemistry*. Editor A. U. Rahman (Mérida, Venezuela: Elsevier), 111–200. doi:10.1016/B978-0-444-63603-4.00004-8

Böhm, M., Stürzebecher, J., and Klebe, G. (1999). Three-Dimensional Quantitative Structure–Activity Relationship Analyses Using Comparative Molecular Field Analysis and Comparative Molecular Similarity Indices Analysis to Elucidate Selectivity Differences of Inhibitors Binding to Trypsin, Thrombin, and Factor Xa. *J. Med. Chem.* 42, 458–477. doi:10.1021/jm981062r

Brandstetter, H., Kühne, A., Bode, W., Huber, R., von der Saal, W., Wirthensohn, K., et al. (1996). X-ray Structure of Active Site-Inhibited Clotting Factor Xa. Implications for Drug Design and Substrate Recognition. *J. Biol. Chem.* 271, 29988–29992. doi:10.1074/jbc.271.47.29988

Cai, Q., Meng, J., Ge, Y., Gao, Y., Zeng, Y., Li, H., et al. (2020). Fishing Antitumor Ingredients by G-Quadruplex Affinity from Herbal Extract on a Three-Phase-Laminar-Flow Microfluidic Chip. *Talanta* 220, 121368. doi:10.1016/j.talanta.2020.121368

Cao, J., Xu, J. J., Liu, X. G., Wang, S. L., and Peng, L. Q. (2016). Screening of Thrombin Inhibitors from Phenolic Acids Using Enzyme-Immobilized Magnetic Beads through Direct Covalent Binding by Ultrahigh-Performance Liquid Chromatography Coupled with Quadrupole Time-Of-Flight Tandem Mass Spectrometry. *J. Chromatogr. A.* 1468, 86–94. doi:10.1016/j.chroma.2016.09.022

Chen, S. D., Gao, J. T., Liu, J. G., Liu, B., Zhao, R. Z., and Lu, C. J. (2015). Five New Diarylheptanoids from the Rhizomes of Curcuma Kwangsiensis and Their Antiproliferative Activity. *Fitoterapia* 102, 67–73. doi:10.1016/j.fitote.2015.02.004

Chinese Pharmacopoeia Commission (2020). *Pharmacopoeia of the People's Republic of China*. Beijing: China Medical Science Press.

Gurbel, P. A., Bliden, K. P., Turner, S. E., Tantry, U. S., Gesheff, M. G., Barr, T. P., et al. (2016). Cell-Penetrating Pepducin Therapy Targeting PAR1 in Subjects with Coronary Artery Disease. *Arterioscler. Thromb. Vasc. Biol.* 36, 189–197. doi:10.1161/ATVBAHA.115.306777

He, J. B., Yan, Y. M., Ma, X. J., Lu, Q., Li, X. S., Su, J., et al. (2011). Sesquiterpenoids and Diarylheptanoids from Nidus Vespae and Their Inhibitory Effects on Nitric Oxide Production. *Chem. Biodivers* 8, 2270–2276. doi:10.1002/cbdv.201000366

He, L., Qin, Z., Li, M., Chen, Z., Zeng, C., Yao, Z., et al. (2018). Metabolic Profiles of Ginger, A Functional Food, and its Representative Pungent Compounds in Rats by Ultraperformance Liquid Chromatography Coupled with Quadrupole Time-Of-Flight Tandem Mass Spectrometry. *J. Agric. Food Chem.* 66, 9010–9033. doi:10.1021/acs.jafc.8b03600

Jagadeeswaran, P., Cooley, B. C., Gross, P. L., and Mackman, N. (2016). Animal Models of Thrombosis from Zebrafish to Nonhuman Primates: Use in the Elucidation of New Pathologic Pathways and the Development of Antithrombotic Drugs. *Circ. Res.* 118, 1363–1379. doi:10.1161/CIRCRESAHA.115.306823

Jirásek, P., Amslinger, S., and Heilmann, J. (2014). Synthesis of Natural and Non-natural Curcuminoids and Their Neuroprotective Activity against Glutamate-

Induced Oxidative Stress in HT-22 Cells. *J. Nat. Prod.* 77, 2206–2217. doi:10.1021/np500396y

Jivishov, E., Nahar, L., and Sarker, S. D. (2020). "Nephroprotective Natural Products," in *Medicinal Natural Products: A Disease-Focused Approach*. Annual Reports in Medicinal Chemistry. Editors S. D. Sarker and L. Nahar (Baku, Azerbaijan: Academic Press), 251–271. doi:10.1016/bs.armc.2020.02.003

Lan, Z., Zhang, Y., Zhang, Y., Liu, F., Ji, D., Cao, H., et al. (2021). Rapid Evaluation on Pharmacodynamics of Curcumae Rhizoma Based on Micro-NIR and Benchtop-NIR. *J. Pharm. Biomed. Anal.* 200, 114074. doi:10.1016/j.jpba.2021.114074

Lee, C. J., and Ansell, J. E. (2011). Direct Thrombin Inhibitors. *Br. J. Clin. Pharmacol.* 72, 581–592. doi:10.1111/j.1365-2125.2011.03916.x

Lewis, B. E., Wallis, D. E., Berkowitz, S. D., Matthai, W. H., Fareed, J., Walenga, J. M., et al. (2001). Argatroban Anticoagulant Therapy in Patients with Heparin-Induced Thrombocytopenia. *Circulation* 103, 1838–1843. doi:10.1161/01.cir.103.14.1838

Li, G., Zhou, R., Zhao, X., Liu, R., and Ye, C. (2018). Correlation between the Expression of IL-18 and D-eep V-enous T-hrombosis. *Int. J. Mol. Med.* 42, 111–200. doi:10.3892/ijmm.2018.3682

Li, J., Liao, C. R., Wei, J. Q., Chen, L. X., Zhao, F., and Qiu, F. (2011). Diarylheptanoids from Curcuma Kwangsiensis and Their Inhibitory Activity on Nitric Oxide Production in Lipopolysaccharide-Activated Macrophages. *Bioorg. Med. Chem. Lett.* 21, 5363–5369. doi:10.1016/j.bmcl.2011.07.012

Li, J., Zhao, F., Li, M. Z., Chen, L. X., and Qiu, F. (2010). Diarylheptanoids from the Rhizomes of Curcuma Kwangsiensis. *J. Nat. Prod.* 73, 1667–1671. doi:10.1021/np100392m

Li, N., Wang, L., Zu, L., Wang, K., Di, L., and Wang, Z. (2012). Antioxidant and Cytotoxic Diarylheptanoids Isolated from Zingiber Officinale Rhizomes. *Chin. J. Chem.* 30, 1351–1355. doi:10.1002/cjoc.201200121

Liu, H., Yan, Q., Zou, D., Bu, X., Zhang, B., Ma, X., et al. (2018). Identification and bioactivity evaluation of ingredients from the fruits of Amomum tsaoko Crevost et Lemaire. *Phytochemistry Lett.* 28, 111–115. doi:10.1016/j.phytol.2018.10.007

Liu, S., Li, S., Yuan, D., Wang, E., Xie, R., Zhang, W., et al. (2021). Protease Activated Receptor 4 (PAR4) Antagonists: Research Progress on Small Molecules in the Field of Antiplatelet Agents. *Eur. J. Med. Chem.* 209, 112893. doi:10.1016/j.ejmech.2020.112893

Liu, Y., and Nair, M. G. (2012). Curcuma Longa and Curcuma Mangga Leaves Exhibit Functional Food Property. *Food Chem.* 135, 634–640. doi:10.1016/j.foodchem.2012.04.129

Matsumoto, T., Nakamura, S., Fujimoto, K., Ohta, T., Ogawa, K., Yoshikawa, M., et al. (2015). Structure of Diarylheptanoids with Antiallergic Activity from the Rhizomes of Curcuma Comosa. *J. Nat. Med.* 69, 142–147. doi:10.1007/s11418-014-0870-8

Matsumoto, T., Nakamura, S., Nakashima, S., Yoshikawa, M., Fujimoto, K., Ohta, T., et al. (2013). Diarylheptanoids with Inhibitory Effects on Melanogenesis from the Rhizomes of Curcuma Comosa in B16 Melanoma Cells. *Bioorg. Med. Chem. Lett.* 23, 5178–5181. doi:10.1016/j.bmcl.2013.07.010

Naghavi, M., Abajobir, A. A., Abbafati, C., Abbas, K. M., Abd-Allah, F., Abera, S. F., et al. (2017). Global, Regional, and National Age-Sex Specific Mortality for 264 Causes of Death, 1980-2016: a Systematic Analysis for the Global Burden of Disease Study 2016. *Lancet* 390, 1151–1210. doi:10.1016/S0140-6736(17)32152-9

Nair, A. S., and Paliwal, A. (2021). "13-Systems Pharmacology and Molecular Docking Strategies Prioritize Natural Molecules as Antiinflammatory Agents," in *Inflammation And Natural Products*. Editors S. Gopi, A. Amalraj, A. Kunnumakkara, and S. Thomas (Kerala, India: Academic Press), 283–319. doi:10.1016/B978-0-12-819218-4.00016-X

Nongonierma, A. B., and Fitzgerald, R. J. (2018). Enhancing Bioactive Peptide Release and Identification Using Targeted Enzymatic Hydrolysis of Milk Proteins. *Anal. Bioanal. Chem.* 410, 3407–3423. doi:10.1007/s00216-017-0793-9

O'Donoghue, M. L., Bhatt, D. L., Wiviott, S. D., Goodman, S. G., Fitzgerald, D. J., Angiolillo, D. J., et al. (2011). Safety and Tolerability of Atopaxar in the Treatment of Patients with Acute Coronary Syndromes: the Lessons from Antagonizing the Cellular Effects of Thrombin–Acute Coronary Syndromes Trial. *Circulation* 123, 1843–1853. doi:10.1161/CIRCULATIONAHA.110.000786

Poole, R. M., and Elkinson, S. (2014). Vorapaxar: First Global Approval. *Drugs* 74, 1153–1163. doi:10.1007/s40265-014-0252-2

Qin, Q., Wang, B., Wang, J., Chang, M., Xia, T., Shi, X., et al. (2019). A Comprehensive Strategy for Studying Protein-Metabolite Interactions by Metabolomics and Native Mass Spectrometry. *Talanta* 194, 63–72. doi:10.1016/j.talanta.2018.10.010

Qin, S., Ren, Y., Fu, X., Shen, J., Chen, X., Wang, Q., et al. (2015). Multiple Ligand Detection and Affinity Measurement by Ultrafiltration and Mass Spectrometry Analysis Applied to Fragment Mixture Screening. *Anal. Chim. Acta* 886, 98–106. doi:10.1016/j.aca.2015.06.017

Suksamrarn, A., Ponglikitmongkol, M., Wongkrajang, K., Chindaduang, A., Kittidanairak, S., Jankam, A., et al. (2008). Diarylheptanoids, New Phytoestrogens from the Rhizomes of Curcuma Comosa: Isolation, Chemical Modification and Estrogenic Activity Evaluation. *Bioorg. Med. Chem.* 16, 6891–6902. doi:10.1016/j.bmc.2008.05.051

Summers, R. L., and Sterling, S. A. (2016). Emergent Bleeding in Patients Receiving Direct Oral Anticoagulants. *Air Med. J.* 35, 148–155. doi:10.1016/j.amj.2016.01.001

Sun, M., Ding, R., Ma, Y., Sun, Q., Ren, X., Sun, Z., et al. (2021). Cardiovascular Toxicity Assessment of Polyethylene Nanoplastics on Developing Zebrafish Embryos. *Chemosphere* 282, 131124. doi:10.1016/j.chemosphere.2021.131124

Tao, W., Xu, X., Wang, X., Li, B., Wang, Y., Li, Y., et al. (2013). Network Pharmacology-Based Prediction of the Active Ingredients and Potential Targets of Chinese Herbal Radix Curcumae Formula for Application to Cardiovascular Disease. *J. Ethnopharmacol.* 145, 1–10. doi:10.1016/j.jep.2012.09.051

Tao, Y., Cai, H., Li, W., and Cai, B. (2015). Ultrafiltration Coupled with High-Performance Liquid Chromatography and Quadrupole-Time-Of-Flight Mass Spectrometry for Screening Lipase Binders from Different Extracts of Dendrobium Officinale. *Anal. Bioanal. Chem.* 407, 6081–6093. doi:10.1007/s00216-015-8781-4

van Ryn, J., Goss, A., Hauel, N., Wienen, W., Priepke, H., Nar, H., et al. (2013). The Discovery of Dabigatran Etexilate. *Front. Pharmacol.* 4, 12. doi:10.3389/fphar.2013.00012

Vanucci-Bacqué, C., and Bedos-belval, F. (2021). Anti-inflammatory Activity of Naturally Occuring Diarylheptanoids - A Review. *Bioorg. Med. Chem.* 31, 115971. doi:10.1016/j.bmc.2020.115971

Vranckx, P., White, H. D., Huang, Z., Mahaffey, K. W., Armstrong, P. W., Van De Werf, F., et al. (2016). Validation of BARC Bleeding Criteria in Patients with Acute Coronary Syndromes: The TRACER Trial. *J. Am. Coll. Cardiol.* 67, 2135–2144. doi:10.1016/j.jacc.2016.02.056

Wang, A. K., Geng, T., Jiang, W., Zhang, Q., Zhang, Y., Chen, P. D., et al. (2020a). Simultaneous determination of twelve quinones from Rubiae radix et Rhizoma before and after carbonization processing by UPLC-MS/MS and their antithrombotic effect on zebrafish. *J. Pharm. Biomed. Anal.* 191, 113638. doi:10.1016/j.jpba.2020.113638

Wang, L., Liang, Q., Zhang, Y., Liu, F., Sun, Y., Wang, S., et al. (2021). iTRAQ-Based Quantitative Proteomics and Network Pharmacology Revealing Hemostatic Mechanism Mediated by Zingiberis Rhizome Carbonisata in Deficiency-Cold and Hemorrhagic Syndrome Rat Models. *Chem. Biol. Interact.* 343, 109465. doi:10.1016/j.cbi.2021.109465

Wang, S., Huai, J., Shang, Y., Xie, L., Cao, X., Liao, J., et al. (2020b). Screening for Natural Inhibitors of 5-lipoxygenase from Zi-Shen Pill Extract by Affinity Ultrafiltration Coupled with Ultra Performance Liquid Chromatography-Mass Spectrometry. *J. Ethnopharmacol.* 254, 112733. doi:10.1016/j.jep.2020.112733

Wang, Y., Wang, W., Xu, H., Sun, Y., Sun, J., Jiang, Y., et al. (2017). Non-Lethal Sonodynamic Therapy Inhibits Atherosclerotic Plaque Progression in ApoE-/- Mice and Attenuates Ox-LDL-Mediated Macrophage Impairment by Inducing Heme Oxygenase-1. *Cell Physiol Biochem* 41, 2432–2446. doi:10.1159/000475913

Wei, H., Zhang, X., Tian, X., and Wu, G. (2016). Pharmaceutical Applications of Affinity-Ultrafiltration Mass Spectrometry: Recent Advances and Future Prospects. *J. Pharm. Biomed. Anal.* 131, 444–453. doi:10.1016/j.jpba.2016.09.021

Wu, Z. Y., Zhang, H., Yang, Y. Y., and Yang, F. Q. (2020). An Online Dual-Enzyme Co-immobilized Microreactor Based on Capillary Electrophoresis for Enzyme Kinetics Assays and Screening of Dual-Target Inhibitors against

Thrombin and Factor Xa. *J. Chromatogr. A.* 1619, 460948. doi:10.1016/j.chroma.2020.460948

Xie, L., Fu, Q., Shi, S., Li, J., and Zhou, X. (2021). Rapid and Comprehensive Profiling of α-glucosidase Inhibitors in Buddleja Flos by Ultrafiltration HPLC-QTOF-MS/MS with Diagnostic Ions Filtering Strategy. *Food Chem.* 344, 128651. doi:10.1016/j.foodchem.2020.128651

Xie, L., Lee, D. Y., Shang, Y., Cao, X., Wang, S., Liao, J., et al. (2020). Characterization of Spirostanol Glycosides and Furostanol Glycosides from Anemarrhenae Rhizoma as Dual Targeted Inhibitors of 5-lipoxygenase and Cyclooxygenase-2 by Employing a Combination of Affinity Ultrafiltration and HPLC/MS. *Phytomedicine* 77, 153284. doi:10.1016/j.phymed.2020.153284

Yang, M., Cooley, B. C., Li, W., Chen, Y., Vasquez-vivar, J., Scoggins, N. O., et al. (2017). Thrombosis And Hemostasis Platelet CD36 Promotes Thrombosis by Activating Redox Sensor ERK5 in Hyperlipidemic Conditions. *Blood* 129, 2917–2927. doi:10.1182/blood-2016-11-750133

Yang, M. H., Chin, Y. W., Chae, H. S., Yoon, K. D., and Kim, J. (2014a). Anti-adipogenic Constituents from *Dioscorea Opposita* in 3T3-L1 Cells. *Biol. Pharm. Bull.* 37, 1683–1688. doi:10.1248/bpb.b14-00216

Yang, M. H., Chin, Y. W., Yoon, K. D., and Kim, J. (2014b). Phenolic Compounds with Pancreatic Lipase Inhibitory Activity from Korean Yam (Dioscorea Opposita). *J. Enzyme Inhib. Med. Chem.* 29, 1–6. doi:10.3109/14756366.2012.742517

Yang, M. H., Yoon, K. D., Chin, Y. W., Park, J. H., and Kim, J. (2009). Phenolic Compounds with Radical Scavenging and Cyclooxygenase-2 (COX-2) Inhibitory Activities from Dioscorea Opposita. *Bioorg. Med. Chem.* 17, 2689–2694. doi:10.1016/j.bmc.2009.02.057

Zhang, L., Yang, Z., Wei, J., Su, P., Pan, W., Zheng, X., et al. (2017a). Essential Oil Composition and Bioactivity Variation in Wild-Growing Populations of Curcuma Phaeocaulis Valeton Collected from China. *Ind. Crops Prod.* 103, 274–282. doi:10.1016/j.indcrop.2017.04.019

Zhang, Q., Yang, Y. X., Li, S. Y., Wang, Y. L., Yang, F. Q., Chen, H., et al. (2017b). An Ultrafiltration and High Performance Liquid Chromatography Coupled with Diode Array Detector and Mass Spectrometry Approach for Screening and Characterizing Thrombin Inhibitors from Rhizoma Chuanxiong. *J. Chromatogr. B Analyt Technol. Biomed. Life Sci.* 1061-1062, 421–429. doi:10.1016/j.jchromb.2017.07.050

Zhang, T.-T., Lu, C.-L., and Jiang, J.-G. (2015). Antioxidant and anti-tumour evaluation of compounds identified from fruit of Amomum tsaoko Crevost et Lemaire. *J. Funct. Foods* 18, 423–431. doi:10.1016/j.jff.2015.08.005

Zhang, Y., Ruan, J., Li, J., Chao, L., Shi, W., Yu, H., et al. (2017c). Bioactive Diarylheptanoids and Stilbenes from the Rhizomes of Dioscorea Septemloba Thunb. *Fitoterapia* 117, 28–33. doi:10.1016/j.fitote.2017.01.004

Zhao, D., Liu, J., Wang, M., Zhang, X., and Zhou, M. (2019). Epidemiology of Cardiovascular Disease in China: Current Features and Implications. *Nat. Rev. Cardiol.* 16, 203–212. doi:10.1038/s41569-018-0119-4

Zheng, X., Pu, P., Ding, B., Bo, W., Qin, D., and Liang, G. (2021). Identification of the Functional Food Ingredients with Antithrombotic Properties via Virtual Screen and Experimental Studies. *Food Chem.* 362, 130237. doi:10.1016/j.foodchem.2021.130237

Zhou, W., Guo, Z., Yu, L., Zhou, H., Shen, A., Jin, Y., et al. (2018). On-line Comprehensive Two-Dimensional Liquid Chromatography Tandem Mass Spectrometry for the Analysis of Curcuma Kwangsiensis. *Talanta* 186, 73–79. doi:10.1016/j.talanta.2018.04.014

Zhou, Y., Xie, M., Song, Y., Wang, W., Zhao, H., Tian, Y., et al. (2016). Two Traditional Chinese MedicinesCurcumae RadixandCurcumae Rhizoma: An Ethnopharmacology, Phytochemistry, and Pharmacology Review. *Evidence-Based Complement. Altern. Med.* 2016, 1–30. doi:10.1155/2016/4973128

Zhu, X. Y., Liu, H. C., Guo, S. Y., Xia, B., Song, R. S., Lao, Q. C., et al. (2016). A Zebrafish Thrombosis Model for Assessing Antithrombotic Drugs. *Zebrafish* 13, 335–344. doi:10.1089/zeb.2016.1263

Conflict of Interest: The authors declare that the research was conducted in the absence of any commercial or financial relationships that could be construed as a potential conflict of interest.

Publisher's Note: All claims expressed in this article are solely those of the authors and do not necessarily represent those of their affiliated organizations, or those of the publisher, the editors, and the reviewers. Any product that may be evaluated in this article, or claim that may be made by its manufacturer, is not guaranteed or endorsed by the publisher.

frontiers in Pharmacology

ORIGINAL RESEARCH
published: 03 January 2022
doi: 10.3389/fphar.2021.725186

Dangshen Erling Decoction Ameliorates Myocardial Hypertrophy *via* Inhibiting Myocardial Inflammation

Yigang Zhong[1,2†], Liuying Chen[3†], Miaofu Li[2], Lian Chen[2], Yufeng Qian[2], Chaofeng Chen[2], Yi Wang[1] and Yizhou Xu[2,3]**

[1]Pharmaceutical Informatics Institute, College of Pharmaceutical Sciences, Zhejiang University, Hangzhou, China, [2]Department of Cardiology, Affiliated Hangzhou First People's Hospital, Zhejiang University School of Medicine, Hangzhou, China, [3]Zhejiang Chinese Medical University, Hangzhou, China

Myocardial hypertrophy plays an essential role in the structural remodeling of the heart and the progression to heart failure (HF). There is an urgent need to understand the mechanisms underlying cardiac hypertrophy and to develop treatments for early intervention. Dangshen Erling decoction (DSELD) is a clinically used formula in Chinese medicine for treating coronary heart disease in patients with HF. However, the mechanism by which DSELD produces its cardioprotective effects remains largely unknown. This study explored the effects of DSELD on myocardial hypotrophy both *in vitro* and *in vivo*. *In vitro* studies indicated that DSELD significantly ($p < 0.05$) reduced the cross-sectional area of the myocardium and reduced elevated lactate dehydrogenase (LDH), tumor necrosis factor (TNF)-α, and interleukin (IL)-6 levels in the induced H9C2 cell model to study inflammation. *In vivo* experiments revealed that DSELD restores cardiac function and significantly reduces myocardial fibrosis in isoproterenol (ISO)-induced HF mouse model ($p < 0.05$). In addition, DSELD downregulated the expression of several inflammatory cytokines, such as granulocyte-macrophage colony-stimulating factor (GM-CSF), granulocyte CSF (G-CSF), IL-1α, IL-1β, IL-3, IL-5, IL-7, IL-12, IL-13, and TNF-α in HF ($p < 0.05$). Further analysis of the cardiac tissue demonstrated that DSELD produces its anti-inflammatory effects *via* the Toll-like receptor (TLR)4 signaling pathway. The expression of TLR4 downstream proteins such as matrix metalloproteinase-9 (MMP9) and myeloid differentiation factor-88 (MyD88) was among the regulated targets. In conclusion, these observations suggest that DSELD exerts antihypertrophic effects by alleviating the inflammatory injury *via* the TLR4 signaling pathway in HF and thus holds promising therapeutic potentials.

Keywords: myocardial hypertrophy, heart failure, Dangshen Erling decoction, inflammation, TLR4 signaling pathway

OPEN ACCESS

Edited by:
Mirko Baruscotti, University of Milan, Italy

Reviewed by:
Songül Karakaya, Atatürk University, Turkey
Maryam Rameshrad, North Khorasan University of Medical Sciences, Iran

****Correspondence:***
Yizhou Xu
qqyzxu@hotmail.com
Yi Wang
zjuwangyi@zju.edu.cn

[†]These authors have contributed equally to this work

Specialty section:
This article was submitted to Ethnopharmacology, a section of the journal Frontiers in Pharmacology

Received: *15 June 2021*
Accepted: *18 November 2021*
Published: *03 January 2022*

Citation:
Zhong Y, Chen L, Li M, Chen L, Qian Y, Chen C, Wang Y and Xu Y (2022) Dangshen Erling Decoction Ameliorates Myocardial Hypertrophy via Inhibiting Myocardial Inflammation. Front. Pharmacol. 12:725186. doi: 10.3389/fphar.2021.725186

INTRODUCTION

Heart failure (HF) is one of the most common forms of cardiac dysfunction caused by various cardiac diseases such as coronary heart disease, hypertension, arrhythmia, and viral myocarditis. HF is characterized by consistent pathological myocardial hypertrophy leading to increasing mortality and morbidity worldwide (Adamo et al., 2020). Pathological myocardial hypertrophy is characterized by enlarged cardiomyocytes and thickened ventricular walls that are the typical features of cardiac

remodeling in HF (Tham et al., 2015). Initially, this adaptive change is to maintain the normal ejection fraction of the heart under increased pressure load; however, sustained pathological overload induces these changes to progress gradually into irreversible damage to the cardiac structure and function (Oka et al., 2014). Therefore, sustained myocardial hypertrophy is the key to HF. Recently, several studies suggest that persistent myocardial inflammation is the hallmark of myocardial hypertrophy (Geng et al., 2019; Zhang et al., 2020b; Zhu et al., 2020).

The inflammatory process in the myocardium manifests as a systemically chronic low-intensity reaction (Rogero and Calder, 2018). During this process, cardiomyocytes secrete various molecules including pro-inflammatory cytokines, colony-stimulating factor (CSF), and chemokines contributing to the infiltration of inflammatory cells into the myocardial interstitial tissue (Yang et al., 2016; Martini et al., 2019). In the sterile (non-infectious) inflammation of the myocardium, the pattern recognition receptor (PRR) is triggered by the damage-associated molecular patterns (DAMPs) such as endogenous tissue damage signaling molecules (Paul-Clark et al., 2012). Toll-like receptor (TLR)4, a member of the PRR family, has been most extensively studied due to its essential role in regulating cardiac inflammation (Dange et al., 2014; Deng et al., 2018). Current elucidation indicates that the development of myocardial hypertrophy is related to the TLR4 signaling pathway (Deng et al., 2018; Singh et al., 2019; Lu et al., 2020).

Traditional Chinese medicine (TCM), especially the formula that comprises several herbs containing complex compounds at specific ratios and doses, has been used effectively as alternative and complementary therapies in cardiovascular diseases in China and many other Asian countries, with a unique theoretical system (Jia et al., 2020). It has been widely applied to prevent and treat HF for more than 2,000 years (Hao et al., 2017; Liu et al., 2018). There is an increasing number of traditional herbal formulas such as Qili Qiangxin capsules that have been proven to be clinically effective for HF (Li et al., 2013). Dangshen Erling decoction (DSELD) is a traditional Chinese herbal formula with a clinical application of strengthening Qi, reinforcing the spleen, and promoting kidney function. It consists of six medicinal herbs, such as *Codonopsis pilosula* (Franch.) Nannf. (Dangshen), *Atractylodes macrocephala* Koidz. (Baizhu), *Smilax glabra* Roxb. (Fuling), *Saposhnikovia divaricata* (Turcz. ex Ledeb.) Schischk. (Fangfeng), *Gynochthodes officinalis* (F.C. How) Razafim. and B. Bremer (Bajitian), and *Glycyrrhiza glabra* L. (Gancao). Our previous study demonstrated that DSELD displayed various pharmacological effects, including antiapoptotic effects and mitochondrial protection (Zhong et al., 2020). High-performance liquid chromatography–mass spectrometry analysis for the structural components of the DSELD extract preliminarily identified 42 compounds, four of them have anti-inflammatory properties (tanshinone II, liquiritigenin, cimifugin, and scopoletin) (Zhong et al., 2020). Therefore, we speculated that DSELD suppresses inflammation to ameliorate myocardial hypertrophy in HF. However, further studies were needed to elucidate the underlying mechanism.

This study explores the effects and the underlying mechanism of DSELD in treating cardiac hypertrophy using *in vivo* and *in vitro* models. The results demonstrate that DSELD ameliorates myocardial hypertrophy *via* inhibiting the TLR4-mediated myocardial inflammation.

MATERIALS AND METHODS

Chemicals and Reagents

The ingredients of DSELD described previously were provided by the Hangzhou First People's Hospital (Hangzhou, China) (Zhong et al., 2020). Its composition is shown in **Table 1**. The herbal mixture was first extracted in water (1:8, w/v) twice by reflux for 2 h each time. After the extraction, the solutions were mixed, filtered, and concentrated. The final extract was concentrated to 0.83 g/ml of crude herb extract in water. The major components of DSELD were measured by liquid chromatography coupled with mass spectrometry to ensure consistency between batches (**Supplementary Figure S1**).

Lipopolysaccharide (LPS; from *Escherichia coli* strain), isoprenaline hydrochloride [isoproterenol (ISO)], MTT assay kit, dimethyl sulfoxide (DMSO), and tetramethyl rhodamine methyl ester (TMRM) were purchased from Sigma Chemical Co. (St. Louis, MO, USA). Alexa Fluor 488 Phalloidin, anti-TLR4 (No. 14358), anti-nuclear factor (NF)-κB (No. 8242), anti-α-Tubulin (No. 3873), anti-β-actin (No. 4970) were purchased from Cell Signaling Technology (Danvers, MA, USA). Anti-matrix metalloproteinase (MMP)9 (No. ab38898) and anti-myeloid differentiation factor (MyD)88 (No. ab 2064) were purchased from Abcam (Cambridge, MA, USA). The nitric oxide (NO) assay and lactate dehydrogenase (LDH) cytotoxicity assay kits were purchased from Beyotime Biotechnology (Shanghai, China). The tumor necrosis factor (TNF)-α ELISA kit, interleukin (IL)-6 ELISA kit, and bicinchoninic acid (BCA) assay kit were purchased from Thermo Fisher Scientific (Eugene, OR, USA). The NT-proBNP ELISA kit was purchased from Yubo Biotechnology (Shanghai, China). Assays were run based on manufacturer's instructions.

Isoproterenol-Induced Cardiac Hypertrophy Model in Mice

A total of 60 male C57/BL6 mice each weighing more than 20 g and between 8 and 10 weeks of age with the specific pathogen-free (SPF) grade were purchased from Shanghai Slac Laboratory Animal Co., Ltd. (Shanghai, China). Mice were randomly divided into the vehicle (saline) group (n = 20) and the ISO group (n = 40). Each mouse received either 5 mg/kg/day ISO (ISO group) or saline (Vehicle group) by subcutaneous injection for 4 weeks. At the same time, half of the mice in the ISO group were randomly selected for DSELD treatment (n = 20). The treatment group received a gavage of DSELD at a dosage of 1.28 g (crude herbs)/kg (calculated based on body surface area) for 4 weeks. Transthoracic echocardiography was performed to evaluate the heart function at the end of the fourth week. Afterward, the blood was collected for the detection of the NT-proBNP and

TABLE 1 | The composition of Dangshen Erling decoction (DSELD).

Species	Herbal name	Part used	Dosage (g)	Ratio (%)
Codonopsis pilosula (Franch.) Nannf.	Dangshen	Root	30	36.14
Smilax glabra Roxb.	Fuling	Kernel	15	18.07
Atractylodes macrocephala Koidz.	Baizhu	Root	10	12.05
Saposhnikovia divaricata (Turcz. ex Ledeb.) Schischk.	Fangfeng	Root	10	12.05
Gynochthodes officinalis (F.C. How) Razafim. and B. Bremer	Bajitian	Root	10	12.05
Glycyrrhiza glabra L.	Gancao	Root	8	9.64
Total			83	100

inflammatory cytokines. Subsequently, the animals were sacrificed by cervical dislocation, and the hearts were collected for further examination.

Echocardiography

Isoflurane (inhaled)-anesthetized mice were subjected to 2-dimensional M-mode and B-mode echocardiography (Vevo TM 2100; Visual Sonics, Canada) to evaluate cardiac function. The ejection fraction (EF) and fractional shortening (FS) were measured as previously reported (Zhang et al., 2020b).

Histological Examination and Immunofluorescence Analysis

The heart was cut into 5-μm cross-sections to analyze the cardiac structure by hematoxylin–eosin (H&E) staining and fibrosis by Sirius Red staining. All stained sections were observed under an inverted microscope. Image Pro Plus 6.0 software (Media Cybernetics, Rockville, MD, USA) was used to map and analyze the area of fibrosis of the Sirius Red staining cross-sections by the software mapping module.

For immunofluorescence staining, cardiac tissues were frozen sectioned into 30-μm slices and blocked with 5% bovine serum albumin (BSA) for 0.5 h. After washing, the tissue sections were incubated with fluorescently labeled MPP9 antibody (1:250), MyD88 antibody (1:250), and NF-κB antibody (1:250). Image Pro Plus 6.0 software (Media Cybernetics) was used to analyze the fluorescence intensity.

Detection of Inflammatory Cytokine Profile in Cardiac Hypertrophy Model

About 50–100 mg myocardial tissue from different experimental groups were collected to perform multiple cytokine assays by Hangzhou AiTing Biological Technology Co., Ltd. (Hangzhou, China).

Measuring Nitric Oxide in RAW264.7 Macrophage Culture

The RAW264.7 macrophages used in this study were obtained from the Cell Bank of Type Culture Collection of the Chinese Academy of Sciences (Shanghai, China). The RAW264.7 macrophages were cultured in Dulbecco's modified Eagle's medium (DMEM) with 10% fetal bovine serum (FBS; pre-inactivated at 56°C for 30 min), penicillin (100 U/ml), and streptomycin (100 μg/ml) at 37°C under 5% CO_2 and 95% air. The effects of DSELD on LPS-activated RAW264.7 macrophages were evaluated after cells were exposed to (1 μg/ml) LPS for 24 h with or without DSELD (Zhang et al., 2018). DSELD at 50 μg/ml was administered to treatment groups as previously described (Zhong et al., 2020). The cell supernatants were collected and stored at -20°C to measure NO concentration using a commercial ELISA kit.

Measuring Lactate Dehydrogenase, Tumor Necrosis Factor-α, and Interleukin-6 in H9C2 Cell Culture

The H9C2 cells used in this study were obtained from Nanjing Beretti Biological Technology Co., Ltd. (Nanjing, China), and cultured in DMEM with 10% FBS, penicillin (100 U/ml), and streptomycin (100 μg/ml) at 37°C, 5% CO_2 and 95% air. The macrophage-conditioned media (CM) stimulation model was conducted as previously described (Li et al., 2016). To evaluate the effects of DSELD on the CM-stimulated H9C2 cells, the H9C2 cells were incubated with CM and treated with DSELD at 50 μg/ml for 24 h. The cell supernatants were collected for detection of LDH, TNF-α, and IL-6.

Measurement of Cell Viability

MTT assay was used to assess cell viability. The H9C2 cells were seeded onto 96-well plates at a density of 5×10^4/well. Then, 100 μl of MTT (5 mg/ml) was added to each well for 4 h. The optical density (OD) was measured at a wavelength of 580 nm after adding DMSO.

High-Content Screening Assay

H9C2 cell monolayers were incubated with 100 nM TMRM for 45 min at 37°C to monitor the TMRM fluorescence (Branco et al., 2013). Cell monolayers were then fixed with cold 4% paraformaldehyde for 30 min, followed by 1% Triton X-100 treatment for 10 min. After three washes with phosphate buffered saline (PBS), the cells were incubated in a mixture of Alexa Fluor 488 Phalloidin (1:20) and Hoechst (1:1,000) at room temperature for 10 min (Guo et al., 2020). The ImageXpress Micro® Confocal High-Content Imaging System (Molecular Devices, LLC, San Jose, CA, USA) was used to acquire images. The analysis module of the MetaXpress® High-Content Image and Analysis Software (Molecular Devices) was used to analyze the images. The cell cross-sectional area was normalized to the nucleus count.

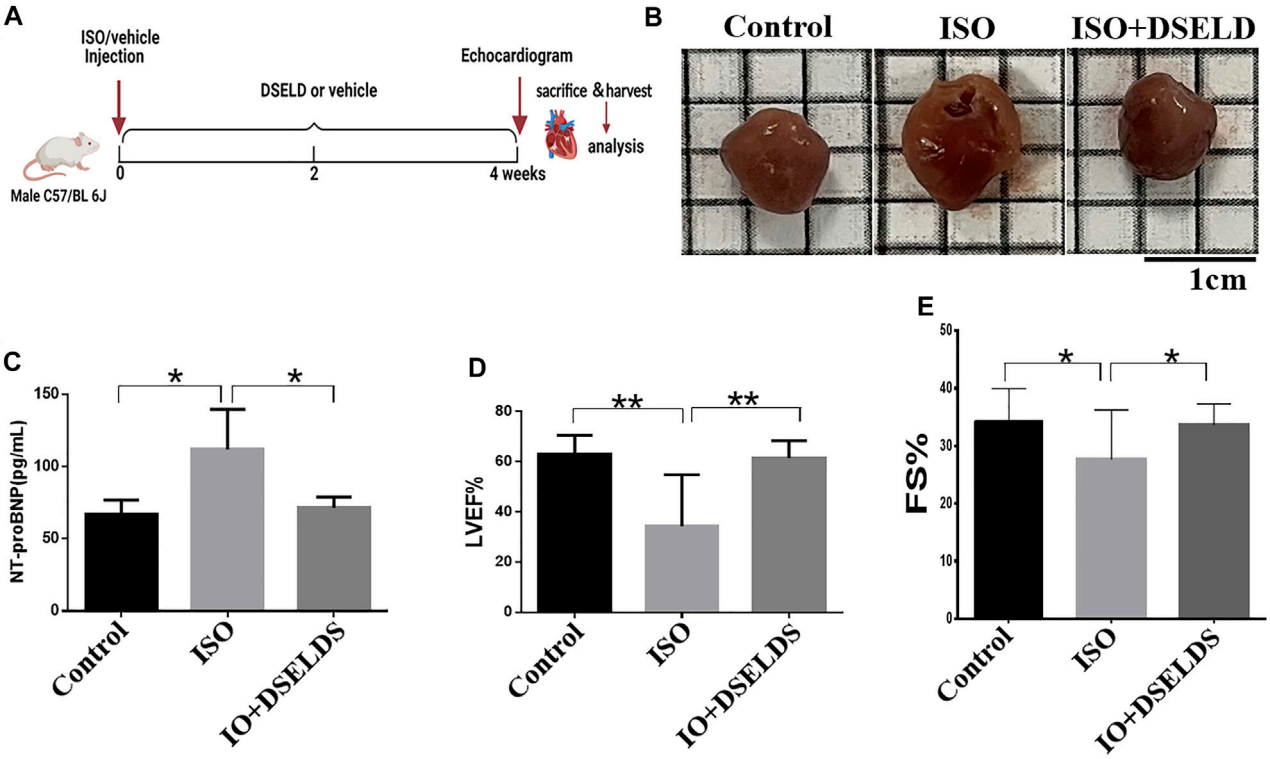

FIGURE 1 | Dangshen Erling decoction (DSELD) improves cardiac function. **(A)** Establishment of heart failure (HF) mouse model. **(B)** The representative images of the heart from the isoproterenol (ISO)-induced HF mice with or without DSELD (1.28 g/kg) treatment. (**C–E**) NT-proBNP, left ventricular ejection fraction (LVEF), and fractional shortening (FS) in the ISO-induced HF mice with or without DSELD (1.28 g/kg) treatment, n = 9–10. *p < 0.05, **p < 0.01.

Western Blot Analysis

Cardiac tissues were lysed using radioimmunoprecipitation assay (RIPA) buffer [50 mM Tris–HCl pH 7.4, 150 mM NaCl, 1% NP-40, and 0.1% sodium dodecyl sulfate (SDS)] containing a protease inhibitor cocktail (Sigma, St. Louis, MO, USA). H9C2 cells were digested by trypsin, and the collected cells were prepared for cell lysis, and proteins were extracted according to the manufacturer's instruction. Western blotting was performed to detect the levels of various proteins in heart tissue or H9C2 cell lysates quantified by BCA assay. A 12% SDS polyacrylamide gel electrophoresis (SDS-PAGE) was used to separate the proteins. Then, the proteins were transferred to polyvinylidene fluoride (PVDF) membrane (Millipore, Burlington, MA, USA). After blocking with 10% skim milk, the membranes were incubated with primary antibodies (TLR4 1:1,000; NF-κB 1:1,000; α-tubulin 1:1,000; β-actin 1:1,000; MMP9 1:1,000; MyD88 1:1,000) at 4°C overnight. After incubation with the appropriate secondary antibodies at room temperature for 1 h, signals were visualized using the enhanced chemiluminescence (ECL) Plus Western blotting detection reagents (Bio-Rad) for 1 min at room temperature. The bands in the membrane were visualized, and densitometric analysis of band intensity was performed using the ChemiDoc Touch Imaging System and Image Lab software (Bio-Rad, Hercules, CA, USA).

Statistical Analysis

The continuous variables were shown as mean ± SD. Statistical analyses were performed using one-way analysis (ANOVA) of variance. Tukey's and Dunnett's tests were applied for multiple comparisons between groups. GraphPad Prism seven software (GraphPad Software, San Diego, CA, USA) was used to carry out the statistical analysis. $p < 0.05$ was considered statistically significant.

RESULTS

Dangshen Erling Decoction Attenuated Cardiac Hypertrophy in the Mouse Model of Heart Failure

To evaluate the effects of DSELD on cardiac hypertrophy, DSELD was intragastrically administered at a dose of 1.28 g/kg in the ISO-induced mouse model for 4 weeks (**Figure 1A**). The ISO-treated mice showed enlarged hearts compared to the control mice (**Figure 1B**). Moreover, the NT-proBNP, an important indicator of HF, was significantly upregulated compared with the control group (**Figure 1C**). Echocardiography revealed that left ventricular ejection fraction (LVEF) and fractional shortening (FS) decreased in the ISO group (**Figures 1D, E**), indicating that heart functions were severely damaged in this group. After

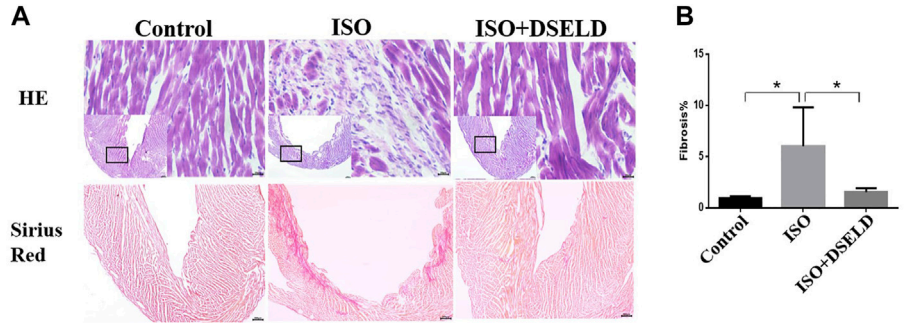

FIGURE 2 | Dangshen Erling decoction (DSELD) attenuates ventricular remodeling. **(A)** Typical histological images of the mouse cardiac tissue from the different groups were stained with H&E (×400) and Sirius Red (×40). **(B)** Quantification of cardiac fibrosis in the different groups of mice, n = 4. *p < 0.05, **p < 0.01.

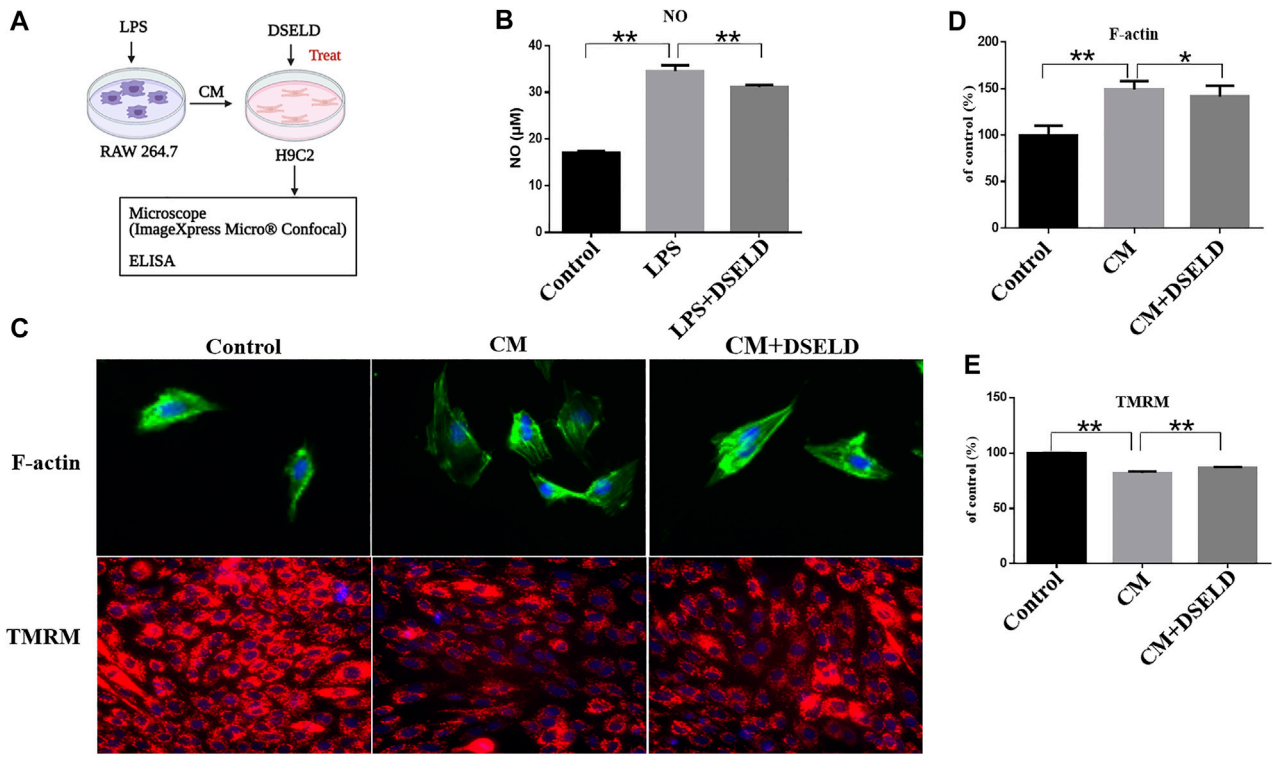

FIGURE 3 | Dangshen Erling decoction (DSELD) protects from myocardial hypertrophy and mitochondrial permeability transition pore (mPTP) in the conditioned media (CM)-induced inflammation in H9C2 cells. **(A)** The operation mode diagram of the RAW264.7 and H9C2 cells. **(B)** RAW264.7 cells were incubated with lipopolysaccharide (LPS; 1 μg/ml) with or without DSELD (50 μg/ml) for 24 h, and nitric oxide (NO) secretion was detected in cell supernatant by ELISA. **(C)** Representative fluorescent images of cardiomyocytes from the different groups [green: phalloidin, red: tetramethyl rhodamine methyl ester (TMRM), and blue: DAPI]. **(D)** The relative area was corrected by the nucleus and normalized to control (F-actin, ×400). **(E)** The fluorescence intensity to control (TMRM, ×200). *p < 0.05, **p < 0.01.

DSELD administration for 4 weeks, the size of the enlarged heart decreased, and the NT-proBNP, EF, and FS of the treated group were significantly restored. These investigations showed that DSELD exhibited cardioprotective properties in HF and almost completely recovered heart function.

Cardiac tissue morphology by H&E and Sirius Red staining was examined using microscopy. The structures of the left ventricle in the ISO-treated group showed large necrotic areas obvious by H&E staining (**Figure 2A**). Furthermore, the adjacent cardiomyocytes were arranged randomly. Sirius Red staining revealed that the total cardiac fibrosis area in the ISO-induced group was enlarged by approximately 5-fold compared to that of the control group (**Figure 2B**). However, DSELD treatment significantly suppressed the pathological changes including

myocardial remodeling and fibrosis caused by ISO. These results proved that DSELD could prevent the ISO-induced damages of the cardiac structure and the proliferation of collagen fibers.

Dangshen Erling Decoction Alleviated the Conditioned Media-Induced Myocardial Hypertrophy in H9C2 Cells

To further investigate the effect of DSELD in ameliorating myocardial hypertrophy, we next established the myocardial hypertrophy model of macrophage-CM-stimulated H9C2 cells (Li et al., 2016; Zhang et al., 2018) (**Figure 3A**). The RAW264.7 macrophage cells were stimulated with 1 μg/ml LPS. After LPS stimulation, RAW264.7 macrophages secreted nearly twice the amount of NO as that of the control DMEM-treated cells (**Figure 3B**), affirming that LPS stimulation of RAW264.7 macrophages was effective. DSELD treatment reduced NO levels, thus inhibiting the effect of LPS stimulation on RAW264.7 macrophages. Then, the supernatants were obtained from the RAW264.7 cells after LPS stimulation for 24 h to imitate the inflammatory environment, as performed for H9C2 cells stimulated by CM (Zhang et al., 2018). The antihypertrophy effects of DSELD (50 μg/ml) on cardiac cells were investigated while establishing the CM-induced myocardial hypertrophy model.

High-Content Imaging System assay was used to evaluate the beneficial effect of DSELD on myocardial hypertrophy and mitochondrial permeability transition pore (mPTP) in the CM-stimulated myocardial hypertrophy model. Evaluation was done with or without DSELD (50 μg/ml) treatment. As shown in **Figures 3C and D**, the average of cardiomyocyte cross-sectional area after CM stimulation significantly enlarged by approximately 50% in comparison to that of the control group. This result showed the successful establishment of the CM-stimulated hypertrophic cardiomyocyte model. However, DSELD treatment reduced the size of CM-induced cardiomyocytes, suggesting the critical role of DSELD in protecting against CM-induced myocardial hypertrophy. Moreover, CM-induced cardiomyocytes exhibited an inferior TMRM fluorescence ability that inversely correlated to the opening of mPTP. Additionally, DSELD significantly potentiated TMRM fluorescence ability in the CM-stimulated H9C2 cell model, demonstrating a decrease in mPTP opening that protected against CM-induced damages in the mitochondrial membrane permeability (**Figures 3C, E**). These results indicate that CM-induced inflammation promotes myocardial hypertrophy as well as the opening of the mPTP, while DSELD alleviates myocardial hypertrophy and restores the mPTP damage in the CM-stimulated H9C2 cells.

Dangshen Erling Decoction Alleviates Myocardial Injury Induced by Conditioned Media

To confirm the antihypertrophy effect of DSELD on inflamed cardiomyocytes, inflammatory markers were evaluated in hypertrophied H9C2 cells. The results show that CM aggravated H9C2 cell death, while DSELD treatment protected cell viability **(Figure 4A)**. The levels of inflammatory markers including LDH, TNF-α, and IL-6 were significantly elevated after CM induction but were suppressed by DSELD treatment (**Figures 4B–D)**. Consistently, the myocardial injury induced by CM was obvious. This damage was related to the inflammatory microenvironment of cardiomyocytes that could be rescued by DSELD treatment.

Dangshen Erling Decoction Downregulates the Multiple Inflammatory Cytokines in the Mouse Model of Cardiac Failure

To further confirm the anti-inflammatory effect of DSELD *in vivo*, multiple inflammatory cytokines were evaluated in the cardiac tissue (**Figure 5A**). The data show that granulocyte-macrophage CSF (GM-CSF), granulocyte CSF (G-CSF), IL-1α, IL-1β, IL-3, IL-5, IL-7, IL-12, IL-13, and TNF-α decreased significantly in the treated group vs. the ISO group **(Figures 5B–N)**. However, some other inflammatory cytokines such as IL-2, IL-9, and interferon (INF)-γ were elevated in DSELD group vs. the ISO group. Notably, increased levels of some cytokines such as IL-1α, IL-1β, and TNF-α have been reported previously in HF compared with controls and were suggested as markers of inflammatory progression in HF (Vistnes et al., 2010). The results of this study indicate that DSELD exhibits an inhibitory effect on multiple inflammatory cytokines in the myocardial tissue.

Dangshen Erling Decoction Alleviates Myocardial Hypertrophy by Inhibiting the Toll-Like Receptor 4 Signaling Pathway

Previous studies suggest that TLR4 signaling pathway plays a critical role in the release of inflammatory cytokines (Zhang et al., 2020a). Therefore, we hypothesized that DSELD protects the cardiomyocytes from inflammation by inhibiting the TLR4 signaling pathway. To verify this notion, further investigation into the changes of key molecules in this signaling pathway with or without DSELD treatment was done, and the expressions of the TLR4, MyD88, and MMP9 in the cardiac tissue were detected (Wang et al., 2016; Wang et al., 2019). Western blot analysis revealed an increase in the protein levels of TLR4, MMP9, MyD88, and NF-κB in the ISO-induced group (**Figure 6**). However, DSELD treatment significantly inhibited the levels of these proteins, indicating that DSELD regulates inflammation by inhibiting the TLR4 signaling pathway.

In situ immunofluorescence evaluation revealed similar results (**Figure 7**). The fluorescence of MMP9, MyD88, and NF-κB in the heart was significantly potentiated, demonstrating the upregulated expressions of these proteins in the ISO-induced myocardial tissue compared to the control group. Furthermore, the fluorescence intensity decreased significantly after DSELD treatment. It also proved that DSELD suppresses the inflammatory process in myocardial hypertrophy by regulating the expressions of these key proteins in the TLR4 signaling

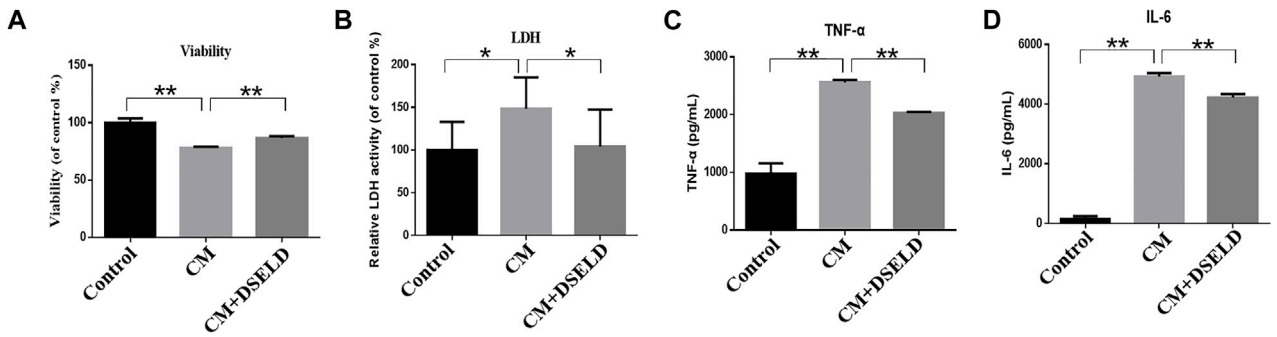

FIGURE 4 | Dangshen Erling decoction (DSELD) inhibits conditioned media (CM)-induced inflammation in the H9C2 cells. **(A)** H9C2 cell viability was evaluated by MTT assay 24 h after incubation with CM. **(B–D)** The elevation of lactate dehydrogenase (LDH), tumor necrosis factor (TNF)-α, and interleukin (IL)-6 from different groups. *p < 0.05, **p < 0.01.

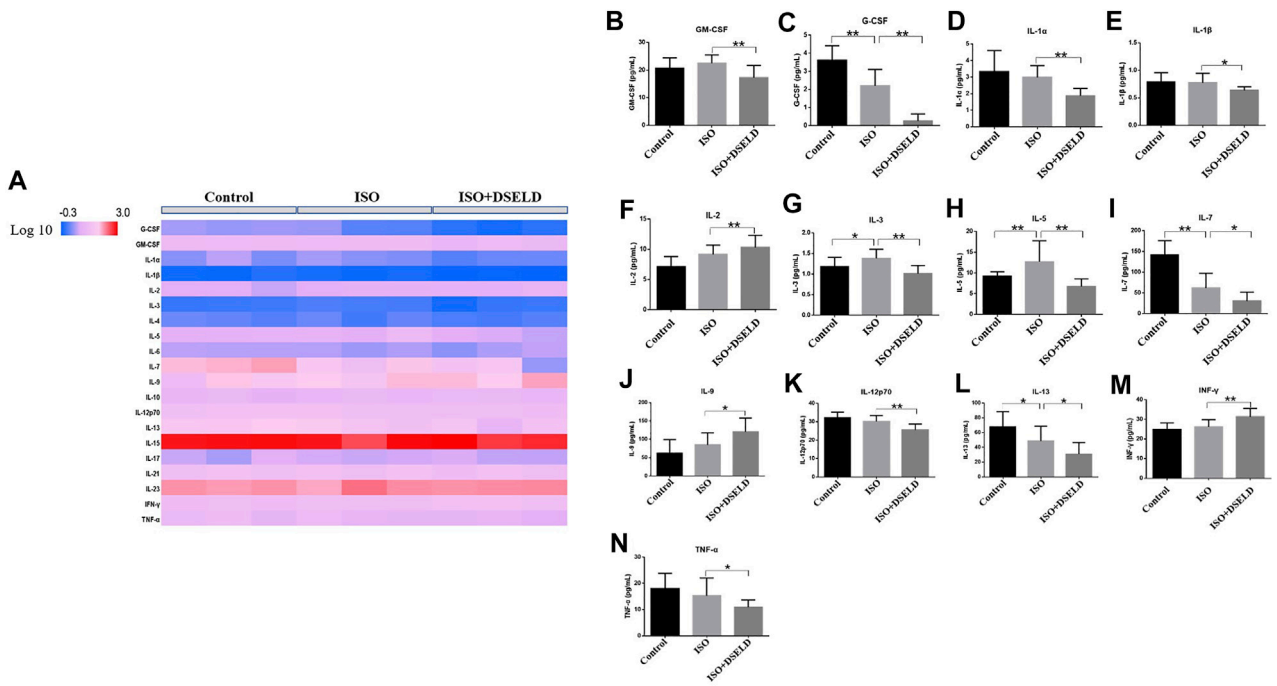

FIGURE 5 | Multiple inflammatory cytokines in heart failure (HF). **(A)** Cytokine profiling of heart samples obtained from the different treatment groups. **(B–N)** Cytokine concentrations in heart samples from different treatment groups of mice, n = 4. *p < 0.05, **p < 0.01.

pathway. Taken together, the results indicate that DSELD alleviates myocardial hypertrophy by inhibiting the expressions of TLR4 signaling pathway-associated proteins.

DISCUSSION

Our previous study shows that the chemical composition of DSELD has anti-inflammatory properties and evaluates its cardioprotective effects and antiapoptotic potentials in H9C2 cells (Zhong et al., 2020). In this work, comprehensive *in vitro* and *in vivo* experiments are conducted to investigate the mechanisms by which DSELD exerts its antihypertrophic properties. The main findings of this study are as follows: 1) DSELD protects H9C2 cells from CM-induced injuries; 2) DSELD restores the cardiac functions and reverses the pathological damages in a mouse model of myocardial hypertrophy; 3) DSELD modulates the levels of multiple inflammatory cytokines; 4) DSELD inhibits inflammation by downregulating the expression of inflammatory proteins such as MyD88 and MMP9, key components of the TLR4 signaling pathway.

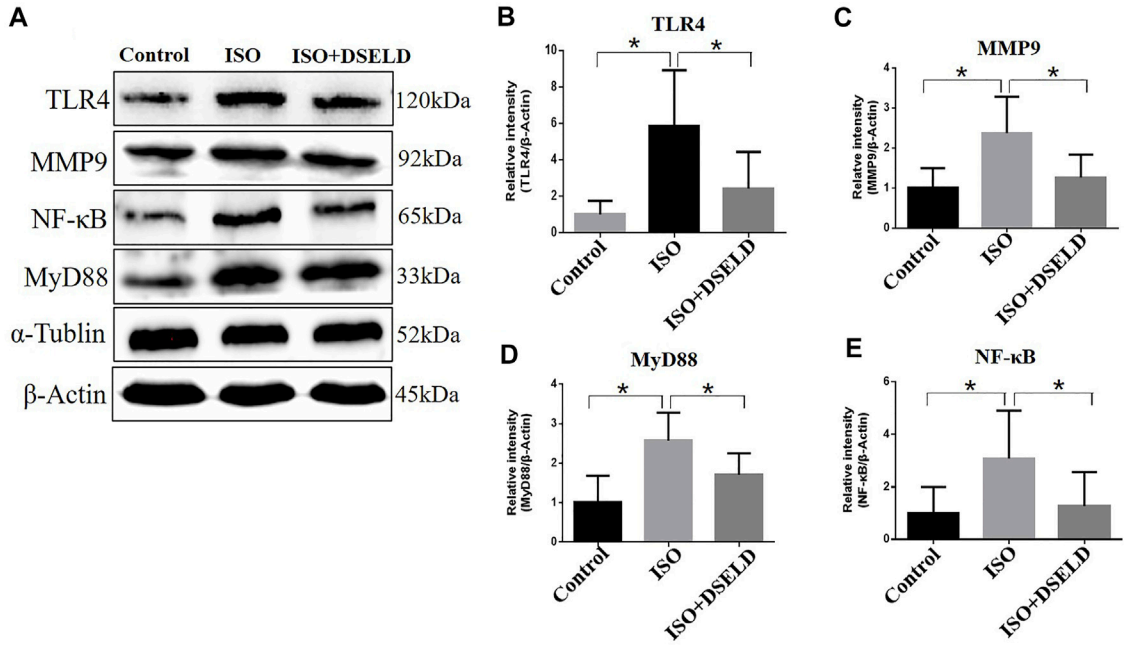

FIGURE 6 | Dangshen Erling decoction (DSELD) inhibits the expressions of Toll-like receptor (TLR)4 signaling pathway proteins. **(A)** Western blot of TLR4, matrix metalloproteinase (MMP)9, nuclear factor (NF)-κB, and myeloid differentiation factor (MyD)88 proteins and **(B–E)** relative expression in the heart samples normalized to control. n = 4. *p < 0.05, **p < 0.01.

Cardiac hypertrophy in the adult heart is manifested as an increase in the size instead of the number of cardiomyocytes obviously because the cardiomyocytes cannot proliferate after birth (Nakamura and Sadoshima, 2018). In our work, the macrophage-CM stimulation was used to establish a successful *in vitro* cardiac hypertrophy model. The cross-sectional area of cardiomyocytes enlarged after LPS-triggered CM stimulation (**Figures 3C, D**). The results also show that CM stimulation elevates the levels of LDH, TNF-α, and IL-6. Infiltration of these inflammatory mediators results in myocardial hypertrophy and fibrosis followed by progression into ventricular remodeling (Ismahil et al., 2014; Shimizu and Minamino, 2016; Bacmeister et al., 2019).

In addition, this study demonstrates that CM stimulation affects the opening of mPTP detected by TMRM staining (**Figures 3C, E**). The weak fluorescence intensity indicates prolonged opening of mPTP. Prolonged mPTP opening leads to mitochondrial energy metabolism disorder, destruction of organelle structure, and typical necrotic cell death, which finally leads to cardiac dysfunction (Kwong and Molkentin, 2015). In our study, the weakest fluorescence intensity of the TMRM was observed in the CM-induced H9C2 cell model, indicating that mPTP is also damaged by inflammation after CM treatment.

Many recent studies suggest that inflammation plays an essential role in promoting HF, and the progression of pathological cardiac remodeling is dependent partly on autoimmune injuries of the heart (Burchfield et al., 2013; Ismahil et al., 2014; Adamo et al., 2020). In this study, ISO-induced myocardial hypertrophy mouse model was used as an *in vivo* model to evaluate DSELD cardioprotective potentials. In addition to monitoring NT-proBNP, EF, FS, and heart structure, multiple cytokine assays were performed on cardiac tissue instead of serum to evaluate the levels of multiple inflammatory cytokines. The results of these assays indicate that multiple inflammatory cytokines such as GM-CSF, G-CSF, IL-1α, IL-1β, IL-3, IL-5, IL-7, IL-12, IL-13, and TNF-α were significantly decreased in the DSELD group vs. the ISO group (**Figure 5**). It has been reported that these cytokines are associated with the activation of $CD4^+$ T cells, which play a pro-inflammatory role during chronic inflammation of HF (Quast et al., 2017). Interestingly, among these inflammatory cytokines, the levels of the G-CSF, IL-7, and IL-13 decreased following ISO treatment. The activation of $CD4^+$ T cells in the myocardial inflammatory microenvironment may lead not only to an increase of chronic inflammatory cytokines but also to an increase of other anti-inflammatory cytokines like IL-17A, which potentially counteracts the pro-inflammatory cytokines, such as G-CSF (Dick and Epelman, 2016). This regulation may be closely related to the timing of cardiac inflammation. For example, the expression level of G-CSF increases rapidly after myocardial ischemia–reperfusion injury (acute inflammation), peaks at day 1, and decreases thereafter (Fan et al., 2019). As inflammation becomes chronic, IL-17A starts to gradually increase to further reduce the G-CSF and suppress myocardial inflammation. IL-7 is not only an inflammatory cytokine but also a hematopoietic growth factor secreted by bone marrow stromal cells whose expression is regulated by the hematopoietic ability of bone marrow (Nguyen et al., 2017). Bone marrow dysfunction is a poor complication of HF leading to the deficiency of hematopoietic growth factor including IL-7 (Westenbrink et al., 2010; Ruifrok et al., 2011). In our study, ISO-induced HF may be associated with the decreased IL-7 levels.

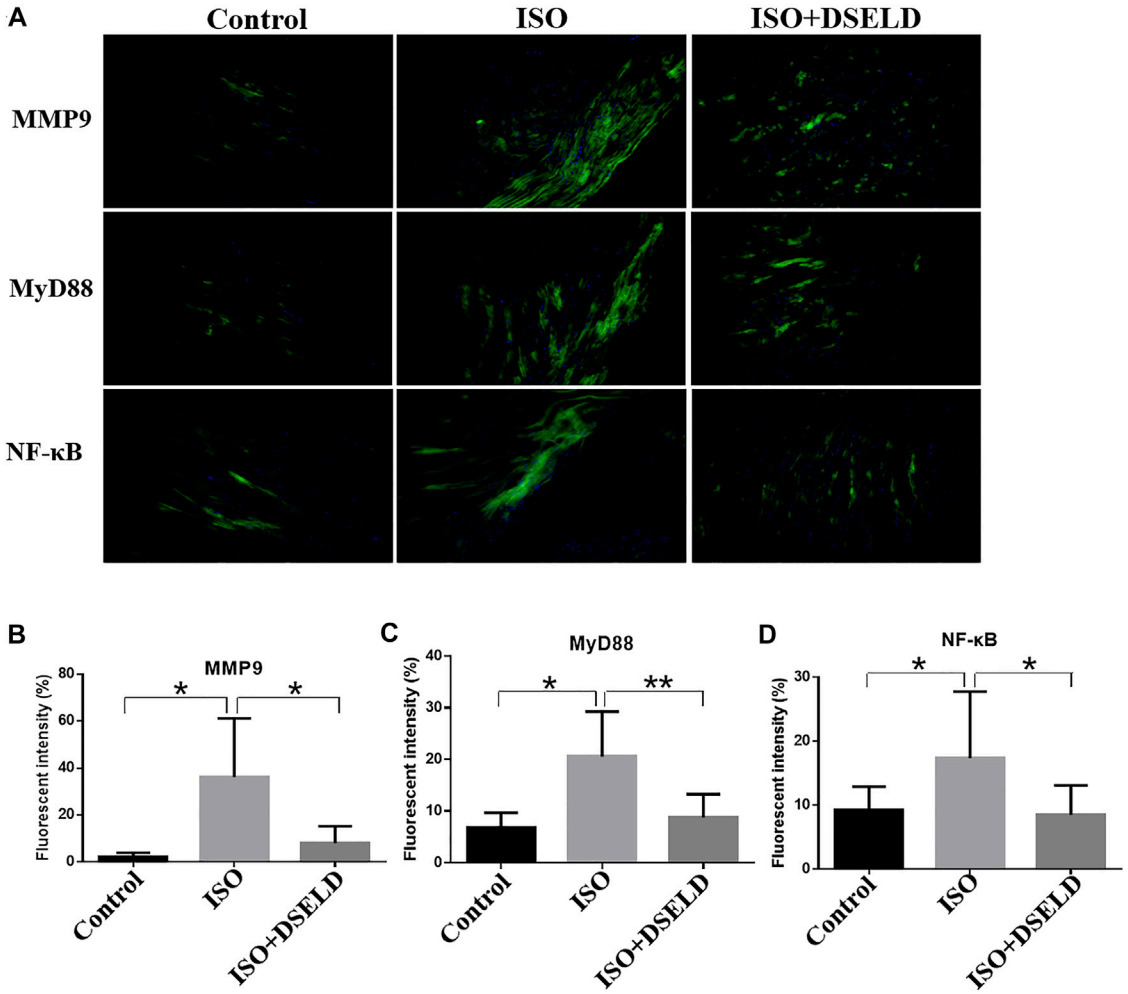

FIGURE 7 | Dangshen Erling decoction (DSELD) attenuates cardiac inflammation by inhibiting the expression of members in the Toll-like receptor (TLR)4 signaling pathway in the cardiac tissue. **(A)** Representative immunofluorescence images of the heart samples from different treatment groups [green: matrix metalloproteinase (MMP)9, myeloid differentiation factor (MyD)88, and nuclear factor (NF)-κB proteins; blue: DAPI, ×200]. **(B–D)** Quantification of the relative fluorescence intensity from different groups of mice, n = 4. *p < 0.05, **p < 0.01.

Meanwhile, insufficient IL-7 may lead to the dysfunction of innate lymphocyte cell, which collectively lead to impair the cytokines it secretes such as IL-13 (Soong et al., 2014). Furthermore, multiple $CD4^+$ T cell-associated cytokines were analyzed as dynamic profiles at different stages of HF development (Wang et al., 2018; Yuan et al., 2019). Moreover, studies have shown that the activation of $CD4^+$ T cells after trauma was TLR4-dependent (Bock et al., 2018). Therefore, we hypothesized that the regulation of these cytokines is associated with the TLR4 signaling pathway (Shi et al., 2006; Gitlin et al., 2020). We further verified the expression of TLR4 signaling pathway molecules with or without DSELD in the myocardial hypertrophy model. The *in vivo* study results show that DSELD not only promoted heart functions and decreased the levels of multiple cytokines but also inhibited the expression of TLR4 pathway-associated proteins.

The TLR4 signal pathway plays an essential role in inflammation (Andersson and Tracey, 2011). TLR4 is the first mammalian Toll protein in the TLR family to be characterized. It is expressed in immune-related cells, including monocytes, macrophages, dendritic cells, as well as adipocytes, enterocytes, and muscle cells to control the inflammatory and immunological responses (Kuzmich et al., 2017). Under stimulation by inflammation-causing substances like LPS, TLR4 induces the production of multiple cytokines including TNF-α and IL-1β, which, in turn, work as endogenous inflammatory inducers by interacting with receptors on target cells (Lancaster et al., 2018; Rogero and Calder, 2018). Several studies revealed that TLR4 is a pivotal modulator of myocardial inflammation, and the high expression of TLR4 is a risk factor for HF (Frantz et al., 1999; Földes et al., 2008; Liu et al., 2015; Rogero and Calder, 2018).

The mechanism by which TLR4 influences myocardial hypertrophy mainly involves the MyD88-dependent pathway and MMP9-dependent pathway (Yang et al., 2016). The MyD88-dependent pathway is initiated after TLR4 activation, thus inducing many transcription factors such as NF-κB. The activation of NF-κB contributes to the expression of inflammatory cytokines like IL-6 and TNF-α (Xu et al., 2020). Supportively, our

results demonstrated the high expression of MyD88, NF-κB, and MMP9 in mice with myocardial hypertrophy. Importantly, DSELD treatment significantly downregulates the expressions of MyD88, NF-κB, and MMP9, revealing that the antihypertrophic effects of the drug may work through suppressing the activated TLR4 pathway.

CONCLUSION

In summary, our study demonstrates that DSELD could protect against myocardial hypertrophy by inhibiting myocardial inflammation. The antihypertrophic mechanism of DSELD might be mediated by the suppression of the TLR4 signaling pathway. But further study is needed to determine which compound in the formula is the major active component. Our findings provide new insight to further understand the pharmacological mechanism of DSELD and bring new therapeutic candidates in the management of HF.

DATA AVAILABILITY STATEMENT

The original contributions presented in the study are included in the article/**Supplementary Material**. Further inquiries can be directed to the corresponding authors.

ETHICS STATEMENT

This animal study was approved by the Animal Care Committee of Zhejiang Chinese Medical University.

AUTHOR CONTRIBUTIONS

YZ, LYC, and ML conducted the experiments and wrote the article. LC, YQ, and CC were involved in parts of the experiments. YZ, LYC, and YX revised the article. YX and YZ conceived the hypothesis, designed the experiments, and reviewed the article. YW helped in guiding the revision. All authors reviewed and approved the final article.

FUNDING

This research was funded by the Zhejiang Traditional Chinese Medicine Science and Technology Plan 363 (No. 2019ZQ038) and Hangzhou Medical and Health Technology Project (No. Z20200135).

ACKNOWLEDGMENTS

The authors are grateful for the support from Pharmaceutical Informatics Institute, College of Pharmaceutical Sciences, Zhejiang University.

SUPPLEMENTARY MATERIAL

The Supplementary Material for this article can be found online at: https://www.frontiersin.org/articles/10.3389/fphar.2021.725186/full#supplementary-material

REFERENCES

Adamo, L., Rocha-Resende, C., Prabhu, S. D., and Mann, D. L. (2020). Reappraising the Role of Inflammation in Heart Failure. *Nat. Rev. Cardiol.* 17, 269–285. doi:10.1038/s41569-019-0315-x

Andersson, U., and Tracey, K. J. (2011). HMGB1 Is a Therapeutic Target for Sterile Inflammation and Infection. *Annu. Rev. Immunol.* 29, 139–162. doi:10.1146/annurev-immunol-030409-101323

Bacmeister, L., Schwarzl, M., Warnke, S., Stoffers, B., Blankenberg, S., Westermann, D., et al. (2019). Inflammation and Fibrosis in Murine Models of Heart Failure. *Basic Res. Cardiol.* 114, 19. doi:10.1007/s00395-019-0722-5

Bock, M., Bergmann, C. B., Jung, S., Kalbitz, M., Relja, B., Huber-Wagner, S., et al. (2018). The Posttraumatic Activation of CD4+ T Regulatory Cells Is Modulated by TNFR2- and TLR4-dependent Pathways, but Not by IL-10. *Cell Immunol* 331, 137–145. doi:10.1016/j.cellimm.2018.06.009

Branco, A. F., Sampaio, S. F., Wieckowski, M. R., Sardão, V. A., and Oliveira, P. J. (2013). Mitochondrial Disruption Occurs Downstream from β-adrenergic Overactivation by Isoproterenol in Differentiated, but Not Undifferentiated H9c2 Cardiomyoblasts: Differential Activation of Stress and Survival Pathways. *Int. J. Biochem. Cel Biol* 45, 2379–2391. doi:10.1016/j.biocel.2013.08.006

Burchfield, J. S., Xie, M., and Hill, J. A. (2013). Pathological Ventricular Remodeling: Mechanisms: Part 1 of 2. *Circulation* 128, 388–400. doi:10.1161/CIRCULATIONAHA.113.001878

Dange, R. B., Agarwal, D., Masson, G. S., Vila, J., Wilson, B., Nair, A., et al. (2014). Central Blockade of TLR4 Improves Cardiac Function and Attenuates Myocardial Inflammation in Angiotensin II-Induced Hypertension. *Cardiovasc. Res.* 103, 17–27. doi:10.1093/cvr/cvu067

Deng, K. Q., Zhao, G. N., Wang, Z., Fang, J., Jiang, Z., Gong, J., et al. (2018). Targeting Transmembrane BAX Inhibitor Motif Containing 1 Alleviates Pathological Cardiac Hypertrophy. *Circulation* 137, 1486–1504. doi:10.1161/CIRCULATIONAHA.117.031659

Dick, S. A., and Epelman, S. (2016). Chronic Heart Failure and Inflammation: What Do We Really Know? *Circ. Res.* 119, 159–176. doi:10.1161/CIRCRESAHA.116.308030

Fan, Q., Tao, R., Zhang, H., Xie, H., Lu, L., Wang, T., et al. (2019). Dectin-1 Contributes to Myocardial Ischemia/Reperfusion Injury by Regulating Macrophage Polarization and Neutrophil Infiltration. *Circulation* 139, 663–678. doi:10.1161/CIRCULATIONAHA.118.036044

Földes, G., Von Haehling, S., Okonko, D. O., Jankowska, E. A., Poole-Wilson, P. A., and Anker, S. D. (2008). Fluvastatin Reduces Increased Blood Monocyte Toll-like Receptor 4 Expression in Whole Blood from Patients with Chronic Heart Failure. *Int. J. Cardiol.* 124, 80–85. doi:10.1016/j.ijcard.2006.12.024

Frantz, S., Kobzik, L., Kim, Y. D., Fukazawa, R., Medzhitov, R., Lee, R. T., et al. (1999). Toll4 (TLR4) Expression in Cardiac Myocytes in normal and Failing Myocardium. *J. Clin. Invest.* 104, 271–280. doi:10.1172/JCI6709

Geng, Z., Fan, W. Y., Zhou, B., Ye, C., Tong, Y., Zhou, Y. B., et al. (2019). FNDC5 Attenuates Obesity-Induced Cardiac Hypertrophy by Inactivating JAK2/STAT3-Associated Inflammation and Oxidative Stress. *J. Transl Med.* 17, 107. doi:10.1186/s12967-019-1857-8

Gitlin, A. D., Heger, K., Schubert, A. F., Reja, R., Yan, D., Pham, V. C., et al. (2020). Integration of Innate Immune Signalling by Caspase-8 Cleavage of N4BP1. *Nature* 587, 275–280. doi:10.1038/s41586-020-2796-5

Guo, R., Liu, N., Liu, H., Zhang, J., Zhang, H., Wang, Y., et al. (2020). High Content Screening Identifies Licoisoflavone A as a Bioactive Compound of Tongmaiyangxin Pills to Restrain Cardiomyocyte Hypertrophy via Activating Sirt3. *Phytomedicine* 68, 153171. doi:10.1016/j.phymed.2020.153171

Hao, P., Jiang, F., Cheng, J., Ma, L., Zhang, Y., and Zhao, Y. (2017). Traditional Chinese Medicine for Cardiovascular Disease: Evidence and Potential

Mechanisms. *J. Am. Coll. Cardiol.* 69, 2952–2966. doi:10.1016/s0415-6412(17)30083-8

Ismahil, M. A., Hamid, T., Bansal, S. S., Patel, B., Kingery, J. R., and Prabhu, S. D. (2014). Remodeling of the Mononuclear Phagocyte Network Underlies Chronic Inflammation and Disease Progression in Heart Failure: Critical Importance of the Cardiosplenic axis. *Circ. Res.* 114, 266–282. doi:10.1161/CIRCRESAHA.113.301720

Jia, Q., Wang, L., Zhang, X., Ding, Y., Li, H., Yang, Y., et al. (2020). Prevention and Treatment of Chronic Heart Failure through Traditional Chinese Medicine: Role of the Gut Microbiota. *Pharmacol. Res.* 151, 104552. doi:10.1016/j.phrs.2019.104552

Kuzmich, N., Sivak, K., Chubarev, V., Porozov, Y., Savateeva-Lyubimova, T., and Peri, F. (2017). TLR4 Signaling Pathway Modulators as Potential Therapeutics in Inflammation and Sepsis. *Vaccines (Basel)* 5, 34. doi:10.3390/vaccines5040034

Kwong, J. Q., and Molkentin, J. D. (2015). Physiological and Pathological Roles of the Mitochondrial Permeability Transition Pore in the Heart. *Cell Metab* 21, 206–214. doi:10.1016/j.cmet.2014.12.001

Lancaster, G. I., Langley, K. G., Berglund, N. A., Kammoun, H. L., Reibe, S., Estevez, E., et al. (2018). Evidence that TLR4 Is Not a Receptor for Saturated Fatty Acids but Mediates Lipid-Induced Inflammation by Reprogramming Macrophage Metabolism. *Cel Metab* 27, 1096–1110.e5. doi:10.1016/j.cmet.2018.03.014

Li, C., Wang, J., Wang, Q., Zhang, Y., Zhang, N., Lu, L., et al. (2016). Qishen Granules Inhibit Myocardial Inflammation Injury through Regulating Arachidonic Acid Metabolism. *Sci. Rep.* 6, 36949. doi:10.1038/srep36949

Li, X., Zhang, J., Huang, J., Ma, A., Yang, J., Li, W., et al. (2013). A Multicenter, Randomized, Double-Blind, Parallel-Group, Placebo-Controlled Study of the Effects of Qili Qiangxin Capsules in Patients with Chronic Heart Failure. *J. Am. Coll. Cardiol.* 62, 1065–1072. doi:10.1016/j.jacc.2013.05.035

Liu, H., Chen, X., Zhao, X., Zhao, B., Qian, K., Shi, Y., et al. (2018). Screening and Identification of Cardioprotective Compounds from Wenxin Keli by Activity Index Approach and *In Vivo* Zebrafish Model. *Front. Pharmacol.* 9, 1288. doi:10.3389/fphar.2018.01288

Liu, L., Wang, Y., Cao, Z. Y., Wang, M. M., Liu, X. M., Gao, T., et al. (2015). Up-regulated TLR4 in Cardiomyocytes Exacerbates Heart Failure after Long-Term Myocardial Infarction. *J. Cel Mol Med* 19, 2728–2740. doi:10.1111/jcmm.12659

Lu, X., He, Y., Tang, C., Wang, X., Que, L., Zhu, G., et al. (2020). Triad3A Attenuates Pathological Cardiac Hypertrophy Involving the Augmentation of Ubiquitination-Mediated Degradation of TLR4 and TLR9. *Basic Res. Cardiol.* 115, 19. doi:10.1007/s00395-020-0779-1

Martini, E., Kunderfranco, P., Peano, C., Carullo, P., Cremonesi, M., Schorn, T., et al. (2019). Single-Cell Sequencing of Mouse Heart Immune Infiltrate in Pressure Overload-Driven Heart Failure Reveals Extent of Immune Activation. *Circulation* 140, 2089–2107. doi:10.1161/CIRCULATIONAHA.119.041694

Nakamura, M., and Sadoshima, J. (2018). Mechanisms of Physiological and Pathological Cardiac Hypertrophy. *Nat. Rev. Cardiol.* 15, 387–407. doi:10.1038/s41569-018-0007-y

Nguyen, V., Mendelsohn, A., and Larrick, J. W. (2017). Interleukin-7 and Immunosenescence. *J. Immunol. Res.* 2017, 4807853. doi:10.1155/2017/4807853

Oka, T., Akazawa, H., Naito, A. T., and Komuro, I. (2014). Angiogenesis and Cardiac Hypertrophy: Maintenance of Cardiac Function and Causative Roles in Heart Failure. *Circ. Res.* 114, 565–571. doi:10.1161/CIRCRESAHA.114.300507

Paul-Clark, M. J., George, P. M., Gatheral, T., Parzych, K., Wright, W. R., Crawford, D., et al. (2012). Pharmacology and Therapeutic Potential of Pattern Recognition Receptors. *Pharmacol. Ther.* 135, 200–215. doi:10.1016/j.pharmthera.2012.05.007

Quast, C., Alter, C., Ding, Z., Borg, N., and Schrader, J. (2017). Adenosine Formed by CD73 on T Cells Inhibits Cardiac Inflammation and Fibrosis and Preserves Contractile Function in Transverse Aortic Constriction-Induced Heart Failure. *Circ. Heart Fail.* 10, e003346. doi:10.1161/CIRCHEARTFAILURE.116.003346

Rogero, M. M., and Calder, P. C. (2018). Obesity, Inflammation, Toll-like Receptor 4 and Fatty Acids. *Nutrients* 10, 432. doi:10.3390/nu10040432

Ruifrok, W. P., Qian, C., Silljé, H. H., Van Goor, H., Van Veldhuisen, D. J., Van Gilst, W. H., et al. (2011). Heart Failure-Associated Anemia: Bone Marrow Dysfunction and Response to Erythropoietin. *J. Mol. Med. (Berl)* 89, 377–387. doi:10.1007/s00109-010-0710-6

Shi, H., Kokoeva, M. V., Inouye, K., Tzameli, I., Yin, H., and Flier, J. S. (2006). TLR4 Links Innate Immunity and Fatty Acid-Induced Insulin Resistance. *J. Clin. Invest.* 116, 3015–3025. doi:10.1172/JCI28898

Shimizu, I., and Minamino, T. (2016). Physiological and Pathological Cardiac Hypertrophy. *J. Mol. Cel Cardiol* 97, 245–262. doi:10.1016/j.yjmcc.2016.06.001

Singh, M. V., Cicha, M. Z., Nunez, S., Meyerholz, D. K., Chapleau, M. W., and Abboud, F. M. (2019). Angiotensin II-Induced Hypertension and Cardiac Hypertrophy Are Differentially Mediated by TLR3- and TLR4-dependent Pathways. *Am. J. Physiol. Heart Circ. Physiol.* 316, H1027–H1038. doi:10.1152/ajpheart.00697.2018

Soong, L., Wang, H., Shelite, T. R., Liang, Y., Mendell, N. L., Sun, J., et al. (2014). Strong Type 1, but Impaired Type 2, Immune Responses Contribute to Orientia Tsutsugamushi-Induced Pathology in Mice. *Plos Negl. Trop. Dis.* 8, e3191. doi:10.1371/journal.pntd.0003191

Tham, Y. K., Bernardo, B. C., Ooi, J. Y., Weeks, K. L., and Mcmullen, J. R. (2015). Pathophysiology of Cardiac Hypertrophy and Heart Failure: Signaling Pathways and Novel Therapeutic Targets. *Arch. Toxicol.* 89, 1401–1438. doi:10.1007/s00204-015-1477-x

Vistnes, M., Christensen, G., and Omland, T. (2010). Multiple Cytokine Biomarkers in Heart Failure. *Expert Rev. Mol. Diagn.* 10, 147–157. doi:10.1586/erm.10.3

Wang, X., Guo, Z., Ding, Z., and Mehta, J. L. (2018). Inflammation, Autophagy, and Apoptosis after Myocardial Infarction. *J. Am. Heart Assoc.* 7, e008024. doi:10.1161/JAHA.117.008024

Wang, Y., Liu, J., Kong, Q., Cheng, H., Tu, F., Yu, P., et al. (2019). Cardiomyocyte-specific Deficiency of HSPB1 Worsens Cardiac Dysfunction by Activating NFκB-Mediated Leucocyte Recruitment after Myocardial Infarction. *Cardiovasc. Res.* 115, 154–167. doi:10.1093/cvr/cvy163

Wang, Y. H., Chen, K. M., Chiu, P. S., Lai, S. C., Su, H. H., Jan, M. S., et al. (2016). Lumbrokinase Attenuates Myocardial Ischemia-Reperfusion Injury by Inhibiting TLR4 Signaling. *J. Mol. Cel Cardiol* 99, 113–122. doi:10.1016/j.yjmcc.2016.08.004

Westenbrink, B. D., Voors, A. A., De Boer, R. A., Schuringa, J. J., Klinkenberg, T., Van Der Harst, P., et al. (2010). Bone Marrow Dysfunction in Chronic Heart Failure Patients. *Eur. J. Heart Fail.* 12, 676–684. doi:10.1093/eurjhf/hfq061

Xu, G. R., Zhang, C., Yang, H. X., Sun, J. H., Zhang, Y., Yao, T. T., et al. (2020). Modified Citrus Pectin Ameliorates Myocardial Fibrosis and Inflammation via Suppressing Galectin-3 and TLR4/MyD88/NF-Kb Signaling Pathway. *Biomed. Pharmacother.* 126, 110071. doi:10.1016/j.biopha.2020.110071

Yang, Y., Lv, J., Jiang, S., Ma, Z., Wang, D., Hu, W., et al. (2016). The Emerging Role of Toll-like Receptor 4 in Myocardial Inflammation. *Cell Death Dis* 7, e2234. doi:10.1038/cddis.2016.140

Yuan, D., Tie, J., Xu, Z., Liu, G., Ge, X., Wang, Z., et al. (2019). Dynamic Profile of CD4+ T-Cell-Associated Cytokines/Chemokines Following Murine Myocardial Infarction/Reperfusion. *Mediators Inflamm.* 2019, 9483647. doi:10.1155/2019/9483647

Zhang, P., Yang, M., Chen, C., Liu, L., Wei, X., and Zeng, S. (2020a). Toll-Like Receptor 4 (TLR4)/Opioid Receptor Pathway Crosstalk and Impact on Opioid Analgesia, Immune Function, and Gastrointestinal Motility. *Front. Immunol.* 11, 1455. doi:10.3389/fimmu.2020.01455

Zhang, Y., Chen, W., and Wang, Y. (2020b). STING Is an Essential Regulator of Heart Inflammation and Fibrosis in Mice with Pathological Cardiac Hypertrophy via Endoplasmic Reticulum (ER) Stress. *Biomed. Pharmacother.* 125, 110022. doi:10.1016/j.biopha.2020.110022

Zhang, Y., Li, C., Meng, H., Guo, D., Zhang, Q., Lu, W., et al. (2018). BYD Ameliorates Oxidative Stress-Induced Myocardial Apoptosis in Heart Failure Post-Acute Myocardial Infarction via the P38 MAPK-CRYAB Signaling Pathway. *Front. Physiol.* 9, 505. doi:10.3389/fphys.2018.00505

Zhong, Y., Li, M., Zhang, X., Chen, L., Wang, Y., and Xu, Y. (2020). Dissecting Chemical Composition and Cardioprotective Effects of Fuzhengkangfu Decoction against Doxorubicin-Induced Cardiotoxicity by LC-MS and Bioinformatics Approaches. *ACS Omega* 5, 14051–14060. doi:10.1021/acsomega.0c01494

Zhu, W., Wu, R. D., Lv, Y. G., Liu, Y. M., Huang, H., and Xu, J. Q. (2020). BRD4 Blockage Alleviates Pathological Cardiac Hypertrophy through the Suppression of Fibrosis and Inflammation via Reducing ROS Generation. *Biomed. Pharmacother.* 121, 109368. doi:10.1016/j.biopha.2019.109368

Conflict of Interest: The authors declare that the research was conducted in the absence of any commercial or financial relationships that could be construed as a potential conflict of interest.

Publisher's Note: All claims expressed in this article are solely those of the authors and do not necessarily represent those of their affiliated organizations or those of the publisher, the editors, and the reviewers. Any product that may be evaluated in this article, or claim that may be made by its manufacturer, is not guaranteed or endorsed by the publisher.

frontiers in Pharmacology

ORIGINAL RESEARCH
published: 18 January 2022
doi: 10.3389/fphar.2021.784041

Curcumin Ameliorates Cardiac Fibrosis by Regulating Macrophage-Fibroblast Crosstalk *via* IL18-P-SMAD2/3 Signaling Pathway Inhibition

Jing Zhao[1,2,3], *Yongjian Chen*[1,2], *Qiming Chen*[1,2], *Tingting Hong*[1,2], *Zhiwei Zhong*[1,2,3], *Junhua He*[1,2,3] *and Cheng Ni*[1]*

[1]Department of Cardiology of the Second Affiliated Hospital, Zhejiang University School of Medicine, Hangzhou, China, [2]Cardiovascular Key Laboratory of Zhejiang Province, Hangzhou, China, [3]Clinical Research Center of the Second Affiliated Hospital, Zhejiang University School of Medicine, Hangzhou, China

Ethnopharmacological relevance: Curcumin is a bright yellow chemical produced by plants of the *Curcuma longa* species. Chemically, curcumin is a diarylheptanoid, belonging to the group of curcuminoids. The therapeutic potential of curcumin has been widely investigated, including its utilization in various of cardiovascular diseases. However, its effect in cardiac remodeling post myocardial infarction and underlying mechanism remains to be uncover.

Aim: To evaluate the therapeutic effect and underlying mechanism of curcumin on cardiac fibrosis after myocardial infarction *via* macrophage-fibroblast crosstalk.

Methods: Male C57BL/6 (C57) mice were subjected to left anterior descending coronary artery ligation to establish myocardial infarction and intragastrically fed vehicle or curcumin (50 mg/kg or 100 mg/kg) for 4 weeks. In parallel, neonatal rat cardiac fibroblasts were isolated and co-cultured with liposaccharide (LPS^- or LPS^+) curcumin-treated macrophages, followed by TGF-β stimulation for 24 h. Cardiac function was determined by 2-dimensional echocardiography, and cardiac fibrosis was measured by picrosirius red staining. Apoptosis of macrophages was investigated by flow cytometry; all pro-fibrotic protein expression (EDA-Fibronectin, Periostin, Vimentin, and α-SMA) as well as TGF-βR1 downstream signaling activation reflected by phosphorylated SMAD2/3 (*p*-SMAD2 and *p*-SMAD3) were demonstrated by western blotting.

Results: Curcumin significantly ameliorated the inflammation process subsequent to myocardial infarction, reflected by decreased expression of $CD68^+$ and $CD3^+$ cells, accompanied by dramatically improved cardiac function compared with the placebo group. In addition, cardiac fibrosis is inhibited by curcumin administration. Interestingly, no significant reduction in fibrotic gene expression was observed when isolated cardiac fibroblasts were directly treated with curcumin *in vitro;* however, pro-fibrotic protein expression was significantly attenuated in CF, which was co-cultured with LPS-stimulated macrophages under curcumin treatment compared with the placebo group.

OPEN ACCESS

Edited by:
Yi Wang,
Zhejiang University, China

Reviewed by:
Guanwei Fan,
Tianjin University of Traditional Chinese Medicine, China
Firdos Ahmad,
University of Sharjah, United Arab Emirates

****Correspondence:***
Cheng Ni
cescni@zju.edu.cn

Specialty section:
This article was submitted to Ethnopharmacology, a section of the journal Frontiers in Pharmacology

Received: *27 September 2021*
Accepted: *20 December 2021*
Published: *18 January 2022*

Citation:
Zhao J, Chen Y, Chen Q, Hong T, Zhong Z, He J and Ni C (2022) Curcumin Ameliorates Cardiac Fibrosis by Regulating Macrophage-Fibroblast Crosstalk via *IL18-P-SMAD2/3 Signaling Pathway Inhibition. Front. Pharmacol. 12:784041. doi: 10.3389/fphar.2021.784041*

Mechanistically, we discovered that curcumin significantly downregulated pro-inflammatory cytokines in macrophages, which in turn inhibited IL18 expression in co-cultured cardiac fibroblasts using bulk RNA sequencing, and the TGF-β1-*p*-SMAD2/3 signaling network was also discovered as the eventual target downstream of IL18 in curcumin-mediated anti-fibrosis signaling.

Conclusion: Curcumin improves cardiac function and reduces cardiac fibrosis after myocardial infarction. This effect is mediated by the inhibition of macrophage-fibroblast crosstalk in the acute phase post-MI and retrained activation of IL18-TGFβ1-*p*-SMAD2/3 signaling in cardiac fibroblasts.

Keywords: myocardial infarction, curcumin, cardiac fibrosis, interleukin-18, transforming growth factor beta receptor-1

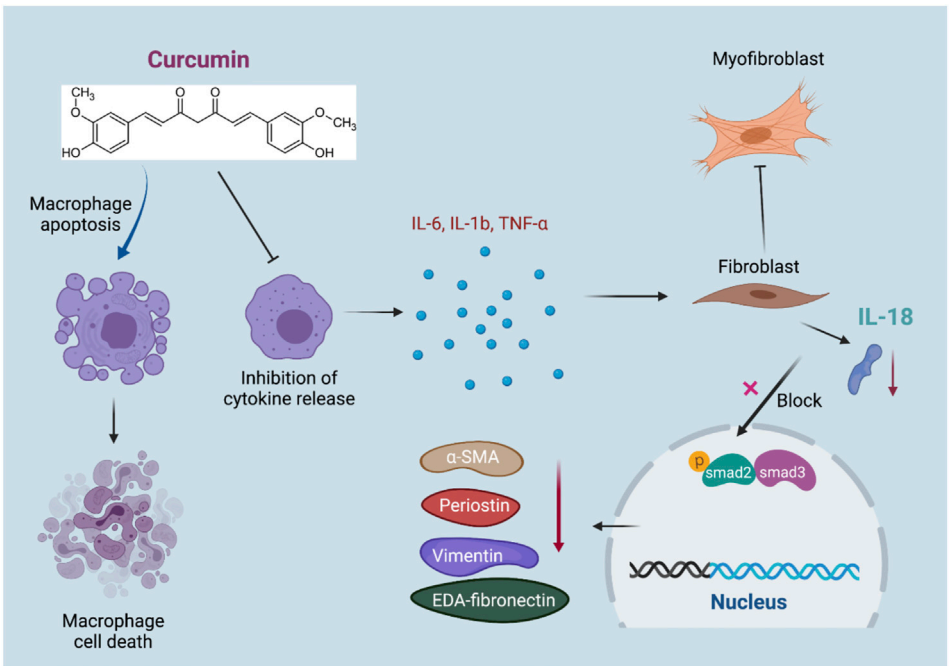

GRAPHICAL ABSTRACT |

INTRODUCTION

Cardiovascular diseases, especially ischemic heart disease, remain the leading cause of death worldwide. Although early reperfusion therapy for acute myocardial infarction (MI) can effectively salvage ischemic myocardium, a considerable portion of cardiomyocytes may still experience irreversible necrosis and loss, followed by ventricular remodeling and cardiac insufficiency, which compromises the long-term survival of patients with MI (Tallquist and Molkentin, 2017). Hence, it is crucial to develop effective therapies for adverse cardiac fibrosis subsequent to MI.

Monocytes and macrophages play a critical role in regulating fibrotic responses in various tissues, including cardiac tissue after ischemic stimulation (Wynn and Vannella, 2016). The normal adult mammalian myocardium contains a relatively small population of resident macrophages (Epelman et al., 2014)' (Heidt et al., 2014) which have been suggested to play a role in cardiac homeostasis by facilitating atrioventricular conduction (Hulsmans et al., 2017). Following injury, resident cardiac macrophages derived from embryonic yolk sac cells are replaced by an abundant population of monocyte-derived macrophages (Epelman et al., 2014), recruited through the

activation of chemokine-dependent pathways (Dewald et al., 2003). Macrophages in injured hearts are highly heterogeneous and exhibit functional and phenotypic versatility that enables them to participate in a wide range of processes, including inflammation regulation, fibrosis, matrix remodeling, angiogenesis, and regeneration (Honold and Nahrendorf, 2018). Thus, subsets of activated macrophages may regulate fibrosis by serving as a major source of cytokines and growth factors with fibrogenic properties, secretion of proteases that participate in matrix remodeling, and production of matricellular proteins. Pro-inflammatory cytokines (such as IL-1β, IL-6, and TNF-α) secreted in many cardiac fibrotic conditions may promote a fibrogenic macrophage phenotype by inducing transcription of members of the TGF-β superfamily.

Turmeric is acquired from Curcuma long L, a tuberous herbaceous perennial plant with yellow flowers and wide leaves, which is a member of ginger family and grows in tropical climate (Prasad et al., 2014). Unlike cinnamon, turmeric has not any different kinds. Curcumin is a symmetric molecule consisting of two similar aromatic rings that contain O-methoxy phenolic groups connected by a carbon linker with an α, β-unsaturated β-diketone moiety (Priyadarsini, 2014). Curcumin's health benefits has been well-established, including anti-tumor, anti-viral, anti-oxidative stress, anti-inflammatory, anti-microbial, hypoglycemic etc. Therapeutically, curcumin exhibits promising potential in preclinical as well as clinical studies and is currently in human trials for a variety of conditions, including metabolic syndrome, nonalcoholic fatty liver disease, atherosclerosis, liver cirrhosis, depression, psoriasis, and Alzheimer's disease (Kocaadam and Şanlier, 2017). The immunomodulatory functions of curcumin arise due to its interactions with cellular and molecular components during inflammatory reactions. Dietary exposure to 40 mg/kg curcumin for 5 weeks showed enhanced IgG levels in rats, suggesting an improvement in immune function after curcumin intervention (South et al., 1997). Curcumin has also been shown to regulate macrophage polarization by increasing the M2 phenotype marker CD163 together with the anti-inflammatory cytokine IL-10 and decreasing the M1 phenotype marker CD86 along with the pro-inflammatory cytokines TNF-α and IL-6 (Li et al., 2017).

Inflammasomes play an important role in mediating fibrosis in cardiac fibroblasts, which are commonly initiated through NLRP3 activation and response and in turn are amplified by IL-18 secretion (Elliott and Sutterwala, 2015). Due to the increased IL-18 level, the synthesis and secretion of TGF-β1 and cytokines can be promoted through autocrine signaling, leading to further inflammatory activation and phosphorylation of SMAD2/3, which initiates fibrogenesis waterfall reactions.

To summarize, our study aimed to unveil the therapeutic effect of curcumin in alleviating IL-18-*p*-SMAD2/3–induced cardiac fibrosis subsequent to MI, which is mediated by the inhibition of inflammation-induced macrophage-fibroblast crosstalk.

MATERIALS AND METHODS

Chemical Materials

Curcumin (65% purity) and lipopolysaccharide (99% purity) were purchased from Sigma-Aldrich (#C1386 and #L2630, St. Louis, MO, United States), respectively. Recombinant human transforming growth factor-β (TGF-β1, PeproTech, NJ, United States). Raw 264.7 cells were obtained from the American Type Culture Collection (ATCC) (China). Neonatal rat cardiac fibroblasts (NRCFs) were isolated from P0–P3 neonatal rats using the Neonatal Heart Dissociation Kit mouse and rat (#130-098-373) (Miltenyi, United States) in accordance with the manufacturer's protocols. Dulbecco's modified Eagle's medium (DMEM) (#8121348) was obtained from Gibco (Thermo Fisher Scientific, Inc.) Fetal bovine serum (FBS) was obtained from BI (#2053264) (Biological Industries, Inc.), phosphate buffered saline (PBS) (#2104140103), Trypsin (#BC-CE-005-100 ml) and Penicillin/Streptomycin (#BC-CE-007-100 ml) were obtained from (Nanjing BioChannel Biotechnology Co., Ltd, China) and *In Situ* Cell Death Detection Kit, Fluorescein was obtained from Roche Diagnostics (Roche Applied Science, Indianapolis, IN, United States). Annexin V-FITC Apoptosis Detection Kit (#CA1020) was supplied by Beijing Solarbio (Beijing, China). Antibodies against Cleaved-caspase 3 (#9661), *p*-SMAD2 (#3108), and SMAD2/3 (#8685) were purchased from Cell Signaling Technology, Inc. EDA-Fibronectin (#6328), Periostin (#14041), Vimentin (#92547), α-SMA (#5694), *p*-SMAD3 (#52903), CD68 (#125212), CD3 (#16669) and Troponin I (#47003)were purchased from Abcam, Inc. ECL western blot detection kits (#FD8020)**.** were purchased from FD bio Science Biological Technology Co., Ltd (China). A cell counting kit-8 (CCK-8) dye was purchased from Biosharp, Inc. Isoflurane was obtained from RWD Life Science Co., Ltd. Picro Sirius Red (#BP-DL030) was obtained from Sbjbio (Nanjing SenBeiJia Biological Technology Co., Ltd.). ELISA kit was used to quantify IL-18 (#ml002816) (Shanghai Enzyme-linked Biotechnology Co., Ltd.).

Animals and Experimental Design

Forty male C57/BL/6J mice weighing 20-25 g were purchased from the Zhejiang Experimental Animal Center (Hangzhou, China). All experiments were approved by the Ethical Committee of Zhejiang University and all surgical procedures were performed by experienced technician sin a blinded manner. Mice were acclimatized to the standard conditions with 12 h lighting cycle, 25 ± 2°C temperature, free access to water and standard chow for 1 week. Then, they were sorted into four groups of 10 mice per group. Group 1 (sham) received dimethylsulfoxide (DMSO-saline) for 28 days intragastrically (i.g.) as a vehicle for curcumin. Group 2 (MI + DMOS) was treated with MI.Group 3 was treated with curcumin 50 mg/kg/day i.g. for 28 days after MI. Group 4 was treated with curcumin 100 mg/kg/day i.g. for 28 days after MI. The appropriate dose (50 mg/kg and 100 mg/kg) was selected (Wang et al., 2019; He et al., 2020). MI was induced by ligation of the left anterior descending coronary

artery. The MI model was established as described previously (Hu et al., 2008).

Echocardiograpic Studies

During 4 weeks treatment, mice was anaesthetized (1.5–2% isoflurane mixed with 98% air condition) and transthoracic echocardiography was performed with a 40 MHz transducer (Vevo 2100 Imaging System, VisualSonics, FUJIFILM, Canada). Two-dimensional B-mode and M-mode measurements in the long-axis view level include left ventricular end-diastolic dimension (LVID,d), left ventricular end-systolic dimension (LVID,s), interventricular septal wall thickness in diastole (IVS,d) and in systole (IVS,s), and left ventricular posterior wall thickness in diastole (LVPW,d) and in systole (LVPW,s). Left ventricular ejection fraction and fractional shortening were automatically calculated by the echocardiographic system (Xiao et al., 2018).

Immunohistochemical Staining

Mouse hearts 7 days post-MI were dehydrated in 30% sucrose solution, embedded in Tissue-Tek OCT compound, snap-frozen in dry ice, and then cut into 7 μm sections. The sections were then stained with a *In Situ* Cell Death Detection Kit (Roche Applied Science, CH), CD3, CD68, Troponin I (Abcam, United Kingdom), and DAPI (Vector Laboratories, Burlingame, CA, United States).

Mouse hearts 28 days post-MI were fixed in 10% formalin-PBS, then paraffin embedded, and cut into 3 μm sections. After deparaffinization, rehydration and tissue antigen recovery, the sections were stained with Periostin (R&D, United States), Troponin I (Abcam, United Kingdom), and DAPI (Vector Laboratories, Burlingame, CA, United States).

Picro Sirius Red Staining

After deparaffinization, sections were stained with Sirius Red. Tissue damage was scored by calculating the scar circumference, including both internal and external scar diameters. The sirius red–stained sections were scanned with a microscope digital camera (Olympus Instrument, United States), and Biotechnologies, China). The percentage of fibrotic area was calculated as the mean value of the endocardial and epicardial length of the whole fibrotic area in proportion to the mean length of the endocardial and epicardial left ventricle using Image using Image Pro Plus software version 6.0.

Macrophage Culture and Drug Treatment

Mouse macrophage-like Raw 264.7 cells were acquired from the ATCC and cultured in DMEM with 10% FBS and 1% Penicillin/Streptomycin at 37°C with 5% CO_2. After 2 days, the medium was replaced, and nonadherent cells were discarded.

Cytotoxicity Test

Raw 264.7 cell viability was examined using the CCK-8 assay (Bio-sharp, China) in accordance with the manufacturer's protocols. Cells were treated with liposaccharides (LPS 1 μg/ml) or LPS with curcumin at different concentrations (0.1, 1, 10, 20, and 50 μM) and the appropriate dose (10μM, 20 μM) was selected refer the previous studies (Gao et al., 2015; Chun-Bin et al., 2020). Then Cells were seeded in a 96-well plate at a density of 8×10^3 cells/well. Following treatment, 10 μL of CCK-8 solution was added to each well and incubated for 2 h. Survival Ratio was calculated according to the following equation: cell survival = [(As-Ab)/(Ac-Ab)] ×100%, where As = treated group, Ac = normal group, and Ab = vehicle control group. The absorbance of each well was measured at 450 and 630 nm using a microplate reader (Spark TECAN, Switzerland). All data were calculated from triplicate samples.

Cell Apoptosis

Raw 264.7 cells were treated with 1 μg/ml LPS or LPS with curcumin (10 and 20 μM). Cell apoptosis was evaluated by flow cytometry with Annexin V-FITC and PI staining (CytoFlex, Beckman Coulter, Germany). The flow cytometry assay was examined in accordance with the manufacturer's protocols.

Cell Co-culture Scheme

NRCFs were isolated from P0–P3 neonatal rats using the Neonatal Heart Dissociation Kit mouse and rat (Miltenyi, United States) in accordance with the manufacturer's protocols. Raw 264.7 cells were first seeded in 0.4 μm Transwell chamber (#3412), after treatment in low-glucose DMEM with serum deprivation overnight, NRCFs were stimulated with 10 ng/ml TGF-β and then co-cultured with 1 μg/ml LPS or 1 μg/ml LPS with 20 μM curcumin, respectively.

Plasmid Transfection

NRCFs in each group were seeded in a 6-well plate at 2×10^5 cells per well and cultured in FBS free medium overnight. NRCFs were transfected for 48 h with 2 μg of the IL18 mimic (IL-18 rat, Shanghai GenePharma Co., Ltd, China) to overexpress IL18 using X-tremeGENE HP DNA Transfection Reagent according to the manufacturer's instructions. Real-time fluorescent quantitative polymerase chain reaction (RT-qPCR) and enzyme-linked immunosorbent assay (ELISA) were used to quantify IL-18 transfection efficiency. Conditioned medium was collected from transfected cell medium and analyzed according to the manufacturer's instructions.

Extraction and Quantitative RT-PCR

Total RNA was isolated from three replicates per group after treatment using the TRIzol method, 2 μg of total RNA was reverse-transcribed to cDNA using Evo M-MLV RT Premix for qPCR method according to the manufacturer's instructions (AG). And resultant cDNA samples were subjected to qPCR on LightCycler® 480 PCR System (Roche) using SYBR® Green Premix Pro Taq HS qPCR Kit (AG). The upstream and downstream primers of IL6, IL-1β, and TNF-α were designed and synthesized by Tsingke Biotechnology Co., Ltd. The primer sequences used were as follows:

Mouse-IL-6, forward (5′-GAGGATACCACTCCCAACAGACC-3′) and reverse (5′-AAGTGCATCATCGTTGTTCATACA-3′); mouse-IL-1β, forward (5′-CCAGCTTCAAATCTCACAGCAG-3′) and reverse (5′-CTTTGGGTATTGCTTGGGATC-3′); mouse-TNFα, forward (5′-CGGAGTCCGGGCAGGT-3′)

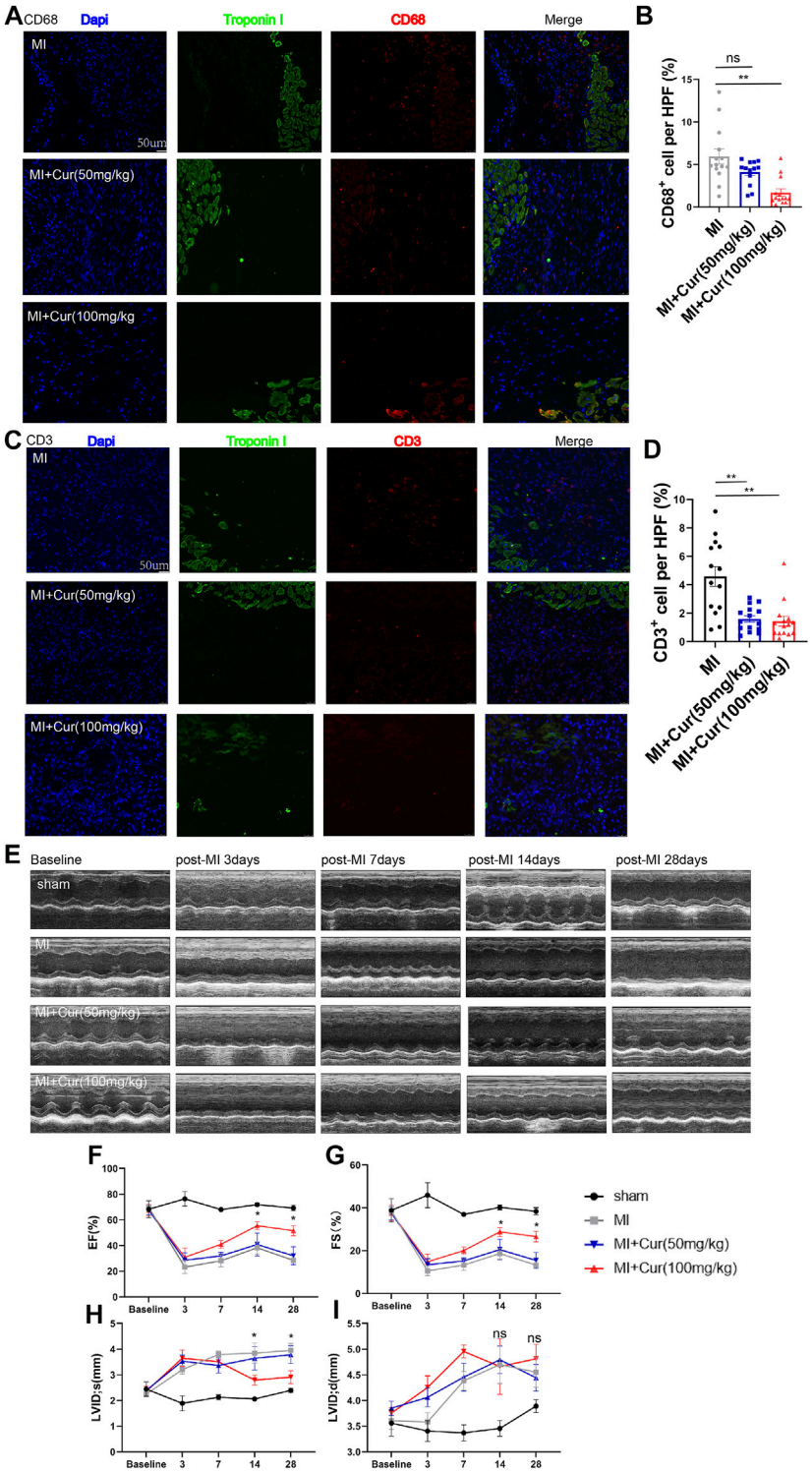

FIGURE 1 | Curcumin administration ameliorates inflammatory response in acute phase post-MI and preserves long-term cardiac function **(A).** Macrophage counts reflected by CD68 staining (red) in peri-infarct heart samples harvested 7 days post-MI from C57 mice in respective group (MI, MI + Cur 50 mg/kg, MI + Cur 100 mg/kg). Troponins were identified by green coloring; statistical data are summarized in **(B).** n = 4-5 in each group **(C).** T cell counts reflected by CD3 staining (red) in peri-infarct heart samples harvested 7 days post-MI from C57 mice (MI, MI + Cur 50 mg/kg, MI + Cur 100 mg/kg). Troponins were identified by green coloring; statistical data are summarized in **(D).** n = 4-5 in each group **(E).** M-mode representative graphs from echocardiography conducted on MI, MI + Cur 50 mg/kg, MI + Cur 100 mg/kg, respectively. Echocardiography were conducted at baseline and 3, 7, 14, and 28 days post-MI. Cardiac function reflected by left ventricle ejection fraction (LVEF%) and left ventricle fraction shortening (LVFS%) in each group (MI, MI + Cur 50 mg/kg, MI + Cur 100 mg/kg) are plotted in **(F)** and **(G)**. n = 5 in each group **(H-I).** Left ventricular internal dimension in systolic phase (LVID s) and Left ventricular internal dimension in diastolic phase (LVID d) in each group at different timepoint were also plotted in **(H)** and **(I)**. MI: myocardial infarction. Results are mean with SEM. NS = no significance between groups, $^{*}p < 0.05$, $^{**}p < 0.01$.

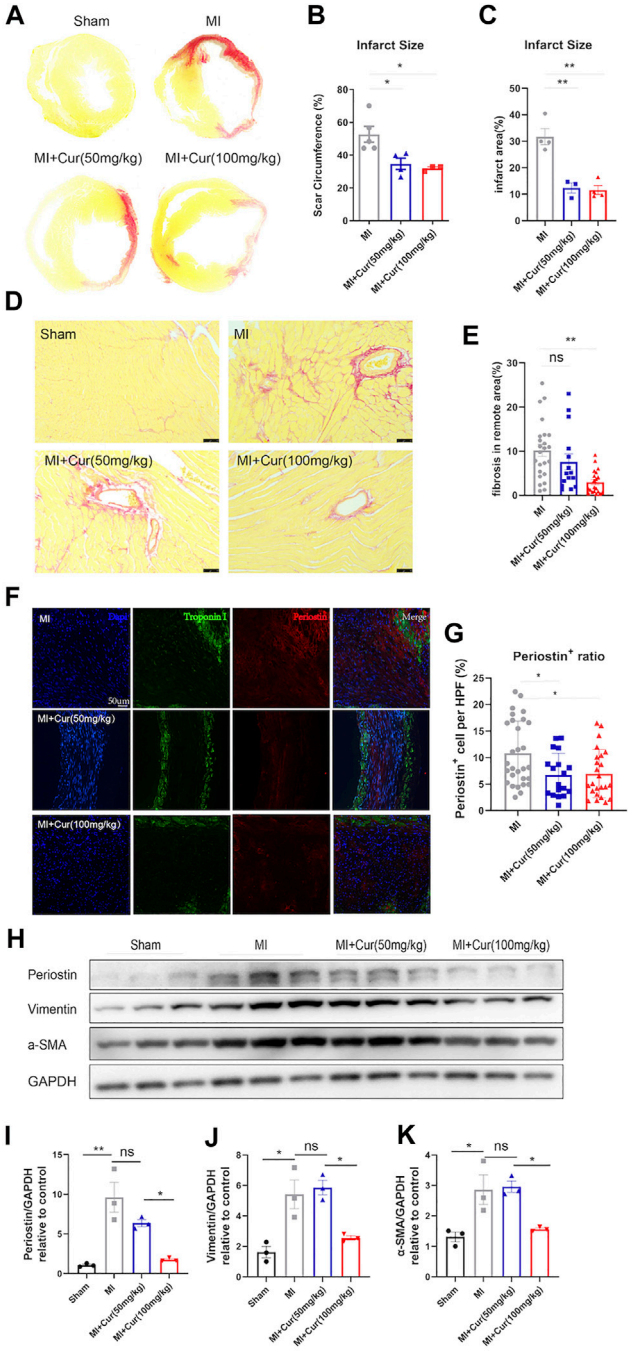

FIGURE 2 | Curcumin reduces scar formation and ameliorates adverse cardiac remodeling in post-MI rats in long-term prospects **(A-B)**. Representative images of sirius red staining of whole heart cross section in rat heart from all groups, as indicated **(A) (B)** Statistical analysis of scar circumference in each group (means with SEM). n = 3–5 per group **(C)** Statistical analysis of infarct area in each group (means with SEM). n = 3–5 per group **(D-E).** Sirius red staining of non-infarcted area in all groups (Sham, MI, MI + Cur 50 mg/kg, MI + Cur 100 mg/kg), scale bar = 100 μm n = 5 per each group **(D)**. Collagen summary and statistics are plotted in **(E) (F-G).** Collagen deposition and content within MI segments measured by Periostin$^+$ cells within MI segment; Periostin (red) indicates myofibroblasts that secrete

(*Continued*)

FIGURE 2 | collagen, and Troponin I was stained green. Representative images are displayed in **(F)**, summary data are plotted in **(G)**, n = 4–5 in each group **(H-K)**. Western blot analysis of pro-fibrotic protein expression (Periostin, Vimentin, α-SMA) in each group (Sham, MI, MI + Cur 50 mg/kg, MI + Cur 100 mg/kg), bands are shown in **(H)**, statistics of each protein of Periostin are plotted in **(I)**, Vimentin in **(J)**, α-SMA in **(K)**. Results are mean with SEM, NS = no significance between groups, $^*p < 0.05$, $^{**}p < 0.01$, n.

and reverse (5′- GCTGGGTAGAGAATGGATGAACA-3′); mouse-GAPDH, forward (5′-TGGCCTTCCGTGTTCCTAC-3′) and reverse (5′- GAGTTGCTGTTGAAGTCGCA-3′); rat-IL-18, forward (5′-TCAGACCACTTTGGCAGACT-3′) and reverse (5′- GATTCGTTGGCTGTTCGGTC-3′) rat-GAPDH, forward (5′-AAAGGGTCATCACCCGCC-3′) and reverse (5′-AGTGATGGCATGGACTGTGG-3′).

Western Blot Analysis

The cells seeded in the 6-well plates were collected, lysed in 2.5×sodium dodecyl sulfate (SDS) gel loading buffer (30 mM Tris-HCl, pH 6.8, 1% SDS, 0.05% bromphenol blue, 12.5% glycerol, and 2.5% mercaptoethanol) and boiled for 30 min; then, 20 μL of the protein was loaded onto 8% concentrated gel for protein electrophoresis separation. After that, the protein was transferred to the PVDF membrane (Millipore, Boston, MA), which was then blocked using 5% skim milk powder for 1 h at room temperature. Then, the membranes were incubated with primary antibodies specific for Cleaved-caspase 3, *p*-SMAD2, SAMD2/3(Cell Signaling Technology), EDA-Fibronectin, Periostin, Vimentin, α-SMA, *p*-Smad3 (Abcam), gapdh (#KC-5G5), and β-actin (#KC-5A08) (KangChen, Shanghai) at 4°C overnight, washed with PBST, and further incubated with a secondary antibody for 1 h. Finally, the immunoreactive protein was detected by a chemiluminescence assay (AI680RGB, GE HealthCare, United States) using the FDbio-Dura ECL kit (FDbio Science Biological Technology Co., LTD, China).

Statistical Analysis

All results were expressed as value ±standard error of the mean (SEM). Significant differences between two groups were determined by the Student's t-test, and One-way ANOVA test was used for multiple comparisons, two-way ANOV test was conducted in multiple group with different time points. $p < 0.05$, $p < 0.01$, was considered statistically significant present *, **, respectively. Statistical calculations were carried out using GraphPad Prism 9.0. The sample size was ≥5 in each group for *in vivo* animal studies, and ≥3 in each group for *in vitro* studies.

RESULTS

Curcumin Resists Inflammation Response Post-MI and Supports Subsequent Cardiac Function

To test the effect of curcumin on MI, we performed MI surgery by permanent ligation of the left anterior descending artery followed

by intragastric administration of curcumin for 7 days or 28 days. In parallel, a placebo post-MI group was also established. At 7 days post-MI surgery, we discovered significantly inhibited inflammation activation reflected by reduced $CD68^+$ and $CD3^+$ cells detected in the peri-infarcted area in the curcumin group compared with the placebo group, while no difference in $CD68^+$ and $CD3^+$ cell counts was observed between the high-dose curcumin group (100 mg/kg) and the low-dose curcumin group (50 mg/kg) (**Figures 1A–D**). In addition, cardiac function in the MI + curcumin group exhibited significant improvement compared with the placebo group 1 month after MI, with no obvious change observed 7 days post-MI between the two groups, as demonstrated by ejection fraction (EF%) and fraction shortening (FS%) (**Figures 1E–G**), in addition, the chamber of left ventricle in systolic phase was dramatically decreased in MI + curcumin group compared with MI group (LVID s), while no significant change were detected between groups in diastolic phase (LVID d) (**Figures 1H,I**). To summarize, the administration of curcumin after MI significantly ameliorated inflammation in the acute phase; however, curcumin exerted a protective effect by preserving long-term cardiac function only after MI, which suggested that the reduced inflammation activation might be related to adverse cardiac remodeling mediated by curcumin intake.

Curcumin Ameliorates Cardiac Fibrosis and Reverses Adverse Remodeling Post-MI

As previously indicated, curcumin delivery significantly improved long-term cardiac function after MI in C57 mice. To determine what yields this beneficial effect, we conducted TUNEL and picro sirius red staining and, surprisingly, discovered no significant reduction in anti-apoptotic effect on cardiomyocyte within border area in the curcumin-treated group compared with the placebo group 7 days after MI (**Supplementary Figure S1A,B**). However, we observed dramatically reduced scar formation reflected by picro sirius red staining in both scar circumference and infarct size dimension in curcumin group compared with the placebo group (**Figures 2A–C**). More importantly, we discovered significant ameliorated fibrosis within non-infarcted area in MI + curcumin group compared with MI group using the dosage of 100 mg/kg (**Figures 2D,E**), indicating the robust anti-fibrotic role of curcumin post MI. In addition, we conducted immunostaining on MI segments using periostin to verify cardiac myofibroblast enrichment and collagen deposition, revealing significantly decreased $periostin^+$ cell expression within MI segment in Curcumin group (**Figures 2F,G**), western blot results also confirmed the therapeutic utilization of Curcumin in inhibiting pro-fibrotic protein expression as displayed by ameliorated Periostin, Vimentin, and α-SMA expression (**Figure 2H–K**). The results presented above indicate that the use of curcumin following MI significantly improved cardiac function by inhibiting excessive collagen deposition and scar formation.

Curcumin Promotes Macrophage Apoptosis Under LPS Stimulation *in vitro* Accompanied by Inhibited Pro-inflammatory Cytokine Secretion

It is known that LPS significantly activate inflammation and mobilize macrophage proliferation as well as M1 polarization. To further investigate the mechanism of curcumin in anti-inflammatory processes, we performed LPS stimulation on macrophage *in vitro* for 24 h followed by Curcumin administration, CCK8 test revealed dramatic inhibited macrophage proliferation when dosage was 20 uM, indicating Curcumin might exerted anti-proliferation or pro-apoptotic effect in macrophages under LPS stimulation (**Figure 3A**). Flow cytometry was conducted to determine whether curcumin promoted macrophage apoptosis under LPS stimulation. As shown in **Figures 3B,C**, curcumin significantly increased macrophage apoptosis under LPS stimulation compared with LPS only also using 20 uM dosage. In addition, the cleaved-caspase three protein level, which acts as a marker of apoptosis, was also significantly up-regulated in the curcumin-treated macrophages with LPS group compared with LPS only reflected by western blot (**Figures 3D,E**). Furthermore, macrophage activation could induce the secretion of pro-inflammatory cytokines such as IL-6, IL1β, and TNF-α to initiate an immune response to ischemic injury, thus aggravating cardiomyocyte apoptosis; however, curcumin treatment significantly inhibited pro-inflammatory cytokine secretion in macrophages with LPS group compared with LPS only, as reflected by reduced IL-6, IL-1β, and TNF-α secretion especially at 20 uM concentration (**Figures 3F–H**). These data indicate that the administration of curcumin on macrophages under LPS stimulation exerted both pro-apoptotic effects in macrophages and anti-inflammatory effects by reducing cytokine release from macrophages, which could be greatly beneficial post-MI.

Curcumin Exerts Anti-Fibrotic Effects via Macrophage-Fibroblast Crosstalk

As previously mentioned, curcumin has also been shown to regulate macrophage polarization by increasing anti-inflammatory cytokine IL-10 levels and decreasing the M1 phenotype marker CD86 along with the pro-inflammatory cytokines TNF-α and IL-6. To validate whether curcumin exerted an inhibitory effect on cardiac fibrosis by alleviating inflammation-induced fibrosis or by directly suppressing cardiac fibroblast *trans*-differentiation and collagen secretion, we co-cultured macrophages under LPS stimulation with isolated primary neonatal rat cardiac fibroblasts *in vitro* followed by TGF-β stimulation in NRCF for 24 h, Surprisingly, we discovered that curcumin administration in macrophages with LPS stimulation significantly mitigated collagen synthesis from co-cultured NRCF, which was revealed by pro-fibrotic protein expression (α-SMA, Vimentin, Periostin, and EDA-Fibronectin) (**Figure 4A,C–F**). In contrast, we did not observe a significant change in fibrosis protein expression when curcumin

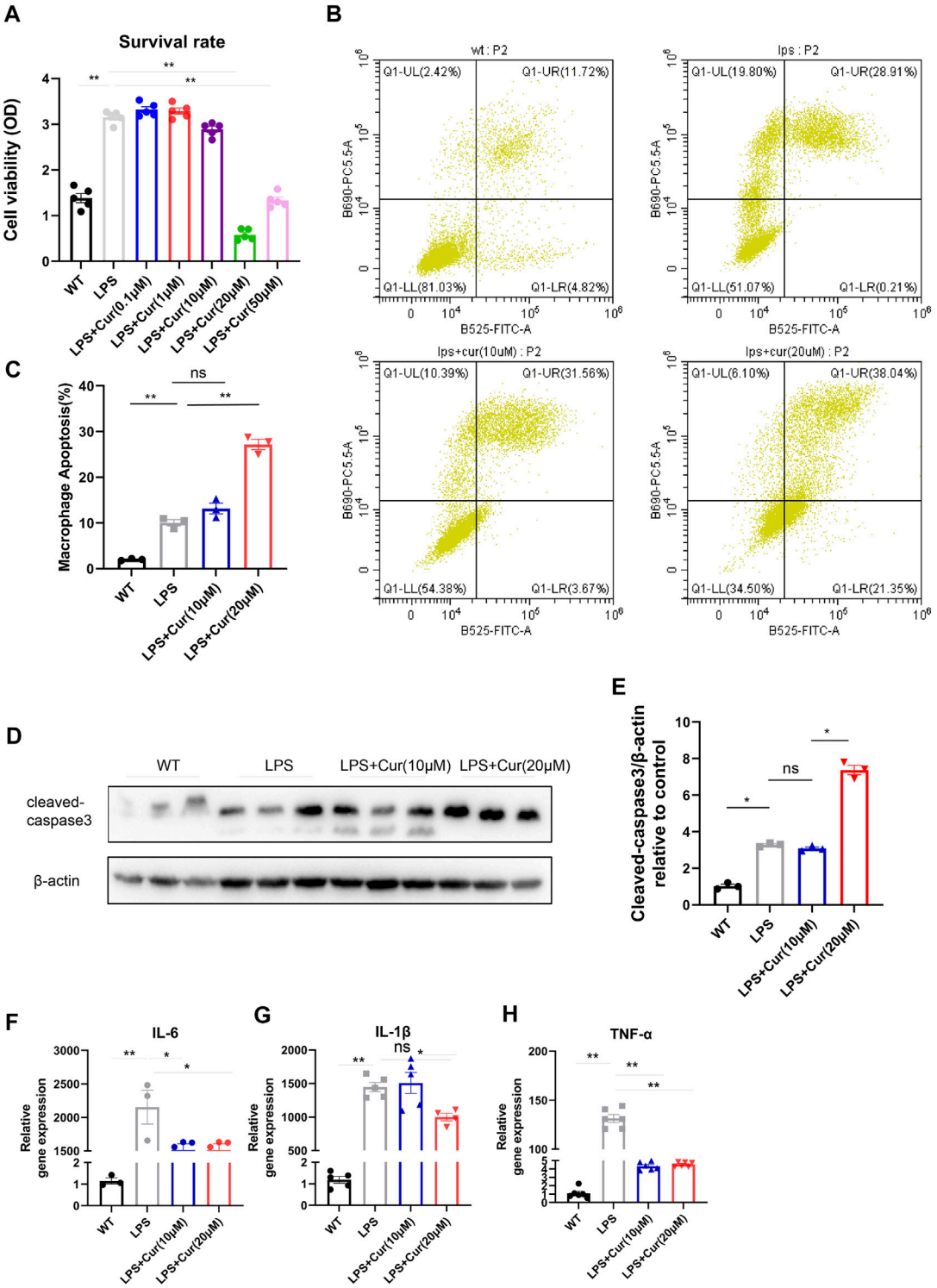

FIGURE 3 | Curcumin promotes macrophage apoptosis *in vitro* and restrain pro-inflammatory cytokine secretio **(A).** Macrophage survival was identified by CCK-8 analysis in respective groups (WT, LPS, LPS + Cur 0.1, 1, 10, 20, and 50 μM) **(B-C)**. Macrophage apoptosis was determined by flow cytometry in respective groups (WT, LPS, LPS + Cur 10 and 20 μM), summary data are displayed in **(C) (D–E).** Pro-apoptotic protein cleaved-caspase three identification by western blot were conducted in respective groups (WT, LPS, LPS + Cur 10 μM and LPS + Cur 20 μM), original bands are displayed in **(D)** and summary data were illustrated in **(E) (F–H).** Pro-inflammatory cytokine detected by qPCR from cell in each group (WT, LPS, LPS + Cur 10 μM and LPS + Cur 20 μM), summary data of IL-6 was plotted in **(F)**, IL-1b in **(G)** and TNF-α in **(H)**. Results are mean with SEM, NS = no significance between groups, $^{*}p < 0.05$, $^{**}p < 0.01$.

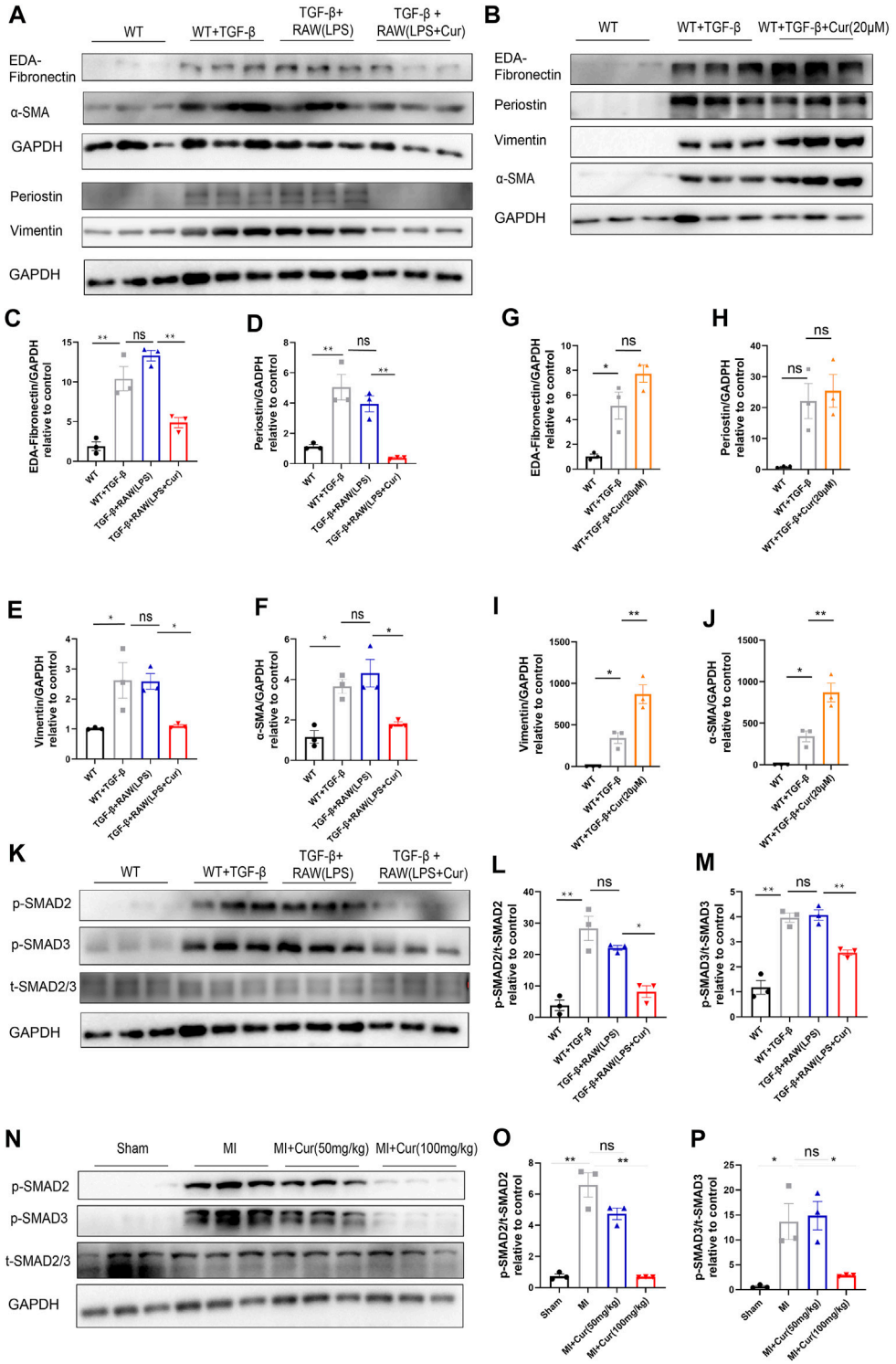

FIGURE 4 | Curcumin inhibits cardiac fibrosis by regulating macrophage-fibroblast crosstalk instead of directly suppressing cardiac fibroblast *trans*-differentiation **(A).** Fibrotic protein expression in different NRCF group (WT, WT + TGF-β, TGF-β+RAW (LPS), TGF-β+RAW (LPS + Cur)) respectively, fibrotic protein is defined as EDA-Fibronectin, periostin, vimentin and α-SMA **(B).** Fibrotic protein expression in different NRCF group (WT, WT + TGF-β, WT + TGF-β+Cur) respectively **(C-F).** Summary data of protein expression are displayed in **(A)**, EDA-fibronectin are plotted in **(C)**, periostin is plotted in **(D)**, vimentin is plotted in **(E)** and α-SMA is plotted in **(F)** **(G–J)**. Summary data of protein expression displayed in **(B)**, EDA-Fibronectin was plotted in **(G),** periostin was plotted in **(H)**, vimentin is plotted in **(I)** and α-SMA in **J)** **(K–M).** TGF-βR1 downs-stream signaling identification by western blot in each group (WT, WT + TGF-β, TGF-β+RAW (LPS), TGF-β+RAW (LPS + Cur)); phosphorylated SMAD2 and SMAD3 were determined as key factors underlying TGF-βR1 signaling to promote fibrosis procedure. Western blot bands are displayed in **(K)**, and summarized data are plotted in **(L-M)** **(N-P)** Phosphorylation level of SMAD2/3 in respective groups (Sham, MI, MI + Cur 50 mg/kg, MI + Cur 100 mg/kg) 1 month after MI were detected by western blotting, bands are shown in **(N)**, and summarized data are plotted in **(O–P)**. Results are mean with SEM, NS = no significance between groups, $^{*}p < 0.05$, $^{**}p < 0.01$.

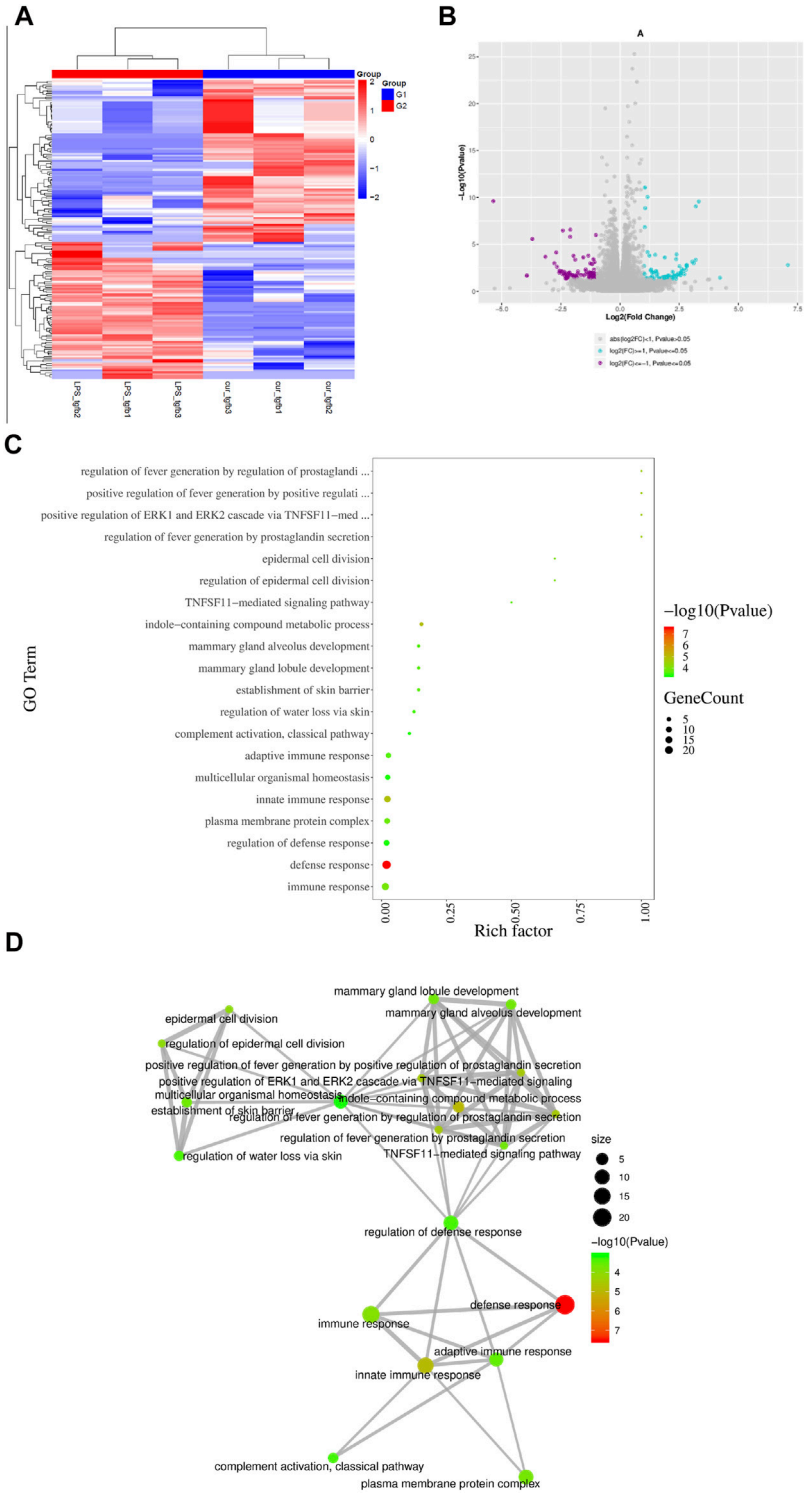

FIGURE 5 | IL-18 plays significant role in curcumin-mediated anti-fibrotic effect screened from mRNA sequencing **(A).** Difference gene heat map between two NRCF group (TGF-β+RAW (LPS), TGF-β+RAW (LPS + Cur)). N = 3 in each group **(B).** Volcano plots indicating up-regulated genes and down-regulated genes between two groups. Purple dots represent down-regulated genes, blue dots represent up-regulated genes, and grey dots represent no significant change. **(C–D).** GO signaling pathway enrichment analysis summary from respective groups. Different colors and dot sizes indicate gene number and gene alteration, respectively. Mutual correlation among all signaling enrichment observations are displayed in **(D)**.

TABLE 1 | Top 10 up and down-regulated genes enriched in inflammation response pathway. (NRCF, co-cultured with PBS-treated macrophages with TGF-β, administration) vs (NRCF, co-cultured with curcumin-treated macrophages with TGF-β, administration).

Gene ID	Gene symbol	FDR	Fold of change log2 (NRCF vs NRCF + Cur)	Up-down
ENSRNOG00000015615	Tnfrsf11a	0.034	3.197800686	up
ENSRNOG00000009848	IL-18	0.035	2.94645754	up
ENSRNOG00000009471	Epsti1	0.014	2.812906485	up
ENSRNOG00000006314	Zbp1	0.043	2.79906252	up
ENSRNOG00000017606	P2rx1	0.0024	2.720746936	up
ENSRNOG00000018798	Bcan	0.025	2.66189736	up
ENSRNOG00000025603	Adgrf2	0.0017	2.581454723	up
ENSRNOG00000001923	Tprg1	0.043	2.558506757	up
ENSRNOG00000010270	Espn	0.036	2.548806342	up
ENSRNOG00000017602	IL-34	0.025	2.386965316	up
ENSRNOG00000020492	Ubbp4	0.0098	–5.355885393	down
ENSRNOG00000036622	Glyatl1	0.012	–2.777779252	down
ENSRNOG00000026296	Saxo2	0.0086	–2.569574924	down
ENSRNOG00000008807	Rp1	0.021	–2.561298476	down
ENSRNOG00000028404	Ppp1r1b	0.0015	–2.430345144	down
ENSRNOG00000010263	Cldn11	0.036	–2.365653939	down
ENSRNOG00000009269	Cga	0.0142	–2.325447584	down
ENSRNOG00000021039	Fam83e	0.048	–2.320912344	down
ENSRNOG00000011334	Tmem63c	0.039	–2.279315173	down
ENSRNOG00000012906	Bcas1	0.017	–2.254907096	down

was directly added to NRCF treated with TGF-β for 24 h compared with the TGF-β only group (**Figure 4B,G–J**). Mechanistically, we discovered decreased phosphorylation of SMAD2/3 in the curcumin-macrophage co-cultured NRCF group compared to NRCF without curcumin treatments, as reflected by the *p*-SMAD2/3 to total SMAD2/3 ratio (**Figure 4K–M**), importantly, we also discovered down-regulated phosphorylation of SMAD2/3 in hearts from post-MI with curcumin treated group compared with MI group, indicating the consistent role in anti-phosphorylation of curcumin towards SMAD2/3(**Figure 4N–P**). In summary, the administration of curcumin only inhibited LPS-stimulated macrophage-fibroblast crosstalk induced excessive collagen deposition, this effect is mediated by the inhibition of SMAD2/3 phosphorylation, while in NRCF with TGF-β stimulation, curcumin delivery was unable to reverse established pro-fibrotic protein expression.

Curcumin Alleviates Cardiac Fibroblast Trans-differentiation by Inhibiting IL-18 Expression Promoted by Macrophage-Fibroblast Crosstalk

To elucidate the detailed mechanism of the identified curcumin-mediated anti-fibrosis effect, we performed bulk mRNA sequencing in NRCF co-cultured with curcumin-treated macrophages and NRCF co-cultured with PBS-treated macrophages; 776 genes were downregulated and 1,467 genes were upregulated in the curcumin group compared with the PBS group (**Figures 5A,B**). Gene enrichment from GO pathway analysis revealed that both immune and defense response signaling were mostly activated and altered between the two groups and that these two signaling pathways were classified and regulated by defense response regulation, indicating the pivotal utilization of curcumin in alleviating an overreactive immune response (**Figures 5C,D**), the top 10 up-regulated and down-regulated genes enriched in immune response signaling are listed in **Table 1**. Among all altered genes enriched in immune response signaling, IL-18 was found to be the top-ranked gene that was significantly down-regulated in the curcumin group, considering the established pro-fibrotic effect mediated by inflammosome-secreted IL-18 and NLRP3 activation. We speculated that the anti-fibrosis effect exerted by curcumin was mediated by mitigating IL-18 expression and secretion in cardiac fibroblasts.

IL-18 Overexpression Neutralizes Anti-Fibrotic Effect in NRCF Co-cultured With Curcumin-Treated Macrophage

Previously, we identified IL-18 as a central molecule in mediating LPS-treated macrophage-activated myofibroblast *trans*-differentiation on NRCF, while curcumin administration significantly ameliorated this process. Hence, to test whether compensation of IL-18 in NRCF after co-culture reverses the anti-fibrotic effect of curcumin, we constructed an IL-18 overexpression plasmid and transfected it into TGF-β-stimulated NRCF after co-culture with LPS and curcumin double-treated macrophages. We discovered significantly upregulated IL-18 gene expression and considerable transfection efficacy, as demonstrated by RT-PCR and immunofluorescence (**Supplementary Figure S2A,B**). Furthermore, IL-18 protein expression levels were determined

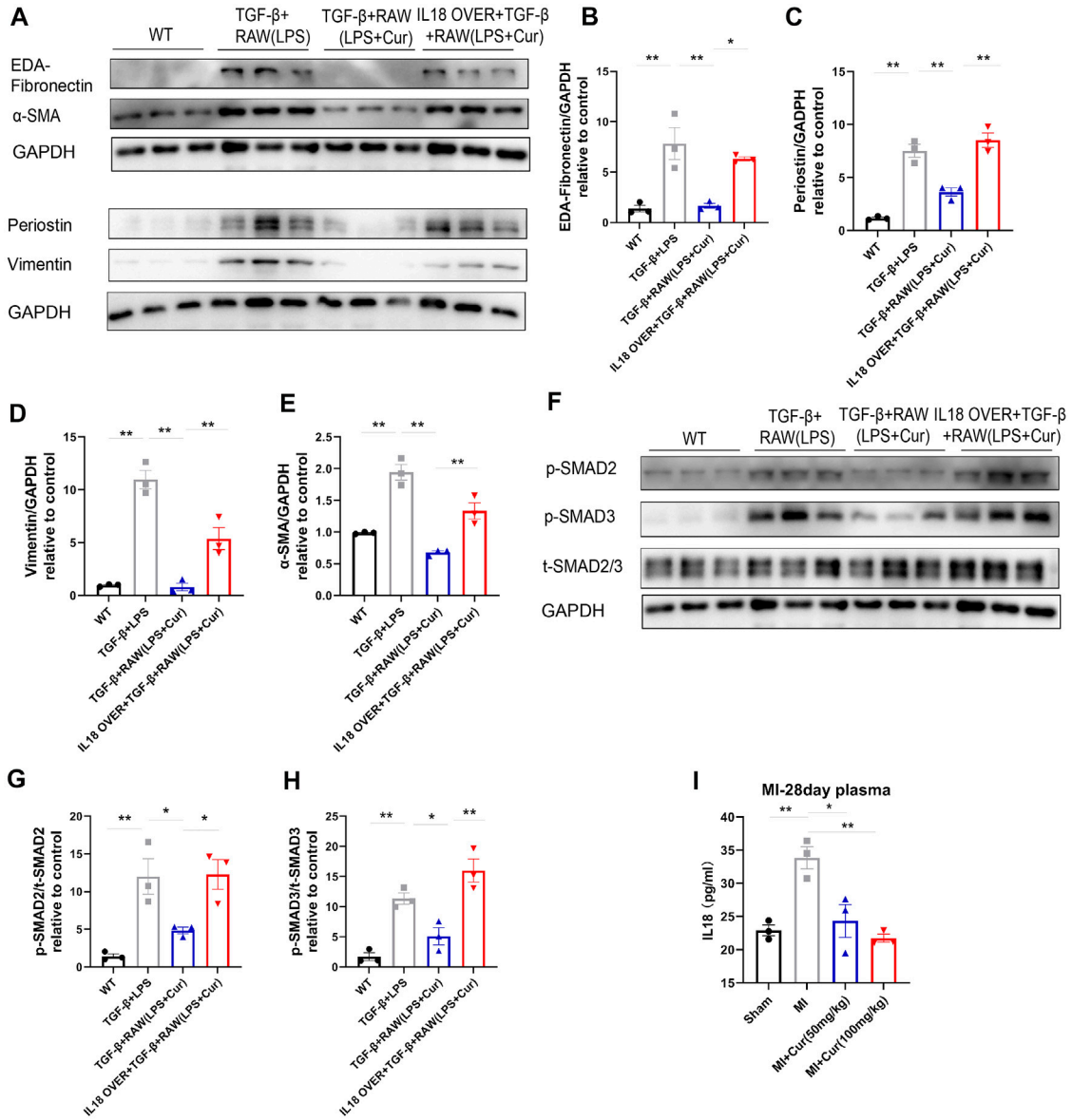

FIGURE 6 | IL-18 compensation represses curcumin-induced inhibition of SMAD2/3 phosphorylation and fibrotic gene expression **(A–E).** Fibrotic protein expression in different NRCF groups (WT, TGF-β+RAW (LPS), TGF-β+RAW (LPS + Cur), IL18 over + TGF-β+RAW (LPS + Cur)) respectively, fibrotic proteins are defined as EDA-Fibronectin, Periostin, Vimentin, and α-SMA. Summary data of protein expression are displayed in **(B–E)**. EDA-Fibronectin is plotted in **(B),** Periostin is plotted in **(C)**, Vimentin is plotted in **(D)** and α-SMA in **(E) (F-H).** Phosphorylation level of SMAD2/3 in different NRCF groups (WT, TGF-β+RAW (LPS), TGF-β+RAW (LPS + Cur), IL18 over + TGF-β+RAW (LPS + Cur)) identified by western blot is illustrated in **(F)**. Summary data are plotted in **(G)** for *p*-SMAD2 and **(H)** for *p*-SMAD3 **(I).** IL-18 content in plasma from different groups (Sham, MI, MI + Cur 50 mg/kg, MI + Cur 100 mg/kg) were identified by ELISA kit, summary data are plotted. Results are mean with SEM, NS = no significance between groups, $^{*}p < 0.05$, $^{**}p < 0.01$.

by ELISA in the supernatant collected from NRCF, indicating successful overexpression after plasmid transfection (**Supplementary Figure S2C**). As expected, IL-18 overexpression in NRCF significantly reversed the curcumin-mediated anti-fibrotic effect, as shown by the expression of fibrotic genes (i.e., EDA-Fibronectin, Periostin, Vimentin, and α-SMA) were detected by western blot analysis (**Figure 6A–E**) more importantly, SMAD2/3 phosphorylation, which was inhibited by curcumin treatment, rebounded by IL-18 overexpression in NRCF (**Figure 6F–H**). Furthermore, IL-18 content was also discovered to be significantly down-regulated in plasma from MI + curcumin group compared with MI group using ELISA, which is consistent with the outcome from unbiased transcriptome analysis as well as *in vitro* findings above (**Figure 6I**). From these findings, we conclude that IL-18-*p*-SMAD2/3 signaling plays a critical role in the curcumin-mediated anti-fibrosis mechanism in TGF-β-stimulated NRCF co-cultured with LPS-treated macrophages.

DISCUSSION

Cardiac fibrosis, characterized by intersection and collagen deposition within the cardiac interstitium due to net accumulation of extracellular matrix (ECM) proteins, is a common pathophysiological manifestation in most myocardial diseases (Berk et al., 2007)' (Kong et al., 2014). In general, the extent of fibrotic remodeling is closely associated with adverse organ outcomes. Myocardial fibrosis is not necessarily the primary cause of dysfunction. In many circumstances, cardiac fibrosis is the result of a reparative process that is activated in response to cardiomyocyte injury. In humans or other adult mammals, quiescent fibroblasts sustained dynamic balance with cardiomyocytes in healthy status; however, these cells have strong potential in repairing injured myocardium; thus, after pathological conditions, loss of a significant number of cardiomyocytes triggers a reparative program, leading to the formation of fibrous tissue. For example, in acute MI, the sudden death of many cardiomyocytes initiates an intense inflammatory reaction, ultimately leading to the replacement of dead myocardium with a collagen-based scar (Frangogiannis, 2012).

Cardiac fibrosis in response to ischemic injury can be divided into three stages: acute early response, proliferation, and late maturation. Inflammation plays a pivotal role in the acute early response, which initiates subsequent repair and acts as a "sentinel." Macrophages are activated immune-cells in early phase post infarction that secrete various cytokines and are intimately correlated with the activation of cardiac fibroblast, initiating "macrophage-fibroblast crosstalk." Pro-inflammatory activation of cardiac fibroblasts is associated with inflammasome induction, which leads to caspase stimulation and IL-1β secretion by macrophages (Kawaguchi et al., 2011)' (Sandanger et al., 2013). In cultured rat heart fibroblasts, higher gelatinase activity was observed in response to stimulation with IL-1β, and tumor necrosis factor α (TNF-α). Interleukin-1β and tumor necrosis factor alpha decreased collagen synthesis and increased matrix metalloproteinase activity in cardiac fibroblasts *in vitro*, and they also differentially regulated the production of tissue inhibitors of metalloproteinases. After ischemia reperfusion–induced heart injury, IL-1 receptor 1-deficient mice showed decreased accumulation of macrophages in the infarcted myocardium and diminished early inflammatory and pro-fibrotic responses (Bujak et al., 2007) suggesting downregulation of cardiac repair in a case of disrupted IL-1-dependent signaling. IL-1β inhibits fibroblast proliferation by inducing cell cycle arrest during the G1/S transition (Palmer et al., 1995). However, extended exposure of cardiac fibroblasts to inflammatory cytokines, such as IL-1β, was observed in the prolonged inflammatory phase post-MI. The long-term action of IL-1 β on cardiac fibroblasts delays or prevents the transition from the pro-inflammatory stage to the proliferative phase of heart repair, which may induce adverse remodeling and heart failure by reducing heart contractility and promoting cardiomyocyte apoptosis (Bujak and Frangogiannis, 2009). In contrast to IL-1β, TNF-α may indirectly induce the profibrotic activity of fibroblasts by increasing the expression of type 1 angiotensin II (AT1) receptors. Indeed, most inflammatory cytokines that cooperate in the pro-inflammatory activation of cardiac fibroblasts can demonstrate effects on fibrotic fibroblast activity. In our study, we revealed that macrophages secreting IL-1β, TNF-α, and IL-6 play a significant role in mediating cardiac fibroblast *trans*-differentiation, which is in accordance with the conclusions derived from the aforementioned previous studies.

Curcumin has roles in various cardiovascular diseases, including ischemic heart, pressure overload heart, and metabolic disorder-related cardiac diseases. It is well-established that curcumin can directly exerts cardio-protective effect by targeting cardiomyocyte through various of signaling pathway, like disrupts the p300/GATA4 complex and represses agonist-and p300-induced hypertrophic responses in cardiomyocytes (Morimoto et al., 2008)or activates the autophagy by upregulating AMPK and JNK1 to alleviate the apoptosis of cardiomyocytes under ischemic stimulation (Yao et al., 2018). However, in our study, we did not confirm the therapeutic effect of curcumin directly in cardiomyocytes, which reflected by the fact that no significant change in cardiomyocyte apoptosis was found in curcumin treated group in mice heart 7 days after MI compared with MI only. In addition, previous studies have also reported that the administration of curcumin in ischemic diseases can salvage the functionality of endothelium (Pu et al., 2013), in our study, we also detected the quantity of CD31 and vWF in ischemic border area but demonstrated no significant difference in the presence or absence of curcumin 28 days after MI (data not shown). The findings illustrated above strongly hints that the regulation of cardiac fibrosis by curcumin may play pivotal role in improving cardiac function after MI. Although it has been well-validated that curcumin inhibits inflammation and anti-ROS as described previously, in a number of studies, curcumin was reported to be directly associated with collagen deposition and fibroblast proliferation. In ischemia-reperfusion (I/R) model, curcumin has been shown to function in regulating both ECM construction and anti-oxidative stress. The downregulated expression of TGF-β1 and *p*-SMAD2/3 and the upregulation of SMAD7 contributed to this therapeutic effect (Wang et al., 2012). To our surprise, we did not observe obvious inhibition of cardiac fibroblast *trans*-differentiation via direct treatment of curcumin with NRCF, and phosphorylated SMAD2/3 levels were found to be equal in the presence or absence of curcumin in NRCF, indicating that curcumin only inhibited cardiac fibrosis through macrophages in our study.

The TGF-β1/SMADs signaling pathway has been found to play an important role in inducing and exacerbating the pathological process of myocardial fibrosis after MI (Walton et al., 2017). Specifically, upon binding with the TGF-β1 receptor on the surface of myocardial fibroblasts, TGF-β1 stimulates phosphorylation of downstream SMADs protein (mainly SMAD2/3) and translocation into the nucleus in combination with SMAD4, induces myocardial fibroblast proliferation, phenotypic transformation, and collagen synthesis and ultimately promotes extracellular matrix formation and myocardial fibrosis. In our study, we demonstrated that cardiac fibroblasts received pro-fibrotic cytokines secreted from activated macrophages, thereby enhancing the expression level of IL-18, which in turn promotes phosphorylated SMAD2/3 and subsequent nuclear translocation of *p*-SMAD2/3, which could be inhibited by curcumin administration on macrophages.

This study had several limitations. First, we detected significantly decreased $CD3^+$ cells in the acute phase post-MI; however, the effect of curcumin on $CD3^+$ cells have not been clarified in this study, as T cells have relatively less connection with fibrosis procedure post injury; however, it is worth studying in the future. Second, the polarization of macrophages (monocytes) post-MI needs to be validated in future studies because both M1 type macrophages (which secrete IL-6, IL1β, and TNF-α) and M2 type macrophages, which serve as reparative forms post injury, can initiate cardiac fibrosis. Finally, because IL-18 serves mostly as a secreted cytokine to exert its biological function, it is to be identified whether IL-18 directly promotes SMAD2/3 nuclear translocation using a genetic knock-out/knock-in animal model.

In summary, our study revealed that the administration of curcumin significantly ameliorated inflammation in the acute phase, as reflected by the promotion of macrophage apoptosis, accompanied by decreased pro-inflammatory cytokine secretion, including IL-6, IL1b, and TNF-α. The alteration of macrophage status is subsequently linked with resident cardiac fibrosis, resulting in decreased expression of IL-18 in fibroblasts and hampered phosphorylation of SMAD2/3 in cardiac fibroblasts, reduced excessive collagen synthesis, and preserved long-term cardiac function post-MI. These findings suggest that curcumin has potential as a potent therapeutic target in treating adverse remodeling in ischemic heart disease.

DATA AVAILABILITY STATEMENT

The datasets presented in this study can be found in online repositories. The names of the repository/repositories and accession number(s) can be found in the article/**Supplementary Material**.

ETHICS STATEMENT

The animal study was reviewed and approved by the second affliated hospital of zhejiang university school of medicine ethics committee. Written informed consent was obtained from the owners for the participation of their animals in this study.

AUTHOR CONTRIBUTIONS

NC organized and designed this study and wrote the manuscript, ZJ orchestrated the whole study and performed data analysis, YC and ZZ did all pathology studies, JH did the flow cytometry experiments, QC and TH helped with the animal model. All authors contributed to the revision of the manuscript and approved the final version.

FUNDING

This work was supported by grants from National Natural Science Foundation of China (No.81900328 for CN), the Fellowship of China Postdoctoral Science Foundation (No. 2020T130587 and No. 2019M652120 for CN) and the Fundamental Research Funds for the Central Universities (No. 2019FZA7007 for CN).

SUPPLEMENTARY MATERIAL

The Supplementary Material for this article can be found online at: https://www.frontiersin.org/articles/10.3389/fphar.2021.784041/full#supplementary-material

REFERENCES

Berk, B. C., Fujiwara, K., and Lehoux, S. (2007). ECM Remodeling in Hypertensive Heart Disease. *J. Clin. Invest.* 117 (3), 568–575. doi:10.1172/JCI31044

Bujak, M., and Frangogiannis, N. G. (2009). The Role of IL-1 in the Pathogenesis of Heart Disease. *Arch. Immunol. Ther. Exp. (Warsz)* 57 (3), 165–176. doi:10.1007/s00005-009-0024-y

Bujak, M., Ren, G., Kweon, H. J., Dobaczewski, M., Reddy, A., Taffet, G., et al. (2007). Essential Role of Smad3 in Infarct Healing and in the Pathogenesis of Cardiac Remodeling. *Circulation* 116 (19), 2127–2138. doi:10.1161/CIRCULATIONAHA.107.704197

Chun-Bin, S., Yi, Y., Qin-Yi, W., Yang, L., Jing-Ze, Y., Hai-Jing, X., et al. (2020). The Main Active Components of Curcuma Zedoaria Reduces Collagen Deposition in Human Lung Fibroblast via Autophagy. *Mol. Immunol.* 124, 109–116. doi:10.1016/j.molimm.2020.05.017

Dewald, O., Frangogiannis, N. G., Zoerlein, M., Duerr, G. D., Klemm, C., Knuefermann, P., et al. (2003). Development of Murine Ischemic Cardiomyopathy Is Associated with a Transient Inflammatory Reaction and Depends on Reactive Oxygen Species. *Proc. Natl. Acad. Sci. U S A.* 100 (5), 2700–2705. doi:10.1073/pnas.0438035100

Elliott, E. I., and Sutterwala, F. S. (2015). Initiation and Perpetuation of NLRP3 Inflammasome Activation and Assembly. *Immunol. Rev.* 265 (1), 35–52. doi:10.1111/imr.12286

Epelman, S., Lavine, K. J., Beaudin, A. E., Sojka, D. K., Carrero, J. A., Calderon, B., et al. (2014). Embryonic and Adult-Derived Resident Cardiac Macrophages Are Maintained through Distinct Mechanisms at Steady State and during Inflammation. *Immunity* 40 (1), 91–104. doi:10.1016/j.immuni.2013.11.019

Frangogiannis, N. G. (2012). Regulation of the Inflammatory Response in Cardiac Repair. *Circ. Res.* 110 (1), 159–173. doi:10.1161/CIRCRESAHA.111.243162

Gao, S., Zhou, J., Liu, N., Wang, L., Gao, Q., Wu, Y., et al. (2015). Curcumin Induces M2 Macrophage Polarization by Secretion IL-4 And/or IL-13. *J. Mol. Cel Cardiol* 85, 131–139. doi:10.1016/j.yjmcc.2015.04.025

He, X., Li, G., Chen, Y., Xiao, Q., Yu, X., Yu, X., et al. (2020). Pharmacokinetics and Pharmacodynamics of the Combination of Rhein and Curcumin in the Treatment of Chronic Kidney Disease in Rats. *Front. Pharmacol.* 11, 573118. doi:10.3389/fphar.2020.573118

Heidt, T., Courties, G., Dutta, P., Sager, H. B., Sebas, M., Iwamoto, Y., et al. (2014). Differential Contribution of Monocytes to Heart Macrophages in Steady-State and after Myocardial Infarction. *Circ. Res.* 115 (2), 284–295. doi:10.1161/CIRCRESAHA.115.303567

Honold, L., and Nahrendorf, M. (2018). Resident and Monocyte-Derived Macrophages in Cardiovascular Disease. *Circ. Res.* 122 (1), 113–127. doi:10.1161/CIRCRESAHA.117.311071

Hu, X., Yu, S. P., Fraser, J. L., Lu, Z., Ogle, M. E., Wang, J. A., et al. (2008). Transplantation of Hypoxia-Preconditioned Mesenchymal Stem Cells Improves Infarcted Heart Function via Enhanced Survival of Implanted Cells and Angiogenesis. *J. Thorac. Cardiovasc. Surg.* 135 (4), 799–808. doi:10.1016/j.jtcvs.2007.07.071

Hulsmans, M., Clauss, S., Xiao, L., Aguirre, A. D., King, K. R., Hanley, A., et al. (2017). Macrophages Facilitate Electrical Conduction in the Heart. *Cell* 169 (3), 510–e20. doi:10.1016/j.cell.2017.03.050

Kawaguchi, M., Takahashi, M., Hata, T., Kashima, Y., Usui, F., Morimoto, H., et al. (2011). Inflammasome Activation of Cardiac Fibroblasts Is Essential for Myocardial Ischemia/reperfusion Injury. *Circulation* 123 (6), 594–604. doi:10.1161/CIRCULATIONAHA.110.982777

Kocaadam, B., and Şanlier, N. (2017). Curcumin, an Active Component of Turmeric (Curcuma Longa), and its Effects on Health. *Crit. Rev. Food Sci. Nutr.* 57 (13), 2889–2895. doi:10.1080/10408398.2015.1077195

Kong, P., Christia, P., and Frangogiannis, N. G. (2014). The Pathogenesis of Cardiac Fibrosis. *Cell Mol Life Sci* 71 (4), 549–574. doi:10.1007/s00018-013-1349-6

Li, B., Hu, Y., Zhao, Y., Cheng, M., Qin, H., Cheng, T., et al. (2017). Curcumin Attenuates Titanium Particle-Induced Inflammation by Regulating Macrophage Polarization *In Vitro* and *In Vivo*. *Front. Immunol.* 8, 55. doi:10.3389/fimmu.2017.00055

Morimoto, T., Sunagawa, Y., Kawamura, T., Takaya, T., Wada, H., Nagasawa, A., et al. (2008). The Dietary Compound Curcumin Inhibits P300 Histone Acetyltransferase Activity and Prevents Heart Failure in Rats. *J. Clin. Invest.* 118 (3), 868–878. doi:10.1172/JCI33160

Palmer, J. N., Hartogensis, W. E., Patten, M., Fortuin, F. D., and Long, C. S. (1995). Interleukin-1 Beta Induces Cardiac Myocyte Growth but Inhibits Cardiac Fibroblast Proliferation in Culture. *J. Clin. Invest.* 95 (6), 2555–2564. doi:10.1172/JCI117956

Prasad, S., Gupta, S. C., Tyagi, A. K., and Aggarwal, B. B. (2014). Curcumin, a Component of golden Spice: from Bedside to Bench and Back. *Biotechnol. Adv.* 32 (6), 1053–1064. doi:10.1016/j.biotechadv.2014.04.004

Priyadarsini, K. I. (2014). The Chemistry of Curcumin: from Extraction to Therapeutic Agent. *Molecules* 19 (12), 20091–20112. doi:10.3390/molecules191220091

Pu, Y., Zhang, H., Wang, P., Zhao, Y., Li, Q., Wei, X., et al. (2013). Dietary Curcumin Ameliorates Aging-Related Cerebrovascular Dysfunction through the AMPK/uncoupling Protein 2 Pathway. *Cell Physiol Biochem* 32 (5), 1167–1177. doi:10.1159/000354516

Sandanger, Ø., Ranheim, T., Vinge, L. E., Bliksøen, M., Alfsnes, K., Finsen, A. V., et al. (2013). The NLRP3 Inflammasome Is Up-Regulated in Cardiac Fibroblasts and Mediates Myocardial Ischaemia-Reperfusion Injury. *Cardiovasc. Res.* 99 (1), 164–174. doi:10.1093/cvr/cvt091

South, E. H., Exon, J. H., and Hendrix, K. (1997). Dietary Curcumin Enhances Antibody Response in Rats. *Immunopharmacol Immunotoxicol* 19 (1), 105–119. doi:10.3109/08923979709038536

Tallquist, M. D., and Molkentin, J. D. (2017). Redefining the Identity of Cardiac Fibroblasts. *Nat. Rev. Cardiol.* 14 (8), 484–491. doi:10.1038/nrcardio.2017.57

Walton, K. L., Johnson, K. E., and Harrison, C. A. (2017). Targeting TGF-β Mediated SMAD Signaling for the Prevention of Fibrosis. *Front. Pharmacol.* 8, 461. doi:10.3389/fphar.2017.00461

Wang, N. P., Wang, Z. F., Tootle, S., Philip, T., and Zhao, Z. Q. (2012). Curcumin Promotes Cardiac Repair and Ameliorates Cardiac Dysfunction Following Myocardial Infarction. *Br. J. Pharmacol.* 167 (7), 1550–1562. doi:10.1111/j.1476-5381.2012.02109.x

Wang, Q., Ye, C., Sun, S., Li, R., Shi, X., Wang, S., et al. (2019). Curcumin Attenuates Collagen-Induced Rat Arthritis via Anti-inflammatory and Apoptotic Effects. *Int. Immunopharmacol* 72, 292–300. doi:10.1016/j.intimp.2019.04.027

Wynn, T. A., and Vannella, K. M. (2016). Macrophages in Tissue Repair, Regeneration, and Fibrosis. *Immunity* 44 (3), 450–462. doi:10.1016/j.immuni.2016.02.015

Xiao, C., Wang, K., Xu, Y., Hu, H., Zhang, N., Wang, Y., et al. (2018). Transplanted Mesenchymal Stem Cells Reduce Autophagic Flux in Infarcted Hearts via the Exosomal Transfer of miR-125b. *Circ. Res.* 123 (5), 564–578. doi:10.1161/CIRCRESAHA.118.312758

Yao, Q., Ke, Z. Q., Guo, S., Yang, X. S., Zhang, F. X., Liu, X. F., et al. (2018). Curcumin Protects against Diabetic Cardiomyopathy by Promoting Autophagy and Alleviating Apoptosis. *J. Mol. Cel Cardiol* 124, 26–34. doi:10.1016/j.yjmcc.2018.10.004

Conflict of Interest: The authors declare that the research was conducted in the absence of any commercial or financial relationships that could be construed as a potential conflict of interest.

The handling editor declared a shared parent affiliation with the authors at the time of the review.

frontiers in Pharmacology

ORIGINAL RESEARCH
published: 08 February 2022
doi: 10.3389/fphar.2021.834192

Stachytine Hydrochloride Improves Cardiac Function in Mice with ISO-Induced Heart Failure by Inhibiting the α-1,6-Fucosylation on N-Glycosylation of β1AR

Panwei Hu[1†], Shuting Guo[1†], Songru Yang[1], Sining Wang[2], Sai Wang[1], Xiaoli Shan[3], Pei Zhao[3], Wei Guo[4], Ming Xu[5], Chen Zhang[4], Rong Lu[1] and Huihua Chen[6*]*

[1]School of Basic Medical Science, Shanghai University of Traditional Chinese Medicine, Shanghai, China, [2]Department of Comprehensive Internal Medicine, Tongde Hospital of Zhejiang Province, Hangzhou, China, [3]Public Laboratory Platform, School of Basic Medical Science, Shanghai University of Traditional Chinese Medicine, Shanghai, China, [4]Department of Pathology, Shanghai University of Traditional Chinese Medicine, Shanghai, China, [5]Department of Physiology, Shanghai University of Traditional Chinese Medicine, Shanghai, China, [6]Teaching and Research Department of Basic Theory of Traditional Chinese Medicine, Shanghai University of Traditional Chinese Medicine, Shanghai, China

OPEN ACCESS

Edited by:
Ling Zhang,
Zhejiang Chinese Medical University, China

Reviewed by:
Keyang Zhu,
Ningbo University, China
Mingbao Lin,
Chinese Academy of Medical Sciences and Peking Union Medical College, China

***Correspondence:**
Huihua Chen
chenhuihua@shutcm.edu.cn
Rong Lu
lurong@shutcm.edu.cn

[†]These authors have contributed equally to this work and share first authorship

Specialty section:
This article was submitted to Ethnopharmacology, a section of the journal Frontiers in Pharmacology

Received: 13 December 2021
Accepted: 31 December 2021
Published: 08 February 2022

Citation:
Hu P, Guo S, Yang S, Wang S, Wang S, Shan X, Zhao P, Guo W, Xu M, Zhang C, Lu R and Chen H (2022) Stachytine Hydrochloride Improves Cardiac Function in Mice with ISO-Induced Heart Failure by Inhibiting the α-1,6-Fucosylation on N-Glycosylation of β1AR. Front. Pharmacol. 12:834192. doi: 10.3389/fphar.2021.834192

Background: Cardiovascular diseases have become a major public health problem that seriously threatens human health. The cumulative effects of various cardiovascular events will eventually develop into chronic heart insufficiency and even heart failure, and the β1 adrenergic receptor signal pathway plays an important role in this process. Stachytine hydrochloride is the main active ingredient of Yimucao, which is a traditional Chinese medicine used to treat gynecological diseases. Modern studies have found that stachytine hydrochloride has a good cardioprotective effect, but it is still unclear whether stachytine hydrochloride has an effect on the β1 adrenergic receptor signal pathway. The purpose of this study is to explore the effect of stachytine hydrochloride on the β1 adrenergic receptor signal pathway.

Method: In this study, a continuous infusion of isoproterenol (40 mg/kg/day) was administered to mice and ventricular myocytes explored the potential mechanism of stachytine hydrochloride (12 mg/kg/day) on the β1 adrenergic receptor signal pathway in the heart. Evaluate changes in cardiac morphology and function by echocardiography, cardiac hemodynamics, and histological methods, and detect molecular changes by Western blot and immunofluorescence. Treat primary cultured adult mouse or neonatal rat ventricular myocytes with or without isoproterenol (0.1 μMol), PNGase F (10^{-2} units/ml),

Abbreviations: β1AR, β1 adrenergic receptors; AMVMs, adult mouse ventricular myocytes; BW, body weight; cAMP, cyclic adenosine monophosphate; dP/dtmax, peak rate of pressure rise; dP/dtmin, peak rate of pressure decline; EF, ejection fraction; ELISA, enzyme-linked immunosorbent assay; FUT8, α-1,6-fucosyltransferase; GPCRs, G protein-coupled receptors; HW, heart weight; ISO, isoproterenol; LCA, lens Culinaris Agglutinin; LW, lung weight; MGAT3, β-1,4-mannosylglycoprotein 4-β-N-acetylglucosaminyltransferase; MGAT4a.α-1,3-mannosyl-glycoprotein 4-β-N-acetylglucosaminyltransferase A; NRVMs, neonatal rat ventricular myocytes; PBS, phosphate-buffered saline; PCA, principal component analysis; Pmax, maximum left ventricular pressure; Pmin, minimum left ventricular pressure; PNGF, PNGase F; PKA, protein kinase A; Sta, stachytine hydrochloride; SW, stroke work; Tau, relaxation time constant; TL, tibial length; TTP, time to peak; Vmax, max of volume; Vmin, min of volume.

and stachytine hydrochloride (10 μMol) at different time points. Detect α-1,6-fucosylation on N-glycosylation, calcium transient, contraction, and relaxation function and related signals.

Results: Stachytine hydrochloride reduces cardiac remodeling and modulates hemodynamic parameters during chronic β1 adrenergic receptor activation *in vivo*. The N-glycosylation of β1 adrenergic receptors decreased after continuous isoproterenol stimulation, while stachytine hydrochloride can increase the N-glycosylation of β1AR in the heart of mice with isoproterenol-induced heart failure. Decreased N-glycosylation of β1 adrenergic receptors will downregulate the cAMP/PKA signal pathway and inhibit myocardial excitation and contraction coupling. Stachytine hydrochloride significantly reduced isoproterenol-induced cardiac N-linked glycoproteins with α-1,6-fucosylation.

Conclusion: Our results show that stachytine hydrochloride inhibits the synthesis of α-1,6-fucosylation on the N-terminal sugar chain by reducing α-1,6-fucosyltransferase (FUT8) and α-1,3-mannosyl-glycoprotein 4-β-N-acetylglucosaminyltransferase A (MGAT4a), upregulating the N-glycosylation level on β1 adrenergic receptors, and maintaining cAMP/PKA signal pathway activation.

Keywords: heart failure, stachydrine hydrochloride, β1 adrenergic receptors, N-glycosylation, α-1,6-fucosylation

INTRODUCTION

G protein-coupled receptors (GPCRs), also known as seven-pass transmembrane receptors, are the largest family of receptors on the cell membrane (Bjarnadóttir et al., 2006). They can be activated by many ligands and have become important targets for the diagnosis and treatment of various diseases. GPCRs can undergo many kinds of post-translational modifications, such as glycosylation, phosphorylation, and ester acylation. Among them, glycosylation is a very common post-translational modification of membrane proteins in living cells (Chuh et al., 2016), and N-glycosylation is the most common glycosylation modification. N-glycosylation modification may be very important for the expression and folding of membrane proteins on the cell surface (Dennis et al., 2009) and affect the expression level of many kinds of GPCRs on the cell membrane surface (He et al., 2002; Dennis et al., 2009; Soto and Trejo, 2010).

Leonurus japonicus Houtt. (Yimucao) is a traditional Chinese medicine. It is often used to treat gynecological diseases because it promotes blood circulation to remove blood stasis and induces diuresis to alleviate edema (Miao et al., 2019). Modern experiments and clinical studies have shown that Yimucao can relieve myocardial ischemia, increase coronary blood flow, and improve heart function. Because it can improve hemodynamics and hemorheology, it has a protective effect on protecting the cardiovascular system (Liu et al., 2012). Our research group conducted a series of studies on the effect of stachytine hydrochloride (Sta), the main active component of Yimucao, and found that Sta can inhibit norepinephrine (Zhang et al., 2014), phenylephrine (Zheng et al., 2020), and TAC-induced myocardial hypertrophy; reduce calcium leakage; maintain calcium homeostasis; inhibit myocardial fibrosis (Liu et al., 2019); and improve cardiac function (Chen et al., 2020). However, the molecular target of Sta is still unclear.

Under physiological conditions, β1AR can bind to and activate Gs protein after being activated. Then, the synthesis of cyclic adenosine monophosphate (cAMP) increases, which activates protein kinase A (PKA) and downstream signaling molecules to enhance myocardial contractility. During the development of heart failure, the continuous increase of catecholamines in the blood promotes the abnormality of the β-adrenergic receptor system. The content of β1 adrenergic receptors in the heart was significantly downregulated, the density of β1AR on the cell membrane was downregulated by 50%, while β2AR did not show this change (Bristow et al., 1982; Bristow et al., 1986; Bristow et al., 1993). Relevant studies have shown that N-glycosylation on β1AR may regulate receptor dimerization on the cell membrane surface by reducing receptor expression (He et al., 2002). Whether Sta regulates the N-glycosylation of myocardial β1AR and maintains the stable number of β1AR, thereby improving the contractile function of the heart, is the focus of this article.

MATERIALS AND METHODS

Chemicals and Reagents

Stachydrine hydrochloride (purity > 98%) was purchased from the National Institutes for Food and Drug Control (Beijing, China). All the other drugs were from Sigma-Aldrich (St Louis, MO, United States), except for those mentioned.

Animal Manipulation

All procedures in C57BL/6J mice and neonatal Wistar rats were approved by the Animal Care and Use Committee of Shanghai

University of Traditional Chinese Medicine (SCXK2016-0011). All animal care and experimental protocols were in compliance with the *Guide for the Care and Use of Laboratory Animals* (NIH, 8th Edition, 2011). Adult male C57BL/6J mice (age, 7 weeks) were purchased from the Shanghai Laboratory Animal Center (Shanghai, China). Animals were housed in an individually vented cage system under a controlled 12-h-light/dark cycle with free access to food and water. Isoprenaline (40 mg/kg/day, ISO group) or vehicle (saline, Sham group) were infused subcutaneously to mice with mini-osmotic pumps (Alzet model 1002, Durect, Cupertino, CA, United States) for 14 days. Sta was orally administered at a constant dose of 12 mg/kg/day to the ISO-infused (ISO + Sta) group and saline-infused (Sham + Sta) group. After experiment completion, mice were euthanized by cervical dislocation. Their hearts were immediately snap-frozen in liquid nitrogen as soon as they were removed during the heart operation and stored at −80°C until use.

Adult Mouse Ventricular Myocytes Culture and Treatment

After mice were anesthetized by intraperitoneal injection with 1% pentobarbital sodium, the Langendorff constant flow perfusion system was used to intubate aorta in mice, and then collagenase type II (#17101015, Thermo Fisher Scientific, United States) was used to perfuse heart. The myocardial tissue was cut into small pieces; thereafter, myocardial cells were obtained after repeated gentle blowing and beating. Isolated cardiomyocytes were inoculated in a 35-mm glass bottom dish wrapped with laminin (#23017015, Thermo Fisher Scientific, United States) and attached to the wall in a 5% CO_2 incubator at 37°C for 2 h. The blank control was given with serum-free M199 medium (GIBCO, United States), while PNGase F (10^{-2} units/ml) purchased from NEB were administered to the experiment group for 2 h. After treatment, under the stimulation conditions of bright field and 1 Hz field, the motion of myocardial sarcomere was tracked by using Si-H optical sarcomere spacing system (WPI, United States) according to the change of gray value of myocardial sarcomere. The systolic and diastolic functions of single myocardial cells were calculated by Micro-Manger 1.4 software (University of California San Francisco).

Neonatal Rat Ventricular Myocytes Culture and Treatment

Primary mouse cardiomyocytes were isolated from Wistar rats within 24 h of birth by serial enzymatic digestion. When the neonatal rats were decapitated, their hearts were quickly excised and placed in phosphate buffer saline. After cleaning and removing the atrial tissue, the ventricles were chopped with scissors and digested using a solution containing collagenase II and 0.25% trypsin (#25200072, Thermo Fisher Scientific, United States). Cells were plated on six-well plates or confocal dishes and maintained in DMEM/F12 medium (GIBCO, United States), containing 10% fetal bovine serum for 48 h at 37°C in a 5% CO_2 incubator as described previously.

For *in vitro* experiments, in order to determine the most effective time of glycosylation, neonatal rat cardiomyocytes were exposed to isoprenaline at several time points (0, 15, 30, 60, 360, and 720 min). When the optical time of administration was confirmed, cardiomyocytes were dosed to the following groups: control group (Con), Con + Sta (10 μMol) group, ISO (0.1 μMol) group, and ISO (0.1 μMol) + Sta (10 μMol) group. In all *in vitro* assays, the cells were incubated with DMEM/F12 without fetal bovine serum for synchronization.

Transcriptome Library Construction and Sequencing

Total mRNAs in Con and ISO groups were extracted from mouse ventricular tissue using TRIzol (Life Technologies, Carlsbad, CA, United States). The mRNA-seq libraries were prepared using the Hieff NGS™ MaxUp Dual-mode mRNA Library Prep Kit for Illumina® (YEASEN, 12301ES96, Shanghai, China); then, the Illumina sequencing platform HiSeq X Ten (Illumina, Shanghai OE Biotech Co., Ltd.) was used to sequence these libraries. HISAT2 software was selected to map the filtered sequenced reads to the reference genome, TPM (Transcripts per kilobase of exon per million mapped reads) were calculated as follows. The differential genes (DEGs) were next determined with DESeq2 R package following the standard |log FC | > 1 and adjusted p-value < 0.05. R package clusterProfiler were used to perform GO function enrichment analysis and KEGG pathway enrichment analysis. The data presented in the study was deposited in the NCBI SRA BioProject repository, and the accession number was PRJNA793393.

Western Blot Assay and Antibodies

Membrane protein and cytoplasmic protein in myocardial tissue were extracted using a Mem-PER Plus Membrane Protein Extraction kit (#89842, Thermo Fisher Scientific, United States). Cardiomyocytes in a six-well plate were rinsed with phosphate-buffered saline (PBS) before being scraped and lysed in RIPA assay (#P0013B, Beyotime, Beijing, China) buffer supplemented with protease inhibitor cocktail and phosphatase inhibitor cocktail II (Roche, Mannheim, Germany). After centrifugation at 14,000 g for 20 min, 40 μg of the supernatant protein was obtained and subsequently divided into two same portions. Lysis was added into the first portion (without PNGaseF) to make the same volume with the second portion. While on the second portion, 20 μg of protein is denatured with 1x Glycoprotein Denaturing Buffer at 100°C for 10 min according to their respective processing protocols. After the addition of 10× NP-40 and GlycoBuffer two into the second group, 1 μl of PNGase F (20 μg/unit) was added and the reaction mix is incubated for 2 h at 37°C. Finally, all samples were prepared for electrophoresis by the addition of 5× loading buffer and boiled for 10 min. Then, protein lysates were separated using 10% polyacrylamide gel and transferred to polyvinylidene fluoride membranes (EMD Millipore, Billerica, MA, United States) on Mini Trans-Blot Cell (Bio-Rad Laboratories, Hercules, CA, United States) blocked with BSA (Weiao Biotechnology Co, Shanghai, China). Membranes were blocked in 5% BSA (Weiao Biotechnology Co, Shanghai, China) for 1 h at room temperature and successively incubated with primary antibodies

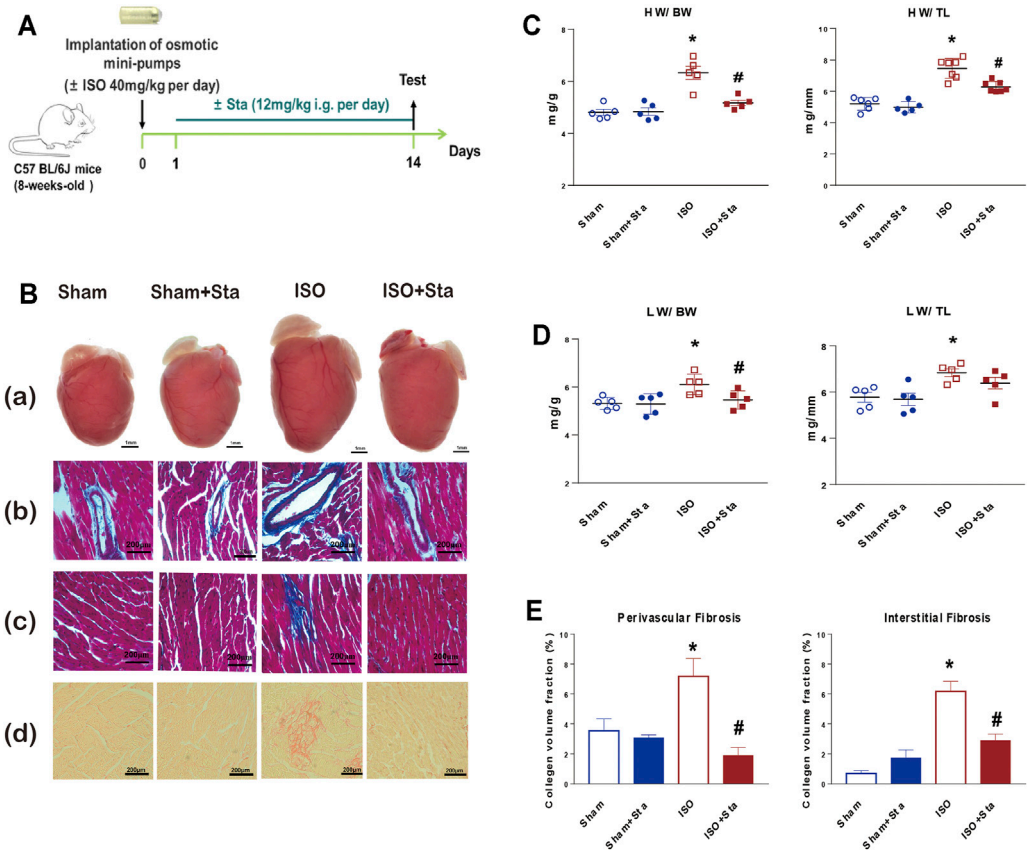

FIGURE 1 | Stachydrine hydrochloride reduces cardiac remodeling induced by ISO in mice. **(A)** Timeline diagram of phenylephrine in mice. **(B)** Cardiac images: **(a)** comparison of heart size in mice that underwent Sham, Sham + Sta, ISO only, or ISO + Sta treatment; **(b, c)** collagen deposition was further recorded using Masson staining on 6-μm-thick heart sections; **(d)** collagen deposition was further recorded using Sirius red staining on 6-μm-thick heart sections. **(C)** HW:BW and HW:TL ($n = 5$ in each group). **(D)** LW:BW and LW:TL ($n = 5$ in each group). **(E)** Quantification of cardiac perivascular and interstitial fibrosis ($n = 5$ in each group). The data are expressed as mean ± standard error of mean, $^{*}p < 0.05$ vs. Sham; $^{\#}p < 0.05$ vs. ISO. ISO, isoproterenol; Sta, stachydrine hydrochloride; HW, heart weight; BW, body weight; LW, lung weight; TL, tibial length.

overnight at 4°C. GAPDH was employed as the internal reference. The following primary antibodies were used in Western blot assay: Anti-beta 1 Adrenergic Receptor (β1AR) (1:1,000, ab3442, Abcam, Cambridge, CB, United Kingdom) and Anti-GAPDH (1: 3,000, #97166, Cell Signaling Technology, Beverly, MA, United States). Membranes were incubated with appropriate secondary antibody for 1 h at room temperature. Secondary antibody was selected as follows: HRP Goat Anti-Rabbit IgG (1:3,000, AS014, Abclonal, Wuhan, China) or HRP Goat Anti-Mouse IgG (1:5,000, AS014, Abclonal, Wuhan, China). Signal was detected using the ECL system (Image Quant LAS 4000, Amersham Biosciences, GE Healthcare, Diegem, Belgium) according to the manufacturer's instructions.

Lens Culinaris Agglutinin Lectin Blot Assay and Antibodies

Protein sample preparation and SDS-PAGE procedures were performed as Western blot. The following antibodies were used in lectin blot: LCA (Biotinylated-LCA) (1:1,000, B-1045-5, VectorLab, Burlingame, VT, United States) and Streptavidin-HRP (1:3000, #3999, Cell Signaling Technology, Beverly, MA, United States).

Immunofluorescence

The cardiac tissues in different groups were prepared into frozen sections for immunofluorescence analysis. For cellular immunofluorescence, cells were washed three times with PBS. When the samples were prepared and fixed with 4% PFA for 10 min, 5% BSA was used to block for 1 h before the addition of primary antibodies. The primary antibodies were as follows: LCA (Fluorescein-LCA) (1:1,000, FL-1041-5, VectorLab, Burlingame, VT, United States) and β1AR (1:100, ab3442, Abcam, Cambridge, CB, United Kingdom). Secondary antibodies coupled with Alexa Fluor 594-conjugated Goat Anti-Rabbit (1:200, AS039, Abclonal, Wuhan, China) were used, and nuclei counterstaining was performed using DAPI (1:1,000, Beyotime, Beijing, China) for 10 min at room temperature for cell nuclei staining.

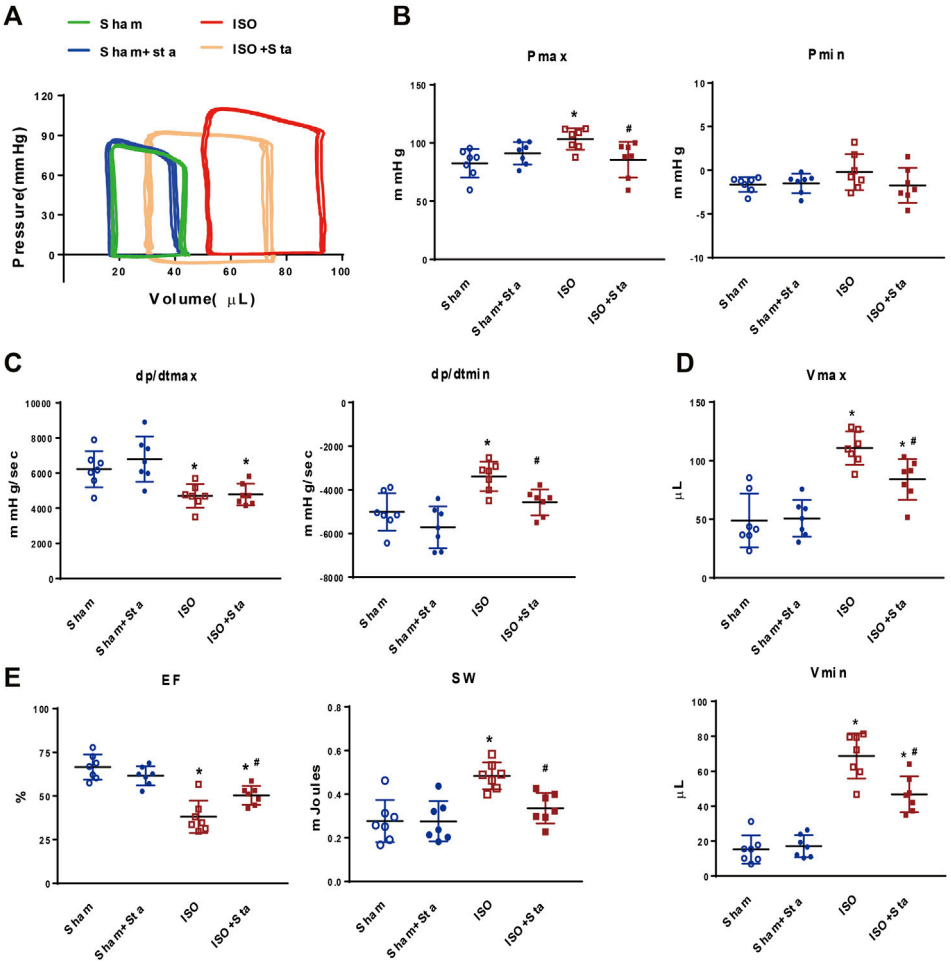

FIGURE 2 | Stachydrine hydrochloride modulates hemodynamic parameters during chronic β1AR activation *in vivo*. **(A)** Representative images of hemodynamic parameters. **(B)** Quantification of Pmax and Pmin ($n = 7$ mice per experimental group). **(C)** Quantification of dP/dtmax and dP/dtmin ($n = 7$ mice per experimental group). **(D)** Quantification of Vmax and Vmin ($n = 7$ mice per experimental group). **(E)** Quantification of EF and SW ($n = 7$ mice per experimental group). Hemodynamic parameters were recorded and measured at 2 weeks after surgery. The data are expressed as mean ± standard error of mean, $^{*}p < 0.05$ versus Sham; $^{\#}p < 0.05$ versus ISO. ISO, isoproterenol; Sta, stachydrine hydrochloride; Pmax, maximum left ventricular pressure; Pmin, minimum left ventricular pressure; dP/dtmax, peak rate of pressure rise; dP/dtmin, peak rate of pressure decline; Vmax, max of volume; Vmin, min of volume; EF: left ventricle ejection fraction; SW, stroke work.

Subsequently, samples were washed with 0.5% PBST three times for 3 min each time and sealed with an anti-fluorescence quencher (P0126, Beyotime, Beijing, China).

cAMP Levels Assay

To assess cAMP concentration, H9C2 cells were plated in 384-well plates at a density of 5,000/well and incubated overnight at 37°C; on the following day, the cell culture medium was replaced with drug-containing medium according to different groups. After completion of the addition, the cAMP level was quantified using the cAMP-Glo™ Assay Kit (#V1501, Promega, United States) following the manufacturer's instructions.

PKA Activity Assay

NRVMs (5×10^5 cells/well) were isolated and seeded in a six well plate, following treatment with different agents, and total protein was harvested using lysis buffer containing phosphatase inhibitor and protease inhibitor. Immediately after, soluble proteins samples were obtained by taking the supernatant after centrifugation of the lysate at 12,000 rpm for 20 min at 4°C. Then, the supernatant was assayed for protein concentration by BCA (Beyotime, China) and their protein concentrations were all adjusted to 1 μl by lysis buffer. Finally, the supernatant protein samples' PKA activity was measured by using ProFluor PKA assay (#V1240, Promega, United States) following the kit instructions.

Enzyme-Linked Immunosorbent Assay

On completion of animal experiments, blood was collected in sterile tubes and then the mice were sacrificed immediately. After remaining still for 2 h in room temperature, the blood was centrifugated at 3,000 rpm for 10 min and the serum was

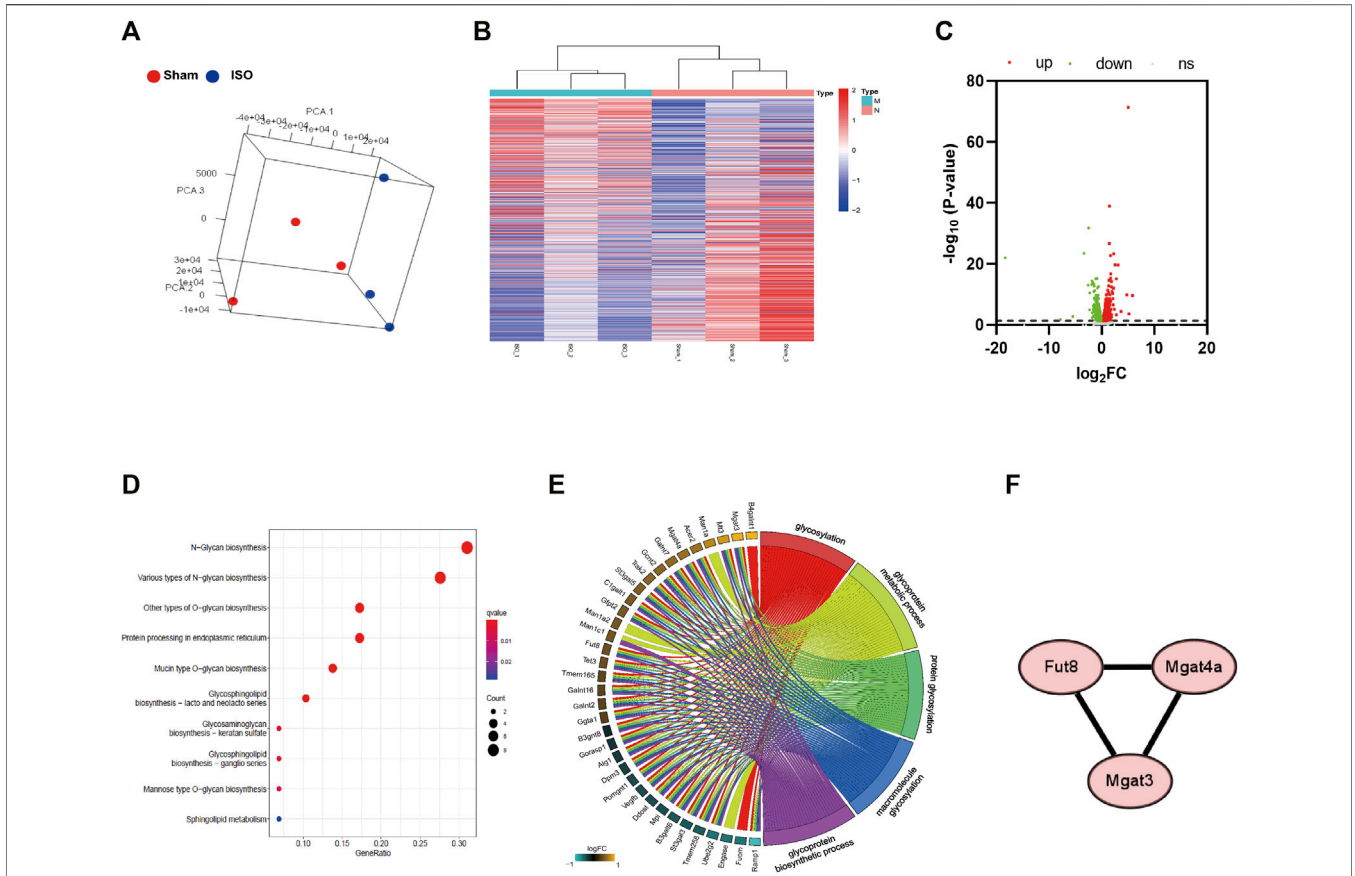

FIGURE 3 | Transcriptome analysis of heart tissue in mice with ISO-induced heart failure. **(A)** Principal Componet Analysis to visualize similarities and differences among samples. **(B,C)** Heatmap and Volcano plot indicates upregulated and downregulated genes with differential mRNA abundance in the ISO group relative to the Sham group measured using RNA sequencing. **(D)** KEGG pathway analysis was performed by mapping N-type glycosylated genes in GO enrichment. **(E)** Gene regulation network was plotted based on the number of enriched genes in GO term. **(F)** Differential genes involved in transferase during N-glycosylation synthesis between Sham and ISO groups. *n* = 5 mice per experimental group. ISO, isoproterenol; Sta, stachydrine hydrochloride.

TABLE 1 | KEGG pathway analysis was performed by mapping N-type glycosylated genes in GO enrichment.

Id	Description	Gene ratio	Gene symbol
mmu00510	N-Glycan biosynthesis	9/43	Man1a/Fut8/Man1c1/Ddost/Man1a2/Mgat4a/Mgat3/Dpm3/Alg1
mmu00513	Various types of N-glycan biosynthesis	8/43	Man1a/Fut8/Man1c1/Ddost/St3gal3/Man1a2/Mgat4a/Alg1
mmu00514	Other types of O-glycan biosynthesis	5/43	St3gal3/C1galt1/Galnt16/Galnt2/Galnt7
mmu00512	Mucin type O-glycan biosynthesis	4/43	C1galt1/Galnt16/Galnt2/Galnt7
mmu00601	Glycosphingolipid biosynthesis—lacto and neolacto series	3/43	St3gal3/Gcnt2/Ggta1
mmu04141	Protein processing in endoplasmic reticulum	5/43	Man1a/Man1c1/Ddost/Ube2g2/Man1a2
mmu00533	Glycosaminoglycan biosynthesis—keratan sulfate	2/43	Fut8/St3gal3
mmu00604	Glycosphingolipid biosynthesis—ganglio series	2/43	St3gal5/B4galnt1
mmu00515	Mannose type O-glycan biosynthesis	2/43	St3gal3/Pomgnt1
mmu01250	Mannose type O-glycan biosynthesis	2/43	Gfpt2/Mpi
mmu00600	Sphingolipid metabolism	2/43	Acer2/B4galt6
mmu00520	Amino sugar and nucleotide sugar metabolism	2/43	Gfpt2/Mpi

separated. FUT8, β-1,4-mannosylglycoprotein 4-β-N-acetylglucosaminyltransferase (MGAT3), and MGAT4a levels in serum were measured by ELISA (ELISA kit for mouse FUT8, ELISA kit for mouse MGAT3, ELISA kit for mouse MGAT4a, MEIMIAN, China) according to the manufacturer's instructions.

Statistical Analysis

The data were shown as means ± standard deviations, and statistical analysis and plotting were conducted using GraphPad Prism 7 software (GraphPad, San Diego, CA, United States). All measurements were carried out at least three times. Two groups' data analysis was compared using *t*-test, and multiple group

TABLE 2 | Gene regulation network was plotted based on the number of enriched genes in GO term.

Id	Description	Gene ratio	Gene symbol
GO: 0070085	Glycosylation	31/43	Fut8/Ddost/Tmem258/Ube2g2/Gorasp1/Tmem165/Gfpt2/St3gal3/St3gal5/Mgat4a/Mgat3/Dpm3/Tet3/Vegfb/Acer2/C1galt1/Trak2/Galnt16/Mpi/Gcnt2/Alg1/B4galnt1/Pomgnt1/Ggta1/Galnt2/Galnt7/Mt3/Ramp1/B3galt6/B3gnt8/Fuom
GO: 0009100	Glycoprotein metabolic process	33/43	Man1a/Fut8/Man1c1/Ddost/Tmem258/Ube2g2/Gorasp1/Tmem165/Gfpt2/St3gal3/Man1a2/St3gal5/Mgat4a/Mgat3/Dpm3/Tet3/Vegfb/Acer2/C1galt1/Trak2/Galnt16/Mpi/Gcnt2/Alg1/Pomgnt1/Ggta1/Galnt2/Galnt7/Mt3/Ramp1/B3galt6/B3gnt8
GO: 0006486	Protein glycosylation	29/43	Fut8/Ddost/Tmem258/Ube2g2/Gorasp1/Tmem165/Gfpt2/St3gal3/St3gal5/Mgat4a/Mgat3/Dpm3/Tet3/Vegfb/Acer2/C1galt1/Trak2/Galnt16/Mpi/Gcnt2/Alg1/Pomgnt1/Ggta1/Galnt2/Galnt7/Mt3/Ramp1/B3galt6/B3gnt8
GO: 0043413	Macromolecule glycosylation	29/43	Fut8/Ddost/Tmem258/Ube2g2/Gorasp1/Tmem165/Gfpt2/St3gal3/St3gal5/Mgat4a/Mgat3/Dpm3/Tet3/Vegfb/Acer2/C1galt1/Trak2/Galnt16/Mpi/Gcnt2/Alg1/Pomgnt1/Ggta1/Galnt2/Galnt7/Mt3/Ramp1/B3galt6/B3gnt8

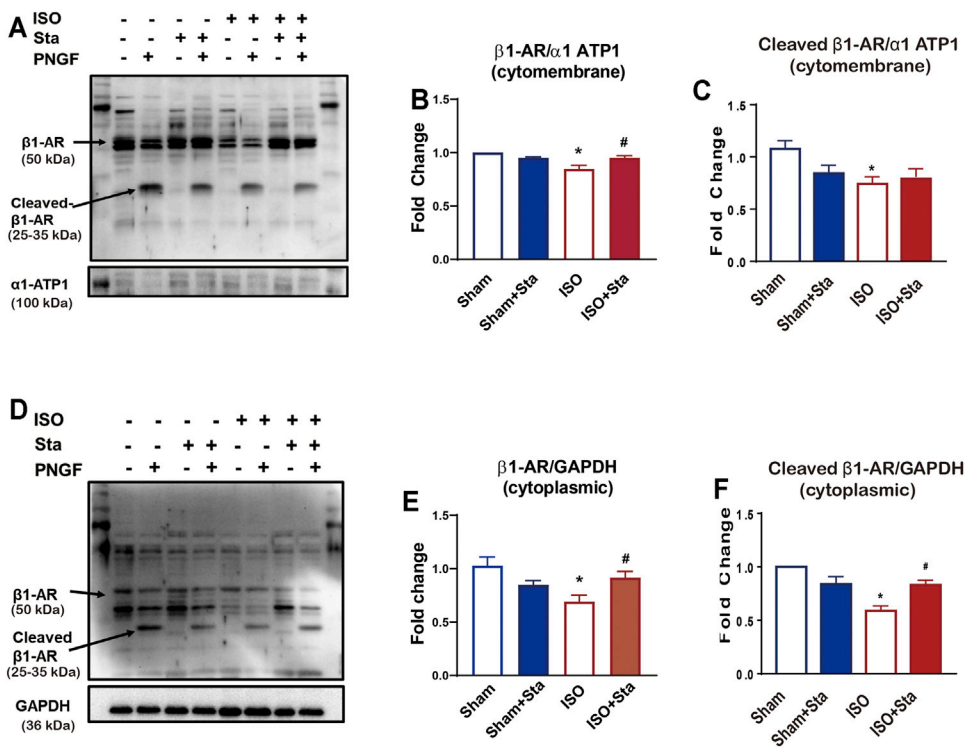

FIGURE 4 | Stachydrine hydrochloride or Sta can increase the N-glycosylation of β1AR in the heart of mice with ISO-induced heart failure. **(A)** Representative Western blot of N-glycosylation of β1AR on the cell membrane of heart tissue after PNGase F digestion. **(B,C)** Quantification of β1AR and N-glycosylation of β1AR on the cell membrane. **(D)** Representative Western blot of N-glycosylation of β1AR in the cytoplasm of heart tissue after PNGase F digestion. **(E,F)** Quantification of β1AR and N-glycosylation of β1AR in cytoplasmic. $n = 3$ mice per experimental group. The data are expressed as mean ± standard error of mean, $^{*}p < 0.05$ versus Sham; $^{\#}p < 0.05$ versus ISO. β1AR, β1 adrenergic receptors; ISO, isoproterenol; Sta, stachydrine hydrochloride.

comparisons were conducted using one-way ANOVA test. Statistically significant difference was set at $p < 0.05$.

RESULTS

Sta Reduces Cardiac Remodeling Induced by ISO in Mice

C57BL/6J mice treated with either ISO or vehicle for 14 days in the presence of Sta (from day 1 to day 14) or its vehicle are shown in **Figure 1A**. Sta prevented ISO-induced increase in HW:BW, HW:TL, and LW/BW (**Figures 1B(a)–D**). Since fibrosis is an important factor in cardiac remodeling, Masson and picrosirius red staining were used to determine cardiac collagen deposition. Histological results showed that ISO significantly induced increased interstitial and perivascular fibrosis compared with the sham group. Sta treatment significantly suppressed cardiac fibrosis elicited by ISO (**Figures 1B(b–d),E**). HW/BW, HW/TL, LW/BW, LW/TL, and interstitial and perivascular fibrosis were similar at baseline in the vehicle and Sta-treated mice (**Figure 1**).

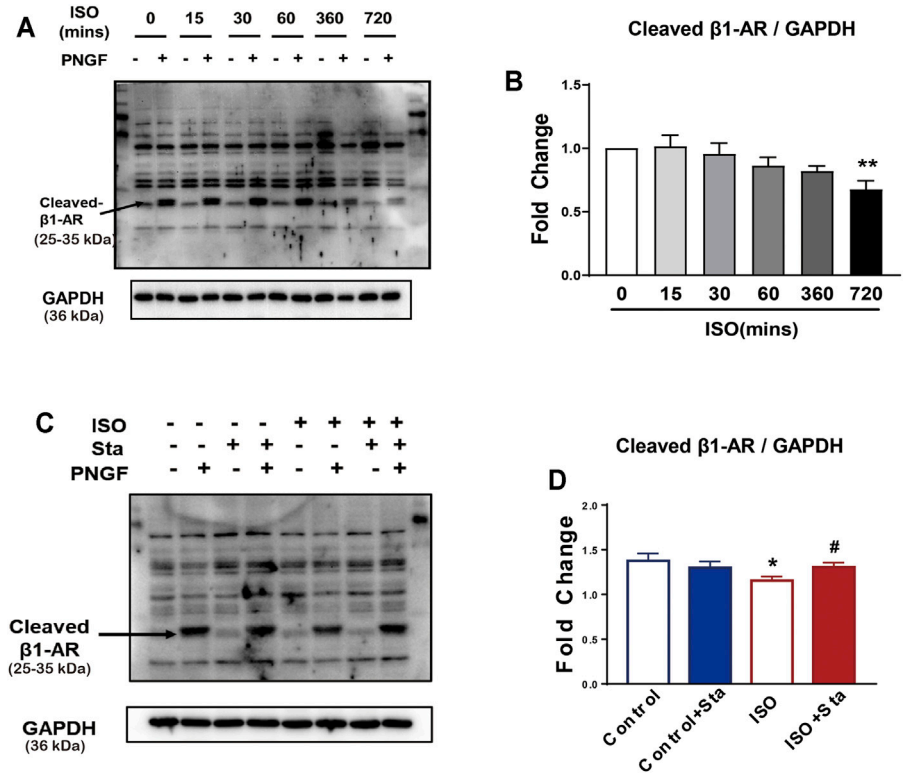

FIGURE 5 | The N-glycosylation of β1AR decreased after continuous ISO stimulation, while stachydrine hydrochloride can increase its expression *in vitro*. **(A)** Representative Western blot of N-glycosylation of β1AR after PNGase F digestion exposed to ISO at different time points in NRVMs (from three independent experiments). **(B)** Quantification of cardiac N-glycosylation of β1AR. **(C)** Representative Western blot of Sta on N-glycosylation of β1AR exposed to ISO at 720 min (from three independent experiments). **(D)** Quantification of cardiac N-glycosylation of β1AR. The data are expressed as mean ± standard error of mean, $^{*}p < 0.05$ versus control; $^{\#}p < 0.05$ versus ISO. β1AR, β1 adrenergic receptors; ISO, isoproterenol; Sta, stachydrine hydrochloride; NRVMs, neonatal rat ventricular myocytes.

Sta Modulates Hemodynamic Parameters During Chronic β1AR Activation *In Vivo*

According to PV loop analysis, ISO significantly elevated the left ventricular pressure (Pmax) and volume (Vmax and Vmin) and stroke work (SW). In addition, ISO induces a decline in cardiac systolic function (dP/dtmax and EF) and diastolic function (dP/dtmin). However, Sta treatment reduced the increase in the Pmax, Vmax, Vmin, dP/dtmin, and SW, and increased ISO-induced EF reduction (**Figure 2**). There was no significant difference in hemodynamic parameters between Sham and Sham + Sta groups.

Transcriptome Analysis of Heart Tissue in Mice With ISO-Induced Heart Failure

By conducting Principal Component Analysis (PCA) between the Sham and ISO groups, we found that the gene expression profile in each group could be clearly distinguished (**Figure 3A**). After comparing transcriptome analyses between Sham and ISO groups, 2,605 differentially expressed genes were identified, including 1,085 upregulated and 1,520 downregulated genes; then, the expression heatmap and volcano plot were presented in **Figures 3B,C**. Next, N-type glycosylated process category analysis was performed by mapping genes to GO enrichment; according to the results, 10 pathways were enriched significantly, especially in N-glycan-related processes (**Figure 3D** and **Table 1**). To assess the regulatory roles of the genes included in the GO process, gene regulation network was plotted based on the number of enriched genes in GO term (**Figure 3E** and **Table 2**). Then, on the foundation of STRING database and MCODE plugin, hub genes in the N-glycan GO process were scrutinized. Finally, FUT8, MGAT3, and MGAT4a were selected as the significantly differential genes in the N-type glycosylated process between Sham and ISO groups (**Figure 3F**).

Sta Increases the N-Glycosylation of β1AR in the Heart of Mice With ISO-Induced Heart Failure

β1AR plays an important role in the excitation–contraction coupling of the heart. In order to verify whether Sta can improve heart function by inhibiting the N-glycosylation of β1AR in ISO-induced heart failure mice, we performed Western blotting experiments in mice heart tissues. We separate the heart tissue protein into membrane protein and cytoplasmic protein to detect the N-terminal glycosylation

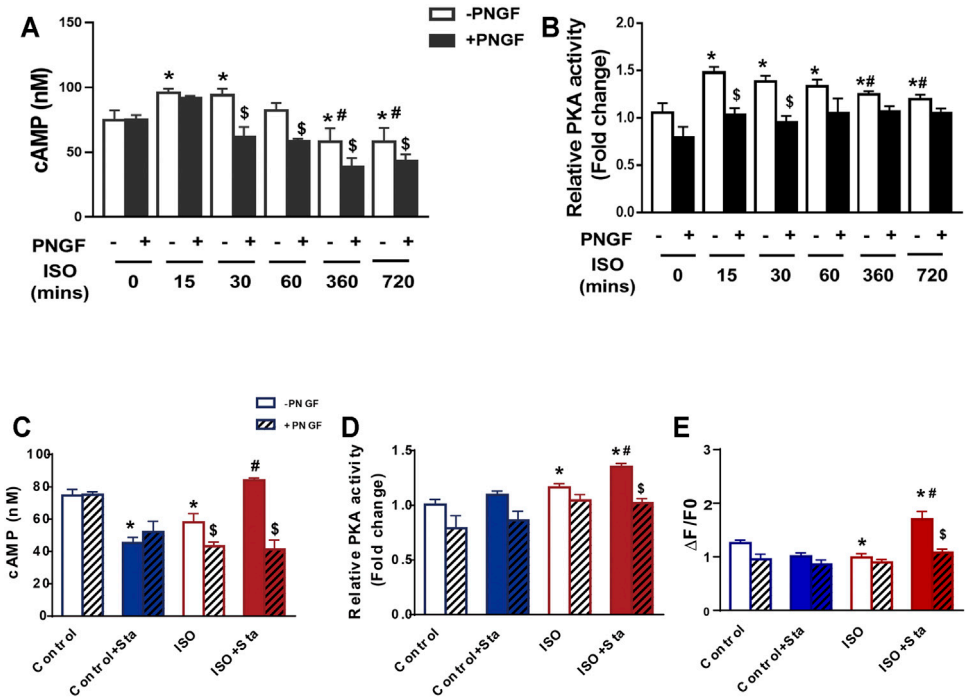

FIGURE 6 | Decreased N glycosylation of β1AR will downregulate the β1AR/cAMP/PKA signal pathway. **(A)** Quantification of cAMP production after PNGase F digestion exposed to ISO at different time points in H9C2 cells (from three independent experiments). **(B)** Quantification of PKA activity after PNGase F digestion exposed to ISO at different time points in NRVMs (from three independent experiments). **(C,D)** Quantification of Sta on cAMP production and PKA activity exposed to ISO at 720 min (from three independent experiments). **(E)** Quantification of Ca^{2+} transient parameters exposed to ISO at 720 min in AMVMs (n = 15 cells from 3 mice in each group). The data are expressed as mean ± standard error of mean, $^{*}p < 0.05$ versus control; $^{\#}p < 0.05$ versus ISO; $\$p < 0.05$ versus -PNGF. AMVMs, adult mouse ventricular myocytes; ISO, isoproterenol; Sta, stachydrine hydrochloride; NRVMs, neonatal rat ventricular myocytes.

expression of β1AR. There were multiple bands (antibody was polyclonal antibody), and the molecular weight of 50 kDa of β1AR was in accordance with the calculated molecular size. After PNGase F digestion, the approximately 25–35 kDa bands, in agreement with the monomer size, turned into one straight density band, indicating that the deglycosylated β1AR was mainly retained as a monomer (**Figure 4**). As shown in **Figures 4B,C**, the expression of β1AR and N-terminal glycosylation of β1AR on the cell membrane of the ISO group were decreased ($p < 0.05$). Among the cytoplasmic proteins, the expression of β1AR (**Figures 4E**) and N-glycosylation of β1AR (**Figure 4F**) was also downregulated in the ISO group ($p < 0.05$), while stachydrine hydrochloride can increase the N-glycosylation of β1AR induced by ISO ($p < 0.05$). Although Sta cannot significantly increase the expression of N-glycosylation of β1AR on the cell membrane surface, it can indeed maintain the number of β1AR on the cytoplasm and cell membrane ($p < 0.05$).

The N-Glycosylation of β1AR Decreased After Continuous ISO Stimulation, While Sta Increases Its Expression *In Vitro*

To explore the time–effect relationship of ISO (0.1 μMol) on N-glycosylation, we detected the expression of N-glycosylation at different time points (0, 15, 30, 60, 360, and 720 min) of ISO in NRVMs. Western blotting for β1AR in whole cell lysate at different time points of ISO treatment. The results showed that N-glycosylation was time-dependent, and the longer the time, the more N glycosylation. Compared with 0 min, the N-glycosylation of β1AR of ISO in 720 min was significantly decreased ($p < 0.05$) (**Figures 5A,B**). The diminution of N-glycosylation of β1AR induced by ISO stimulation for 720 min was inhibited by Sta (10 μMol) ($p < 0.05$) (**Figures 5C,D**).

Decreased N-Glycosylation of β1AR Will Downregulate the β1AR/cAMP/PKA Signal Pathway and Inhibit Myocardial Excitation and Contraction Coupling

We conducted the following experiments: we detected the cAMP expression and PKA activity in NRVMs and myocardial systolic function in AMVMs at different time points (0, 15, 30, 60, 360, and 720 min). The results showed that with the prolongation of ISO stimulation time, the content of cAMP, activation of PKA, and amplitude of sarcomere contraction were decreased ($p < 0.05$). After PNGase F is added, the content of cAMP, activation of PKA, and amplitude of sarcomere contraction decrease rapidly ($p < 0.05$) (**Figures 6A,B** and **Figure 7A**).

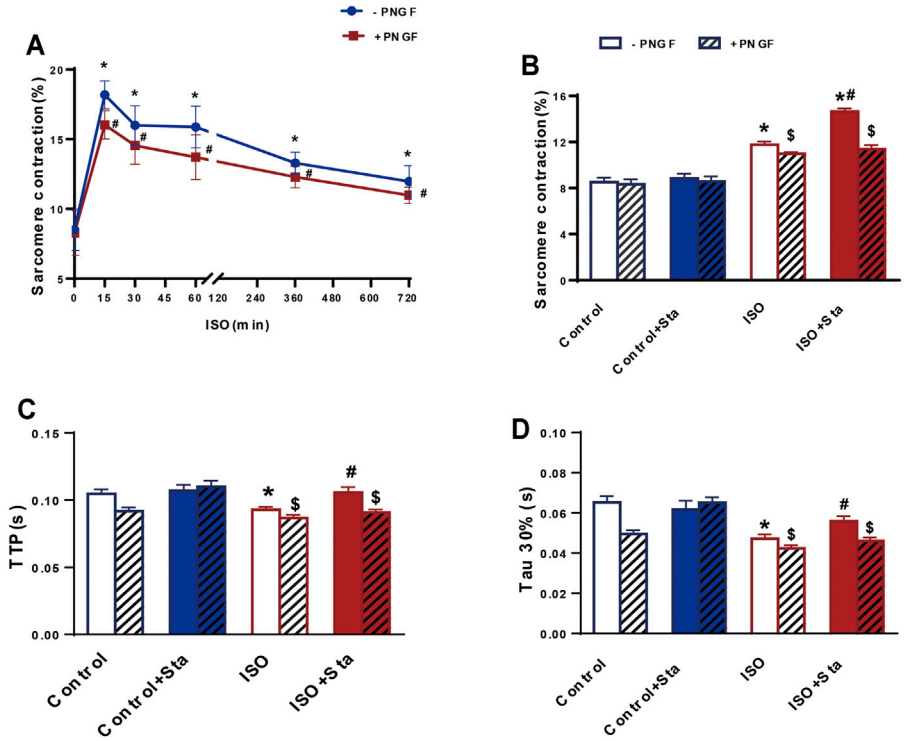

FIGURE 7 | Stachydrine hydrochloride improves myocardial contraction and diastolic function decline caused by continuous ISO stimulation by regulating N-glycosylation. **(A)** Quantification of sarcomere contraction after PNGase F digestion exposed to ISO at different time points in AMVMs ($n > 30$ cells from 3 mice in each group). **(B–D)** Quantification of Sta on sarcomere contraction, TTP and Tau 30% in AMVMs exposed to ISO at 720 min ($n > 20$ cells from 3 mice in each group). The data are expressed as mean ± standard error of mean, *$p < 0.05$ versus control; #$p < 0.05$ versus ISO; \$$p < 0.05$ versus -PNGF. AMVMs, adult mouse ventricular myocytes; ISO, isoproterenol; Sta, stachydrine hydrochloride; Tau, relaxation time constant; TTP, time to peak.

We tested the effects of Sta on cAMP, PKA, calcium transients, and myocardial contraction and diastolic function when ISO was applied for 720 min. Compared with the ISO group, the ISO + Sta group can significantly increase the cAMP content, PKA activity, and amplitude of calcium transient ($p < 0.05$). After adding PNGase F, the effect of Sta on the increase of cAMP, PKA, and Ca^{2+} transients disappeared ($p < 0.05$) (**Figures 6C–E**). The downstream biological effects of cAMP/PKA/Ca^{2+} signaling pathway regulation are myocardial contraction and diastolic function. **Figures 7B–D** show that Sta can slow down the decrease in sarcomere contraction amplitude, time to peak (TTP), and sarcomere relaxation time constant (Tau) caused by continuous ISO stimulation ($p < 0.05$). After adding PNGase F to shear N-glycosylation, these effects of Sta disappear ($p < 0.05$).

Sta Significantly Reduced ISO-Induced Cardiac N-Linked Glycoproteins With α-1,6-Fucosylation

LCA is an important tool for the study of glycoproteins with N-linked glycans; the main glycoproteins that are profiled by lectins are core α-1,6-fucose glycans. To verify the expression differences in N-linked glycoproteins with α-1,6-fucosylation, lectin affinity histochemical analysis is presented in **Figures 8**, **9**.

As shown in **Figures 8A,B**, with the prolongation of ISO action time, the α-1,6-fucosylation levels gradually increased. Compared with 0 min, the α-1,6-fucosylation expression level of ISO in 720 min was significantly increased ($p < 0.05$). To measure the degree of N-linked glycoproteins with α-1,6-fucosylation, we measured the ratio of cleaved LCA to LCA. Then, the control group without PNGase F was homogenized. We also found that after 720 min of ISO action, N-linked glycoproteins with α-1,6-fucosylation increased significantly ($p < 0.05$) (**Figures 8C,D**). The increase of α-1,6-fucosylation levels induced by ISO at 720 min was significantly reduced by stachydrine hydrochloride ($p < 0.05$) (**Figures 8C,D**). The lectin affinity histochemical analysis on NRVMs is shown in **Figure 8G**. α-1,6-fucosylation is mainly distributed around the nuclear membrane. Compared with the control group, the fluorescence brightness of α-1,6-fucosylation increased after 720 min of ISO exposure, indicating that the expression of α-1,6-fucosylation increased. Sta can inhibit the increase in α-1,6-fucosylation induced by ISO. However, after adding PNGase F, the green fluorescence around the nuclear membrane of each group disappeared.

Images of FITC-labeled LCA lectin affinity fluorescence histopathology sections. All the images of the sections showed

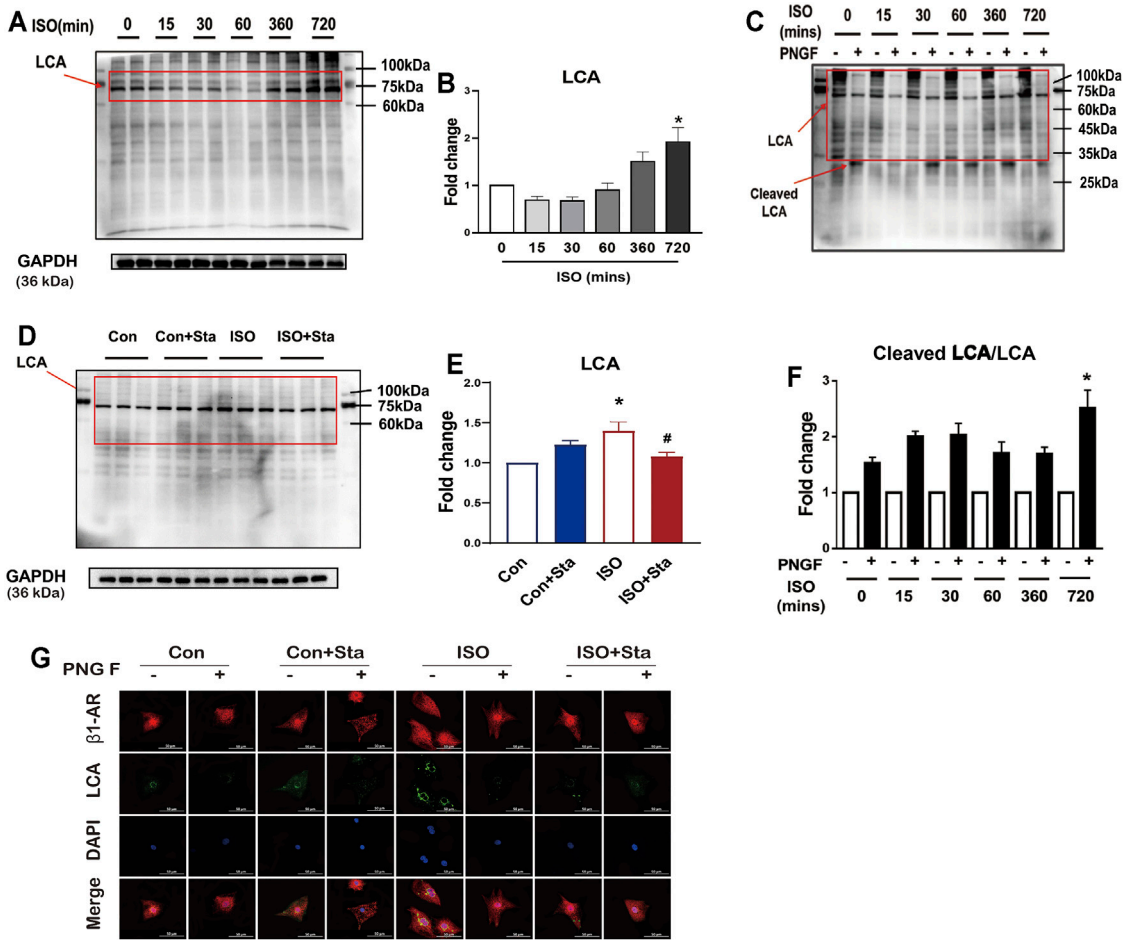

FIGURE 8 | Stachydrine hydrochloride reduced ISO-induced cardiac N-linked glycoproteins with α-1,6-fucosylation *in vitro*. **(A,B)** Representative Western blot and quantification of LCA exposed to ISO at different time points in NRVMs (from three independent experiments). **(C,D)** Representative Western blot and quantification of LCA after PNGase F digestion exposed to ISO at different time points in NRVMs (from three independent experiments). **(E,F)** Representative Western blot and quantification of Sta on cAMP production and PKA activity exposed to ISO at 720 min (from three independent experiments). **(G)** Representative immunofluorescence of LCA and β1AR exposed to ISO at different time points in NRVMs. The data are expressed as mean ± standard error of mean, $^{*}p < 0.05$ versus control; $^{\#}p < 0.05$ versus ISO. ISO, isoproterenol; Sta, stachydrine hydrochloride; NRVMs, neonatal rat ventricular myocytes.

that the extracellular and interstitial matrix were obviously stained. In addition, we found that the green fluorescence of LCA staining was coincident with the blue fluorescence of the nucleus. From the fluorescence intensity, we can see that the α-1,6-fucosylation in the ISO group myocardium was upregulated significantly compared with the sham group. Compared with the ISO group, the fluorescence of the ISO + Sta group was relatively weak (**Figure 9A**). In order to determine the distribution of α-1,6-fucosylation in cells, we extracted cytoplasmic proteins and cell membrane proteins. Through LCA lectin blot, we found that the expression of α-1,6-fucosylation (both cytoplasmic proteins and membrane proteins) in the ISO group increased, while Sta could inhibit the increase of myocardium protein α-1,6-fucosylation residues on N-glycosylation ($p < 0.05$) (**Figures 9B–E**). Consistent with the results of transcriptome analysis, the expression of FUT8, MAGT3, and MAGT4a in the serum of ISO mice was upregulated, while Sta could inhibit the expression of FUT8 and MAGT4a ($p < 0.05$) (**Figures 9F,G**).

DISCUSSION

Protein glycosylation is a posttranslational modification essential for protein functions such as proper folding, targeting to cellular compartments, and modulating receptor/ion channel activities (Ohtsubo and Marth, 2006; Ednie et al., 2019). The oligosaccharides of cell surface glycoproteins can regulate recognition processes, such as signal transduction, cell adhesion, immune response, and host–pathogen interactions. If the glycoprotein changes slightly, it will change the biological function (Zhao et al., 2018). In this study, we first found that Sta can inhibit ISO-induced cardiac hypertrophy and improve cardiac function in

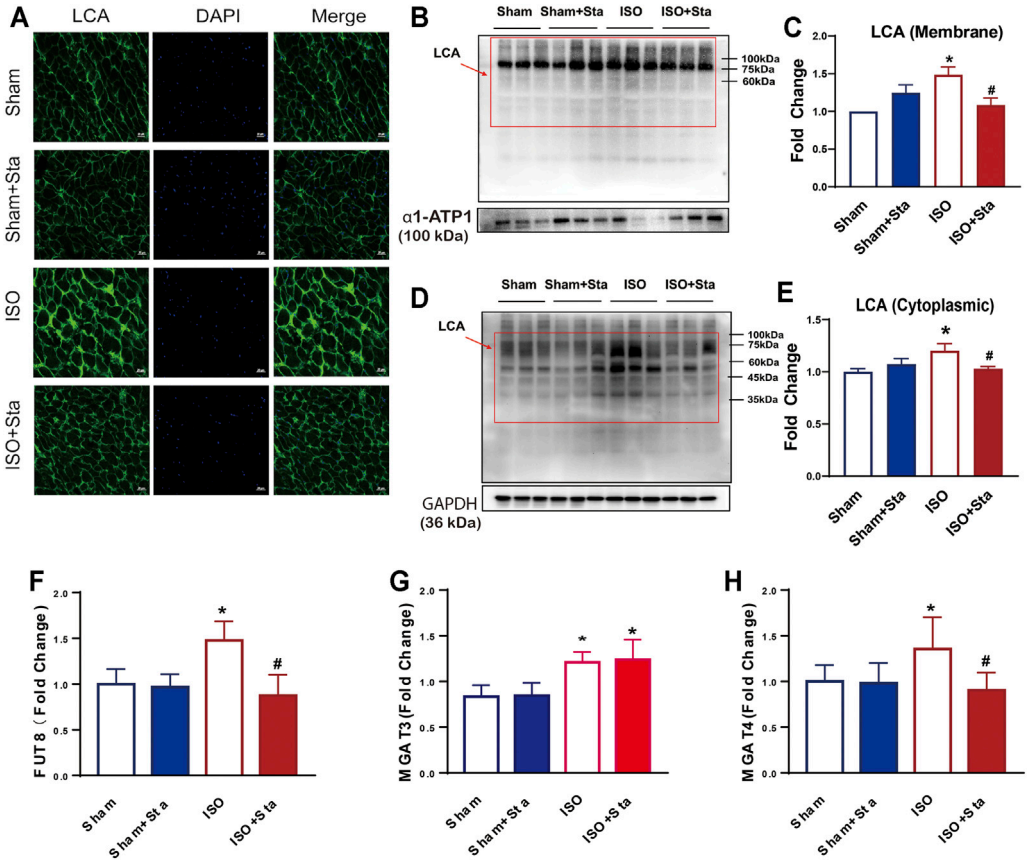

FIGURE 9 | Stachydrine hydrochloride inhibits the expression of FUT8 and MAGT4a to reduced α-1,6-fucosylation. **(A)** Images of FITC-labeled Lens culinaris agglutinin (LCA) lectin affinity fluorescence histopathology sections. **(B–E)** Representative Western blot and quantification of LCA exposed to ISO at 2 weeks on the cell membrane and in cytoplasmic. **(F–H)** FUT8, MGAT3, and MGAT4a expression measurement with ELISA kits. $n = 5$ mice per experimental group. The data are expressed as mean ± standard error of mean, $^{*}p < 0.05$ versus Sham; $^{\#}p < 0.05$ versus ISO. FUT8, α-1,6-fucosyltransferase; LCA, Lens culinaris agglutinin; MGAT3, β-1,4-mannosylglycoprotein 4-β-N-acetylglucosaminyltransferase; MGAT4a.α-1,3-mannosyl-glycoprotein 4-β-N-acetylglucosaminyltransferase A; ISO, isoproterenol; Sta, stachydrine hydrochloride.

mice with ISO-induced heart failure. Then, through transcriptomics analysis, we found that many N-glycosylation regulatory signaling pathways in the ISO group have changed. Therefore, our hypothesis is whether Sta improves heart function by regulating N-glycosylation.

There are three subtypes of βAR: β1AR, β2AR, and β3AR. All of these subtypes couple to Gs and therefore increase cellular cAMP levels when stimulated with agonist (Steinberg, 2018; Alhayek and Preuss, 2021). β1AR is found in a variety of tissues but is particularly highly expressed in the heart, where it mediates the bulk of the effects of epinephrine on cardiac function. Glycosylation modulates interactions of receptors and ligands with themselves, coregulatory molecules, and distinct membrane domains of intact cells, thereby altering signal transduction (Ednie et al., 2019). Studies have reported that blocking the N-glycosylation of β1AR will reduce the potency of isoproterenol in cyclic AMP generation assays, and reduce the expression of β1AR on the cell surface and dimerization (He et al., 2002). In the ISO model, we found that the expression of β1AR in the myocardial cell membrane and cytoplasm decreased. At the same time, we also found that the β1AR N-glycosylation of cell membrane proteins and cytoplasmic proteins of heart tissues in the ISO group was decreased significantly. In addition, we verified that continuous ISO stimulation can reduce the N-glycosylation level of β1AR *in vitro*, which is consistent with the results of previous reports.

In vivo experiments revealed that Sta can increase the reduction of β1AR in the cell membrane and cytoplasm induced by ISO, and Sta can increase the N-glycosylation level of β1AR in the cytoplasm. *In vitro* experiments also found that Sta can increase the decrease in N-glycosylation of β1AR induced by ISO. Does Sta improve the cardiac function of the ISO model related to maintaining the amount of β1AR and regulating N-glycosylation?

We know that the β1AR/cAMP/PKA signaling pathway plays an important role in the coupling of myocardial excitation and contraction. Is the decline in heart function caused by long-term continuous stimulation of ISO related to the decreased expression of N-glycosylation on β1AR? Subsequently, we tested whether the downregulation of N-glycosylation on β1AR affects its downstream cAMP/PKA signaling pathway. Continuous stimulation of ISO caused the downregulation of cAMP, PKA, and myocardial contractile function, and the downregulation trend was consistent with the downregulation trend of N-glycosylation on β1AR.

After cutting or not cutting N-glycosylation with PNGase F, we observed the effect of ISO on cAMP, PKA, and myocardial contractile function at different times. We found that when the N-glycosylation is not sheared, the effect of prolonging the action time of ISO on the cAMP, PKA, and myocardial contractile function is to promote first, and then gradually decreases, with the lowest at 720 min. The above results indicate that the N-glycosylated cleavage of the β1AR receptor will affect the contraction and relaxation of the downstream cardiomyocytes. After shearing N-glycosylation, the shrinkage of ISO decreases even more. Sta can increase the cAMP, PKA, calcium signal, and the downregulation of myocardial contraction and relaxation function caused by the continuous stimulation of ISO. However, after cutting N-glycosylation, the protective effect of Sta also disappeared. Therefore, we infer that the protective effect of Sta on the β1AR/cAMP/PKA signaling pathway is achieved by upregulating the N-glycosylation of β1AR. What is the mechanism by which Sta regulates N-glycosylation?

LCA is an important tool for the study of glycoproteins with N-linked glycans (Zhao et al., 2018). This lectin recognizes sequences containing α-1,6-fucose structures and also identifies additional sugars as part of the receptor structure (André et al., 2009). Studies have shown that the upregulation of α-1,6-fucosylation expression can cause abnormalities in cardiac structure and function (Zhao et al., 2018). To determine whether Sta improves cardiac function by regulating α-1,6-fucosylation, we use LCA lectin to analyze the differences in glycans between groups. LCA lectin electrophoresis showed that the α-1,6-fucosylation expression of cardiomyocytes and tissues increased significantly after continuous ISO stimulation, and the N-glycosylation of both cell membrane proteins and cytoplasmic proteins was significantly increased. We speculate that the upregulation of α-1,6-fucosylation may result in the downregulation of N-glycosylation on β1AR. Sta can inhibit the increase in α-1,6-fucosylation induced by ISO, thereby increasing the number of β1AR, maintaining the basis of cAMP/PKA signaling pathway, and improving myocardial function.

There are several N-glycan branching enzymes such as N-acetyl-glucosaminyltransferases GnT-I, II, III, IV, V, VI, IX (Vb), and FUT8, and a modifying enzyme, β-galactoside α-2,6 sialyltransferase 1. These enzymes are intimately associated with various diseases and biological functions by modifying target proteins (Taniguchi et al., 2021). Through transcriptome analysis, we found that among the enzymes related to N-glycosylation in the ISO model, the gene expression levels of FUT8, MAGT3, and MAGT4a increased significantly. Does Sta inhibit α-1,6-fucosylation by inhibiting these three transferases? We found that Sta could inhibit the expression of FUT8 and MAGT4a.

This study verified that when ISO was continuously stimulated, the expression of N-glycosylation on β1AR gradually decreased, the expression of LCA linked to N-glycosyl gradually increased, and cAMP/PKA and downstream signaling pathways gradually decreased. We have also verified the effect of downregulation of N-glycosylation on β1AR on cAMP/PKA and downstream signaling pathways. However, how the upregulation of LCA directly causes downregulation of N-glycosylation on β1AR has not been verified. This is also a technical difficulty. This is the shortcoming of this research.

CONCLUSION

In summary, we determined the contribution of Sta in isoproterenol-induced heart failure through α-1,6-fucosylation linked by N-glycosylation. The underlying mechanism may be related to the inhibition of the synthesis of α-linked mannose residues on the N-terminal sugar chain by reducing FUT8 and MGAT4a. Our results reveal the molecular mechanism of Sta in the prevention and treatment of heart failure, and highlight the important role of N-glycosylation on β1AR in the progression of heart failure. It provides a new idea for elucidating the cardiovascular protective effect of the traditional Chinese medicine monomer Sta.

DATA AVAILABILITY STATEMENT

The transcriptome library construction and sequencing data presented in the study was deposited in the NCBI SRA BioProject repository, and the accession number was PRJNA793393.

ETHICS STATEMENT

The animal study was reviewed and approved by the Animal Care and Use Committee of Shanghai University of Traditional Chinese Medicine.

AUTHOR CONTRIBUTIONS

RL and HC conceived and designed the experiments. PH and SG performed the *in vivo* experiments. SY, SaW, and XS performed the *in vitro* experiments and analyzed the experimental results. WG and PZ isolated heart experiments and analyzed the data. SiW and MX performed transcriptome analysis experiments. HC and CZ drafted this manuscript.

FUNDING

This work was supported by the National Natural Science Foundation of China (Grant number 82074054), the Youth Program of National Natural Science Foundation of China (Grant number 81903831), the Natural Science Foundation of Shanghai (Grant number 19ZR1457600), and Shanghai Municipality: Shanghai Chenguang Program (Grant number 19CG48).

REFERENCES

André, S., Kozár, T., Kojima, S., Unverzagt, C., and Gabius, H. J. (2009). From Structural to Functional Glycomics: Core Substitutions as Molecular Switches for Shape and Lectin Affinity of N-Glycans. *Biol. Chem.* 390, 557–565. doi:10.1515/BC.2009.072

Bjarnadóttir, T. K., Gloriam, D. E., Hellstrand, S. H., Kristiansson, H., Fredriksson, R., and Schiöth, H. B. (2006). Comprehensive Repertoire and Phylogenetic Analysis of the G Protein-Coupled Receptors in Human and Mouse. *Genomics* 88, 263–273. doi:10.1016/j.ygeno.2006.04.001

Bristow, M. R., Ginsburg, R., Minobe, W., Cubicciotti, R. S., Sageman, W. S., Lurie, K., et al. (1982). Decreased Catecholamine Sensitivity and Beta-Adrenergic-Receptor Density in Failing Human Hearts. *N. Engl. J. Med.* 307, 205–211. doi:10.1056/NEJM198207223070401

Bristow, M. R., Ginsburg, R., Umans, V., Fowler, M., Minobe, W., Rasmussen, R., et al. (1986). Beta 1- and Beta 2-Adrenergic-Receptor Subpopulations in Nonfailing and Failing Human Ventricular Myocardium: Coupling of Both Receptor Subtypes to Muscle Contraction and Selective Beta 1-receptor Down-Regulation in Heart Failure. *Circ. Res.* 59, 297–309. doi:10.1161/01.RES.59.3.297

Bristow, M. R., Minobe, W. A., Raynolds, M. V., Port, J. D., Rasmussen, R., Ray, P. E., et al. (1993). Reduced Beta 1 Receptor Messenger RNA Abundance in the Failing Human Heart. *J. Clin. Invest.* 92, 2737–2745. doi:10.1172/JCI116891

Chen, H. H., Wang, S. N., Cao, T. T., Zheng, J. L., Tian, J., Shan, X. L., et al. (2020). Stachydrine Hydrochloride Alleviates Pressure Overload-Induced Heart Failure and Calcium Mishandling on Mice. *J. Ethnopharmacol.* 248, 112306. doi:10.1016/j.jep.2019.112306

Chuh, K. N., Batt, A. R., and Pratt, M. R. (2016). Chemical Methods for Encoding and Decoding of Posttranslational Modifications. *Cell Chem. Biol.* 23, 86–107. doi:10.1016/j.chembiol.2015.11.006

Dennis, J. W., Lau, K. S., Demetriou, M., and Nabi, I. R. (2009). Adaptive Regulation at the Cell Surface by N-Glycosylation. *Traffic* 10, 1569–1578. doi:10.1111/j.1600-0854.2009.00981.x

Ednie, A. R., Parrish, A. R., Sonner, M. J., and Bennett, E. S. (2019). Reduced Hybrid/complex N-Glycosylation Disrupts Cardiac Electrical Signaling and Calcium Handling in a Model of Dilated Cardiomyopathy. *J. Mol. Cel. Cardiol.* 132, 13–23. doi:10.1016/j.yjmcc.2019.05.001

He, J., Xu, J., Castleberry, A. M., Lau, A. G., and Hall, R. A. (2002). Glycosylation of Beta(1)-Adrenergic Receptors Regulates Receptor Surface Expression and Dimerization. *Biochem. Biophys. Res. Commun.* 297, 565–572. doi:10.1016/S0006-291X(02)02259-3

Liu, X., Shan, X., Chen, H., Li, Z., Zhao, P., Zhang, C., et al. (2019). Stachydrine Ameliorates Cardiac Fibrosis through Inhibition of Angiotensin II/Transformation Growth Factor β1 Fibrogenic Axis. *Front. Pharmacol.* 10, 538. doi:10.3389/fphar.2019.00538

Liu, X. H., Pan, L. L., and Zhu, Y. Z. (2012). Active Chemical Compounds of Traditional Chinese Medicine Herba Leonuri: Implications for Cardiovascular Diseases. *Clin. Exp. Pharmacol. Physiol.* 39, 274–282. doi:10.1111/j.1440-1681.2011.05630.x

Miao, L.-L., Zhou, Q.-M., Peng, C., Liu, Z.-H., and Xiong, L. (2019). Leonurus Japonicus (Chinese Motherwort), an Excellent Traditional Medicine for Obstetrical and Gynecological Diseases: A Comprehensive Overview. *Biomed. Pharmacother.* 117, 109060. doi:10.1016/j.biopha.2019.109060

Ohtsubo, K., and Marth, J. D., 2006. Glycosylation in Cellular Mechanisms of Health and Disease. *Cell* 126, 855–867. doi: doi: doi:10.1016/j.cell.2006.08.019

Soto, A. G., and Trejo, J. (2010). N-linked Glycosylation of Protease-Activated Receptor-1 Second Extracellular Loop: A Critical Determinant for Ligand-Induced Receptor Activation and Internalization. *J. Biol. Chem.* 285, 18781–18793. doi:10.1074/jbc.M110.111088

Steinberg, S. F. (2018). Beta1-Adrenergic Receptor Regulation Revisited. *Circ. Res.* 123, 1199–1201. doi:10.1161/CIRCRESAHA.118.313884

Taniguchi, N., Ohkawa, Y., Maeda, K., Harada, Y., Nagae, M., Kizuka, Y., et al. (2021). True Significance of N-Acetylglucosaminyltransferases GnT-III, V and α1,6 Fucosyltransferase in Epithelial-Mesenchymal Transition and Cancer. *Mol. Aspects Med.* 79, 100905. doi:10.1016/j.mam.2020.100905

Zhang, C., Shan, X. L., Liao, Y. L., Zhao, P., Guo, W., Wei, H. C., et al. (2014). Effects of Stachydrine on Norepinephrine-Induced Neonatal Rat Cardiac Myocytes Hypertrophy and Intracellular Calcium Transients. *BMC Complement. Altern. Med.* 14, 474. doi:10.1186/1472-6882-14-474

Zhao, Q., Jia, T. Z., Cao, Q. C., Tian, F., and Ying, W. T. (2018). A Crude 1-DNJ Extract from Home Made Bombyx Batryticatus Inhibits Diabetic Cardiomyopathy-Associated Fibrosis in Db/db Mice and Reduces Protein N-Glycosylation Levels. *Int. J. Mol. Sci.* 19. doi:10.3390/ijms19061699

Zheng, J., Tian, J., Wang, S., Hu, P., Wu, Q., Shan, X., et al. (2020). Stachydrine Hydrochloride Suppresses Phenylephrine-Induced Pathological Cardiac Hypertrophy by Inhibiting the Calcineurin/nuclear Factor of Activated T-Cell Signalling Pathway. *Eur. J. Pharmacol.* 883, 173386. doi:10.1016/j.ejphar.2020.173386

Conflict of Interest: The authors declare that the research was conducted in the absence of any commercial or financial relationships that could be construed as a potential conflict of interest.

Publisher's Note: All claims expressed in this article are solely those of the authors and do not necessarily represent those of their affiliated organizations, or those of the publisher, the editors, and the reviewers. Any product that may be evaluated in this article, or claim that may be made by its manufacturer, is not guaranteed or endorsed by the publisher.

frontiers in Pharmacology

ORIGINAL RESEARCH
published: 21 February 2022
doi: 10.3389/fphar.2022.828061

Calycosin as a Novel PI3K Activator Reduces Inflammation and Fibrosis in Heart Failure Through AKT–IKK/STAT3 Axis

Xiaoping Wang[1†], Weili Li[2†], Yawen Zhang[1], Qianbin Sun[2], Jing Cao[1], NanNan Tan[1], Shuangjie Yang[1], Linghui Lu[1], Qian Zhang[1], Peng Wei[1], Xiao Ma[3,4], Wei Wang[1,2,5,6] and Yong Wang[1,2,5,6,3,4]**

[1]School of Chinese Medicine, Beijing University of Chinese Medicine, Beijing, China, [2]School of Life Sciences, Beijing University of Chinese Medicine, Beijing, China, [3]Department of Biochemistry and Molecular Biology, Mayo Clinic, Rochester, MN, United States, [4]Department of Cardiovascular Medicine, Mayo Clinic, Rochester, MN, United States, [5]Beijing Key Laboratory of TCM Syndrome and Formula, Beijing, China, [6]Key Laboratory of Beijing University of Chinese Medicine, Ministry of Education, Beijing, China

OPEN ACCESS

Edited by:
Yi Wang,
Zhejiang University, China

Reviewed by:
Guanwei Fan,
Tianjin University of Traditional Chinese Medicine, China
Zhi Yong Du,
Capital Medical University, China

***Correspondence:**
Yong Wang
doctor_wangyong@163.com
Wei Wang
wangwei26960@126.com

†These authors have contributed equally to this work

Specialty section:
This article was submitted to Ethnopharmacology, a section of the journal Frontiers in Pharmacology

Received: 02 December 2021
Accepted: 24 January 2022
Published: 21 February 2022

Citation:
Wang X, Li W, Zhang Y, Sun Q, Cao J, Tan N, Yang S, Lu L, Zhang Q, Wei P, Ma X, Wang W and Wang Y (2022) Calycosin as a Novel PI3K Activator Reduces Inflammation and Fibrosis in Heart Failure Through AKT–IKK/STAT3 Axis. Front. Pharmacol. 13:828061. doi: 10.3389/fphar.2022.828061

Aim: Inflammation and fibrosis have been shown to be critical factors in heart failure (HF) progression. Calycosin (Cal) is the major active component of *Astragalus mongholicus Bunge* and has been reported to have therapeutic effects on the cardiac dysfunction after myocardial infarction. However, whether Cal could ameliorate myocardial infarction (MI)-induced inflammation and fibrosis and precise mechanisms remain uncertain. The aim of this study is to explore the role of Cal in HF and to clarify the underlying mechanisms.

Methods: For *in vivo* experiments, rats underwent left anterior descending artery ligation for heart failure model, and the cardioprotective effects of Cal were measured by echocardiographic assessment and histological examination. RNA-seq approach was applied to explore potential differential genes and pathways. For further mechanistic study, proinflammatory-conditioned media (conditioned media)-induced H9C2 cell injury model and TGFβ-stimulated cardiac fibroblast model were applied to determine the regulatory mechanisms of Cal.

Results: In the *in vivo* experiments, echocardiography results showed that Cal significantly improved heart function. GO and reactome enrichment revealed that inflammation and fibrosis pathways are involved in the Cal-treated group. KEGG enrichment indicated that the PI3K–AKT pathway is enriched in the Cal-treated group. Further experiments proved that Cal alleviated cardiomyocyte inflammatory responses evidenced by downregulating the expressions of phosphorylated IκB kinase α/β (*p*-IKKα/β), phosphorylated nuclear factor kapa B (*p*-NFκB), and tumor necrosis factor α (TNFα). Besides, Cal effectively attenuated cardiac fibrosis through the inhibitions of expressions and depositions of collagen I and collagen III. In the *in vitro* experiments, the phosphatidylinositol three kinase (PI3K) inhibitor LY294002 could abrogate the anti-inflammation and antifibrosis therapeutic effects of Cal, demonstrating that the cardioprotective effects of Cal were mediated through upregulations of PI3K and serine/threonine kinase (AKT).

Conclusion: Cal inhibited inflammation and fibrosis via activation of the PI3K–AKT pathway in H9C2 cells, fibroblasts, and heart failure in postacute myocardial infarction rats.

Keywords: heart failure, calycosin, myocardial fibrosis, inflammation, PI3K–Akt pathway

INTRODUCTION

Despite recent advances in the therapies of cardiovascular disorders, heart failure (HF) remains a major cause of morbidity and mortality worldwide, which brings great burden on healthcare costs (Rhee and Lavine, 2020). Most often, HF is caused by myocardial infarction (MI) and typically associated with cardiac remodeling (Humeres and Frangogiannis, 2019). Notably, inflammation and fibrosis play crucial roles in the pathophysiology of HF (Bacmeister et al., 2019). Thus, there is an urgent need to develop novel anti-inflammatory and antifibrosis HF therapies.

Inflammation plays an important role in HF. After myocardial infarction, inflammatory response in remote remodeling myocardial segments is activated (Prabhu and Frangogiannis, 2016). Nuclear factor kappa-B (NFκB) is a crucial heterodimeric transcription factor in inflammatory responses, which is regulated by the IκB kinase (IKK) complex (Israël, 2010). Studies have shown that the persistently activated NFκB pathway in HF progression mediated the excessive release of various inflammatory cytokines such as tumor necrosis factor α (TNFα) and interleukin-1 (IL-1) (Wang et al., 2020a). Herein, the IKK-NF-κB pathway is believed to be one of the most attractive targets for HF.

Myocardial pathological remodeling is the major reason for decreased cardiac function HF (Frangogiannis, 2014). Massive sudden loss of cardiomyocytes induced by inflammatory response overwhelms the limited regenerative capacity of the myocardium, resulting in the formation of a collagen-based scar (Prabhu and Frangogiannis, 2016). Along this line, the imbalance of myocardial extracellular matrix (ECM) deposition and degradation promotes the collagen fiber replacement in necrotic myocardial tissue, which contributes to scar tissue accumulation and cardiac fibrosis. Matrix metalloproteinase 9 (MMP-9) could degrade the ECM and plays an important role in the compensation of myocardial fibrosis (Medeiros et al., 2017). Signal transducer and activator of transcription 3 (STAT3), a member of STAT family, is a transcription factor, which can inhibit the degradation of ECM and regulate myocardial fibrosis (Wang et al., 2019; Singh et al., 2021). Therefore, STAT3–MMP9 are promising antifibrosis targets for HF therapeutic strategies.

Phosphatidylinositol three kinase (PI3K)-serine/threonine kinase (AKT) is an important signaling pathway that can protect the heart against cardiac injuries (Wu et al., 2016). PI3K belongs to a conserved family of lipid kinases and is the primary regulator of AKT activation (Chong et al., 2015). It is reported that PI3K could phosphorylate IKK into active form and subsequently activate downstream target NFκB to activate the inflammatory responses (Li et al., 2018). Meanwhile, evidence have shown that activation of PI3K could decrease the level of STAT3 phosphorylation to reduce the fibrosis (Lee et al., 2019). Collectively, the PI3K–AKT signaling pathway plays a crucial role in inflammation response and cardiac fibrosis.

Calycosin (Cal) is one of the major active ingredients in the plant *Astragalus mongholicus* Bunge (Efferth et al., 2016) and has emerged as a highly valued herb to treat cardiovascular diseases. Liu et al. have proven that Cal attenuates myocardial ischemia–reperfusion injury by activating JAK2/STAT3 signaling pathway via the regulation of IL-10 secretion in mice (Liu et al., 2020). Huang et al. have reported that Cal reduces infarct size, oxidative stress, and preserve heart function in an isoproterenol-induced myocardial infarction model (Huang et al., 2020). Zhai et al. revealed that Cal ameliorates doxorubicin-induced cardiotoxicity by suppressing oxidative stress and inflammation via the sirtuin 1-NOD-like receptor protein three pathway (Zhai et al., 2020). However, whether Cal could alleviate MI-induced HF remains unknown. Herein, the left anterior descending (LAD) artery ligation-induced HF rat model was conducted to investigate efficacy evaluation. To explore the mechanism of action of Cal, we applied an RNA-seq approach. Intriguingly, the inflammation and fibrosis pathways are significantly enriched. Furthermore, we performed proinflammatory conditioned media (CM)-induced H9C2 cell lines and TGFβ-stimulated cardiac fibroblasts to verify the precise molecular mechanisms.

MATERIALS AND METHODS

Reagents and chemicals

Calycosin was purchased from the Nature Standard Technical Service Co., Ltd. (Shanghai, China). Fosinopril, DMEM, FBS, trypsin, penicillin, streptomycin, sodium cacodylate buffer, and DAPI were purchased from the Beijing BioDee Biotechnology Co., Ltd. (Beijing, China). Paraformaldehyde (4%) and saline (0.9%) were from Applygen Technology Inc. (Beijing, China). Dimethyl sulfoxide (DMSO) was acquired from Sigma-Aldrich LLC (Shanghai, China). LY294002 was purchased from Abmole China Branch. All other chemicals were purchased from commercial sources.

Animal experiments, grouping, and model establishment

After 1 week of acclimation, Sprague–Dawley (SD) male rats (220 g) obtained from the Beijing Vital River Laboratory Animal Technology Co., Ltd. were randomly divided into four groups (number/each group = 8): sham group, model group, calycosin (Cal) treatment group, and fosinopril treatment group. Rats in the sham group underwent sham surgery, while HF was induced in other rats by direct left anterior descending (LAD) artery ligation as described in our previous study (Zhang

et al., 2018). Based on our previous literature (Zhang et al., 2019; Wang et al., 2020a), 24 h after surgery, the acute myocardial infarction model was established, and the drug treatment was started. Rats in the Cal group were treated with Cal at a dosage of 80 mg/kg per day (Li et al., 2020). Rats in the fosinopril group were treated with fosinopril at a dosage of 4.67 mg/kg per day (Wang et al., 2020b). Rats in the sham group and model group were treated with the same volume of distilled water. All the drugs and distilled water were orally administrated with an amount of l ml/100 g for 28 days. It is reported that based on available clinical evidence, fosinopril is an effective and well-tolerated option for the management of patients with heart failure (Davis et al., 1997). For this reason, we set the fosinopril group as a positive control. During the whole procedure, the total mortality of the rats was 30%; most deaths occurred during surgery or after surgery, possibly owing to acute pump failure or fatal arrhythmia. This study conforms to the Guide for the Care and Use of Laboratory Animals published by the US National Institutes of Health (NIH publication no. 85–23, revised 1996), and it was approved by the Institutional Animal Care and Use Committee at the Beijing University of Chinese Medicine (consent number: BUCM20200914-YW).

Echocardiographic assessment

Transthoracic echocardiography was performed by using a Vevo 2100 instrument (VisualSonics, Canada) equipped with an MS-400 imaging transducer. The echocardiographic measurements were performed under general anesthesia with 1% pentobarbital sodium. M-mode tracings were recorded through the anterior and posterior left ventricular (LV) walls at the papillary muscle level. Heart functions were assessed by related parameters including left ventricular internal dimension—systole (LVID; s), left ventricular internal dimension—diastole (LVID; d), ejection fraction (EF), and fractional shortening (FS). Three cardiac cycles were recorded for the measurements.

Histological examination

Hearts were cut horizontally through the mid region to create cross sections of both the left and right ventricles, and the apex part was fixed with 4% paraformaldehyde. Then the tissues were embedded in paraffin and cut into 5-μm sections. After deparaffinized by xylene and rehydrated via different grades of ethanol, the sections were stained with hematoxylin–eosin (HE) staining and Masson staining to assess overall pathological changes. Digital images were observed under a microscope at ×400 magnification (Leica Biosystems Richmond, Inc.). Inflammatory cell rate is evaluated by the area of inflammatory cell infiltration using HE staining images. In brief, we selected the region of inflammatory cell infiltration in Image Pro Plus software, then calculated the area of this region as the area of inflammatory cell infiltration of this picture. Then we calculated the area of inflammatory cell infiltration of eight HE views (magnification = original × 400) in the same group. The intensity of inflammatory cell infiltration in other groups was calculated and compared. The collagen volume fraction was also analyzed by Image Pro Plus software in the infarcted border zone. Eight separate images (magnification = original × 400) of Masson staining sections were selected, and collagen volume fraction (CVF) was calculated using the following formula: CVF = collagen area / total visual area × 100%, to assess the degree of cardiac fibrosis.

Detection of serum biomarkers

The serum was collected from fresh blood and centrifuged at 3,000 × *g* for 10 min at 4°C. The concentrations of serum NTpro-BNP, malondialdehyde (MDA), interleukin-1 (IL-1), and TNFα were detected by enzyme-linked immunosorbent assay.

Immunohistochemistry assay

Heart sections were deparaffinized and blocked with 5% goat serum for 1.5 h at room temperature. After washing three times with PBS, the sections were incubated with primary antibodies: rabbit polyclonal anti-TNFα antibody (1:500; Abcam; ab220210), rabbit polyclonal anti-collagen I antibody (1:500; Abcam; ab34710), and rabbit polyclonal anti-collagen III antibody (1: 500; Abcam; ab7778) at 4°C overnight, and then were incubated with a secondary antibody. Finally, the sections were stained with diaminobenzidine (DAB).

Ribonucleic acid preparation

In our previous report, RNA-seq was applied in HF rats, the same model as this research (Gao et al., 2020). According to the evaluation results of cardiac function, the difference of intergroup in each group was not significant by comparing with pair-matching *t* test, so we chose three animals per group by random sampling. Total RNA of the cardiac tissues was extracted using TRIzol Reagent® (Invitrogen, Carlsbad, CA, USA). Extracted RNA was digested with dnase to remove contaminating genomic DNA, and the quality of RNA was evaluated by RNA Nano 6000 Assay Kit of the Agilent Bioanalyzer 2100 system (Agilent Technologies, CA, USA). RNA was purified using poly-T oligo-attached magnetic beads, then reverse transcribed into cDNA. After cDNA was ligated with adaptors, PCR amplification was applied with Phusion High-Fidelity DNA polymerase, universal PCR primers, and index (X) primer, and build the library of each sample. The library was sequenced on Illumina Hiseq4000 platform and 150-bp paired-end reads. Quality control and alignment were performed with rat reference sequences. Subsequently, read counts of each gene were computed as raw gene expression.

Differential expression analysis; GO, reactome, and KEGG pathway enrichment

Using the R package "DESeq2," differentially expressed genes (DEG) were identified with a p-value <0.05 and |log2 (foldchange)| >1 in the R version 3.5.1 software. Furthermore, GO, reactome, and KEGG pathway enrichment were performed using the R package "clusterProfiler" with $p < 0.05$ (R version 3.5.1 software).

H9C2 cell culture and cell viability

Cell used in the present study were purchased from the China Infrastructure of Cell Line Resources (Institute of Basic Medical Sciences, Chinese Academy of Medical Sciences) and cultured in

Dulbecco's modified Eagle medium (DMEM, Hyclone, USA) supplemented with 10% fetal bovine serum (FBS, Corning, USA), as well as a mixture of penicillin (100 U/ml, Corning, USA) and streptomycin (100 μg/ml, Gibco, USA) at 37°C in a humidified atmosphere of 5% CO_2. To evaluate the cytotoxicity of Cal in H9C2 cells, cells were cultured in 96-well plates at a density of 6×10^3 cells/well and subjected to different concentrations (2.5, 5, 10, and 20 μM) of Cal treatments. Referring to the inflammatory cell model in our previous study (Li et al., 2016), RAW264.7 cells were subjected to lipopolysaccharide (LPS) (1 μg/ml) for 24 h. Then cell supernatants for conditioned media (CM) were collected for the next experiments. To investigate the effects of Cal on CM-stimulated cardiomyocytes, H9C2 cells were precultured with Cal for 6 h, then stimulated with CM (with/without Cal) for 24 h. CCK-8 was applied to detect the cell viability at 450 nm under a microplate reader.

Isolation and cardiac fibroblast culture

Cardiac fibroblasts were isolated from neonatal SD rats using mixed enzymatic digestion (0.06% trypsin/0.04% collagenase type II in D-PBS without Ca^{2+}/Mg^{2+}). Then fibroblasts were separated from cardiomyocytes by differential adhesion for about 90 min. The adherent cells are fibroblasts. Cells at passages 2–6 were cultured with serum-free media for about 24 h and subsequently stimulated with 20 ng/ml of TGF-β1 (PeproTech, USA) and Cal or LY294002 for 24 h.

Detection for supernatant biomarkers

Levels of tumor necrosis factor-α (TNF-α) and IL-1 in cell supernatant were assessed by following the protocols of commercially available kits (NanjingJiancheng, China). The content was expressed as pg/ml.

Evaluation of mitochondrial transmembrane potential

Mitochondrial membrane potential (MMP) in different groups were evaluated by the JC-1 staining kit (Beyotime Biotechnology, China). H9C2 cells were cultured on laser confocal dishes and then induced by CM. Different groups of H9C2 cells were incubated with JC-1 probe for 30 min at 37°C in the dark. After washing three times with PBS, the images were scanned by laser confocal microscopy (Leica Microsystems GmbH). Image ProPlus (IPP) software was applied to calculate and analyze the ratio of aggregates/monomers fluorescence intensity.

Detection of reactive oxygen species

ROS was assessed by a commercial assay using fluorescent probe DCFH-DA. H9C2 cells were induced by CM in the presence or absence of Cal and LY294002, and then observed at excitation and emission wavelengths of 488 and 525 nm under a fluorescence microscope (Leica Microsystems GmbH).

Cell immunofluorescence

H9C2 cells were grown onto confocal dishes for the specified experiment time, fixed with 4% paraformaldehyde for 12 min followed by 0.5% Triton X-100 for 20 min, and blocked with normal goat serum for 1.5 h. Then cells were incubated with NFκB antibody overnight at 4°C. After three times of washing, cells were incubated with the secondary antibody at room temperature for 1.5 h in the dark. After being washed three times, cells were counterstained with 5 μg/ml of DAPI for 20 min. Images were then obtained under a confocal microscope. For α-SMA immunofluorescence, anti-α-SMA antibody (1A4, Santa Cruz Biotech) and an Alexa–Fluor 488-labeled secondary antibody (Molecular Probes) were used.

Western blot analysis

Heart tissues and H9C2 cells were homogenized in RIPA lysis buffer and quantified by the bicinchoninic acid (BCA) method. A total of 50 μg of protein was separated by 10% sodium dodecyl sulfate polyacrylamide gel electrophoresis (SDS-PAGE) gel and then transferred to a PVDF membrane. After being blocked in a solution of TBST with 5% skimmed milk for 1.5 h at room temperature, the membranes were incubated overnight at 4°C with the following primary antibodies: anti-*p*-NFκB (ab97726; Abcam, USA), NFκB (CST8242, Cell Signaling Technology, Germany), antiTNFα antibody (ab183218; Abcam, USA), anti-p-STAT3 (ab76315; Abcam, USA), STAT3 (ab68153; Abcam, USA), MMP-9 (ab38898; Abcam, USA), PI3K (ab182651; Abcam, USA), AKT (ab182729; Abcam, USA), *p*-AKT (CST4060, Cell Signaling Technology, Germany), *p*-IKKα/β (CST2697T, Cell Signaling Technology, Germany), IKKα (CST2682, Cell Signaling Technology, Germany), IKKβ (CST8943, Cell Signaling Technology, Germany), and anti-GAPDH (ab8245, Abcam, 1:5,000) at 4°C overnight. Afterward, membranes were washed and incubated with specific horseradish peroxidase (HRP)-conjugated secondary antibodies (goat antirabbit IgG 1:12,000 and goat antimouse IgG 1:5,000) for 1 h. The blots were visualized with enhanced chemiluminescent (ECL) plus Western blotting detection reagent (GE Healthcare, UK) for 1 min at room temperature without light, and then captured and analyzed by UVP BioImaging Systems (Bio-Rad, Hercules, CA, USA). Furthermore, protein expressions were normalized based on GAPDH level, and grayscale analysis was performed by the Image-Lab software.

Statistical analysis

Statistical analysis was performed with the SPSS software (SPSS version 22.0) or GraphPad Prism 7. All data were presented as the mean ± standard deviation (SD). Data were carried out by Dunnett's test and one-way analysis of variance (ANOVA) to compare differences among multiple groups. *p*-Values less than 0.05 were considered statistically significant.

RESULTS

Efficacy evaluation after calycosin treatment in heart failure model

After 28 days of treatments, echocardiography was implemented to examine cardiac function. The results indicated that rats in the model group had significantly lower values of EF and FS, while

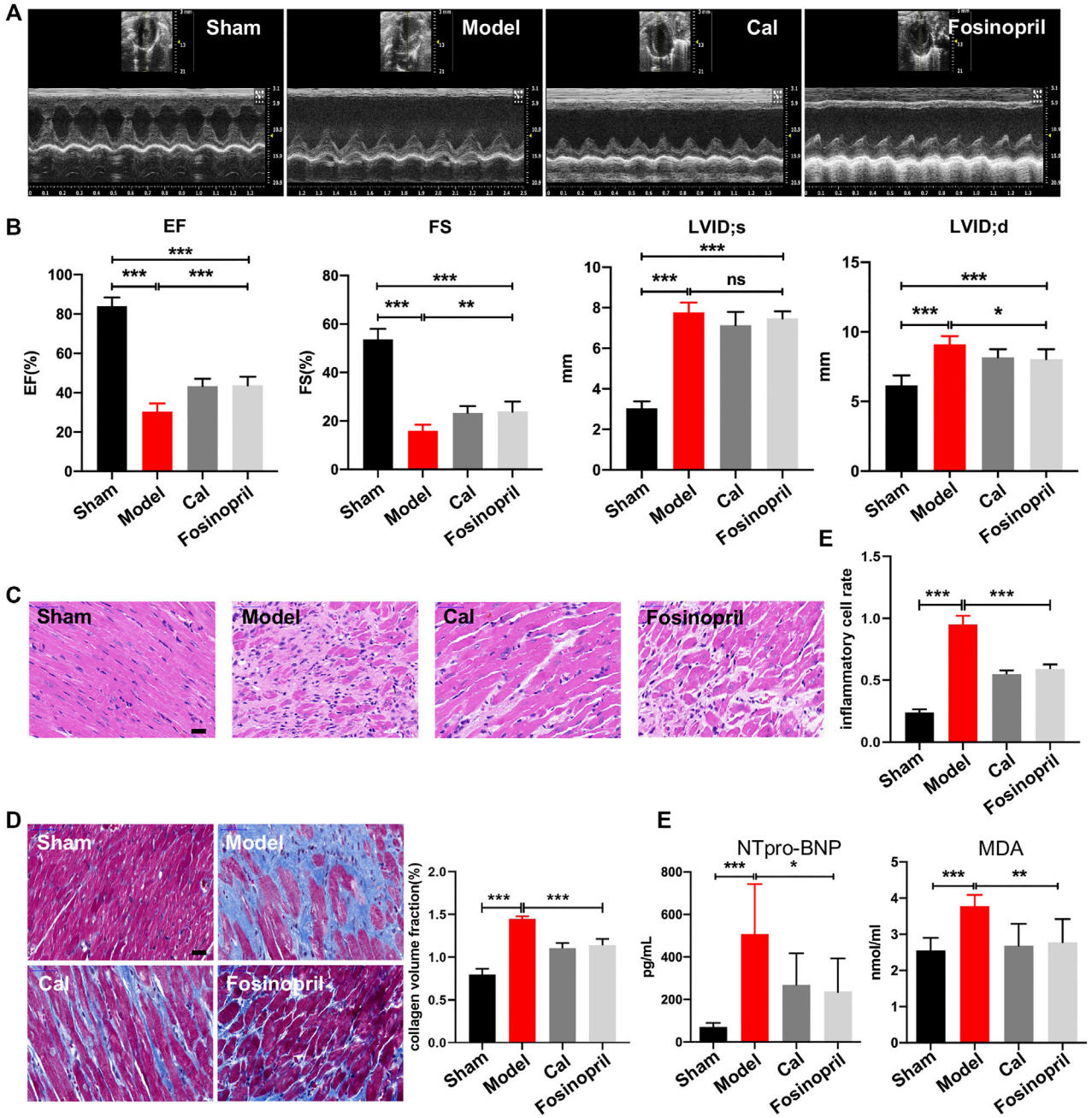

FIGURE 1 | Calycosin (Cal) protected heart function against heart failure (HF) in rats. **(A)** Representative images of echocardiography representing the changes in cardiac function. **(B)** Echocardiographic analysis showed that Cal and fosinopril treatment could increase ejection fraction (EF) and fractional shortening (FS), and decrease left ventricle internal dimension—diastole (LVID; d) values, while there were no significances on left ventricle internal dimension—systole (LVID; s). **(C)** Hematoxylin–eosin (HE) staining showed that Cal and fosinopril treatment protected against the inflammation injury; scale bar = 50 μm. Quantification of inflammatory cell infiltration (%) showed that Cal and fosinopril treatment decreased the inflammatory cell rate. **(D)** Masson staining and quantification of collagen volume fraction (CVF) showed that Cal and fosinopril treatment reduced collagen deposition and alleviated myocardial fibrosis; scale bar = 50 μm. **(E)** Levels of serum NTpro-BNP and MDA in the different groups. Data are presented as the mean ± standard error of three independent experiments ($N = 8$ per group, $^{*}p < 0.05$, $^{**}p < 0.01$, and $^{***}p < 0.001$).

the diameters on LVID; s and LVID; d were longer than that in the sham group, revealing that the HF model was successfully induced. After treatment with Cal and fosinopril, both EF and FS were increased significantly compared with the model group, suggesting that the left ventricular function was improved by Cal and fosinopril treatment. Additionally, compared with the model group, LVID; d in Cal and fosinopril groups were reduced significantly, while LVID; s in Cal and fosinopril groups were

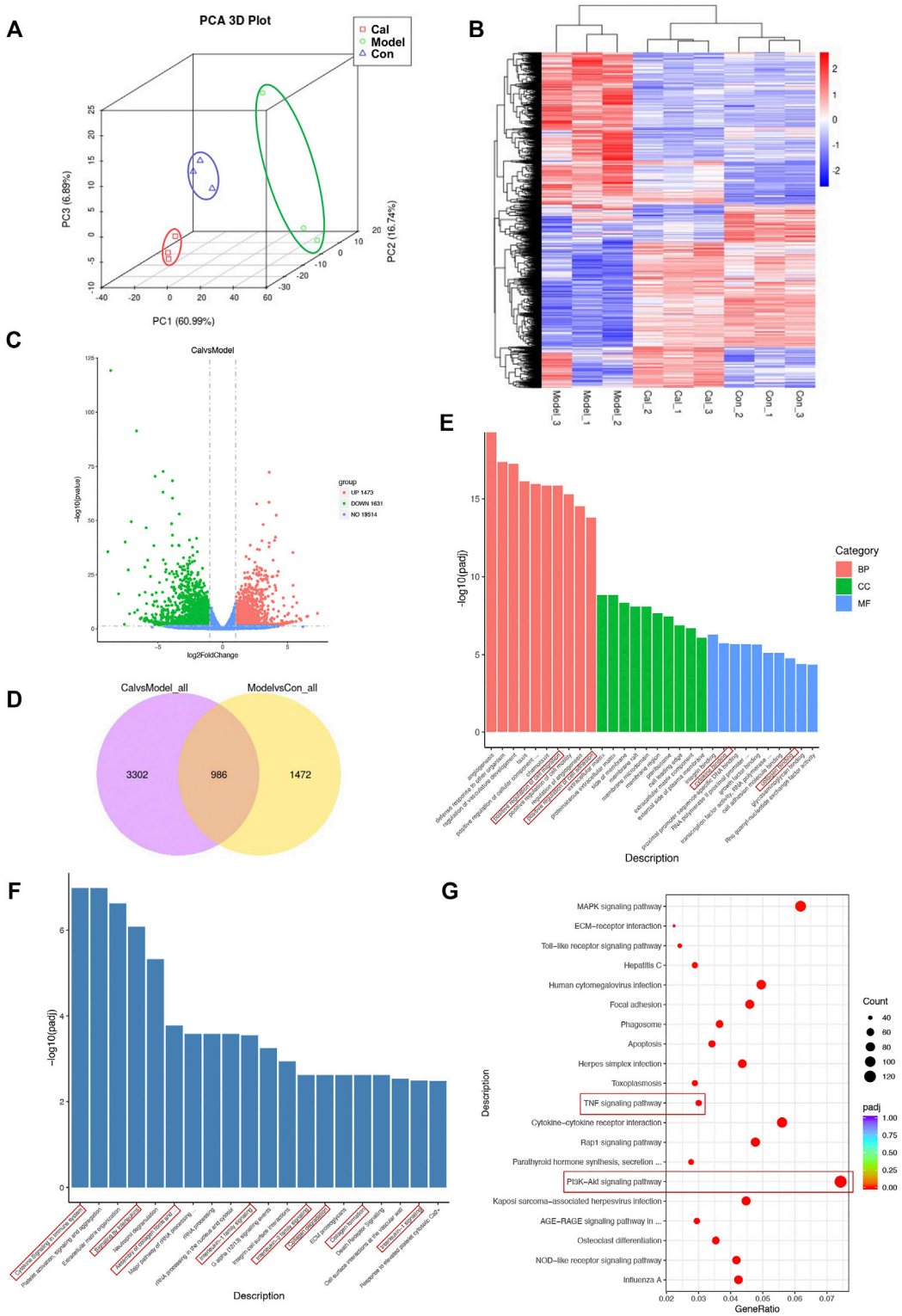

FIGURE 2 | Functional analysis of the differentially expressed genes (DEGs). **(A)** Principal component analysis (PCA) was used for visualizing RNA-seq between the different groups. **(B)** Heatmap of total DEGs between the different groups. **(C)** Volcano plots of DEGs between the Cal-treated group and the model group. The *x*-axis represents log2 (fold change) and the *y*-axis represents –log10 (padj). Red dots represent log2 > 1 and *p*-value < 0.05. Green dots are log2 < –1 and *p*-value < 0.05. **(D)** The 986 common DEGs were identified by Venn diagram. **(E)** The identified DEGs (Cal group vs. model group) were used for various Gene Ontology enrichment analysis including biological process (BP), cellular component (CC), and molecular functions (MF). The identified DEGs (Cal group vs. model group) were used for reactome **(F)** and KEGG **(G)** pathway classification analysis. *N* = 3 per group.

of no statistical significance (**Figures 1A, B**). The pathological changes in heart tissue were detected by H&E staining. As shown in **Figure 1C**, the left ventricular areas of the rats in the sham group were clearly visible, with the myocardial fibers arranged neatly and no inflammatory cell infiltration exerted in the myocardial interstitial space. However, in the heart tissue of rats in the model group, a significantly increased infiltration of inflammatory cell was present, myocardial fibers in the infarcted area were almost dissolved, and the myocardial stripes disappeared. Treatment with Cal and fosinopril rescued hearts from inflammatory cell infiltration and improved these pathological changes obviously (**Figure 1C**). Besides, Masson staining showed that there was obvious extensive collagen deposition in the border zone of the infarction in HF rats, whereas treatment with Cal and fosinopril significantly reduced contents of collagen deposition (**Figure 1D**). In addition, compared with the model group, Cal and fosinopril significantly reduced the serum levels of NTpro-BNP and MDA, which are the biomarkers of cardiac injury in HF (**Figure 1E**). These data indicated the protective effects of Cal and fosinopril on cardiac function.

Identification of differentially expressed genes associated with calycosin treatment

We utilized RNA-Seq to determine the effect of Cal on the cardiac transcriptome. Principal component analysis (PCA) was used for visualizing RNA-seq between different groups (**Figure 2A**). A hierarchical cluster heatmap between different groups illustrated the differentially expressed genes (DEGs) (**Figure 2B**). Compared with the model group, a total of 3,104 DEGs (1,473 upregulated and 1,631 downregulated genes) satisfied $|\log2\ (\text{foldchange})| > 1$ and the adjusted *p*-value less than 0.05 in the Cal-treated group (**Figure 2C**). Besides, the 986 key targets of Cal treatment against the HF model were obtained by overlapping the 4,288 targets of Cal treatment and 2,458 targets of HF model with a Venn diagram (**Figure 2D**). Furthermore, the identified 3,104 DEGs (Cal group vs. model group) were further used for Gene Ontology and functional pathway enrichment analysis. Intriguingly, enrichment analyses of GO annotations and reactome pathways revealed that the DEGs are related to inflammatory response and fibrosis in the Cal treatment group compared with the model group (**Figures 2E, F**). Besides, KEGG enrichment analysis of 3,104 DEGs showed that the involved pathway of Cal treatment was mainly composed of the PI3K–Akt signaling pathway, TNF signaling pathway, cytokine–cytokine receptor interaction, and MAPK signaling (**Figure 2G**). In conclusion, the integrated RNA-seq results suggested that the cardioprotective effects of Cal may owe to anti-inflammation and antifibrosis.

Effects of calycosin on myocardial inflammation via IKKs-NFκB pathway

The IKKs-NFκB pathway is considered as the initiation of inflammatory cascade. WB results implied that expressions of IKKα/β and NFκB remained relatively unaltered among different groups, while the expression levels of phosphorylated IKKα/β (*p*-IKKα/β) and NFκB (*p*-NFκB) increased significantly in the model group. After treatment with Cal, the expressions of *p*-IKKα/β and *p*-NFκB were reduced significantly, while only *p*-NFκB was decreased markedly in the fosinopril group (**Figure 3A**). The expression of downstream target activated by NFκB was further detected. Protein level of TNFα in the model group was increased, whereas Cal and fosinopril treatment suppressed the expression of TNFα (**Figure 3A**). Additionally, immunohistochemistry results showed that IOD of TNFα in the model group was upregulated significantly. After treatment with Cal and fosinopril, IOD of TNF was decreased (**Figure 3B**). Besides, Cal and fosinopril significantly reduced the serum levels of TNFα (**Figure 3C**) and IL-1 (**Figure 3D**). Collectively, these data indicated that Cal and fosinopril could alleviate inflammatory responses in HF rats.

Effects of calycosin on myocardial fibrosis via STAT3-MMP9 pathway

To investigate the effects of Cal and fosinopril on antifibrosis, the contents of collagen I and III in the cardiac tissue were determined by IHC. Results showed that IOD of collagen I and III in the model group were increased, compared with that in the sham group. After treatment with Cal and fosinopril, IODs of collagens I (**Figure 4A**) and III (**Figure 4B**) were both reduced. These results demonstrated that Cal and fosinopril could effectively attenuate cardiac fibrosis through the inhibition of expressions and depositions of collagen I and collagen III. Recent evidence indicates that the sustained activation of STAT3 signaling after MI may contribute to adverse remodeling and progression to heart failure (Nural-Guvener et al., 2015). MMP-9 is involved in post-MI repair and remodeling by regulating ECM metabolism and processing inflammatory mediators (Frangogiannis, 2017). The results showed that expressions of phosphorylated STAT3 (p-STAT3) and MMP-9 were upregulated in the model group, and Cal and fosinopril impressively inhibited the expressions of p-STAT3 and MMP-9 compared with the model group (**Figure 4C**).

PI3Ks are kinases that are responses for different types of membrane receptors, which have been observed to be activated in many cardiovascular diseases such as heart failure, hypertension, and atherosclerosis (Ghigo et al., 2013). *In vivo* results implied that the expressions of PI3K and *p*-AKT in the model group were decreased, while after treatment with Cal and fosinopril, the expressions were both upregulated remarkably (**Figure 4D**). Besides, transcriptome analysis revealed that the mRNA level of Pik3cd was significantly increased under Cal treatment, compared with the model group (**Figure 4E**). The Cal treatment dramatically downregulated the mRNA levels of mmp9, tnf, and nfap (NFκB activating protein), respectively (**Figure 4E**).

Anti-inflammation effects of calycosin via PI3K–AKT signaling pathway in cardiomyocytes

To further confirm the regulatory mechanism of Cal on inflammation and to better simulate the pathological

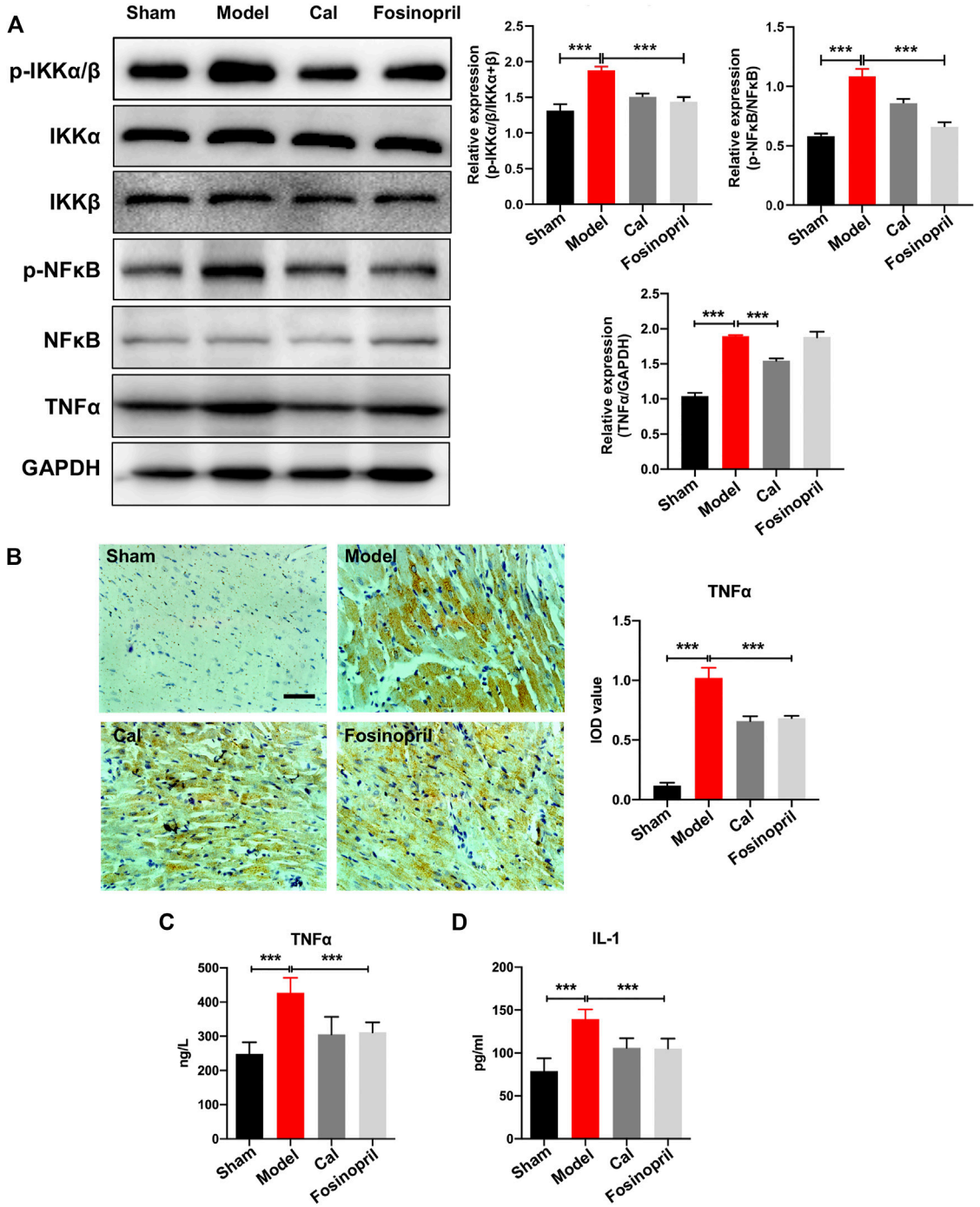

FIGURE 3 | Effects of Cal on myocardial inflammatory via IKKs-NFκB pathway. **(A)** Western blot bands of *p*-IKKα/β, *p*-NFκB, and TNFα and their quantitative results in HF rats, Cal could downregulate the expressions of *p*-IKKα/β, *p*-NFκB, and TNFα, while fosinopri did not decrease *p*-NFκB expression. **(B)** IHC images of TNFα and quantitative results in different groups. Levels of serum TNFα **(C)** and IL-1 **(D)** in the different groups. Data are presented as the mean ± standard error of three independent experiments. (*N* = 3 per group, ** $p < 0.01$, and *** $p < 0.001$).

environment of cardiomyocytes under inflammatory condition in HF, we applied a macrophage conditioned media (CM)-stimulated cardiomyocyte model described in our previous study (Li et al., 2016). Cell viability was reduced dramatically, and cell injury had occurred as characterized by induction of ROS and mitochondria damage. H9C2 cell, an embryonic cardiomyocyte cell line, was selected here owing to its robust and fast reaction to various stimuli. As shown in **Figures 5A, B**, treatment with 1–25 μM Cal proved to be effective, and 5 μM Cal showed the best protective effect on cell viability. So, 5 μM Cal

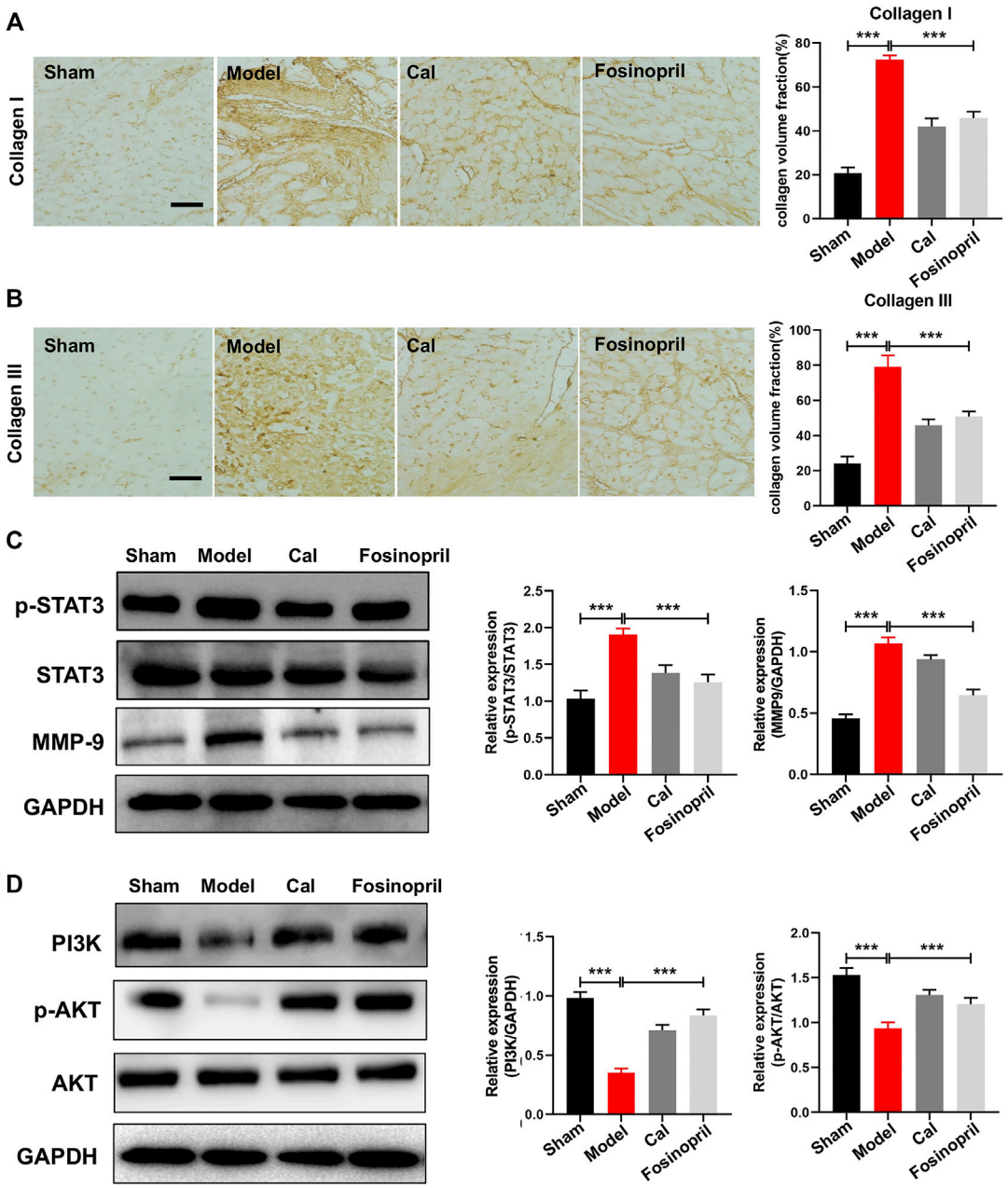

E

SYMBOL	Mean Expression	log2FoldChange	*p*-value	padj
Pik3cd	792.45	2.82 ↑	0.0030	0.0218
mmp9	188.12	-1.68 ↓	0.0031	0.0274
nfap	452.42	-1.26 ↓	0.0033	0.0439
tnf	321.29	-1.14 ↓	0.0036	0.0474

FIGURE 4 | Effects of Cal on myocardial fibrosis via the STAT3–MMP9 pathway. IHC images of collagen I **(A)** and III **(B)** in HF rats. Quantitative results of types I and III collagen content with IOD value; Cal and fosinopril could significantly reduce the collagen deposition compared with the model group. **(C)** Western blot bands of p-STAT3 and MMP-9 and their quantitative results in HF rats; Cal and fosinopril could downregulate the expressions of p-STAT3 and MMP-9. **(D)** Western blot bands of PI3K, *p*-AKT, and AKT and their quantitative results in HF rats. **(E)** The differentially expressed genes between the Cal group and the model group. The arrows represent the upregulated or downregulated expression of gene. Data are presented as the mean ± standard error of three independent experiments. ($N = 3$ per group, $^{**}p < 0.01$, $^{***}p < 0.001$).

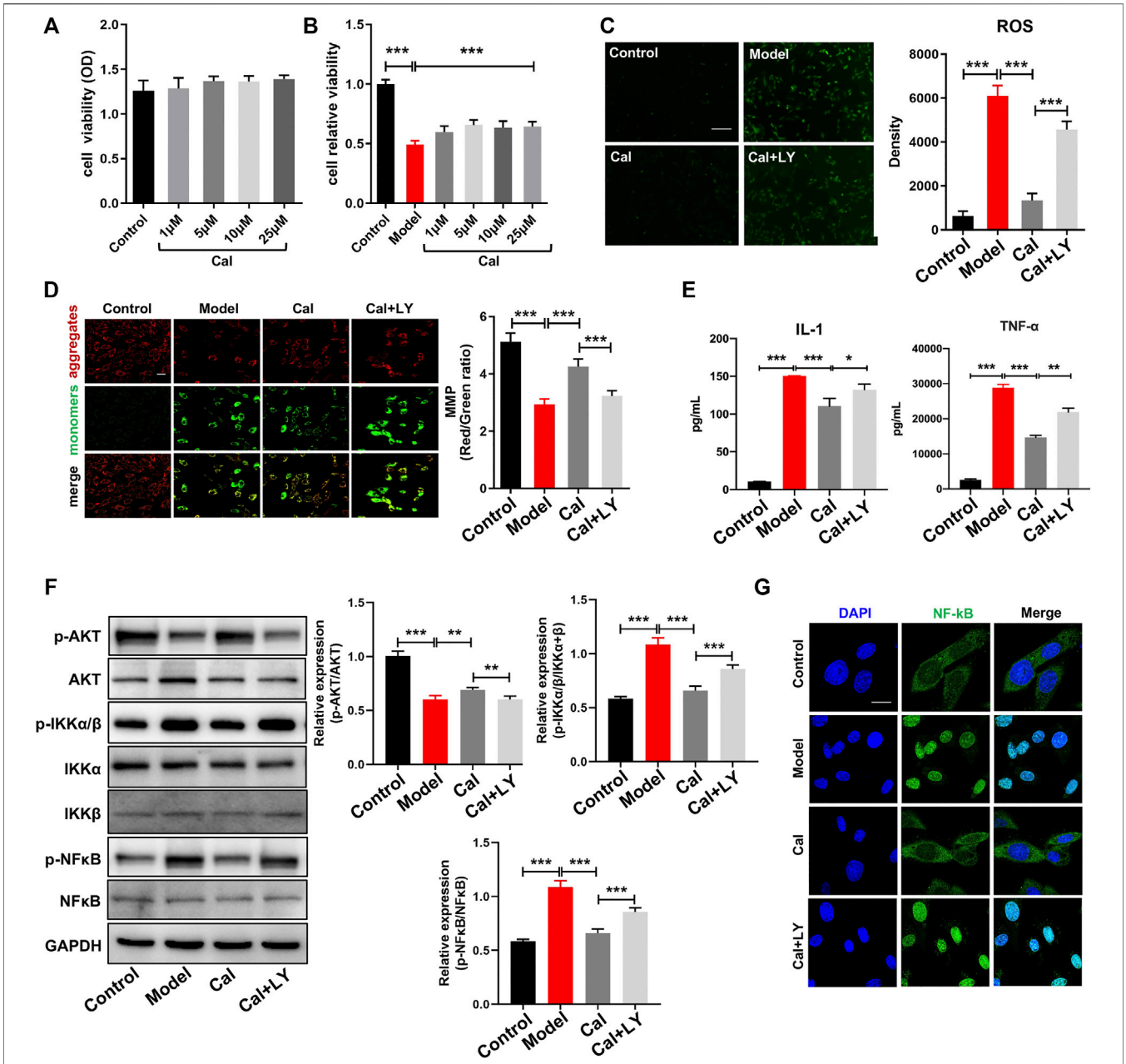

FIGURE 5 | Anti-inflammation effects of Cal via the PI3K–AKT signaling pathway in cardiomyocytes. CCK8 assay was used to determine cell injury. **(A)** Cal (1–25 μM) has no cytotoxicity on H9C2 cells compared with the control group. **(B)** Conditioned media (CM)-induced cellular injury in H9C2 cells and Cal (5 μM) increased cell viability significantly. **(C)** reactive oxygen species (ROS) staining in the different groups, $N = 12$. (D) Mitochondrial membrane potential (MMP) was determined by JC-1 probe (400×, scale bar = 100 μm), $N = 12$. **(E)** The release of IL-1 and TNF-α in H9C2 cell supernatants was detected by ELISA assay, $N = 12$. **(F)** Western blot bands of *p*-AKT, *p*-IKKα/β, and *p*-NFκB and quantitative results in cells. **(G)** Immunofluorescence staining of NFκB under different treatments; scale bar = 50 μm. $N = 20$ cells per group. Data are presented as the mean ± standard error of three independent experiments. $^{*}p < 0.05$, $^{**}p < 0.01$, $^{***}p < 0.001$.

was the optimal concentration applied in the subsequent experiments. During the inflammatory phase of heart failure, myocardial cell death and hypoxia trigger the overgeneration of reactive oxygen species (ROS) and the damage of the mitochondria. ROS staining showed that Cal dramatically reduced the level of ROS (**Figure 5C**). The evaluation of mitochondrial transmembrane potential (MMP) was conducted by JC-1 probe (Zhang et al., 2021). The results suggested that the ratio of aggregates/monomers increased in response to Cal, suggesting that the MMP returned to normal (**Figure 5D**). Besides, Cal significantly reduced the release of TNFα and IL-1 (**Figure 5E**). Intriguingly, LY294002, an inhibitor of PI3K, compromised these protective effects of Cal in CM-induced H9C2 cells.

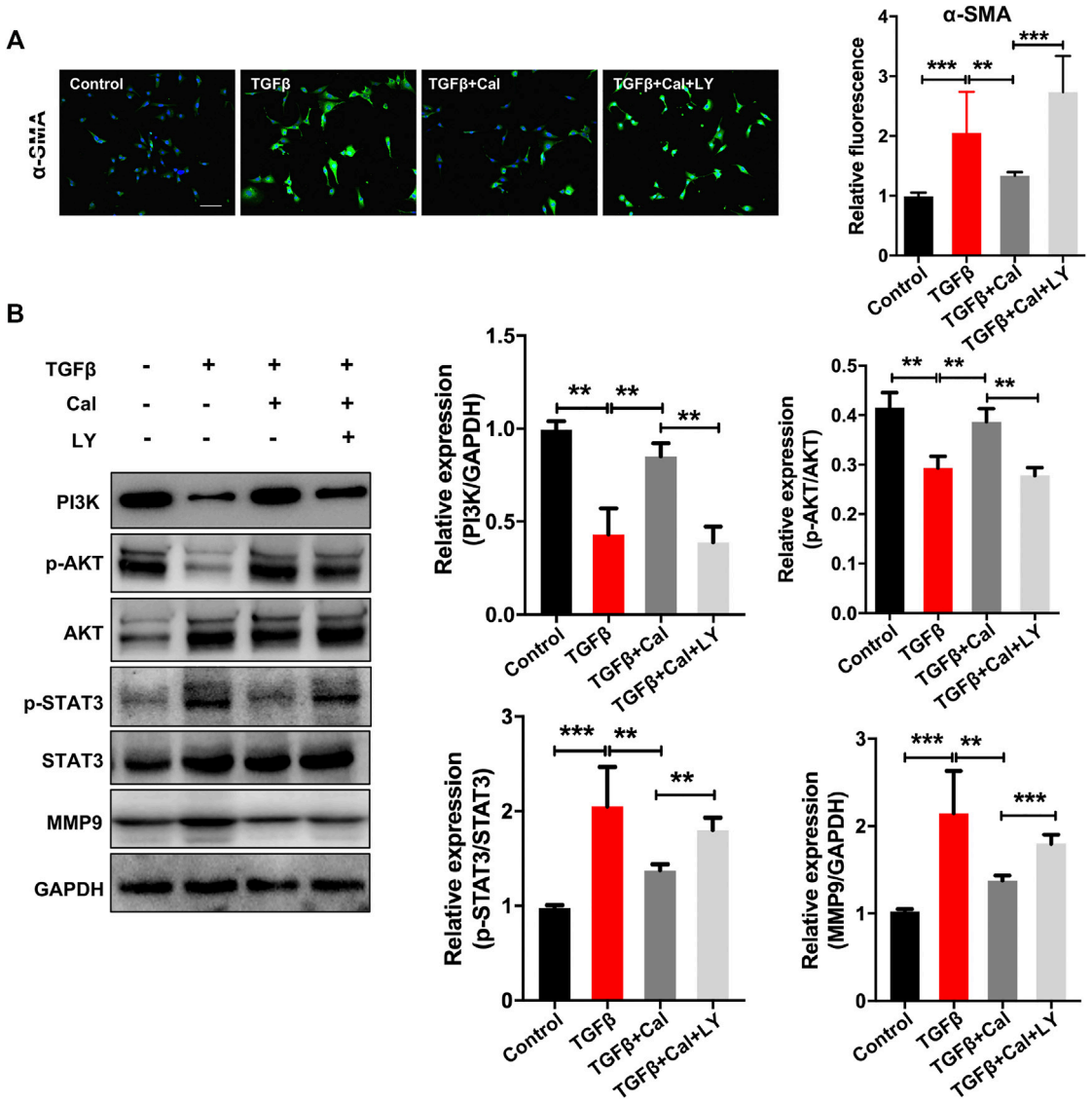

FIGURE 6 | Cal regulated the TGFβ-activated PI3K–Akt signaling pathway in cardiac fibroblasts. **(A)** Representative images of α-SMA immunoassay in each group. Scale bar = 50 μm. *N* = 20 cells per group. **(B)** Western blot bands of PI3K, AKT, STAT3, and MMP9 and their quantitative results in cells. Data are presented as the mean ± standard error of three independent experiments. **p* < 0.05, ***p* < 0.01, ****p* < 0.001.

As the PI3K–AKT pathway plays a vital role in regulating the inflammation, we compared the expression levels of *p*-AKT, *p*-IKKα/β, and *p*-NFκB in CM-induced H9C2 cells with or without Cal treatment. WB results implied that expression of *p*-AKT was impressively reduced in the model group, while treatment with Cal could promote the expression of *p*-AKT (**Figure 5F**). Besides, the expressions of *p*-IKKα/β and *p*-NFκB were both markedly increased in the model group compared with the control group, while treatment with Cal downregulated their expressions, respectively (**Figure 5F**). Immunofluorescence results also showed that Cal treatment inhibited nuclear translocation of NFκB (**Figure 5G**). To further explore the anti-inflammation effect of Cal on the PI3K–AKT pathway, LY294002, an inhibitor of PI3K, was added together with Cal. Intriguingly, LY294002 suppressed the expression of *p*-AKT. Furthermore, the regulation on *p*-IKKα/β, NFκB activation, ROS level, MMP, and proinflammatory cytokine level by Cal was also eliminated by LY294002 (**Figures 5D–G**), indicating that Cal protected against CM-induced injury in H9C2 cells partly by targeting on the PI3K–AKT pathway. Collectively, these results demonstrated that Cal could alleviate inflammation by activating PI3K–AKT pathway in cardiomyocytes.

Antifibrosis effects of calycosin via PI3K–AKT signaling pathway in cardiac fibroblasts

The effects of Cal on TGFβ-stimulated cardiac fibroblasts were further investigated. Cardiac fibroblasts were incubated with

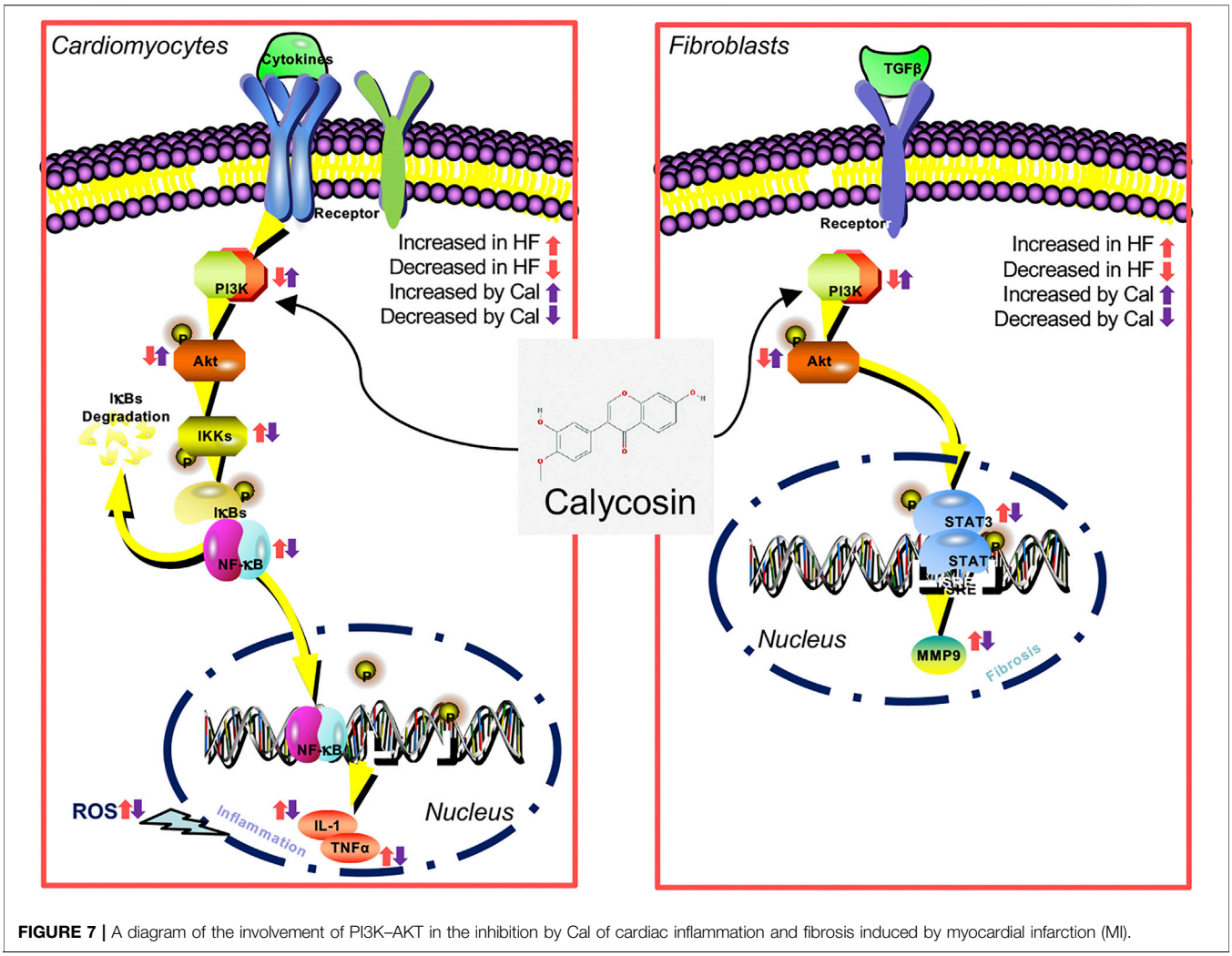

FIGURE 7 | A diagram of the involvement of PI3K–AKT in the inhibition by Cal of cardiac inflammation and fibrosis induced by myocardial infarction (MI).

TGFβ at a concentration of 20 ng/ml for 24 h. TGFβ induces transformation of fibroblast to myofibroblast, which is the main producer of collagens and is characterized by the presence of α-smooth muscle actin (α-SMA). Our results showed that α-SMA expression was increased in TGFβ-stimulated cells, suggesting that fibroblasts were phenotypically transformed into myofibroblasts (**Figure 6A**). Cal treatment suppressed TGFβ-induced expression of α-SMA, dramatically reduced the expressions of p-STAT3 and MMP-9, and upregulated the expressions of PI3K and *p*-AKT compared with the model group (**Figures 6A, B**). While cotreatment with LY294002 abolished these effects. These data suggested that Cal could block the transformation of fibroblast to myofibroblast, thereby suppressing cardiac fibrosis via the PI3K–AKT pathway.

DISCUSSION

The main goal of this research was to explore the relationship between the PI3K–AKT signaling pathway and the potential anti-inflammation/antifibrosis effects of Cal on HF in rats and in H9C2 cells. Our study provided a novel approach and mechanism for the treatment of HF. The main findings are as follows: 1) Cal ameliorated cardiac functions and alleviated pathological changes in an HF rat model. 2) Cal inhibited excessive release of proinflammatory cytokines by inhibiting IKK-NFκB-mediated inflammatory pathway in cardiomyocytes. 3) Cal blocked the transformation of fibroblast to myofibroblast through the inhibition of STAT3-MMP9 signaling. 4) These regulative effects were accessed by targeting the PI3K–AKT pathway.

HF is typically associated with myocardial fibrosis. Here, inflammation and fibrosis are thought to play critical roles. Activation of an inflammatory reaction and the subsequent secretion of inflammatory cytokines, such as TNFα, facilitate the recruitment and activation of more inflammatory cells to the developing lesion (Huang and Frangogiannis, 2018). Cardiac fibrosis is characterized by an increased amount and a disrupted composition of the fibrillar/collagen-rich ECM. Excessive fibroblast activation may lead to expansion of the fibrotic scar area, which increases myocardial stiffness and promotes diastolic dysfunction (Kong et al., 2018). In our HF rat model, levels of TNFα and IL-1 elevated significantly. In addition, cardiac remodeling characteristics

were observed, such as cardiomyocyte derangement, infiltrated inflammatory cells, as well as abnormal deposition of collagen. Therefore, inflammation and fibrosis are interesting targets for innovative heart failure treatments. The exciting part is that Cal treatment rescued hearts from inflammatory cell infiltration and maintained original morphology as well as reduced contents of collagen deposition in HF models. Furthermore, Cal treatment could reverse the abnormal elevation of serums TNFα level and IL-1 level in HF rats.

To investigate the potential mechanisms of Cal, RNA-seq is applied. GO significant enrichment analysis identified that anti-inflammation and antifibrosis effects are involved in Cal treatment, and the PI3K–AKT signaling pathway is regulated by Cal to ameliorate the cardiac function of HF according to KEGG enrichment analysis. A few studies have reported changes in PI3K signaling in HF (Ghigo et al., 2017; Durrant and Hers, 2020), There is controversy in the literature as some studies reported an activation, while others reported an inhibition of PI3K (Hao et al., 2020). Collectively, our findings can give a deeper insight on the therapeutic mechanisms of Cal in treating HF.

To further investigate the underlying mechanism of anti-inflammation and antifibrosis, a CM-induced H9C2 cell model and a TGFβ-induced cardiac fibroblast model were conducted, respectively. In cardiomyocytes, Cal significantly improved cell viability, inhibited ROS production, and restored MMP against CM-induced injury. Besides, results showed that Cal could downregulate levels of *p*-IKKα/β, *p*-NFκB, TNFα, and IL-1, demonstrating that Cal has a regulative efficacy on anti-inflammation pathway in cardiomyocytes. In cardiac fibroblasts, Cal showed a marked effect on myocardial fibrosis evidenced by decreased α-SMA expression. Besides, Cal could decrease the protein levels of p-STAT3 and MMP-9. These results indicated that Cal could alleviate inflammatory responses and attenuate cardiac fibrosis to exert cardioprotection against HF. The upstream pathways of inflammation and fibrosis were further demonstrated. Cal could enhance the expression of PI3K, then activate *p*-AKT expression dramatically. LY294002, an inhibitor of PI3K, was then added together with Cal, to further validate the effect of Cal on the PI3K–AKT pathway. Results indicated that the protective effects and relative protein levels of *p*-AKT, *p*-IKKα/β, and *p*-NFκB were abrogated by LY294002 in cardiomyocytes. In addition, cotreatment with LY294002 also abolished the effects of Cal on α-SMA, p-STAT3, and MMP9 levels in cardiac fibroblasts. Collectively, these data indicated that Cal exerted anti-inflammation and antifibrosis effects against HF through the PI3K–AKT pathway.

CONCLUSION

This study implies that Cal reduces cardiac inflammation and fibrosis via the PI3K–AKT signaling pathway in H9C2 cells, fibroblasts, and heart failure postacute myocardial infarction rats (**Figure 7**). Cal, as a novel PI3K activator, reduces inflammation and fibrosis in heart failure through the AKT–IKK/STAT3 axis. These findings aid our understanding on the therapeutic mechanisms by which Cal exerts cardioprotection.

Our work still includes some limitations. In our previous study, 1–10 μg/ml of LPS had no effects on the production of NO and LDH in H9C2 cells, indicating that LPS is not an ideal agent for inducing inflammation in H9C2 cells (Li et al., 2016). As cytokines released from macrophages play an important role in the progression of inflammation in ischemic heart tissue (Li et al., 2016), we concluded that cytokines contained in the conditioned medium used to stimulate H9C2 cells is critical. To determine whether the conditioned medium contain LPS is important, and we would perform mass spectrometry analysis in our future study. Since TGFβ is not an equivalent stimulus to the *in vivo* HF model. In order to replicate the *in vivo* and HF phenotype more appropriately, methodologically, we will use fibroblasts cultured from sham rats and HF rats to make our conclusions much more compelling and powerful. Besides, we will include the fosinopril group in the RNA seq and *in vitro* data. In addition, we will carry out experiments to explore whether LY can blunt the impact of Cal *in vivo*.

DATA AVAILABILITY STATEMENT

The datasets presented in this study can be found in online repositories. The names of the repository/repositories and accession number(s) can be found below: https://www.ncbi.nlm.nih.gov/, https://www.ncbi.nlm.nih.gov/geo/query/acc.cgi?acc=GSE184649.

ETHICS STATEMENT

The animal study was reviewed and approved by the Institutional Animal Care and Use Committee at the Beijing University of Chinese Medicine.

AUTHOR CONTRIBUTIONS

XW, WL, and QZ contributed to the conception and design of the experiment. SY, NT, and PW contributed to the animal experiments. QS, JC, and YZ contributed to the cell culture. XM revised the manuscript. YW, WW, and LL were responsible for the financial support, manuscript revision and final approval of the manuscript. All authors have read and agreed with the manuscript.

FUNDING

This work was financially supported by grants from the National Natural Science Foundation of China (No. 82174364, 81,822,049) and Beijing University of Chinese Medicine New Teacher Starting Foundation (2021-JYB-XJSJJ014).

ACKNOWLEDGMENTS

The authors thank the members of their laboratory and their collaborators for their research work.

REFERENCES

Bacmeister, L., Schwarzl, M., Warnke, S., Stoffers, B., Blankenberg, S., Westermann, D., et al. (2019). Inflammation and Fibrosis in Murine Models of Heart Failure. *Basic Res. Cardiol.* 114 (3), 19. doi:10.1007/s00395-019-0722-5

Chong, E., Chang, S. L., Hsiao, Y. W., Singhal, R., Liu, S. H., Leha, T., et al. (2015). Resveratrol, a Red Wine Antioxidant, Reduces Atrial Fibrillation Susceptibility in the Failing Heart by PI3K/AKT/eNOS Signaling Pathway Activation. *Heart Rhythm* 12 (5), 1046–1056. doi:10.1016/j.hrthm.2015.01.044

Davis, R., Coukell, A., and McTavish, D. (1997). Fosinopril. A Review of its Pharmacology and Clinical Efficacy in the Management of Heart Failure. *Drugs* 54 (1), 103–116. doi:10.2165/00003495-199754010-00012

Durrant, T. N., and Hers, I. (2020). PI3K Inhibitors in Thrombosis and Cardiovascular Disease. *Clin. Transl Med.* 9 (1), 8. doi:10.1186/s40169-020-0261-6

Efferth, T., Shan, L., and Zhang, Z.-W. (2016). Tonic Herbs and Herbal Mixtures in Chinese Medicine. *World J. Tradit Chin. Med.* 2 (1), 10–25. doi:10.15806/j.issn.2311-8571.2015.0037

Frangogiannis, N. G. (2017). The Extracellular Matrix in Myocardial Injury, Repair, and Remodeling. *J. Clin. Invest.* 127 (5), 1600–1612. doi:10.1172/JCI87491

Frangogiannis, N. G. (2014). The Inflammatory Response in Myocardial Injury, Repair, and Remodelling. *Nat. Rev. Cardiol.* 11 (5), 255–265. doi:10.1038/nrcardio.2014.28

Gao, S., Zhang, Q., Tian, C., Li, C., Lin, Y., Gao, W., et al. (2020). The Roles of Qishen Granules Recipes, Qingre Jiedu, Wenyang Yiqi and Huo Xue, in the Treatment of Heart Failure. *J. Ethnopharmacol* 249, 112372. doi:10.1016/j.jep.2019.112372

Ghigo, A., Laffargue, M., Li, M., and Hirsch, E. (2017). PI3K and Calcium Signaling in Cardiovascular Disease. *Circ. Res.* 121 (3), 282–292. doi:10.1161/CIRCRESAHA.117.310183

Ghigo, A., Morello, F., Perino, A., and Hirsch, E. (2013). Therapeutic Applications of PI3K Inhibitors in Cardiovascular Diseases. *Future Med. Chem.* 5 (4), 479–492. doi:10.4155/fmc.13.11

Hao, Q., Zhang, F., Wang, Y., Li, Y., and Qi, X. (2020). Cardiac Contractility Modulation Attenuates Chronic Heart Failure in a Rabbit Model via the PI3K/AKT Pathway. *Biomed. Res. Int.* 2020, 1625362. doi:10.1155/2020/1625362

Huang, J., Shen, H., Jiang, M., Huang, L., Yuan, Y., and Wang, Q. (2020). Calycosin Reduces Infarct Size, Oxidative Stress and Preserve Heart Function in Isoproterenol-Induced Myocardial Infarction Model. *Pak J. Pharm. Sci.* 33 (3Special), 1341–1347.

Huang, S., and Frangogiannis, N. G. (2018). Anti-inflammatory Therapies in Myocardial Infarction: Failures, Hopes and Challenges. *Br. J. Pharmacol.* 175 (9), 1377–1400. doi:10.1111/bph.14155

Humeres, C., and Frangogiannis, N. G. (2019). Fibroblasts in the Infarcted, Remodeling, and Failing Heart. *JACC Basic Transl Sci.* 4 (3), 449–467. doi:10.1016/j.jacbts.2019.02.006

Israël, A. (2010). The IKK Complex, a central Regulator of NF-kappaB Activation. *Cold Spring Harb Perspect. Biol.* 2 (3), a000158. doi:10.1101/cshperspect.a000158

Kong, P., Shinde, A. V., Su, Y., Russo, I., Chen, B., Saxena, A., et al. (2018). Opposing Actions of Fibroblast and Cardiomyocyte Smad3 Signaling in the Infarcted Myocardium. *Circulation* 137 (7), 707–724. doi:10.1161/CIRCULATIONAHA.117.029622

Lee, T. M., Harn, H. J., Chiou, T. W., Chuang, M. H., Chen, C. H., Chuang, C. H., et al. (2019). Preconditioned Adipose-Derived Stem Cells Ameliorate Cardiac Fibrosis by Regulating Macrophage Polarization in Infarcted Rat Hearts through the PI3K/STAT3 Pathway. *Lab. Invest.* 99 (5), 634–647. doi:10.1038/s41374-018-0181-x

Li, C., Wang, J., Wang, Q., Zhang, Y., Zhang, N., Lu, L., et al. (2016). Qishen Granules Inhibit Myocardial Inflammation Injury through Regulating Arachidonic Acid Metabolism. *Sci. Rep.* 6, 36949. doi:10.1038/srep36949

Li, D., Zhao, L., Li, Y., Kang, X., and Zhang, S. (2020). Gastro-Protective Effects of Calycosin against Precancerous Lesions of Gastric Carcinoma in Rats. *Drug Des. Devel Ther.* 14, 2207–2219. doi:10.2147/DDDT.S247958

Li, Y., Xia, J., Jiang, N., Xian, Y., Ju, H., Wei, Y., et al. (2018). Corin Protects H2O2-Induced Apoptosis through PI3K/AKT and NF-Kb Pathway in Cardiomyocytes. *Biomed. Pharmacother.* 97, 594–599. doi:10.1016/j.biopha.2017.10.090

Liu, Y., Che, G., Di, Z., Sun, W., Tian, J., and Ren, M. (2020). Calycosin-7-O-β-D-glucoside Attenuates Myocardial Ischemia-Reperfusion Injury by Activating JAK2/STAT3 Signaling Pathway via the Regulation of IL-10 Secretion in Mice. *Mol. Cel Biochem* 463 (1-2), 175–187. doi:10.1007/s11010-019-03639-z

Medeiros, N. I., Gomes, J. A. S., and Correa-Oliveira, R. (2017). Synergic and Antagonistic Relationship between MMP-2 and MMP-9 with Fibrosis and Inflammation in Chagas' Cardiomyopathy. *Parasite Immunol.* 39 (8). doi:10.1111/pim.12446

Nural-Guvener, H., Zakharova, L., Feehery, L., Sljukic, S., and Gaballa, M. (2015). Anti-Fibrotic Effects of Class I HDAC Inhibitor, Mocetinostat Is Associated with IL-6/Stat3 Signaling in Ischemic Heart Failure. *Int. J. Mol. Sci.* 16 (5), 11482–11499. doi:10.3390/ijms160511482

Prabhu, S. D., and Frangogiannis, N. G. (2016). The Biological Basis for Cardiac Repair after Myocardial Infarction: From Inflammation to Fibrosis. *Circ. Res.* 119 (1), 91–112. doi:10.1161/CIRCRESAHA.116.303577

Rhee, A. J., and Lavine, K. J. (2020). New Approaches to Target Inflammation in Heart Failure: Harnessing Insights from Studies of Immune Cell Diversity. *Annu. Rev. Physiol.* 82, 1–20. doi:10.1146/annurev-physiol-021119-034412

Singh, R., Kaundal, R. K., Zhao, B., Bouchareb, R., and Lebeche, D. (2021). Resistin Induces Cardiac Fibroblast-Myofibroblast Differentiation through JAK/STAT3 and JNK/c-Jun Signaling. *Pharmacol. Res.* 167, 105414. doi:10.1016/j.phrs.2020.105414

Wang, Q., Qu, X., Zheng, L., and Wang, H. (2021). Thymic Stromal Lymphopoietin Alleviates Fibrosis after Myocardial Infarction through Regulating STAT3. *Panminerva Med.* 63. doi:10.23736/s0031-0808.19.03683-8

Wang, X., Guo, D., Li, W., Zhang, Q., Jiang, Y., Wang, Q., et al. (2020a). Danshen (Salvia Miltiorrhiza) Restricts MD2/TLR4-MyD88 Complex Formation and Signalling in Acute Myocardial Infarction-Induced Heart Failure. *J. Cel Mol Med* 24 (18), 10677–10692. doi:10.1111/jcmm.15688

Wang, X., Meng, H., Wang, Q., Shao, M., Lu, W., Chen, X., et al. (2020b). Baoyuan Decoction Ameliorates Apoptosis via AT1-CARP Signaling Pathway in H9C2 Cells and Heart Failure post-acute Myocardial Infarction Rats. *J. Ethnopharmacol* 252, 112536. doi:10.1016/j.jep.2019.112536

Wu, M. P., Zhang, Y. S., Zhou, Q. M., Xiong, J., Dong, Y. R., and Yan, C. (2016). Higenamine Protects Ischemia/reperfusion Induced Cardiac Injury and Myocyte Apoptosis through Activation of β2-AR/PI3K/AKT Signaling Pathway. *Pharmacol. Res.* 104, 115–123. doi:10.1016/j.phrs.2015.12.032

Zhai, J., Tao, L., Zhang, S., Gao, H., Zhang, Y., Sun, J., et al. (2020). Calycosin Ameliorates Doxorubicin-Induced Cardiotoxicity by Suppressing Oxidative Stress and Inflammation via the Sirtuin 1-NOD-like Receptor Protein 3 Pathway. *Phytother Res.* 34 (3), 649–659. doi:10.1002/ptr.6557

Zhang, L., Fu, R., Duan, D., Li, Z., Li, B., Ming, Y., et al. (2021). Cyclovirobuxine D Induces Apoptosis and Mitochondrial Damage in Glioblastoma Cells through ROS-Mediated Mitochondrial Translocation of Cofilin. *Front. Oncol.* 11, 656184. doi:10.3389/fonc.2021.656184

Zhang, Q., Shao, M., Zhang, X., Wang, Q., Guo, D., Yang, X., et al. (2018). The Effect of Chinese Medicine on Lipid and Glucose Metabolism in Acute Myocardial Infarction through PPARγ Pathway. *Front. Pharmacol.* 9, 1209. doi:10.3389/fphar.2018.01209

Zhang, X., Wang, Q., Wang, X., Chen, X., Shao, M., Zhang, Q., et al. (2019). Tanshinone IIA Protects against Heart Failure post-myocardial Infarction via AMPKs/mTOR-dependent Autophagy Pathway. *Biomed. Pharmacother.* 112, 108599. doi:10.1016/j.biopha.2019.108599

Conflict of Interest: The authors declare that the research was conducted in the absence of any commercial or financial relationships that could be construed as a potential conflict of interest.

frontiers in Pharmacology

CLINICAL TRIAL
published: 18 March 2022
doi: 10.3389/fphar.2022.831208

Efficacy and Mechanism of Buyang Huanwu Decoction in Patients With Ischemic Heart Failure: A Randomized, Double-Blind, Placebo-Controlled Trial Combined With Proteomic Analysis

Mingjun Zhu[1†], Jingjing Wei[2†], Ying Li[3†], Yongxia Wang[1], Junguo Ren[3], Bin Li[1], Bo Ma[3], Xinlu Wang[1], Lijie Qiao[2], Cheng Zhou[2] and Jianxun Liu[3*]*

[1]First Affiliated Hospital of Henan University of CM, Zhengzhou, China, [2]Henan University of Chinese Medicine, Zhengzhou, China, [3]Beijing Key Laboratory of Pharmacology of Chinese Materia Region, Institute of Basic Medical Sciences, Xiyuan Hospital, China Academy of Chinese Medical Sciences, National Clinical Research Center of Cardiovascular Disease of Traditional Chinese Medicine, Beijing, China

OPEN ACCESS

Edited by:
Yi Wang,
Zhejiang University, China

Reviewed by:
Min Wu,
China Academy of Chinese Medical Sciences, China
Jianxin Chen,
Beijing University of Chinese Medicine, China

***Correspondence:**
Mingjun Zhu
zhumingjun317@163.com
Jianxun Liu
liujx0324@sina.com

[†]These authors have contributed equally to this work

Specialty section:
This article was submitted to Ethnopharmacology, a section of the journal Frontiers in Pharmacology

Received: 08 December 2021
Accepted: 04 March 2022
Published: 18 March 2022

Citation:
Zhu M, Wei J, Li Y, Wang Y, Ren J, Li B, Ma B, Wang X, Qiao L, Zhou C and Liu J (2022) Efficacy and Mechanism of Buyang Huanwu Decoction in Patients With Ischemic Heart Failure: A Randomized, Double-Blind, Placebo-Controlled Trial Combined With Proteomic Analysis. Front. Pharmacol. 13:831208. doi: 10.3389/fphar.2022.831208

Objective: Buyang Huanwu Decoction (BYHW), a famous herbal prescription in traditional Chinese medicine (TCM), has been used for 200 years for treating ischemic heart failure (IHF). This study aims to assess the efficacy and safety of BYHW combined with guideline-guided pharmacotherapy in patients with IHF and explore the biological mechanism by which BYHW exerts its efficacy.

Methods: In the multicenter, double-blind, randomized controlled trial, a total of 80 patients with IHF were randomized to receive BYHW or placebo for 3 months. The primary efficacy endpoints were New York Heart Association (NYHA) classification, TCM syndrome scores, N-terminal pro-B-type natriuretic peptide (NT-ProBNP), whereas the mechanism exploration endpoints included energy metabolism parameters and coagulation function parameters. In addition, we performed the proteomic study of the serum of patients after treatment by label-free quantification technology to verify the candidate target proteins and pathways.

Results: After 3 months of treatment, the NYHA classification, TCM syndrome scores, and the percentage of subjects with at least 30% reduction in NT-ProBNP were significantly improved in the BYHW group, compared with the control group ($p < 0.05$); BYHW treatment also significantly regulated blood glucose, blood lipid levels, ameliorated energy metabolism and improved coagulation function parameters. There

Abbreviations: 6MWD, 6-minute walk distance; ATP, adenosine triphosphate; ADP, adenosine diphosphate; APOC1, Apolipoprotein C-I; APOC2, Apolipoprotein C-II; APTT, activation time of partial thromboplastin; BYHW, Buyang Huanwu Decoction; CPB2, Carboxypeptidase B2; F13A1, Coagulation factor XIII A; FGB, fibrinogen beta; FGG, fibrinogen gamma; FIB, fibrinogen; GLU, glucose; HDL-C, high density lipoprotein cholesterol; ICAM1, intercellular adhesion molecule1; IHF, ischemic heart failure; LDL-C, low density lipoprotein cholesterol; LVEF, left ventricular ejection fraction; NT-ProBNP, N-terminal pro-B-type natriuretic peptide; NYHA, New York Heart Association; PT, prothrombin time; TC, total cholesterol; TCM, traditional Chinese medicine; TG, triglyceride; TT, thrombin time.

were no significant differences in safety endpoints between the two groups. In addition, we obtained 56 differentially expressed proteins by proteomics, including 20 upregulated proteins and 36 downregulated proteins. Bioinformatic analysis revealed the mechanism of BYHW treatment was significantly related to complement and coagulation cascades, cholesterol metabolism, NF-kappa B signaling pathway, PI3K-Akt signaling pathway, and metabolic pathways. Among these differentially regulated proteins, fibrinogen gamma (FGG), fibrinogen beta (FGB), Carboxypeptidase B2 (CPB2), Coagulation factor XIII A (F13A1), Intercellular adhesion molecule1 (ICAM1), Apolipoprotein C-II(APOC2), Apolipoprotein C-I(APOC1), and CD44 were found to be signature proteins associated with the efficacy of BYHW against IHF.

Conclusion: BYHW treatment can further improve cardiac dysfunction and clinical symptoms in IHF based on standard therapy without apparent adverse effects. Additionally, BYHW may play a therapeutic role in IHF by improving energy metabolism and regulating coagulation function through multiple targets and pathways.

Keywords: ischemic heart failure, Buyang Huanwu decoction, randomized controlled trial, proteomics, energy metabolism, coagulation function

Clinical Trial Registration: clinicaltrials.gov, identifier NCT02875639

1 INTRODUCTION

Ischemic heart failure (IHF) remains a significant cause of morbidity and mortality worldwide. More than 37.7 million patients suffer from HF worldwide, and about 70% of HF can trace back to ischemic heart disease (Ziaeian and Fonarow, 2016; Elgendy et al., 2019). More than 8.9 million patients with HF have been in China, and coronary heart disease has become the dominant primary disease in Chinese patients (Ma et al., 2020). With the development of early reperfusion strategies, including coronary stent implantation and drug therapy, the short-term mortality after acute myocardial infarction has been significantly reduced. However, the prevalence of IHF has been increasing year by year. After myocardial infarction, about 40%–56% of patients will have decreased cardiac function, about 25%–33% of patients will develop HF (Minicucci et al., 2011). Therefore, it is essential to effectively improve patients' clinical symptoms and quality of life with IHF to prevent or reverse cardiac remodeling.

In recent years, clinical randomized controlled trials have confirmed the safety and effectiveness of traditional Chinese medicine (TCM) in treating IHF (Li et al., 2013). According to the TCM theory, the leading causes of IHF are deficiency of heart-qi and blood stasis. The theory further defines the Buyang Huanwu Decoction (BYHW) as a classic prescription for supplementing heart-qi and activating blood circulation. To specify, BYHW consists of seven commonly used Chinese herbal medicines, all registered in the Chinese Pharmacopoeia:

Astragali Radix (*Astragalus membranaceus* (Fisch.) Bge. var. mongholicus (Bge.), Hsiao or *Astragalus membranaceus* (Fisch.) Bge., Leguminosae), Paeoniae Radix Rubra (*Paeonia lactiflora* PalL or Paeonia veitchii Lynch, Ranunculaceae), Radix Angelicae Sinensis (*Angelica sinensis* (Oliv.) Diels., Umbelliferae), Rhizoma Chuanxiong (*Ligusticum chuanxiong* Hort., Umbelliferae), Flos Carthami (*Carthamus tinctorius* L., Feverfew), Pheretima (*Pheretima aspergillum* (E. Perrier) or Pheretima vulgaris Chen or *Pheretima guillelmi* (Michaelsen) or *Pheretima pectinifera* Mkhaeken, Megascolecidae), and Persicae Semen (*Prunus persica* (L) Batsch or *Prunus davidiana* (Carr.) Franch., Rosaceae).

The Preparation and assay methods of BYHW followed the guidelines of the Pharmaceutical standards of the Ministry of Health of the People's Republic of China. By using the method of liquid chromatography tandem-mass spectrometry (LC-MS/MS), we identified 11 compounds from the BYHW granules. (Please see **Supplementary Material** for more information). Previous studies have shown that BYHW can regulate lipid metabolism, improve hemorheology, enhance plaque stability, and protect cardiac function (Wang et al., 2011; Chen et al., 2021). Although numerous clinical trials reported the efficacy of BYHW in treating IHF (Wu et al., 2021), the underlying mechanism of BYHW in treating IHF remains unclear.

Proteomics is a discipline based on mass spectrometry technology. The research thinking of proteomics is very similar to the holistic and multi-targeted view of TCM. By characterizing Disease symptoms at the molecular level by detecting the protein expression and modification of clinical samples, the discipline offers a new approach and theoretical support for Chinese medicine's clinical diagnosis and treatment (Wei et al., 2019).

In this paper, we ensure the clinical trial meets the standards of randomized, multicenter, double-blind, and placebo-controlled. Our objective is to evaluate the efficacy and safety of BYHW combined under the guidelines for IHF pharmacotherapy and to reveal the biological mechanism by label-free quantification proteomics.

2 METHODS

2.1 Trial Design

A multicenter, randomized, double-blind, placebo-controlled, parallel-group clinical study was conducted in China from June 2016 to December 2019 to reveal the therapeutic mechanism of BYHW in the treatment of IHF (qi deficiency and blood stasis syndrome). The trial consisted of 80 subjects from three clinical trial sites in Henan Province, China, including The First Affiliated Hospital of Henan University of Chinese Medicine, Henan Province Hospital of TCM, and Zhengzhou Hospital of TCM. This study observed the World Medical Association's Declaration of Helsinki and the regulations and guidelines of China on Good Clinical Practice. The trail obtained ethical approval from the Ethics Committee of the First Affiliated Hospital of Henan University of Chinese Medicine (Approval number: 2015HL-045-01). This study has been registered with the US Clinical Trials Registry (https://clinicaltrials.gov; identifier NCT02875639).

2.2 Participants

2.2.1 Inclusion Criteria

1) Age 40 to 75; 2) Patients with ischemic heart failure: left ventricular ejection fraction (LVEF) less than or equal to 45% measured by echocardiography in modified Simpson method; History of myocardial infarction with or without percutaneous coronary intervention or coronary artery bypass grafting; Coronary angiography or coronary computed tomography angiography shows ≥50% stenosis in at least one main coronary artery with or without revascularization, which the researcher thinks is closely related to HF; With or without dyspnea, fatigue and fluid retention (edema); 3) Qi deficiency and blood stasis syndrome (Ren et al., 2012); 4) New York Heart Association (NYHA) Class II to III; 5) Submitted informed consent.

2.2.2 Exclusion Criteria

1) Combine the pulmonary embolism, or acute coronary syndrome, or acute cerebrovascular disease; 2) Combine other heart diseases: valvular heart disease, dilated cardiomyopathy, hypertension heart disease, pulmonary heart disease, congenital heart disease; 3) Severe hepatic and renal dysfunction, malnutrition, malignant tumor; 4) Psychosis and drug abuse; 5) Absolute contraindications to TCM; 6) Being pregnant, planning for pregnancy or breastfeeding.

2.3 Interventions

Before registration, the trial provided informed consent to all eligible patients in written form. Subsequently, all registered patients underwent a screening process for 1 week. During this period, the patients received western medicine treatments according to their clinical conditions under the Guidelines for Heart Failure established by the American College of Cardiology Foundation/American Heart Association or the Chinese Medical Association (Yancy et al., 2013; Cardiovascular Society Heart Failure Group of Chinese Medical Association, 2018). Western medicine treatments included diuretics, angiotensin-converting enzyme inhibitors or angiotensin receptor blockers, β-receptor blockers, aldosterone receptor antagonists, digoxin, and vasodilators. After rigorous screening, the trial randomly assigned stable subjects to either the experimental or control group. In addition to their standardized western medicine, patients assigned to the experimental or control group took BYHW or placebo, respectively, for 3 months. The composition of BYHW was 60 g of Astragali Radix, 15 g of Paeoniae Radix Rubra, 20 g of Radix Angelicae Sinensis, 12 g of Rhizoma Chuanxiong, 12 g of Pheretima, 12 g of Flos Carthami, and 12 g of Persicae Semen, totaling 143 g of the crude drug. Its formula granules (19.4 g) were prepared in the same proportion by Sanjiu Medical & Pharmaceutical Co., Ltd. (Shenzhen, China), with a TCM simulant as the placebo. They were similar to each other in strength, appearance, and odor. The investigational drug (granules in 19.4 g) was orally given to the patients twice a day, 1 pack per dosing. The trial did not apply additional Chinese herbs other than BYHW or placebo. The investigational drug was taken routinely for 3 months unless not allowed due to specific clinical circumstances. Patients were free to withdraw from the trial when necessary.

2.4 Outcomes

The primary efficacy endpoints included NYHA classification, TCM syndrome scores, NT-ProBNP. The efficacy standard was developed under the Principles for Clinical Research of New Drugs of Traditional Chinese Medicine in the Treatment of Heart Failure (Wang et al., 2019). The secondary efficacy endpoints included a 6-minute walk distance (6MWD) and LVEF. Mechanism exploration endpoints included energy metabolism indexes [Adenosine Diphosphate (ADP)/Adenosine Triphosphate (ATP) Ratio; Glucose (GLU); total cholesterol (TC); triglyceride (TG); high-density lipoprotein cholesterol (HDL-C); low-density lipoprotein cholesterol (LDL-C)], and coagulation function parameters [Prothrombin time (PT); Activation time of partial thromboplastin (APTT); Fibrinogen (FIB); and Thrombin Time (TT)]. The safety endpoints included tests of blood, urine, Electrolytes (K, Na, Cl), Hepatic and renal function. The above endpoints were observed and recorded once at months 0 and 3, respectively, during the treatment period. The adverse events (AEs)/adverse drug reactions (ADRs) record form was truthfully completed during the trial.

2.5 Sample Size

The sample used to explore the efficacy and mechanism was small in terms of size. According to expert opinions, the minimum sample size required for enrollment subjects in this study was 30 cases in each group. Considering a dropout rate of about 20% in each group, the sample size in each group was chosen to be 40 cases. Therefore, we enrolled 80 patients in this study and subsequently randomized the patients in a 1:1 ratio to the BYHW and control groups.

2.6 Randomization

The randomization procedure was designed by the Data Manager, Xiyuan Hospital of China Academy of Chinese

Medical Sciences, using SAS statistical software. Block randomization was performed using the PROC PLAN process (block length of 10, in 8 blocks). The resulting random numbers were hidden in sealed opaque envelopes by investigators not involved in the recruitment. The therapists were responsible for sequentially opening the randomized envelopes and allocating the subjects accordingly. Patients, participants, and the study statistician were all blinded to treatment allocation. Each group of TCM investigational drug and TCM simulants passed the drug inspection and were entrusted to China Resources Sanjiu Medical & Pharmaceutical Co., Ltd., for manufacturing. An independent drug administrator was responsible for the delivery and distribution of the drugs used in the study.

2.7 Proteomics Analysis

2.7.1 Preparation of Serum Samples

The study randomly chose 30 patients from each group among all subjects who completed the trial. The same amount of serum from 10 participants, five male and five female, was mixed, and the operation was repeated three times. After freezing, the serum was thawed at room temperature. The serum underwent shaking for 1 min, with 50 μl taken as a sample to be transferred into the EP tube. The high-abundance protein removal kit was transferred to a 10 kDa ultrafiltration tube and concentrated to 50 μl, which was replaced into an 8 mol L^{-1} solution system. The final concentration of 50 mmol L^{-1} 1,4-DTT was used for reduction, alkylation (dark) using a final concentration of 100 mmol L^{-1} IAA, and subsequent urea displacement by 50 mmol L^{-1} NH_4CO_3 solutions, followed by incubation at 95°C for 10 min, enzymatic digestion (37°C, 16 h) using trypsin added at 1:50 mass ratio of enzyme to substrate, terminated by adding 0.1% FA. Protein concentration was identified by the bicinchoninic acid method.

2.7.2 Main Instrument and Reagents

The instrument and reagents involved in the study were purchased from the following organizations:

Easy nLC 1,000 nA Upgrade Liquid Chromatograph: Thermo Fisher, United States. Q Exactive Plus (QE Plus): Thermo Fisher, United States. Chromatographic water: Hangzhou Wahaha Group Co., Ltd., China. Urea: Affymetrix, United States. Sequencing grade Trypsin: Promega, United States. Formic Acid (FA), Dithiothreitol (DTT), and acetonitrile (ACN): Thermo Fisher, United States. Iodoacetamide (IAA): GE Healthcare, United States. Ammonium Bicarbonate: Amresco, United States.

2.7.3 LC-MS/MS Analysis

The samples went through an Easy nLC 1,000 nL liquid chromatography. The flow phase A was 0.1% FA and double steam water, the flow phase B was 0.1% FA and ACN, gradient elution: 0~3 min, 3%–6% B; 3–78 min, 6%–22% B; 78–79 min, 22%–100% B; 79~107 min, 100% B. The flow rate is 400 nL min^{-1}. Mass spectrometry was performed on a QE Plus mass spectrometer in data-dependent acquisition mode. The resolution of the first-order mass spectrum was set to 70,000, the scan range was m/z 300-1,800, the automatic gain control value was 3 × 106, and the injection time was 50 ms. The resolution of the secondary mass spectrum was set to 17,500, the automatic gain control value was 1×10^5, the injection time was 45 ms, and the impact energy was 27 NCE. The standard for the second collection was set to the top 20 most intense ions as parent ions before Orbitrap detection. Each sample was repeated three times by mass spectrometry.

2.7.4 Protein Identification and Quantitative Analysis

The RAW data obtained by mass spectrometry were imported into Proteome Discoverer software for protein identification. The protein database was from UniProt (http://www.uniprot.org/). The parameters were established as follows:

Confidence of peptide: high
Maximum number of protein leakage sites: 2
Length range of peptide: 6–144 amino acids
Mass deviation of parent ion: ± 10
Mass deviation of fragment ion: 0.02
Fixed modification: cysteine iodoacetamide
Variable modification: methionine oxidation and N-acetylation
False discovery rate of peptide library search: 1%

The RAW data was evaluated by Maxquant software via quantitative analysis, and the protein database was the same as above. Below were the standards of the parameters:

Maximum number of protein leakage sites: 2
Fixed modification: cysteine iodoacetamide
Variable modification: methionine oxidation and N-acetylation
Mass deviation of precursor ions: ± 20
Fragment ion mass deviation: 0.02
Minimum detectable peptide: 7 amino acids
False discovery rate of peptide library search: 1%.

2.7.5 Bioinformatics Analysis

The study identified proteins with a statistically significant and fold change >1.5 as differentially expressed proteins. Function and pathway enrichment analyses were performed by searching the differentially expressed proteins against the Gene Ontology (GO) (http://www.geneontology.org/) and Kyoto Encyclopedia of Genes and Genomes (KEGG) (http://www.genome.jp/kegg/pathway.html) database. For protein-protein interaction analysis, the study referred to the Search Tool for the Retrieval of Interacting Genes/Proteins (STRING) (https://string-db.org/).

2.8 Statistical Analysis

All statistical analyses were performed using SAS statistical software version 9.2 (SAS Institute). The baseline characteristics of all subjects who received randomized treatment were analyzed according to the Full Analysis Set (FAS) principle. The data of subjects who completed all trials were examined based on the Per Protocol Set (PPS) principle. Continuous variables were presented as the mean ± standard deviation (SD). Under the condition of normal distribution and

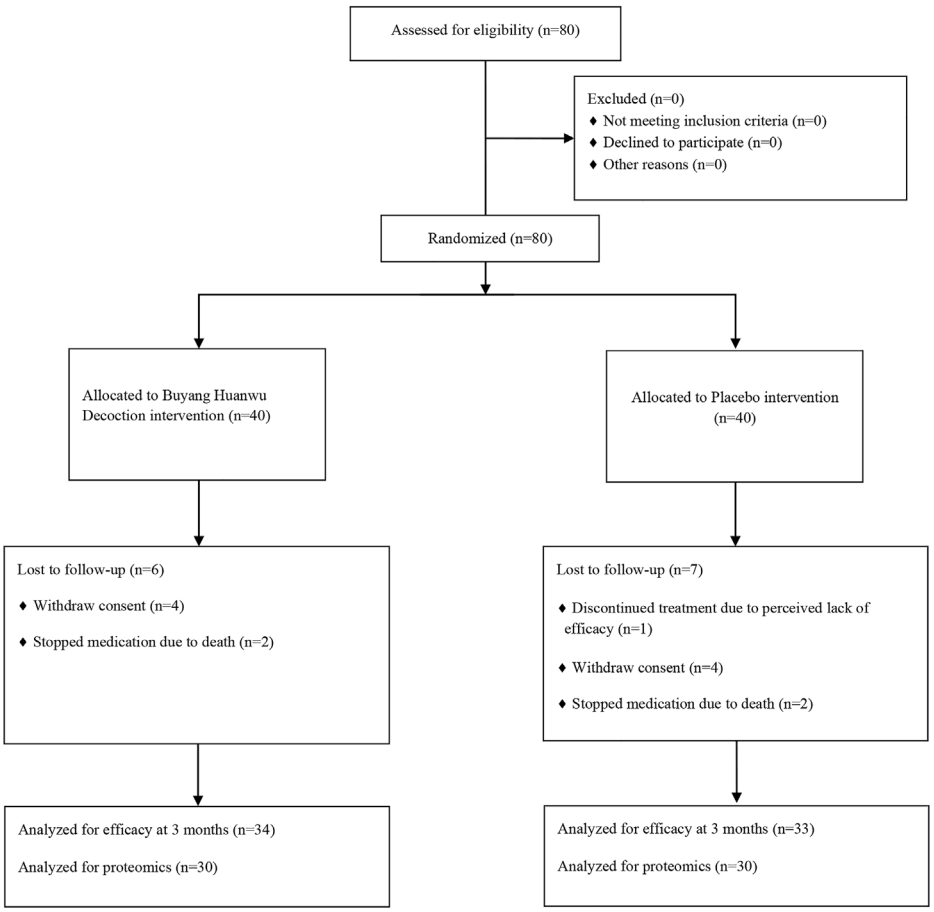

FIGURE 1 | Flow diagram of patient selection and trial design.

equal variance, the t-test was applied to compare the two groups while the Wilcoxon rank-sum test was used as an alternative; binary variables expressed as frequency or percentage were estimated using chi-square or Fisher exact test. $p < 0.05$ was considered statistically significant.

3 RESULTS

3.1 Clinical Characteristics

The study contained, in total, 80 patients with IHF. After the strict screening process, 80 patients with IHF were finally included and randomized to the control and BYHW groups (**Figure 1**). Among the participants, 67 patients completed the 3-month treatment period. During the trial, a total of 9 subjects dropped out (4 in the BYHW group and 5 in the control group), causing an 11.25% dropout rate. The main reason for dropout was that the subjects were unwilling or unable to continue the clinical trial and voluntarily requested to withdraw. In addition, 4 patients died due to their disease worsening (2 in the BYHW group and 2 in the control group). There was no significant difference in demographics, vital signs, medical history, background drug information, NYHA classification, and TCM syndrome scores between the two groups ($p > 0.05$; **Table 1**).

3.2 Comparison of Efficacy Endpoints Between the BYHW and Control Groups

After 3 months, BYHW treatment significantly improved NYHA classification by 55.88% compared with the 36.36% increase observed in the control group ($p = 0.038$); Similarly, BYHW treatment showed high efficacy (70.59%) in improving TCM syndrome scores compared with the 48.48% increase observed in the control group ($p = 0.036$) (See details in **Table 2**).

As shown in **Table 3**, there was no significant difference in NT-ProBNP, 6 MWD, and LVEF between the two groups before and after treatment ($p > 0.05$); compared with the same group before treatment, BYHW treatment significantly improved NT-ProBNP, 6 MWD, and LVEF as the control group ($p < 0.01$). In addition, 76.00% of subjects from the BYHW group had a decrease in NT-ProBNP of at least 30% compared with 48.10% of subjects from the control group ($p < 0.05$).

TABLE 1 | Baseline characteristics of participants between the BYHW and control groups.

Characteristic	BYHW (*n* = 40)	Control (*n* = 40)	*p* value
Basic information			
Age (years)	64.68 ± 7.89	64.93 ± 8.13	0.889
Male n (%)	27 (67.50%)	26 (65.00%)	0.813
Female n (%)	13 (32.50%)	14 (35.00%)	
BMI (kg/cm^2)	24.72 ± 3.70	24.27 ± 3.60	0.584
SBP (mmHg)	129.40 ± 17.35	127.80 ± 17.70	0.684
DBP (mmHg)	80.22 ± 9.94	77.50 ± 11.15	0.252
Heart rate (bpm)	69.65 ± 7.75	66.72 ± 7.74	0.097
Respiratory rate (times/min)	18.50 ± 1.15	18.63 ± 1.24	0.628
Medical history n (%)			
History of hypertension	13 (44.80%)	20 (48.80%)	0.112
History of diabetes	8 (27.60%)	9 (22.00%)	0.785
Hyperlipidemia	5 (17.20%)	7 (17.10%)	0.531
Treatment n (%)			
Antiplatelet	37 (92.50)	35 (87.50%)	0.456
Beta-blockers	19 (47.50%)	28 (70.00%)	0.041
ACEI/ARB	17 (42.5%)	12 (30.00%)	0.271
Calcium antagonists	3 (7.50%)	7 (17.50%)	0.176
Statins	32 (80.00%)	33 (82.50%)	0.775
Diuretics	13 (32.50%)	10 (25.00%)	0.459
Aldosterone receptor antagonist	11 (27.50%)	12 (30.00%)	0.812
Nitric acid lipid	9 (22.50%)	11 (27.50%)	0.606
Digoxin	8 (20.00%)	4 (10.00%)	0.21
Clinical index			
TCM syndrome score	14.65 ± 3.16	15.75 ± 4.28	0.1948
NYHA classification			
II n (%)	25 (62.5%)	25 (62.5%)	1
III n (%)	15 (37.5%)	15 (37.5%)	

BYHW, Buyang Huanwu decoction; BMI, body mass index; SBP, systolic blood pressure; DBP, diastolic blood pressure; ACEI, angiotensin converting enzyme inhibitors; ARB, angiotensin receptor blocker; TCM, traditional Chinese medicine; NYHA, New York Heart Association.

TABLE 2 | Comparison of NYHA classification and TCM syndrome scores efficiency between BYHW and control groups after 3 months of treatment.

	Excellent	Valid	Invalid	Worsened	Effective rate (%)	*p* value
NYHA classification efficiency						
BYHW (*n* = 34)	16	3	13	2	55.88	0.038
Control (*n* = 33)	12	0	12	9	36.36	
TCM syndrome scores efficiency						
BYHW (*n* = 34)	6	18	10	0	70.59	0.036
Control (*n* = 33)	9	7	16	1	48.48	

TABLE 3 | Comparison of change in NT-ProBNP, 6 MWD and LVEF between BYHW and control groups after 3 months of treatment.

	BYHW (*n* = 34)	Control (*n* = 33)	*p* value
NT-ProBNP (pg/ml)			
Before treatment	2017.67 ± 3,094.69	1954.26 ± 2,690.37	0.904
After treatment	1,211.03 ± 1,663.36**	1931.23 ± 4,307.86*	0.406
Proportion of patients with a reduction in NT-proBNP at least 30% (%)	76.00%	48.10%	0.039
LVEF (%)			
Before treatment	41.09 ± 8.05	42.22 ± 7.85	0.563
After treatment	49.12 ± 9.82**	47.62 ± 10.25**	0.543
6 MWD (m)			
Before treatment	372.10 ± 85.24	363.82 ± 97.72	0.712
After treatment	435.91 ± 68.62**	399.88 ± 126.03*	0.149

*NT-proBNP, N-terminal pro-B-type natriuretic peptide; LVEF, left ventricular ejection fraction; 6 MWD, 6-minute walking distance; compared with the same group before treatment, *p < 0.05, **p < 0.01.*

TABLE 4 | Comparison of change in energy metabolism indexes between BYHW and control group after 3 months of treatment.

	BYHW (n = 34)	Control (n = 33)	p value
ADP/ATP Ratio			
Before treatment	1.43 ± 2.80	1.00 ± 0.69	0.395
After treatment	0.76 ± 0.47*	0.80 ± 0.76	0.796
GLU (mmol/L)			
Before treatment	7.99 ± 4.00	6.40 ± 2.12	0.046
After treatment	6.42 ± 1.90**	5.46 ± 1.79**	0.039
TC (mmol/L)			
Before treatment	4.01 ± 1.06	4.34 ± 1.21	0.24
After treatment	3.55 ± 0.81*	3.98 ± 0.92	0.05
TG (mmol/L)			
Before treatment	1.66 ± 1.20	1.70 ± 0.92	0.891
After treatment	1.51 ± 0.63	1.76 ± 1.22	0.294
HDL-C (mmol/L)			
Before treatment	1.18 ± 0.29	1.11 ± 0.21	0.264
After treatment	1.29 ± 0.29	1.20 ± 0.22	0.128
LDL-C (mmol/L)			
Before treatment	2.50 ± 0.75	2.57 ± 0.91	0.74
After treatment	2.09 ± 0.68**	2.42 ± 0.73	0.064

*ADP, adenosine diphosphate; ATP, adenosine triphosphate; GLU, glucose; TC, total cholesterol; TG, triglyceride; LDL-C, low density lipoprotein cholesterol; HDL-C, high density lipoprotein cholesterol, *p < 0.05, **p < 0.01.*

TABLE 5 | Comparison of change in coagulation function indexes between BYHW and control group after 3 months of treatment.

	BYHW (n = 34)	Control (n = 33)	p value
PT (s)			
Before treatment	12.18 ± 1.34	11.92 ± 1.55	0.473
After treatment	12.83 ± 2.39	12.00 ± 1.76	0.112
APTT (s)			
Before treatment	31.14 ± 4.14	30.99 ± 5.38	0.898
After treatment	34.30 ± 7.23*	32.30 ± 8.03	0.287
FIB (g/L)			
Before treatment	3.44 ± 0.75	3.43 ± 1.00	0.95
After treatment	2.83 ± 0.48**	3.08 ± 0.59*	0.054
TT (s)			
Before treatment	14.79 ± 2.37	14.87 ± 2.91	0.907
After treatment	16.28 ± 2.13**	15.07 ± 2.65	0.043

*PT, prothrombin time; APTT, activation time of partial thromboplastin; FIB, fibrinogen; TT, thrombin time; compared with the same group before treatment, *p < 0.05, **p < 0.01.*

3.3 Comparison of Mechanism Exploration Endpoints Between the Buyang Huanwu Decoction and Control Groups

From the data in **Table 4**, there was no significant difference in ADP/ATP Ratio, TC, TG, HDL-C, and LDL-C between the two groups before and after treatment ($p > 0.05$). When compared with the same group before treatment, there was a significant improvement in ADP/ATP Ratio, TC and LDL-C in the BYHW group ($p < 0.05$), but hardly any difference in the control group ($p > 0.05$). In addition, GLU varied distinctly between the two groups before and after treatment ($p < 0.05$).

As shown in **Table 5**, there was no prominent difference in PT, APTT, FIB, and TT at baseline between the two groups ($p > 0.05$). After 3 months, BYHW treatment dramatically improved TT compared with the control group ($p < 0.05$); compared with the same group before treatment, BYHW treatment notably improved APTT, FIB, and TT ($p < 0.05$).

3.4 Safety Evaluation

No significant difference in laboratory indicators between the BYHW and the control groups ($p > 0.05$; Please see **Supplementary Material**) was shown in the study. In addition, no significant ADRs were reported in the two groups during the trial. However, 4 patients died during the trial, all of whom died due to their disease deterioration unrelated to the investigational product. We recorded it in detail and made a report of it.

3.5 Proteomics Analysis

3.5.1 Protein Quantification and Data Quality Control

Proteomics analysis displayed 267 non-redundant proteins from serum samples in the two groups. Among these proteins, there were a total of 208 proteins in both groups, accounting for 77.9% of the total proteins identified (see **Figure 2A**). The Pearson correlation between samples is shown in **Figure 2B**. The results show that the correlation coefficient between the two groups was low. The noticeable difference in the Pearson correlation coefficient within each group indicated that the samples between the two groups are relatively independent.

3.5.2 Identification of Differentially Expressed Proteins

In order to further explore the potential effect of BYHW on IHF, $p < 0.05$ (Student's t-test) and folding change >1.5 were used as the analysis criteria. Compared with the control group, the study identified 56 differentially expressed proteins in the BYHW group, including 20 upregulated proteins and 36 downregulated proteins (Please see **Supplementary Material**). The volcanic map was further drawn according to the significance level and fold change value. In **Figure 3A**, the red dot represents the upregulated protein, the blue dot represents the downregulated protein, and the gray dot represents the non-differentially expressed gene. The heat map of cluster analysis showed that BYHW treatment caused notable changes in protein levels in the two groups (as shown in **Figure 3B**).

3.5.3 Functional Classification of Differentially Expressed Proteins

GO analysis was performed using the OmicShare tools (https://www.omicshare.com/tools). GO covers three domains: biological process, molecular function, and cellular component, and the top 20 GO terms of each category were shown in **Figure 4**. The cellular component enrichment terms indicated that most of the differentially expressed proteins were located in the extracellular region, extracellular region part, extracellular space, immunoglobulin complex (**Figure 4A**). The analysis found that the molecular functions of the differentially expressed proteins mainly included antigen binding, signaling receptor binding, immunoglobulin receptor binding, lipase inhibitor activity (see **Figure 4B**). Biological processes mainly involved protein activation cascade, complement activation, immune response, humoral immune response (see **Figure 4C**).

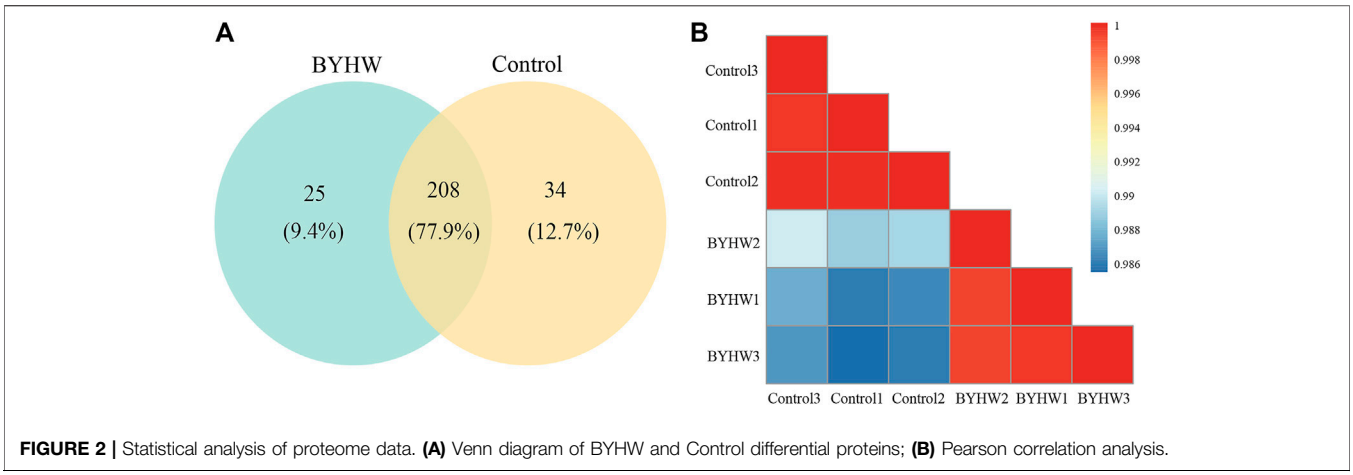

FIGURE 2 | Statistical analysis of proteome data. **(A)** Venn diagram of BYHW and Control differential proteins; **(B)** Pearson correlation analysis.

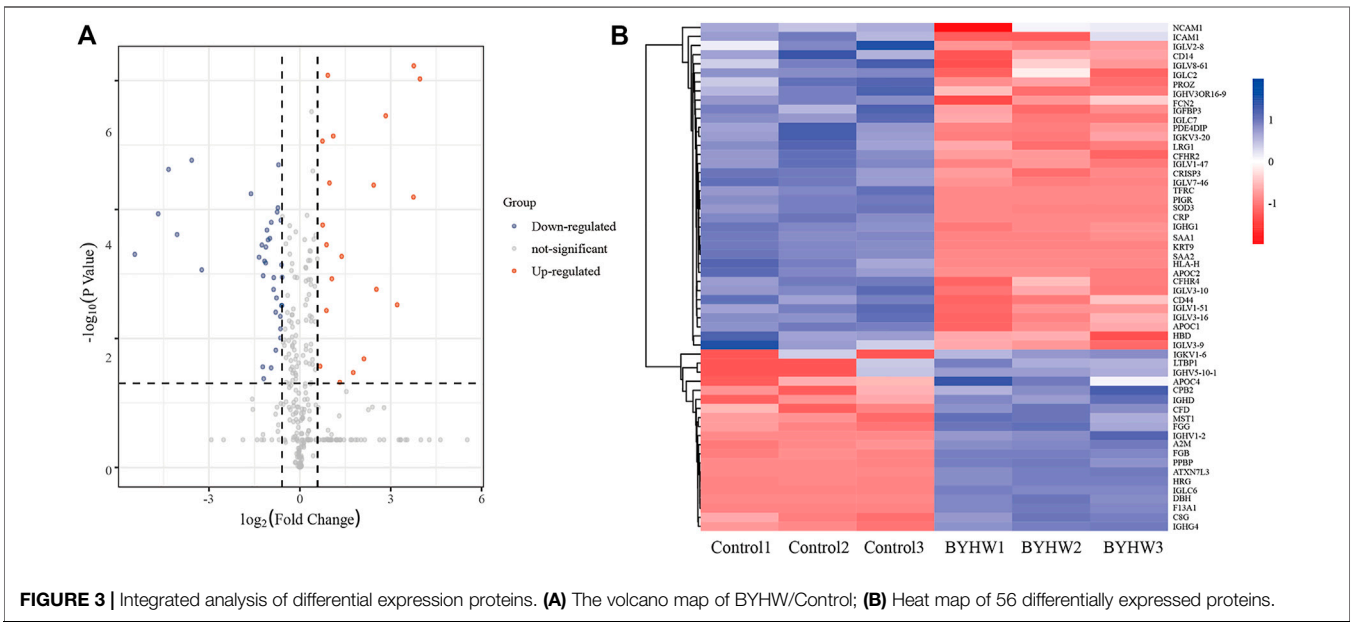

FIGURE 3 | Integrated analysis of differential expression proteins. **(A)** The volcano map of BYHW/Control; **(B)** Heat map of 56 differentially expressed proteins.

3.5.4 Biological Pathway Analysis of Differentially Expressed Proteins

We performed a pathway enrichment analysis using the DAVID classification system (https://david.ncifcrf.gov/summary.jsp) and KEGG databases. The top 20 relevant pathways were shown in **Figure 5A**, and the coordinate ruler with the number of genes outside the circle; The second circle is the number of background genes and *p*-value. The more genes, the longer the bar will be. The redder the color, the smaller the *p*-value; The third circle is the total number of genes in each classification; The fourth circle represents the rich factor of each category (Qie et al., 2020). The differential proteins were associated with various biological pathways, including complement and coagulation cascades (ko04610), cholesterol metabolism (ko04979), NF-kappa B signaling pathway (ko04064), PI3K-Akt signaling pathway (ko04151), and metabolic pathways (ko01100).

3.5.5 Protein-Protein Interaction Analysis of Differentially Expressed Proteins

The protein functions usually interact with each other to complete a series of biological processes in organisms. We thus applied the STRING database to predict all the protein interactions enriched in the pathway. Furthermore, we created a protein interaction network diagram to discover the critical nodes of BYHW treatment in the process of IHF. Set the highest confidence level, and the strongest connectivity included fibrinogen gamma (FGG), fibrinogen beta (FGB), Carboxypeptidase B2 (CPB2), Coagulation factor XIII A (F13A1), Intercellular adhesion molecule1 (ICAM1), Apolipoprotein C-II (APOC2), Apolipoprotein C-I (APOC1), CD44, suggesting that these proteins could be critical factors for BYHW intervention at the protein level (see **Figure 5B**).

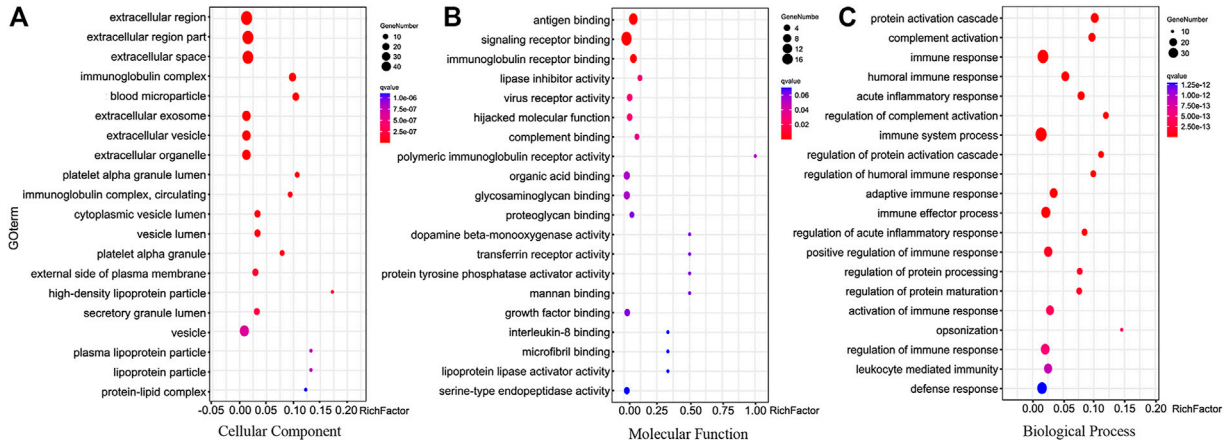

FIGURE 4 | Biological function analysis of differentially expressed proteins. **(A)** Top 20 cellular component enrichment terms. **(B)** Top 20 molecular function enrichment terms. **(C)** Top 20 biological process enrichment terms.

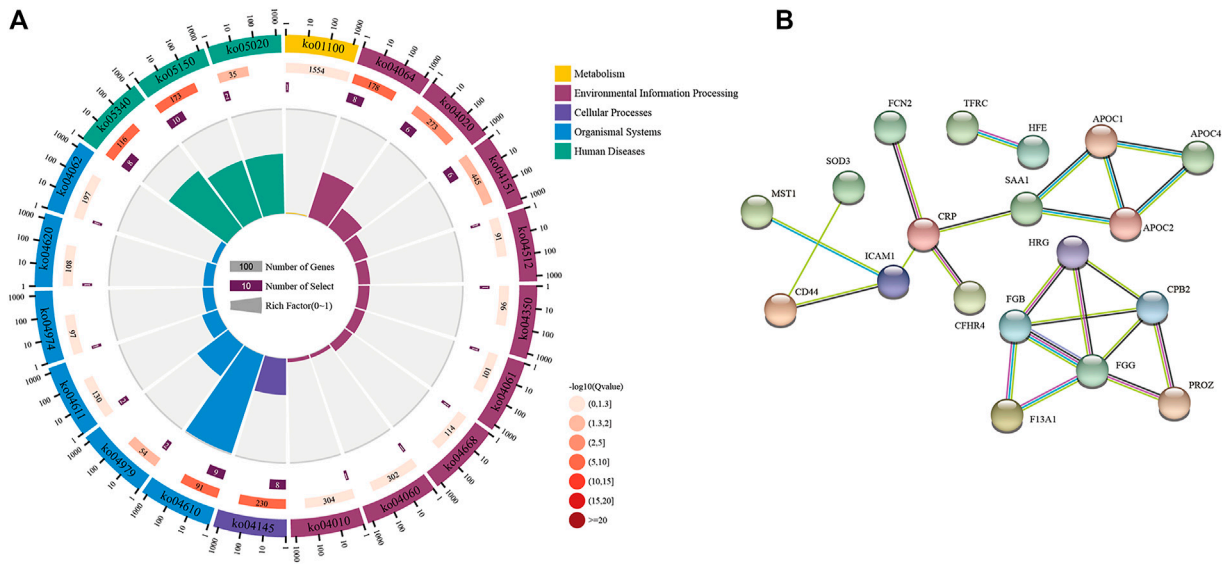

FIGURE 5 | Pathway enrichment results and interaction relationship of different expressed proteins. **(A)** Top 20 biological pathway analysis of differentially expressed proteins; **(B)** Protein-protein interaction network differentially expressed proteins.

4 DISCUSSION

At present, modern medicine has reached a standstill for the pharmaceutical treatment of IHF. Based on the original effective neuroendocrine suppression, the role of drugs in further reducing the mortality and disability rate is more and more limited, while non-drug treatment is challenging to promote due to issues including technology, cost, and indication. Therefore, it is essential to develop new therapies to treat patients with IHF. BYHW was first published in *Yilin Gaicuo* by Wang Qingren, a famous doctor in the Qing Dynasty. It is a classical representative compound of supplementing qi and promoting blood circulation. According to the theory of "treating different diseases with the same therapy" in TCM, BYHW is applied to treat cardiovascular diseases and other diseases of qi deficiency and blood stasis syndrome with notable effects (Li et al., 2014).

In this study, we assessed the effectiveness and safety of BYHW in treating IHF for the first time through a randomized controlled trial with multiple endpoints. The combined results showed that BYHW significantly improved the clinical symptoms and cardiac function of IHF patients, ameliorated energy metabolism, and regulated coagulation function. We evaluated the clinical efficacy of BYHW in IHF by observing NYHA Classification, TCM syndrome scores, NT-proBNP, 6MWD, and LVEF. The results showed that BYHW significantly improved NYHA classification, TCM syndrome scores, and the percentage of subjects with at least 30% reduction in NT-

ProBNP compared with the placebo; BYHW treatment significantly improved NT-ProBNP, 6 MWD, and LVEF compared with those before treatment. These findings suggested that BYHW, in combination with other standard therapies, may be a better cure for patients with IHF. As IHF is a complex syndrome, patients with IHF will display multiple symptoms, including dysregulation of the neuro-endocrine-immune network, energy metabolism disorders, and imbalance of coagulation mechanism (González et al., 2011). The results also showed that BYHW treatment significantly improved ADP/ATP Ratio, GLU, TC, LDL-C, APTT, FIB, and TT compared with those before treatment. We inferred that the therapeutic mechanism of BYHW may be related to the regulation of blood glucose and blood lipid levels, the improvement of energy metabolism and anticoagulant activity, and the reduction of the risk of thrombosis. Notably, almost patients included in the study tolerated well, and we tentatively assume that BYHW is relatively safe and does not increase the incidence of adverse effects. We also found that although most patients received guideline-guided heart failure therapy (ACEI/ARB, β-blockers, and Aldosterone receptor antagonist) at baseline, their proportion was lower than expected in global heart failure trials, which may reflect the gap in the actual treatment of patients with heart failure in most Asian countries.

In the present study, we investigated the underlying mechanism of BYHW on regulating serum proteome using label-free quantification. After screening and identification, we finally obtained 56 differentially expressed proteins, including 20 upregulated proteins and 36 downregulated proteins. The GO enrichment analysis revealed that these proteins were mainly located in the extracellular region, extracellular region part, extracellular space, and immunoglobulin complex. They participated in biological processes such as protein activation cascade, complement activation, immune response, and humoral immune response. KEGG pathway analysis showed that the pathways in which these differential proteins were mainly involved included complement and coagulation cascades, cholesterol metabolism, PI3K-Akt signaling pathway, NF-kappa B signaling pathway, and metabolic pathways.

The complement system is initially classified as a part of innate immunity. It is a strict self-regulatory system composed of the liquid phase, cell surface, and intracellular proteins. In the blood circulation, complements and coagulation cascades form a tight and complex network. They activate and regulate each other and jointly regulate immune monitoring and tissue homeostasis. Dysregulation of complements and coagulation cascades can lead to the progression of different clinical diseases (Luo et al., 2020). Other than our research, multiple studies have revealed that Chinese medicine can play a role in treating cardiovascular diseases through complement and coagulation cascades (Wang P et al., 2020; Wang, J et al., 2020). Atherosclerosis (AS) is one of the leading causes of cardiovascular disease. Research has shown that Cholesterol metabolism and dyslipidemia are involved in the occurrence of AS (Ke and Shen, 2019), which may have a direct or indirect adverse effect on the long-term prognosis of myocardial infarction. The reason may be the degree of ischemic injury, or the subsequent events (e.g., recurrent myocardial infarction) increase the risk of HF (Gerber et al., 2016). PI3K/Akt signaling pathway plays an essential role in angiogenesis. In other words, PI3K acts as a crucial signal for regulating cell metabolism, proliferation, and apoptosis. It also plays a vital role in the activation of the Akt-dependent signaling pathway. A variety of vasoactive factors can be controlled by Akt activation (Lin et al., 2015). The PI3K/Akt signaling pathway regulates inhibits oxidative stress, improves cardiac dysfunction and hemodynamics, and alleviates myocardial fibrosis (Zhong et al., 2020). NF-kappa B is an essential nuclear transcription factor involved in regulating cell differentiation and apoptosis in organisms and controlling inflammatory and immune responses. Activation of the NF-kappa B signaling pathway may be associated with aggravation of heart failure (Li et al., 2018). Previous studies have also shown that BYHW can inhibit NF-kappa B signaling pathway and adjust blood lipid levels to treat AS (Liu et al., 2020).

Based on the observation of the protein-protein interaction functional network, we discovered that FGG, FGB, CPB2, F13A1, ICAM1, APOC2, APOC1, and CD44 were located in the center of the network, serving as a hub to interact with other proteins. The proteins mainly participated in a variety of biological processes, including coagulation systems and energy metabolism. Moreover, fibrinogen level plays an essential role in coagulation, hemostasis, and inflammation, a recognized risk factor for cardiovascular diseases. Fibrinogen circulates as a dimer in the plasma, consisting of three pairs of polypeptide chains alpha, beta, and gamma encoded by fibrinogen alpha (FGA), FGB, and FGG genes (Simurda et al., 2020). In addition, fibrinogen acts as a crucial agent in treating IHF: it can promote platelet aggregation, promote the growth, proliferation, and contraction of smooth muscle and endothelial cells. It also increase blood viscosity and peripheral resistance, causing endothelial cell damage. More importantly, fibrinogen promotes red blood cell adhesion and thrombosis, which are crucial for the occurrence of cardiovascular diseases (Kunutsor et al., 2016). Previous studies have also shown that TCM could regulate FGA and FGG levels to improve coagulation function and play a role in treating coronary heart disease (Wang, J et al., 2020). As for CPB2, it inactivates a variety of inflammatory mediators by removing c-terminal arginine. It also removes c-terminal lysine from partially degraded fibrin, thereby reducing tissue plasminogen activator and plasminogen binding to clots, eventually reducing plasmin formation (Claesen et al., 2021). Evidence showed that the CPB2 level in the thrombus site in patients with acute myocardial infarction is exceptionally high, and it is helpful to the thrombus dynamics of plaque rupture site (Leenaerts et al., 2015). Additionally, we discovered that BYHW could upregulate CPB2 by proteomics, which plays a beneficial role in treating IHF. The F13A1 protein found in BYHW affects many physiological processes and plays a crucial role in balancing thrombus formation and dissolution. Pharmacological studies have shown that F13A1 may be a promising drug target for developing new anticoagulants with limited bleeding risk (Al-Horani and Kar, 2020). As for ICAM1, other studies defined the protein's crucial role in the development of heart failure by participating in the process of inflammation and apoptosis (Patel et al., 2020). ICAM1 has the potential as a biomarker and therapeutic target for post-acute myocardial infarction heart failure (Lino et al., 2019). Numerous drugs for heart failure can inhibit the expression of ICAM and have anti-inflammatory effects (Krychtiuk et al., 2015), which matched with the results of our study. Based on previous studies, many apolipoproteins seem involved in ventricular remodeling and HF worsening (Jang et al., 2020). APOC2 is a component of

chylomicrons, very LDL, LDL, and HDL. The existing evidence supports the significant correlation between APOC2 and coronary artery stenosis (Ku et al., 2020). APOC1 is directly related to cardiovascular physiology by controlling plasma lipid levels (Fuior and Gafencu, 2019). In addition, APOC1 is the only known endogenous cholesteryl ester transfer protein inhibitor, and this constitutive effect of APOC1 is impaired in coronary artery disease with dyslipidemia (Sacks et al., 2020). Likewise, our study showed that BYHW may regulate APOC1 and APOC2, further improving energy metabolism and playing a therapeutic role. CD44 is a widely expressed transmembrane glycoprotein involved in various cell functions, including cell adhesion, migration, proliferation, and differentiation. The defect of the CD44 signal cascade may play an essential role in the pathogenesis of adverse remodeling after myocardial infarction (Frangogiannis, 2019). In addition, CD44, hyaluronan, and their interactions are indispensable in developing myocardial fibrosis and cardiac remodeling after myocardial infarction, accelerating the progress of heart failure (Suleiman et al., 2018). These core proteins could be closely related to the development of IHF, and BYHW could play a therapeutic role in IHF through these targets.

Our study has some limitations. To begin with, we only detected the serum proteome of patients after treatment and need to further examine the serum proteome changes at other time points. In addition, the chemical composition of TCM is complex, and the practical components of BYHW that play a therapeutic role deserve to be further studied.

5 CONCLUSION

In conclusion, BYHW could further improve cardiac dysfunction and clinical symptoms in patients with IHF, ameliorate energy metabolism and regulate coagulation function in the context of standard medical treatment for IHF. We also demonstrated the safety of BYHW in clinical application. Proteomics analysis showed that BYHW may exert therapeutic effects on IHF by improving energy metabolism and regulating coagulation function through multiple targets (FGG, FGB, CPB2, F13A1, ICAM1, APOC2, APOC1, and CD44) and pathways (complement and coagulation cascades, cholesterol metabolism, NF-kappa B signaling pathway, PI3K-Akt signaling pathway, and metabolic pathways). This study greatly expands our knowledge, provides scientific support for the potential therapeutic mechanism of BYHW in treating IHF, and offers a possible alternative for the prevention and treatment of IHF.

DATA AVAILABILITY STATEMENT

The datasets presented in this study can be found in online repositories. The name of the repository and accession number can be found below: ProteomeXchange; PXD029771.

ETHICS STATEMENT

The studies involving human participants were reviewed and approved by the Ethics Committee of the First Affiliated Hospital of Henan University of Chinese Medicine (Approval number: 2015HL-045-01). The patients/participants provided their written informed consent to participate in this study.

AUTHOR CONTRIBUTIONS

MZ and JL conceived and designed this study. MZ, JW, and YL wrote the paper and analyzed the data. YW, BL, and XW provided essential methodological suggestions and revised the manuscript. JR and BM made contributions to proteomics experiments. LQ and CZ were responsible for coordinating the study. All authors read and approved the final manuscript.

FUNDING

The National Basic Research Program of China (2015CB554401), the Ministry of Science and Technology of the People's Republic of China's Key Projects during the 13th Five-Year Plan Period (2019YFC1710003), the National Natural Science Foundation of China (82074226 and 82030120), the Chinese Medicine Evidence-Based Capacity Building Project of State Administration of Traditional Chinese Medicine (2019XZZX-XXG003), and Innovation Team and Talents Cultivation Program of National Administration of Traditional Chinese Medicine (Grant No. ZYYCXTD-C-202007) supported the study.

SUPPLEMENTARY MATERIAL

The Supplementary Material for this article can be found online at: https://www.frontiersin.org/articles/10.3389/fphar.2022.831208/full#supplementary-material

REFERENCES

Al-Horani, R. A., and Kar, S. (2020). Factor XIIIa Inhibitors as Potential Novel Drugs for Venous Thromboembolism. *Eur. J. Med. Chem.* 200, 112442. doi:10.1016/j.ejmech.2020.112442

Cardiovascular Society Heart Failure Group of Chinese Medical Association (2018). Heart Failure Professional Committee of Chinese Medical Doctor Association, and Editorial Committee of Chinese Journal of Cardiology Chinese Guidelines for the Diagnosis and Treatment of Heart Failure 2018. *Chin. J. Cardiol.* 46, 760–789. doi:10.3760/cma.j.issn.0253-3758.2018.10.004

Chen, S., Wang, Y., Liang, C., Li, J., Li, Y., Wu, Q., et al. (2021). Buyang Huanwu Decoction Ameliorates Atherosclerosis by Regulating TGF-β/Smad2 Pathway to Promote the Differentiation of Regulatory T Cells. *J. Ethnopharmacol* 269, 113724. doi:10.1016/j.jep.2020.113724

Claesen, K., Mertens, J. C., Leenaerts, D., and Hendriks, D. (2021). Carboxypeptidase U (CPU, TAFIa, CPB2) in Thromboembolic Disease:

What Do We Know Three Decades after its Discovery? *Ijms* 22 (2), 883. doi:10.3390/ijms22020883

Elgendy, I. Y., Mahtta, D., and Pepine, C. J. (2019). Medical Therapy for Heart Failure Caused by Ischemic Heart Disease. *Circ. Res.* 124 (11), 1520–1535. doi:10.1161/CIRCRESAHA.118.313568

Frangogiannis, N. G. (2019). Cardiac Fibrosis: Cell Biological Mechanisms, Molecular Pathways and Therapeutic Opportunities. *Mol. Aspects Med.* 65, 70–99. doi:10.1016/j.mam.2018.07.001

Fuior, E. V., and Gafencu, A. V. (2019). Apolipoprotein C1: Its Pleiotropic Effects in Lipid Metabolism and beyond. *Int. J. Mol. Sci.* 20 (23), 5939. doi:10.3390/ijms20235939

Gerber, Y., Weston, S. A., Enriquez-Sarano, M., Manemann, S. M., Chamberlain, A. M., Jiang, R., et al. (2016). Atherosclerotic Burden and Heart Failure after Myocardial Infarction. *JAMA Cardiol.* 1 (2), 156–162. doi:10.1001/jamacardio.2016.0074

González, A., Ravassa, S., Beaumont, J., López, B., and Díez, J. (2011). New Targets to Treat the Structural Remodeling of the Myocardium. *J. Am. Coll. Cardiol.* 58 (18), 1833–1843. doi:10.1016/j.jacc.2011.06.058

Jang, A. Y., Han, S. H., Sohn, I. S., Oh, P. C., and Koh, K. K. (2020). Lipoprotein(a) and Cardiovascular Diseases - Revisited. *Circ. J.* 84 (6), 867–874. doi:10.1253/circj.CJ-20-0051

Ke, C., and Shen, Y. (2019). Letter by Ke and Shen Regarding Article, "Long-Term Association of Low-Density Lipoprotein Cholesterol with Cardiovascular Mortality in Individuals at Low 10-Year Risk of Atherosclerotic Cardiovascular Disease: Results from the Cooper Center Longitudinal Study". *Circulation* 139 (18), 2190–2191. doi:10.1161/CIRCULATIONAHA.118.038328

Krychtiuk, K. A., Watzke, L., Kaun, C., Buchberger, E., Hofer-Warbinek, R., Demyanets, S., et al. (2015). Levosimendan Exerts Anti-inflammatory Effects on Cardiac Myocytes and Endothelial Cells *In Vitro*. *Thromb. Haemost.* 113 (2), 350–362. doi:10.1160/TH14-06-0549

Ku, E. J., Cho, K. C., Lim, C., Kang, J. W., Oh, J. W., Choi, Y. R., et al. (2020). Discovery of Plasma Biomarkers for Predicting the Severity of Coronary Artery Atherosclerosis by Quantitative Proteomics. *BMJ Open Diabetes Res. Care* 8 (1), e001152. doi:10.1136/bmjdrc-2019-001152

Kunutsor, S. K., Kurl, S., Zaccardi, F., and Laukkanen, J. A. (2016). Baseline and Long-Term Fibrinogen Levels and Risk of Sudden Cardiac Death: A New Prospective Study and Meta-Analysis. *Atherosclerosis* 245, 171–180. doi:10.1016/j.atherosclerosis.2015.12.020

Leenaerts, D., Bosmans, J. M., van der Veken, P., Sim, Y., Lambeir, A. M., and Hendriks, D. (2015). Plasma Levels of Carboxypeptidase U (CPU, CPB2 or TAFIa) Are Elevated in Patients with Acute Myocardial Infarction. *J. Thromb. Haemost.* 13 (12), 2227–2232. doi:10.1111/jth.13135

Li, J. H., Liu, A. J., Li, H. Q., Wang, Y., Shang, H. C., and Zheng, G. Q. (20142014). Buyang Huanwu Decoction for Healthcare: Evidence-Based Theoretical Interpretations of Treating Different Diseases with the Same Method and Target of Vascularity. *Evid. Based Complement. Alternat Med.* 2014, 506783. doi:10.1155/2014/506783

Li, L., Hao, J., Jiang, X., Li, P., and Sen, H. (2018). Cardioprotective Effects of Ulinastatin against Isoproterenol-Induced Chronic Heart Failure through the PI3K-Akt, P-38 MAPK and NF-Kb- P-athways. *Mol. Med. Rep.* 17 (1), 1354–1360. doi:10.3892/mmr.2017.7934

Li, X., Zhang, J., Huang, J., Ma, A., Yang, J., Li, W., et al. (20132013). A Multicenter, Randomized, Double-Blind, Parallel-Group, Placebo-Controlled Study of the Effects of Qili Qiangxin Capsules in Patients with Chronic Heart Failure. *J. Am. Coll. Cardiol.* 6262 (1212), 10651065–10721072. doi:10.1016/j.jacc.2013.05.035

Lin, Z., Zhou, P., von Gise, A., Gu, F., Ma, Q., Chen, J., et al. (2015). Pi3kcb Links Hippo-YAP and PI3K-AKT Signaling Pathways to Promote Cardiomyocyte Proliferation and Survival. *Circ. Res.* 116 (1), 35–45. doi:10.1161/CIRCRESAHA.115.304457

Lino, D. O. C., Freitas, I. A., Meneses, G. C., Martins, A. M. C., Daher, E. F., Rocha, J. H. C., et al. (2019). Interleukin-6 and Adhesion Molecules VCAM-1 and ICAM-1 as Biomarkers of post-acute Myocardial Infarction Heart Failure. *Braz. J. Med. Biol. Res.* 52 (12), e8658. doi:10.1590/1414-431X20198658

Liu, B., Song, Z., Yu, J., Li, P., Tang, Y., and Ge, J. (2020). The Atherosclerosis-Ameliorating Effects and Molecular Mechanisms of BuYangHuanWu Decoction. *Biomed. Pharmacother.* 123, 109664. doi:10.1016/j.biopha.2019.109664

Luo, S., Hu, D., Wang, M., Zipfel, P. F., and Hu, Y. (2020). Complement in Hemolysis- and Thrombosis- Related Diseases. *Front. Immunol.* 11, 1212. doi:10.3389/fimmu.2020.01212

Ma, J., Chen, T., Wu, S., Yang, C., Bai, M., Shu, K., et al. (2019). iProX: an Integrated Proteome Resource. *Nucleic Acids Res.* 47 (D1), D1211–D1217. doi:10.1093/nar/gky869

Ma, L. Y., Chen, W. W., Gao, R. L., Liu, L. S., Zhu, M. L., Wang, Y. J., et al. (2020). China Cardiovascular Diseases Report 2018: an Updated Summary. *J. Geriatr. Cardiol.* 17 (1), 1–8. doi:10.11909/j.issn.1671-5411.2020.01.001

Minicucci, M. F., Azevedo, P. S., Polegato, B. F., Paiva, S. A., and Zornoff, L. A. (2011). Heart Failure after Myocardial Infarction: Clinical Implications and Treatment. *Clin. Cardiol.* 34 (7), 410–414. doi:10.1002/clc.20922

Patel, R. B., Colangelo, L. A., Reiner, A. P., Gross, M. D., Jacobs, D. R., Launer, L. J., et al. (2020). Cellular Adhesion Molecules in Young Adulthood and Cardiac Function in Later Life. *J. Am. Coll. Cardiol.* 75 (17), 2156–2165. doi:10.1016/j.jacc.2020.02.060

Qie, C., Jiang, J., Liu, W., Hu, X., Chen, W., Xie, X., et al. (2020). Single-cell RNA-Seq Reveals the Transcriptional Landscape and Heterogeneity of Skin Macrophages in Vsir-/- Murine Psoriasis. *Theranostics* 10 (23), 10483–10497. doi:10.7150/thno.45614

Ren, Y., Zhang, M., Chen, K., You, S., Li, J., Guo, L., et al. (2012). Clinical and Epidemiological Investigation of TCM Syndromes of Patients with Coronary Heart Disease in China. *Evid. Based Complement. Alternat Med.* 2012, 714517. doi:10.1155/2012/714517

Sacks, F. M., Liang, L., Furtado, J. D., Cai, T., Davidson, W. S., He, Z., et al. (2020). Protein-Defined Subspecies of HDLs (High-Density Lipoproteins) and Differential Risk of Coronary Heart Disease in 4 Prospective Studies. *Arterioscler Thromb. Vasc. Biol.* 40 (11), 2714–2727. doi:10.1161/ATVBAHA.120.314609

Simurda, T., Brunclikova, M., Asselta, R., Caccia, S., Zolkova, J., Kolkova, Z., et al. (2020). Genetic Variants in the FGB and FGG Genes Mapping in the Beta and Gamma Nodules of the Fibrinogen Molecule in Congenital Quantitative Fibrinogen Disorders Associated with a Thrombotic Phenotype. *Int. J. Mol. Sci.* 21 (13), 4616. doi:10.3390/ijms21134616

Suleiman, M., Abdulrahman, N., Yalcin, H., and Mraiche, F. (2018). The Role of CD44, Hyaluronan and NHE1 in Cardiac Remodeling. *Life Sci.* 209, 197–201. doi:10.1016/j.lfs.2018.08.009

Wang, J., Zhang, Y., Liu, Y. M., Yang, X. C., Chen, Y. Y., Wu, G. J., et al. (2020). Uncovering the Protective Mechanism of Huoxue Anxin Recipe against Coronary Heart Disease by Network Analysis and Experimental Validation. *Biomed. Pharmacother.* 121, 109655. doi:10.1016/j.biopha.2019.109655

Wang, P., Huang, H., Chen, B., Su, Y., Shi, P., and Yao, H. (2020). Systems Pharmacology Dissection of Mechanisms of Dengzhan Xixin Injection against Cardiovascular Diseases. *Chem. Pharm. Bull. (Tokyo)* 68 (9), 837–847. doi:10.1248/cpb.c20-00122

Wang, W. R., Lin, R., Zhang, H., Lin, Q. Q., Yang, L. N., Zhang, K. F., et al. (2011). The Effects of Buyang Huanwu Decoction on Hemorheological Disorders and Energy Metabolism in Rats with Coronary Heart Disease. *J. Ethnopharmacol* 137 (1), 214–220. doi:10.1016/j.jep.2011.05.008

Wang, X., Zhao, Z., Mao, J., Du, T., Chen, Y., Xu, H., et al. (20192019). Randomized, Double-Blinded, Multicenter, Placebo-Controlled Trial of Shenfu Injection for Treatment of Patients with Chronic Heart Failure during the Acute Phase of Symptom Aggravation (Yang and Qi Deficiency Syndrome). *Evid. Based Complement. Alternat Med.* 2019, 9297163. doi:10.1155/2019/9297163

Wei, J., Guo, F., Zhang, M., Xian, M., Wang, T., Gao, J., et al. (2019). Signature-oriented Investigation of the Efficacy of Multicomponent Drugs against Heart Failure. *FASEB J.* 33 (2), 2187–2198. doi:10.1096/fj.201800673RR

Wu, X. B., Tian, Y. Q., Tian, P. P., Chen, H. W., and Li, J. (2021). Systematic Review and Sequential Analysis on Efficacy of Modified Buyang Huanwu Tang in Treatment of Chronic Heart Failure. *Chin J. Exp. Tradit Med Formul* 27 (1), 188–195. doi:10.13422/j.cnki.syfjx.20202112

Yancy, C. W., Jessup, M., Bozkurt, B., Butler, J., Casey, D. E., Jr, Drazner, M. H., et al. (2013). 2013 ACCF/AHA Guideline for the Management of Heart Failure: Executive Summary: a Report of the American College of Cardiology Foundation/American Heart Association Task Force on Practice Guidelines. *Circulation* 128 (16), 1810–1852. doi:10.1161/CIR.0b013e31829e8807

Zhong, S., Guo, H., Wang, H., Xing, D., Lu, T., Yang, J., et al. (2020). Apelin-13 Alleviated Cardiac Fibrosis via Inhibiting the PI3K/Akt Pathway to Attenuate Oxidative Stress in Rats with Myocardial Infarction-Induced Heart Failure. *Biosci. Rep.* 40 (4), BSR20200040. doi:10.1042/BSR20200040

Ziaeian, B., and Fonarow, G. C. (2016). Epidemiology and Aetiology of Heart Failure. *Nat. Rev. Cardiol.* 13 (6), 368–378. doi:10.1038/nrcardio.2016.25

Conflict of Interest: The authors declare that the research was conducted in the absence of any commercial or financial relationships that could be construed as a potential conflict of interest.

The reviewer MW declared a shared parent affiliation with the author(s) YL, JR, BM, and JL to the handling editor at the time of review.

Publisher's Note: All claims expressed in this article are solely those of the authors and do not necessarily represent those of their affiliated organizations, or those of the publisher, the editors and the reviewers. Any product that may be evaluated in this article, or claim that may be made by its manufacturer, is not guaranteed or endorsed by the publisher.

frontiers | Frontiers in Pharmacology

ORIGINAL RESEARCH
published: 09 June 2022
doi: 10.3389/fphar.2022.862709

Molecular Mechanism of Naringenin Against High-Glucose-Induced Vascular Smooth Muscle Cells Proliferation and Migration Based on Network Pharmacology and Transcriptomic Analyses

Wenjun He[1,2,3†], *Yanming Wang*[1,2,4†], *Rui Yang*[1,2,4], *Huihui Ma*[1,2,4], *Xuqing Qin*[1,2,4], *Meijuan Yan*[1,2,3], *Yi Rong*[1,2,4], *Yufang Xie*[1,2,4], *Li Li*[1], *Junqiang Si*[1,2,4], *Xinzhi Li*[1,2,3*] *and Ketao Ma*[1,2,4*]

[1]*Key Laboratory of Xinjiang Endemic and Ethnic Diseases, Ministry of Education, Shihezi University School of Medicine, Shihezi, China,* [2]*NHC Key Laboratory of Prevention and Treatment of Central Asia High Incidence Diseases, First Affiliated Hospital, Shihezi University School of Medicine, Shihezi, China,* [3]*Department of Pathophysiology, Shihezi University School of Medicine, Shihezi, China,* [4]*Department of Physiology, Shihezi University School of Medicine, Shihezi, China*

Although the protective effects of naringenin (Nar) on vascular smooth muscle cells (VSMCs) have been confirmed, whether it has anti-proliferation and anti-migration effects in high-glucose-induced VSMCs has remained unclear. This study aimed to clarify the potential targets and molecular mechanism of Nar when used to treat high-glucose-induced vasculopathy based on transcriptomics, network pharmacology, molecular docking, and *in vivo* and *in vitro* assays. We found that Nar has visible anti-proliferation and anti-migration effects both *in vitro* (high-glucose-induced VSMC proliferation and migration model) and *in vivo* (type 1 diabetes mouse model). Based on the results of network pharmacology and molecular docking, vascular endothelial growth factor A (VEGFA), the proto-oncogene tyrosine-protein kinase Src (Src) and the kinase insert domain receptor (KDR) are the core targets of Nar when used to treat diabetic angiopathies, according to the degree value and the docking score of the three core genes. Interestingly, not only the Biological Process (BP), Molecular Function (MF), and KEGG enrichment results from network pharmacology analysis but also transcriptomics showed that phosphatidylinositol-3-kinase (PI3K)/protein kinase B (Akt) is the most likely downstream pathway involved in the protective effects of Nar on VSMCs. Notably, according to the differentially expressed genes (DEGs) in the transcriptomic analysis, we found that cAMP-responsive element binding protein 5 (CREB5) is a downstream protein of the PI3K/Akt pathway that participates in VSMCs proliferation and migration. Furthermore, the results of molecular experiments *in vitro* were consistent with the bioinformatic analysis. Nar significantly inhibited the protein expression of the core targets (VEGFA, Src and KDR) and downregulated the PI3K/Akt/CREB5 pathway. Our results indicated that Nar exerted anti-proliferation and anti-migration effects on high-glucose-induced VSMCs through decreasing expression of the target protein VEGFA, and then downregulating the PI3K/Akt/CREB5 pathway, suggesting its potential for treating diabetic angiopathies.

Keywords: diabetic angiopathies, naringenin, network pharmacology, transcriptomics, molecular docking

OPEN ACCESS

Edited by:
Yi Wang,
Zhejiang University, China

Reviewed by:
Hemant Giri,
Oklahoma Medical Research Foundation, United States
Yan Yang,
Southwestern Medical University, China
Jiang Jianping,
The First Affiliated Hospital of Zhejiang Chinese Medical University, China

***Correspondence:**
Ketao Ma
maketao@hotmail.com
Xinzhi Li
lixinzhi@shzu.edu.cn

†These authors have contributed equally to this work

Specialty section:
This article was submitted to Ethnopharmacology, a section of the journal Frontiers in Pharmacology

Received: *26 January 2022*
Accepted: *20 April 2022*
Published: *09 June 2022*

Citation:
He W, Wang Y, Yang R, Ma H, Qin X, Yan M, Rong Y, Xie Y, Li L, Si J, Li X and Ma K (2022) Molecular Mechanism of Naringenin Against High-Glucose-Induced Vascular Smooth Muscle Cells Proliferation and Migration Based on Network Pharmacology and Transcriptomic Analyses. Front. Pharmacol. 13:862709. doi: 10.3389/fphar.2022.862709

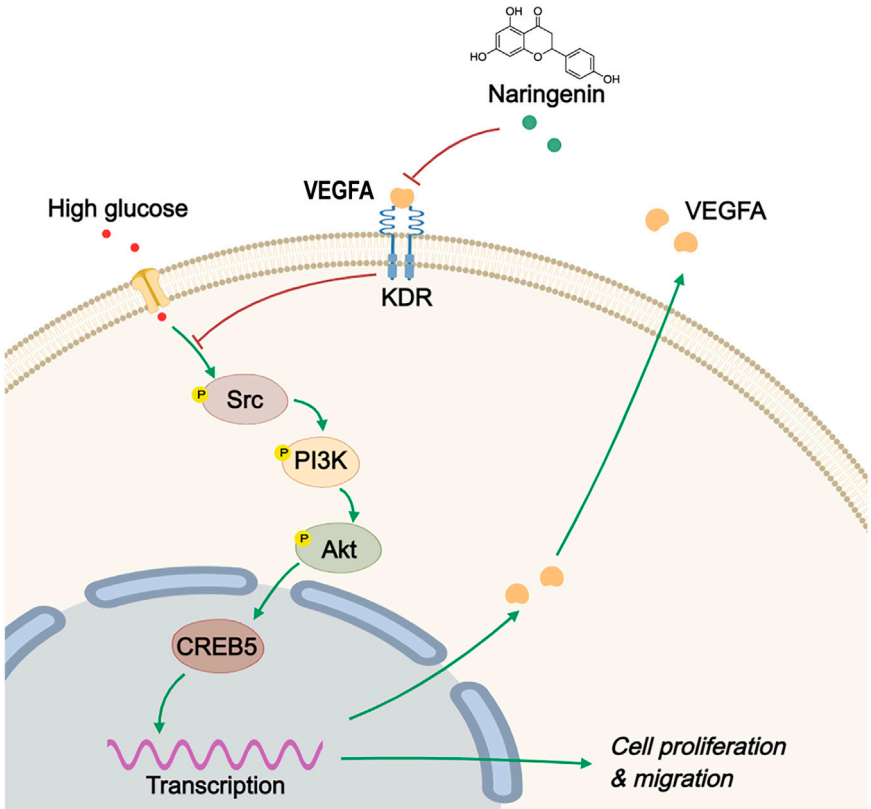

GRAPHICAL ABSTRCAT | Schematic diagram of the protective effect of Nar on high-glucose-induced VSMCs proliferation and migration via inhibiting PI3K/Akt/CREB5 signaling pathway. High glucose could activate PI3K/Akt/CREB5 signaling pathway, leading to excessive proliferation and migration of VSMCs, but Nar could downregulated PI3K/Akt/CREB5 pathway through inhibiting the expression of VEGFA, which located on the upstream of PI3K/Akt signaling pathway, and inhibiting the expression of p-PI3K, p-Akt and CREB5 at the same time, which demonstrated that Nar has an anti-proliferation and anti-migration effect on high-glucose-induced VSMCs through inhibiting PI3K/Akt/CREB5 signaling pathway.

1 INTRODUCTION

The morbidity of diabetes characterized by abnormally elevated glucose is increasing year by year across the world, making it one of the most serious burdens on healthcare resources globally (Forbes and Cooper, 2013). The diabetic complications that arise with the progression of diabetes are major causes of low quality of life and high mortality among patients, which include retinopathy, nephropathy, neuropathy, myocardial infarction, and cerebrovascular disease (Deshpande et al., 2008). In particular, cardiovascular diseases (CVDs) due to microvascular and macrovascular lesions are major causes of death in diabetics. The anomalous blood glucose level is closely related to such vascular lesions. Under normal physiological conditions, vascular smooth muscle cells (VSMCs) tend to accumulate at the G0/G1 phase of the cell cycle, which is characterized by low proliferation, and an ordered, differentiated, and contractile phenotype for achieving contractile and synthetic function (Bruemmer and Law, 2003). However, under pathological conditions, VSMCs have a more pronounced ability to proliferate and migrate (Jiang et al., 2017). Numerous studies have reported that chronic hyperglycemia is directly responsible for the initiation and exacerbation of a transition in vascular phenotype from the normal, stabilized contractile phenotype to the synthetic phenotype with the development and progression of diabetes (Shi et al., 2020). Additionally, the excessive proliferation of VSMCs can lead to the development and exacerbation of hypertension, atherosclerosis, and restenosis (Ran et al., 2021). Therefore, modification of the VSMC phenotype is a potential treatment strategy for various vascular diseases in diabetic patients.

Naringenin (Nar) (PubChem CID: 932) is a member of the flavonoids obtained from citrus fruits, including grapefruit, orange, and tomato (Arafah et al., 2020). Evidence has shown that it has various pharmacological activities, including anti-inflammatory, anti-tumor, anti-bacterial, anti-diabetic, anti-oxidant, immunomodulatory, hepatoprotective, and cardiovascular protective effects (Den Hartogh and Tsiani, 2019). Salehi et al. reported a clinical trial that showed that, through long-term daily supplementation with grapefruit (containing naringenin glycoside), the endothelial function of 48 healthy menopausal women was improved (Salehi et al., 2019). In addition, Chen et al. reported that Nar can inhibit

VSMC proliferation and migration by upregulating HO-1 expression in a TNF-α-induced VSMC proliferation model (Chen et al., 2012). Moreover, Lee et al. found that both Nar and naringin had protective effects on the cardiovascular system by inhibiting MMP expression and Akt activity in a TNF-α-induced VSMC proliferation model (Lee et al., 2009). These studies indicate that Nar has potential beneficial effects on VSMCs. However, whether Nar has beneficial effects on high-glucose-induced VSMC proliferation and migration remains unclear. Therefore, in the present study, we further explored the effect of Nar on VSMC proliferation and migration induced by high glucose, and examined the possible molecular mechanisms involved by combining network pharmacology and transcriptomics. Our findings demonstrated that Nar could attenuate the high-glucose-induced proliferation and migration of VSMCs through inhibiting VEGFA target expression and downregulating the PI3K/Akt/CREB5 signaling pathway, which indicated Nar's potential for treating vascular lesions in diabetic vessels.

2 MATERIALS AND METHODS

2.1 Materials

Naringenin (Nar) (≥ 95%, N5893), streptozotocin (STZ) were purchased from Sigma (Sigma Aldrich, United States). Anti-PCNA (1:1000, ab29) and anti-OPN (1:500, ab63856) were purchased from Abcam. Anti-MMP2 (1:1000, bs-4605R) and anti-MMP9 (1:1000, bsm-54040R) were obtained from Bioss Biotechnology Co., LTD. (Beijing, China). Anti-α-SMA (1:1000, BM0002), anti-VEGFA (1:1000, BA0407) and anti-VEGFR2/KDR (1:1000, A00901-3) were purchased from Boster Biological Technology Co. Ltd. (Shanghai, China). Anti-CREB5 (1:1000, G420) was purchased from Santa cruz. The following antibodies: PI3K (1:1000, 4249), p-PI3K (1:500, 17366), Akt-pan (1:1000, 4685), p-Akt (Ser 473) (1:1000, 4060), Src (1:1000, 36D10), and p-Src (1:1000, D49G4) were obtained from CST. EdU Imaging kit was purchased from APE × Bio (United States). Trypsin, Dulbecco's Modified Eagle's Medium (DMEM) and fetal bovine serum (FBS) were purchased from GIBCO.

2.2 Animals and Model Preparation

Male C57BL/6 mice aged 6–8 weeks (20 ± 2 g) were obtained from Hengzhao Biotechnology Co., Ltd. All animal experiments were performed in accordance with standard animal research guidelines. Mice were housed under a 12 h light/12 h dark cycle in a temperature-controlled room, and maintained on standard chow and tap water ad libitum.

To establish the diabetic model, 48 mice were randomly assigned to two groups. The Control group contained 12 mice and the diabetic group 36. After fasting for 12 h, mice in the diabetic group were intraperitoneally injected with streptozotocin (STZ, Sigma) (40 mg/kg body wt.) dissolved in sodium citrate buffer (pH 4.2) for 5 consecutive days (Nikolic et al., 2014). Control mice were injected with an equal volume of buffer solution. Three days after injection with STZ, mice with non-fasting blood glucose levels > 16.6 mmol/L were considered to have been successfully induced to develop diabetes and used for subsequent experiments.

Thirty-six diabetic mice were randomly divided into three groups: a model group (DM), a low-dose Nar group (DM + LN) (25 mg/kg), and a high-dose Nar group (DM + HN) (75 mg/kg) (Zhang et al., 2018). Nar was dissolved in saline (Wang et al., 2016), and intragastrically administered once a day for 12 weeks. The model and control mice were intragastrically administered an equal volume of saline. After 12 weeks of treatment, all mice were euthanized, and the thoracic aorta was isolated and used for subsequent experiments.

2.3 Cell Culture and Treatments

The primary Sprague-Dawley rat VSMCs were isolated from the thoracic aorta of male rats by the tissue adherence method, and characterized by smooth muscle-specific α-actin staining, as described previously (Sun et al., 2016). Only cells at passages 3-6 were used for the *in vitro* experiment. The VSMCs were cultured in DMEM (normal glucose) containing 10% FBS and 1% antibiotic-antimycotic (containing penicillin, streptomycin, and amphotericin B) at 37°C in a 5% CO2 and 95% air incubator, as described previously (Hashim et al., 2006).

2.4 Hematoxylin–Eosin Staining

The thoracic aorta was isolated and fixed in 4% paraformaldehyde, embedded in paraffin, and transversely cut into 5 μm sections with a cryostat. The sections were subjected to hematoxylin–eosin (HE) staining (Fan et al., 2012) and then imaged with a light microscope. Media thickness, lumen diameter, and their ratio were measured as indicators of vascular remodeling.

2.5 Immunohistochemistry

Immunohistochemical analysis was conducted as previously described (Ren et al., 2020). The thoracic aorta was prefixed, and the paraffin-embedded sections were washed with PBS, blocked with blocking buffer, and treated with primary antibodies for 24 h at 4°C, then primary antibodies were washed out, followed by incubation with the secondary antibodies for 30 min at room temperature. Positive cells were visualized using 3,3-diaminobenzidine. Then, images were obtained with an Olympus microscope.

2.6 Evaluation of Vascular Smooth Muscle Cells Proliferation

The proliferation ability of VSMCs was assessed by CCK-8 assay, 5-ethynyl-2′-deoxyuridine (EdU) incorporation assay, and PCNA expression (Ren et al., 2017). Cells were seeded into 96-well plates (5×10^4/ml) for 24 h. After 24 h of starvation in serum-free medium, the cells were then exposed to normal glucose, high glucose (25 mmol/L), or high glucose with various doses of Nar (50, 100, and 150 μmol/L) for 24 h (Wu et al., 2020). Appropriate amount of Nar was dissolved in DMSO, making it at the

concentration of 1 mmol/L, which was then diluted with the corresponding DMEM into 50, 100 and 150 μmol/L. After cultivation, 10 μL of CCK-8 (APE × Bio) was added to each well. After incubation at 37°C in a 5% CO2 atmosphere for 2.5 h, absorbance was examined by a microplate reader (Thermo Fisher) at 450 nm. For the EdU incorporation assay, cells were seeded in six-well plates and cultured up to 80–95% density, followed by starvation and incubation with diverse DMEM or Nar for 24 h. EdU incorporation assay was performed in accordance with the manufacturer's instructions. EdU-positive cells were examined by flow cytometry (FCM). Besides, PCNA, acting on chromatin as a platform for various proteins in the processes of DNA replication, was detected by western blot as a marker of cell proliferation.

2.7 Cell Migration Assay

For the wound scratch assay, VSMCs were seeded into six-well plates and cultured up to 80–90% confluence, the cells were then starved in starvation medium for 24 h. A single scratch wound was generated using a 1 mL pipette tip, after which the cells were subjected to different stimulations for an additional 12, 24, or 48 h. Cell migration was assessed by measuring scratch area with ImageJ software.

A modified transwell assay in 24-well plates was used to analyze VSMC migration. VSMCs (5×10^4/ml) were resuspended in serum-free medium and 200 μL was added to the upper chamber. The lower chamber was filled with 500 μL of DMEM (10% FBS) with normal glucose, high glucose, and/or different concentrations of Nar. After 24 h of incubation, cells migrated to the lower face of the chamber. The number of migrated cells was clarified by violet staining, as described previously (Zhang et al., 2019).

2.8 Immunofluorescence Analysis

Immunofluorescence analysis was performed as previously described (Zang et al., 2019). Briefly, VSMCs were plated on glass coverslips in six-well plates, cultured up to 40–50% confluence, and treated with 4% paraformaldehyde for 20 min. They were then washed with PBS and permeabilized with 0.2% Triton X-100 for 5 min, blocked with 5% BSA at room temperature for 30 min, and incubated with the primary antibodies (1:100) overnight at 4°C. The cells were washed with PBS and incubated with FITC/TRITC-conjugated fluorescence secondary antibody (1:500) for 2 h at 37°C. The nuclei were stained with DAPI (1:1000) for 15 min at room temperature. Immunofluorescence images were acquired with an Olympus cellSens Entry (Olympus, Tokyo, Japan).

2.9 qRT-PCR

Total RNA of each group of VSMCs was extracted using the miRNA isolation Kit (Omega, United States) and quantified using the NanoDrop one Spectrophotometer (Thermo-Fisher, United States). cDNA was carried out using a cDNA synthesis Kit (Thermo-Fisher, United States) according to the instructions. Quantitative Reverse Transcriptase PCR (qRT-PCR) samples were prepared using SYBR Green PCR Kit (500), and amplified by using LightCycler96 Real-time fluorescent quantitative PCR Instrument (Roche, Switzerland). Relative mRNA expression was normalized to the control mRNA expression using the ΔΔCt method.

2.10 Western Blotting

Cellular protein was extracted from the diversely treated VSMCs with radioimmune precipitation assay (RIPA) lysis buffer, as previously reported (Jia et al., 2019). Protein concentration was measured using a bicinchoninic acid (BCA) protein assay kit. Equal amounts of the protein samples were separated by 10% or 12% SDS-PAGE and transferred to a PVDF membrane, followed by blocking with 5% BSA or dry milk in Tris-buffered saline (TBS) for 2 h at room temperature. The primary antibodies (1:1000 dilution) were incubated overnight at 4°C; after washing with TBST (TBS containing 0.1% Tween 20) three times for 10 min each, treatment with the secondary antibodies was applied (1:10,000 dilution; Zhongshan Jinqiao, China) for 2 h. Following three washes with TBST, the membranes were incubated with enhanced chemiluminescence (ECL) reagent and exposed to the Odyssey Infrared Imaging System. Images were analyzed by ImageJ software.

2.11 Collection of Nar's Potential Targets

The molecular structure of Nar was confirmed using PubChem (https://pubchem.ncbi.nlm.nih.gov/), which was imported into the Swiss Target Prediction database (http://swisstargetprediction.ch/) and TargetNet database (http://targetnet.scbdd.com) for compound target prediction analysis (Ai et al., 2020).

2.12 Collection of Diabetic Angiopathy-Related Disease Target Genes

The term "diabetic angiopathies" was used as a keyword to acquire important target genes of diabetic angiopathies with the following databases: DisGeNET (https://www.disgenet.org/), GeneCards database (https://www.genecards.org/), OMIM database (https://www.omim.org/), and the Comparative Toxicogenomics Database (CTD, http://ctdbase.org/) (Xiao et al., 2021). Then, the UniProt database (https://www.uniprot.org/) was used to convert the target name into an official gene symbol by inputting the target name and limiting the species to human beings (Xiao et al., 2021). Finally, the database search results were integrated and the duplicates were deleted to acquire all target genes of diabetic angiopathies.

2.13 Common Target Acquisition and PPI Network Construction

The common targets of diabetic angiopathies and Nar were used in the OmicShare tools (https://www.omicshare.com/) to create a Venn map. They were then used in the String database (https://string-db.org/) to obtain the relevant information of protein–protein interactions (PPI), which was subsequently

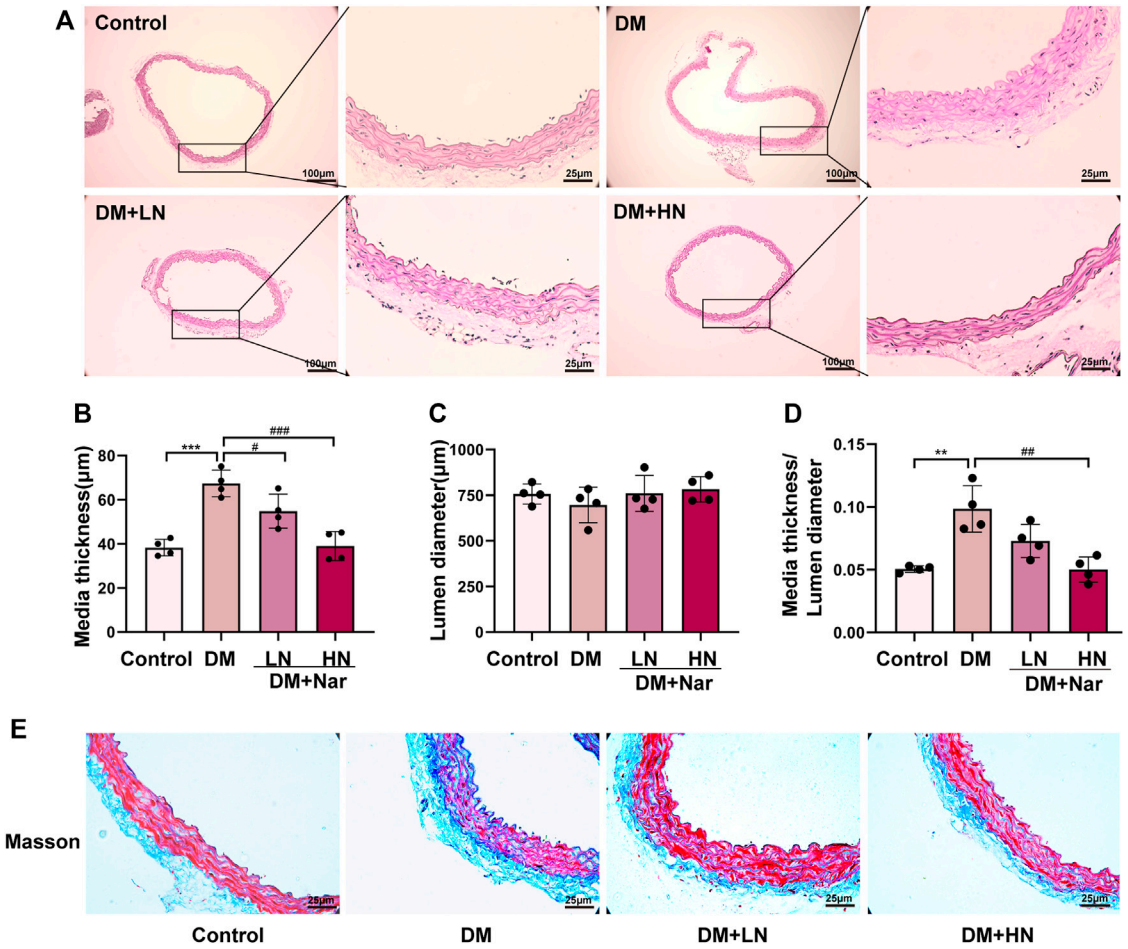

FIGURE 1 | Protective effect of Nar against diabetic angiopathies *in vivo*. **(A)** HE staining of thoracic aorta from diverse groups of mice. **(B)** Bar graph of media thickness of aorta in diverse groups. **(C)** Bar graph of lumen diameter of aorta in diverse groups **(D)** Bar graph of HE staining analysis the ratio of media thickness/lumen diameter in aorta. $^{**}p < 0.01$, $^{***}p < 0.001$ compared with Control group, $^{\#}p < 0.05$, $^{\#\#}p < 0.01$, $^{\#\#\#}p < 0.001$, compared with HG group. **(E)** Representative images of Masson's staining of the aorta (magnification: 400×).

demonstrated and visualized by Cytoscape 3.7.0 software. Meanwhile, the degree values of proteins and the key proteins within the PPI network were acquired using Cytoscape 3.7.0 software.

2.14 Functional Enrichment Analysis

GO and KEGG pathway analyses of the common proteins were performed using DAVID database (https://david.ncifcrf.gov/) as Excel and bubble charts. The results were sorted according to *p* value and count value.

2.15 RNA Extraction and Analysis of Transcriptomic Sequencing

RNA samples were extracted from diversely treated VSMCs ($n = 3$) using Trizol reagent, as previously described (Sun et al., 2021). VSMCs were incubated in different DMEM for 24 h as follows: high glucose (HG group) and high glucose with Nar (100 μmol/L) (Nar group). Then, the RNA samples were analyzed by NovelBio (Shanghai, China).

2.16 PPI Network and Pathway Enrichment Analysis of Transcriptomic Sequencing

The differentially expressed genes (DEGs) were acquired from transcriptomic sequencing by comparing the Nar group with the HG group, which are potential targets of Nar in the treatment of diabetic angiopathies. To analyze the information on the interactions of the candidate DEGs, String database (https://string-db.org/) and Cytoscape 3.7.0 software were used. The KEGG pathways were analyzed according to the results of the transcriptomic sequencing.

2.17 Molecular Docking

Molecular docking was performed to analyze the interaction between Nar and core targets, which was conducted using

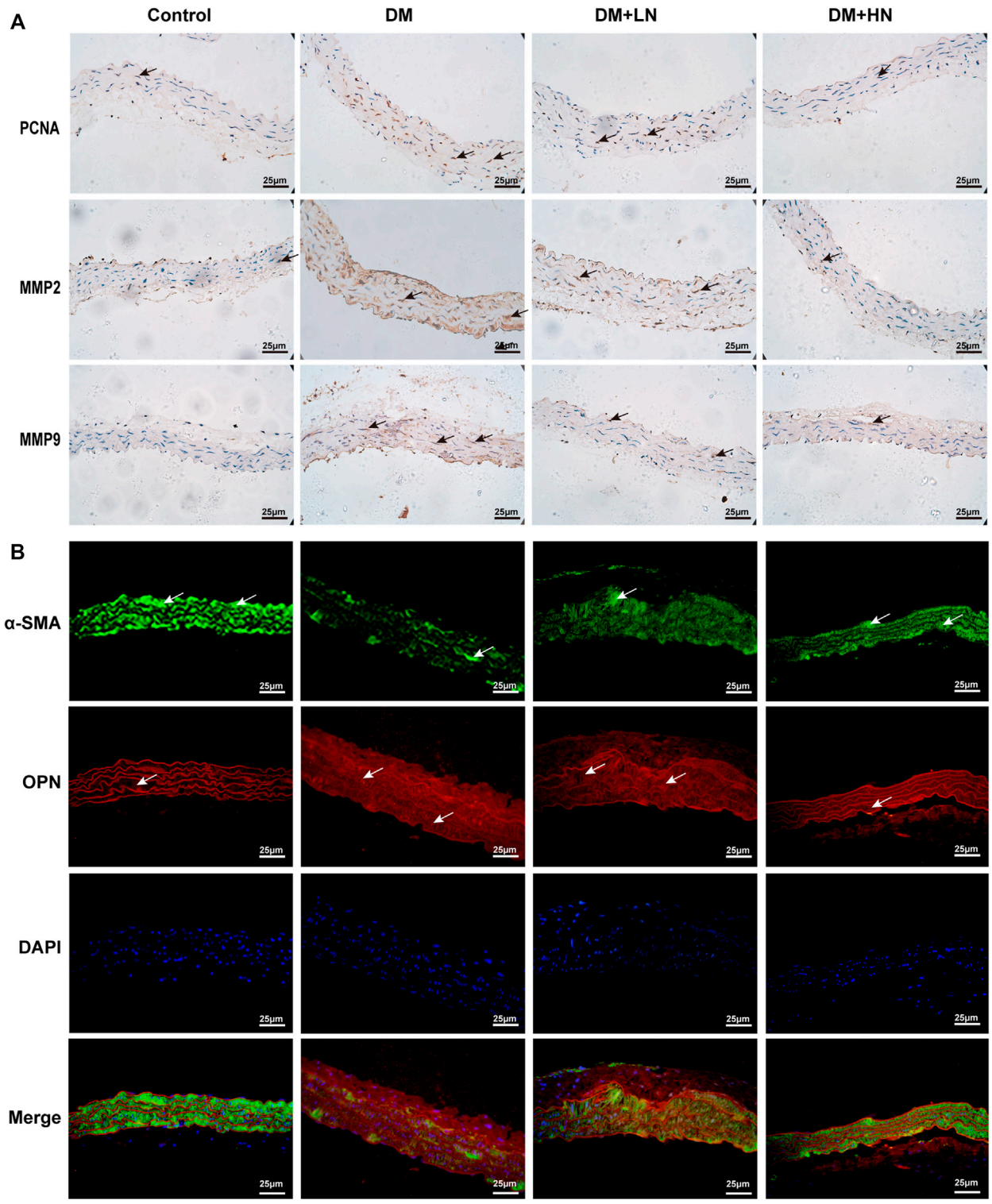

FIGURE 2 | (A) Nar inhibited diabetes induced VSMCs' proliferation, migration and phenotype switching *in vivo*. Immunohistochemical analysis of PCNA, MMP2, and MMP9 expression in the aorta in diverse groups (magnification: 400×). **(B)** Immunofluorescence staining of α-SMA and OPN expression in diverse groups of mice.

LibDock. The complexes of the targets were downloaded from the Protein Data Bank (PDB) database according to PDBbind benchmark dataset (version 2020, www.pdbbind.org.cn) (Ren et al., 2018; Rezaei et al., 2022), and the cognate ligand docking and inhibitor ligand docking were performed as the positive control test. The 3D structures of Nar and inhibitors were

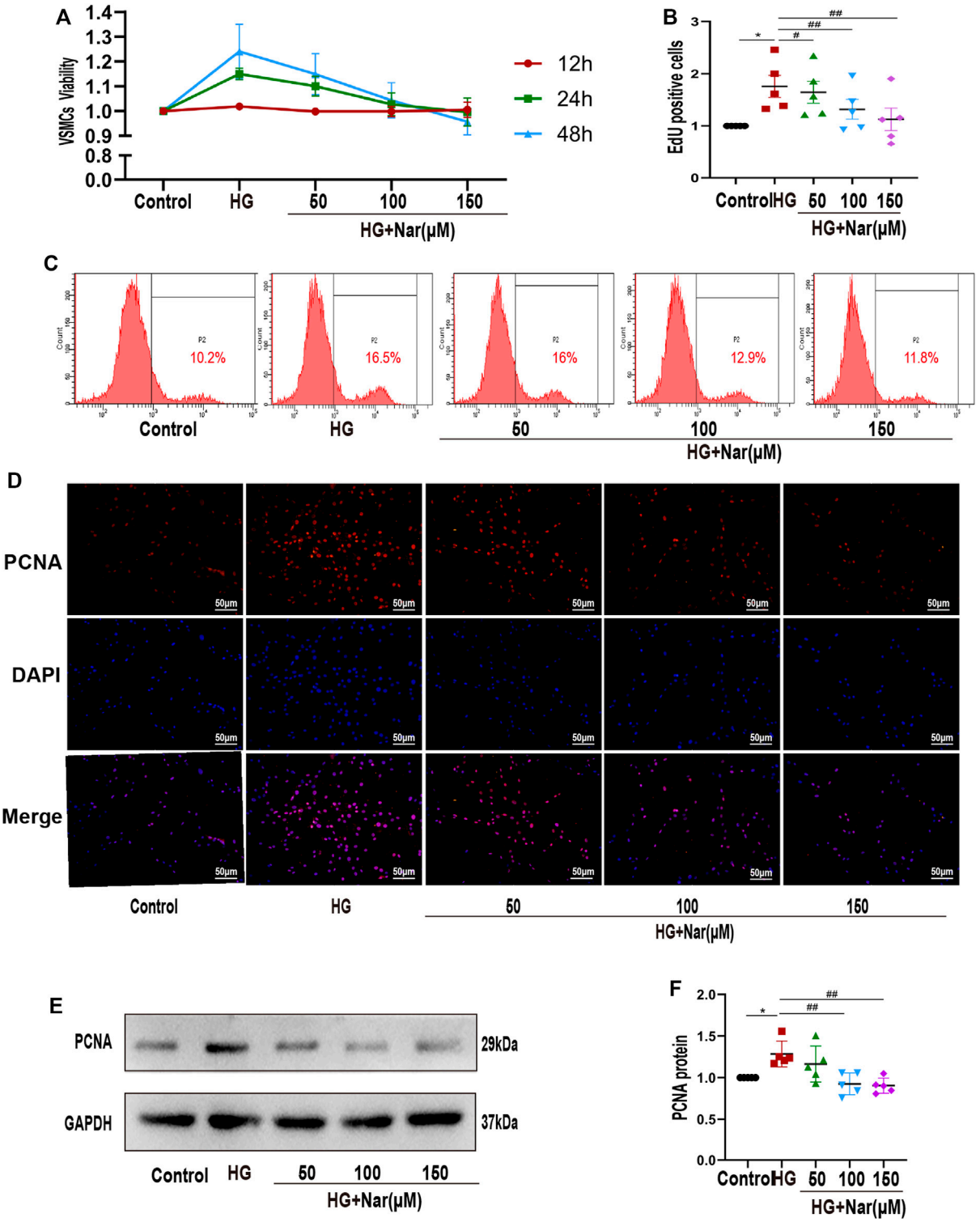

FIGURE 3 | Nar inhibited high-glucose-induced VSMC proliferation. **(A)** CCK-8 assay showed that Nar reduced the viability of high-glucose-induced VSMCs at 24 and 48 h, $p < 0.05$. **(B,C)** Flow cytometry showed a lower cell proliferation rate in the Nar group than in the HG group. **(D)** Immunofluorescent staining of PCNA (magnification: 200×). **(E,F)** Western blot analysis showed PCNA expression associated with different treatments of VSMCs, $^{*}p < 0.05$ compared with Control group, $^{\#\#}p < 0.01$ compared with HG group.

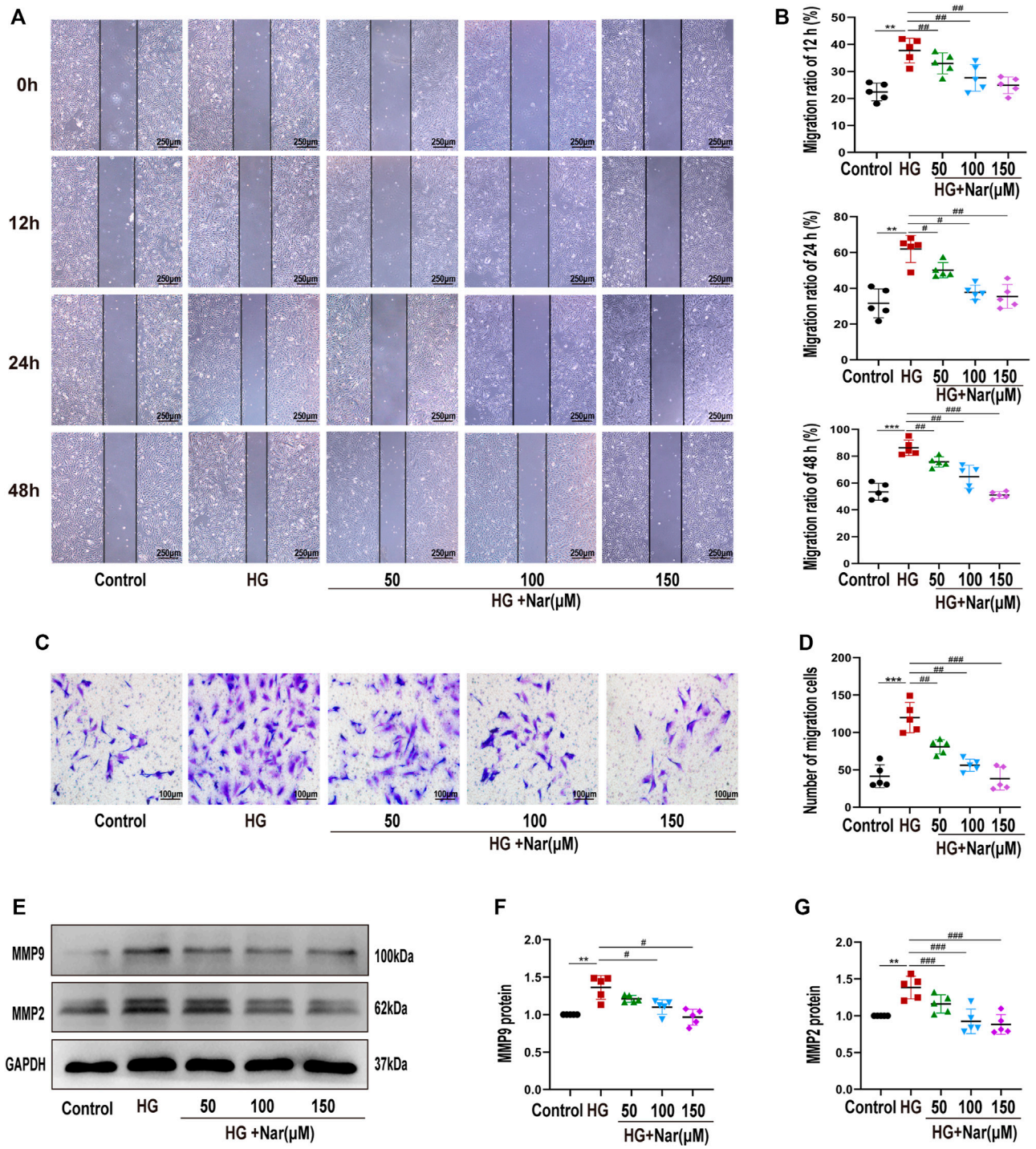

FIGURE 4 | Nar inhibited high-glucose-induced VSMC migration. **(A,B)** Wound healing assay of VSMC migration at 12, 24, and 48 h (magnification: 40×). **(C,D)** Transwell migration assay of Control group, HG group, and groups with diverse doses of Nar (magnification: 200×). **(E–G)** Western blot analysis of MMP2 and MMP9 expression. $^{**}p < 0.01$ compared with Control group, $^{\#\#}p < 0.01$ compared with HG group.

downloaded from the PubChem database (https://pubchem.ncbi.nlm.nih.gov/). Docking programs were operated using LibDock with protein-molecules interactions, a higher LibDock score means a greater capacity for ligand-protein binding, as obtained in Discovery Studio 2016 (Li et al., 2021). The binding results were visualized as 3D and 2D diagrams using Discovery Studio Visualization version 4.5 (Accelrys, Inc., San Diego, CA, United States).

2.18 Statistical Analysis

Trials were directed in a double-blinded and randomized fashion. All data are presented as mean ± SD. Student's paired *t*-test was used for comparisons between two groups. One-way ANOVA was used for multiple comparisons. $p < 0.05$ was considered statistically significant.

3 RESULTS

3.1 Protective Effect of Nar Against Diabetic Angiopathies *in vivo*

Firstly, type 1 diabetic C57BL/6 mice model was used to assess the effect of Nar on diabetic vascular remodeling. After being injected with STZ for consecutive 5 days, 36 mice with blood glucose > 16.6 mmol/L were considered diabetic and randomly divided into three groups, DM group, DM + LN group and DM + HN group. According to the blood glucose and body weight monitoring, the blood glucose of DM group was significantly increased for continuous 12 weeks compared with Control group, but the blood glucose of Nar group including DM + LN and DM + HN group had no significant differences compared with DM group (**Supplementary Figure 1A**). At the same time, the body weight of DM group was significantly decreased compared with Control group, and the body weight of DM + LN and DM + HN were consistent with DM group (**Supplementary Figure 1B**).

According to HE staining, it revealed a higher media thickness of aorta in DM group, compared with Control group, and the media thickness of aorta in DM + LN and DM + HN group was significantly less than DM group (**Figures 1A–D**). At the same time, Masson's trichrome staining showed a severer fibrosis in DM group, which was alleviated significantly after treatment with Nar (**Figure 1E**).

Whether Nar has the effect of anti-proliferation and anti-migration on VSMCs, immunochemistry staining was exerted to detect the expression of related proteins, PCNA, MMP2, and MMP9. According to the result of immunochemistry staining, the expression of PCNA, MMP2, and MMP9 were increased in DM group, and treatment with Nar (DM + LN, DM + HN) decreased the expression of PCNA, MMP2, and MMP9 (**Figure 2A**).

Moreover, to confirm the effect of Nar reversed VSMCs dedifferentiation, immunofluorescence staining was used to detected the expression of α-SMA, a marker of characteristic contractile phenotype of VSMC, and OPN, a marker of synthetic phenotype of VSMCs. As shown in **Figure 2B**, there was a lower expression of α-SMA in DM group compared with Control group, but a higher expression in DM + LN and DM + HN groups compared with DM group, on the contrary, the expression of OPN was highly increased in DM group, and reduced significantly in DM + LN and DM + HN groups.

3.2 Nar Inhibited High-Glucose-Induced Vascular Smooth Muscle Cells Proliferation

Firstly, VSMC was isolated and characterized as shown in **Supplementary Figure 2A,B**, and only passages 3 to passages 6 were used in cell experiments. To evaluate the influence of Nar on VSMCs under high-glucose conditions, we first confirmed the cytotoxic effects of Nar on VSMCs at 200 μmol/L, but not at other concentrations (50, 100, and 150 μmol/L) (**Supplementary Figure 2C**). Then, VSMCs were stimulated with a high level of glucose along with different concentrations of Nar (50, 100, and 150 μmol/L) for 24 h to examine cell proliferation by CCK-8 assay and flow cytometry. CCK-8 assay showed that high glucose can lead to higher viability of VSMCs, while Nar decreased the high glucose-induced cell viability (**Figure 3A**). Flow cytometry indicated that Nar at concentrations of 50, 100, and 150 μmol/L inhibited the high-glucose-induced proliferation of VSMCs (**Figures 3B,C**). At the same time, incubation with a high level of glucose induced the upregulation of PCNA, considered a marker of cellular proliferation, and Nar suppressed the upregulation of PCNA as reflected by the fluorescence intensity (**Figure 3D**) and protein expression (**Figures 3E,F**) in high glucose-incubated VSMCs.

3.3 Nar Inhibited High-Glucose-Induced Vascular Smooth Muscle Cells Migration

Next, to explore whether Nar abrogated VSMCs migration in response to high glucose, wound healing assay and transwell assay were exerted. As shown in **Figures 4A,D**, incubation of VSMCs with high glucose resulted in an increase of their scratch area, however, Nar counteracted the high-glucose-induced migration of VSMCs, as evidenced by wound healing assay (**Figures 4A,B**) and Transwell migration assay (**Figures 4C,D**). Markers such as MMP9 and MMP2 are considered to be involved in cell migration (Shen et al., 2021). Consistent with this, treatment with Nar mitigated the upregulation of MMP9 and MMP2 protein levels in high-glucose-incubated VSMCs (**Figures 4E–4G**).

3.4 Nar Abrogated High-Glucose-Induced Vascular Smooth Muscle Cells Dedifferentiation

VSMCs dedifferentiation plays a vital role in the proliferation and migration of VSMCs as well as vascular dysfunction. To detect whether Nar affected high-glucose-induced VSMC dedifferentiation, we examined the expression of α-SMA and OPN of VSMCs in terms of fluorescence intensity and protein levels. Our results indicated that high glucose can induce the change of VSMC phenotype from differentiated to dedifferentiated cells, as evidenced by the increased expression of OPN, a marker of a synthetic phenotype, along with decreased expression of α-SMA, a marker of a contractile phenotype. As shown in **Figures 5A,C,D**, the expression of α-SMA was significantly reduced, and after treating with different concentrations of Nar, the expression of α-SMA was gradually increased. Simultaneously, as shown in **Figures 5B,C,E**, the expression of OPN was significantly increased, while decreased after incubation with diverse concentrations of Nar. Our results demonstrated that incubation with Nar significantly antagonized the VSMCs dedifferentiation response to high glucose.

3.5 Results of Network Pharmacology Analysis

3.5.1 Collection of Nar Targets and Diabetic Angiopathy Targets

According to the Swiss target prediction database and TargetNet database, 190 Nar-related targets were collected. A total of 3213

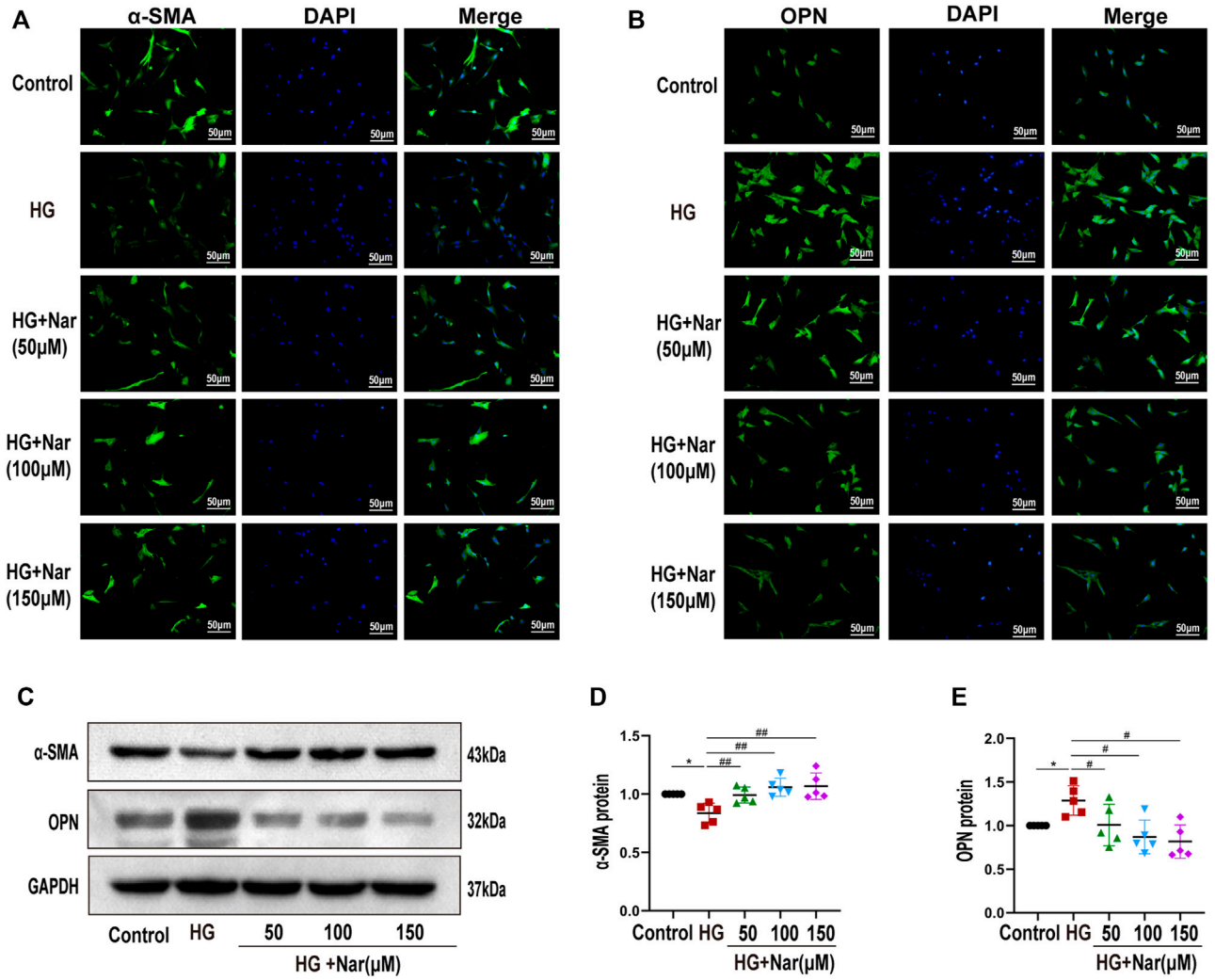

FIGURE 5 | Nar abrogated high-glucose-induced VSMC dedifferentiation. **(A,B)** Immunofluorescent staining of α-SMA and OPN (magnification: 200×). **(C–E)** Western blot analysis of α-SMA and OPN expression. $^{*}p < 0.05$ compared with Control group, $^{\#}p < 0.05$, $^{\#\#}p < 0.01$ compared with HG group.

diabetic angiopathy-related genes were acquired from the GeneCards, OMIM, DisGeNet, and CTD databases after removing duplicate genes, and 102 common targets were obtained, as shown in **Figure 6A**. The PPI network of these 102 potential targets was constructed via the String database, according to the degree, top 50 of them were visualized using Cytoscape 3.7.0 as shown in **Figure 6B**. The top 10 proteins were as follows, VEGFA (degree 51), PTGS2 (degree 47), Src (degree 45), ESR1 (degree 41), HSP90AA1 (degree 37), AR (degree 34), APP (degree 33), KDR (degree 30), PIK3CA (degree 29) and MMP2 (degree 27).

3.5.2 GO and KEGG Pathway Analyses

To identify the possible mechanism by which Nar suppresses diabetic angiopathies, 102 predicted targets were subjected to GO and KEGG enrichment analyses. GO enrichment analysis including biological process (BP) and molecular function (MF) analysis identified the involvement of the targets in the response to phosphatidylinositol-3-phosphate biosynthetic process, extracellular matrix disassembly, and phosphatidylinositol 3-kinase activity, among others, which are closely related to cell proliferation and migration (**Figures 6C,D**). According to the *p*-values ($p < 0.05$) and count values, the top 20 KEGG pathways involved in the alleviation of diabetic angiopathies by Nar were identified as major pathways (**Figure 6E**) intimately associated with proliferation and migration, including the VEGF signaling pathway and PI3K-Akt signaling pathway.

3.6 Results of Transcriptomic Sequencing and Data Analysis

3.6.1 DEGs Reversed by Nar

To further explore the mechanism by which Nar acts against diabetic angiopathies, we conducted transcriptomic sequencing on VSMC samples incubated with high glucose (HG) or high glucose with Nar (Nar). A total of 711 DEGs showed

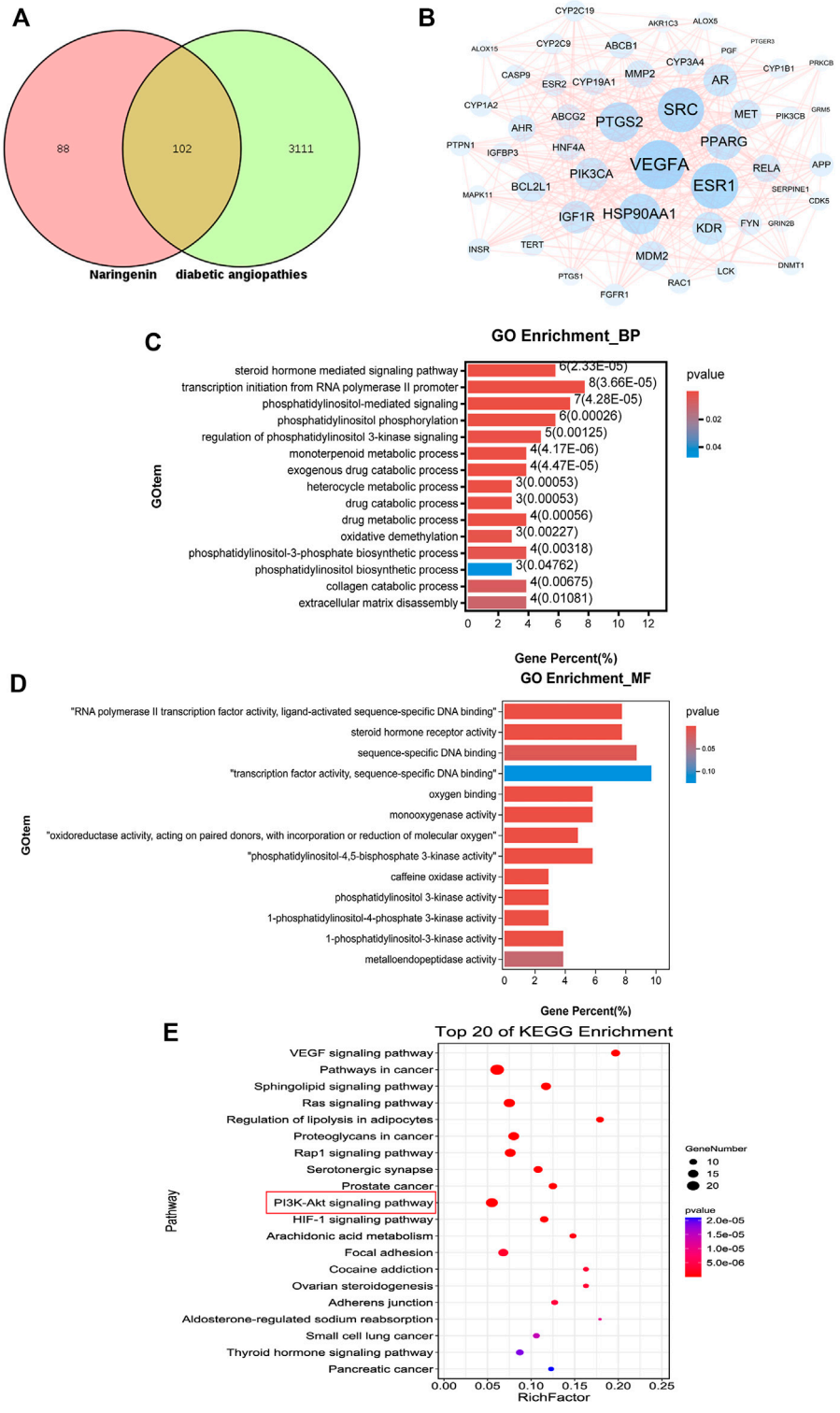

FIGURE 6 | Results of network pharmacology analysis. **(A)** Venn diagram shows the number of common targets between Nar and diabetic angiopathies. **(B)** Protein–protein interaction (PPI) network of the common targets according to degree value analyzed by Cytoscape software. **(C)** GO enrichment (BP) analysis of network pharmacology. **(D)** GO enrichment (MF) analysis of network pharmacology. **(E)** Top 20 most enriched KEGG categories for the common targets shows the vital Nar-related signaling pathway against diabetic angiopathies according to network pharmacology analysis.

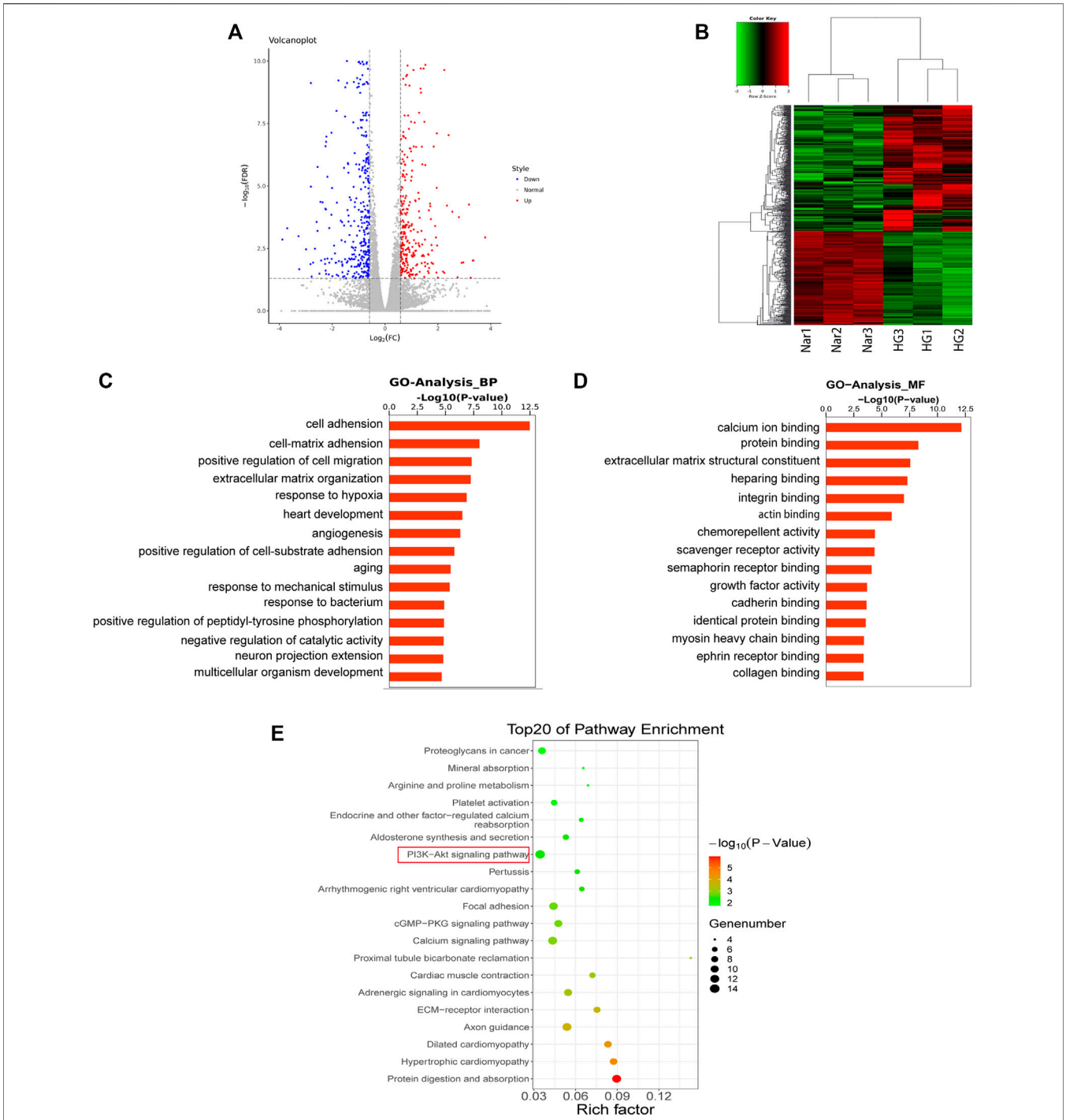

FIGURE 7 | Results of transcriptomic sequencing and data analysis **(A)** A volcano plot indicates the mRNA expression profile of the Nar group vs the HG group. **(B)** Heatmap shows the clustering of mRNAs between the Nar and HG groups of VSMCs. Up- and downregulated genes are colored in red and blue, respectively. **(C)** GO enrichment (BP) analysis of transcriptomic analysis. **(D)** GO enrichment (MF) analysis of transcriptomic analysis. **(E)** Top 20 most enriched KEGG categories for the downregulated genes shows the vital Nar-related signaling pathway against diabetic angiopathies according to transcriptomic analysis.

significant change of expression due to Nar compared with the level with HG ($p < 0.05$, $|\text{Log2FC}| > 0.585$), 303 of which were upregulated and 408 were downregulated in the Nar group (**Figures 7A,B**).

3.6.2 GO and KEGG Pathway Analyses

GO and KEGG enrichment analyses of the above-mentioned up- and downregulated DEGs were conducted. The GO enrichment of downregulated genes was shown in **Figures 7C,D**, which

TABLE 1 | LibDock analysis of core targets bound with different molecules.

Target	PDB	LibDock score		
		Naringenin	Cognate ligand	Inhibitor
VEGFA	1VPP	98.7813	99.4048	117.326
Src	5XP7	104.866	128.602	111.639
KDR	3VHK	111.412	120.848	121.494

identified cell–matrix adhesion, positive regulation of migration, and angiogenesis, factors that are intimately related to cell proliferation and migration.

The results of KEGG enrichment analysis of 408 downregulated DEGs were listed in **Figure 7E**, which identified the cGMP/PKG signaling pathway and PI3K/Akt signaling pathway were closely related to cell proliferation and migration. Interestingly, we found that the same KEGG pathway, namely, the PI3K/Akt pathway, was identified both in network pharmacology and transcriptomic analyses, indicating its potentially vital role in Nar's effects against VSMC proliferation and migration induced by high glucose. Thus, the PI3K/Akt signaling pathway was regarded as the key pathway of Nar protected against diabetic angiopathies.

The genes enriched in the PI3K/Akt pathway were listed in **Supplementary Table 1**, including ITGA4, TNC, IGF1, and CREB5 et al., among them, CREB5, which was found in the downstream part of this pathway and was downregulated by Nar. At the same time, VEGFA, Src and KDR, located in the upstream part of the PI3K/Akt pathway, were identified as key targets included among the top 10 targets from the network pharmacology analysis.

3.7 Results of Molecular Docking Analysis

Molecular docking was carried out to investigate the potential binding modes and interactions between Nar and its key targets VEGFA (PDB: 1VPP), Src (PDB: 5XP7), and KDR (PDB: 3VHK). As shown in **Table 1**, the LibDock score between VEGFA and Nar was 98.7813, and the LibDock score between VEGFA and inhibitors (PTC299 and Erdafitinib) were 99.4048 and 117.326. As to Src, it had LibDock score of 104.866 interacted with Nar, 128.602 interacted with its cognate ligand (8C6), and 111.639 interacted with the specific inhibitor (Src inhibitor 1). And the interaction between KDR and Nar was evaluated based on the dock score of 111.412

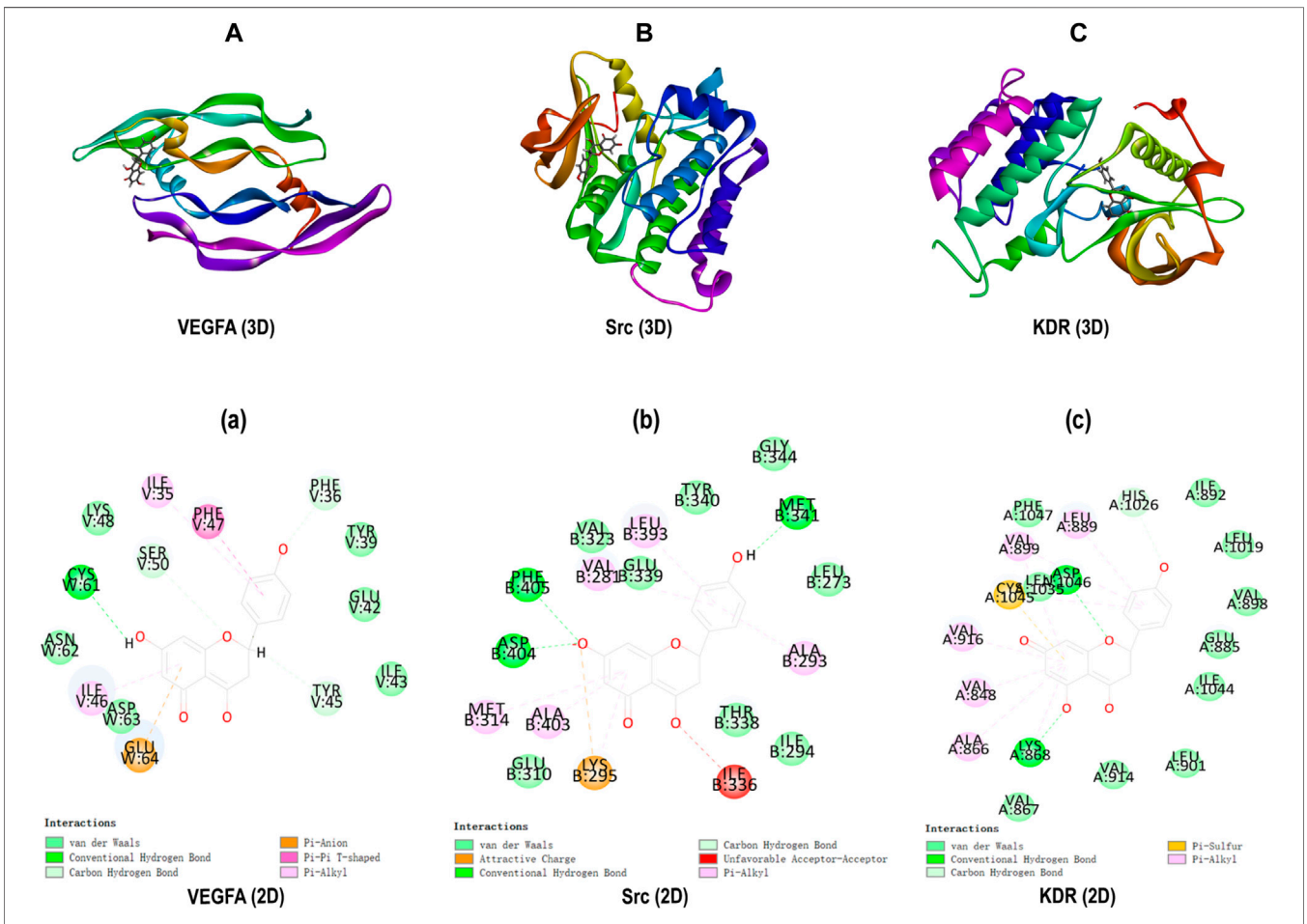

FIGURE 8 | Molecular docking. **(A-C)** 3D docking for Nar in the active binding pocket of VEGFA, Src and KDR. **(a-c)** 2D interaction patterns between Nar and VEGFA, Src and KDR.

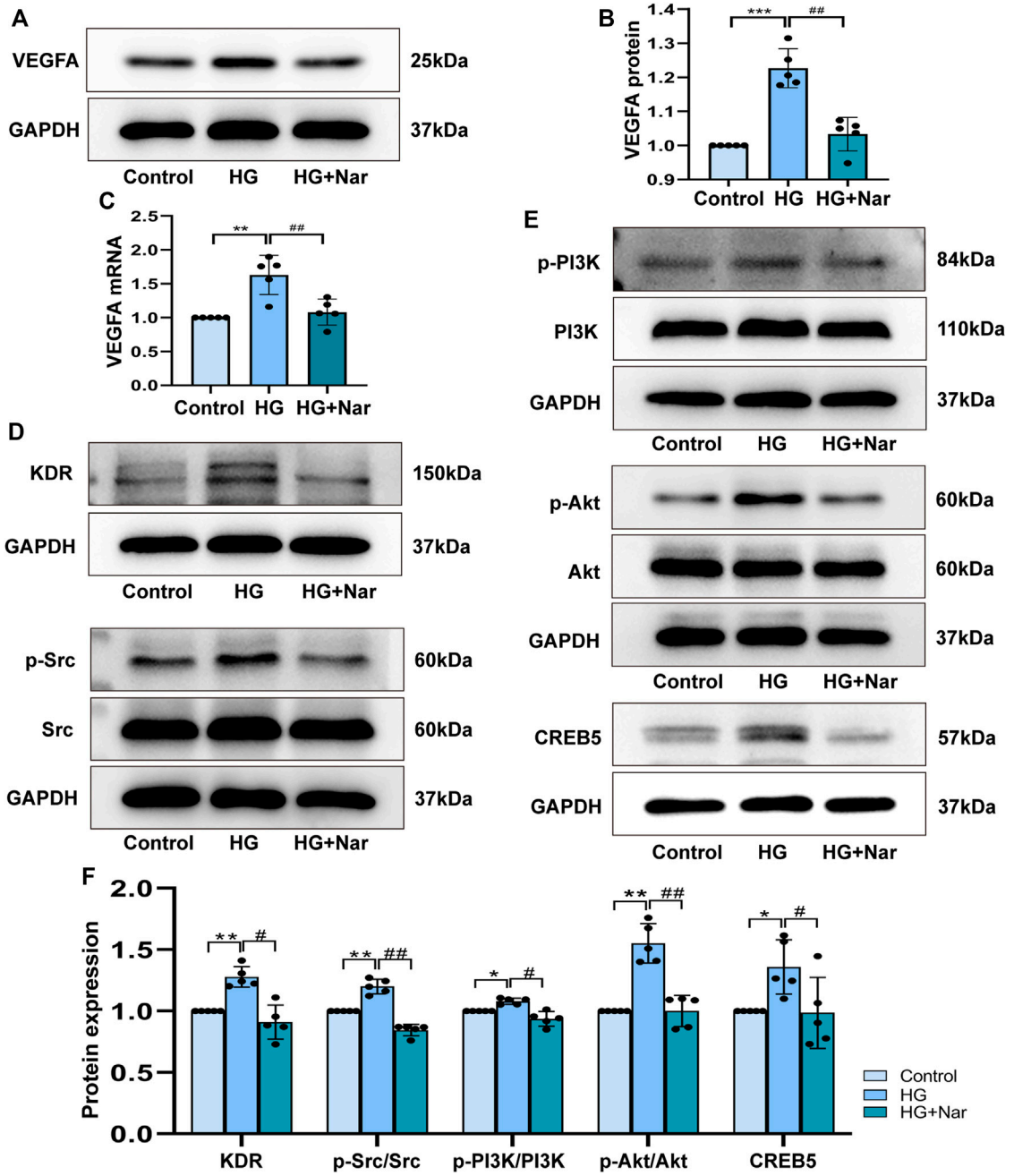

FIGURE 9 | Nar down-regulated the expression of core target VEGFA and PI3K/Akt/CREB5 signaling pathway. **(A)** Western blot detected the protein expression of VEGFA. **(B)** Analysis of VEGFA protein expression. **(C)** Analysis of VEGFA mRNA expression. **(D,E)** Nar suppressed KDR, p-Src, p-PI3K, p-Akt and CREB5 expression which upregulated by HG group. **(F)** Bar graph showed related protein expression analysis. $^{*}p < 0.05$, $^{**}p < 0.01$ compared with Control group, $^{\#}p < 0.05$, $^{\#\#}p < 0.01$ compared with HG group.

interacted with Nar, 120.848 interacted with cognate ligand (BPK), and 121.494 interacted with specific inhibitor (Linifanib). So, comparing the LibDock Score of VEGFA Src, and KDR bound with different molecules, the LibDock Score of Src and KDR bound with Nar had no significant differences with those of Src and KDR bound with their cognate ligands and inhibitors, which demonstrated that Nar had good binding affinity with Src and KDR. At the same time, the LibDock Score of VEGFA bound with Nar had no significant differences with those of VEGFA bound with its specific inhibitors, which illustrated that Nar had good binding affinity with VEGFA (**Table 1**).

The interactions among proteins and molecules were shown in **Figure 8**, according to **Figures 8A,a**, the interactions between Nar and VEGFA included the formation of π-anion interaction

with GLU64 residue, π-π stacked interaction with PHE47 residue, π-Alkyl interaction with ILE35 and ILE46 residues, and conventional hydrogen bond form with its ASP63 residue. In addition, as shown in **Figures 8B,b**, the attractive charge interaction with LYS295 residue, unfavorable acceptor-acceptor interaction with ILE336 residue, π-alkyl interaction with LEU393, VAL281, MET314, et al. residues, and hydrogen bond with PHE405, ASP404 and MET341 residues were involved in the interactions between Nar and Src. Besides, **Figures 8C** showed Nar could interact with KDR through π-sulfur interaction with CYS1045 residue, hydrogen bond with ASP1046 and LYS868 residues, and π-alkyl interaction with LEU889, VLA899, ALA866, et al. residues.

3.8 Regulatory Effect of Nar on PI3K/Akt/CREB5 Signaling Pathway

To identify whether Nar could inhibit VEGFA directly, qRT-PCR was used to detected mRNA expression of VEGFA, the primer sequences as follows, VEGFA: forward 5′-CCCTGGCTTTAC TGCTGTACC-3′; reverse 5′-CTTCATGGGCTTTCTGCT CCC-3′. GAPDH: forward 5′-GACATGCCGCCTGGAGAA AC-3′; reverse 5′-AGCCCAGGATGCCCTTTAGT-3′. At the same time, VEGFA protein expression was detected. As shown in **Figures 9A–C**, high glucose could induce high expression of VEGFA, and Nar could downregulate the mRNA and protein expression of VEGFA. To confirm that the anti-proliferation and anti-migration effects of Nar were related to PI3K/Akt/CREB5 signaling pathway, the expression of related proteins, including KDR, Src, p-Src, PI3K, p-PI3K, Akt, p-Akt, and CREB5 was detected. The results showed that the expression of KDR, p-Src, p-PI3K, p-Akt, and CREB5 was significantly upregulated by high glucose, and downregulated by Nar in the presence of high glucose (**Figures 9D–F**).

4 DISCUSSION

In diabetic patients, the excessive proliferation of VSMCs induced by abnormally elevated blood glucose can cause and exacerbate macrovascular and microvascular diseases, such as hypertension, atherosclerosis, and restenosis (Kay et al., 2016). Acute increases of reactive oxygen species (ROS) and inflammatory cytokines caused by chronic hyperglycemia in diabetic patients have devastating effects on vascular function (Chapple et al., 2013). Additionally, the gradual accumulation of superfluous metabolites (free fatty acids, glycation end products, O-GlcNAcylation, etc.) may also promote the extreme differentiation, proliferation, and migration of VSMCs (Byon and Kim, 2020; Shi et al., 2020). The prevention and treatment of diabetic vascular complications mainly includes the following aspects: self-management and drug therapy, including antihyperglycemic, lipid-regulating, antihypertensive and anti-platelet drugs. In addition, our findings may provide new consideration for the molecular mechanism underlying the action of naringenin.

Nar, a compound with various pharmacological activities, like anti-inflammatory, anti-tumor, anti-diabetic and anti-proliferation effects. Some small-scale clinical studies have showed that the naringenin with a dosage ranging between 600 and 800 μmol/L/day has the ability to improve endothelial function in different patient groups. For example, Rendeiro et al., reported that the flow-mediated dilatation of brachial artery was improved after long-term daily supplementation with orange flavanone beverages in clinic study (Rendeiro et al., 2016). Habauzit et al. reported that endothelial dysfunction was improved after supplementation with long-term daily grapefruit juice/day containing about 480 μmol/L naringenin glycoside (Habauzit et al., 2015). Besides, Rebello et al., found that the single doses of 150, 300, 600, and 900 mg of naringenin was safe and tolerant in small-scale healthy adults (Rebello et al., 2020). These previous studies have provided valid basis for the clinical application of Nar.

α-Smooth muscle actin (α-SMA), as a particularly contractile protein, is a specific gene marker of smooth muscle cells (SMCs) (Goumans and Ten Dijke, 2018). Osteopontin (OPN) is involved not only in the metastatic phenotype but also in the synthetic phenotype of VSMCs, and can be highly activated under particular physiological and pathological conditions such as inflammation and imbalanced immunity (Denhardt et al., 2003; Zhang M. et al., 2020). Under physiological conditions, VSMCs preferentially adopt the differentiated and contractile phenotype, rather than the dedifferentiated and synthetic phenotype. Conversely, under pathological conditions, VSMCs can transform into the synthetic phenotype characterized by the high expression of OPN and low expression of α-SMA (Lin et al., 2018). In our study, we first found that Nar clearly decreased the media thickness and fibrosis of the aortic arch and modified the promiscuous and disordered smooth muscle cells in a type 1 diabetic (T1D) mouse model (**Figures 1A–E**).

Substantial evidence has shown that the transformation of VSMCs to a phenotype involving high synthesis contributes to increased proliferation, migration, and excessive production of extracellular matrix. Therefore, we continued to examine the effect of Nar on the proliferation and migration of VSMCs induced by high glucose. Proliferating cell nuclear antigen (PCNA), as a marker of VSMC proliferation, is an important factor in regulating DNA replication, DNA repair, sister-chromatid cohesion, and cell cycle control prominent inflammatory mediators, are a family of zinc-containing proteolytic enzymes that are involved in various processes, including growth, migration, angiogenesis, and metastasis of cancer cells (Strzalka and Ziemienowicz, 2011; Pittayapruek et al., 2016). MMP2 and MMP9 belong to gelatinases of MMPs' main subgroups. MMP2 has been considered to be a potential mediator of VSMC migration, which can facilitate such migration by inducing a switch from a contractile to a synthetic phenotype (Belo et al., 2015). MMP9 is not only a biomarker of cancer cell invasion and tumor metastasis and expressed in various cancer cells, but also participates in the development of cardiovascular disease, lung disease, and diabetes (Mondal et al., 2020). In this study, immunohistochemical analysis showed that Nar significantly reduced the expression of PCNA, MMP2, and MMP9 proteins in the T1D model (**Figure 2A**). Simultaneously, we found that Nar not only significantly inhibited the proliferation by reducing the expression of

PCNA and the number of Edu-positive cells (**Figure 3**), but also restrained the migration by decreasing the expression of MMP2 and MMP9 in the model of proliferating and migrating VSMCs induced by high glucose (**Figure 4**). Additionally, Nar significantly altered the dedifferentiation by upregulating α-SMA expression and downregulating OPN expression both *in vivo* (T1D model) (**Figure 2B**) and *in vitro* (high-glucose-induced VSMCs) (**Figure 5**) experiments. These results indicated that Nar not only significantly inhibited cell proliferation and migration but also modified the phenotype from a dedifferentiated and synthetic phenotype to a differentiated and contractile one both *in vivo* and *in vitro*.

To further explore the potential molecular mechanism behind the anti-proliferation and anti-migration effects of Nar on VSMCs, a transcriptomic approach was initially used to predict the potential signaling pathway. For transcriptomic sequencing analysis, 303 upregulated genes and 408 downregulated genes were found to be involved in the protective effect of Nar on VSMCs. The GO enrichment results for the differentially expressed genes (DEGs) showed particular associations with the biological processes of positive regulation of cell migration, extracellular matrix organization, and angiogenesis (**Figures 7C,D**). Meanwhile, the KEGG results of transcriptomic sequencing analysis showed that the PI3K/Akt signaling pathway et al. were involved in the protective effect of Nar on VSMCs (**Figure 7E**). Network pharmacology is another bioinformatic approach that has been considered as a novel research method for identifying putative targets and pharmacological mechanisms (Wei et al., 2016). Therefore, we also explored the potential targets and signaling pathways by using a network pharmacology-based method. Notably, GO enrichment analysis showed that the 102 overlaps between Nar and diabetic angiopathies were particularly related to the regulation of phosphatidylinositol 3-kinase signaling, including phosphatidylinositol-3-phosphate biosynthetic process and phosphatidylinositol 3-kinase activity (**Figures 6C,D**). Furthermore, KEGG pathway enrichment analysis provided the same result that the PI3K/Akt signaling pathway participated in the effects of Nar against diabetic angiopathies as in the network pharmacology and transcriptomic sequencing analyses (**Figures 6E**, **7E**). Substantial evidence has indicated that the PI3K/Akt signaling pathway, MAPK signaling pathway, cytokine-cytokine receptor interaction, and cGMP/PKG signaling pathway are related to vasculopathy (Wang et al., 2013; Karar and Maity, 2011; Loppnow et al., 2011; Zhou et al., 2021). These reports are consistent with our results. Additionally, as shown in **Figure 6A**, there were 102 targets overlapping between drug targets (Nar) and disease targets (diabetic angiopathies) in the Venn diagram (**Figure 6A**), with VEGFA (degree 51), Src (degree 45), and KDR (degree 30) being the core targets according to the degree value in the PPI network (**Figure 6B**). Vascular endothelial growth factor A (VEGFA) is closely related to the proliferation and migration of endothelial cells by participating in angiogenesis by binding to KDR (VEGFR2) (Claesson-Welsh and Welsh, 2013). Src, as a downstream target of VEGFR, plays an important role in the regulation of angiogenesis by binding its SH2 domain to a tyrosine autophosphorylation site on EGFR (Park et al., 2007; Schenone et al., 2007). The interaction of VEGFA and VEGFR2 has been shown to contribute to abnormal angiogenesis by regulating various pathways, including proliferation through the PLC-γ/PKC/RAF/MEK/ERK signaling pathway, vascular permeability and survival via the PI3K/Akt signaling pathway, and migration through the p38-MAPK signaling pathway (Zhang A. et al., 2020). Considering the consistent results of transcriptomic analysis, network pharmacology analysis, and the scientific evidence obtained to date, we speculated that the core targets of VEGFA, Src and KDR, and the PI3K/Akt signaling pathway might be involved in the anti-proliferation and anti-migration effects of Nar.

For the core targets of VEGFA, Src and KDR, we initially used molecular docking to evaluate the binding affinity, and positive control test was performed as the benchmark. As shown in **Figure 8** and **Table 1**, according to the LibDock score of proteins interacted with different ligands, Nar had good binding affinity with VEGFA, Src and KDR. Then, we continued to analyze the expression of VEGFA, Src and KDR, the results showed that Nar prominently reduced the mRNA and protein expression of VEGFA (**Figures 9A–C**), indicating VEGFA was inhibited by Nar directly. According to **Figures 9D,F**, the protein expression of Src and KDR was significantly downregulated by Nar, which consistent with the results of molecular docking. VEGFA, an important subunit of the VEGF family in vascular, was found in the upstream of PI3K/Akt pathway. The synthesis and secretion of VEGFA is greatly associated with the progression of many angiogenesis diseases (Doronzo et al., 2012). According to previous studies, VEGFA was high expressed in high glucose induced VSMCs, and the inhibition of VEGFA abrogated excessive VSMCs proliferation and migration (Natarajan et al., 1997; Chen et al., 2014). Besides, Chan KC, et al., and Wen X, et al. proved that PI3K/Akt could be activated by high glucose, resulting in a promotive cell proliferation and migration (Chan et al., 2012; Wen et al., 2022). These studies indicated that VEGFA mediated PI3K/Akt pathway could take part in the high glucose induced endothelial dysfunction.

It is reported that the overexpression of cAMP-responsive element binding protein 5 (CREB5) promotes the proliferation and migration of different cancer cells. Specifically, CREB5 has been shown to promote cell proliferation and correlate with a poor prognosis in hepatocellular carcinoma, while the lncRNA SNHG5 affects the cell proliferation, metastasis, and migration of colorectal cancer through regulating miR-132–3p/CREB5 (Wu et al., 2018). According to the DEGs identified in the transcriptomic analysis, we found that CREB5 was particularly associated with the PI3K/Akt pathway and significantly upregulated in the VSMCs induced by high glucose. However, the high level of CREB5 in the model of proliferating and migrating VSMCs induced by high glucose was clearly downregulated by Nar. Consistent with the results of transcriptomic analysis, the protein level of CREB5 was significantly reduced by Nar (**Figures 9E,F**). To the best of our knowledge, we are the first to discover that CREB5 is involved in the proliferation and migration of VSMCs induced by high glucose. Additionally, CREB5 has a close relationship with the PI3K/Akt pathway. Huang et al. reported that this

pathway was upstream of CREB5, which participated in the proliferation, migration, and invasion of breast cancer (Huang et al., 2019). Hiroya et al. found that human coronary artery smooth muscle cells (CASMCs) preferentially proliferate rather than undergo apoptosis in a manner dependent on the downregulated expression of the bcl-2 gene family (bcl-xl and bfl-1/A1) through the PI3K and MAPK pathways in high-glucose-stimulated human CASMCs (Sakuma et al., 2002). VSMCs could undergo phenotypic transformation and increase their ability to migrate and proliferate through upregulation of the ERK1/2 and PI3K/Akt signaling pathways stimulated by high glucose (Shi et al., 2015). In a similar study, Fan et al. showed that the injection of hong jing tian could improve proliferation and migration by inhibiting the Akt pathway in high-glucose-induced vascular smooth muscle cells (Fan et al., 2019). In addition, Zhou et al. found that arctiin could attenuate the proliferation and arrest the cell cycle in the G0/G1 phase by inactivating VEGF and the PI3K/Akt signaling pathway in high-glucose-induced human retinal capillary endothelial cells (Zhou et al., 2020). These studies are consistent with our results. The experiments in the current study demonstrated that Nar could ameliorate the proliferation and migration by decreasing the expression of VEGFA proteins, and downregulating the downstream PI3K/Akt and CREB5 pathway.

5 CONCLUSION

In summary, in this study transcriptomic sequencing, network pharmacology analysis, and in the vitro and vivo experimental validation were used to illustrate the potential mechanism behind the anti-proliferation and anti-migration effects of Nar in a model of high-glucose-stimulated VSMCs. The obtained results showed that Nar can significantly attenuate the proliferation and migration of these cells, which might be achieved by inhibiting the expression of its target VEGFA, and then downregulating the PI3K/Akt/CREB5 pathway.

DATA AVAILABILITY STATEMENT

The original contributions presented in the study are included in the article/**Supplementary Material**, further inquiries can be directed to the corresponding authors.

ETHICS STATEMENT

The animal study was reviewed and approved by Shihezi University.

AUTHOR CONTRIBUTIONS

WH accomplished the experiments, wrote the paper and drew the figures; YW wrote and revised the paper, created the tables; RY sorted the data of animal experiments; HM fed animals and completed diabetic mice model; XQ accomplished cell culture; MY accomplished Masson staining and sorted the data; YR analyzed the data of network pharmacology; YX analyzed the data of transcriptomic sequencing; LL and JS did the molecular docking; XL and KM directed the research and revised the paper.

FUNDING

This work was supported by the Foundation for the National Natural Science Foundation of China (Nos. 81860085 and 81860286), the Corps Science and Technology Cooperation Project of China (No. 2020BC004), and the Central Research Institute Fund of Chinese Academy of Medical Sciences (No. 2020-PT330-003), and the Autonomous Region Postgraduate Innovation Project (No. XJ 2021G129).

ACKNOWLEDGMENTS

We are grateful to the Key Laboratory of Xinjiang Endemic and Ethnic Diseases, NHC Key Laboratory of Prevention and Treatment of Central Asia High Incidence Diseases, the Department of Physiology and Pathophysiology of Shihezi University School of Medicine.

SUPPLEMENTARY MATERIAL

The Supplementary Material for this article can be found online at: https://www.frontiersin.org/articles/10.3389/fphar.2022.862709/full#supplementary-material

REFERENCES

Ai, Z., Zhou, S., Li, W., Wang, M., Wang, L., Hu, G., et al. (2020). "Fei Yan No. 1" as a Combined Treatment for COVID-19: An Efficacy and Potential Mechanistic Study. *Front. Pharmacol.* 11, 581277. doi:10.3389/fphar.2020.581277

Arafah, A, Rehman, M., Mir, T., Wali, A., Ali, R., Qamar, W., et al. (2020). Multi-Therapeutic Potential of Naringenin (4',5,7-Trihydroxyflavonone): Experimental Evidence and Mechanisms. *Plants (Basel)*, 9, 1784. doi:10.3390/plants9121784

Belo, V. A., Guimarães, D. A., and Castro, M. M. (2015). Matrix Metalloproteinase 2 as a Potential Mediator of Vascular Smooth Muscle Cell Migration and Chronic Vascular Remodeling in Hypertension. *J. Vasc. Res.* 52, 221–231. doi:10.1159/000441621

Bruemmer, D., and Law, R. E. (2003). Thiazolidinedione Regulation of Smooth Muscle Cell Proliferation. *Am. J. Med.* 115, 87S–92S. doi:10.1016/j.amjmed.2003.09.014

Byon, C. H., and Kim, S. W. (2020). Regulatory Effects of O-GlcNAcylation in Vascular Smooth Muscle Cells on Diabetic Vasculopathy. *J. Lipid Atheroscler.* 9, 243–254. doi:10.12997/jla.2020.9.2.243

Chan, K. C., Wu, C. H., Huang, C. N., Lan, K. P., Chang, W. C., and Wang, C. J. (2012). Simvastatin Inhibits Glucose-Stimulated Vascular Smooth Muscle Cell Migration Involving Increased Expression of RhoB and a Block of Ras/Akt Signal. *Cardiovasc. Ther.* 30, 75–84. doi:10.1111/j.1755-5922.2010.00226.x

Chapple, S. J., Cheng, X., and Mann, G. E. (2013). Effects of 4-Hydroxynonenal on Vascular Endothelial and Smooth Muscle Cell Redox Signaling and Function in Health and Disease. *Redox Biol.* 1, 319–331. doi:10.1016/j.redox.2013.04.001

Chen, J., Dai, M., and Wang, Y. (2014). Paeonol Inhibits Proliferation of Vascular Smooth Muscle Cells Stimulated by High Glucose via Ras-Raf-Erk1/2 Signaling Pathway in Coculture Model. *Evidence-Based Complementary Altern. Med.* 2014, 484269. doi:10.1155/2014/484269

Chen, S., Ding, Y., Tao, W., Zhang, W., Liang, T., and Liu, C. (2012). Naringenin Inhibits TNF-α Induced VSMC Proliferation and Migration via Induction of HO-1. *Food Chem. Toxicol.* 50, 3025–3031. doi:10.1016/j.fct.2012.06.006

Claesson-Welsh, L., and Welsh, M. (2013). VEGFA and Tumour Angiogenesis. *J. Intern. Med.* 273, 114–127. doi:10.1111/joim.12019

Den Hartogh, D. J., and Tsiani, E. (2019). Antidiabetic Properties of Naringenin: A Citrus Fruit Polyphenol. *Biomolecules* 9. doi:10.3390/biom9030099

Denhardt, D. T., Mistretta, D., Chambers, A. F., Krishna, S., Porter, J. F., Raghuram, S., et al. (2003). Transcriptional Regulation of Osteopontin and the Metastatic Phenotype: Evidence for a Ras-Activated Enhancer in the Human OPN Promoter. *Clin. Exp. Metastasis* 20, 77–84. doi:10.1023/a:1022550721404

Deshpande, A. D., Harris-Hayes, M., and Schootman, M. (2008). Epidemiology of Diabetes and Diabetes-Related Complications. *Phys. Ther.* 88, 1254–1264. doi:10.2522/ptj.20080020

Doronzo, G., Viretto, M., Russo, I., Mattiello, L., Anfossi, G., and Trovati, M. (2012). Effects of High Glucose on Vascular Endothelial Growth Factor Synthesis and Secretion in Aortic Vascular Smooth Muscle Cells from Obese and Lean Zucker Rats. *Int. J. Mol. Sci.* 13, 9478–9488. doi:10.3390/ijms13089478

Fan, Z., Guo, C., Zhang, Y., Yao, J., Liao, L., and Dong, J. (2019). Hongjingtian Injection Inhibits Proliferation and Migration and Promotes Apoptosis in High Glucose-Induced Vascular Smooth Muscle Cells. *Drug. Des. Devel. Ther.* 13, 4115–4126. doi:10.2147/DDDT.S220719

Fan, Z. D., Zhang, L., Shi, Z., Gan, X. B., Gao, X. Y., and Zhu, G. Q. (2012). Artificial microRNA Interference Targeting AT(1a) Receptors in Paraventricular Nucleus Attenuates Hypertension in Rats. *Gene Ther.* 19, 810–817. doi:10.1038/gt.2011.145

Forbes, J. M., and Cooper, M. E. (2013). Mechanisms of Diabetic Complications. *Physiol. Rev.* 93, 137–188. doi:10.1152/physrev.00045.2011

Goumans, M. J., and Ten Dijke, P. (2018). TGF-β Signaling in Control of Cardiovascular Function. *Cold Spring Harb. Perspect. Biol.* 10. doi:10.1101/cshperspect.a022210

Habauzit, V., Verny, M. A., Milenkovic, D., Barber-Chamoux, N., Mazur, A., Dubray, C., et al. (2015). Flavanones Protect from Arterial Stiffness in Postmenopausal Women Consuming Grapefruit Juice for 6 Mo: A Randomized, Controlled, Crossover Trial. *Am. J. Clin. Nutr.* 102, 66–74. doi:10.3945/ajcn.114.104646

Hashim, S., Li, Y., and Anand-Srivastava, M. B. (2006). Small Cytoplasmic Domain Peptides of Natriuretic Peptide Receptor-C Attenuate Cell Proliferation Through Gialpha Protein/MAP Kinase/PI3-Kinase/AKT Pathways. *Am. J. Physiol. Heart Circ. Physiol.* 291, H3144–H3153. doi:10.1152/ajpheart.00327.2006

Huang, W., Zhao, C., Zhong, H., Zhang, S., Xia, Y., and Cai, Z. (2019). Bisphenol S Induced Epigenetic and Transcriptional Changes in Human Breast Cancer Cell Line MCF-7. *Environ. Pollut.* 246, 697–703. doi:10.1016/j.envpol.2018.12.084

Jia, S., Ma, W. D., Zhang, C. Y., Zhang, Y., Yao, Z. H., Quan, X. H., et al. (2019). Tanshinone IIA Attenuates High Glucose Induced Human VSMC Proliferation and Migration Through miR-21-5p-Mediated Tropomyosin 1 Downregulation. *Arch. Biochem. Biophys.* 677, 108154. doi:10.1016/j.abb.2019.108154

Jiang, D., Yang, Y., and Li, D. (2017). Lipopolysaccharide Induced Vascular Smooth Muscle Cells Proliferation: A New Potential Therapeutic Target for Proliferative Vascular Diseases. *Cell Prolif.* 50. doi:10.1111/cpr.12332

Karar, J., and Maity, A. (2011). PI3K/AKT/mTOR Pathway in Angiogenesis. *Front. Mol. Neurosci.* 4, 51. doi:10.3389/fnmol.2011.00051

Kay, A. M., Simpson, C. L., and Stewart, J. A. (2016). The Role of AGE/RAGE Signaling in Diabetes-Mediated Vascular Calcification. *J. Diabetes Res.* 2016, 6809703. doi:10.1155/2016/6809703

Lee, E. J., Kim, D. I., Kim, W. J., and Moon, S. K. (2009). Naringin Inhibits Matrix Metalloproteinase-9 Expression and AKT Phosphorylation in Tumor Necrosis Factor-Alpha-Induced Vascular Smooth Muscle Cells. *Mol. Nutr. Food Res.* 53, 1582–1591. doi:10.1002/mnfr.200800210

Li, X., Zhao, Y., Chen, B., Zhu, Z., Kang, Q., Husain, T., et al. (2021). Inhalation and Ingestion of Synthetic Musks in Pregnant Women: In Silico Spontaneous Abortion Risk Evaluation and Control. *Environ. Int.* 158, 106911. doi:10.1016/j.envint.2021.106911

Lin, H., Ni, T., Zhang, J., Meng, L., Gao, F., Pan, S., et al. (2018). Knockdown of Herp Alleviates Hyperhomocysteinemia Mediated Atherosclerosis Through the Inhibition of Vascular Smooth Muscle Cell Phenotype Switching. *Int. J. Cardiol.* 269, 242–249. doi:10.1016/j.ijcard.2018.07.043

Loppnow, H., Buerke, M., Werdan, K., and Rose-John, S. (2011). Contribution of Vascular Cell-Derived Cytokines to Innate and Inflammatory Pathways in Atherogenesis. *J. Cell Mol. Med.* 15, 484–500. doi:10.1111/j.1582-4934.2010.01245.x

Mondal, S., Adhikari, N., Banerjee, S., Amin, S. A., and Jha, T. (2020). Matrix Metalloproteinase-9 (MMP-9) and its Inhibitors in Cancer: A Minireview. *Eur. J. Med. Chem.* 194, 112260. doi:10.1016/j.ejmech.2020.112260

Natarajan, R., Bai, W., Lanting, L., Gonzales, N., and Nadler, J. (1997). Effects of High Glucose on Vascular Endothelial Growth Factor Expression in Vascular Smooth Muscle Cells. *Am. J. Physiol.* 273, H2224–H2231. doi:10.1152/ajpheart.1997.273.5.H2224

Nikolic, I., Saksida, T., Mangano, K., Vujicic, M., Stojanovic, I., Nicoletti, F., et al. (2014). Pharmacological Application of Carbon Monoxide Ameliorates Islet-Directed Autoimmunity in Mice via Anti-Inflammatory and Anti-Apoptotic Effects. *Diabetologia* 57, 980–990. doi:10.1007/s00125-014-3170-7

Park, S. I., Shah, A. N., Zhang, J., and Gallick, G. E. (2007). Regulation of Angiogenesis and Vascular Permeability by Src Family Kinases: Opportunities for Therapeutic Treatment of Solid Tumors. *Expert Opin. Ther. Targets* 11, 1207–1217. doi:10.1517/14728222.11.9.1207

Pittayapruek, P., Meephansan, J., Prapapan, O., Komine, M., and Ohtsuki, M. (2016). Role of Matrix Metalloproteinases in Photoaging and Photocarcinogenesis. *Int. J. Mol. Sci.* 17. doi:10.3390/ijms17060868

Ran, F., Li, W., Qin, Y., Yu, T., Liu, Z., Zhou, M., et al. (2021). Inhibition of Vascular Smooth Muscle and Cancer Cell Proliferation by New VEGFR Inhibitors and Their Immunomodulator Effect: Design, Synthesis, and Biological Evaluation. *Oxid. Med. Cell Longev.* 2021, 8321400. doi:10.1155/2021/8321400

Rebello, C. J., Beyl, R. A., Lertora, J. J. L., Greenway, F. L., Ravussin, E., Ribnicky, D. M., et al. (2020). Safety and Pharmacokinetics of Naringenin: A Randomized, Controlled, Single-Ascending-Dose Clinical Trial. *Diabetes Obes. Metab.* 22, 91–98. doi:10.1111/dom.13868

Ren, X., Shi, Y. S., Zhang, Y., Liu, B., Zhang, L. H., Peng, Y. B., et al. (2018). Novel Consensus Docking Strategy to Improve Ligand Pose Prediction. *J. Chem. Inf. Model* 58, 1662–1668. doi:10.1021/acs.jcim.8b00329

Ren, X. S., Tong, Y., Ling, L., Chen, D., Sun, H. J., Zhou, H., et al. (2017). NLRP3 Gene Deletion Attenuates Angiotensin II-Induced Phenotypic Transformation of Vascular Smooth Muscle Cells and Vascular Remodeling. *Cell Physiol. Biochem.* 44, 2269–2280. doi:10.1159/000486061

Ren, X. S., Tong, Y., Qiu, Y., Ye, C., Wu, N., Xiong, X. Q., et al. (2020). MiR155-5p in Adventitial Fibroblasts-Derived Extracellular Vesicles Inhibits Vascular Smooth Muscle Cell Proliferation via Suppressing Angiotensin-Converting Enzyme Expression. *J. Extracell. Vesicles* 9, 1698795. doi:10.1080/20013078.2019.1698795

Rendeiro, C., Dong, H., Saunders, C., Harkness, L., Blaze, M., Hou, Y., et al. (2016). Flavanone-Rich Citrus Beverages Counteract the Transient Decline in Postprandial Endothelial Function in Humans: A Randomised, Controlled, Double-Masked, Cross-Over Intervention Study. *Br. J. Nutr.* 116, 1999–2010. doi:10.1017/S0007114516004219

Rezaei, M. A., Li, Y., Wu, D., Li, X., and Li, C. (2022). Deep Learning in Drug Design: Protein-Ligand Binding Affinity Prediction. *IEEE/ACM Trans. Comput. Biol. Bioinf.* 19, 407–417. doi:10.1109/tcbb.2020.3046945

Sakuma, H., Yamamoto, M., Okumura, M., Kojima, T., Maruyama, T., and Yasuda, K. (2002). High Glucose Inhibits Apoptosis in Human Coronary Artery Smooth Muscle Cells by Increasing Bcl-xL and bfl-1/A1. *Am. J. Physiol. Cell Physiol.* 283, C422–C428. doi:10.1152/ajpcell.00577.2001

Salehi, B., Fokou, P., Sharifi-Rad, M., Zucca, P., Pezzani, R., Martins, N., et al. (2019). The Therapeutic Potential of Naringenin: A Review of Clinical Trials. *Pharmaceuticals* 12, 11. doi:10.3390/ph12010011

Schenone, S., Manetti, F., and Botta, M. (2007). SRC Inhibitors and Angiogenesis. *Curr. Pharm. Des.* 13, 2118–2128. doi:10.2174/138161207781039580

Shen, J., Zhu, X., Wu, Z., Shi, Y., and Wen, T. (2021). Uvangoletin, Extracted from Sarcandra Glabra, Exerts Anticancer Activity by Inducing Autophagy and Apoptosis and Inhibiting Invasion and Migration on Hepatocellular Carcinoma Cells. *Phytomedicine Int. J. Phytotherapy Phytopharm.* 94, 153793.

Shi, J., Yang, Y., Cheng, A., Xu, G., and He, F. (2020). Metabolism of Vascular Smooth Muscle Cells in Vascular Diseases. *Am. J. Physiol. Heart Circ. Physiol.* 319, H613–H631. doi:10.1152/ajpheart.00220.2020

Shi, L., Ji, Y., Jiang, X., Zhou, L., Xu, Y., Li, Y., et al. (2015). Liraglutide Attenuates High Glucose-Induced Abnormal Cell Migration, Proliferation, and Apoptosis of Vascular Smooth Muscle Cells by Activating the GLP-1 Receptor, and Inhibiting ERK1/2 and PI3K/Akt Signaling Pathways. *Cardiovasc. Diabetol.* 14, 18. doi:10.1186/s12933-015-0177-4

Strzalka, W., and Ziemienowicz, A. (2011). Proliferating Cell Nuclear Antigen (PCNA): A Key Factor in DNA Replication and Cell Cycle Regulation. *Ann. Bot.* 107, 1127–1140. doi:10.1093/aob/mcq243

Sun, H. J., Zhao, M. X., Ren, X. S., Liu, T. Y., Chen, Q., Li, Y. H., et al. (2016). Salusin-β Promotes Vascular Smooth Muscle Cell Migration and Intimal Hyperplasia After Vascular Injury via ROS/NFκB/MMP-9 Pathway. *Antioxid. Redox Signal* 24, 1045–1057. doi:10.1089/ars.2015.6475

Sun, X., Qiao, N., Zhang, X., Zang, L., Zhao, D., and Zhu, X. (2021). First Report of Natural Infection of Zucchini by Tomato Chlorosis Virus and Cucurbit Chlorotic Yellows Virus in China. *Plant Dis.*, PDIS05200932PDN. doi:10.1094/PDIS-05-20-0932-PDN

Wang, C., Fan, R. Q., Zhang, Y. X., Nie, H., and Li, K. (2016). Naringenin Protects Against Isoniazid- and Rifampicin-Induced Apoptosis in Hepatic Injury. *World J. Gastroenterol.* 22, 9775–9783. doi:10.3748/wjg.v22.i44.9775

Wang, J., Yang, K., Xu, L., Zhang, Y., Lai, N., Jiang, H., et al. (2013). Sildenafil Inhibits Hypoxia-Induced Transient Receptor Potential Canonical Protein Expression in Pulmonary Arterial Smooth Muscle via cGMP-PKG-Pparγ Axis. *Am. J. Respir. Cell Mol. Biol.* 49, 231–240. doi:10.1165/rcmb.2012-0185OC

Wei, S., Niu, M., Wang, J., Wang, J., Su, H., Luo, S., et al. (2016). A Network Pharmacology Approach to Discover Active Compounds and Action Mechanisms of San-Cao Granule for Treatment of Liver Fibrosis. *Drug Des. Devel. Ther.* 10, 733–743. doi:10.2147/DDDT.S96964

Wen, X., XI, Y., Zhang, Y., Jiao, L., Shi, S., Bai, S., et al. (2022). DR1 Activation Promotes Vascular Smooth Muscle Cell Apoptosis via Up-Regulation of CSE/H S Pathway in Diabetic Mice. *FASEB J. Official Publ. Fed. Am. Soc. Exp. Biol.* 36, e22070. doi:10.1096/fj.202101455r

Wu, J., Wang, S. T., Zhang, Z. J., Zhou, Q., and Peng, B. G. (2018). CREB5 Promotes Cell Proliferation and Correlates with Poor Prognosis in Hepatocellular Carcinoma. *Int. J. Clin. Exp. Pathol.* 11, 4908–4916.

Wu, Y., Zhang, M., Xu, C., Chai, D., Peng, F., and Lin, J. (2020). Anti-Diabetic Atherosclerosis by Inhibiting High Glucose-Induced Vascular Smooth Muscle Cell Proliferation via Pin1/BRD4 Pathway. *Oxid. Med. Cell Longev.* 2020, 4196482. doi:10.1155/2020/4196482

Xiao, Y., Liu, Y., Lai, Z., Huang, J., Li, C., Zhang, Y., et al. (2021). An Integrated Network Pharmacology and Transcriptomic Method to Explore the Mechanism of the Total Rhizoma Coptidis Alkaloids in Improving Diabetic Nephropathy. *J. Ethnopharmacol.* 270, 113806. doi:10.1016/j.jep.2021.113806

Zang, Y. H., Chen, D., Zhou, B., Chen, A. D., Wang, J. J., Gao, X. Y., et al. (2019). FNDC5 Inhibits Foam Cell Formation and Monocyte Adhesion in Vascular Smooth Muscle Cells via Suppressing NFκB-Mediated NLRP3 Upregulation. *Vasc. Pharmacol.* 121, 106579. doi:10.1016/j.vph.2019.106579

Zhang, A., Fang, H., Chen, J., He, L., and Chen, Y. (2020a). Role of VEGF-A and LRG1 in Abnormal Angiogenesis Associated with Diabetic Nephropathy. *Front. Physiol.* 11, 1064. doi:10.3389/fphys.2020.01064

Zhang, J., Deng, B., Jiang, X., Cai, M., Liu, N., Zhang, S., et al. (2019). All-Trans-Retinoic Acid Suppresses Neointimal Hyperplasia and Inhibits Vascular Smooth Muscle Cell Proliferation and Migration via Activation of AMPK Signaling Pathway. *Front. Pharmacol.* 10, 485. doi:10.3389/fphar.2019.00485

Zhang, J., Qiu, H., Huang, J., Ding, S., Huang, B., Wu, Q., et al. (2018). Naringenin Exhibits the Protective Effect on Cardiac Hypertrophy via EETs-PPARs Activation in Streptozocin-Induced Diabetic Mice. *Biochem. Biophys. Res. Commun.* 502, 55–61. doi:10.1016/j.bbrc.2018.05.119

Zhang, M., Li, F., Wang, X., Gong, J., Xian, Y., Wang, G., et al. (2020b). MiR-145 Alleviates Hcy-Induced VSMC Proliferation, Migration, and Phenotypic Switch Through Repression of the PI3K/Akt/mTOR Pathway. *Histochem. Cell Biol.* 153, 357–366. doi:10.1007/s00418-020-01847-z

Zhou, H., Simion, V., Pierce, J., Haemmig, S., Chen, A., and Feinberg, M. (2021). LncRNA-MAP3K4 Regulates Vascular Inflammation Through the P38 MAPK Signaling Pathway and Cis-Modulation of MAP3K4. *FASEB J. Official Publ. Fed. Am. Soc. Exp. Biol.* 35, e21133. doi:10.1096/fj.202001654rr

Zhou, M., Li, G., Zhu, L., Zhou, H., and Lu, L. (2020). Arctiin Attenuates High Glucose-Induced Human Retinal Capillary Endothelial Cell Proliferation by Regulating ROCK1/PTEN/PI3K/Akt/VEGF Pathway *In Vitro*. *J. Cell Mol. Med.* 24, 5695–5706. doi:10.1111/jcmm.15232

Conflict of Interest: The authors declare that the research was conducted in the absence of any commercial or financial relationships that could be construed as a potential conflict of interest.

Publisher's Note: All claims expressed in this article are solely those of the authors and do not necessarily represent those of their affiliated organizations, or those of the publisher, the editors and the reviewers. Any product that may be evaluated in this article, or claim that may be made by its manufacturer, is not guaranteed or endorsed by the publisher.

frontiers | Frontiers in Pharmacology

CLINICAL TRIAL
published: 16 June 2022
doi: 10.3389/fphar.2022.829416

Panax notoginseng Saponins Alleviate Coronary Artery Disease Through Hypermethylation of the miR-194-MAPK Pathway

*Lian Duan, Yongmei Liu, Jun Li, Yun Zhang, Yan Dong, Chao Liu and Jie Wang**

Department of Cardiology, Guang Anmen Hospital, Beijing, China

Background: *Panax notoginseng* saponins (PNS) may have an inhibitory effect against coronary artery disease (CAD); however, the mechanism is unclear. Recent research has begun to evaluate the role of epigenetics in CAD. Our team found that hypomethylation of miR-194 could be an important mechanism of CAD.

Purpose: The aim of this study was to investigate the effect of PNS against CAD and evaluate whether the mechanism is related to methylation of mi-R194.

Methods: We conducted a randomized controlled trial with a double-blind placebo design on 84 patients with CAD. Treatment was continued for 4 weeks, and the clinical effect of PNS on CAD was observed. Methylation of miR-194, its promoter, and the key nodes of the MAPK pathway were measured by pyrosequencing and qRT-PCR. We then conducted a pharmacological analysis of the active components of PNS. The effects of PNS on oxidized human umbilical vein endothelial cells and the methylation of miR-194, its promoter, and the key nodes of the MAPK pathway were measured *in vitro* through methylation-specific PCR (MSPCR), qRT-PCR, Western blot analysis, and annexin V/propidium iodide apoptosis assay.

Results: PNS improved symptoms of CAD. High-density lipoprotein and white blood cell count demonstrated significant changes after treatment in the PNS group. No significant difference was observed between miR-194 and mRNA MAPK, FAS, RAS, and FOS in the PNS group after treatment. However, some notable trends were observed in these genes. The targets of PNS were predicted by the pharmacological components. Some targets were found to be differentially expressed genes in CAD sequencing. Six genes, including MAPK1, RAS, and FASL, were common targets of PNS in CAD sequencing. Correlations were observed between genes in the interaction network and clinical parameters. *In vitro*

OPEN ACCESS

Edited by:
Ling Zhang,
Zhejiang Chinese Medical University, China

Reviewed by:
Yong Wang,
Beijing University of Chinese Medicine, China
Hai-Gang Zhang,
Army Medical University, China

****Correspondence:***
Jie Wang
wangjiedoctor2015@163.com

Specialty section:
This article was submitted to Ethnopharmacology, a section of the journal Frontiers in Pharmacology

Received: *05 December 2021*
Accepted: *06 May 2022*
Published: *16 June 2022*

Citation:
Duan L, Liu Y, Li J, Zhang Y, Dong Y, Liu C and Wang J (2022) Panax notoginseng Saponins Alleviate Coronary Artery Disease Through Hypermethylation of the miR-194-MAPK Pathway. Front. Pharmacol. 13:829416. doi: 10.3389/fphar.2022.829416

Abbreviations: CAD, coronary artery disease; c-Jun, Jun proto-oncogene; DMEM, Dulbecco's modified Eagle medium; DBP, diastolic blood pressure; ECG, electrocardiogram; FASL, Fas cell surface death receptor ligand; FOS, Fos proto-oncogene; HGB, hemoglobin; HDL, high-density lipoprotein; LDL, low-density lipoprotein cholesterol; MAPK, mitogen-activated protein kinase; miRNA, microRNA; MSPCR, methylation-specific PCR; PNS, *Panax notoginseng* saponins; PI, propidium iodide; qRT-PCR, quantitative real-time PCR; RAS, rat sarcoma; SBP, systolic blood pressure; TCM, traditional Chinese medicine; TC, total cholesterol; TG, triglycerides; UA, unstable angina; WBC, white blood cell.

experiments confirmed that PNS could change the methylation of miR-194, its promoter, and MAPK, FAS, RAS, and FOS. Intervention with PNS is likely to improve apoptosis.

Conclusion: We reported the regulation of miR-194 promoter, miR-194, and MAPK methylation by PNS through cell experiments and a randomized controlled trial. PNS can be used for intervention in CAD by targeting the miR-194 promoter-miR-194-MAPK signaling pathway.

Clinical Trial Registration: https://www.clinicaltrials.gov/, NCT03083119.

Keywords: ***Panax notoginseng*** **saponins, coronary artery disease, DNA methylation, miRNA, MAPK**

INTRODUCTION

Despite massive efforts to develop cardiovascular treatments, coronary artery disease (CAD) remains the leading cause of mortality and morbidity in the world (Douglas et al., 2016). In recent years, traditional Chinese medicine (TCM) has received widespread attention. *Panax notoginseng* (Burkill) F.H.Chen [Araliaceae] is particularly popular among patients with CAD because many studies have demonstrated the inhibitory effects of this plant against CAD. *Panax notoginseng* saponins (PNS) are the main active ingredient in this plant (Duan et al., 2017). PNS has multiple effects on CAD, including anti-inflammation, regulation of lipid metabolism and the coagulation system, anti-apoptosis, pro-angiogenesis, anti-atherosclerosis, and anti-myocardial ischemia (Zhang et al., 2016; Shen et al., 2017; Zhou et al., 2018; Xiong et al., 2020; Wang et al., 2021). Long-term use of PNS can effectively reduce the end point of CAD and improve angina pectoris, electrocardiogram (ECG), and lipid metabolism, illustrating that PNS is a potential agent against CAD (Duan et al., 2018).

Recent research has begun to discover the role of epigenetics in cardiovascular disease development. According to our previous research (Rupérez et al., 2021), miR-194 promoter-methylation-miR-194-mitogen-activated protein kinase (MAPK) could be biomarkers of CAD.

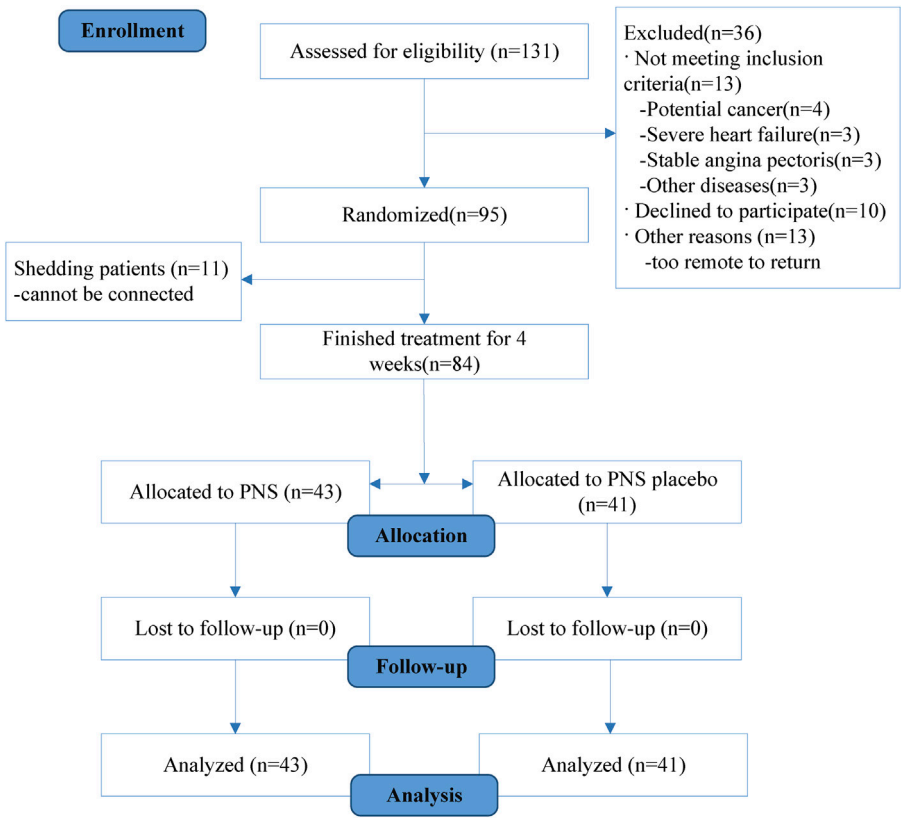

FIGURE 1 | Trial protocol timeline as described in detail in the Materials and Methods section.

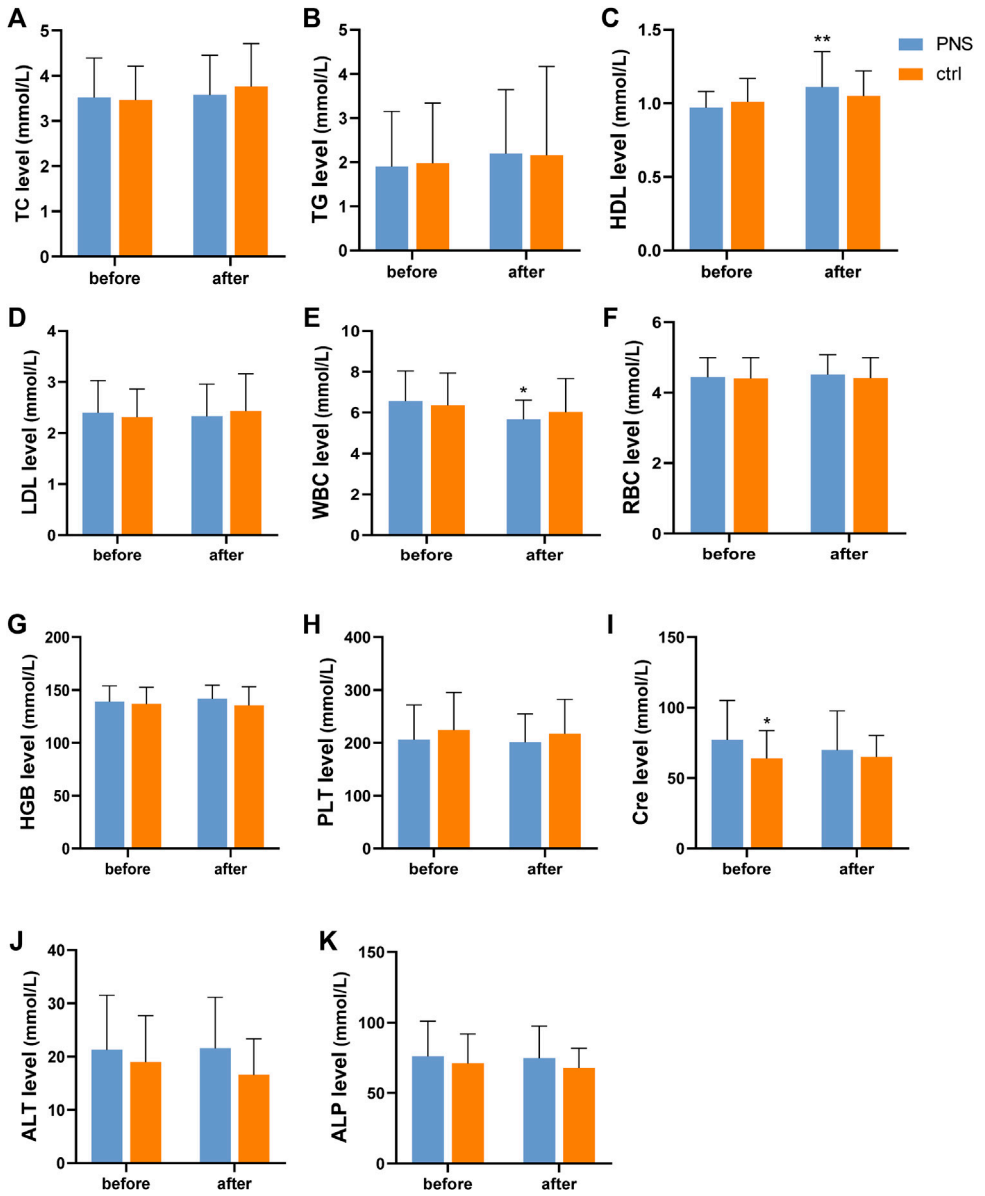

FIGURE 2 | Cell experimental protocol as described in detail in the Materials and Methods section.

MATERIALS AND METHODS

Participant Recruitment and Sample Collection

The study population consisted of 84 patients presenting within 15 days of an unstable angina (UA) event at Guang Anmen Hospital. Patients were included if they had a coronary angiography to estimate the extent of CAD for all subjects according to the criteria defined by the American Heart Association. Those with at least one major epicardial vessel with >50% stenosis were defined as CAD subjects, while those with <50% stenosis were defined as control subjects (Austen et al., 1975; Zhao et al., 2019). Finally, those aged 45–75 years were included. The exclusion criteria consisted of an index event due to uncontrolled hypertension and/or blood pressure remaining ≥180/110 mmHg despite treatment, New York Heart Association class III or IV congestive heart failure irrespective of ejection fraction, or class II heart failure with left ventricular ejection fraction ≤40% persisting at the end of the run-in period despite treatment, severe valvular heart disease, arrhythmia, cardiomyopathy, stable angina pectoris, clinically apparent liver; kidney; hematological system; nervous system; or mental disease, malignancy (except for nonmelanoma skin cancer) within the preceding 3 years, and inability to provide informed consent or comply with study requirements.

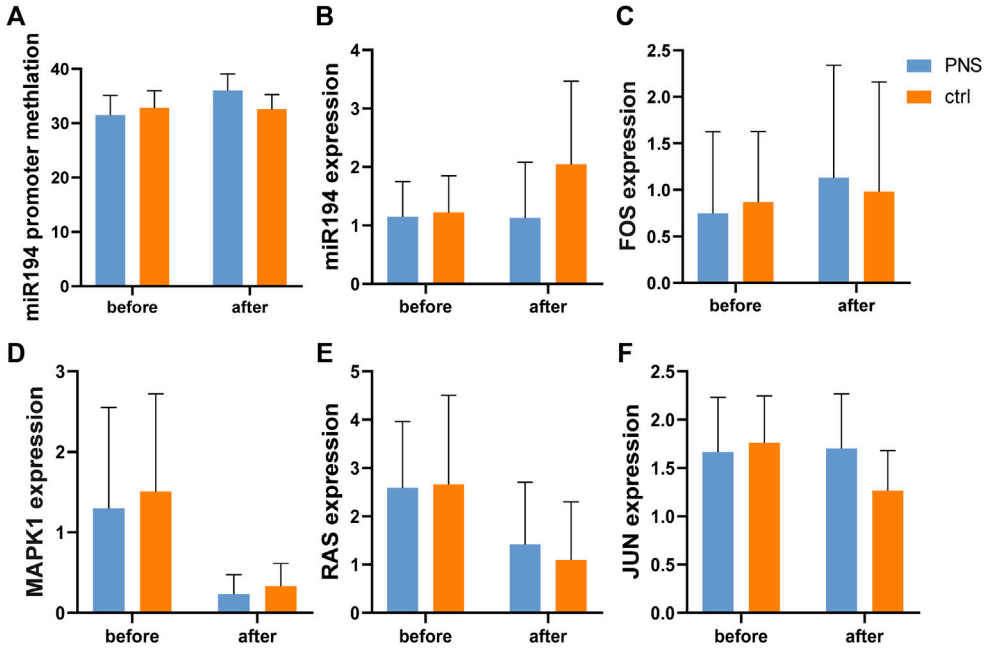

FIGURE 3 | Study participant flow diagram.

TABLE 1 | Comparison of characteristics between PNS and the placebo group.

	PNS (n = 43)	Placebo (n = 41)
Age (years)	65.39 ± 8.68	63.63 ± 7.05
Sex (male, %)	28 (65%)	32 (78%)
Smoking history [n (%)]	5 (12%)	5 (12%)
Hypertension [n (%)]	22 (51%)	26 (63%)
Diabetes [n (%)]	17 (40%)	16 (39%)
TC (mmol/L)	3.63 ± 0.90	3.65 ± 0.68
TG (mmol/L)	1.95 ± 1.26	2.25 ± 1.48
LDL-C (mmol/L)	2.65 ± 0.87	2.52 ± 0.75
HDL-C (mmol/L)	0.99 ± 0.16	1.04 ± 0.51
Aspirin administration [n (%)]	31 (72%)	28 (68%)
Statin administration [n (%)]	28 (65%)	29 (70%)

TC: total cholesterol; TG: triglycerides; LDL-C: low-density lipoprotein cholesterol; HDL-C: high-density lipoprotein cholesterol.

TABLE 2 | Adverse cardiovascular events 60 days after treatment between PNS and the placebo group.

	PNS (n = 43)	Placebo (n = 41)
Death [n (%)]	0 (0%)	0 (0%)
Myocardial infarction [n (%)]	0 (0%)	0 (0%)
Stroke [n (%)]	0 (0%)	0 (0%)
Readmission due to angina [n (%)]	2 (5%)	2 (5%)

The study protocol was approved by the institutional ethics committee of Guang Anmen Hospital, Beijing, and is registered at *Clinical Trials* (identifier: NCT03083119) (https://www.clinicaltrials.gov/). All patients provided written informed consent.

A standardized questionnaire was applied to assess smoking history, hypertension, and diabetes among study subjects. Smoking history was classified as either "no smoking" or "smoking" (including both former and current smokers). Hypertension status was classified as either "non-hypertension" or "hypertension" (including the previous diagnosis of hypertension and systolic blood pressure (SBP) ≥ 140 mmHg and/or diastolic blood pressure (DBP) ≥ 90 mmHg currently). Diabetes status was classified as either "non-diabetes" or "diabetes" (including previous diagnosis of diabetes and fasting blood glucose ≥7.0 mmol/L or postprandial blood glucose ≥11.1 mmol/L) (Ge et al., 2016).

Blood samples of patients on an empty stomach for 12 h were drawn in the morning within 24 h after admission. Blood of the outpatients and controls was drawn in the morning of the second day after admission. Specifically, 4 ml of venous blood was collected and placed in an EDTA tube. Peripheral blood mononuclear cells (PBMCs) were centrifuged within 6 h.

Randomization and Blinding

SPSS 19.0 software was used to randomly generate the 1:1 allocation scheme of the subjects. Drugs with corresponding numbers were given, according to the order of treatment. A random card was made to record the distribution plan and then sealed in an opaque envelope. A double-blind design was used in this study, and PNS and PNS placebo were numbered as group 1 or group 2. According to the drug distribution method of double-blind experiments, the drugs were packed in the same box with different drug numbers. The blind bottom was made in duplicate and managed by a specially assigned person. After completion of

TABLE 3 | (Panel A) Length of angina attacks; (Panel B) Frequency of angina attacks.

Panel A	N	Before (min/time)	After (min/time)
PNS	41	8.95 ± 1.13	2.50 ± 1.26$^{\triangle\triangle}$
Placebo	43	8.53 ± 1.36	4.33 ± 1.05$^{**\#\#}$
Panel B	**n**	**Before (times/wk)**	**After (times/wk)**
PNS	41	7.15 ± 4.23	1.24 ± 1.08$^{\triangle}$
Placebo	43	8.24 ± 5.15	2.14 ± 1.26*

*$^{\triangle}p < 0.05$ and $^{\triangle\triangle}p < 0.01$, significantly different from the PNS group before. *$p < 0.05$ and **$p < 0.01$, significantly different from the placebo group before. $^{\#}p < 0.05$ and $^{\#\#}p < 0.01$, significantly different from the PNS group after.*

the trial, the data from group 1 and group 2 were statistically analyzed.

Study Treatment

This study used a double-blind, placebo design (Xuesaitong soft capsule and Xuesaitong soft capsule placebo). The main ingredient of the Xuesaitong capsule is PNS. The experimental group was treated with Xuesaitong capsules based on conventional drugs, and two capsules (0.66 g) were given twice a day. The placebo group was treated with Xuesaitong placebo capsules (specifications: 0.33 g × 12 s × 2 board, Kunming Torch Pharmaceutical Group Co., Ltd.). Xuesaitong soft capsule or Xuesaitong soft capsule placebo was administered 0.5 h after conventional drugs. Treatment continued for 4 weeks. Treatment was not combined with other Chinese decoctions or proprietary Chinese medicines during the trial. Furthermore, all subjects were strongly recommended to receive other concomitant secondary prevention medications, according to practice guidelines (Roffi et al., 2016). All participants underwent follow-up examinations 28 and 60 days after treatment (**Figure 1**).

The Xuesaitong capsule (State medical permit Z19990022, specifications: 0.33 g × 12 s × 2 board, Kunming Torch Pharmaceutical Group Co., Ltd.) batch number was 20150417, and each capsule contained 60 mg of medicine. The composition was 5.4 mg R1, 31.8 mg Rg1, and 17.2 mg Rb1. The placeboes were glue pills filled with starch and caramel pigment and had an identical look, color, and weight to XSTSC.

Study treatment was administered on a background of conventional drugs, including antiplatelet, anticoagulant, statin, vasodilator, diuretic, hypotension, and hypoglycemic drugs, and the combination drugs were allowed before and during clinical trials (including emergency treatment drugs) in accordance with the diagnosis and treatment procedures. Drugs prohibited before and during the clinical trial included other Chinese patent medicines and traditional Chinese medicine decoctions not provided in this study.

Verification of the Methylation Level of Related Sites by Pyrosequencing

The reaction system was set up for bisulfite transformation, which was carried out on a 9700 PCR instrument with a hot cover, and the DNA was frozen and preserved after treatment. For PCR (PyroMark PCR kit) amplification, the single-chain PCR products were purified, and the primers were annealed. The PCR products were retained for pyrosequencing on the PyroMark ID instrument, and the assay was established by PyroMark cytidine-phosphate-guanosine software. The related items were prepared and sequenced, and the results were analyzed.

Detection of the miR-194 Promoter Methylation Level by Methylation-Specific PCR (MSPCR)

The genomic DNA of tissue or peripheral blood was extracted using the phenol chloroform method. DNA concentration, OD260, OD280, and OD260/OD280 were measured using a nanodrop 1000 spectrophotometer. The DNA sample OD260/OD280 used in this experiment was 1.8–1.9, which was regarded as qualified DNA. The DNA samples were treated with bisulfite, amplified by PCR, and reacted with a self-analysis platform. The 384-pore plate was put into the sample adding instrument. After the parameter setting was complete, the sample could be spotted on the chip. After sampling, the chip was placed in the mass spectrometer, and methylation analysis was performed according to the molecular weight difference of C and T bases in the fragment. The methylation ratio of mass spectrometry was obtained by EpiTYPER software version 1.0 (Sequenom, San Diego, CA, United States).

Real-Time Fluorescence Quantitative PCR

Cells were collected and treated 72 h later. The total RNA was extracted using the TRIzol method and then reverse transcribed into cDNA for PCR. For PCR, cDNA was diluted 10 times with 4 μL SYBR Green, 5 μL primer, 0.2 μL + primer (10 μmol/L), 0.2 μL each, and 0.6 μL water for a total of 10 μL. PCR was performed at 95°C for 5 min, 95°C for 10 s, and 60°C for 20 s for a total of 50 cycles and then at 5°C for 10 s, 60°C for 10 s, and 40°C for 30 s. The CT values of the target and control genes were automatically collected by using the fluorescence quantitative analyzer, and the relative mRNA expression was calculated and counted by $2^{-\triangle\triangle Ct}$.

Detection of the Protein Expression by Western Blot Analysis

Cells were collected, and the protein was extracted using a one-step animal cell active protein extraction kit (Sango Biotechnology, Shanghai, China, product No. c500022), and the protein concentration was detected using a Bradford protein detection kit (Sango Biotechnology, Shanghai, China, product No. c503031). Western blot analysis was carried out on the fully based automated system (San Jose, CA, United States). Two main antibodies were purchased: anti-ERK1 (Abcam, ab32537, 1:50 dilution) and goat anti-rabbit anti-β-tubulin (ProteinSimple, cell signaling, 2148, 1:400 dilution). We used β-tubulin as the internal parameter and prepared 100 mm dithiothreitol, 5× master mix, ladder, luminol-s, and peroxide premixed solution, respectively,

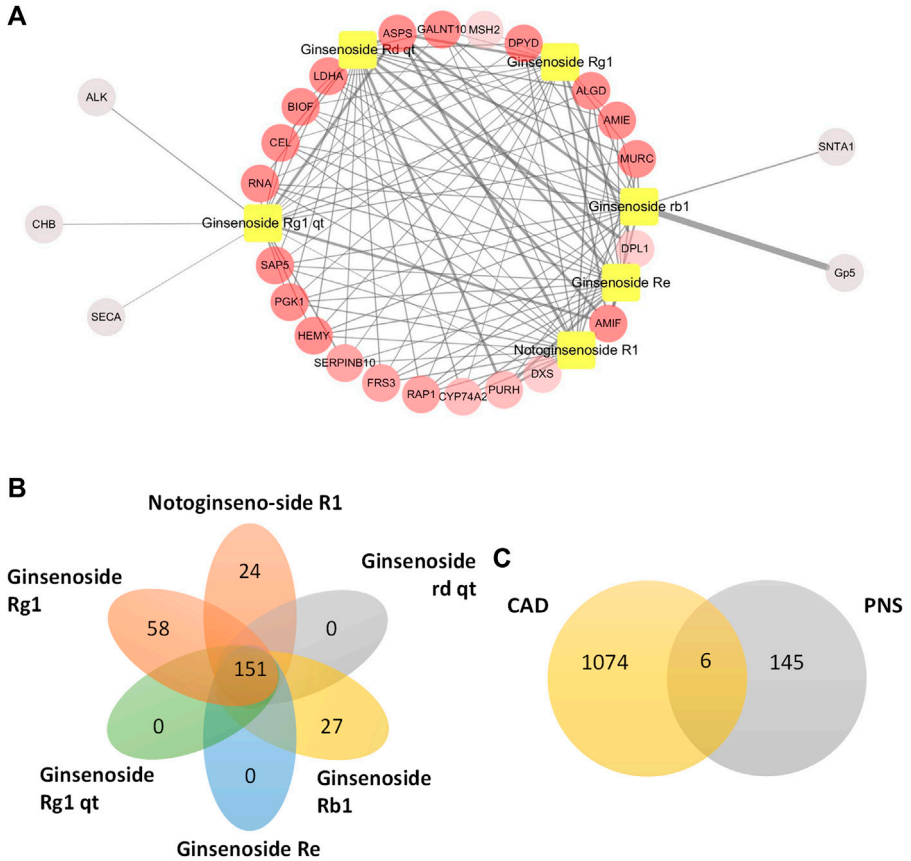

FIGURE 4 | Blood tests before and after treatment in the PNS and placebo groups. $p < 0.05$ and $^{**}p < 0.01$, significantly different from the PNS group before.

according to the instructions. Then, we diluted the previously extracted protein with the 5× master mix to a solution with a final concentration of 0.2 mg/ml and denatured the solution at 95°C for 5 min. The sample and antibody were added to the board according to the instructions and tested on the computer.

Cell Culture and Grouping

HUVECs were cultured in Dulbecco's modified Eagle medium (DMEM) containing 10% fetal bovine serum, 100 U/mL penicillin, and 100 mg/L streptomycin. The medium was cultured in an incubator with 5% CO_2 at 37°C and changed daily. The third to eighth generation cells were used in all experiments. The HUVECs grew to about 80% fusion. After centrifugation, 1.5 ml DMEM (4°C precooling) containing 10% dimethyl sulfoxide was added to the cell precipitation. After blowing and mixing, it was transferred to a 2-ml cell cryopreservation tube and stored in a 80°C refrigerator.

HUVECs were divided into three groups: a control group, an H_2O_2 model group, and an H_2O_2 model + PNS group. The H_2O_2 model group was treated with 100 μmol/L H_2O_2 for 3 h, and the H_2O_2 model + PNS group was treated with 100 μmol/L H_2O_2 for 3 h and then 30 mg/L PNS for 24 h. Cell samples were collected 24 h after treatment with H_2O_2 for 3 h (**Figure 2**). The standard of PNS was provided by the National Institutes for Food and Drug Control and included 26.3% Rg1, 27.0% Rb1, 7.4% R1, 3.7% Re, and 7.6% Rd. The concentration of PNS was 30 μg/ml.

Annexin V/Propidium Iodide (PI) Apoptosis Assay

The HUVECs were divided into groups, as shown in **Figure 2**. Then, 48 h after infection with Lenti-Vector Control and Lenti-Bmi1-shRNA and 24 h after treatment with cisplatin, we centrifuged the cells at 1000 r/min for 5 min. We counted 1×10^6 cells and added 100 μL of binding buffer into a 1.5 ml centrifuge tube. Then, 5 μL of annexin V was incubated, and 3 μL of PI was added. Apoptosis was analyzed by flow cytometry with 400 μL binding buffer.

Statistical Analysis

SPSS software version 19.0 was used for statistical analysis. Data are expressed as the mean ± standard deviation. For comparisons of two groups, an independent sample *t*-test was used to analyze normal distributions, and a rank-sum test was used to analyze non-normal distributions. For multiple comparisons, the quantitative data on normal distributions were analyzed using variance analysis and a Q test, while those of non-normal distributions were analyzed using a nonparametric test.

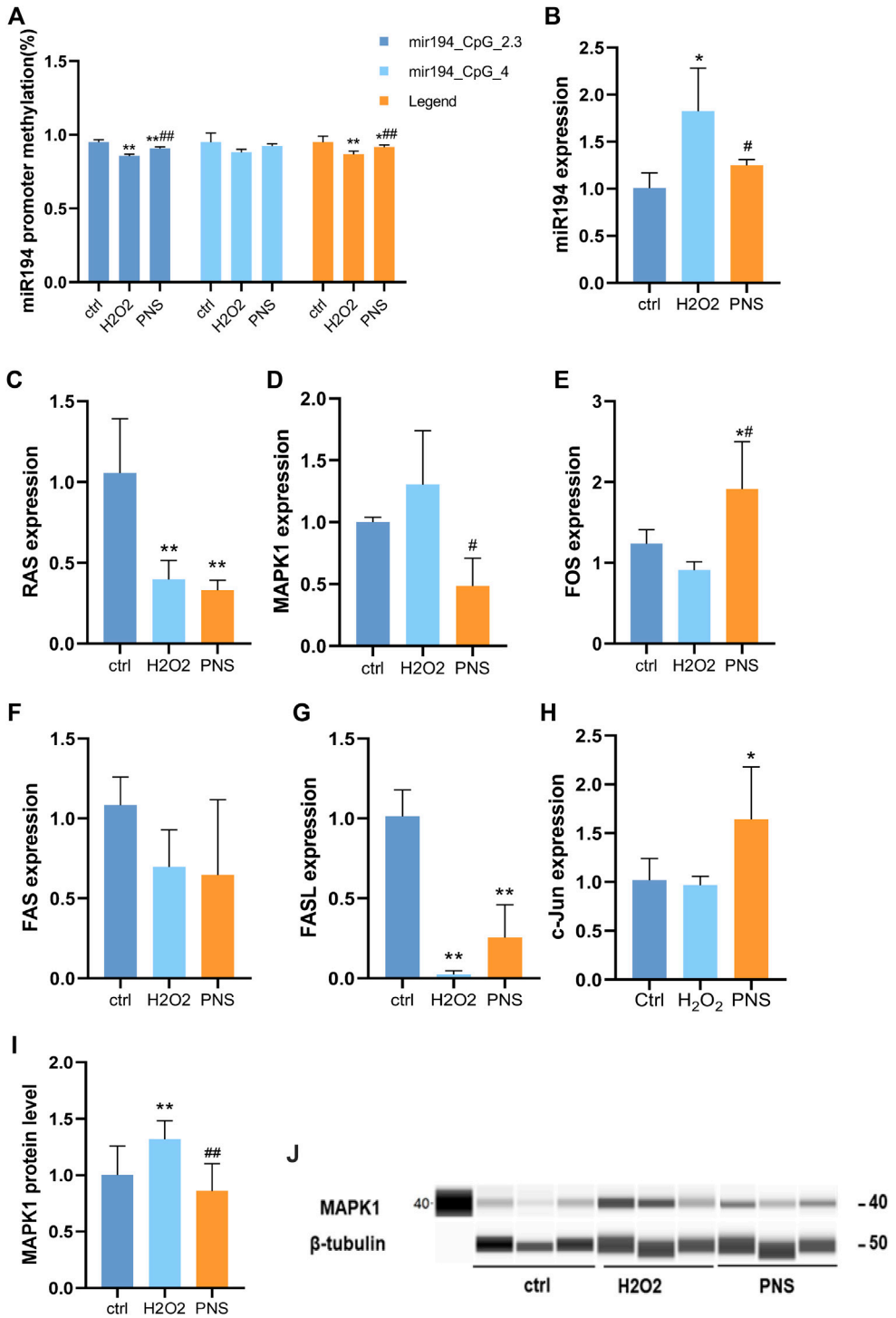

FIGURE 5 | Prediction of PNS targets by pharmacological analysis. **(A)** Top 20 potential targets of PNS. The relationship of the top 20 best matching genes of PNS was exhibited by Cytoscape. Yellow squares indicate the main ingredients of PNS. The circles indicate the potential targets. The nodes with a higher degree appear redder in color. The nodes with a higher fit value have thicker edges. **(B)** Common targets of the main ingredients of PNS. **(C)** Common targets of PNS potential targets and CAD-related genes.

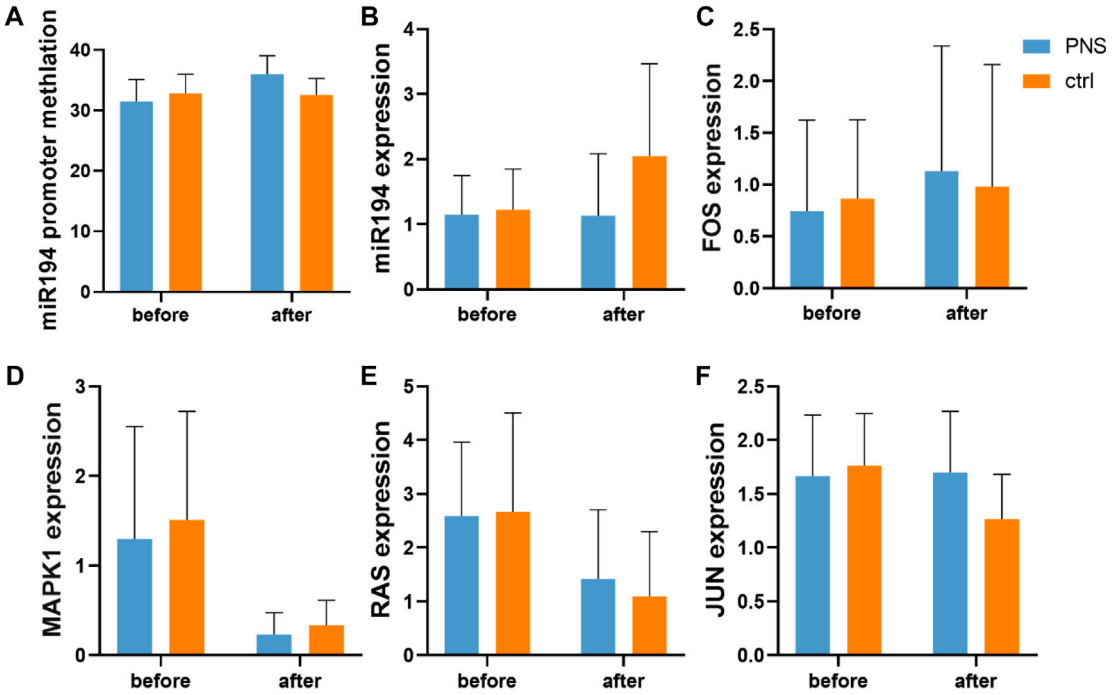

FIGURE 6 | Expression of key genes in the miR-194 promoter-miR914-MAPK pathway according to pyrosequencing and PCR.

RESULTS

PNS Had an Effect Against CAD

This study included 95 patients with CAD. During the study period, 11 patients were shed, and 84 patients completed the study (**Figure 3**. Statistical analysis was conducted on the personal and clinical data on the 84 patients, including sex, age, smoking history, diabetes status, hypertension status, blood glucose, total cholesterol, and triglycerides. No significant difference was observed between the PNS and placebo groups before treatment regarding demographics, diabetes status, hypertension, blood glucose, total cholesterol, or low-density lipoprotein cholesterol ($p > 0.05$) (**Table 1**).

We also observed the incidence of cardiovascular adverse events within 60 days after treatment. No difference was observed between the two groups (**Table 2**).

Questionnaires were filled out on the day of admission and 4 weeks after treatment to calculate the occurrence of angina attacks in the two groups. The length of angina attacks was significantly reduced in both groups. However, treatment with PNS led to a significantly greater reduction than the placebo. Additionally, both groups had a significant decrease in the frequency of angina attacks after treatment, although no significant difference was observed in the groups (**Table 3A**, **Table 3B**).

Routine blood and biochemical examination were measured on days 1 and 30 after enrollment. HDL significantly increased ($p < 0.01$) after treatment in the PNS group (**Figure 4C**). In other aspects of blood lipids, no significant difference was observed between the two groups before and after treatment (**Figure 4A,B,D**). Additionally, the white blood cell (WBC) count decreased significantly after PNS treatment, which confirmed the anti-inflammatory effect of PNS (**Figure 4E**). Meanwhile, hemoglobin (HGB) levels increased in the PNS group and decreased in the placebo group (**Figure 4G**). Kidney and liver functions were similar before and after treatment in the two groups (**Figure 4I–K**). However, the Cre level decreased in the PNS group (**Figure 4I**).

Prediction of PNS Targets

Five main active ingredients in PNS were identified in the Chinese Pharmacopoeia (2015 edition), namely, notoginsenoside R1, ginsenoside Rg1, ginsenoside Re, ginsenoside Rd, and ginsenoside Rb1. Then, the Traditional Chinese Medicine Systems Pharmacology Database and Analysis Platform were used to evaluate the pharmacokinetic-related properties of PNS. Through the PharmMapper database, potential targets of the five active ingredients were predicted. Then, 4 ml venous blood from patients with CAD and controls was collected and placed in EDTA tubes. DNA was extracted from centrifuged PBMCs. We sequenced the captured bisulfite transformed DNA samples using Illumina HiSeq2500 and Roche SeqCap Epi methylation enrichment kits. Then, we found genes related to CAD and identified the top 300 potential targets of every active component. We obtained 429 targets of the six molecules and found that these six main ingredients of PNS shared some common targets. The top 20 potential targets were extracted according to their fit value. Notably, the potential targets of each molecule were closely interrelated (**Figure 5A**). A total of 151

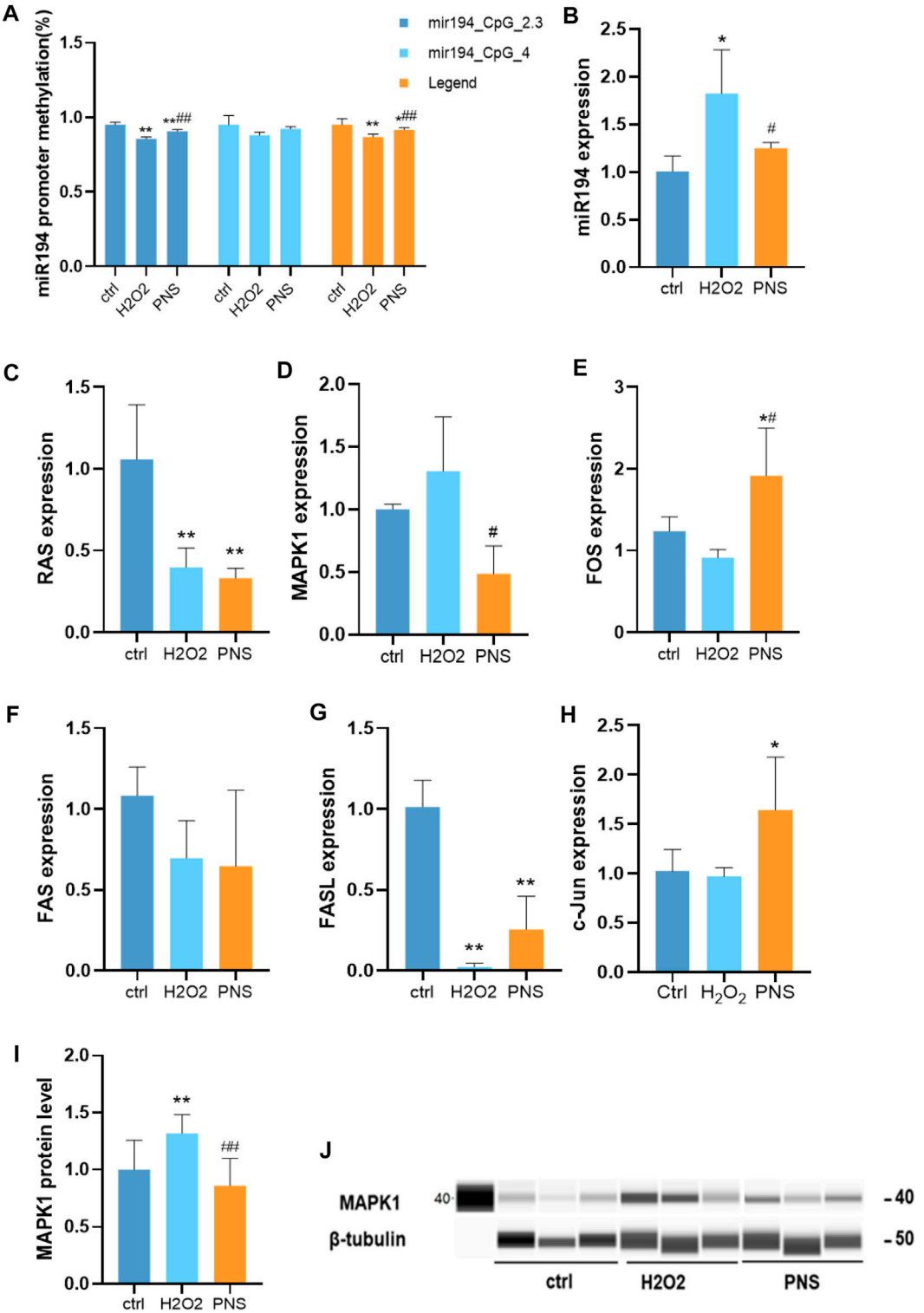

FIGURE 7 | Expression of key genes in the miR-194 promoter-miR-194-MAPK pathway by MSPCR, qRT-PCR, and Western blotting *in vitro* **(A)** DNA methylation level of the miR-194 promoter by MSPCR; **(B)** miR-194 expression; **(C)**RAS expression; **(D)** MAPK1 expression; **(E)** FOS expression; **(F)** FAS expression; **(G)** FASL expression; **(H)** c-Jun expression; **(I)** MAPK1 protein level; and **(J)** MAPK1 protein.

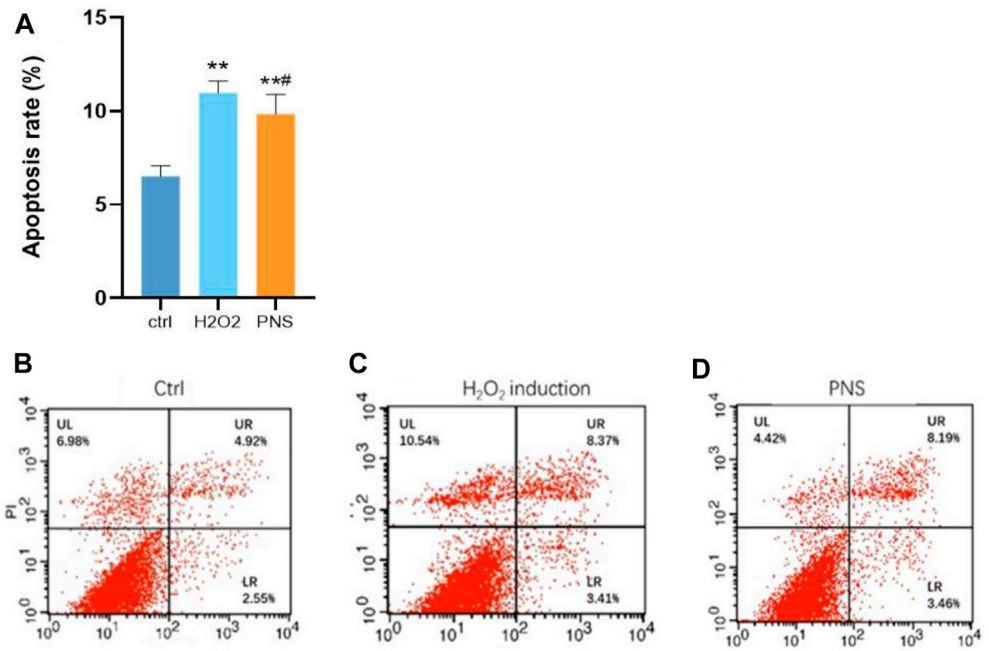

FIGURE 8 | Annexin V/PI apoptosis assay results. **(A)** Level of apoptosis in HUVECs; **(B)** control group; **(C)** H_2O_2 group; and **(D)** PNS group. $^{*}p < 0.05$ and $^{**}p < 0.01$, significantly different from the control group. $^{\#}p < 0.05$, significantly different from the H_2O_2 group.

common targets of the main ingredients of PNS were selected for further investigation (**Figure 5B**). Six genes were common targets of PNS in CAD sequencing, namely, *NOTCH1*, *ECE1*, *SOCS3*, *MAPK1*, *RAS*, and Fas cell surface death receptor ligand (FASL) (**Figure 5C**).

PNS Changes Hypomethylation of miR-194

According to the gene test, the level of methylation of miR-194 was similar before treatment in the two groups, and after treatment, no significant difference was observed (**Figure 6A**). However, the level of DNA methylation in the miR-194 promoter region increased in the PNS group after treatment but not in the placebo group.

The expression levels of the key nodes in the PNS and placebo groups were obtained using qRT-PCR and compared. No significant difference was observed between the two groups before and after treatment. However, while no significant difference in the expression of miR-194 was observed in the PNS group after treatment, that of the placebo group increased (**Figure 6B–E**). In addition, there was no significant difference between mRNA RAS, Fos proto-oncogene (FOS), MAPK1, and Jun proto-oncogene (c-Jun) after treatment.

Effects of PNS on DNA Methylation, miRNA, and Target Genes Related to Oxidative Damage in HUVECs

The methylation level always was changed in the early stage of life or by the influence of a long time in general. However, PNS could change the trend of methylation. We observed that miR-194 in HUVECs was hypermethylated by H_2O_2, and miR-194 was hypomethylated by PNS treatment (**Figures 7A**, **4B**). Then, by qRT-PCR, we detected the expression level of miR-194 and found that it was upregulated in H_2O_2 HUVECs and downregulated in PNS-treated cells, which was the opposite trend of miR-194 methylation (**Figure 7B**). Thus, hypomethylation of the gene would lead to overexpression, and hypermethylation would inhibit expression, which was consistent with normal results of methylation.

Compared with the H_2O_2 group, MAPK1 was upregulated, and FAS, c-Jun, RAS, FOS, and FASL were downregulated (**Figure 7C–G**). However, after PNS intervention, MAPK1 expression was significantly downregulated, while FOS and FASL expressions were upregulated compared to H_2O_2-induced HUVECs. The results of PCR conformed to the targets of the pharmacological analysis, MAPK1, FASL, and RAS.

In addition, we performed Western blot analysis to detect the MAPK1 expression. The results generally resembled those of the mRNA expression of the key genes. In the H_2O_2 group, MAPK1 was upregulated; however, after PNS intervention, MAPK1 was downregulated compared to the levels in H_2O_2-induced HUVECs.

PNS Protects HUVECs From Apoptosis by H_2O_2 Induction

Using annexin V/PI apoptosis assay, we observed that apoptosis was differentially upregulated in oxidative HUVECs (**Figure 8A**). With the intervention of PNS, the apoptosis rate significantly decreased. Presumably, PNS plays an important role in damaged cells during the early stages of injury (Figure 8A–D).

DISCUSSION

According to previous research, a randomized controlled trial was conducted to observe the clinical effects and changes in key nodes of the miR-194 promoter-miR-194-MAPK signaling pathway. A total of 84 patients with CAD were collected and randomly divided into two groups (the PNS group and placebo group). In terms of the length of angina pectoris attacks, both groups demonstrated a significant decrease after treatment, and the PNS group had a larger reduction. In the comparison of blood lipids, HDL changed significantly after treatment in the PNS group. We previously conducted a meta-analysis including 17 studies with a total of 2,315 patients with UA. We found that PNS had a promising therapeutic effect on the reduction of the primary end point, frequency, and duration of angina attacks in patients with UA (Yang et al., 2014; Duan et al., 2018).

In our previous research, we identified a unique DNA methylation-miRNA-mRNA regulatory network for CAD. We also identified key signaling pathways in this network, including the miR-194 promoter-miR-194-MAPK signaling pathway in CAD by pyrosequencing, MSPCR, qRT-PCR, and Western blotting analysis. Moreover, miR-194 is one of the hepatic-enriched miRNAs. In addition, it is upregulated in the serum of patients with myocardial infarction and is closely correlated with impaired cardiac function (Matsumoto et al., 2013). In addition, miR194 was increased in a lipopolysaccharide-induced H9c2 cardiomyocyte injury model. It also promoted cardiomyocyte apoptosis and participated in myocardial injury induced by endotoxemia (Zhai and Ding, 2018). The upregulation of circulating miR194 levels was found to be closely correlated with impaired human cardiac function, including ejection fraction and NT-proBNP levels. In addition, miR194 sponges could improve obesity-mediated cardiac dysfunction *in vivo* (Nie et al., 2018). The expression of miR194 degraded coronary vascular tissues and endothelial cells of rats with atherosclerosis (Li et al., 2021). Meanwhile, silencing miR-194-5p could alleviate doxorubicin-induced cardiotoxicity *via* PAK2 *in vitro* and *in vivo*. Moreover, inhibition of miR-194-5p or the overexpression of PAK2 reduced DOX-induced apoptosis of cardiomyocytes. Silencing of miR-194-5p also improved DOX-induced cardiac dysfunction (Fa et al., 2022). Moreover, activation of 5′AMP-activated protein kinase (AMPK)-p21-activated kinase 2 (PAK2) signaling attenuated ER stress and myocardial apoptosis induced by ischemia/reperfusion injury (Xu et al., 2020). Finally, the phosphorylation level of MAPK was elevated by miR-194 (Latouche et al., 2016; Bai et al., 2017; Niu et al., 2018; Liu et al., 2021). Similarly, in our cell experiment, miR-194 was upregulated in H_2O_2-induced HUVECs and decreased by PNS treatment.

No significant difference was observed in miR-194 levels in the PNS group after treatment; however, in the placebo group, these levels increased. In addition, no significant difference was observed in mRNA RAS, FOS, MAPK1, or c-Jun after treatment. However, RAS expression decreased after treatment, and the decrease was more obvious in the placebo group. Moreover, FOS in the PNS group had an increasing trend, but the placebo group did not. MAPK1 decreased after treatment, but there were no differences between the two groups. In addition, c-Jun did not change significantly in the PNS group, while in the placebo group, there was a significant downward trend.

We found that PNS can improve the symptoms of patients with CAD. In addition, we observed that PNS in traditional Chinese medicine affects DNA methylation-miRNA-mRNA. Using pharmacological analysis, some of the PNS targets were found to be differentially expressed genes in CAD sequencing. Six genes were common targets of PNS in CAD sequencing, including NOTCH1, ECE1, SOCS3, MAPK1, RAS, and FASL. Additionally, genes in the interaction network and clinical parameters were correlated. Meanwhile, *in vitro* experiments demonstrated that the key nodes in the miR-194 promoter-miR-194-MAPK signaling pathway in CAD are changed by PNS. A previous study reported that PNS conferred profound protection through the downregulation of MAPK (Luo et al., 2021; Yang et al., 2022). Finally, intervention with PNS is likely to improve apoptosis.

The present study has several limitations. First, the sample size of the randomized controlled trial was relatively small. Second, the samples came from the same hospital, and using samples from different regions may be beneficial. Third, while miR-194 and its target gene demonstrated a trend from PNS treatment, the change was not significant, likely because the intervention time with PNS was not long enough. In the future, a larger, multicenter study with a longer intervention period is warranted to confirm the clinical efficacy of PNS.

In conclusion, in a randomized controlled clinical trial, PNS alleviated CAD and changed the key nodes of the miR-194 promoter-miR-194-MAPK signaling pathway. PNS also acted on this pathway *in vitro*. PNS are important for the intervention of CAD, and the miR-194 promoter-miR-194-MAPK signaling pathway is likely to be a therapeutic target of PNS for CAD.

DATA AVAILABILITY STATEMENT

The original contributions presented in the study are included in the article/supplementary material; further inquiries can be directed to the corresponding author.

ETHICS STATEMENT

The studies involving human participants were reviewed and approved by the institutional ethics committee of Guang Anmen Hospital.

AUTHOR CONTRIBUTIONS

LD, YML, and JW contributed to the conception of the study. The protocol of the research was drafted by LD, YML, and JW. The manuscript was revised by JL. The samples were collected and

detected by LD, CL, and YML. The randomization and blind method were managed by YD. The in vitro experiment was conducted by LD, YZ, and YD. JW and YD analyzed the results and ensured that no errors occurred during the study. All authors have read and agreed to the publication of this version of the manuscript.

FUNDING

This work was supported by the National Natural Science Foundation of China (Nos. 81473561 and 81904185) and the Excellent Young Scientific and Technological Talents of China Academy of Chinese Medicine Sciences (No. ZZ14-YQ-015).

ACKNOWLEDGMENTS

The authors thank Wang Li from Beijing Children's Hospital for technical guidance in MSP, Qi Xin from the pathology department of Guang'anmen Hospital for guidance in AV/PI, and the Ouyi company for technical guidance in pyrosequencing. The authors apologize to colleagues whose work was not cited due to space limitations or our oversight.

REFERENCES

Austen, W. G., Edwards, J. E., Frye, R. L., Gensini, G. G., Gott, V. L., Griffith, L. S., et al. (1975). A Reporting System on Patients Evaluated for Coronary Artery Disease. Report of the Ad Hoc Committee for Grading of Coronary Artery Disease, Council on Cardiovascular Surgery, American Heart Association. *Circulation* 51 (4 Suppl. l), 5–40. doi:10.1161/01.cir.51.4.5

Bai, M., Zhang, M., Long, F., Yu, N., Zeng, A., and Zhao, R. (2017). Circulating microRNA-194 Regulates Human Melanoma Cells via PI3K/AKT/FoxO3a and P53/p21 Signaling Pathway. *Oncol. Rep.* 37 (5), 2702–2710. doi:10.3892/or.2017.5537

Douglas, L., Mann, D. P. Z., Libby, P., and Bonow, R. O. (2016). *Braunwald's Heart Disease*. 9th ed.. Boston: Elsevier, 886.

Duan, L., Xiong, X., Hu, J., Liu, Y., Li, J., and Wang, J. (2017). Panax Notoginseng Saponins for Treating Coronary Artery Disease: A Functional and Mechanistic Overview. *Front. Pharmacol.* 8, 702. doi:10.3389/fphar.2017.00702

Duan, L., Xiong, X., Hu, J., Liu, Y., and Wang, J. (2018). Efficacy and Safety of Oral Panax Notoginseng Saponins for Unstable Angina Patients: A Meta-Analysis and Systematic Review. *Phytomedicine* 47, 23–33. doi:10.1016/j.phymed.2018.04.044

Fa, H., Xiao, D., Chang, W., Ding, L., Yang, L., Wang, Y., et al. (2022). MicroRNA-194-5p Attenuates Doxorubicin-Induced Cardiomyocyte Apoptosis and Endoplasmic Reticulum Stress by Targeting P21-Activated Kinase 2. *Front. Cardiovasc Med.* 9, 815916. doi:10.3389/fcvm.2022.815916

Ge, P. C., Chen, Z. H., Pan, R. Y., Ding, X. Q., Liu, J. Y., Jia, Q. W., et al. (2016). Synergistic Effect of Lipoprotein-Associated Phospholipase A2 with Classical Risk Factors on Coronary Heart Disease: A Multi-Ethnic Study in China. *Cell Physiol. Biochem.* 40 (5), 953–968. doi:10.1159/000453153

Latouche, C., Natoli, A., Reddy-Luthmoodoo, M., Heywood, S. E., Armitage, J. A., and Kingwell, B. A. (2016). MicroRNA-194 Modulates Glucose Metabolism and its Skeletal Muscle Expression Is Reduced in Diabetes. *PloS one* 11 (5), e0155108. doi:10.1371/journal.pone.0155108

Li, Y., Geng, Y., Zhou, B., Wu, X., Zhang, O., Guan, X., et al. (2021). Long Non-coding RNA GAS5 Worsens Coronary Atherosclerosis through MicroRNA-194-3p/TXNIP Axis. *Mol. Neurobiol.* 58 (7), 3198–3207. doi:10.1007/s12035-021-02332-x

Liu, B., Lin, L., Yu, S., Xia, R., and Zheng, L. (2021). Long Non-coding RNA H19 Acts as a microRNA-194 Sponge to Inhibit the Apoptosis and Promote the Proliferation of Hypertrophic Scar Fibroblasts. *Can. J. Physiol. Pharmacol.* 99 (12), 1288–1297. doi:10.1139/cjpp-2021-0351

Luo, H., Vong, C. T., Tan, D., Zhang, J., Yu, H., Yang, L., et al. (2021). Panax Notoginseng Saponins Modulate the Inflammatory Response and Improve IBD-like Symptoms via TLR/NF-[Formula: See Text]B and MAPK Signaling Pathways. *Am. J. Chin. Med.* 49 (4), 925–939. doi:10.1142/S0192415X21500440

Matsumoto, S., Sakata, Y., Suna, S., Nakatani, D., Usami, M., Hara, M., et al. (2013). Circulating P53-Responsive microRNAs Are Predictive Indicators of Heart Failure after Acute Myocardial Infarction. *Circ. Res.* 113 (3), 322–326. doi:10.1161/CIRCRESAHA.113.301209

Nie, H., Pan, Y., and Zhou, Y. (2018). Exosomal microRNA-194 Causes Cardiac Injury and Mitochondrial Dysfunction in Obese Mice. *Biochem. Biophys. Res. Commun.* 503 (4), 3174–3179. doi:10.1016/j.bbrc.2018.08.113

Niu, T., Jin, L., Niu, S., Gong, C., and Wang, H. (2018). Lycium Barbarum Polysaccharides Alleviates Oxidative Damage Induced by H2O2 through Down-Regulating MicroRNA-194 in PC-12 and SH-Sy5y Cells. *Cell Physiol. Biochem.* 50 (2), 460–472. doi:10.1159/000494159

Roffi, M., Patrono, C., Collet, J. P., Mueller, C., Valgimigli, M., Andreotti, F., et al. (2016). 2015 ESC Guidelines for the Management of Acute Coronary Syndromes in Patients Presenting without Persistent ST-Segment Elevation: Task Force for the Management of Acute Coronary Syndromes in Patients Presenting without Persistent ST-Segment Elevation of the European Society of Cardiology (ESC). *Eur. Heart J.* 37 (3), 267–315. doi:10.1093/eurheartj/ehv320

Rupérez, C., Ferrer-Curriu, G., Cervera-Barea, A., Florit, L., Guitart-Mampel, M., Garrabou, G., et al. (2021). Meteorin-like/Meteorin-β Protects Heart against Cardiac Dysfunction. *J. Exp. Med.* 218 (5), e20201206. doi:10.1084/jem.20201206

Shen, Q., Li, J., Zhang, C., Wang, P., Mohammed, A., Ni, S., et al. (2017). Panax Notoginseng Saponins Reduce High-Risk Factors for Thrombosis through Peroxisome Proliferator-Activated Receptor -γ Pathway. *Biomed. Pharmacother.* 96, 1163–1169. doi:10.1016/j.biopha.2017.11.106

Wang, W., Yang, L., Song, L., Guo, M., Li, C., Yang, B., et al. (2021). Combination of Panax Notoginseng Saponins and Aspirin Potentiates Platelet Inhibition with Alleviated Gastric Injury via Modulating Arachidonic Acid Metabolism. *Biomed. Pharmacother.* 134, 111165. doi:10.1016/j.biopha.2020.111165

Xiong, L. L., Qiu, D. L., Xiu, G. H., Al-Hawwas, M., Jiang, Y., Wang, Y. C., et al. (2020). DPYSL2 Is a Novel Regulator for Neural Stem Cell Differentiation in Rats: Revealed by Panax Notoginseng Saponin Administration. *Stem Cell Res. Ther.* 11 (1), 155. doi:10.1186/s13287-020-01652-4

Xu, L., Cai, Y., Wang, Y., and Xu, C. (2020). Meteorin-Like (METRNL) Attenuates Myocardial Ischemia/Reperfusion Injury-Induced Cardiomyocytes Apoptosis by Alleviating Endoplasmic Reticulum Stress via Activation of AMPK-PAK2 Signaling in H9C2 Cells. *Med. Sci. Monit.* 26, e924564. doi:10.12659/MSM.924564

Yang, L., Wang, H., Wang, P., Gao, M., Huang, L., Cui, X., et al. (2022). De Novo and Comparative Transcriptomic Analysis Explain Morphological Differences in Panax Notoginseng Taproots. *BMC genomics* 23 (1), 86. doi:10.1186/s12864-021-08283-w

Yang, X., Xiong, X., Wang, H., and Wang, J. (2014). Protective Effects of Panax Notoginseng Saponins on Cardiovascular Diseases: A Comprehensive Overview of Experimental Studies. *Evid. Based Complement Alternat. Med.* 2014, 204840. doi:10.1155/2014/204840

Zhai, Y., and Ding, N. (2018). MicroRNA-194 Participates in Endotoxemia Induced Myocardial Injury via Promoting Apoptosis. *Eur. Rev. Med. Pharmacol. Sci.* 22 (7), 2077–2083. doi:10.26355/eurrev_201804_14739

Zhang, J. S., Zhang, B. X., Du, M. M., Wang, X. Y., and Li, W. (2016). Chinese Preparation Xuesaitong Promotes the Mobilization of Bone Marrow Mesenchymal Stem Cells in Rats with Cerebral Infarction. *Neural Regen. Res.* 11 (2), 292–297. doi:10.4103/1673-5374.177738

Zhao, C. H., Cao, H. T., Zhang, J., Jia, Q. W., An, F. H., Chen, Z. H., et al. (2019). DNA Methylation of Antisense Noncoding RNA in the INK Locus (ANRIL) Is Associated with Coronary Artery Disease in a Chinese Population. *Sci. Rep.* 9 (1), 15340. doi:10.1038/s41598-019-51921-3

Zhou, Z., Wang, J., Song, Y., He, Y., Zhang, C., Liu, C., et al. (2018). Panax Notoginseng Saponins Attenuate Cardiomyocyte Apoptosis through Mitochondrial Pathway in Natural Aging Rats. *Phytother. Res.* 32 (2), 243–250. doi:10.1002/ptr.5961

Conflict of Interest: The authors declare that the research was conducted in the absence of any commercial or financial relationships that could be construed as a potential conflict of interest.

Publisher's Note: All claims expressed in this article are solely those of the authors and do not necessarily represent those of their affiliated organizations, or those of the publisher, the editors, and the reviewers. Any product that may be evaluated in this article, or claim that may be made by its manufacturer, is not guaranteed or endorsed by the publisher.

frontiers | Frontiers in Pharmacology

ORIGINAL RESEARCH
published: 27 June 2022
doi: 10.3389/fphar.2022.842671

Wuwei Qingzhuo San Ameliorates Hyperlipidemia in Mice Fed With HFD by Regulating Metabolomics and Intestinal Flora Composition

Shasha Ge[1,2†], *Cuiping Liao*[1,2†], *Duna Su*[3], *Tunuo Mula*[4], *Zhula Gegen*[4], *Zhiyong Li*[5] *and Ya Tu*[1,2*]

[1]Experimental Research Center, China Academy of Chinese medical sciences, Beijing, China, [2]Development Research Center of TCM, China Academy of Chinese Medical Science, Beijing, China, [3]Chi Feng an Ding Hospital, Chifeng, China, [4]College of Mongolian Medicine and Pharmacy, Inner Mongolia Minzu University, Tongliao, China, [5]Institute of Chinese Materia medica, China Academy of Chinese medical sciences, Beijing, China

Hyperlipidemia is one of the most common metabolic disorders that threaten people's health. Wuwei Qingzhuo San (WQS) is a traditional Mongolian medicine prescription, which is widely used in Mongolia for the treatment of hyperlipidemia. Our previous studies found that it has hypolipidemic and hepatoprotective effects on hyperlipidemic hamsters. However, the underlying lipid-lowering mechanisms of WQS and its relationship with intestinal flora are not yet clear. In this study, 16 S rRNA gene sequencing and metabolomics were performed to investigate the action mechanism of WQS on hyperlipidemic mice induced by a high-fat diet (HFD). As a result, metabolic pathway enrichment analysis revealed that the intervention of WQS had obviously modulated the metabolism of α-linolenic acid and linoleic acid and the biosynthesis of bile acids. 16 S rRNA sequencing showed that WQS had altered the composition of the intestinal microbiota in hyperlipidemic mice fed with HFD and, especially, adjusted the relative abundance ratio of Firmicutes/*Bacteroides*. These findings provide new evidence that WQS can improve HFD-induced hyperlipidemia by regulating metabolic disorders and intestinal flora imbalance.

Keywords: hyperlipidemia, Wuwei Qingzhuo San, metabolomics, 16S rRNA gene sequencing, intestinal microbiota

OPEN ACCESS

Edited by:
Ling Zhang,
Zhejiang Chinese Medical University, China

Reviewed by:
Min Wu,
China Academy of Chinese Medical Sciences, China
Almagul Kushugulova,
Nazarbayev University, Kazakhstan

***Correspondence:**
Ya Tu
tuya126@126.com

[†]*These authors have contributed equally to this work*

Specialty section:
This article was submitted to Ethnopharmacology, a section of the journal Frontiers in Pharmacology

Received: *24 December 2021*
Accepted: *16 May 2022*
Published: *27 June 2022*

Citation:
Ge S, Liao C, Su D, Mula T, Gegen Z, Li Z and Tu Y (2022) Wuwei Qingzhuo San Ameliorates Hyperlipidemia in Mice Fed With HFD by Regulating Metabolomics and Intestinal Flora Composition. Front. Pharmacol. 13:842671. doi: 10.3389/fphar.2022.842671

1 INTRODUCTION

Hyperlipidemia is a condition that incorporates various acquired and inherited diseases, which have been described as an elevated level of lipid in the body (Hill and Bordoni, 2021). It is also considered a high-risk factor for atherosclerosis plaque and vascular disease that may ultimately lead to death (Mach et al., 2019). The incidence of hyperlipidemia in Chinese adults reaches 40% (Committee, C. A. D. G. R. J., 2016), and more than 3 million adults in the United States and Europe have been diagnosed with hyperlipidemia. Therefore, it is necessary to make early diagnoses and prevention in order to reduce morbidity and mortality.

Wuwei Qingzhuo San (WQS) is a traditional Mongolian prescription with a long clinical history (Bai, 1992), which was first recorded in the "BaiFang Chapter." This prescription is composed of five traditional Chinese medicines, including *Punica granarum* L. (shiliu), *Carthamus tinctorius* L. (honghua), *Wurfbainia vera (Blackw.)* Myristica fragrans Houtt.(doukou), Neolitsea cassia (L.)

Kosterm (rougui), and *Piper longum* L (biba). It has the effect of "relieving stagnation to promoting stomach fire (开郁消食)" and "Eliminating Phlegm and Producing Essence (清浊生华)" (Commission, C. P., 2020), which can be used to treat indigestion induced by overeating, abdominal distension, and diarrhea or some metabolic disease. It was found that the five herbs of WQS contain tannins, alkaloids, flavonoids, organic acids, and other components (Kumar et al., 2011; Ge et al., 2021) which have good effects in anti-inflammatory, immunomodulatory, and metabolic regulation. Our previous studies found that WQS has an attractive hypolipidemic and hepatoprotective effect in the hyperlipidemic hamster (Li et al., 2020), and associated endogenous metabolites in biological fluids were analyzed qualitatively and quantitatively using metabolomics (Hu and Xu, 2014). But its mechanism of regulation of cholesterol metabolism remains to be studied. Therefore, this study will focus on serum metabolomics to elaborate on how WQS regulates lipid metabolism.

Interestingly, recent research has found gut microbiota can maintain the physiological functions of the intestine, regulate diet, and host metabolism, and reduce the occurrence of metabolic disorders, so it is considered to be a regulator of host metabolism (Wang et al., 2020). Accumulating literature indicates that intestinal flora is related to the occurrence of chronic metabolic disorders (Lazar et al., 2019). Moreover, these five herbs in WQS are raw material medicine, which is different from the traditional Chinese prescription that needs to go through traditional processing techniques such as water extracting, so WQS will firstly go through catabolism of intestinal flora after oral administration, following the small molecular compounds are absorbed into the blood. Therefore, the study of the relationship between WQS and the gut microbiota is of some significance for the study of the hypolipidemic mechanism of this prescription.

In our previous study, it was predicted that WQS increases cholesterol catabolism through the upregulation of CYP7A1 and inhibits hepatic HMGCR expression through the upregulation of p-AMPK, thereby inhibiting cholesterol synthesis and lowering blood lipids(Li et al., 2020). Therefore, we extended our previous study to detect endogenous metabolites in mouse serum by UPLC-QTOF/MS-based serum metabolomics to determine whether the lipid-lowering mechanism of WQS is related to endogenous substances. Meanwhile, hyperlipidemia is closely related to intestinal flora, and the imbalance of intestinal flora will lead to changes in endogenous substances. The regulatory effect of WQS on the gut microbiota was also investigated by using 16 S rRNA gene sequencing. These studies provide a more comprehensive understanding of the mechanism by which WQS mediates therapeutic effects in HFD-induced hypolipidemic mice by regulating intestinal flora.

2 MATERIALS AND METHODS

2.1 Materials and Animals

Wuwei Qingzhuo San was purchased from FuXin Mongolian Medicine Co., Ltd., (SFDA approval number: Z21020300, Inner Mongolia, China). It consists of *Punica granarum* L., *Carthamus tinctorius* L., *Wurfbainia vera (Blackw.)* Myristica fragrans Houtt.(doukou), Neolitsea cassia (L.) Kosterm, and *Piper longum* L with the mixed proportion of the respective compounds being 8:4:1:1:1. According to the traditional record of Mongolian medicine habit, the drug's raw materials are often crushed into a powder and taken with water. Hence, WQS (Batch number: 20200614) in this study was dissolved in 0.5% carboxymethyl cellulose (CMC) buffer solution and prepared as a drug suspension before use.

Thirty male apolipoprotein E-deficient ($Apoe^{-/-}$) on a C57BL/6J background mouse (8-week-old, weighting 18–22 g) were provided from Beijing Vital River Laboratory Animal Technology Co., Ltd. (SCXK-2011-0011). The animal experiment was approved by the animal committee of Medical Experimental Center, China Academy of Chinese Medical Sciences.

2.2 Animal Administration

Thirty male $apoe^{-/-}$ mice were caged in controlled conditions of temperature (22 ± 2°C) and relative humidity (60 ± 5%) with a 12 h light/dark cycle for 7 days. Ten mice were fed normal chow as a normal control group (NC group, n = 10). Other apoe–/– mice were fed a high-fat diet (10% lard, 10% sucrose, 0.2% cholesterol, 0.5% bile salts, and 79.3% standard chow) as the HFD model group (HFD model group, n = 20) throughout the experimental period. After 4 weeks of HFD feeding, blood samples were collected from the orbital vein. The kit of Nanjing Jiancheng Institute of Bioengineering (Nanjing, China) was used to quantitatively determine the content of TC, TG, HDL-C, and LDL-C in the serum. Thereafter, according to the levels of blood lipid, these 20 mice in the HFD model group were randomly divided into two groups as follows: mice fed a high-fat diet as the HFD group (n = 10), and mice fed a high-fat diet + WQS as the WQS group (0.598 g/kg/day, n = 10). All mice were sacrificed after 6 weeks of WQS administration, serum samples were collected after centrifugation at 3,000 rpm for 15min. Ceca contents were washed from the cecum with 1.0 ml of cold Milli-Q water. All samples were stored at -80°C before analysis.

2.3 Serum Metabolomic

2.3.1 Sample Preparation

Serum metabolomic analysis was performed on all mice in each group due to take into account the individual differences of mice in each group. The 50 μL serum samples were mixed with 200 μL methanol-acetonitrile solution (2:1, v/v) and sonicated for 5 min, then incubated for 20 min at -20°C freezers, the incubation solution was then centrifuged for 10 min (14,000 rpm, -4°C), and 200 μL of supernatant was injected into the LC/MS system for analysis. Furthermore, equal aliquots of the processed supernatants from each sample as the quality control (QC) sample.

2.3.2 UPLC-Q-TOF/MS Analysis

Chromatographic separation was performed on a 1,290 Infinity series UPLC System (Agilent Technologies) with a UPLC BEH

C_{18} column (2.1 × 100 mm, 1.7 μm, Waters). The mobile phase consisted of 0.1% formic acid aqueous (mobile phase A), and 0.1% formic acid acetonitrile (mobile phase B), and the gradient elution program with a flow rate of 0.4 ml min^{-1} was listed as follows: mobile phase B maintaining at 5% (0.00–0.50 min), from 5 to 30% (0.50–1.50 min), from 30 to 60% (1.50–4.00 min), from 60 to 99% (4.00–5.00 min) and maintaining at 95% (5.00–7.50 min).

Mass spectrometry information of small molecules was collected by the Q-TOF-MS spectrometer with an ESI source in negative or positive ion mode. The following MS conditions were used: the capillary voltage and cone voltage were 2.0 kV and 40 V, the desolvation gas temperature and source temperature were 440 and 115°C, and the flow rate of desolvation gas and cone gas was 80 L/h and 50 L, respectively, and the scan range was 50–1,000 m/*z*. The system control and data analysis were performed by Waters Progenesis QI v2.2 (Nonlinear Dynamics).

2.3.3 Data Processing and Multivariate Analysis

The original data of UPLC-Q-TOF-MS/MS were processed by Progenesis QI v2.2 (Nonlinear Dynamics from Waters) combined with the SIMCA program (version 14.0, Sweden). PLS-DA, OPLS-DA, and PCA were carried out. And the value of R^2X or R^2Y and Q^2 were used to evaluate the quality of the model. By default, SIMCA was used for seven rounds of cross-validation throughout the experiment to determine the most reasonable number of endogenous components and prevent excessive model fitting. And the OPLS-DA results needed further confirmation by a permutation evaluation (200 times). The value of P determined by the student's test was used to select potential biomarkers. The biomarkers were identified by Progenesis QI MetaScope software and compared with the Human Metabolome Database (http://hmdb.ca/) based on accurate mass and specific MS^2 fragments. Pathway enrichment analysis was performed on the MetaboAnalyst website (http://www.metaboanalyst.ca/) based on the KEGG database (Kyoto Encyclopedia of Genes and Genomes, http://www.kegg.jp/kegg/pathway.html).

2.4 Intestinal Flora Analysis

Metagenomic DNA from the contents in the cecum was extracted by MagPure Soil DNA LQ Kit (TransGen Biotech, Beijing, China) according to the manufacturer's protocols. The bacteria DNA concentration and purity were estimated by a Nanodrop NC2000 spectrophotometer (Thermo Fisher Scientific Inc., USA). The hypervariable V3 -V4 region of bacteria 16 S rDNA genes was amplified by PCR with the primers (338 F: 5′-ACTCCTACG GGAGGCAGCA) and primers (806 R: 5′GGACTACHVGGGTWTCTAAT). PCR was conducted using the following program: 98°C for 5 min, 24 cycles for 30 s at 98°C, 52°C for 30 s, 72°C for 45 s, 72°C for 5 min on an Eppendorf thermocycler. Amplification was confirmed by 2% agarose gel electrophoresis, PCR products were purified by the VAHTSTM DNA Clean Beads (Vazyme, Nanjing, China) and were quantified by the Quant-iT PicoGreen dsDNA Assay Kit on a quantitative Microplate reader (BioTek, FLx800). The V3-V4 region of bacterial 16 S rRNA genes was sequenced with the NovaSeq 6,000 platform (Illumina, USA) according to the manufacturer's specifications. In addition, the clustering sequences were binned into operational taxonomic units (OTUs) with a 97% similarity cutoff using Vsearch (v2.13.4) (Rognes et al., 2016). Alpha diversity metrics (Chao1, Observed species, Shannon, Simpson index) and beta-diversity metrics (unweighted UniFrac (Lozupone and Knight, 2005) were respectively estimated by QIIME2 and the BrayCurtis distance algorithm.

2.5 Statistical Analysis

SPSS software (version 16.0) was used to analyze the data by one-way ANOVA and expressed as mean ± SD. Tukey's multiple comparison test was used to identify significant treatment differences. Spearman correlation analysis was performed to determine the relationship between variables. $p < 0.05$ is considered to be statistically significant.

3 RESULTS

3.1 WQS Administration Alleviates Hyperlipidemia in High-Fat-Diet Mice

Male $apoe^{-/-}$ mice developed hyperlipidemia after 10 weeks of HFD feeding. The weight (**Figure 1A**), liver index (**Figure 1B**), and blood lipid (**Figures 1C–F**) of mice with a high-fat diet were increased significantly, indicating that a diet-induced hyperlipidemia mice model was successfully established. After 6 weeks of WQS treatment, body weight and liver index were decreased, but there was no significant difference compared with the HFD group. In addition, the TC, TG, and LDL-c levels were markedly increased in the HFD group, but these were significantly decreased in the WQS group, especially on TC levels ($p < 0.01$). These results indicate that WQS effectively improved dyslipidemia in hyperlipidemia mice induced by continuous consumption of HFD.

3.2 WQS-Modulated Serum Metabolomic Profiling in HFD Mice

The representative base peak chromatogram (BPI) of serum samples from the NC, HFD, and WQS groups, and the BPI of QC samples in positive and negative ion modes are presented in **Supplementary Figure S1** and **Supplementary Table S1**. The results of PCA showed that the three groups were clear separated in the positive and negative ion modes (**Figures 2**, **3**). It indicates that serum biochemical disturbances occurred in hyperlipidemia mice, and the metabolic pattern changes significantly after oral administration of WQS. In addition, the WQS group was close to the NC group, which means that hyperlipidemia in mice showed the greatest improvement after oral administration of WQS (**Figures 2A–B**).

The score plot of OPLS-DA analysis showed obvious differences in metabolic characteristics among the groups, as shown in **Figures 2C–E**, especially the WQS group was distinguished from the HFD group. In addition, the permutation plot helped to obtain risk assessment of incorrect

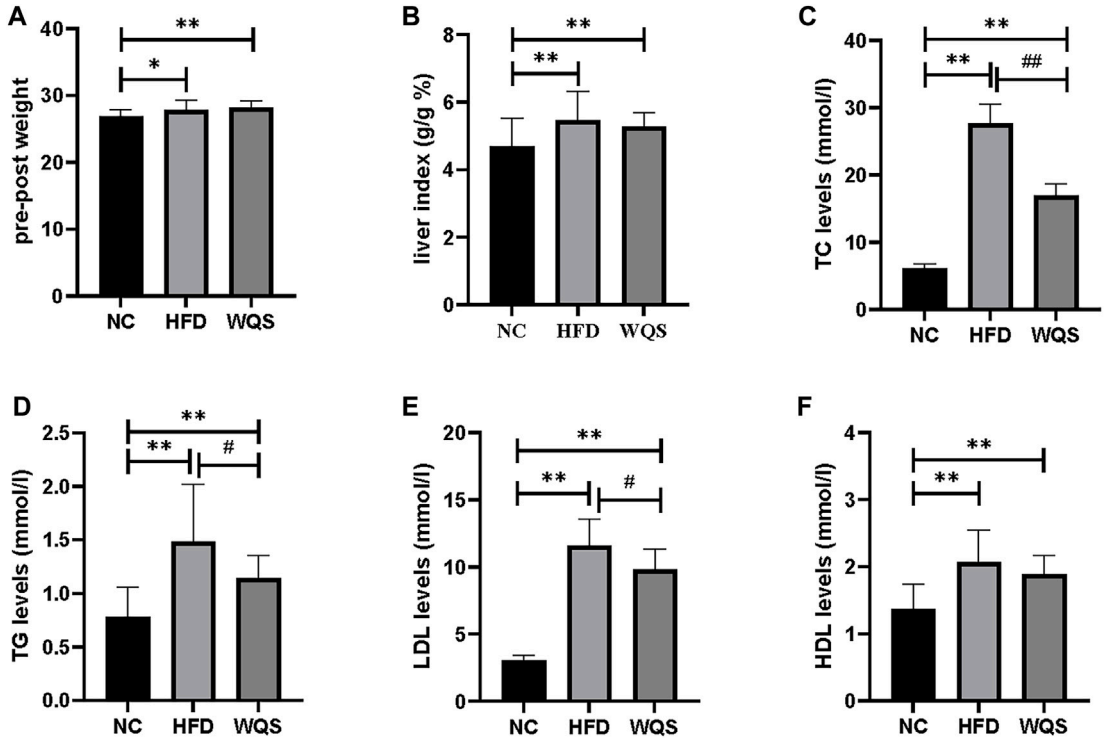

FIGURE 1 | Effects of WQS on HFD-induced hyperlipidemia in mice. Relative change of **(A)** body weight; **(B)** liver index; **(C)** TC levels in serum; **(D)** TG levels in serum; **(E)** LDL-C levels in serum; **(F)** HDL-C levels in serum.

results from OPLS-DA. The 200 times permutation tests showed that all established OPLS-DA models are credible and have no over-fitting because the R^2 and Q^2 values of the random permutation experiment were lower than the corresponding original values, and the regression line of Q^2 had a negative intercept.

S- plot and ANOVA tests were conducted to reveal the potential biomarkers that contribute the most to the difference between groups. The points farthest from zero on the *X*-axis and *Y*-axis contributed the most to the difference between groups, and the metabolites with VIP> 1.5 and $p < 0.05$ are considered potential biomarkers (**Figure 3**). According to predefined criteria and the handling method, a total of 12 potential biomarkers were identified. The differences in the relative levels among the three groups were revealed by the cluster analysis of the heat maps of all metabolites, as shown in **Figure 4A**. Compared with the NC group, twelve metabolites were upregulated significantly in the HFD group, including 3-beta-hydroxy-4beta-methyl-5alpha-cholest-7-ene-4alpha-carbaldehyde, 9-oxo-13-hydroxy-11-octadecenoic acid, 9S-10 R-Epoxy-6Z-octadecene, deoxycholic acid, lagodeoxycholic, neoabietic acid, N-palmitoyl phenylalanine, PE (18:2 (9Z, 12Z)/0:0), secosterol-A, and trihydroxycoprostanoic acid. The levels of neoabietic acid-1, and Alpha-Linolenic acid were downregulated significantly. However, the levels of these metabolites in the WQS group were reversed and returned to normal or near to normal levels compared with the HFD group. Therefore, they were considered the potential biomarkers of the lipid-lowering effect of WQS. The Spearman correlation in these identified metabolites is shown in **Figure 4B**. In addition, the KEGG pathway annotation results of the metabolites showed that α-linolenic acid and linoleic acid metabolism and bile acid biosynthesis pathways were enriched, which might be possible pathways for WQS's lipid-lowering.

3.3 WQS Supplementation Modulated Gut Microbial Community Composition

High-throughput 16 S rRNA sequencing combined with diversity analysis was used to investigate the influence of WQS on the intestinal microbial composition of HFD-fed mice. We drew the microbial classification tree based on the taxonomic annotations of species with OUT clustering and added the grouping abundance data of each taxa node to the graph in the form of a pie chart (**Supplementary Figure S2A**), and the threshold was set at the relative abundance of 0.5%, the taxa nodes whose relative abundance is greater than these thresholds at the same classification level.

The Alpha diversity results showed that a significant decrease in the richness of intestinal bacteria was observed in the HFD group measured by the Chao index and the observed species index compared to the NC group at the OTU level. However, the abundance of bacterial communities was increased after oral administration of WQS compared with the NC group ($p <$

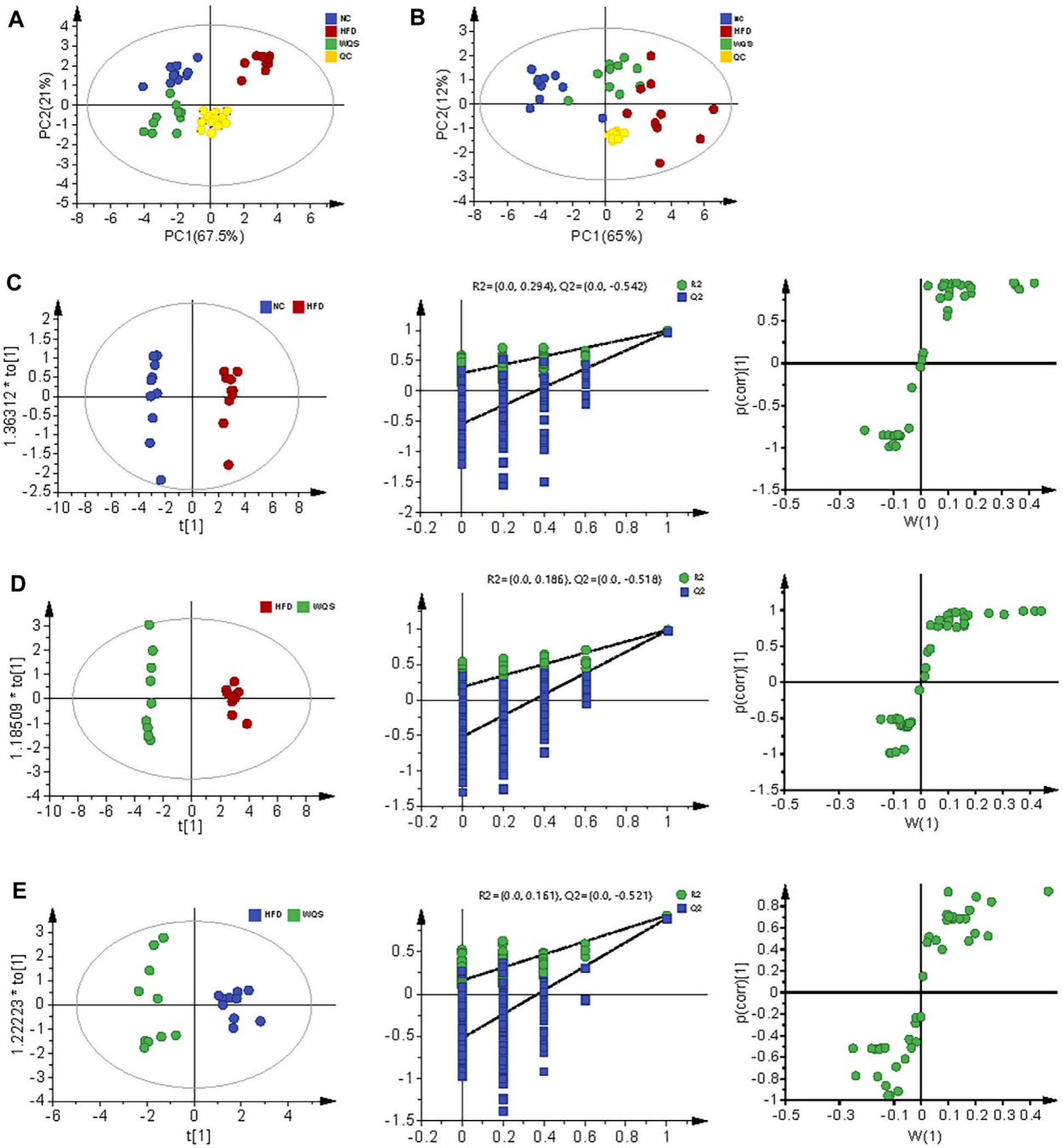

FIGURE 2 | PCA for plasma from NC, HFD, and WQS groups in the positive **(A)** and negative **(B)** ESI mode. OPLS-DA score scatter plots, permutation test of OPLS-DA model, and S plots for NC group **(C)**, HFD group **(D)**, and WQS group **(E)** in the positive ESI mode.

0.01 in **Supplementary Figure S2B**). Meanwhile, the microbial community diversity of the HFD group decreased as measured by the Simpson and Shannon diversity index, but there was no statistical difference (**Supplementary Figure S2B**). The unweighted UniFrac analysis based on PCoA and NMDS analysis was conducted to compare similarities between intestinal microbial communities. The results revealed a notable separation of the microbial structure among the three groups (**Supplementary Figures S2C,D**). There was a significant difference among the three groups (R2 = 0.36, p = 0.001, adonis analysis), and observations of bacterial composition indicated that the high-fat diet altered the composition of the fecal microbiota, which had a considerable separation in microbial community with distance clustering to the NC group. Meanwhile,

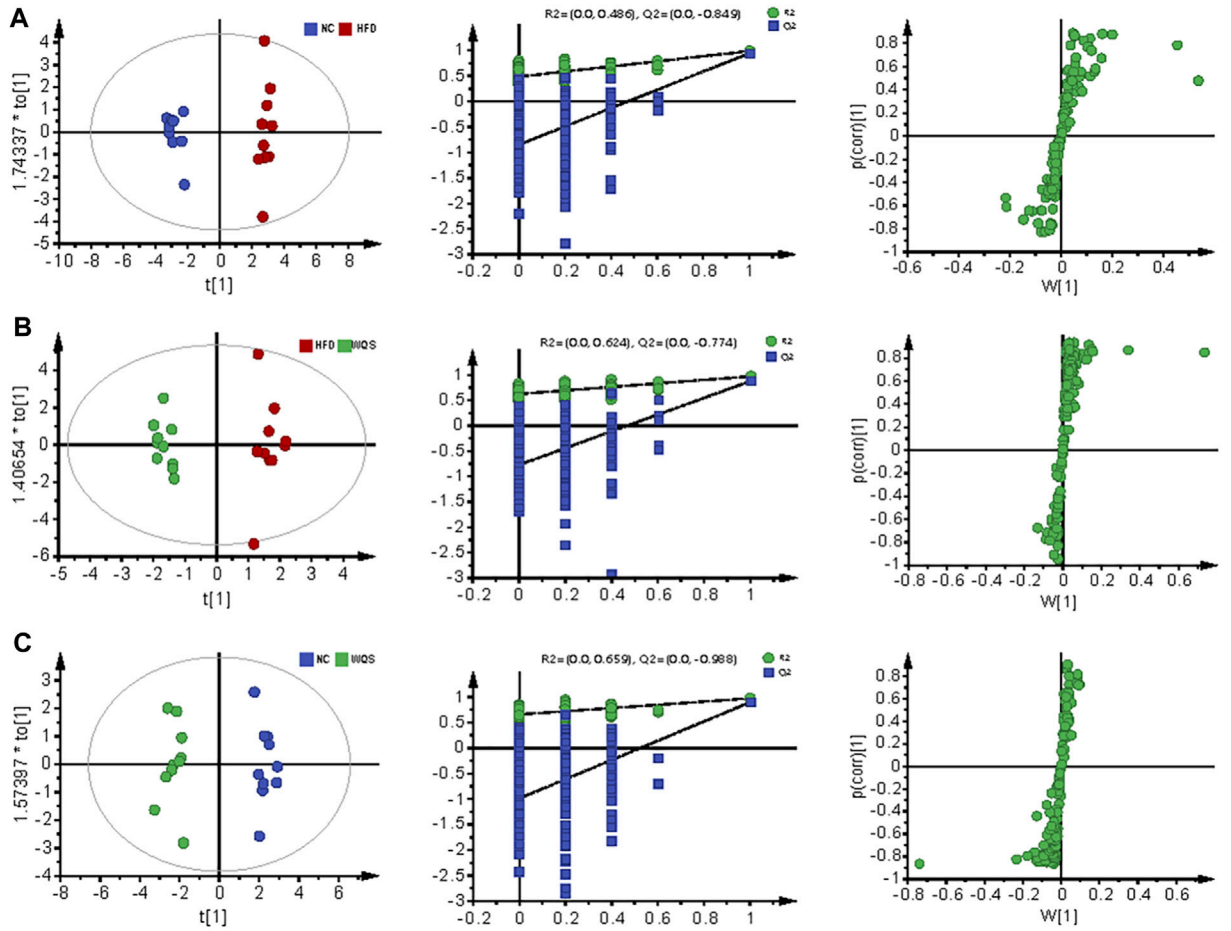

FIGURE 3 | Serum metabolomic profiling by UPLC-QTOF MS in negative ion modes. OPLS-DA score scatter plots, permutation test of OPLS-DA model, and S plots for NC group **(A)**, HFD group **(B)**, and WQS group **(C)** in the negative ESI mode.

the microbial community of the WQS group was significantly separated from that of the HFD group, which indicated that WQS supplementation induced a remarkable change in gut microbial structure compared with the HFD group.

The results of OTUs statistical analysis showed that the structure of fecal bacteria was different among the three groups. As presented in **Figure 5A**, all three groups have four dominant phyla (Firmicutes, Bacteroidetes, Proteobacteria, and Actinobacteria) with different relative abundances. A significant rise in Firmicutes and a significant decline in *Bacteroides* and Proteobacteria were observed in the HFD group by comparing with the NC group. However, these changes were reversed after the oral administration of WQS. At the genus level, the relative abundance of Muribaculaceae, Blautia, [Eubacterium]_fissicatena_group, Lachnospiraceae_NK4A136_group, *Bacteroides*, and Ruminococcaceae_UCG-014_ was relatively lower, but the abundance of Bilophila, Roseburia, Lachnoclostridium, [Ruminococus]_torques_group, and Allobaculum was relatively higher in the HFD group.

To identify the most significant differences in specific gut microbial taxa from phyla to genera associated with different dietary interventions. LEfSe analysis was performed to analyze the microbial community. The results indicated that there are 125 rich differential taxa among the three groups (**Figure 5B**), (LDA>2, $p < 0.05$), including 70 genera. At the genus level, Muribaculaceae, Lachnospiraceae_NK4A136_group, Ruminococcaceae_UCG_014, and Novosphingobium and Lactococcus were dominant in the NC group. However, the HFD group was dominated by Rumencoccus __torques_group, Lachnoclostridium, Anaerotruncus, Pelomonas, and Brevundimonas. Therefore, the changes in these strains might be related to the pathogenesis of hyperlipidemia. The WQS group was dominated by Bilophila, Roseburia, Ruminiclostridium_9, Holdemania, and Dubosiella, these bacteria can be considered intestinal indicators for WQS to improve HFD-induced hyperlipidemia. The cladogram in **Figure 5C** further demonstrates the specific intestinal microbial taxa related to WQS treatment.

PICRUSt 2 (Phylogenetic Investigation of Communities by Reconstruction of Unobserved States) was used to study the changes in intestinal microbial function in HFD mice. Based on the KEGG database, PICRUSt displayed a total of six pathways

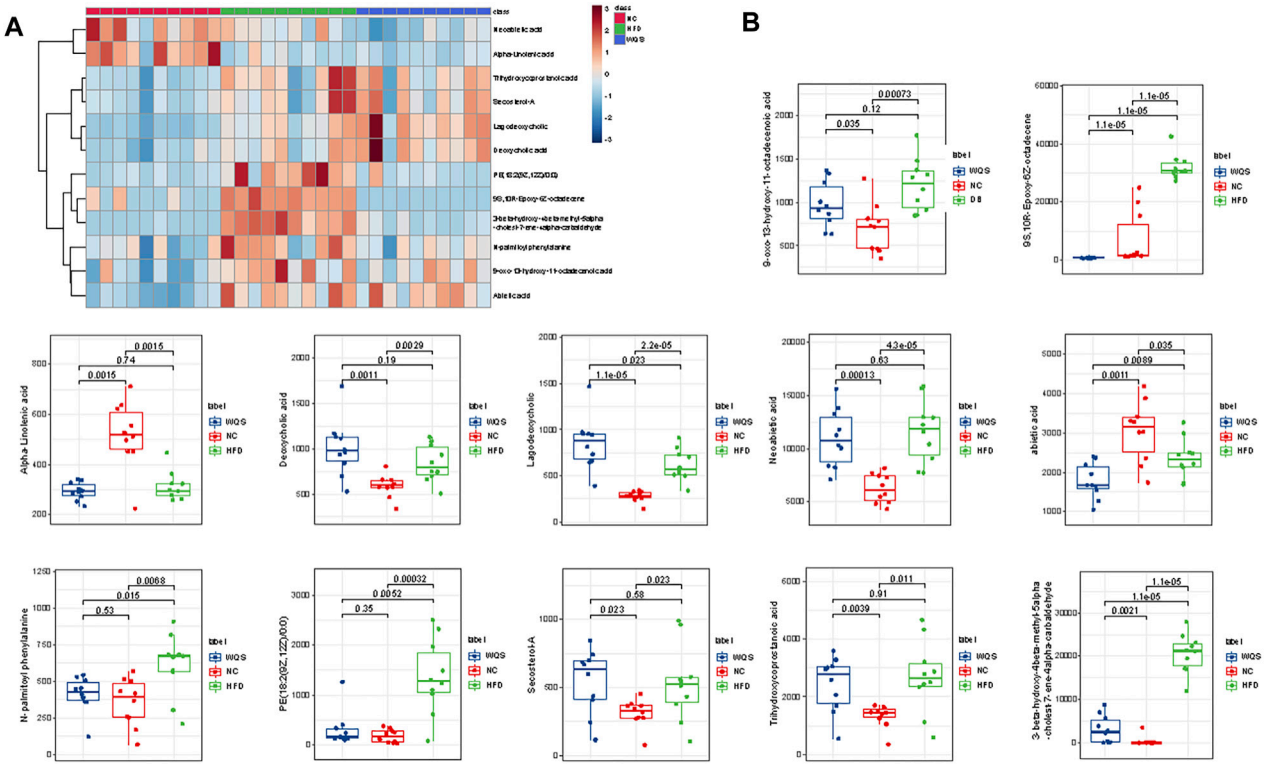

FIGURE 4 | Heatmap to visualize the abundance of biomarkers in each group. **(A)** hierarchical clustering heat map of the 12 differential metabolites, with the degree of change marked with red (upregulation) and blue (downregulation); **(B)** 12 metabolites with differential abundance.

of biological metabolism in Level 1 pathways (**Figure 5D**): cellular processes, environmental information processing, genetic information processing, human diseases, metabolism, and organismal systems. Metabolism and genetic information processing were dominant among them. At KEGG pathway level 2, it mainly included amino acid metabolism, carbohydrate metabolism, and metabolism of cofactor vitamin. HFD mice decreased 8 pathways and increased 12 pathways compared with the NC group.

3.4 Correlation Between Specific Microbial Taxa and Metabolic Parameters in Mice

To observe the relationship between metabolites and intestinal flora more intuitively, Spearman correlation analysis was performed on the three groups. At the phylum level (**Figure 6A**), Neoabietic acid showed negative relationships with Tenericutes, Bacteroidetes, and Patescibacteria. Similarly, at the genus level (**Figure 6B**), Secosterol-A, Trihydroxycoprostanoic acid, Deoxycholic acid, and Lagodeoxycholic showed negative relationships with Lachnoclostridium, unclassified_Lachnospiraceae, and uncultured_Lachnospiraceae. Meanwhile, Neoabietic acid-1 and 9 S, 10 R-Epoxy-6Z-octadecene showed negative relationships with Ruminococcaceae_UCG-014, Lachnospiraceae_NK4A136_group, and Muribaculaceae while positively related with Lachnoclostridium, [Ruminococcus]_torques_group, Roseburia, Ruminiclostridium_9, Dubosiella, and Holdemania. In addition, Alpha-Linolenic acid and PE (18:2 (9Z, 12Z)/0:0) correlated positively with Ruminiclostridium_9 and Roseburia.

4 DISCUSSION

Hyperlipidemia is a potentially harmful disease, which will cause cardiovascular diseases with high mortality (Nelson, 2013). It will endanger people's lives and health if patients do not receive timely medical treatment, bringing a heavy burden to the national medical insurance. At present, the main treatment of hyperlipidemia is a statin (Karr, 2017), but due to genetic and ethnic differences, while effective, it causes a markedly increased risk of myopathy (Sathasivam, 2012) and rhabdomyolysis (Antons et al., 2006). We still need to actively develop new drugs to deal with it. According to the records of traditional Mongolian medicine, the incidence of hyperlipidemia is due to excessive greasy ingredients in a daily diet and weak "stomach fire" (Zhang and Chang, 2015). Unable to complete normal metabolism to discharge unnecessary dregs, resulting in the continuous accumulation of greasy components in the blood. WQS can enhance the ability of "stomach fire" and "liver movement", and improve the "metabolic power" of the human body (Hasgova, 2015), achieving the effect of cleaning up excess greasy components in blood lipids. Therefore, our study

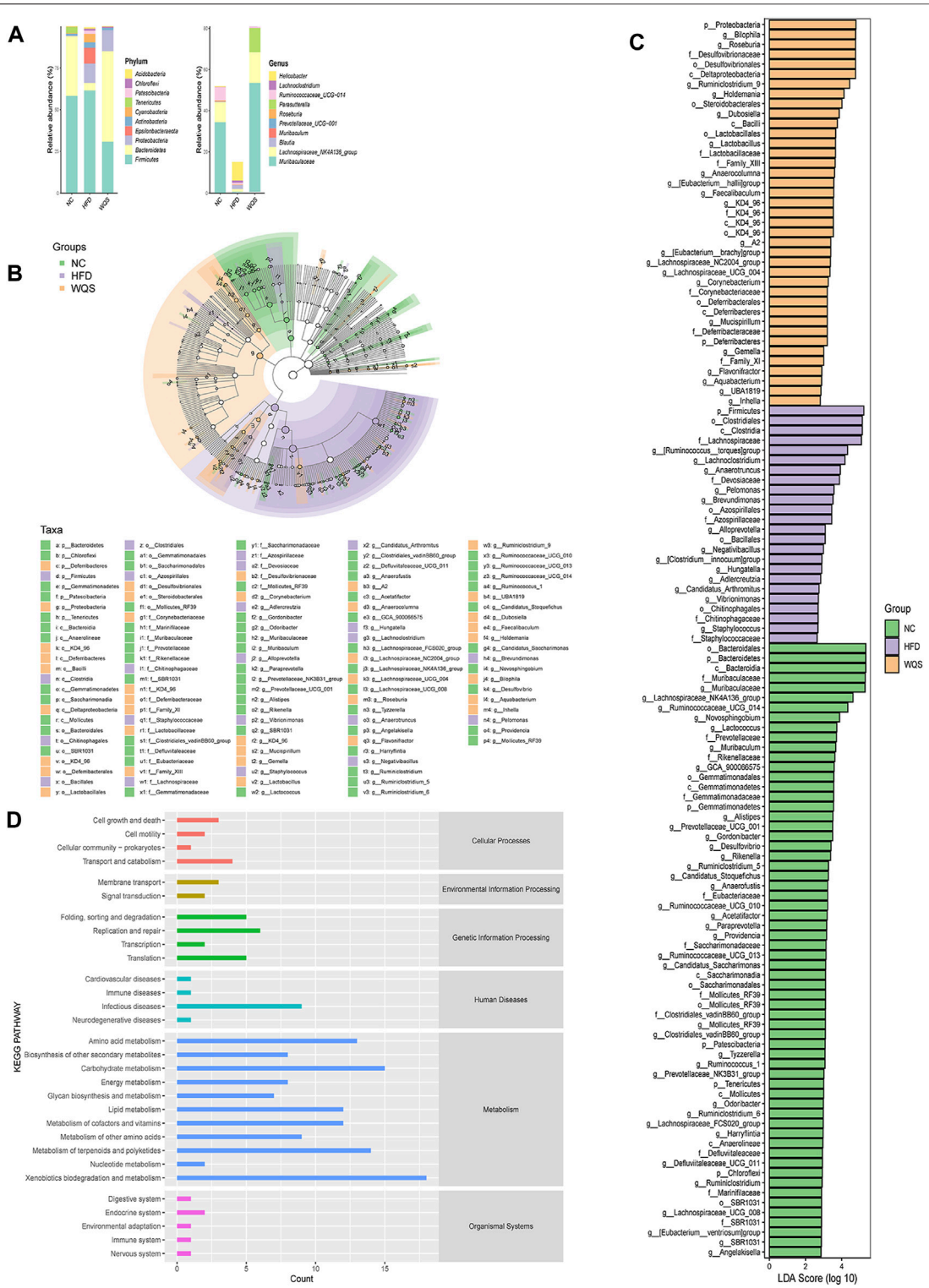

FIGURE 5 | Effects of WQS on the changes of gut microbial composition and identification of most characteristic taxa among groups by linear discriminant analysis (LDA) effect size (LEfSe). **(A)** Composition of the microbial community at the phylum and genus level; **(B)** Most significant difference in gut microbial taxa between groups after LDA. The threshold on the logarithmic LDA score for discriminative features was set to 4.0. The length of the bar of the LDA represents the influence of species abundance on the different effects. **(C)** Cladogram visualizing the output of the LEfSe analysis. (c, class; f, family; g, genus; o, order; p, phylum). **(D)** KEGG pathway enrichment.

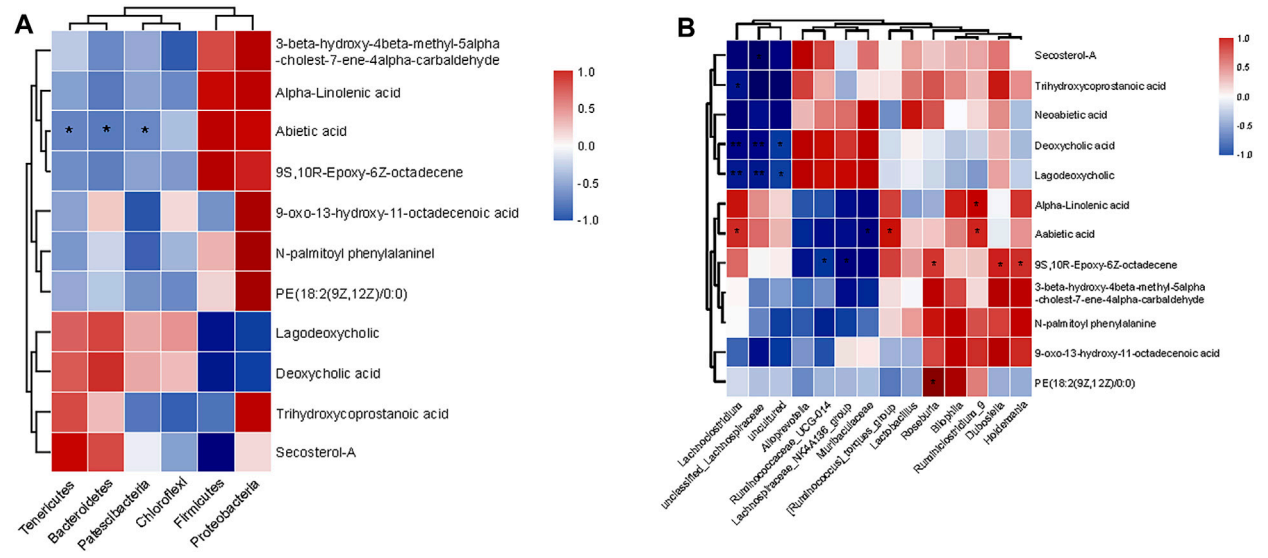

FIGURE 6 | Spearman's correlation between the identified metabolites and microbiota at different levels. **(A)** Correlation at the phylum level. **(B)** Correlation at the genus level.

established a mouse model with hyperlipidemia (Burdge, 2006) and then orally administered WQS to observe changes in metabolism and intestinal bacteria in mice, and the relationship between them, revealing an underlying mechanism of alleviation of hyperlipidemia.

The hyperlipidemia mice model induced by HFD to simulate the clinical situation of patients with hyperlipidemia. ApoE−/− mice fed with a high-fat diet are indeed susceptible to hyperlipidemia were corresponding to previous reports (Fazio and Linton, 2001). By measuring the contents of blood lipids, including TC, TG, and LDL-C, we found that these index in mice fed with a high-fat diet was significantly increased compared with the control group, which proved that the hyperlipidemia mice model was established successfully. However, compared with those of the HFD group, TC and LDL-C levels decreased significantly in the WQS group. Moreover, TG levels decreased but there was no statistical difference. In particular, WQS has a significant decreased the level of TC, a typical hyperlipidemic indicator. All these results confirmed the lipid-lowering effect of WQS. It is worth mentioning that ellagic acid from *Punica granarum* (Ge et al., 2021), piperine and quercetin from *Piper longum* (Yadav et al., 2020) have been reported to have good lipid-regulating effects in WQS.

Through serum metabolomic analysis, we identified some metabolites associated with lipid metabolism in the serum of mice treated with WQS. The cluster analysis results showed that the main differential metabolite pathway was the α-linolenic acid and linoleic acid metabolism pathway in different groups. Linoleic acid (LNA), commonly referred to as omega-6 fatty acid, is a polyunsaturated fatty acid (PUFA) precursor of the longer n-6 fatty acid (Huang, 2006). PUFA α-linoleic acid (ALA) is also a precursor of n-3 fatty acids, called omega-3 fatty acids (Yue et al., 2020). Previous research reported that daily use of α-linolenic acid (ALA) can improve blood lipids in healthy non-obese men and women (Burak et al., 2019). Furthermore, the ALA diet improves blood lipid profile by reducing the levels of TG, TC, LDL, and VLDL-C in patients with hyperlipidemia or hyperglycemia. On the one hand, ALA can reduce the content of cholesterol in plasma and the liver by regulating cholesterol reverse transport (RCT) (Andersen and Fernandez, 2013). On the other hand, it can reduce cholesterol production by inhibiting the activity and mRNA expression of HMG-CoA reductase (Das, 2006). Furthermore, another report showed that ALA significantly decreases liver weight, liver cholesterol levels, and expression of cholesterol synthase (farnesyl pyrophosphate synthase) associated with hyperlipidemia (O'Reilly et al., 2020). There is some evidence that CLA promotes significant changes in HDL metabolism in the body, which has been shown to decrease plasma cholesterol levels and increase high-density lipoprotein levels in mice (den Hartigh, 2019). Moreover, CLA plays an important role in fat deposition in the liver and the development and improvement of insulin resistance (Moon et al., 2009). Interestingly, a report based on the foam cell model showed that CLA notably reduced the levels of both free and conjugated cholesterol, and the foam cell formation is via a PPARγ/LXRα-dependent regulation of cholesterol metabolism (Saini and Keum, 2018), which further confirms their specificity in atherosclerotic protection. Regulating the metabolism of these two fatty acids may be responsible for the effect of WQS on improving blood lipid status in hyperlipidemic mice.

As we all know, changes in the composition of the gut microbiota are closely related to some metabolic diseases, including hyperlipidemia and diabetes (He and You, 2020). In our results, the high-fat diet decreased intestinal bacteria diversity in mice, and the overall α-diversity was improved after WQS treatment in mice on the high-fat diet. Previous studies indicated that the diversity of gut microorganisms is beneficial to human health. The interaction between different types of intestinal flora

can prevent certain strains of gut bacteria from reaching the level of manipulation of the host, thus further preventing the invasion of pathogenic bacteria. In our research, the diversity and composition of the microbiota in the HFD group have changed, with the Firmicutes increased and the *Bacteroides* and Proteobacteria decreased, which is similar to the situation of gut microbiota in obesity (Alcock et al., 2014). The increased abundance of Firmicutes is associated with the accumulation of lipid droplets, promoting fatty acid uptake at the onset of obesity and atherosclerosis (He and You, 2020). Roseburia (Tamanai-Shacoori et al., 2017), Ruminiclostridium (Jo et al., 2021), and *Lactobacillus* (Teng et al., 2020), as beneficial taxa, have high relative abundance in the WQS group, which might be a characteristic parameter that helps to significantly adjust blood lipids and relieve metabolic syndrome. Therefore, we deduced that these bacteria associated with the WQS supplement might be beneficial in decreasing excess cholesterol metabolism and adjusting lipid metabolism disorders in mice.

The balance of intestinal bacteria is closely related to the normal metabolic state of the body. Therefore, we performed serum metabolomics combined with Spearman analysis to observe the correlation of the gut microbiota with serum metabolites. Firmicutes and Proteobacteria displayed negative correlations with ALA, and Bacteroidetes showed positive correlations with ALA. It means that the content of ALA increases with decreasing Firmicutes/Bacteroidetes (F/B) ratio, which may help reduce the effect of a high F/B ratio, such as hyperlipidemia and obesity (Stojanov et al., 2020). Similarly, at the genus level, many genera are strongly correlated with differential metabolites, indicating that intestinal bacteria are indeed involved in the regulation of remodeling metabolism with the WQS intervention. Thus, we deeded that the regulation of blood lipids by WQS is related to the gut microbiota, and changes in the gut microbiota cause fluctuations in the content of endogenous metabolites in hyperlipidemic mice. However, intestinal bacteria could not be identified accurately and adequately by 16 S rRNA sequencing at the species level based on the Illumina platform, and the active constituent of WQS is not clear. Further studies are required to analyze the active compound of WQS and its relationship with key microbial phylotypes and lipid metabolic parameters, and to clarify their biological activities and action mechanism.

5 CONCLUSION

In this study, we found that a high-fat diet in ApoE$^{-/-}$ mice can induce hyperlipidemia, the key strains of bacteria in the gut and serum metabolite had changed dramatically. In HFD-induced hyperlipidemic mice after the oral administration of WQS, their serum lipid profiles had shown improvement and the structure of the gut microbiota had been reshaped. There are thirteen endogenous metabolites in serum that were screened as biomarkers for regulating blood lipids, which have been associated with the alterations of the gut microbiota population. This study made us realize how the key intestinal bacteria strains and important metabolic biomarkers played a profound role in the procession of hyperlipidemia and provided rewarding information to discover new drugs for the treatment and prevention of hyperlipidemia. Although the lipid-lowering effect of WQS has been reported previously (Bai et al., 2017), it is to explain its underlying pharmacological mechanism from the insight of metabolomics and to explore the relationship of the intestinal flora with WQS in the treatment of hyperlipidemia for the first time. The finding of this research is helping further to explore the in-depth molecular mechanisms and promote WQS clinical application.

DATA AVAILABILITY STATEMENT

The datasets presented in this study can be found in online repositories. The names of the repository/repositories and accession number(s) can be found at: NCBI with BioProject ID PRJNA812319.

ETHICS STATEMENT

The animal study was reviewed and approved by the Medical Experimental Center, China Academy of Chinese Medical Sciences.

AUTHOR CONTRIBUTIONS

SG and CL conducted data collection and processing and wrote the manuscript; DS, MT, and ZG carried out experiments and collected the samples; ZL supervised all the experiments and edited the manuscript; and YT designed the entire study and received funding and edited the manuscript.

FUNDING

The work was supported by the Ministry of Science and Technology of China (Grant number 2018YFC1708202) and the National Natural Science Foundation of China (NSFC; Grant number 81274192). And the Natural Science Foundation of Tianjin (20JCQNJC00320).

SUPPLEMENTARY MATERIAL

The Supplementary Material for this article can be found online at: https://www.frontiersin.org/articles/10.3389/fphar.2022.842671/full#supplementary-material

REFERENCES

Alcock, J., Maley, C. C., and Aktipis, C. A. (2014). Is Eating Behavior Manipulated by the Gastrointestinal Microbiota? Evolutionary Pressures and Potential Mechanisms. *Bioessays* 36 (10), 940–949. doi:10.1002/bies.201400071

Andersen, C. J., and Fernandez, M. L. (2013). Dietary Approaches to Improving Atheroprotective HDL Functions. *Food Funct.* 4 (9), 1304–1313. doi:10.1039/c3fo60207a

Antons, K. A., Williams, C. D., Baker, S. K., and Phillips, P. S. (2006). Clinical Perspectives of Statin-Induced Rhabdomyolysis. *Am. J. Med.* 119 (5), 400–409. doi:10.1016/j.amjmed.2006.02.007

Bai, Q. (1992). *Encyclopedia of Chinese Medicine Mongolian Medicine*. Shanghai: Shanghai Scientific and Technical Publishers, 212.

Bai, Y. C., and Bao, G. H. (2017). Experimental Study on Blood Lipid-Lowering Efficacy of Mongolian Medicine Wuwei Qingzhuo Powder. *World Latest Med. Inf. Dig.* 17 (34), 191.

Burak, C., Wolffram, S., Zur, B., Langguth, P., Fimmers, R., Alteheld, B., et al. (2019). Effect of Alpha-Linolenic Acid in Combination with the Flavonol Quercetin on Markers of Cardiovascular Disease Risk in Healthy, Non-obese Adults: a Randomized, Double-Blinded Placebo-Controlled Crossover Trial. *Nutrition* 58, 47–56. doi:10.1016/j.nut.2018.06.012

Burdge, G. C. (2006). Metabolism of Alpha-Linolenic Acid in Humans. *Prostagl. Leukot. Essent. Fat. Acids* 75 (3), 161–168. doi:10.1016/j.plefa.2006.05.013

Commission, C. P. (2020). *Chinese Pharmacopoeia*, 1. Beijing, China: China Medical Science Press, 648.

Committee, C. A. D. G. R. J. (2016). Guidelines for Prevention and Treatment of Dyslipidemia in Chinese Adults (Reviced 2016). *Chin. circulation J.* 31 (10), 937–953.

Das, U. N. (2006). Biological Significance of Essential Fatty Acids. *J. Assoc. Physicians India* 54 (R), 309–319.

den Hartigh, L. J. (2019). Conjugated Linoleic Acid Effects on Cancer, Obesity, and Atherosclerosis: A Review of Pre-clinical and Human Trials with Current Perspectives. *Nutrients* 11 (2), 370. doi:10.3390/nu11020370

Fazio, S., and Linton, M. F. (2001). Mouse Models of Hyperlipidemia and Atherosclerosis. *Front. Biosci.* 6 (March), D515–D525. doi:10.2741/Fazio

Ge, S., Duo, L., Wang, J., GegenZhula, J., Yang, J., Li, Z., et al. (2021). A Unique Understanding of Traditional Medicine of Pomegranate, Punica Granatum L. And its Current Research Status. *J. Ethnopharmacol.* 271, 113877. doi:10.1016/j.jep.2021.113877

Hasgova, A. (2015). Effect of Mongolian Medicine Wuwei Qingzhuo Powder on Lipid Metabolism in Rats with Hyperlipidemia [J]. *Chin. J. Ethn. Med.* 21 (01), 37–38. doi:10.16041/j.cnki.cn15-1175.2015.01.028

He, Y. J., and You, C. G. (2020). The Potential Role of Gut Microbiota in the Prevention and Treatment of Lipid Metabolism Disorders. *Int. J. Endocrinol.* 2020, 8601796. doi:10.1155/2020/8601796

Hill, M. F., and Bordoni, B. (2021). *Hyperlipidemia*. StatPearls. Available at: https://connect.ebsco.com/s/article/Why-did-the-link-I-clicked-from-a-website-outsi.

Hu, C., and Xu, G. (2014). Metabolomics and Traditional Chinese Medicine. *TrAC Trends Anal. Chem.* 61, 207–214. doi:10.1016/j.trac.2014.06.007

Jo, J. K., Seo, S. H., Park, S. E., Kim, H. W., Kim, E. J., Kim, J. S., et al. (2021). Gut Microbiome and Metabolome Profiles Associated with High-Fat Diet in Mice. *Metabolites* 11 (8), 482. doi:10.3390/metabo11080482

Kapoor, R., and Huang, Y.-S. (2006). Gamma Linolenic Acid: An Antiinflammatory Omega-6 Fatty Acid. *Curr. Pharm. Biotechnol.* 7 (6), 531–534. doi:10.2174/138920106779116874

Karr, S. (2017). Epidemiology and Management of Hyperlipidemia. *Am. J. Manag. Care.* 23 (9 Suppl. l), S139.

Kumar, S., Kamboj, J., Suman, S., and Sharma, S. (2011). Overview for Various Aspects of the Health Benefits of Piper Longum Linn. Fruit. *J. Acupunct. Meridian Stud.* 4 (2), 134–140. doi:10.1016/S2005-2901(11)60020-4

Lazar, V., Ditu, L. M., Pircalabioru, G. G., Picu, A., Petcu, L., Cucu, N., et al. (2019). Gut Microbiota, Host Organism, and Diet Trialogue in Diabetes and Obesity. *Front. Nutr.* 6, 21. doi:10.3389/fnut.2019.00021

Li, J., Wang, C., Song, L., Cai, S., Li, Z., and Tu, Y. (2020). The Potential Mechanism of Wuwei Qingzhuo San against Hyperlipidemia Based on TCM Network Pharmacology and Validation Experiments in Hyperlipidemia Hamster. *Evidence-Based Complementary Altern. Med.* 2020, 1–14. doi:10.1155/2020/5369025

Lozupone, C., and Knight, R. (2005). UniFrac: a New Phylogenetic Method for Comparing Microbial Communities[J]. *Applied and Environmental Microbiology* 71 (12), 8228–8235.

Mach, F., Baigent, C., Catapano, A. L., Koskinas, K. C., Casula, M., Badimon, L., et al. (2019). 2019 ESC/EAS Guidelines for the Management of Dyslipidaemias: Lipid Modification to Reduce Cardiovascular Risk. *Russ. J. Cardiol.* 25, 3826–4205. doi:10.15829/1560-4071-2020-3826

Moon, H. S., Lee, H. G., Seo, J. H., Chung, C. S., Kim, T. G., Choi, Y. J., et al. (2009). Antiobesity Effect of PEGylated Conjugated Linoleic Acid on High-Fat Diet-Induced Obese C57BL/6J (Ob/ob) Mice: Attenuation of Insulin Resistance and Enhancement of Antioxidant Defenses. *J. Nutr. Biochem.* 20 (3), 187–194. doi:10.1016/j.jnutbio.2008.02.001

Nelson, R. H. (2013). Hyperlipidemia as a Risk Factor for Cardiovascular Disease. *Prim. Care* 40 (1), 195–211. doi:10.1016/j.pop.2012.11.003

O'Reilly, M. E., Lenighan, Y. M., Dillon, E., Kajani, S., Curley, S., Bruen, R., et al. (2020). Conjugated Linoleic Acid and Alpha Linolenic Acid Improve Cholesterol Homeostasis in Obesity by Modulating Distinct Hepatic Protein Pathways. *Mol. Nutr. food Res.* 64 (7), e1900599. doi:10.1002/mnfr.201900599

Rognes, T., Flouri, T., Nichols, B., Quince, C., and Mahé, F. (2016). VSEARCH: a Versatile Open Source Tool for Metagenomics. *PeerJ* 4, e2584. doi:10.7717/peerj.2584

Saini, R. K., and Keum, Y. S. (2018). Omega-3 and Omega-6 Polyunsaturated Fatty Acids: Dietary Sources, Metabolism, and Significance - A Review. *Life Sci.* 203, 255–267. doi:10.1016/j.lfs.2018.04.049

Sathasivam, S. (2012). Statin Induced Myotoxicity. *Eur. J. Intern. Med.* 23 (4), 317–324. doi:10.1016/j.ejim.2012.01.004

Stojanov, S., Berlec, A., and Štrukelj, B. (2020). The Influence of Probiotics on the Firmicutes/Bacteroidetes Ratio in the Treatment of Obesity and Inflammatory Bowel Disease. *Microorganisms* 8 (11), 1715. doi:10.3390/microorganisms8111715

Tamanai-Shacoori, Z., Smida, I., Bousarghin, L., Loreal, O., Meuric, V., Fong, S. B., et al. (2017). Roseburia spp.: a Marker of Health? *Future Microbiol.* 12 (2), 157–170. doi:10.2217/fmb-2016-0130

Teng, Y., Wang, Y., Tian, Y., Chen, Y.-y., Guan, W.-y., Piao, C.-h., et al. (2020). Lactobacillus Plantarum LP104 Ameliorates Hyperlipidemia Induced by AMPK Pathways in C57BL/6N Mice Fed High-Fat Diet. *J. Funct. Foods* 64, 103665. doi:10.1016/j.jff.2019.103665

Wang, P. X., Deng, X. R., Zhang, C. H., and Yuan, H. J. (2020). Gut Microbiota and Metabolic Syndrome. *Chin. Med. J. Engl.* 133 (7), 808–816. doi:10.1097/CM9.0000000000000696

Yadav, V., Krishnan, A., and Vohora, D. (2020). A Systematic Review on Piper Longum L.: Bridging Traditional Knowledge and Pharmacological Evidence for Future Translational Research. *J. Ethnopharmacol.* 247, 112255. doi:10.1016/j.jep.2019.112255

Yue, H., Qiu, B., Jia, M., Liu, W., Guo, X. F., Li, N., et al. (2020). Effects of α-linolenic Acid Intake on Blood Lipid Profiles : a Systematic Review and Meta-Analysis of Randomized Controlled Trials. *Crit. Rev. Food Sci. Nutr.* 1-17, 1–17. doi:10.1080/10408398.2020.1790496

Zhang, L. W., and Chang, F. H. (2015). Research Progress on Hypolipidemic Effect of Chinese and Mongolian Medicine. *North. Pharm.* 12 (02), 84–85.

Conflict of Interest: The authors declare that the research was conducted in the absence of any commercial or financial relationships that could be construed as a potential conflict of interest.

The reviewer MW declared a shared parent affiliation with the authors SG, CL, YT to the handling editor at the time of review.

frontiers | Frontiers in Pharmacology

ORIGINAL RESEARCH
published: 05 July 2022
doi: 10.3389/fphar.2022.888522

Total Barley Maiya Alkaloids Prevent Increased Prolactin Levels Caused by Antipsychotic Drugs and Reduce Dopamine Receptor D2 *via* Epigenetic Mechanisms

Yu-Ling Cao[1,2†], Li -Zhu[1†], Hong Zhang[1,2], Jun-Hua Meng[1], Hua-Jun Wu[1], Xiong Wang[1], Jin-Hu Wu[1], Ji-Li Zou[1], Mao-Sheng Fang[3], Jing An[1] and Yong-Gang Chen[1]**

[1]Pharmacy Department of Wuhan University Tongren Hospital (The Third Hospital of Wuhan), Wuhan, China, [2]Medical College of Wuhan University of Science and Technology, Wuhan, China, [3]Department of Psychiatry, Wuhan Mental Health Center, Wuhan, China

OPEN ACCESS

Edited by:
Michael Heinrich,
University College London,
United Kingdom

Reviewed by:
Shelini Surendran,
University of Surrey, United Kingdom
Mohammad Safiqul Islam,
Noakhali Science and Technology
University, Bangladesh

***Correspondence:**
Jing An
503771136@qq.com
Yong-Gang Chen
cyg508@163.com

†These authors have contributed equally to this work and share first authorship

Specialty section:
This article was submitted to Ethnopharmacology, a section of the journal Frontiers in Pharmacology

Received: 03 March 2022
Accepted: 07 June 2022
Published: 05 July 2022

Citation:
Cao Y-L, -Zhu L, Zhang H, Meng J-H, Wu H-J, Wang X, Wu J-H, Zou J-L, Fang M-S, An J and Chen Y-G (2022) Total Barley Maiya Alkaloids Prevent Increased Prolactin Levels Caused by Antipsychotic Drugs and Reduce Dopamine Receptor D2 via Epigenetic Mechanisms. Front. Pharmacol. 13:888522. doi: 10.3389/fphar.2022.888522

Background: The dopamine D2 receptor (DRD2) plays an important role in the increased prolactin (PRL) levels associated with the pathogenesis of antipsychotic drugs (ADs). Elevated prolactin levels can affect people's quality of life. Maiya alkaloids has been used to treat diseases associated with high PRL levels. Maiya, is a processed product of the mature fruits of Hordeum vulgare L. (a gramineous plant) after sprouting and drying and also a common Chinese herbal drug used in the clinic, is traditionally used to treat abnormal lactation, and is currently used clinically for the treatment of abnormal PRL levels.

Aims: Epigenetic mechanisms can be related to DRD2 expression. We investigated the role of DRD2 methylation in the induction of PRL expression by ADs and the mechanism underlying the effects of total barley maiya alkaloids (TBMA) on this induction.

Methods: The methylation rate of DRD2 in 46 people with schizophrenia who took risperidone was detected by MassARRAY sequencing. Humans were long term users of Ris. Seventy Sprague Dawley female rats were divided into seven groups. A rat model of risperidone-induced PRL was established, and the potential protective effects of TBMA and its components [e.g., hordenine (Hor)] on these increased PRL levels were investigated. The PRL concentration was detected by Enzyme-linked immunosorbent assay. PRL, DRD2, and DNA methyltransferase (DNMT1, DNMT3α, and DNMT3β) protein and mRNA expression were detected by western blotting and real-time polymerase chain reaction (RT-PCR), respectively. The positive rate of methylation in the DRD2 promoter region of rats was detected by MassARRAY sequencing.

Results: Clinical studies showed that the positive rate of DRD2 methylation associated with increased PRL levels induced by ADs was significantly higher than in the normal prolactinemia (NPRL) group. *In vivo* and vitro, TBMA and Hor inhibited this induction of PRL expression and increased DRD2 expression by inhibiting the expression of the DNMTs.

Conclusions: TBMA and hordenine increased DRD2 expression by inhibiting DNMT-dependent DRD2 methylation.

Keywords: antipsychotic drugs, total barley maiya alkaloids, dopamine D2 receptor, DNA methylation, prolactin

INTRODUCTION

Schizophrenia is among the global most disabling health conditions (Lee et al., 2016) and affects about 21 million people worldwide (Vos et al., 2016; Li et al., 2018; Jung et al., 2021). People with schizophrenia have a life expectancy 15 years shorter than the general population (Pillinger et al., 2019; Lobo et al., 2021). Antipsychotic drugs (ADs) and psychological consultation are commonly used to treat schizophrenia. However, ADs can cause many side effects, particularly causing an abnormal increase in prolactin (PRL), with an incidence rate as high as 70% (Bostwick et al., 2009; Alosaimi et al., 2018). This increase is often accompanied by amenorrhea, galactorrhea, and infertility (Bostwick et al., 2009), seriously affecting the quality of life.

Previous studies focused on the pathogenesis of PRL increases induced by ADs (Huang et al., 2020). However, given the exacerbated severity of PRL increase caused by ADs, the epigenetic mechanisms involved in this pathogenesis have become an area of interest. DNA methylation is catalyzed by DNA methyltransferases (DNMTs) (Huang et al., 2020) and regulates a variety of biological and pathological processes (Stresemann et al., 2006; Hamidi et al., 2015). DNA methylation is mainly observed in CpG islands and strongly correlates with transcriptional suppression (Antequera and Bird, 1993; Horii and Hatada, 2016). During DNA methylation, methyl groups are transferred by DNA methyltransferases, including DNMT1, DNMT2, DNMT3α, DNMT3β, DNMT3C, and DNMT3L (Robertson, 2001; Barau et al., 2016). DNMT1, DNMT3α, and DNMT3β are the major DNA methyltransferases in animals, maintaining methylation on hemimethylated CpG sites (Borowczyk et al., 2009). DRD2, a regulator of transcriptional responses, modulates PRL expression in the pituitary gland. Therefore, DRD2 inactivation or mutations decreasing DRD2 mRNA or protein expression can result in PRL accumulation, activating PRL transcriptional programs (Céspedes, 2017; Gerra et al., 2021). The noncoding region of DRD2 contains CGG repeat sequences that provide a foundation for methylation. Previous studies revealed that CpG hypermethylation of DRD2 leads to gene inactivation and loss of function in alcohol-exposed rats (Gangisetty et al., 2015). Emerging evidence has demonstrated that DRD2 expression is tightly regulated by DNA methylation. Several studies have reported that the DRD2 methylation rate increases with decreasing DRD2 expression (Tan et al., 2021).

Risperidone (Ris) is a common antipsychotic drug used for treating schizophrenia; however, increases in PRL levels are common after long-term administration, leading to serious adverse reactions, such as amenorrhea, galactorrhea, anovulation and infertility (Zhu et al., 2021). In addition, opioids (Demarest et al., 2015), estrogen (Ni et al., 2021), and contraceptives (Taşkömür and Erten 2021) can increase PRL levels. We hypothesized that the increased PRL levels associated with these drugs and hormones might be related to DRD2 methylation because clinical data showed that AD-induced increases in PRL levels are associated with DRD2 methylation. In China, bromocriptine (Bro), a DRD2 agonist, is the first choice for the clinical treatment of the elevated PRL levels caused by ADs; however, this treatment is accompanied by hallucinations, conscious insanity, digestive system disorders, and other adverse reactions (Chen et al., 2017). Therefore, more suitable therapeutic drugs are needed.

Multiple studies have shown that maiya is an edible traditional Chinese medicine for treating digestive disorders and abnormal PRL levels with fewer side effects than bromocriptine. In a preliminary study, we extracted total barley maiya alkaloids (TBMA) from maiya and found that hordenine (Hor) accounted for 8.58% of the active components in the TBMA (Tao et al., 2021). Previous studies confirmed that TBMA and hordenine were the active ingredients reducing PRL and regulating lactation. In addition, we have shown that TBMA and hordenine can inhibit abnormal PRL secretion by upregulating DRD2 expression (Gong et al., 2021). However, the epigenetic mechanism by which TBMA inhibits PRL secretion and the increased PRL levels associated with ADs has not been clarified. The current study investigated the epigenetic mechanism of PRL inhibition by evaluating the active components in maiya (i.e., TBMA and Hor). To this end, we used a Ris-induced increased PRL rat model and MMQ cells to explore whether TBMA and hordenine could alter DRD2 or its methylation status.

MATERIALS AND METHODS

Human Subjects

This study was comprised of 46 schizophrenic patients taking Ris for a long time. The study has received ethical approval

TABLE 1 | Demographic and clinical characteristics of the two groups.

	HPRL (n = 24)	NPRL (n = 22)	p
Females (n/%)	17 (70.8)	13 (59%)	0.465
Age (years)	31.3 ± 1.26	28.11 ± 3.76	0.154
BMI ($kg{\cdot}m^{-2}$)	20.45 ± 2.16	21.35 ± 5.1	0.732
PRL level before Ris (ng/mL^{-})	16.32 ± 4.39	19.44 ± 5.16	0.231
PRL level after Ris ($ng{\cdot}mL^{-1}$)	83.21 ± 11.19	21.56 ± 1.77	**0.00018*****
Ris dose (mg/day)	3.53 ± 0.97	2.16 ± 1.01	0.79
Smoking (years/%)	2 (8)	5 (22.7)	0.452
Drinking (years/%)	1 (4)	2 (9)	0.112
Psychiatric history (years/%)	16 (66.7)	13 (59)	0.543

Note: Values denote the mean ± standard deviation.

from Pharmacy Department of Wuhan University Tongren Hospital (The Third Hospital of Wuhan). The patients were divided into high PRL level (HPRL) and normal PRL level (NPRL) groups. Normal PRL levels were 2.64–13.13 ng/ml in males and 3.34–26.72 ng/ml in premenopausal females (<50 years). The demographic data of the subjects are provided in **Table 1**. The mean age of the participants is 29.24 ± 2.57. Venous blood samples (200 μl) were collected from the subjects, and genomic DNA was extracted. The DNA solutions were kept at −80°C prior to analysis.

Chemicals and Reagents

The following chemicals and reagents were used in this study: raw maiya (batch number: 20200501, Hubei Pingpong Hongkang Traditional Chinese Medicine Decoction Pieces Co., Ltd., China); TBMA [prepared using a previously established TBMA extraction and purification method (21)], purity: 65.7%; hordenine [$C_{10}H_{15}NO$, MW:165.24, Aladdin Reagent (Shanghai) Co., Ltd., China], purity: ≥99%; Bro ($C_{33}H_{44}BrN_5O_8S$, MW: 750.7, MedChemExpress, United States), purity: >99.98%; Ris (batch number: KFB6W00A, Xian Janssen Pharmaceutical Co., Ltd., China.); 5-Aza-2′deoxycytidine ($C_8H_{12}N_4O_4$, MW:228.21, MedChemExpress, United States), purity: 99.93%.

Animal Model

Specific-pathogen-free (SPF) female Sprague Dawley (SD) rats (200 ± 20 g) were purchased from the Experimental Animal Center of Three Gorges University [Hubei, China; Grant No. SYXK(E)2020–0080]. The experimental protocol was approved by the Ethics Committee of The Third Hospital of Wuhan. All animal experiments complied with the Animal Research: Reporting of *In Vivo* Experiments guidelines and were conducted according to the National Institutes of Health Guide for the Care and Use of Laboratory Animals (NIH Publications No. 8023, revised 1978).

TABLE 2 | The sequences of the real-time PCR primers.

Gene	Sequence
GAPDH	Forward primer: 5′- GACATGCCGCCTGGAGAAAC-3′
	Reverse primer: 5′- AGCCCAGGATGCCCTTTAGT-3′
PRL	Forward primer: 5′- GGTTTGGTCACAACTCCCATCCC -3′
	Reverse primer: 5′- TGGACAATTTGGCACCTCAGGAAC -3′
DRD2	Forward primer: 5′- AAGACGATGAGCCGCAGAAAGC -3′
	Reverse primer: 5′- AGCAGATGATGAACACACCGAGAAC -3′
DNMT1	Forward primer: 5′- TGTTCCTCCTTCTGCCATCAATGTG -3′
	Reverse primer: 5′- CATCGTCCTTAGCGTCGTCGTAAC -3′
DNMT3α	Forward primer: 5′- CGTCACACAGAAGCATATCCAGGAG -3′
	Reverse primer: 5′- CAGGAGGCGGTAGAACTCAAAGAAG -3′
DNMT3β	Forward primer: 5′- GATGGAGATGGTGAAGCGGATGATG -3′
	Reverse primer: 5′- AGGCTGGAGATACTGTTGCTGTTTC -3′

Animal Groups and Drug Administration

Chronic treatment with Ris (0.1 mg/kg/day) causes increased PRL levels in Sprague-Dawley rats (Wang et al., 2018). Bro is a well-known dopamine agonist that suppresses pituitary PRL release in MMQ cells and improves antipsychotic-induced PRL levels in rats (Miranda and Jones, 2007; Bernard et al., 2015; Wei et al., 2017; Zhou et al., 2018; Bernard et al., 2019). It served as a positive control for this study. Seventy rats were randomly assigned into seven treatment groups as follows: 1) blank control, 2) Ris, 3) Ris + Bro (5 mg/kg), Ris + Hor (5 mg/kg), Ris + N-Methyltyramine (N-Methy) (5 mg/kg), Ris + TBMA (3.6 mg/kg), Ris + TBMA (7.2 mg/kg) (n = 10). Ris (0.1 mg/kg) was administered orally at 9:00 a.m. The control group was given a 5% gum arabic solution. Bro, Hor, N- Methy, and TBMA were given orally to their corresponding groups 2 h after Ris administration. Treatment with Ris and the other agents was

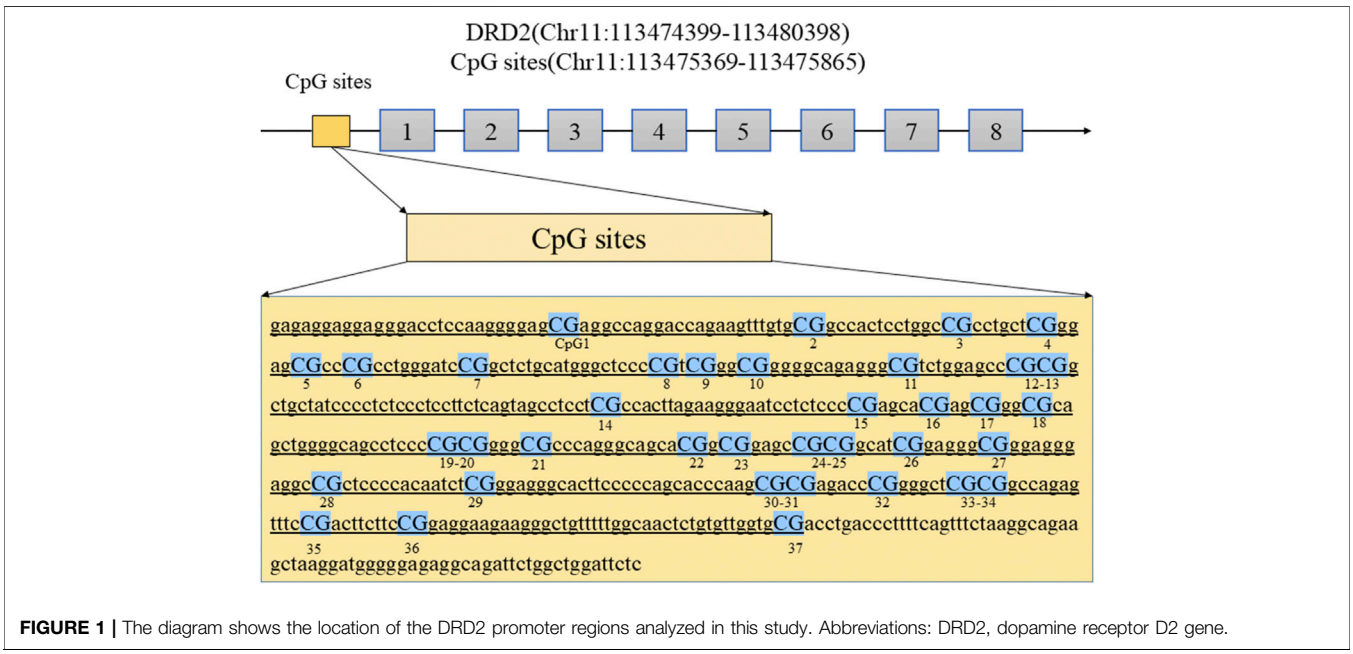

FIGURE 1 | The diagram shows the location of the DRD2 promoter regions analyzed in this study. Abbreviations: DRD2, dopamine receptor D2 gene.

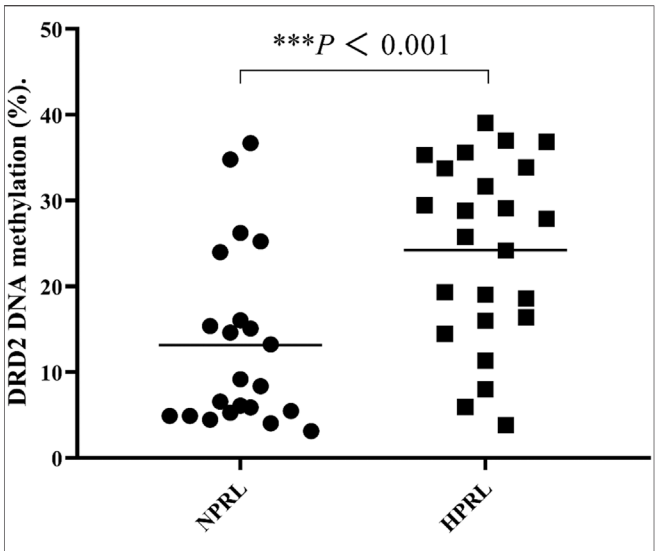

FIGURE 2 | Comparisons of DRD2 DNA methylation (%) between HPRL and NPRL subjects. Each bar represents the mean ± standard error (***p < 0.001 versus NPRL).

performed once daily for 8 weeks. At week 7, fasting blood was collected. At week 8, all animals were fasted and then euthanized by cervical dislocation under anesthesia. The pituitary glands were collected, flash-frozen in liquid nitrogen, and stored at −80°C.

Cell Culture and Treatment Groups

MMQ rat pituitary tumor cells were purchased from Beijing Beina Chuanglian Biotechnology Institute. These cells secrete prolactin and express dopamine receptors and are, thus, an ideal *in vitro* cell model system for our study. The cells (1×10^5) were seeded in 6-well plates. After 24 h, the cells were the treated with Bro, Hor, or TBMA for 72 h. The DNMT inhibitor 5′-AZA was also used to establish the DNMT low-expression cell model.

Enzyme-Linked Immunosorbent Assay

Blood samples were collected retro-orbitally from the rats. The PRL ELISA kit was purchased from LunChangShuo Biotech (Cat. # SU-B30285, Xiamen, China).

Real-Time Fluorescence Quantitative PCR

Total RNA was extracted from the frozen pituitary samples using the Total RNA Kit (batch number: R6934010000C17U031, Omega). cDNA was synthesized using the SweScript RT I First Strand cDNA Synthesis Kit with gDNA Remove). mRNA expression was measured using the Stratagene Mx 3000P Real-Time PCR system (Agilent Technologies, CA, United States). Relative expression was calculated using the $2^{-\Delta\Delta Ct}$ method. All

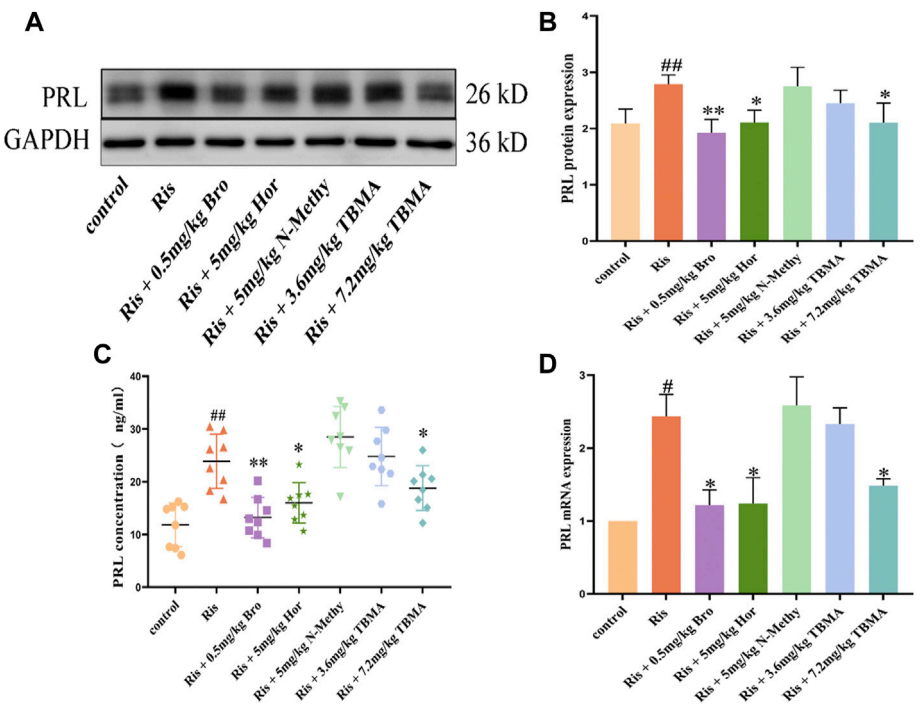

FIGURE 3 | Effects of TBMA, hordenine, and N-methyltyramine on PRL expression. **(A,B)** PRL protein expression determined by western blotting using GAPDH as a loading control. Data are presented as the mean ± SD (n = 3 rats per group). **(C)** PRL concentrations detected by ELIA (n = 8). **(D)** PRL mRNA expression. mRNA expression was determined using RT-PCR (n = 3 rats per group; $^{\#}p < 0.05$ and $^{\#\#}p < 0.01$ versus the control group; $^{*}p < 0.05$ and $^{**}p < 0.01$ versus the Ris group. Bro = bromocriptine; Hor = hordenine; N-Methy = N-methyltyramine; Ris = risperidone; TBMA = total barley maiya alkaloids.

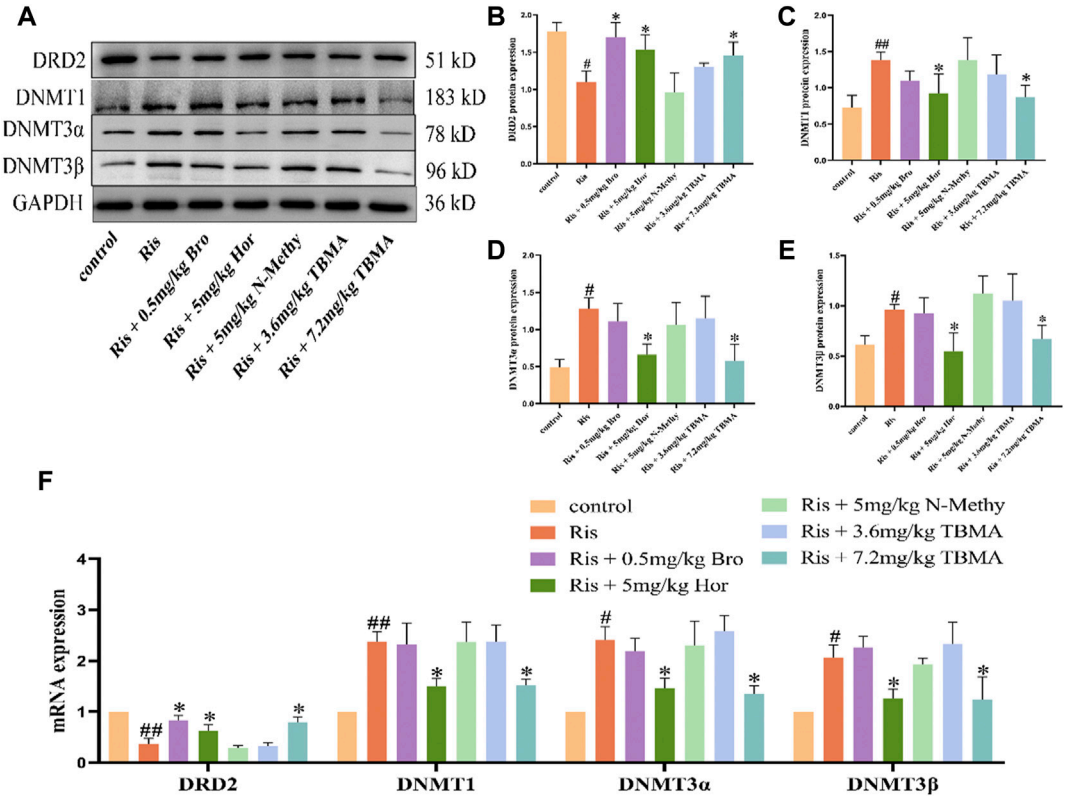

FIGURE 4 | Effects of TBMA, hordenine, and N-methyltyramine on DRD2 and DNMT expression. **(A–E)** DRD2, DNMT1, DNMT3α, and DNMT3β protein expression. GAPDH was used as a loading control. **(F)** DRD2, DNMT1, DNMT3α, and DNMT3β mRNA expression. Data are presented as the mean ± SD. Protein expression in each group was determined using western blotting. mRNA expression in each group was determined using RT-PCR ($n = 3$ rats per group; $^{\#}p < 0.05$ and $^{\#\#}p < 0.01$ versus the control group; $^{*}p < 0.05$ versus the Model group. Bro = bromocriptine; Hor = hordenine; N-Methy = N-methyltyramine; Ris = risperidone; TBMA = total barley maiya alkaloids.

values were normalized to the expression of the housekeeping gene GAPDH. The primer sequences are listed in **Table 2**.

Western Blot Analysis

PRL, DRD2, and DNMTs protein levels in the pituitary samples were determined by western (WB) blot analysis, as previously described (Gong et al., 2021). The antibodies used in this experiment were anti-PRL (1:6000, Affinity, United States), anti-DRD2 (1:1000, Wuhan Proteintech Co., Ltd., China), anti-DNMT1 (1:1000, Wuhan Proteintech Co., Ltd., China), anti-DNMT3α (1:1000, Affinity, United States), and anti-DNMT3β (1:1000, ABclonal, China).

MassARRAY Sequencing

MassARRAY sequencing was used to detect the methylation rate of DRD2. The CpG island of the DRD2 promoter region was sequenced by Huada Gene Technology Co., Ltd. (Beijing, China).

Statistical Analysis

Data are presented as the mean ± standard deviation (SD; normal distribution). Differences between groups were analyzed with the one-way analysis of variance (ANOVA) comparison test using SPSS 22.0 software (SPSS, Chicago, IL, United States). A p-value < 0.05 was considered statistically significant.

RESULTS

Comparison of DRD2 Methylation Rates Between HPRL and NPRL Subjects

Figure 1 illustrates the structure of the DRD2 promoter region with the CpG sites for methylation that may play a central role in gene silencing (**Figure 1**). The demographic data for each group of subjects are shown in **Table 1**. HPRL and NPRL subjects did not differ in sex, age, or BMI ($p > 0.05$). The results of the DRD2 methylation analysis following long-term risperidone monotherapy are shown in **Figure 2**. The positive rate of DRD2 methylation in the HPRL group was significantly higher than in the NPRL group ($p < 0.001$).

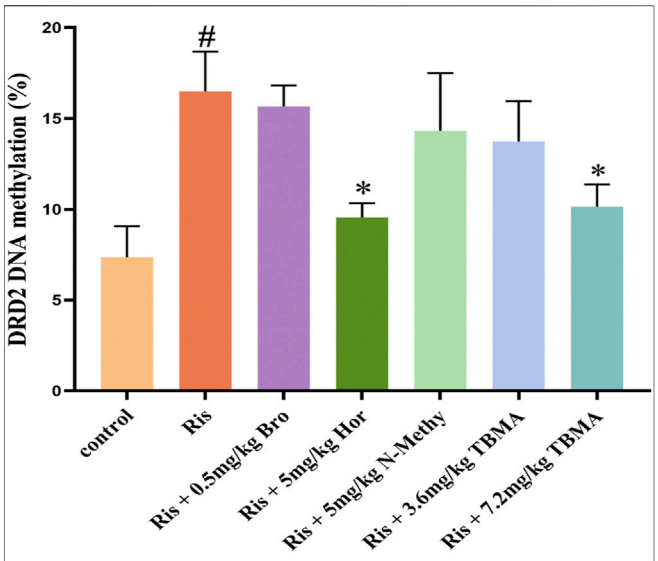

FIGURE 5 | DRD2 methylation status. Data are presented as the mean ± SD ($n = 3$ per group). ($^{\#}p < 0.05$ versus the control group; $^{*}p < 0.05$ versus the Ris group). Bro = bromocriptine; Hor = hordenine; N-Methy = N-methyltyramine; Ris = risperidone; TBMA = total barley maiya alkaloids.

Effects of TBMA and Hordenine on PRL in Ris Induced the PRL Level Increased Rats

Based on the clinical results, we established a rat model of elevated PRL levels by long-term administration of Ris to female rats. These rats were then treated with vehicle, Bro, Hor, N-Methy, or 3.6 mg/kg or 7.2 mg/kg TBMA. The ELISA results showed that Ris increased the fasting serum PRL concentration, and Hor and 7.2 mg/kg TBMA decreased the Ris-induced PRL concentrations (**Figure 3C**). After treatment with Bro, hordenine, or 7.2 mg/kg TBMA, PRL protein (**Figures 3A,B**) and mRNA (**Figure 3D**) expression levels were significantly decreased in the pituitary. In contrast, N-methyltyramine and 3.6 mg/kg TBMA did not affect PRL expression.

TBMA and Hordenine Reversed the Changes in PRL Levels Induced by Ris Concomitant With Decreased DRD2 Expression and Increased DNMTs Expression in the Pituitary

We examined the changes in DRD2 and DNMTs expression in each rat group. DRD2 mRNA expression was downregulated in the Ris group, whereas DNMT1, DNMT3α, and DNMT3β mRNA expression levels were upregulated. Compared to the Ris group, the DRD2 mRNA expression levels in the Ris + Hor (5 mg/kg) group and Ris + TBMA (7.2 mg/kg) group were significantly upregulated, while the mRNA expression levels of the DNMTs were significantly downregulated. Compared with the Ris group, the DRD2 mRNA expression was also significantly upregulated in the Ris + Bro (0.5 mg/kg) group; however, DNMT mRNA expression did not change. Moreover, DRD2 and DNMT mRNA expression did not change in the Ris +5 mg/kg N-methyl and Ris + TBMA (3.6 mg/kg) group (**Figure 4F**). The WB analysis results were consistent with the mRNA results (**Figures 4A–E**). Ris-induced PRL levels could reduce DRD2 levels and increase DNMT mRNA and protein levels in the rat pituitary. Furthermore, hordenine and 7.2 mg/kg TBMA could restore DRD2 levels and reduce DNMT expression. Bro could also increase DRD2 levels. N-methyl and 3.6 mg/kg TBMA had no significant effects on DRD2 or the DNMTs.

DRD2 Methylation Was Significantly Upregulated by Ris and Downregulated by TBMA and Hordenine

To clarify the mechanism underlying decreased DRD2 expression, we investigated whether DRD2 promoter hypermethylation was responsible for this downregulation using MassARRAY sequencing. Ris treatment enhanced DRD2 promoter methylation while significantly decreasing DRD2 expression. In contrast, 7.2 mg/kg TBMA and hordenine upregulated DRD2 expression levels by causing DRD2 promoter demethylation. However, Bro, N-methyltyramine, and 3.6 mg/kg TBMA did not have this effect. Together, these results suggest that the decreased DRD2 expression observed with Ris-induced increased PRL levels resulted from reversible methylation of the DRD2 promoter region (Figure **5**).

TBMA and Hordenine Protected MMQ Cells From Ris-Induced PRL Increased Levels and DRD2 Methylation

To verify the results obtained with the clinical samples and in rats, we further evaluated the effects of Ris, TBMA, and Hor *in vitro* using MMQ cells. Because N-methyltyramine had no effect *in vivo*, only TBMA and hordenine were studied *in vitro*. In this experiment, Ris (10, 20, and 40 μg/ml) was used to induce PRL levels in the MMQ cells. We found that 40 μg/ml Ris increased PRL expression, decreased DRD2 expression, and upregulated the expression levels of DNMT1, DNMT3α, and DNMT3β (**Figures 6A–C**). Treatment with 65.2 μg/ml TBMA or 6.5 μg/ml hordenine abrogated the effects of Ris on PRL, DRD2, and the DNMTs. The lower TBMA concentration had no effect (**Figures 6D–F**). These data were consistent with the rat data demonstrating that TBMA and hordenine could inhibit PRL expression by reversing DRD2 methylation induced by Ris.

The Effects of TBMA and Hordenine on DRD2 Methylation and PRL Expression Was Enhanced by Modulating DNMT Expression

5′AZA is an inhibitor of DNA methyltransferase. Treatment of MMQ cells with different concentrations of 5′ AZA (100 μM, 200 μM, and 400 μM) revealed that 400 μM 5′AZA significantly inhibited the expression of DNMT1, DNMT3α, and DNMT3β while increasing DRD2 levels and inhibiting PRL expression (**Figures 7A–C**). Therefore, 400 μM 5′AZA was selected for the subsequent experiment. Compared to the Ris +5′AZA

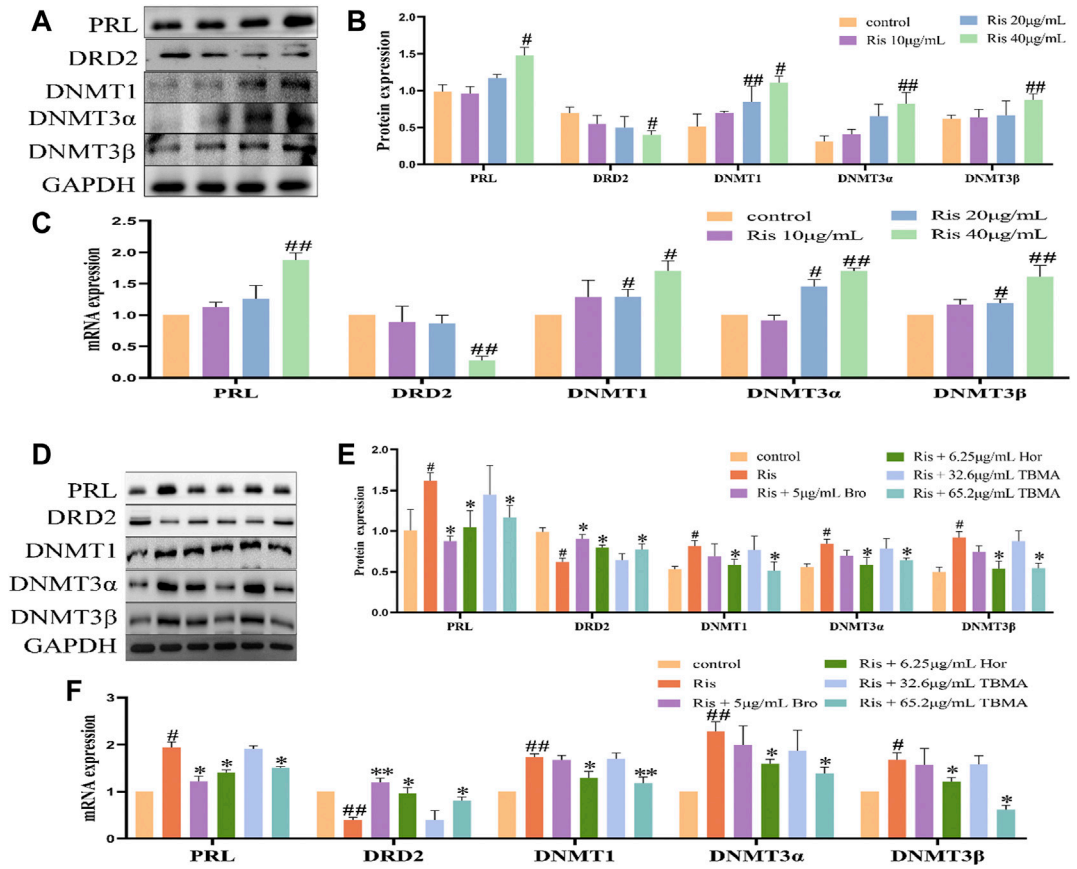

FIGURE 6 | TBMA and hordenine regulated DRD2 DNA methylation. **(A,B)** PRL, DRD2, and DNMT protein expression by western blotting following treatment with different risperidone concentrations ($n = 3$). **(C)** PRL, DRD2, and DNMT mRNA expression levels by RT-PCR following different risperidone concentrations ($n = 3$). **(D,E)** WB was used to detect PRL, DRD2, and DNMT protein expression by western blotting following TBMA or hordenine treatment of MMQ cells ($n = 3$). **(F)** was used to detect the mRNA levels of PRL, DRD2, and DNMT mRNA expression by RT-PCR following TBMA or hordenine treatment of MMQ cells ($n = 3$). Data are presented as the mean ± SD ($^{\#}p < 0.05$ and $^{\#\#}p < 0.01$ versus the control group; $^{*}p < 0.05$ and $^{**}p < 0.01$ versus the Ris group). Hor = hordenine; Ris = risperidone; TBMA = total barley maiya alkaloids.

group, the mRNA and protein expression levels of PRL and the DNMTs were decreased in the Ris +5′AZA +65.2 μg/ml TBMA and Ris +5′AZA +6.5 μg/ml Hor groups and DRD2 expression levels were increased (**Figures 7D–F**), further demonstrating that TBMA and hordenine could enhance DRD2 expression and decrease PRL expression through demethylation.

DISCUSSION

This study investigated the correlation between DRD2 methylation and the ability of TBMA and hordenine to modulate PRL levels increased by ADs. We found that the positive rate of DRD2 methylation in HPRL patients was significantly higher than in NPRL patients after long-term administration of Ris. Ris is a DRD2 antagonist that could reduce DRD2 expression in our studies, indicating that DNA methylation could increase PRL expression by reducing DRD2 expression. Previous studies demonstrated that TBMA and hordenine could inhibit PRL expression by restoring the expression of DRD2 (Gong et al., 2021). Our current study further revealed that TBMA and hordenine could increase DRD2 expression and reduce PRL levels through DRD2 promoter demethylation *in vivo* and *in vitro*. The methylation of specific genes has been associated with transcriptional inactivation (Suzuki and Bird, 2008). Therefore, DRD2 hypermethylation is consistent with the observed decrease in DRD2 expression.

ADs cause abnormal increases in PRL levels (Grigg et al., 2017; Molitch, 2020), which seriously affect the quality of life of patients. To overcome these increased PRL levels, patients are administered bromocriptine or have their dose of ADs reduced and combined with aripiprazole (Rusgis et al., 2021). However, bromocriptine has many adverse side effects, including neurological and digestive system disorders (Rusgis et al., 2021). Reducing the dose of ADs can lead to the recurrence of a patient's condition and affect treatment efficacy. When combined with aripiprazole, it will increase the burden of cognitive function in patients (Jiang et al., 2021). Therefore, the development of new drugs that reduce the increased PRL

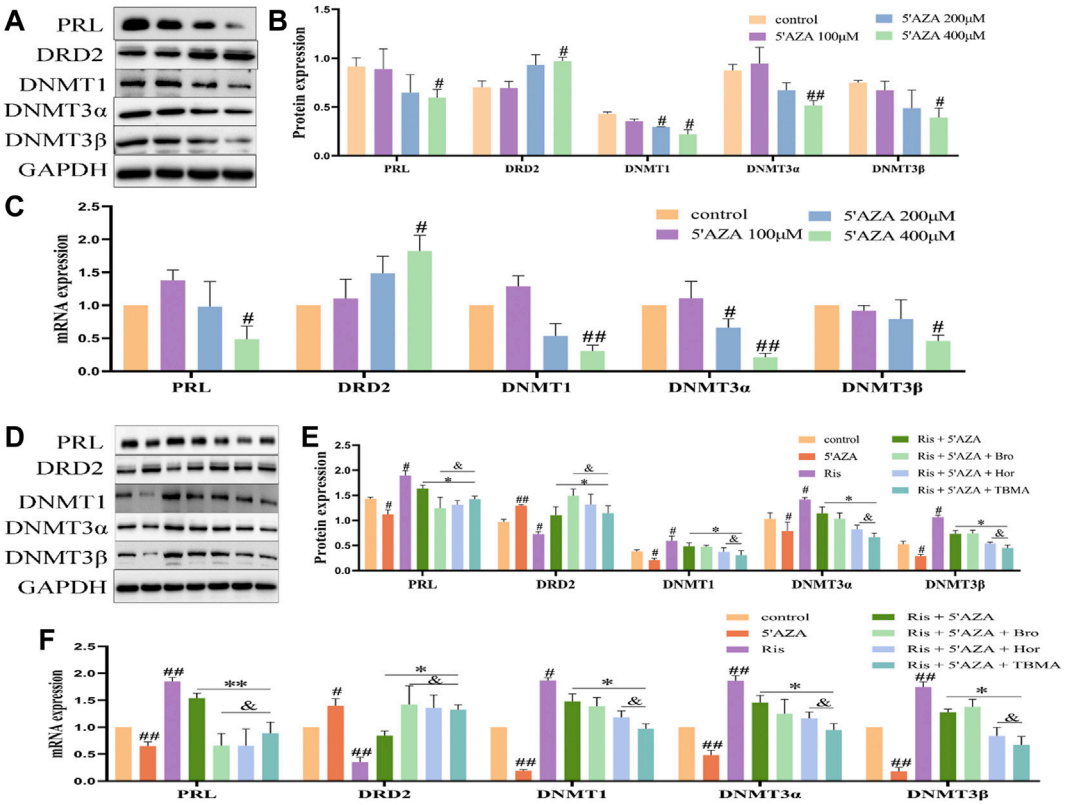

FIGURE 7 | The effects of TBMA and hordenine on DRD2 DNA methylation were enhanced by low DNMT expression levels. **(A,B)** PRL, DRD2, and DNMT protein expression by western blotting following treatment with different 5′AZA concentrations (n = 3). **(C)** PRL, DRD2, and DNMT mRNA expression by RT-PCR following treatment with different 5′AZA concentrations (n = 3; $^{*}p < 0.05$ and $^{**}p < 0.01$ versus the control group. **(D,E)** PRL, DRD2, and DNMT protein expression by western blotting following TBMA or hordenine treatment of MMQ cells (n = 3). **(F)** PRL, DRD2 and DNMT mRNA expression by RT-PCR following TBMA or hordenine treatment of MMQ cells (n = 3). Data are presented as the mean ± SD ($^{\#}p < 0.05$ and $^{\#\#}p < 0.01$ versus the control group; $^{*}p < 0.05$ and $^{**}p < 0.01$ versus the Ris group; $^{\&}p < 0.05$ versus the Ris +5′AZA group. 5′AZA = 5-Aza-2′-deoxycytidine; Hor = hordenine; Ris = risperidone; TBMA = total barley maiya alkaloids.

levels caused by ADs is needed to improve the quality of life of schizophrenic patients.

Epigenetic modifications are most commonly regulated by direct methylation of DNA or post-translational modifications of histones, both of which can promote or repress gene transcription (Asa and Ezzat, 1998; Yoshino et al., 2007). Epigenetic dysregulation, promoter methylation, and silencing of tumor suppressor genes are implicated in pituitary neoplasia (Asa and Ezzat, 1998). Pituitary tumorigenesis often involves genetic mutations in classical oncogenes or tumor suppressor genes (Asa and Ezzat, 2002; Thumfart et al., 2021). DRD2 methylation is closely related to children's psychological trauma (Cespedes et al., 2021) and alcohol dependence (Shirvani-Farsani et al., 2021) and is a marker of schizophrenia (Gangisetty et al., 2015; Molitch, 2020; Lisoway et al., 2021) showed that increased DRD2 promoter methylation is correlated with decreased DRD2 mRNA levels and increased PRL mRNA levels in the pituitary. Many studies have reported that the loss of DRD2 expression accelerates the increase in PRL levels caused by ADs (Gao et al., 2021). As an important active component of TBMA, hordenine has demonstrated agonistic effects on DRD2 improving DRD2 expression levels may be a significant approach to preventing AD-induced increases in PRL levels (Gong et al., 2021).

DNA methylation provides a new therapeutic approach for targeted inhibition of tumor factors and a possible way to overcome cancer drug resistance (Robertson, 2001). Current knowledge regarding the genetic and epigenetic regulation of DRD2 is mainly restricted to the oncology field (Tan et al., 2021). As such, this study is the first to investigate whether DRD2 methylation is involved in the underlying mechanisms of AD-induced increases in PRL levels. We detected the methylation rate of DRD2 in the pituitary of rats with increased PRL levels following treatment with the AD Ris. We found that the methylation rate in the CpG island of the DRD2 promoter region was increased by Ris but could be reversed by TBMA or hordenine treatment. We also found that the expression levels of DNMT1, DNMT3α, and DNMT1β were increased in rats with elevated PRL levels and Ris-treated MMQ cells. The DNMTs are responsible for transferring methyl groups from s-adenosine methionine to the 5′-position of cytosine residues in DNA (Stresemann et al., 2006). In particular, DNMT1 acts as a maintenance methyltransferase, whereas DNMT3α and DNMT3β are *de novo* methyltransferases (Edwards et al.,

2017). Thus, our study revealed that increased DNMT expression might lead to CpG methylation in the DRD2 promoter.

5′-AZA is a nucleoside-based DNMT inhibitor that induces demethylation and gene reactivation. It is a cytosine analog, which is metabolically activated *in vivo* and readily incorporated into DNA during replication (Christman, 2002). We used 5′-AZA to verify the role of DNMT-mediated methylation in regulating DRD2 expression. We found that 5′AZA caused demethylation of the DRD2 promoter and a significant increase in DRD2 expression, consistent with our hypothesis. By decreasing the expression of the DNMTs with 5′AZA, the protective effects of TBMA and hordenine were attenuated. Together, these results confirmed that TBMA and hordenine could improve DRD2 expression and reduce the secretion of PRL by inhibiting its expression mediated by the DNMTs, which is consistent with another study demonstrating that increased DRD2 promoter methylation in the rat pituitary is closely related to decreased DRD2 mRNA levels and increased PRL mRNA levels.

In this study, we found that the positive rate of DRD2 methylation in HPRL patients was significantly higher than in NPRL patients after long-term administration of Ris at the clinical level. Our current study revealed that TBMA and hordenine could increase DRD2 expression and reduce PRL levels through DRD2 promoter demethylation *in vivo* and *in vitro*. However, only 46 patients with schizophrenia were included in the clinical study, which is a small number of cases, so the sample size should be expanded for further study. which will be the focus of our future research.

We also observed the interesting phenomenon that TBMA had a greater effect on DNMT levels than hordenine, suggesting that other unknown components in TBMA can decrease the expression of the DNMTs. In future TBMA studies, we hope to identify these other components and further characterize the specific components regulating DRD2 methylation.

CONCLUSION

Our study clearly indicates that TBMA could reduce the incidence of AD-induced PRL level increases through DRD2 methylation, providing new insights into the epigenetic mechanism of the increased PRL levels caused by chronic AD administration and potential new treatment strategies based on epigenetic regulation. These findings could lay a foundation for future research and clinical intervention. Indeed, clarifying the biological mechanism mediating the relationship between DRD2 methylation and increased PRL levels can bring new and personalized prevention and treatment possibilities, reduce pain, and improve the quality of life.

DATA AVAILABILITY STATEMENT

The raw data supporting the conclusion of this article will be made available by the authors, without undue reservation.

ETHICS STATEMENT

The studies involving human participants were reviewed and approved by Wuhan Third Hospital. The patients/participants provided their written informed consent to participate in this study. The animal study was reviewed and approved by Wuhan Third Hospital. Written informed consent was obtained from the individual(s) for the publication of any potentially identifiable images or data included in this article.

AUTHOR CONTRIBUTIONS

Y-LC, writing of the original draft; L-Z, writing, review, and editing; HZ, data curation; J-HM, methodology; H-JW, methodology; XW, formal analysis; J-HW, formal analysis; J-LZ, methodology; M-SF, methodology; Y-GC, writing, funding acquisition; JA, original draft, funding acquisition.

FUNDING

This work was supported by the Scientific Research Project of Wuhan Health Commission (WZ21Q03); Major Project of Wuhan Health Commission (WZ21M03); Hubei Provincial Central Guidance Local Science and Technology Development Project (2020ZYYD026); Wuhan Applied Basic Frontier Project (2020020601012301).

REFERENCES

Alosaimi, F. D., Fallata, E. O., Abalhassan, M., Alhabbad, A., Alzain, N., Alhaddad, B., et al. (2018). Prevalence and Risk Factors of Hyperprolactinemia Among Patients with Various Psychiatric Diagnoses and Medications. *Int. J. Psychiatry Clin. Pract.* 22 (4), 274–281. doi:10.1080/13651501.2018.1425459

Antequera, F., and Bird, A. (1993). Number of CpG Islands and Genes in Human and Mouse. *Proc. Natl. Acad. Sci. U. S. A.* 90 (24), 11995–11999. doi:10.1073/pnas.90.24.11995

Asa, S. L., and Ezzat, S. (2002). Medical Management of Pituitary Adenomas: Structural and Ultrastructural Changes. *Pituitary* 5 (2), 133–139. doi:10.1023/a:1022320732718

Asa, S. L., and Ezzat, S. (1998). The Cytogenesis and Pathogenesis of Pituitary Adenomas. *Endocr. Rev.* 19 (6), 798–827. doi:10.1210/edrv.19.6.0350

Barau, J., Teissandier, A., Zamudio, N., Roy, S., Nalesso, V., Hérault, Y., et al. (2016). The DNA Methyltransferase DNMT3C Protects Male Germ Cells from Transposon Activity. *Science* 354 (6314), 909–912. doi:10.1126/science.aah5143

Bernard, V., Young, J., and Binart, N. (2019). Prolactin - a Pleiotropic Factor in Health and Disease. *Nat. Rev. Endocrinol.* 15 (6), 356–365. doi:10.1038/s41574-019-0194-6

Bernard, V., Young, J., Chanson, P., and Binart, N. (2015). New Insights in Prolactin: Pathological Implications. *Nat. Rev. Endocrinol.* 11 (5), 265–275. doi:10.1038/nrendo.2015.36

Borowczyk, E., Mohan, K. N., D'Aiuto, L., Cirio, M. C., and Chaillet, J. R. (2009). Identification of a Region of the DNMT1 Methyltransferase that Regulates the

Maintenance of Genomic Imprints. *Proc. Natl. Acad. Sci. U. S. A.* 106 (49), 20806–20811. doi:10.1073/pnas.0905668106

Bostwick, J. R., Guthrie, S. K., and Ellingrod, V. L. (2009). Antipsychotic-induced Hyperprolactinemia. *Pharmacotherapy* 29 (1), 64–73. doi:10.1592/phco.29.1.64

Céspedes, I. C., Ota, V. K., Mazzotti, D. R., Wscieklica, T., Conte, R., Galduróz, J. C. F., et al. (2021). Association between Polymorphism in Gene Related to the Dopamine Circuit and Motivations for Drinking in Patients with Alcohol Use Disorder. *Psychiatry Res.* 295, 113563. doi:10.1016/j.psychres.2020.113563

Céspedes, M. E. (2017). Polimorfismos del receptor D2. *Rev. Argent. Endocrinol. Metab.* 54 (1), 29–36. doi:10.1016/j.raem.2016.12.002

Chen, Y-g., Li, L-j., Guo, H., Zou, J-l., He, J., and Wang, Y-m. (2017). Effects of the Optimal Prescription of Huiru Yizeng on Hyperprolactinemia and Hyperplasia of Mammary Glands in Model Rats. *Med. Her.* 36 (01), 37

Christman, J. K. (2002). 5-Azacytidine and 5-Aza-2'-Deoxycytidine as Inhibitors of DNA Methylation: Mechanistic Studies and Their Implications for Cancer Therapy. *Oncogene* 21 (35), 5483–5495. doi:10.1038/sj.onc.1205699

Demarest, S. P., Gill, R. S., and Adler, R. A. (2015). Opioid Endocrinopathy. *Endocr. Pract.* 21 (2), 190–198. doi:10.4158/EP14339.RA10.4158/EP14339.RA

Edwards, J. R., Yarychkivska, O., Boulard, M., and Bestor, T. H. (2017). DNA Methylation and DNA Methyltransferases. *Epigenetics Chromatin* 10, 23. doi:10.1186/s13072-017-0130-8

Gangisetty, O., Wynne, O., Jabbar, S., Nasello, C., and Sarkar, D. K. (2015). Fetal Alcohol Exposure Reduces Dopamine Receptor D2 and Increases Pituitary Weight and Prolactin Production via Epigenetic Mechanisms. *PLoS One* 10 (10), e0140699. doi:10.1371/journal.pone.0140699

Gao, L., Wu, Z. X., Assaraf, Y. G., Chen, Z. S., and Wang, L. (2021). Overcoming Anti-cancer Drug Resistance via Restoration of Tumor Suppressor Gene Function. *Drug Resist Updat* 57, 100770. doi:10.1016/j.drup.2021.100770

Gerra, M. L., Gerra, M. C., Tadonio, L., Pellegrini, P., Marchesi, C., Mattfeld, E., et al. (2021). Early Parent-Child Interactions and Substance Use Disorder: An Attachment Perspective on a Biopsychosocial Entanglement. *Neurosci. Biobehav Rev.* 131, 560–580. doi:10.1016/j.neubiorev.2021.09.052

Gong, X., Tao, J., Wang, Y., Wu, J., An, J., Meng, J., et al. (2021). Total Barley Maiya Alkaloids Inhibit Prolactin Secretion by Acting on Dopamine D2 Receptor and Protein Kinase A Targets. *J. Ethnopharmacol.* 273, 113994. doi:10.1016/j.jep.2021.113994

Grigg, J., Worsley, R., Thew, C., Gurvich, C., Thomas, N., and Kulkarni, J. (2017). Antipsychotic-induced Hyperprolactinemia: Synthesis of World-wide Guidelines and Integrated Recommendations for Assessment, Management and Future Research. *Psychopharmacol. Berl.* 234 (22), 3279–3297. doi:10.1007/s00213-017-4730-6

Hamidi, T., Singh, A. K., and Chen, T. (2015). Genetic Alterations of DNA Methylation Machinery in Human Diseases. *Epigenomics* 7 (2), 247–265. doi:10.2217/epi.14.80

Horii, T., and Hatada, I. (2016). Regulation of CpG Methylation by Dnmt and Tet in Pluripotent Stem Cells. *J. Reprod. Dev.* 62 (4), 331–335. doi:10.1262/jrd.2016-046

Huang, X., Ren, L., Hou, L., Fan, H., Wang, C., Wang, C., et al. (2020). Paeoniflorin Ameliorates Antipsychotic-Induced Hyperprolactinemia in Rats by Attenuating Impairment of the Dopamine D2 Receptor and TGF-B1 Signaling Pathways in the Hypothalamus and Pituitary. *J. Ethnopharmacol.* 257, 112862. doi:10.1016/j.jep.2020.112862

Jiang, P., Sun, X., Ren, J., Liu, H., Lin, Z., Liu, J., et al. (2021). Effects of the Combination of Second-Generation Antipsychotics on Serum Concentrations of Aripiprazole and Dehydroaripiprazole in Chinese Patients with Schizophrenia. *Gen. Psych.* 34 (2), e100423. doi:10.1136/gpsych-2020-100423

Jung, Y.-S., Kim, Y.-E., Go, D.-S., and Yoon, S.-J. (2021). The Prevalence, Incidence, and Admission Rate of Diagnosed Schizophrenia Spectrum Disorders in Korea, 2008-2017: A Nationwide Population-Based Study Using Claims Big Data Analysis. *PLoS One* 16 (8), e0256221. doi:10.1371/journal.pone.0256221

Lee, W. K., Lim, D., and Park, H. (2016). Disability-Adjusted Life Years (DALYs) for Injuries Using Death Certificates and Hospital Discharge Survey by the Korean Burden of Disease Study 2012. *J. Korean Med. Sci.* 31 Suppl 2 (Suppl. 29859), S200–S207. doi:10.3346/jkms.2016.31.S2.S200

Li, H., Li, J., Yu, X., Zheng, H., Sun, X., Lu, Y., et al. (2018). The Incidence Rate of Cancer in Patients with Schizophrenia: A Meta-Analysis of Cohort Studies. *Schizophr. Res.* 195, 519–528. doi:10.1016/j.schres.2017.08.065

Lisoway, A. J., Chen, C. C., Zai, C. C., Tiwari, A. K., and Kennedy, J. L. (2021). Toward Personalized Medicine in Schizophrenia: Genetics and Epigenetics of Antipsychotic Treatment. *Schizophr. Res.* 232, 112–124. doi:10.1016/j.schres.2021.05.010

Lobo, M. C., Whitehurst, T. S., Kaar, S. J., and Howes, O. D. (2022). New and Emerging Treatments for Schizophrenia: a Narrative Review of Their Pharmacology, Efficacy and Side Effect Profile Relative to Established Antipsychotics. *Neurosci. Biobehav Rev.* 132, 324–361. doi:10.1016/j.neubiorev.2021.11.032

Miranda, T. B., and Jones, P. A. (2007). DNA Methylation: the Nuts and Bolts of Repression. *J. Cell. Physiol.* 213 (2), 384–390. doi:10.1002/jcp.21224

Molitch, M. E. (2020). Dopamine Agonists and Antipsychotics. *Eur. J. Endocrinol.* 183 (3), C11–C13. doi:10.1530/EJE-20-0607

Ni, Y., Chen, Q., Cai, J., Xiao, L., and Zhang, J. (2021). Three Lactation-Related Hormones: Regulation of Hypothalamus-Pituitary axis and Function on Lactation. *Mol. Cell. Endocrinol.* 520, 520, 111084. doi:10.1016/j.mce.2020.111084

Pillinger, T., D'Ambrosio, E., McCutcheon, R., and Howes, O. D. (2019). Correction to: Is Psychosis a Multisystem Disorder? A Meta-Review of Central Nervous System, Immune, Cardiometabolic, and Endocrine Alterations in First-Episode Psychosis and Perspective on Potential Models. *Mol. Psychiatry* 24 (6), 928–794. doi:10.1038/s41380-018-0275-2

Robertson, K. D. (2001). DNA Methylation, Methyltransferases, and Cancer. *Oncogene* 20 (24), 3139–3155. doi:10.1038/sj.onc.1204341

Rusgis, M. M., Alabbasi, A. Y., and Nelson, L. A. (2021). Guidance on the Treatment of Antipsychotic-Induced Hyperprolactinemia when Switching the Antipsychotic Is Not an Option. *Am. J. Health Syst. Pharm.* 78 (10), 862–871. doi:10.1093/ajhp/zxab065

Shirvani-Farsani, Z., Maloum, Z., Bagheri-Hosseinabadi, Z., Vilor-Tejedor, N., and Sadeghi, I. (2021). DNA Methylation Signature as a Biomarker of Major Neuropsychiatric Disorders. *J. Psychiatr. Res.* 141, 34–49. doi:10.1016/j.jpsychires.2021.06.013

Stresemann, C., Brueckner, B., Musch, T., Stopper, H., and Lyko, F. (2006). Functional Diversity of DNA Methyltransferase Inhibitors in Human Cancer Cell Lines. *Cancer Res.* 66 (5), 2794–2800. doi:10.1158/0008-5472.CAN-05-2821

Suzuki, M. M., and Bird, A. (2008). DNA Methylation Landscapes: Provocative Insights from Epigenomics. *Nat. Rev. Genet.* 9 (6), 465–476. doi:10.1038/nrg2341

Tan, Y., Sun, R., Liu, L., Yang, D., Xiang, Q., Li, L., et al. (2021). Tumor Suppressor DRD2 Facilitates M1 Macrophages and Restricts NF-Kb Signaling to Trigger Pyroptosis in Breast Cancer. *Theranostics* 11 (11), 5214–5231. doi:10.7150/thno.58322

Tao, J-h., Gong, X-y., Zou, J-l., and Chen, Y-g. (2020). Simultaneous Determination of Alkaloids and Tricin in Malt Extract by HPLC. *New drugs traditional Chin. Med. Clin. Pharmacol.* 31 (01), 102

Tao, J.-h., Gong, X.-y., Cao, Y.-l., Zhang, Q.-y., Jing, S.-s., Wang, H., et al. (2021). Mechanism of Barley Malt-dependent DRD2 to Treat Hyperprolactinemia Based on UPLC-Q-TOF/MS and Network Pharmacology. *Eur. J. Integr. Med.* 43, 1322. doi:10.1016/j.eujim.2021.101322

Taşkömür, A. T., and Erten, Ö. (2021). The Effect of Tubal Ligation Surgery during Cesarean Operation on Dysmenorrhoea, Dyspareunia and Menstrual Cycle. *J. Gynecol. Obstetrics Hum. Reproduction* 50 (6), 102054. doi:10.1016/j.jogoh.2020.102054

Thumfart, K. M., Jawaid, A., Bright, K., Flachsmann, M., and Mansuy, I. M. (2021). Epigenetics of Childhood Trauma: Long Term Sequelae and Potential for Treatment. *Neurosci Biobehav Rev* 132, 1039. doi:10.1016/j.neubiorev.2021.10.042

Vos, T., Allen, C., Arora, M., Barber, R. M., Bhutta, Z. A., Brown, A., et al. (2016). Global, Regional, and National Incidence, Prevalence, and Years Lived with Disability for 310 Diseases and Injuries, 1990-2015: a Systematic Analysis for the Global Burden of Disease Study 2015. *Lancet* 388 (10053), 1545–1602. doi:10.1016/S0140-6736(16)31678-6

Wang, P-c., Shi, J-f., Song, M-f., Wang, Y-g., and Li, X. (2018). Inhibitory Effect of Raw Malt on Hyperprolactinemia Induced by Risperidone in Female Rats. *Chin. J. Clin. Pharmacol.* 34 (09), 1092

Wei, Y., La, L., Wang, L., Batey, R., Wang, C., and Li, Y. (2017). Paeoniflorin and Liquiritin, Two Major Constituents in Chinese Herbal Formulas Used to Treat Hyperprolactinemia-Associated Disorders, Inhibits Prolactin Secretion in Prolactinoma Cells by Different Mechanisms. *J. Ethnopharmacol.* 204, 36–44. doi:10.1016/j.jep.2017.03.054

Yoshino, A., Katayama, Y., Ogino, A., Watanabe, T., Yachi, K., Ohta, T., et al. (2007). Promoter Hypermethylation Profile of Cell Cycle Regulator Genes in Pituitary Adenomas. *J. Neurooncol* 83 (2), 153–162. doi:10.1007/s11060-006-9316-9

Zhou, X., Ren, L., Yu, Z., Huang, X., Li, Y., and Wang, C. (2018). The Antipsychotics Sulpiride Induces Fatty Liver in Rats via Phosphorylation of Insulin Receptor Substrate-1 at Serine 307-mediated Adipose Tissue Insulin Resistance. *Toxicol. Appl. Pharmacol.* 345, 66–74. doi:10.1016/j.taap.2018.02.023

Zhu, Y., Zhang, C., Siafis, S., Zhuo, K., Zhu, D., Wu, H., et al. (2021). Prolactin Levels Influenced by Antipsychotic Drugs in Schizophrenia: A Systematic Review and Network Meta-Analysis. *Schizophr. Res.* 237, 20–25. doi:10.1016/j.schres.2021.08.013

Conflict of Interest: The authors declare that the research was conducted in the absence of any commercial or financial relationships that could be construed as a potential conflict of interest.

Publisher's Note: All claims expressed in this article are solely those of the authors and do not necessarily represent those of their affiliated organizations, or those of the publisher, the editors and the reviewers. Any product that may be evaluated in this article, or claim that may be made by its manufacturer, is not guaranteed or endorsed by the publisher.

Advantages of publishing in Frontiers

OPEN ACCESS
Articles are free to read for greatest visibility and readership

FAST PUBLICATION
Around 90 days from submission to decision

HIGH QUALITY PEER-REVIEW
Rigorous, collaborative, and constructive peer-review

TRANSPARENT PEER-REVIEW
Editors and reviewers acknowledged by name on published articles

Frontiers
Avenue du Tribunal-Fédéral 34
1005 Lausanne | Switzerland

Visit us: www.frontiersin.org
Contact us: frontiersin.org/about/contact

REPRODUCIBILITY OF RESEARCH
Support open data and methods to enhance research reproducibility

DIGITAL PUBLISHING
Articles designed for optimal readership across devices

FOLLOW US
@frontiersin

IMPACT METRICS
Advanced article metrics track visibility across digital media

EXTENSIVE PROMOTION
Marketing and promotion of impactful research

LOOP RESEARCH NETWORK
Our network increases your article's readership